IMPERIAL COLLEGE LONDON

The role of innate lymphoid cells in mucosal inflammation in paediatric viral bronchiolitis

A thesis submitted for the degree of Doctor of Philosophy

Dawid Swieboda

National Heart & Lung Institute
Imperial College London
Norfolk Place
London W2 1PG

December 2020

Abstract

Background Human respiratory syncytial virus (RSV) is the most common cause of bronchiolitis and acute lower respiratory tract infections (LRTI) among children worldwide. RSV is the leading cause of childhood hospitalisation and a financial burden on national health systems. No vaccine that protects against RSV infection is available. Children with bronchiolitis are at high risk of developing wheeze and asthma later in childhood. Recent data suggest that innate immunity plays a vital role in childhood, especially when maternal antibodies' levels are low and adaptive immune responses are immature. Innate lymphoid cells (ILCs) are among the most recently discovered innate immune cell types that could play a pivotal role in innate responses to RSV bronchiolitis. ILCs have been classified into three groups: ILC1, ILC2 and ILC3 depending on their function, transcription factor expression and phenotype. Although ILC2 numbers have been found to be elevated in bronchiolitis, the phenotypic and functional differences between ILCs from healthy infants and those with bronchiolitis have not been explored.

Hypothesis I propose that ILC frequencies and function are associated with disease severity and aetiology in children with acute lower respiratory tract infection.

Sub-hypothesis 1 ILCs from neonates are functionally different from healthy adult subjects.

Sub-hypothesis 2 Alterations in ILC frequencies and numbers in blood and airway samples are associated with disease severity, pathogen type and load.

Sub-hypothesis 3 Alterations in ILC function are associated with disease severity, pathogen type and load.

Methods To determine differences in ILCs in early life, lymphocyte populations, including ILC subset frequencies and numbers in blood samples collected from adults and neonates were investigated by flow cytometry. To study ILCs in bronchiolitis, blood and upper and lower airway samples were collected from infants with and without a respiratory viral infection. An optimised multicolour immunophenotyping panel (OMIP), intracellular staining panels (ICS) and other systems of analytical approach such as UMAP (Uniform Manifold Approximation and Projection), heatmaps, correlograms and principal component analysis (PCA) were used. ILCs were defined using the following gating strategy: live, single, $CD45^{+}$, lineage negative (CD3, CD14, CD16, CD56, CD1a, CD123 FcεR1α)$^{-}$ and $CD127^{+}$ cells. ILC1 cells were defined as $CD117^{-}CRTH2^{-}$, ILC2 cells were defined as $CRTH2^{+}$ $CD117^{int}$ and ILC3s were defined as $CD117^{+}CRTH2^{-}$. At the same time, other lymphocyte and granulocyte populations were enumerated. Alongside cellular work, using the

Meso Scale Discovery (MSD) platform, 29 immune mediators and cytokines were measured in airway samples.

Results I successfully optimised flow cytometry panels to determine frequencies and function of ILCs in small volumes of difficult to obtain clinical samples. Results suggest that ILC numbers were higher in whole blood obtained from neonates compared to healthy adults (*P*=0.0032), however, they produced significantly less IFN-γ (*P*=0.0015). Furthermore, there were significantly lower numbers of NKT (*P*=0.0001) and MAIT cells (*P*=0.0031) in neonates compared to healthy adults. In bronchiolitis, ILC numbers were significantly decreased in peripheral blood (*P*=0.005) and airways samples (*P*=0.025) obtained from bronchiolitic compared to control subjects; however, their capacity for IFN-γ production was similar between those groups. Interestingly, there was a significantly decreased production of IFN-γ in $CD4^+$ (*P*=0.042) and $CD8^+$ T cells (*P*=0.006) from bronchiolitic compared to control patients. Finally, levels of almost all mediators were higher in bronchiolitic babies than controls, including both type-1, type-2 and type-17 associated cytokines. Only IL-4 production in lower and upper airways was increased in rhinovirus- (RV) but not RSV-associated bronchiolitis (*P*=0.006).

Conclusions Small volumes of whole blood and paediatric respiratory samples can be used for enumerating ILCs (NK cells, ILC1, ILC2, ILC3), granulocytes (eosinophils and neutrophils), T – cells ($CD4^+$ and $CD8^+$), MAIT cells and NKT-like cells. The comparison of neonate and adult functional responses suggests that innate lymphoid cells are mature in early life and might play a pivotal role in the neonatal type-2 bias *via* the production of IL-13. Bronchiolitis was characterised not only by $CD3^+$ T cell but also by $CD3^-$ lymphopenia. ILCs numbers were much lower in infants with bronchiolitis compared to healthy controls; however, ILC had the ability to produce IFN-γ. My data suggest that RSV and RV can lead to different phenotypes of bronchiolitis. Finally, I demonstrated the importance of studying the lower and upper airways simultaneously, discovering that inflammatory signatures were different between these two compartments. For the first time all members of the ILC family were studied in viral bronchiolitis. Determining why some infants develop bronchiolitis and the pathogenesis of lower airway disease in infants could lead to a better understanding of early life immunity and the development of new biomarkers and clinical prophylactics.

Declaration of originality

I certify that this report, and the research to which it refers, are products of my work, conducted from October 2017 onwards at Imperial College London. Any ideas or quotations from published work or otherwise, or from the work of others are fully acknowledged in accordance with the Imperial College policy for Academic Integrity.

Copyright declaration

The copyright of this thesis rests with the author and is made available under a Creative Commons Attribution Non-Commercial No Derivatives licence. Researchers are free to copy, distribute or transmit the thesis on the condition that they attribute it, that they do not use it for commercial purposes and that they do not alter, transform or build upon it. For any reuse or redistribution, researchers must make clear to others the licence terms of the work.

Content

ABSTRACT **2**

DECLARATION OF ORIGINALITY **4**

COPYRIGHT DECLARATION **4**

CONTENT **5**

LIST OF FIGURES **10**

LIST OF TABLES **14**

ABBREVIATIONS **16**

ACKNOWLEDGEMENTS **20**

1. GENERAL INTRODUCTION AND OUTLINE OF THE THESIS **22**

1.1. Bronchiolitis **23**

1.2. Epidemiology of bronchiolitis **24**

1.3. Aetiology of bronchiolitis **25**
1.3.1. Respiratory Syncytial Virus (RSV) 25
1.3.1.1. Classification 26
1.3.1.2. Virion structure, genome and proteins of RSV 26
1.3.1.3. Attachment and fusion glycoprotein of RSV 28
1.3.1.4. RSV cell entry and replication 29

1.4. Non – RSV bronchiolitis, epidemiology **29**
1.4.1. Human Rhinovirus (HRV) 30
1.4.2. Human Metapneumonia Virus (hMPV) 31
1.4.3. Influenza viruses 31
1.4.4. Enteroviruses (EVs) 32
1.4.5. Coronaviruses (CoVs) 32

1.5. Immunity in bronchiolitis **32**
1.5.1. Adaptive responses in bronchiolitis 33
1.5.1.1. T lymphocytes (CD4 and CD8 T cells) 33
1.5.1.2. Unconventional' T cells 34
1.5.1.3. B Cells and immunoglobulins (Ig) 35
1.5.2. Innate responses in bronchiolitis 36
1.5.2.1. Innate barriers 36
1.5.2.2. Neutrophils 37
1.5.2.3. Eosinophils 37
1.5.2.4. Monocytes 38

1.6. Innate lymphoid cells (ILCs) including NK cells **39**
1.6.1. ILC subtypes 40
1.6.2. Group ILC1 - immunology 41
1.6.2.1. NK cell immunology - cytotoxic ILC1s (cILC1s) 41
1.6.2.2. Non-NK ILC1s 43

1.6.3. Group ILC2 immunology 44
1.6.3.1. ILC2s and their immunology 45
1.6.4. Group ILC3 immunology 47
1.6.5. ILCs in infection and homeostasis 48
1.6.5.1. ILCs in viral infections 49
1.6.5.2. ILCs and bronchiolitis in children 50

1.7. Rationale, hypothesis, aims & outline of the thesis 51
1.7.1. Rationale 51
1.7.2. Research proposal 51
1.7.3. Aims 51
1.7.4. Outline of the thesis 52

2. MATERIALS AND METHODS 53

2.1. Materials 54
2.1.1. Consumables 54
2.1.2. Reagents 55
2.1.3. Media and media supplements 56
2.1.4. Commercially available kits 56
2.1.5. Antibodies for cytometry 57
2.1.6. MSD panels 59
2.1.7. Equipment and software 59

2.2. Methods 60
2.2.1. Early Life Lung Infection (ELLI) study - outline 60
2.2.2. Ethical Approval (see Appendix) 61
2.2.3. Consent (see Appendix) 61
2.2.4. Deferred consent (see Appendix) 61
2.2.5. Clinical cohort/patients 62
2.2.6. Clinical data collection 64
2.2.7. Clinical procedures 64
2.2.7.1. Airway samples 65
2.2.7.1.1. Nasosorbtion (NS) 65
2.2.7.1.2. Nasopharyngeal aspirate (NPA) 65
2.2.7.1.3. Tracheal Aspirate (TA) 65
2.2.7.2. Blood samples 66
2.2.7.2.1. Infant blood samples 66
2.2.7.2.2. Adult blood samples 66
2.2.7.2.3. Cord blood samples 66
2.2.8. Samples collection and processing 66
2.2.8.1. Fresh blood samples collection 66
2.2.8.1.1. Adult blood collection 66
2.2.8.1.2. Infants blood collection 66
2.2.8.1.3. Cord blood collection 67
2.2.8.2. Fresh blood sample processing 67
2.2.8.2.1. Plasma collection 67
2.2.8.2.2. PBMC isolation 67
2.2.8.2.3. Freezing samples 68
2.2.8.2.4. Thawing samples 68
2.2.8.3. Fresh airway samples collection 68
2.2.8.3.1. NS collection 68
2.2.8.3.2. NS processing 69
2.2.8.3.3. NPA and TA sample collections 69
2.2.8.3.4. NPA and TA sample processing 70
2.2.9. Assays 70
2.2.9.1. Flow cytometry 70
2.2.9.1.1. Surface staining 70

2.2.9.1.1.1. Fresh whole blood staining 70
2.2.9.1.1.2. Fresh airway samples staining 71
2.2.9.1.2. Intracellular staining 71
2.2.9.1.2.1. Stimulation of PBMCs 71
2.2.9.1.2.2. Surface staining 71
2.2.9.1.2.3. Permeabilisation and intracellular staining 72
2.2.9.1.3. Preparation of compensation beads 72
2.2.9.1.4. Flow cytometry analysis 73
2.2.9.1.5. Deep immunophenotyping analysis 73
2.2.9.1.6. Heatmaps, correlograms and PCA visualisations in R 74
2.2.9.2. Measurement of cytokines via MSD plates 74
2.2.9.3. Statistic and data analysis 75

3. RESULTS 76

3.1. Immunophenotyping leukocytes in a small volume of paediatric samples 77
3.1.1. Introduction for Chapter 3.1 78
3.1.2. Methods for Chapter 3.1 80
3.1.2.1. Blood samples collection and processing 80
3.1.2.2. Airway samples collection and processing 81
3.1.3. Flow cytometry and staining procedures during OMIP optimisation 82
3.1.3.1. Staining protocol for flow cytometry on fresh peripheral blood and blood stabilised with TransFix™ 82
3.1.3.2. Staining protocol for OMIP on airway samples, frozen and red-cell-lysed blood 83
3.1.3.3. Antibodies titration for OMIP on whole blood and airways samples 83
3.1.3.4. Data acquisition 83
3.1.4. Results for Chapter 3.1 84
3.1.4.1. Design and optimisation of staining panel 84
3.1.4.2. Optimisation of staining panel on blood from healthy adult volunteers 92
3.1.4.2.1. Characterizing the impact of RBC lysis before and after staining on the innate cell populations in whole blood 92
3.1.4.2.2. Characterising of the impact of Fc- receptor blocking on RBC-lysed whole blood 93
3.1.4.2.3. The impact of time and fixative reagent on fluorochrome brightness 94
3.1.4.3. Establishing the effect of controlled-rate cryopreservation on whole blood 95
3.1.4.4. The characterisation a Transfix™-based stabilisation technique on whole blood staining 96
3.1.4.4.1. Characterising the effect of time on the preservation of whole blood using Transfix™ 97
3.1.4.5. Optimisation of the staining panel on paediatric airway samples 98
3.1.5. Discussion for Chapter 3.1 102

3.2. Innate lymphocytes are phenotypically and functionally different between adults and neonates 106
3.2.1. Introduction for Chapter 3.2 107
3.2.2. Methods for Chapter 3.2 109
3.2.2.1. Samples collection and processing 109
3.2.2.2. The immune cell populations (OMIP) panel 110
3.2.2.3. Intracellular staining panels for cytokine production 110
3.2.2.3.1. Optimisation and gating strategy for the IFN-γ, IL-13, IL-17A and IL-22 staining panel 110
3.2.2.3.2. NK cell function (Granzyme B) staining panel 116
3.2.2.4. Antibody titration and FMO controls for ICS flow cytometry panels 117
3.2.2.5. Acquisition of flow cytometric data 118
3.2.2.5.1. Deep Immunophenotyping (*t*-SNE and UMAP) 118
3.2.2.6. Statistic and data analysis 119
3.2.3. Results for Chapter 3.2 123
3.2.3.1. Characteristics of study populations for chapter 3.2 123
3.2.3.2. The abundance of different innate and adaptive cells using OMIP in adults and neonates 125
3.2.3.2.1. OMIP study population characteristics 125
3.2.3.2.2. The abundance of innate cell populations in healthy adults and neonates 127
Enumeration of circulating granulocytes in healthy adults and neonates 127
Enumeration of circulating ILCs in healthy adults and neonates 128

Enumeration of circulating NK cells in healthy adults and neonates 130
3.2.3.2.3. The normal abundance of other lymphocyte populations in healthy adults and neonates 131
3.2.3.2.4. Assessment of immune cell populations by UMAP 135
3.2.3.2.5. Assessment of circulatory immune cell populations and their correlations utilising R functions 138
3.2.3.3. The functional phenotype of different innate and adaptive cells determined by intracellular staining for cytokine production 146
3.2.3.3.1. Cytokine production (ICS) panel study population 146
3.2.3.3.2. The functional phenotype of innate cell populations in healthy adults and neonates 147
IFN-, IL-13, IL-17A and IL-22 production in circulating NKs and ILCs (ILC1s, ILC2s, ILC3s) 147
3.2.3.3.3. The functional phenotype of other lymphocyte populations in healthy adults and neonates . 150
IFN-, IL-13, IL-17A and IL-22 production in circulating NKT, CD4⁺ and CD8⁺ T cells 150
3.2.3.3.4. Assessment of the functional phenotype of circulatory cell populations by UMAP 152
3.2.3.3.5. Assessment of circulatory immune cell populations and their correlations utilising R function 158
3.2.3.4. NK cell function (Granzyme B production) 164
3.2.3.4.1. NK cell function (Granzyme B) study population 164
3.2.3.4.2. The functional phenotype of innate and adaptive cell populations in healthy adults and neonates using the Granzyme B panel 165
Granzyme B production and CD57 expression in circulating NK cell populations 165
Granzyme B production and CD57 expression in circulating NKT, CD4⁺ and CD8⁺ T cell populations 168
3.2.3.4.3. Assessment of the functional phenotype of circulatory cell populations by UMAP 168
3.2.3.4.4. Assessment of circulatory immune cell populations and their correlations utilising R in the Granzyme B cohort 171
3.2.4. Discussion for Chapter 3.2 176

3.3. Alterations in frequency, number and function of innate lymphocytes in bronchiolitis 185
3.3.1. Introduction for Chapter 3.3 186
3.3.2. Methods for Chapter 3.3 189
3.3.2.1. Sample collection and processing 189
3.3.2.2. Flow cytometry panels 189
3.3.2.3. Analysis flow cytometry 189
3.3.2.3.1. Deep Immunophenotyping of cytometric data (UMAP) 189
3.3.2.4. Measurement of cytokine levels using the MSD platform 189
3.3.2.5. Statistic and data analysis 190
3.3.3. Results for Chapter 3.3 191
3.3.3.1. Characteristics of study populations for chapter 3.3 191
3.3.3.2. The abundance of different innate and adaptive cells in bronchiolitis 194
3.3.3.2.1. Cohort characteristics for cell enumeration in whole blood 194
3.3.3.2.2. Cohort characteristics for cell enumeration in NPA 194
3.3.3.2.3. Cohort characteristics for cell enumeration in TA 195
3.3.3.2.4. The abundance of cell populations in control and bronchiolitic infants in blood and airway samples 199
Enumeration of granulocytes, lymphocytes and monocytes in control and bronchiolitic infants 199
3.3.3.2.4.1. The abundance of innate cell populations in control and bronchiolitic infants 200
Enumeration of granulocytes in control and bronchiolitic infants 200
Enumeration of ILCs in control and bronchiolitic infants 202
Enumeration of NK cells in control and bronchiolitic infants 205
3.3.3.2.4.2. The abundance of adaptive cell populations in controls and bronchiolitics 206
Enumeration of lymphocytes, CD4⁺ and CD8⁺ T cells in control and bronchiolitic infants 206
Enumeration of MAIT, NKT, Tc2 and Th2 cells in control and bronchiolitic infants 208
3.3.3.2.5. Assessment of the immunome of bronchiolitic infants by UMAP 210
3.3.3.2.6. Assessment of cellular correlations in bronchiolitic infants 217
Correlation of different cell populations in whole blood, NPA and TA immune profiles 217
Correlations between NPA and TA cellular immune profiles 217
Correlation between disease severity and cellular immune profiles 222
3.3.3.3. The functional phenotype of innate and adaptive PBMCs in bronchiolitis and health 226
3.3.3.3.1. Cohort characteristics for the PBMC functional phenotyping 226

3.3.3.3.2. Functional phenotyping reveals alterations in cytokine production in NKT and T cells in bronchiolitis 228
IFN-γ, IL-13, IL-17A and IL-22 production in circulating innate (NK, ILC1s, ILC2s, ILC3s and NKTs) and adaptive ($CD4^+$ and $CD8^+$ T cells) cell populations 228
UMAP confirms IFN-γ, IL-13, IL-17A and IL-22 production in the adaptive and innate populations 229
3.3.3.3.3. Correlations between the age and IFN-γ-producing innate and adaptive cells 232
3.3.3.4. The quantification of mucosal immune mediators in the lower and upper airways 233
3.3.3.4.1. Cohort characteristics of NPA used in immune mediators quantification 233
3.3.3.4.2. Cohort characteristics of TA used in immune mediators quantification 234
3.3.3.4.3. Changes in soluble mediators in the airways of control and bronchiolitic patients 237
Level of selected mediators in the upper airway (NPA) compartment 237
Level of selected mediators in the lower airway (TA) compartment 239
3.3.3.4.4. Cytokine profiles in severe bronchiolitis and healthy controls 241
NPA cytokine immune profile in bronchiolitis and health 241
TA cytokine immune profile in bronchiolitis and health 243
3.3.3.4.5. Assessment of cytokine correlations in bronchiolitic infants 243
Correlations analysis according to age, weight, disease severity 243
Correlations between NPA and TA cytokine immune profiles 245
3.3.4. Discussion for Chapter 3.3 250
Granulocytes in Bronchiolitis 250
Innate Lymphoid Cells in Bronchiolitis 251
Innate and adaptive lymphocytes in bronchiolitis 253
Cytokine production in bronchiolitis 254
Type-2 responses in bronchiolitis 254
Heterogeneity in the immune response in bronchiolitis 256
Strengths and limitations of this study 257

DISCUSSION 260
Why ILCs and bronchiolitis? 261
Tools that matter - OMIP 262
Newborns not so immature 264
Ye olde bronchiolitis and ILCs - new kids on the block 266
Future work 270
Conclusions & final remarks 273

BIBLIOGRAPHY 276

APPENDIX 286

ELLI Ethical Approval 287

ELLI Consent Form (Parents and Guardians) V3.0 294

ELLI PIS Healthy Adults V3.0 296

ELLI PIS Parents and guardians (Infected) V3.0 300

ELLI PIS Parents and guardians (Uninfected) V3.0 305

ELLI Protocol V3.0 311

Figure permission from Nature Springer 329

Publication OMIP-062 336

List of figures

Figure 1.1 Epidemiology of bronchiolitis. 24
Figure 1.2 The structure of RSV. 27
Figure 1.3 Members of the ILC family. 39

Figure 2.2.1 Clinical workflow in the Paediatric Intensive Care Unit (PICU) and Imperial College London (ICL) laboratories, St. Mary's Campus in the ELLI project. 60
Figure 2.2.2 Flow chart indicating the clinical cohorts involved in the ELLI study. 62
Figure 2.2.3 Flow chart indicating the clinical procedures involved in the ELLI study. 65
Figure 2.2.4 Strategies for processing blood samples for flow cytometry. 67
Figure 2.2.5 Airway samples processing, and flow cytometry staining scheme used throughout the study. 69

Figure 3.1.1 Strategies for blood sample processing before immunophenotyping using OMIP. 80
Figure 3.1.2 Strategies for airway sample processing before immunophenotyping. 81
Figure 3.1.3 Example gating strategy and *t*-SNE analysis for visualisation of ILCs (including NK cells), granulocytes, MAIT, NKT-like cells and other T cell populations in paediatric clinical samples. 85
Figure 3.1.4 Exemplified gating strategy on NKT-like cells. 86
Figure 3.1.5 Histograms of CD161 and CD127 expression on ILCs. 86
Figure 3.1.6 The histograms showing antibodies titration used in the optimised FACS panel. ..87
Figure 3.1.7 Live/Dead reagent titration. 88
Figure 3.1.8 Gating strategy for enumeration of lymphocytes and granulocytes in paediatric nasopharyngeal aspirate (NPA) and tracheal aspirate (TA). 90
Figure 3.1.9 Fluorescence Minus one controls (FMOs) for Granulocytes, NK cells, MAITs and ILCs. 91
Figure 3.1.10 Comparison of RBC lysis before and after staining protocol on granulocytes, ILCs and a total number of live cells in fresh human blood. 92
Figure 3.1.11 Impact of Fc blocking on granulocytes and total number of cells in lysed whole blood human samples. 93
Figure 3.1.12 Stained and fixed blood samples can be left up to three days post-staining before performing flow cytometry analysis. 94
Figure 3.1.13 Controlled – rate freezing and storage in liquid N_2 of fresh whole blood reduces the total number of live cells and the number of granulocytes upon recovery. 95
Figure 3.1.14 Comparison of blood processing protocols on whole blood stabilised using a patented Transfix™ reagent. 96
Figure 3.1.15 Transfix™ - a stabilising reagent preserves blood cells and cellular antigens up to 6 days before flow cytometry analysis. 97
Figure 3.1.16 Blood samples stabilised with Transfix™ show a time-dependent decrease in the brightness of CRTH2 staining on ILCs. 99
Figure 3.1.17 Comparison of different processing protocols on lymphocyte and ILC number in tracheal aspirate (TA). 100
Figure 3.1.18 Comparison of different processing protocols on lymphocytes and ILC number in nasopharyngeal aspirate (NPA) using the optimised FACS panel. 101

Figure 3.2.1 Alternative strategies for PBMCs staining during ICS panel optimization. 109

Figure 3.2.2 Example gating strategy for visualisation of IFN-γ, IL-13, IL-17A and IL-22 production (ICS panel) in different populations of ILCs (ILC1, ILC2 and ILC3) and NK cells using (I) stimulated (II) and unstimulated adult PBMCs. 114
Figure 3.2.3 Example gating strategy for visualisation of Granzyme B production and CD57 expression (ICS panel) in NK, NKT, $CD4^+$ and $CD8^+$ T cell populations using adult PBMCs. 115
Figure 3.2.4 Alternative strategies for PBMCs staining during Granzyme B panel optimization. 117
Figure 3.2.5 Titration of antibodies used in optimized ICS and Granzyme B staining panels. 118
Figure 3.2.6 Extra Fluorescence Minus One controls (FMOs) for CD4, ILCs, Lymphocytes and NK cells utilized in optimized ICS and Granzyme B staining panels. 119
Figure 3.2.7 Comparison of deep immune phenotyping strategies (t-SNE and UMAP) for visualisation of ILCs (including NK cells), granulocytes, MAIT, NKT cells and other T cell populations in whole blood from adults and cord blood from neonates. 122
Figure 3.2.8 Flowchart of the study participants used in chapter 3.2 123
Figure 3.2.9 Abundance of granulocytes in whole blood from healthy adults and neonatal cord blood 127
Figure 3.2.10 Abundance of ILCs in the whole blood from healthy adults and cord blood from neonates. 128
Figure 3.2.11 Abundance of NK cells in whole blood from healthy adults and cord blood from neonates. 130
Figure 3.2.12 Abundance of lymphocytes, $CD4^+$ and $CD8^+$ T cells in whole blood from healthy adults and cord blood from neonates. 131
Figure 3.2.13 Abundance of MAIT, NKT, Tc2 and Th2 cells in whole blood from healthy adults and cord blood from neonates 133
Figure 3.2.14 Deep immune phenotyping of CD45+ populations in whole blood in adults and neonates using UMAP reveals cells alterations. 134
Figure 3.2.15 Deep immune phenotyping of ILCs (including NK cells) in whole blood in adults and neonates using UMAP reveals alterations in cell populations 137
Figure 3.2.16 Hierarchical clustering of the cohort of healthy adults and neonates using heatmaps. 139
Figure 3.2.17 The separation healthy adults and neonates using PCA but not by differences in sex 141
Figure 3.2.18 Neonates do not segregate using PCA by sex, weight, vaccination status and gestational age at vaccination. 142
Figure 3.2.19 The correlation between the different cell populations in healthy adults. 144
Figure 3.2.20 The correlation between the different cell populations in healthy neonates using correlograms. 145
Figure 3.2.21 Comparison of production of signature cytokines in stimulated NKs and ILCs from healthy adult and neonate PBMCs. 148
Figure 3.2.22 Comparison of production of signature cytokines in stimulated ILC populations (ILC1s, ILC2s and ILC3s) from healthy adult and neonate PBMCs 149
Figure 3.2.23 Comparison of production of signature cytokines in stimulated NKT, $CD4^+$ and $CD8^+$ T cells from healthy adult and neonate PBMCs. 151
Figure 3.2.24 Deep immune phenotyping of stimulated ILCs (including NK cells), NKT cells and other T cell populations in adult and neonate PBMCs using UMAP reveals alterations in cytokine production 155
Figure 3.2.25 Deep immune phenotyping of stimulated ILCs (ILC1s, ILC2s and ILC3s) and NK cells in adult and neonate PBMCs using UMAP reveals alterations in the cytokine production. 157

Figure 3.2.26 The hierarchical clustering of subjects in the ICS cohort of healthy adults and neonates using heatmap format. 158
Figure 3.2.27 The separation between healthy adults and neonates using PCA using the ICS cohort. 160
Figure 3.2.28 The correlation between different cell populations in the ICS cohort of healthy adults 162
Figure 3.2.29 The correlation between different cell populations in healthy neonates 163
Figure 3.2.30 Comparison of production of Granzyme B and CD57 expression of NK cells from healthy adult and neonatal PBMCs. 166
Figure 3.2.31 Comparison of production of Granzyme B and CD57 expression of NKT, CD4 and CD8 T cells from healthy adult and neonate PBMCs. 167
Figure 3.2.32 Deep immune phenotyping of granzyme B and CD57 expressing NK cells, NKT cells and T cell populations in adult and neonatal PBMCs using UMAP. 170
Figure 3.2.33 Hierarchical clustering and subject and sex signatures in the Granzyme B cohort of healthy adults and neonates using the heatmap format. 172
Figure 3.2.34 The separation of healthy adults and neonates using PCA and not by differences in sex in the Granzyme B cohort. 173
Figure 3.2.35 Correlation between the different cell populations in the Granzyme B cohort of healthy adults 174
Figure 3.2.36 The correlation between the different cell populations in the Granzyme B cohort of healthy neonates 175

Figure 3.3.1 Flowchart of the study participants used in chapter 3.3 191
Figure 3.3.2 Abundance of live cells, granulocytes, lymphocytes and monocytes in whole blood and airway samples from control and bronchiolitic infants. 199
Figure 3.3.3 Abundance of granulocytes in whole blood and airway samples from control and bronchiolitic infants. 201
Figure 3.3.4 Abundance of ILCs in whole blood and airway samples from control and bronchiolitic infants. 204
Figure 3.3.5 Abundance of NK cells in whole blood and airway samples from control and bronchiolitic infants. 205
Figure 3.3.6 Abundance of lymphocytes, $CD4^+$ and $CD8^+$ T cells in whole blood and airway samples from control and bronchiolitic infants. 207
Figure 3.3.7 Abundance of MAIT, NKT, Tc2 and Th2 cells in whole blood and airway samples from control and bronchiolitic infants. 209
Figure 3.3.8 Deep immune phenotyping of $CD45^+$ populations in whole blood and airway samples from control and bronchiolitic infants using UMAP reveals cell alterations. 212
Figure 3.3. 9 Deep immune phenotyping ILCs (including NK cells) in whole blood and airway samples from control and bronchiolitic infants using UMAP reveals cell alterations. 214
Figure 3.3.10 Deep immune phenotyping ILCs (including NK cells) in whole blood from control and bronchiolitic infants using UMAP reveals cells alterations in $CD4^+$ NKs and $CD4^+$ monocytes. 216
Figure 3.3.11 The correlation between different cell populations in bronchiolitic infants 218
Figure 3.3.12 The correlation dependence between the frequencies of the same cell populations in TA and NPA in the bronchiolitic infants. 220
Figure 3.3.13 The correlation dependence between the quantification of the same cell populations in TA and NPA in the bronchiolitic infants. 222
Figure 3.3.14 The correlation between different cell populations and the severity of disease in whole blood and airway samples in bronchiolitic infants. 225

Figure 3.3.15 Comparison of production of signature cytokines in stimulated ILCs (including NKs and ILC1s, ILC2s, ILC3s), NKT, $CD4^+$ and $CD8^+$ T cells from control and bronchiolitic infants' PBMCs.....228
Figure 3.3.16 Deep immune phenotyping of stimulated PBMCs from control and bronchiolitic infants using UMAP reveals alterations in cytokine production in the adaptive but not innate compartment.....231
Figure 3.3.17 The differences in IFN-γ-producing CD4, CD8 and NKT cells between control and bronchiolitic infants cannot be explained by age differences. 232
Figure 3.3.18 Soluble mediators in NPA samples from control and bronchiolitic infants.....238
Figure 3.3.19 Soluble mediators in TA samples from bronchiolitic infants 240
Figure 3.3.20 The hierarchical clustering of the NPA cytokines from control and bronchiolitic infants using heatmap format. 242
Figure 3.3.21 Hierarchical clustering of cytokines in the TA from control and bronchiolitic infants using a heatmap format. 244
Figure 3.3.22 Separation between subjects in PCA analysis of cytokine levels is not associated with the health status, sex or the aetiology of the disease. 247
Figure 3.3.23 The investigation of the correlation dependence between the cytokine levels and the severity of disease in NPA and TA from bronchiolitic infants using MSD data. 249

List of tables

Table 2.1 1 Consumables used throughout this thesis. 54
Table 2.1 2 'Off-shelf' reagents used in this thesis. 55
Table 2.1 3 Media and media supplements used in this thesis. 56
Table 2.1 4Commercially available kits. 57
Table 2.1 5 Antibodies used for surface staining for OMIP, ICS and Granzyme B panels. 57
Table 2.1 6 Antibodies used for intracellular staining in the ICS and Granzyme B panels. 58
Table 2.1 7 MSD panels used for the analysis of soluble mediators in airways supernatants. 59
Table 2.1 8 Equipment used throughout this thesis. 59
Table 2.1 9 Software used throughout this thesis 59
Table 2.2 1 Exclusion criteria for infants and adults in ELLI study 63
Table 2.2 2 Inclusion criteria for infants and adults in ELLI study 64
Table 2.2 3 Inclusion and exclusion criteria for cord blood in ELLI study 64

Table 3.1.1 Extracellular antibodies and their concentrations used in the optimised flow cytometry panel. 82

Table 3.2.1 Extra- and intracellular antibodies and their concentrations used in the optimised IFN-γ, IL-13, IL-22, IL-17A flow cytometry panel. 110
Table 3.2.2 Extra- and intracellular antibodies and their concentrations used in the optimised Granzyme B flow cytometry panel. 111
Table 3.2.3 Adults and neonates' demographics used for Chapter 3.2 123
Table 3.2.4 Demographics and clinical data for neonates used in Chapter 3.2. 124
Table 3.2.5 Adults and neonates' demographics used for the immune cell populations (OMIP) panel. 125
Table 3.2.6 Neonates demographics and clinical data used for the immune cell populations (OMIP) panel. 125
Table 3.2.7 Adults and neonates' demographics used in the optimised IFN-γ, IL-13, IL-22, IL-17A ICS flow cytometry panel. 146
Table 3.2.8 Neonates demographics and clinical data used in the optimised IFN-γ, IL-13, IL-22, IL-17A flow cytometry panel. 147
Table 3.2.9 Demographics of adults and neonates used in the optimised NK cell function (Granzyme B) flow cytometry analysis. 164
Table 3.2.10 Demographics and clinical data of neonates used the NK cell function (Granzyme B) flow cytometry analysis. 165

Table 3.3.1 Control and bronchiolitic infants' demographics used for Chapter 3.3. 193
Table 3.3.2 Control and bronchiolitic infants' demographics used for whole blood enumeration with immune cell population (OMIP) panel in Chapter 3.3. 196
Table 3.3.3 Control and bronchiolitic infants' demographics for NPA enumeration with the immune cell population (OMIP) panel in Chapter 3.3. 197
Table 3.3.4 Control and bronchiolitic infants' demographics used for TA enumeration with immune cell population (OMIP) panel in Chapter 3.3. 198
Table 3.3.5 Control and bronchiolitic infants' demographics used in the optimised IFN-γ, IL-13, IL-22, IL-17A flow cytometry panel (ICS) for Chapter 3.3. 227
Table 3.3.6 Control and bronchiolitic infants' demographics used for NPA analysis with MSD platform in Chapter 3.3. 235

Table 3.3.7 Control and bronchiolitic infants' demographics used for TA analysis with MSD platform in Chapter 3.3. 236

Abbreviations

Abbreviation	Definition
A	
ADCC	Antibody-dependent cell-mediated cytotoxicity
AIDS	Acquired Immune Deficiency Syndrome
LRTI	Lower Respiratory Tract Infection
APC	Antigen-presenting cells
Areg	Amphiregulin
Arg-1	Arginase-1
B	
BAFF	B-cell Activating Factor
BAL	Bronchoalveolar lavage
BALF	Bronchoalveolar Lavage Fluid
BrdU	5-bromo-2'-deoxyuridine
C	
CD	Cluster of Differentiation
CF	Cystic fibrosis
COPD	Chronic Obstructive Pulmonary Disease
CRTH2	Chemoattractant receptor - homologous expressed on Th2 cells
CSF	Cerebrospinal Fluid
CST	Cytometry Setting and Tracking
CXCL8	C-X-C Motif Chemokine Ligand 8
D	
DC	Dendritic cells
DMSO	Dimethyl sulfoxide
E	
ECP	Eosinophil Cationic Protein
EDN	Eosinophil-derived neurotoxin
EDTA	Ethylenediaminetetraacetic acid
EET	Eosinophil Extracellular Traps
EGFR	Epidermal Growth Factor Receptor
ELLI	Early Life Lung Infection
EOS	Eosinophils
ETT	Endotracheal Tube
EV	Enteroviruses
F	
FACS	Fluorescence-Activated Cell Sorting
FASL	Surface-associated FAS (CD95L) ligand
Fc	Fc receptor
FI-RSV	Formalin-Inactivated RSV
FlowSOM	Flow Self-Organizing Maps
FM	Freezing Media
FMO	Fluorescence Minus One
FSC	Forward Side Scatter

G	
GRAN	Granulocytes
GrzmB	Granzyme B
H	
HA	Hemagglutinin
HIV	Human Immunodeficiency Virus
hMPV	Human Metapneumovirus
HSC	Hematopoietic Stem Cell
I	
IBD	Inflammatory Bowel Disease
ICAM-1	Intercellular Adhesion Molecule 1
ICRRU	Imperial Clinical Respiratory Research Unit
ICS	Intracellular Staining
IELs	Intraepithelial lymphocytes
IFN	Interferon
iILC2s	inflammatory ILC2s
IL	Interleukin
ILCs	Innate Lymphoid Cells
iNKT	invariant Natural Killer T
IPF	Idiopathic Pulmonary Fibrosis
IR	Infra-Red
ISG	Interferon-Stimulated Genes
K	
kg	kilogram
KIRs	Killer cells Immunoglobulin-like Receptors
L	
LD	Live/Dead
LDLR	Low-Density Lipoprotein Receptor
Lin neg	Lineage negative
LLOD	Lower Limit of Detection
LRT	Lower Respiratory Tract
LTi	Lymphoid Tissue-inducer
LYM	Lymphocytes
M	
MAIT	Mucosal-Associated Invariant T
matAbs	Maternal antibodies
MCMV	Mouse Cytomegalovirus
MHC	Major Histocompatibility Complex
MIP-3α	Macrophage Inflammatory Protein 3α
MON	Monocytes
MPO	Myeloperoxidase
MSD	Meso Scale Discovery platform
mTOR	mammalian Target Of Rapamycin
N	

NA	Neuraminidase
NU	Neonatal Unit
NCR	Natural-Cytotoxicity-Receptor
NEC	Necrotising Enterocolitis
NET	Neutrophil Extracellular Traps
NHSBT-NCI	NHS Blood Transfer Non-Clinical Issue
NICU	Neonatal Intensive Care Unit
nILC2s	natural ILC2s
NK	Natural killer
NPA	Nasopharyngeal Aspirates
NS	Nasosorption
O	
OMIP	Optimised Multicolour Immunophenotyping Panel
P	
PCA	Principal Component of Analysis
PD-1	Programmed Cell Death 1
PFA	Paraformaldehyde
PGD_2	Prostaglandin D_2
PICU	Paediatric Intensive Care Unit
PMA	Phorbol 12-Myristate 13-Acetate
R	
RAG	Recombination Activating Gene
RBC	Red Blood Cells
RDRP	RNA-dependent RNA polymerase
REC	Research Ethics Committee
RNA	Ribonucleic acid
RORγT	RAR-related Orphan Receptor gamma T
RSV	Respiratory Syncytial Virus
RT	Room Temperature
RV	Rhinovirus
S	
S1P	Sphingosine-1-Phosphate
SAM	Synthetic Absorptive Matrix
SARS-CoV	Severe Acute Respiratory Syndrome-Coronovirus
SCID	Severe Combined Immunodeficiency Disease
scRNA-seq	single-cell RNA sequencing
SeV	Sendai Virus
SOP	Standard Operating Procedure
SP-A	Surfactant Proteins A
SSC	Side Site Scatter

T	
t-SNE	*t*- Stochastic Neighbouring Embedding
TA	Tracheal Aspirate
Tc	$CD8^+$ cytotoxic T cell
TEM	Transmission Electron Microscopy
Th	$CD4^+$ helper T cell
TLR	Toll-Like Receptor
TNFR	Tumour Necrosis Factor Receptor
TRAIL	TNF-Related Apoptosis-Inducing Ligand
T_{regs}	T regulatory cells
Trm	T-resident memory
TSLP	Thymic Stromal Lymphopoietin
U	
UMAP	Uniform Manifold Approximation and Projection
ULOD	Upper Limit of Detection
URTI	Upper Respiratory Tract Infection
W	
WB	Whole Blood
WBC	White Blood Cells
WHO	The World Health Organisation
Other	
γ_c	Common cytokine receptor γ-chain
χ^2 test	Chi-squared test

Acknowledgements

,, I was taught that the way of progress is neither swift nor easy''
Maria Skłodowska – Curie

Writing this thesis was a four-year journey, and I was lucky to have many 'good hearts' along the way and some who made it challenging. It would be impossible to say thank you to all those good hearts beside me over years, but I would love to thank you for those kings and queens that made my journey worth taking.

I would love to thank Dr Fiona Culley, for her support, patience, and invaluable insights since the beginning of this PhD. I have been fortunate to have you as my mentor, supervisor and the one who listened to my never-ending stories during the lockdown. Thank you for being a fantastic scholar and teaching me to be the best I can be in this what I am doing without losing enthusiasm and passion. I have been fortunate to have not one but five supervisors: Dr Ryan Thwaites, Dr Simon Nadel, Prof Trevor Hansel and Prof Peter Openshaw. I am grateful for all the chats, their kindness and erudition. Big thank you, in particular, to Peter and his stories and anecdotes – they made me giggle so many times.

I am particularly grateful to Dr Yanping Guo, Gale Lewis, Sasha Ashbourne – Lewis, Seema Vekaria, Dan Solanki for their guidance, help and chats. I have found all the members of the Respiratory Medicine Section supportive during this PhD project. I am very appreciative of the MRC-Asthma UK Centre for providing the funding for my PhD studies.

Special thanks go to all students in our office: Sophie Sagawe, Freja Kirsebom, Kate Strong, Celia Diaz, who have cheered me; for their encouragements and expertise on wide-range matters. It would be impossible to face another day without them and their light approach towards life, love and work. You are divinities that should be worshipped! I wish you all the best and hope to stay friends forever. Freja, you are my Ariana Grande, and I do not know how I have coped the last year without you; you are such an amazing friend, listener and, foremost, an extraordinary being!

Special thanks have to go to my incredibly devoted and hard-working team of research nurses: Sarah Darnell, Amina 'Farhana' Mehar, Benjamin Walsh, Sobia Mustafa in Clinical Children Research Facility, St. Mary's Hospital, London. It goes without saying that without your work, this PhD would fail, and I was fortunate to have you for keeping a hand on a pulse.

A Mount Everest of gratitude to all my supportive and loving friends Marie Toussaint, Anabel Guedan-Paredez, Maria-Belén Trujillo, Heidi Makrinioti, Neil Andrews, Lukasz Bukowski, Norbert Szymczyk, Piotr Brysik, Radek Leżański, Pawłek Ziomek, Michael Mertens, Maciek Brylewicz, James Maxwell, Sarad Gurung, Anna Wałek, Edilia Hinojosa, Rebecca and Hannah Tyerman *et al*. Extra special gratitude goes to Maria 'Mary' Matuśkiewicz, who has been the biggest and the most faithful fan of mine. You believed from the beginning that I would be the best PhD ever. You woke up a warrior in me who fought to finish this incredible journey, and that is why I am so utterly grateful for your friendship.

Finally, I would love to thank my whole family, including my sisters Angelika and Basia, who has put up with all stories of my life in London. Most of all, my mum Bożena, who has been on my side for better and worse. She taught me to inspire, challenge myself, and I am blessed to be your son- *Dziekuję że jesteś*. Dad, I believe you would be proud of the man I have become, and I truly miss you every day.

Last, but never least, Mother Earth for never stop giving and allowing me to flourish in an abundance of sunshine, stars and miracles that sweeps me off my feet daily.

1.

Introduction

1.1. Bronchiolitis

Bronchiolitis is a potentially life-threatening illness of the lower respiratory tract (LRT). It affects infants and young children [1,2]. The most common causes of bronchiolitis worldwide are infections with respiratory syncytial virus (RSV) and rhinovirus (RV). Children with RSV-related bronchiolitis stay in hospital longer and have a more intense inflammatory response with higher levels of mortality and morbidity compared to RV infection [1,2]. The exact mechanisms of pathogenesis are not very well understood.

Bronchiolitis manifests itself as a combination of cough, wheezing, rhinitis, tachypnoea, hyperinflation and chest retraction. Clinical scores assess severe bronchiolitis, and infants who have severe bronchiolitis are those who require hospitalisation. During bronchiolitis cytotoxic, viral-induced necrosis occurs in the epithelium of the LRT leading to blockage of bronchioles [3]. Data from ultra-high-speed video microscopy and transmission electron microscopy revealed that RSV can directly lead to cilial impairment through mitochondrial damage, and, combined with increased mucus production and the loss of epithelial and ciliated cells, results in decreased mucociliary clearance and increased plugging of airways with mucus and necrotic cell debris [4]. Mucus production is an important arm of innate host defence as it can serve to trap airborne particles, but its production in excess might lead to the obstruction of lower airways and increase the severity of diseases, including bronchiolitis. Besides direct damage of the epithelium by the virus, overexuberant immune responses contribute to the pathogenesis [5]. Immune responses skewed towards type-2 immunity, characterised by the production of type-2 cytokines (IL-4, IL-5 and IL-13), may contribute to lung damage and hyperinflammation in viral infection [6]. It has been documented that children with severe viral bronchiolitis exhibit lung inflammation pronounced with an abundance of T cells, neutrophils, monocytes, and inflammatory mediators that can be pathogenic and lead to the development of the enhanced disease [5].

Although bronchiolitis is considered as a homogeneous illness according to the American Academy of Paediatrics clinical guidelines [2], recent studies of bronchiolitis identified several clinical phenotypes of this illness, suggesting it is a heterogeneous entity [7]. Pathogenesis in bronchiolitis has been an active research area. A lack of vaccine and an expensive antibody-based immune prophylaxis with Palivizumab (a recombinant humanised monoclonal antibody to the RSV fusion protein sold under the brand name Synagis) underlies the need for new biomarkers and treatments in bronchiolitis [5,8].

1.2. Epidemiology of bronchiolitis

Bronchiolitis is a seasonal disease that peaks between mid-December and February in the northern hemisphere, causing winter epidemics [9]. RSV-related bronchiolitis predominantly affects infants below the age of two and poses a significant financial burden on national health services in the UK and worldwide [10]. The World Health Organisation (WHO) estimates that RSV-related infections are associated with 120000 in-hospital deaths (94600 – 149000) and up to 3.2 million hospitalisations annually [11,12]. The overall estimated economic impact of RSV-related healthcare is between $500-$700 million annually in the USA alone (**Figure 1.1**) [13,14].

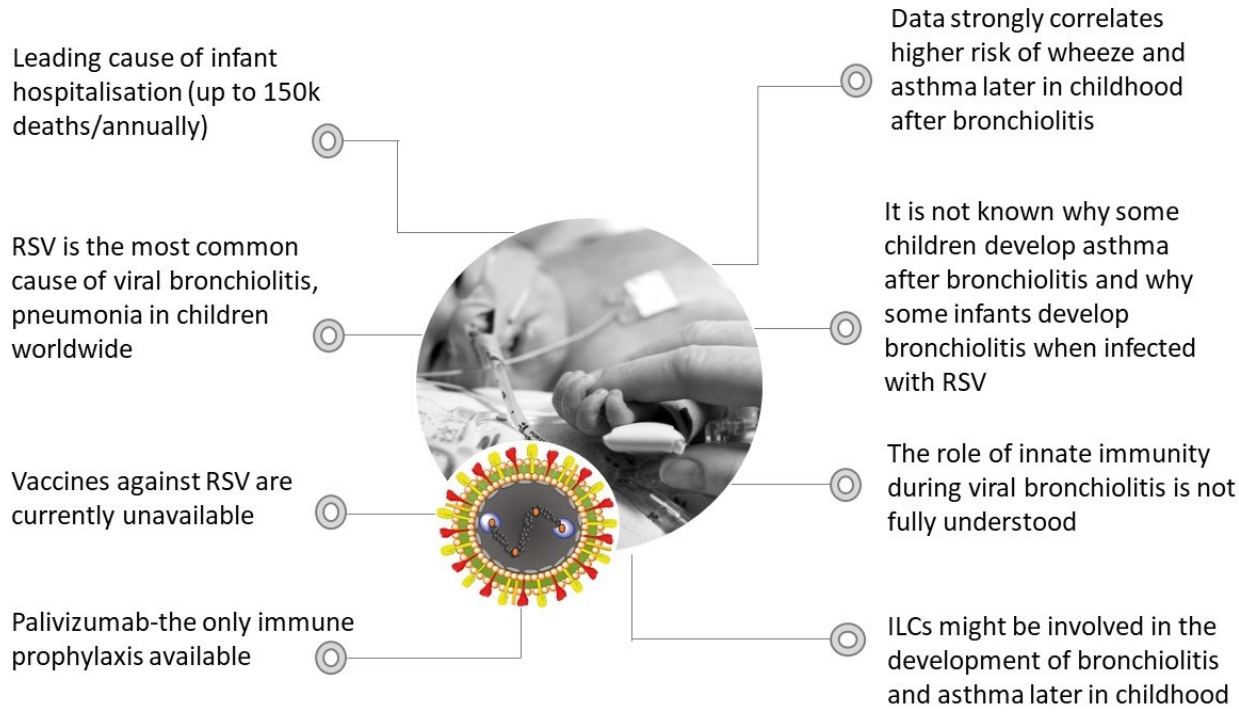


Figure 1.1 Epidemiology of bronchiolitis.

Bronchiolitis is the leading reason for a child under the age of two to be admitted to hospital. This is usually caused by a respiratory syncytial virus (RSV). Children who have had severe bronchiolitis are at a higher risk of developing recurring wheeze and asthma later in childhood. There is no vaccine, and no new treatments have been developed in recent years. I aimed to better understand the immune response to RSV infection, thereby contributing to better treatments or vaccines for RSV disease.

In the developed, high-income world mortality is very low, while in low and middle-income countries (LMICs) paediatric deaths due to bronchiolitis are high even in a hospital setting. The number of RSV-related deaths due to bronchiolitis outside of a hospital is unknown but likely to be high. Data from slums in Argentina, Indonesia and Bangladesh was utilised to estimate the total deaths in a hospital setting using the community – to – hospital death ratio to recalculate the RSV-related mortality adjusted to other confounders such as influenza and pneumococcal infections [12]. This data suggested that the global mortality due to RSV-bronchiolitis might be

underestimated, and additional studies are needed to accurately determine the fatality especially when multi-bacterial and viral co-infections are involved. Mansbach *et al.* (2012) found that 29.8% of a cohort of bronchiolitic children were diagnosed with co-infections with multiple pathogens present, including RSV, RV and other viruses or bacteria [1,2].

In the UK, bronchiolitis is a high morbidity but low mortality disease with a death rate of 1.8 per 100000 children under one year of age [15]. This low death rate reflects progress in supportive intensive care and substantial effort put into prevention of RSV-related bronchiolitis, such as use of the minimal handling approach, educating parents and pre-treatment of high-risk children (infants born prematurely, with congenital heart disease, with pulmonary and/or neuromuscular abnormalities, and immunocompromised) with immunoprophylaxis with Palivizumab (Synagis, a recombinant humanised monoclonal antibody to the RSV fusion protein F) [1,15].

In other high-income countries mortality in babies in and outside the hospital is also low, well studied and mostly involves children below three months of age [5,8,10]. Although only 1-3% of infants infected with RSV require hospitalisation, 2-3% of admitted children require intensive care unit (ICU) treatment and mechanical ventilation [10,16]. Most babies with bronchiolitis recover without complications. Enigmatically, it is not known why some infants (1-2%) develop life-threatening bronchiolitis when others suffer mild infections [10]. There are many risk factors for RSV-induced bronchiolitis. Genetic polymorphisms in innate immune genes, such as variants in CXCL8, IL-4Rα and the 5q31 Th2 cytokine locus are responsible for up to 20% of susceptibility to severe RSV infection [10,17,18]. Other key factors include prematurity, sex, a low cord blood level of vitamin D, maternal smoking, immunodeficiency and poor socio-economic background [5,8–10]. The strongest predictor of the severity of bronchiolitis is the age of the baby. [19]. Infection studies on *L. monocytogenes*, *T. gondii*, *Streptococcus spp.* and RSV highlight the importance of innate deficiencies, particularly in TLR signalling on the susceptibility to infection in the first year of life [20]. Selective immunological amnesia seems to be the main factor which allows RSV to re-infect patients repeatedly throughout life [5].

1.3. Aetiology of bronchiolitis

1.3.1. Respiratory Syncytial Virus (RSV)

The human respiratory syncytial virus (RSV) was first isolated from chimpanzees with coryza in the Walter Reed Army Institute of Research in the USA in 1957. A couple of years later, RSV was recovered from the LRTs of bronchiolitic children admitted to hospital in Baltimore (MD) [21]. Since its discovery, this viral agent has been linked with the development of paediatric bronchiolitis,

and it has been associated with the development of wheeze and asthma later in childhood [10,22]. In healthy adults and the elderly (≥60 years of age), RSV is a cause of upper respiratory tract colds. However, RSV can lead to high morbidity and mortality in older adults. From published data, it is known that RSV-related disease burden in the elderly and immunocompromised adults is similar to non-pandemic influenza A infections [22,23].

1.3.1.1. Classification

RSV, of the *Orthopneumovirus* genus of the *Pneumoviridae* family in the order *Mononegavirales* is responsible for acute lower respiratory tract illness (ALRIs) such as bronchiolitis and pneumonia in children and vulnerable adults worldwide [23–25]. Since RSV can form multinucleated giant cell syncytia in type II respiratory epithelium, the descriptive term RSV (Respiratory Syncytial Virus) was coined [23]. Although there is only one RSV serotype, two main variants have been identified, RSV A and RSV B, based on antigenic reactivity to monoclonal antibodies and genetic differences [24]. Even though both variants co-circulate during annual epidemics, typically, only one of the subtypes is prevalent in the RSV season [25]. It is believed that in the summer months, a reservoir for both circulating variants of RSV may be immunocompromised and chronic obstructive pulmonary disease (COPD) adults [15].

1.3.1.2. Virion structure, genome and proteins of RSV

RSV is an enveloped (**Figure 1.2 A, C**) filamentous virus with a diameter of 150 nm [10]. Its negative-sense, non-segmented, 15.2 kb RNA genome consists of 10 genes (3'-NS1-NS2-N-P-M-SH-G-F-M2-L-5') encoding 11 proteins: structural proteins, such as the nucleocapsid protein (N), phosphoprotein (P), one matrix protein (M), three envelope proteins (F, G, SH), the other M2 matrix protein (M2), the large protein (L) and two non-structural proteins (NS1 and NS2) (**Figure 1.2 B**) [24,26]. The non-structural genes of RSV NS1 and NS2 are the first to be transcribed. Both NS1 and NS2 are expressed early in infection as they stop apoptosis of infected cells, inhibit the induction of alpha/beta interferon (IFN-α/β) and reduce the IFN-orchestrated antiviral state [27,28]. The M2 gene is one of the last transcriptional units of RSV genome and has two overlapping open reading frames (ORFs) for the upstream M2-1 (22 kDa, ORF1, a forward transcription elongation factor) and the downstream M2-2 (11kDa, ORF2, a regulatory transcription/replication switch of the viral RNA) matrix proteins [29,30]. Both, the M2-1 and M2-2 matrix proteins, have an important modulatory function balancing RNA replication and transcription of the RSV genome [31]. The nucleocapsid protein (N) encapsulates viral RNA, forming RNA – N protein complexes as it has an intrinsic capacity for binding non-specifically to

RNA [31]. The nucleoprotein (N) with the phosphoprotein (P), the large polymerase protein (L) and the matrix protein cofactors M2-1 and M2-2 form the helical RNA-dependent RNA polymerase complex required for replication of RSV [31]. The L protein acts as the RNA-dependent RNA polymerase driving viral RNA replication, transcription of mRNA and it is involved in the capping of 5'-mRNA end and the methylation of the cap [24]. The P phosphoprotein is a crucial part of replication and transcription machinery through the interactions with N and L proteins to keep them soluble for a proper assembly of the virion [32].

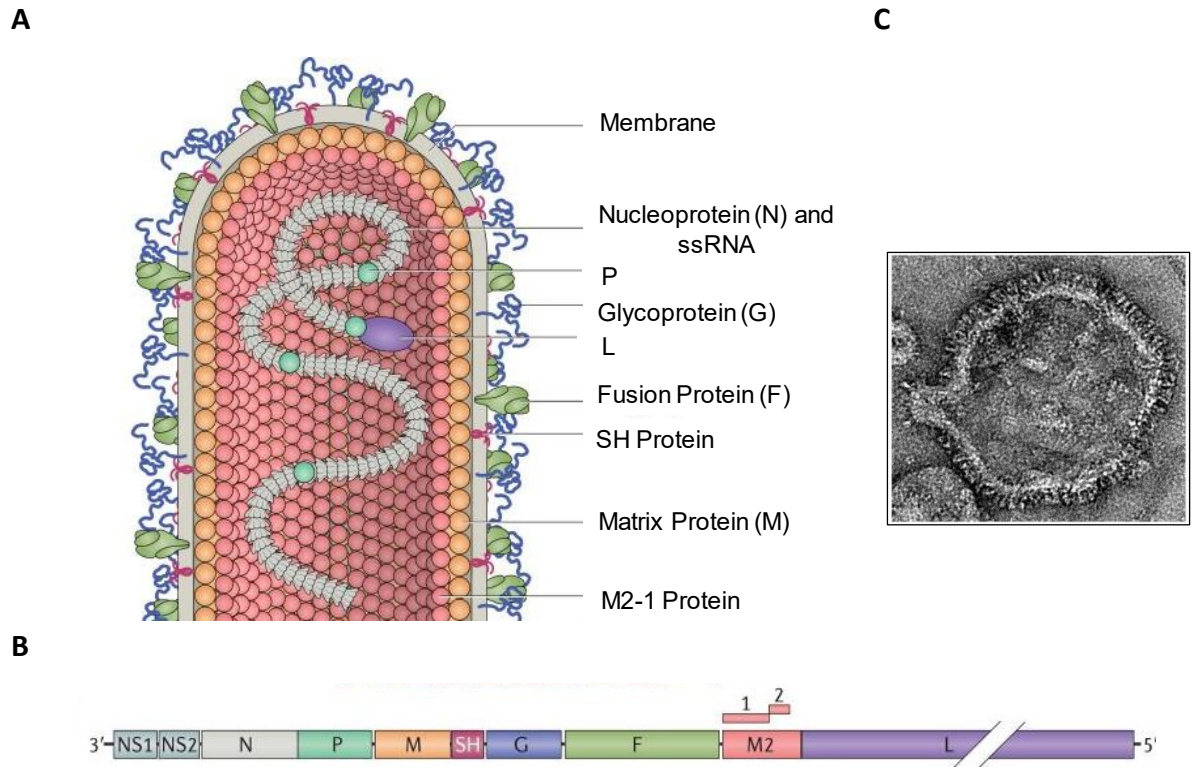


Figure 1.2 The structure of RSV.

(A) RSV, of the *Pneumoviridae* family, is an enveloped, filamentous virus with a diameter of 150 nm. The figure illustrates the mature assembled particle of RSV with the F and G protein being important for infectivity and immune responses. **(B)** The genetic structure of RSV. The 15.2kb non-segmented, negative-stranded, RNA genome consists of 10 genes (3'-NS1-NS2-N-P-M-SH-G-F-M2-L-5') encoding 11 proteins. **(C)** The EM image of a purified RSV particle courtesy of Dr *Weining Wu*. (Adapted by permission from Springer Nature: Nature Review Microbiology, Respiratory syncytial virus and how to block it, Michael B. Battles and Jason S. McLellan, 2019 [23]) (See Appendix).

RSV possess four proteins which are associated with the formation of the viral envelope and virus antigenic properties. The M protein is a non-glycosylated matrix protein that lines the inner surface of the RSV envelope, supports the outer bilayer, and is involved in the proper morphogenesis of the budding virion [32]. The attachment, heavy glycosylated glycoprotein G, the fusion protein F and small hydrophobic SH are the surface proteins of the virion. The G and F protein play a crucial role in entry and immunity to RSV [10,25]. The SH protein is in lesser

abundance than G and F on the surface of RSV; however, it seems to prevent the apoptosis of infected cells [33]. The SH protein (at around 100 amino acids in length) is an example of a virioporin, short amino acid peptides that form oligomers that have an active proton and ion channel activity at low pH. The RSV SH protein can permeabilise plasma membranes by forming pentameric transmembrane structures during RSV infection [33].

1.3.1.3. Attachment and fusion glycoprotein of RSV

RSV G and F proteins have an essential role in establishing the infection. The glycosylated G protein is involved in the attachment of the virion (membrane-anchored form, Gm) to the target epithelial cells and modulating immune responses if produced as a secreted isoform (sG)[34]. The G protein is around 300 amino acids, a transmembrane peptide that has been implicated in pathogenesis during RSV infection [5,23]. The C-terminal ectodomain consists of a 26-amino acid conserved region and a heparin-binding domain flanked by mucin-like domains. The ectodomain is evolutionarily the most variable structural part of G of all RSV proteins. The differences in the mucin-like domains are used to differentiate the two antigenic profiles of RSV (RSV-A and RSV-B) [35]. The conserved region contains a cysteine noose structure with a CX_3C chemokine fraktaline motif that allows binding to the CX_3CR1 receptor. G protein interaction with CX3CR1 on ciliated epithelial cells may mediate RSV infection [36]. Furthermore, this receptor is involved in leukocyte chemotaxis and the membrane-bound or soluble form of the G protein may have immunomodulatory properties [37]. The cysteine noose motif has structural similarity to the fourth domain of the tumour necrosis factor receptor (TNFR) that might alter the antiviral activity of TNF. The N-terminal cytosolic domain of G protein is connected to the transmembrane domain and palmitoylated post-translationally [38].

The fusion (F) protein of RSV is a 574-amino-acid peptide that is a class I viral fusion glycoprotein involved in the formation of syncytia [24]. Nucleolin and IFG1R have been identified as a host receptor for the RSV F glycoprotein [39,40]. To be functionally active, the F protein undergoes proteolysis leading to the production of two subunits, F1 and F1 (C-terminal and N-terminal, respectively), linked by two disulphide covalent bonds and forming the heterodimeric protomer. The trimerization of the protomer yields a mature, spherical shaped F protein in prefusion conformation [23]. The prefusion F protein changes conformation (refolds) into a post-fusion secondary structure that can span the host membrane if the viral and cell membrane are in close proximity [41].

1.3.1.4. RSV cell entry and replication

After the attachment to the host membrane through the G protein and fusion via F protein, conformational changes viral membranes allow RSV particle entry into the host cell. These conformational changes are accomplished via electrostatic interaction of a heparin-binding domain flanked by the mucin-like G protein domains and binding of RSV F protein to nucleolin [24]. After fusion, the RSV genome consisting of the helical ribonucleoprotein complex (RNP) is released into the cytoplasm, where the transcription and translation of the viral genome are led by the large polymerase protein (L) in the 3' to 5' direction in spatially distinct viral inclusion bodies [42]. Roughly 4 hours post-infection viral mRNA can be detected, 12 hours post-infection mRNA and protein synthesis reach its peak [42].

As mentioned before, the L protein acts as the RNA-dependent RNA polymerase driving viral RNA replication, transcription of mRNA, the capping of 5'-mRNA, the methylation of the cap and finally producing new antigenomes for virions [24]. RSV assembly occurs in the proximity of the plasma membrane. The RSV virion encapsulation involves the cytoplasmatic tail of the F protein and the G protein N-terminal end to recruit matrix (M) protein to start budding of the new virion in an actin-dependent manner [43]. The maturation process is associated with the apical membrane, where the budding virions detach and form the 150 nm long filamentous particles in an M-dependent manner. It is reasoned that spherical virions' formation is responsible for lower infectivity due to premature conformational changes of a prefusion F protein into the postfusion stable conformation [44].

1.4. Non – RSV bronchiolitis, epidemiology

RSV-related bronchiolitis is responsible for up to 73% of all cases of acute LRTIs [45]. The second most common viral agent responsible for the hospitalisation of babies with bronchiolitis is human Rhinovirus (HRV). In a multicentre study of the aetiology of acute viral bronchiolitis using nasopharyngeal aspirates (NPA), Mansbach *et al.* (2012) reported that HRV was associated with up to 25.6% of bronchiolitic cases; less than 8% of the incidents were associated with co-infection with HRV, RSV and bacteria [46]. Furthermore, in their study, co-infections with different viral and bacterial pathogens were detected in almost 29.8% of bronchiolitic babies [46]. Among other viral infections, the newly discovered human metapneumovirus (hMPV) is yet another common cause of acute LRTIs in young children, immune-compromised adults and the elderly [47]. Finally, there is growing evidence of other viral agents, such as influenza, enteroviruses and coronaviruses and their importance in paediatric bronchiolitis [48].

There is more data suggesting HRV role in infant bronchiolitis; however, the disease's outcome can differ compared to RSV and HMPV signalling that bronchiolitis can be heterogeneous entity regarding the pathogen type and immune responses. Compared to RSV, children with HRV-bronchiolitis have a different nasopharyngeal metabolome profile. HRV infection was associated with a significant increase of essential and non-essential N – acetylamino acids reflecting on different co-occurring bacterial species [22]. Furthermore, even if the phenotype of bronchiolitis seem to be indistinguishable, children with HRV-bronchiolitis have shorter hospitalisation, different medical histories and an increased risk of wheeze leading to asthma [46].

1.4.1. Human Rhinovirus (HRV)

HRV, of the *Picornaviridae* family is an enterovirus responsible for the common cold and is associated with upper respiratory tract infections (URTIs). In the USA alone, the HRV-related cold is a high financial burden due to absenteeism from work and medical visits. Although HRV was discovered almost 70 years ago, there are no approved antiviral treatments and vaccines currently available on the market. Based on genome sequencing HRV-A, HRV-B and HRV-C species have been identified [49]. Around 160 HRV serotypes (74 serotypes belong to HRV-A group, 25 serotypes fall into HRV-B group, and about 60 strains are identified in HRV-C group) and a high mutability rate hinder vaccine development [50,51]. HRVs have been classified according to the receptor used for the host cell entry. Almost 90% of all HRVs subtypes belong to the 'major group' that uses the cell surface receptor intercellular adhesion molecule 1 (ICAM-1) for cell entry. In contrast, the 'minor group' attaches the low-density lipoprotein receptor (LDLR) on the host cell.. In addition, cadherin-related family member 3 molecule (CDHR3) has been identified as a receptor for the RV-C group [51].

HRV is a 7200 bp single-stranded, positive-sense RNA virus whose genome encodes a large, single protein. This single protein is subsequently cleaved into 11 peptides, including four capsid proteins (VP1-4) and seven non-structural proteins, including RNA-dependent RNA polymerase (RDRP) and the proteases [52]. HRV uses the receptor-mediated clathrin-dependent (the minor group), clathrin-independent (the major group) endocytosis or macropinocytosis for infection of epithelial cells [50]. In the host cytosol, the entire genome is translated into the large polyprotein by the host 40S ribosomal subunit. This polyprotein is then subsequently cleaved by P1, P2 and P3 proteases leading to the production of 11 viral proteins in total [53,54]. Following viral replication, the HRV 3D protein transcribes positive-stranded viral RNA into the negative strands, which are the templates for future viral genome. After replication rounds, the viral genomes are

packed into the newly assembled capsids and released to the environment using extracellular vesicles or cell lysis [49].

1.4.2. Human Metapneumonia Virus (hMPV)

Since its discovery in respiratory patients in 2001, hMPV has been associated with acute respiratory infections in infants and adults. HMPV belongs to the family of *Pneumoviridae,* and its symptoms are similar to those caused by RSV [55]. Like RSV, hMPV infections occur in winter times and overlap with the RSV peaks worldwide being responsible for up to 5%-10% of infant hospitalisation with acute LRTIs [48,56]. Co-infection between RSV and hMPV is often reported; however, little is known about the immune impact of hMPV-related bronchiolitis.

The hMPV genome is single-stranded, negative-sense RNA and contains eight genes (3'-N–P–M–F–M2–SH–G–L-5') that code nine proteins [48]. HMPV is genetically very similar to RSV; however, there is a lack of two non-structural proteins NS1 and NS2. The NS1 and NS2 absence may be the reason for the difference in immunopathology between RSV and hMPV infections as these two proteins are important inhibitors of interferon [55]. Epidemiological data indicate that hMPV infections are severe in young babies [47] leading to a stay in ICU, oxygen supplementation, the need for mechanical ventilation, and a higher risk of asthma and lung diseases.

1.4.3. Influenza viruses

After RSV, HRV and hMPV, influenza viruses are one of the leading causes of acute LRTI infections and hospitalisation among children below the age of 2. Although there are significant advances in the production of more effective vaccines against influenza, this virus still causes yearly outbreaks, has a significant financial impact on healthcare systems worldwide and is a major threat to human health. According to the WHO, influenza is related to epidemics with almost 5 million severe cases and up to 650000 deaths per annum [57]. Bashir et al. (2017) reported in their comprehensive study in Islamabad Pakistan, that influenza was the viral pathogen responsible for up to 30% of all cases of bronchiolitis and pneumonia in children below 2-years of age [58].

The genomes of the influenza viruses (influenza A, B and C) of the *Orthomyxoviridae* family are comprised of eight viral ribonucleoprotein complexes (seven segments for influenza C), containing the negative-sense single-stranded genomic RNA. All influenza viruses have a very similar structure and they are characterised according to their glycoproteins neuraminidase (NA) and hemagglutinin (HA), on the outside of the virion. The accumulation of mutations in the NA and HA proteins is responsible for antigenic drift [59]. The reassortment of HA and NA proteins between different influenza viruses' strains (human and animal ones) is responsible for antigenic

shift. This antigenic shift enables influenza to jump between species. The presence of entirely novel antigenic proteins enables influenza to evade the host's pre-existing adaptive immunity contributing to high immunopathogenicity [59].

1.4.4. Enteroviruses (EVs)

Similarly to HRVs, enteroviruses belong to the *Picornaviridae* family and are divided into three groups (EV-A, EV-B and EV-C). These non-enveloped, positive-sense RNA viruses (with a genome of 7.2-7.5kb) are responsible for upper respiratory infections in people worldwide. Although EVs are very similar to HRV on the genetic level, the viruses are remarkably different. EVs are not restricted to the epithelium of the upper airways. They have vast clinical outcomes from mild disease to ICU admission (from paralysis to encephalopathies, febrile illness to myocarditis) and are a leading cause of meningitis [60]. Outbreaks of enterovirus 68 (EV-D68) infections in Japan, France, the Philippines, the Netherlands and the UK have been implicated in acute respiratory illness and hospitalisation among paediatric patients [61].

1.4.5. Coronaviruses (CoVs)

Coronaviruses are large RNA viruses that have emerged as the causative agent of severe acute respiratory syndrome (SARS-CoV) [62]. Two human coronaviruses, HCoV-OC43 and HCoV-NL63 are common causes of hospitalisation of children and are involved in the development of bronchiolitis and pneumonia in humans worldwide [62]. HCoV-OC43 and HCoV-NL63 were responsible for URTI (8.4%) and LRTI (4.7%) in non-hospitalised children [62].

In a cohort study of 68 Norwegian babies admitted to hospital in the RSV season, infants with CoVs were a less common cause of LRTIs than RSV; however, children affected by CoVs were older and had frequent wheeze with underlying chronic disease [63]. Interestingly, co-infection with RSV and either HCoV-OC43 or HCoV-NL63 manifested itself as bronchiolitis with higher severity, more extended in-hospital stay and affected younger children [63]. Severe acute respiratory syndrome coronavirus 2 (SARS-CoV-2) has been of particular interest since the recent breakout of the pandemic worldwide. Understanding innate mucosal immunity in protection against viral infection with SARS-CoV-2 has been an important part of many studies [64].

1.5. Immunity in bronchiolitis

Innate and adaptive immunity eliminate pathogens and play crucial roles in immune homeostasis and tolerance against pathogens, such as RSV or other viruses and bacteria [65]. There is a continuous debate about the role of adaptive immune responses in infants during severe bronchiolitis. Innate immunity may be relatively important in early childhood and during

bronchiolitis due to limited antigen encounter *in utero* and an immature adaptive response and where there are low levels of maternal antibodies (matAbs) [10,20]. Studies in mice have demonstrated that $CD4^+$ and $CD8^+$ T cells are involved in the clearance of viruses; however, they can also be associated with the development of immunopathology during viral infection and inflammation caused by RSV [5]**.** Overexuberant and unbalanced T cells responses, neutrophilia [66], monocytosis [5] and inflammation of the airways [16] can correlate with severe RSV-related disease. Interestingly, the skewed immune responses towards type-2 responses and inadequate type-1 responses can provide a partial explanation of RSV-related disease severity; however, it does not give an absolute answer.

1.5.1. Adaptive responses in bronchiolitis

1.5.1.1. T lymphocytes (CD4 and CD8 T cells)

T Lymphocytes are a part of adaptive immunity. These cells are referred to as T lymphocytes or T cells due to their origin from thymocytes in the thymus. In contrast to innate immune cells, which can be activated within hours and produce cytokines without being primed or entering tissues, T lymphocytes are adaptive immune cells that need several days to respond in order to become operational [67]. T cells are divided into $CD8^+$ cytotoxic T cells (Tc) and $CD4^+$ helper T cells (Th), respectively. $CD4^+$ T cells recognise antigens presented by Major Histocompatibility Complex (MHC) Class II on antigen-presenting cells (APCs) and, once activated, release cytokines to kill pathogens and provide help to other cells of the immune system. $CD8^+$ T cells recognise antigens presented by Major Histocompatibility Complex (MHC) Class I and kill cells that have been infected or transformed [68].

$CD4^+$ and $CD8^+$ T cells are responsible not only for the clearance of different pathogens but are also associated with the development of immunopathology during infection. In viral bronchiolitis, it is clear that T cells are important for the elimination of virus but can also contribute to immunopathology [18]. In 1960, the first alum-precipitated formalin-inactivated RSV (FI-RSV) vaccine was used in children under two years of age with disastrous results. In vaccinated children, subsequent natural RSV infection leads to cell-mediated, enhanced disease with almost 80% hospitalisation rate due to pneumonia or bronchiolitis [69]. In FI-RSV immunised children, the pathogenic immune responses were characterised by pulmonary inflammation due to the accumulation of T cells and granulocytes. The enhanced model of RSV infection has been repeated in different animal models and has allowed us to understand the mechanisms of the enhanced pathology following FI-RSV vaccination. Data from the murine model suggests that

polarization of CD4 T cells into type 2 (Th2) cells with the formation of immune complexes could provide a partial explanation of the vaccine-enhanced immunopathology [70].

Defective T cells responses can potentially be responsible for RSV susceptibility. Human studies associate the RSV infection with $CD4^+$ and $CD8^+$ T cell-induced apoptosis. Systemic lymphopenia is a risk factor for the severity of RSV infection, especially in the elderly and those on immunosuppressants after organ transplantation with impaired T cell activity [71]. In younger patients with severe RSV-bronchiolitis systemic lymphopenia is pronounced and they require oxygen supplementation and hospitalisation; in fatal cases of RSV-disease, T-cell counts of $CD4^+$ and $CD8^+$ T from the lungs are very low [71]. The low T-cell counts in the severe patients are usually related to high expression of programmed cell death 1 (PD-1) protein in pulmonary $CD8^+$ cells and decreased differentiation of CD8s into $CD69^+$ and $CD103^+$ T-resident memory (T_{rm}) cells via activation of mammalian target of rapamycin (mTOR) [72]. Usually, the CD8 number increases during infection, especially in milder cases of RSV bronchiolitis and decreases in ventilated babies resulting in worse disease outcome [66]. Interestingly, murine studies of $CD4^+$ T cell depletion before RSV infection lead to milder RSV-disease [73].

An immune response skewed away from protective type-1 immunity towards type-2 immunity, characterised by the production of type-2 cytokines (IL-4, IL-5 and IL-13), may contribute to lung damage and hyperinflammation in RSV-infection [6], whereas type-1 immunity characterised by the production of IL-2 and interferon-γ (IFN-γ) is related to virus clearance and improved disease outcome [74].

T_{regs} (T regulatory cells) are another group of CD4 cells that can control the peripheral tolerance in homeostasis and upon environmental insults [75,76]. T_{regs} are $CD4^+$ $CD25^+FoxP3^+$ T cells, making up to 10% of total CD4 T cells and are critical in promoting the resolution of a wide variety of diseases including the RSV infection[5]. Data obtained from a mouse model of RSV infection using 'depletion regulatory T cells' (DREG) mice showed that in the acute RSV infection model, depletion of T_{regs} stimulated viral clearance but increased cytokines and chemokine release leading to influx into the lungs of $CD4^+$, IFN-γ-producing $CD8^+$ T cells and weight loss [77,78].

1.5.1.2. Unconventional' T cells

Innate-like $CD3^+$ T lymphocytes include mucosal-associated invariant T (MAIT) cells, γδT cells, invariant natural killer T (iNKT) and intraepithelial lymphocytes (IELs) [79,80]. These cells can rapidly recognise and become activated by microbial components, environmental agents and stress-induced molecules expressed on cells. In brief, invariant T cells are an example of different

strategies utilised by the immune system to fight with different biological and non-biological agents.

MAIT cells are $CD3^+CD8^+CD161^{high}$ T lymphocytes which in humans express the Vα7.2-Jα33/20/12 chain while in mice Vα19-Jα33 [79,81]. These cells in both humans and mice recognise microbial riboflavin (vitamin B12) precursor 5-Amino-Ribityl-Uracil (5-A-RU), in the context of MR1 [79]. Natural killer T (NKT) cells are $CD3^+$ $CD56^+$ T lymphocytes, most of which express TRAV10-TRAJ18 in humans and TRAV11-TRAJ18 in mice paired with strict TCRβ chains [82]. These TCR bearing NKTs respond to glycolipids presented by an MHC-I-like non-polymorphic protein CD1d [82]. In both cases, MAITs and NKTs are strongly associated with mucosal surfaces and recognition of non-peptide antigens in tissues, such as lungs [83]. A recent longitudinal study of MAIT cells' characterisation indicates their frequency to be 30 times higher in adults than in newborns [84].

1.5.1.3. B Cells and immunoglobulins (Ig)

Similarly to T cells, B lymphocytes are a part of adaptive immunity. These cells are referred to as B lymphocytes due to their origin in the bone marrow B cells have been recognised as a part of humoral immunity for their ability to produce antibodies (Abs) [85]. B cells bind antigen via the B-cell receptor (BCR) and can be activated via TLRs. This allows B cells to act as critical antigen-presenting cells (APC) for T cell activation and are an essential source of cytokines [86,87].

B cell responses can be involved in protection and pathology during RSV infection. RSV-specific antibodies have been found virtually in every child and adult, suggesting the commonality of RSV infection [10]. In infants, levels of maternal RSV-specific antibodies (MatAbs) passed *via* the placenta and colostrum correlates with protection against infection, hospitalisation and the development of severe RSV disease [10]. Moreover, the passive transfer of immunoglobulin (Palivizumab prophylaxis) has remarkable effectiveness in reducing the risk of hospitalisation and RSV-associated severe disease [5]. Although serum neutralising antibodies correlate with protective immunity, it is unknown why antibodies seem to be insufficient in preventing reinfection with RSV throughout life. It is clear from human challenge studies that higher airway IgA correlated with a reduced likelihood of infection [88].

The characteristics of B cells has been determined in early life. B cells, like T cells, can be divided into subsets based on the location, the expression of transcription factors and their functions. In the foetal period, a specific B cell population has been characterised known as B1 cells or 'innate B cells' [89]. B1 cells have a particular role in early childhood as 1) they are fourfold less ubiquitous in adults compared to neonates and 2) they provide rapid and spontaneous production of

natural antibodies without prior infection or immunisation [90]. Moreover, data from infants infected with RSV below the age of 3 suggest fewer somatic mutations in their B cell compartment compared to infants infected after three months [91]. Somatic mutations are an essential part of B cells ability to produce high-affinity neutralising antibodies. Together, fewer somatic mutations in the antibody genes of younger individuals in the B cell compartment might lead to the generation of poorly functional antigen-specific antibodies upon RSV infection [91].

1.5.2. Innate responses in bronchiolitis

1.5.2.1. Innate barriers

Innate responses and the airway epithelial cells play a role in bronchiolitis. The respiratory epithelium provides primary protection against different inhaled environmental stimuli such as bacteria, viruses or non-biological agents [18]. After inhalation and inoculation in the nasal mucosa, pathogens such as viruses can cross the epithelium using different strategies, including transcytosis or direct infection of immune cells [92,93]. Viruses may use cell-to-cell transfer using intracytoplasmatic bridges in order to replicate.

Data from Zhang *et al*. (2002) suggests that the virus is shed exclusively from the luminal (apical) side of ciliated epithelial cells in RSV infection. [94]. RSV has a relatively small cytopathic effect on human respiratory epithelial cells; however, it is important as it is the site of virus replication and the source of type I/III interferons, cytokines, chemokines and antimicrobial proteins [5,10,18]. Interferons limit viral load by driving the production of interferon-stimulated genes (ISG) which can be associated with exuberant inflammatory responses to RSV and disease severity [95]. Antimicrobial proteins such as cathelicidin, β-defensins and surfactant proteins (SP-A) are the first line of defence at the epithelium and can bind to viruses, including RSV [5]. Data from RSV studies using SP-$A^{-/-}$ mice and SP-$A^{+/+}$ controls demonstrated that surfactants play an essential role in controlling RSV clearance and reducing pulmonary infiltration of leukocytes into the airways [96]. Respiratory epithelial cells cooperate with other immune cells such as alveolar macrophages in the lungs. In a mouse model of RSV-induced bronchiolitis exuberant chemokine production leads to neutrophil infiltration into the lungs of infected animals [95]. Furthermore, data from studies in children with RSV bronchiolitis suggest that higher production of chemotactic mediators and the recruitment of innate cells, such as neutrophils and NK cells may be the reason for inappropriate immune responses in the airways of bronchiolitic children and have an impact on disease severity [97–99]. Apart from neutrophils and NK cells, monocytes'

recruitment is important to reduce the viral load via the production of type-1 immune responses [100].

1.5.2.2. Neutrophils

Neutrophils are involved in a plethora of airways diseases such as chronic obstructive pulmonary disease (COPD), cystic fibrosis (CF), severe asthma and are ubiquitous in ventilated children with severe bronchiolitis [71]. Activated, airway neutrophils release neutrophil elastase (NE) and myeloperoxidase (MPO) which can lead to inflammation of the LRT and increased pathogenesis [101]. Neutrophil recruitment to lungs is notably orchestrated via CXCL8 (Interleukin (IL)-8) and CXCL8 peak in lungs from children with RSV-bronchiolitis coincides with the severity of disease [71]. Interestingly, neutrophils may undergo the process of NETosis described as the formation of neutrophil extracellular traps (NETs) during the process of their death [102,103]. NETs formation is a mechanism of innate antimicrobial activity that involves releasing decondensed chromatin (dsDNA, histones and non-histone proteins) to control microbial activity [104]. NETs are present in BAL and nasopharyngeal aspirates (NPA) in severe bronchiolitis [71].

In RSV-induced bronchiolitis, RSV genomic material and proteins (G, F and N of RSV) have been detected within neutrophils. This can be explained by phagocytosis and RSV replication inside neutrophils [105]. In ventilated infants with severe bronchiolitis, neutrophils in BAL and blood express activation markers such as CD18, ICAM-1 and CD11b and are involved in tissue damage [18]. The neutrophilic infiltration and inflammatory mediators are often associated with lung injury due to infection [105] and mechanical ventilation [106]. It is known that neutrophils may contribute to tissue damage in RSV-bronchiolitis in children below the age of six [107]. Data from Lukens *et al*. (2010) of primary RSV infection of 22 infants younger than 52 weeks showed that an influx of neutrophils proceeded the peak of T-cell activation suggesting it might play a key role in the immunopathology of RSV infection [107].

1.5.2.3. Eosinophils

Eosinophils are granulocytes that play a pivotal role in allergic inflammation and allergic diseases, including asthma, allergic dermatitis and parasitic infections [108]. These cells are uncommon in tissues of healthy subjects and appear under pathological conditions through infiltration from the periphery into the tissue upon stimulation with type-2-related cytokines IL-3, IL-4, IL-5 and IL-9 [109]. The migration to the inflammatory sites is regulated through highly expressed CCR3 which binds to chemokines, such as CCL11 (eotaxin), CCL24 (eotaxin-2), CCL7 and CCL13 (MCP-3 and MCP-4, respectively) and CCL5 (RANTES) [109].

In pulmonary diseases such as asthma, the presence of eosinophils is related to bronchial hyperresponsiveness and the severity of disease [109]. The role of eosinophils in RSV bronchiolitis is controversial. Contrary to adenovirus or influenza infections, in RSV-related bronchiolitis, the number of circulating eosinophils during recovery is increased suggesting their role in the recovery process and resolution of infection [110]. Moreover, during the acute phase of disease circulating eosinophils express in abundance the activation marker CD11b; however, no increase in numbers of these cells has been reported [71,110]. Eosinophil cationic protein (ECP) and eosinophil-derived neurotoxin (EDN) have been detected in BAL, NPA and serum of ventilated children with RSV bronchiolitis suggesting their activation in the acute phase of the disease [71]. Interestingly, recently discovered web-like DNA fragments known as eosinophil extracellular traps (EETs) might be involved in the pathophysiology or protection from RSV bronchiolitis. Although the role of EETs and EETosis have been recently documented in the development of allergic asthma, the role of EETosis in RSV-bronchiolitis has not yet been elucidated [104].

1.5.2.4. Monocytes

Monocytes are plastic white blood cells (WBC) which replenish tissue macrophages and dendritic cells (DCs). Monocytes are a very heterogeneous family of cells which upon infection can be recruited into tissues [111]. Primary CD69-positive monocytes have been found in pulmonary tissue of children with severe bronchiolitis [66]. In the periphery, monocytes express an increased level of TLR4 on their surface and decreased level of TLR8 and TNF-α during RSV infection [71]. The Jans *et al.* (2018) study demonstrated upregulation of Siglec-1 production in monocytes from newborns and adults following *in vitro* and *in vivo* RSV infection [112]. Siglec-1 lead to the inhibition of IFN-γ production by T cells in adults but not newborns[112] Siglec-1 is the only Siglec that does not have a signalling motif suggesting cell-to-cell interaction as an operating mode. Siglec-1 inhibition of IFN-γ production by T cells occurred via interaction with CD43 on memory T cells. Although newborn and adults monocytes have a similar expression of Siglec-1 on monocytes, higher expression of CD43 on T cells and the higher number of memory T cells in adults could explain the inhibitory effect of of Siglec-1 on the production of IFN-γ in adults and not newborns [112].

1.6. Innate lymphoid cells (ILCs) including NK cells

Innate lymphoid cells (ILCs) are a recently discovered, heterogeneous population of innate immune cells which ubiquitously populate lymphoid and non-lymphoid tissues and are enriched at every mucosal and tissue barrier thus far examined [65]. In just 10 years there has been growing awareness of their importance in driving, managing and resolution of different pathophysiological conditions.

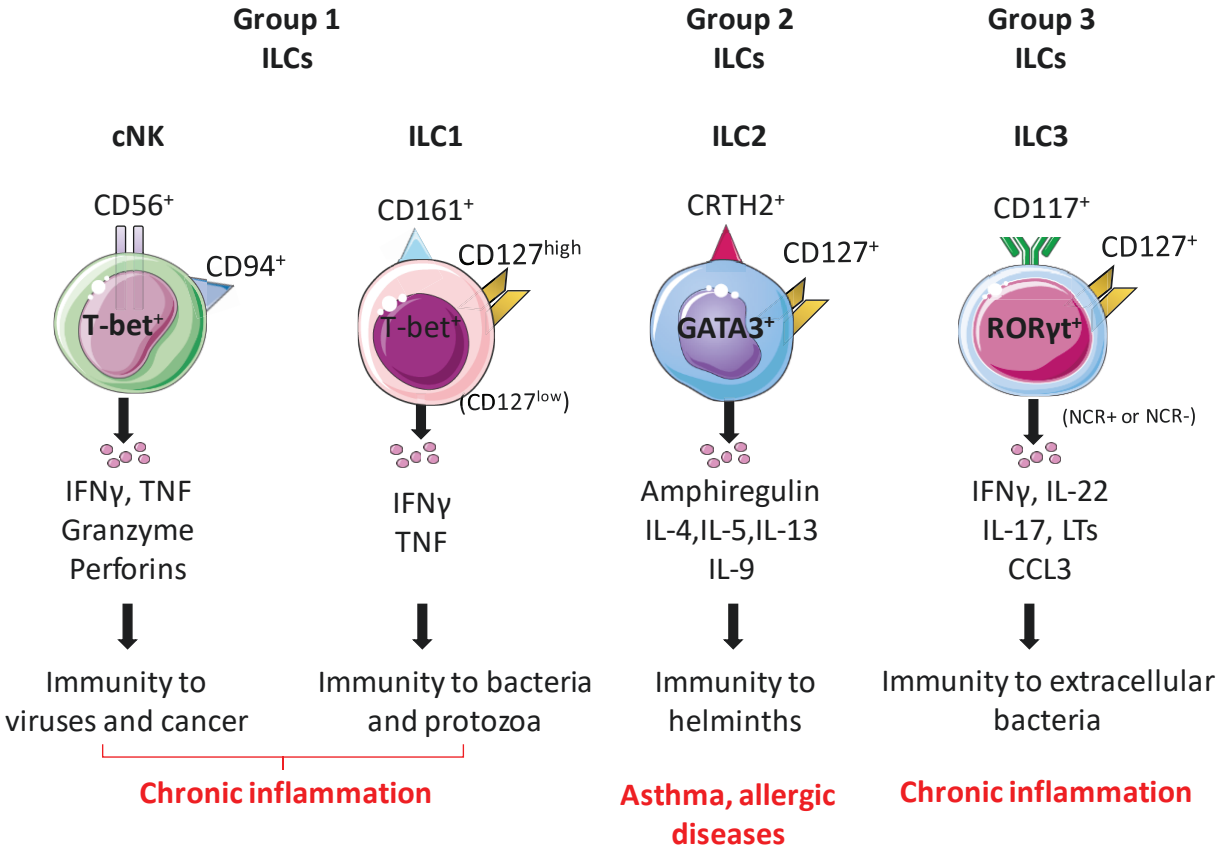


Figure 1.3 Members of the ILC family.

ILCs have a complex phenotype and have been divided into three groups based on their cytokine production and the transcriptional factors important for their function and development: Group 1 ILCs (cytotoxic-NK and non-cytotoxic-ILC1), Group 2 ILCs (ILC2) and Group 3 ILCs (ILC3). ILCs have an essential regulatory function in innate immunity and are characterised by the lack of antigen-specific receptors even though they have typical lymphocyte morphology. ILCs are present throughout the body and enrich mucosal surfaces of the gut, lungs and skin. (Cell pictures courtesy of Servier Medical Art licensed under a Creative Commons Attribution 3.0 Unported License. https://smart.servier.com).

ILCs are among the first cells to respond to environmental stimuli and pathogens because of their strategic location. ILCs are deeply integrated into mucosal sites, such as the lungs, intestines, and other various tissues, including skin, liver, and adipose tissue. There is an ample body of evidence of ILC involvement in regulating and maintaining of immunity and inflammation in the gut [67,113]. ILCs are important in regulating ensuing innate and adaptive

responses in the lungs; for example, ILC-depleted mice infected with influenza have impaired lung function and decreased epithelial integrity [114].

ILCs discovery and investigation have changed how we perceive the role of innate immunity in immunomodulation and how these cells contribute to tissue homeostasis, development and integrity. How ILCs can regulate different pathophysiological and physiological processes has been studied in detail especially regarding the intestinal and lung barrier; however, many questions still need to be addressed to decipher the role of ILCs in different disorders, such as bronchiolitis.

1.6.1. ILC subtypes

The prototypical and most extensively studied ILC populations are natural killer (NK) and lymphoid tissue-inducer (LTi) cells [115,116]. The latter have been shown to help the formation of lymph nodes, whereas NK cells produce interferon-γ (IFN-γ) to spontaneously combat tumours and mediate early anti-viral activity [117,118]. Interestingly, both NK and LTi cells depend on the common cytokine receptor γ-chain (aka γ_c or IL-2Rγ or CD25) and the expression of the helix-loop-helix inhibitor Id-2 during development [119]. Subsequently, other ILC populations have been shown to require γ_c and Id-2 expression for their development, including ILC1s, ILC2s and ILC3s (**Figure 1.3**).

ILC1s, ILC2s and ILC3s are considered to mirror $CD4^+$T helper 1 (Th1), Th2 and Th17 cells, respectively, whereas cytotoxic NK cells may compliment the cytokine profile and function of $CD8^+$T cells [120,121]. Their strategic location at barrier surfaces allows ILCs to respond to any environmental perturbations rapidly without the need to undergo clonal selection, priming and expansion.

The members of the ILC family have classic lymphoid morphology; however, they lack antigen-specific receptor [67,121]. The absence of recombinant activating gene (RAG) – dependent, adaptive antigen receptor, lymphocyte-like morphology and the lack of antigen-presenting surface markers are ''a holy trinity'' of ILCs features [122]. To remove nomenclature difficulties, ILCs have been classified into three groups: ILC1, ILC2 and ILC3 depending on their function, transcription factor expression and phenotype (**Figure 1.3**) [118]. The group 1 ILCs includes both cytotoxic ILCs (cNK cells) and non-cytotoxic ncILC1s. The latter are T-bet^+ cells which produce IFN-γ in response to IL-12 [65]. ILC2s depend on GATA-3 expression and are a source of type 2 cytokines (IL-4, IL-5, IL-9 and IL-13) [123]. Finally, ILC3s can produce IL-17A, IL17F, IL-22, GM-CSF or TNF, depending on

the stimulus, and express the transcriptional factor RORγT [124]. Group 3 ILCs include LTi cells which have different physiological functions.

Recently, another distinct subset of regulatory ILCs (ILCregs) has been identified, and it has been found to play a pivotal role in the resolution of intestinal inflammation in mice and humans. This novel population of innate regulatory ILCs can produce IL-10, and their development is directly related to the expression of *Id-3* expression factor [125]. Using similar protocols Seehus *et al*. (2017) have identified ILC2s producing IL-10 [126]. IL-10^{+} Id-3^{+} ILC_{regs} can suppress the activity of ILC1s and ILC2s and there is evidence using high-resolution single-cell RNA sequencing (scRNA-seq) data of ILC transcription profiles that ILC2 are progenitors of these cells [127]. It is will be crucial to validate the existence of ILC_{reg} with further studies and find them in tissues other than the gut, such as lungs and skin.

1.6.2. Group ILC1 - immunology

Group 1 ILCs represent the oldest member of the ILC family: natural killer (NK) cells. NK cells were discovered almost 40 years ago in mice by Rolf Keissling (1975) and were characterised by the 'natural' capacity to kill Moloney leukaemia cells through a cytotoxic mechanism [115]. ILC1 family includes other innate lymphocytes (referred to as ILC1s) capable of producing type-1 T cell cardinal cytokines (i.e., IFN- γ).

Although both NK cells and ILC1s belong to the same family, there are significant differences between those two subsets of cells. NK cells are abundant in peripheral blood and easily recirculate between different tissues. On the other hand, ILC1s are found in various mucosal sites and seem to have a more tissue-resident phenotype [128]. Moreover, different transcriptional profiles of T-bet and Eomes between NK cells and ILC1s can be the most defining distinction between these two populations: NK are T-bet- and Eomes-dependent, whereas ILC1s need T-bet but not Eomes for their development and function [129].

1.6.2.1. NK cell immunology - cytotoxic ILC1s (cILC1s)

NK cells are found widely in lymphoid and nonlymphoid tissues consistent with their innate sentinel function. In humans, these cells represent from 2% to 18% of total lymphocytes in the periphery [67] and up to 10% of resident lymphocytes in the lung or spleen [130]. Human NK cells have a life span of around two weeks that is in accordance with data from adult mice using continuous labelling with 5-bromo-2'-deoxyuridine (BrdU) of splenic NK cells [131]. Historically, human NK cells have been characterised as dedicated, cytotoxic cells which are believed to be an ancient part of the innate immune system [132].

Based on functional, anatomic and phenotypic features NK cells have been divided into distinct subpopulations in both mice and humans. Since the 1980s, CD56 and CD16 are two major surface markers for NK division which allow delineation of two major subsets: the cytotoxic $CD56^{L}CD16^{+}$ NK cells and the less cytotoxic $CD56^{h}CD16^{-}$ NK cells (both subsets are also known as $CD56^{dim}CD16^{+}$ and $CD56^{bright}CD16^{-}$, respectively) [128]. 80% of NK cells in peripheral blood from a healthy donor are $CD56^{dim}CD16^{+}$ NK1s while less than 15% of total circulating NK cells are $CD56^{bright}CD16^{-}$ [133]. Interestingly, both subtypes express constitutively T-bet and Eomes transcription factors and respond to IL-2 and IL-15 through the production of IFN-γ cytokines and orchestrate cellular cytotoxicity [132]. Recently, different subsets of NK cells have been described among mice and humans regarding the phenotype, localisation and transcriptomic patterns [134]. Crinier et al. (2018) work using high-input pan-genomic, scRNA-seq defined the NK cell heterogeneity across organs and species [135]. This single-cell resolution data strengthens the dichotomy between $CD56^{dim}CD16^{+}$ and $CD56^{bright}CD16^{-}$ in blood and organs between mice and humans; however, new unknown subpopulations with organ-specific features were discovered which differ from non-NK ILC1s [135].

Despite their name, NK cells isolated from the periphery in humans or mouse spleen are hardly killer cellsdue to low levels of Granzyme B and perforin production [136]. Maturation of NK cells involves priming with IL-15, according to mice models [137]. NK cells can recognise 'missing self' by which NK cells kill cells missing the self-MHC class I markers [67].

NK cells must become educated and learn what the normal levels of MHC-I expression are on cells. They are then inhibited from killing if a normal level of MHC 1 expression is detected. If MHC I is missing then they are no longer inhibited and are become killer cells. MHC class-I receptors' ability to interact with MHC class I molecules that are constitutively expressed on healthy cells is the reason for 'self tolerance' and toxicity towards aberrant cells. Two families of inhibitory receptors have been identified; the lectin-like CD94-NKG2A heterodimer in mice and the killer cells immunoglobulin-like receptors (KIRs) in humans [138]. NK cell killing is activated by recognition of ligands on target cells by activating receptors such as NKG2D. Furthermore, the low-affinity IgG receptor CD16 expression on NK cells allows them to target cells opsonised with antibodies through antibody-dependent cell-mediated cytotoxicity (ADCC) [139].

NK cells can eliminate aberrant or virus-infected cells through molecules stored in special cytotoxic granules called secretory lysosomes [128]. These cytotoxic granules contain cytotoxic proteins: perforin and granzymes which facilitate effective cell death of target cells. Apart from

cytotoxic molecules, NK cells can eliminate aberrant cells by mechanisms involving TNF-related apoptosis-inducing ligand (TRAIL) and surface-associated FAS (CD95L) ligand (FASL) [140].

Most of the data about the importance of NK cells in defence against infection come from an animal model of the herpes viruses infection [67]. NK cell deficiency has been described in a small number of cases in humans. NK cells deficiency includes patients with severe combined immunodeficiency disease/syndrome (SCID) but also cases of isolated NK deficiencies [141]. SCID is the name of the group of disorders usually inherited that cause disturbed development in T and B cells via *IL2RG* or *JAK3* deficiency and manifest as severely impaired immune responses [141]. Interestingly, SCID patients with *IL2RG* or *JAK3* deficiency have provided insights into NK redundancy. Although those patients have no or very little circulating NK cells after allogeneic hematopoietic transplant (HSCT) or after *IL2RG* gene therapy, no particular susceptibility to disease was observed among those patients in the follow up from 7 to 39 years after HSCT [141]. This situation leads to the question of whether NK cells are critical for innate immunity or whether humans can adapt to the lack of these cells. It is believed that because of improved hygiene, NK cells defects may have smaller clinical consequences.

1.6.2.2. Non-NK ILC1s

The ILC1 family includes cytotoxic Natural Killer (cNK) and non-NK ILC1s (ILC1) cells (killer and helper ILCs, respectively). The Immunological Genome (ImmGen) Project showed that non-NK ILC1s and cNK cells share gene-expression profiles and they are rather similar cell types. These transcriptomic similarities between NK cells and ILC1s have been the source of heated discussion in the literature [142]. Furthermore, ILC1s became one of the most controversial among all ILC members and their existence has been recently being questioned by another study using CyTOF (Cytometry by Time Of Flight) even though Bernik *et al.* (2013) demonstrated the existence of ILC1s distinct from NK cells in previous experiments [129,143].

To add complexity to the already complex system, non–NK ILC1s, in both human and mice, may consist of a further two groups according to their surface marker (i.e., CD127) and cytotoxic granule production. The first subset of non-NK ILC1s includes $CD127^{+}$, non-cytotoxic ILC1s (ncILC1s also known as helper-ILC1s) while the second one includes intraepithelial ILC1 cells (ieILC1) which are more NK-like [128]. IeILC1s are a unique cell population with a distinct integrin profile, memory-activated-like characteristics, and, a capacity to produce cytotoxic granules [144]. Fuchs et al. (2013) suggested that ieILC1 due to their strategic, intraepithelial location, TGF-β

hallmark, IFN-γ production and CD160 surface marker expression should be regarded a functional counterpart of tissue-resident memory $CD8^+$ T cells [144].

Nc-ILC1s can be found in the lungs, tonsils, spleen, liver, inflamed intestines and the blood [145]. Nc-ILC1s are activated by IL-12, IL-15 and IL-18 to produce type-1 cytokines IFN-γ and tumour necrosis factor-α (TNF-α) [65]. Nc-ILC1s differ from conventional NK cells and ieILC1 as they are predominantly resident cells expressing CD49a (VLA-1) and CD69 tissue-homing markers but lack the CD67L (selectin mediating cNK cells homing into the lymphoid organs) [146]. Furthermore, the significantly higher expression of CXCR6 mRNA on nc-ILC1s compared to cNK cells can play a crucial role in tissue-homing and trafficking of these cells [147]. This tissue-homing phenotype is reminiscent of T_{rm} cells and indicates the importance of nc-ILC1 in preventing from reinfections [148,149].

Nc-ILC1s due to production of IFN-γ are involved in protection against viruses, intracellular bacteria and protozoa. From murine studies of *Toxoplasma gondii* infection, mice lacking nc-ILC1s (T-bet deficient) progressed into severe disease suggesting a non-redundant role of nc-ILC1s in immunity to intracellular infection [150]. T-$bet^{-/-}$ mice failed to produce any IFN-γ and thus, to control the infection with the *T. gondii* parasite. Moreover, in *T. gondii* infection nc-ILC1s, not cNK cells or ILC3s, are the major producer of type-1 cytokines, such as IFN-γ and TNF-α [65,150]. Other mouse studies with *Salmonella enterica* and *Clostridium difficile* infection support nc-ILC1-mediated immunity and their non-redundant role in bacterial infection [151,152].

Similarly, nc-ILC1s were increased during influenza A and mouse cytomegalovirus (MCMV) infections and were ready to produce large quantities of IFN-γ. Tissue-resident nc-ILC1s control early viral infection of MCMV before the response from adaptive immunity and other innate cells. In a mouse model of MCMV infection, genetic ablation of nc-ILC1s leads to increased viral load even if cNK cells were present and fully functioning. It is believed that nc-ILC1s are involved in immunosurveillance of the primary sites of viral infection via the production of IFN-γ in response to IL-12 from tissue-resident XCR1+ dendritic cells [153].

1.6.3. Group ILC2 immunology

Group 2 ILCs (referred later as ILC2s) are at the centre of anti-helminth protection, allergic inflammation, tissue repair and homeostasis [117,154–156]. These cells play an important role in the initiation and exacerbation of type 2 responses via the production of cardinal type 2-associated cytokines (IL-5, IL-13) upon stimulation with IL-25 (aka IL-17E) [157], the IL-1 family member IL-33 [158] and TSLP [154,159]. Other studies suggest that along with IL-5 and IL-13, ILC2s produce IL-4 and

IL-9 upon some specific conditions; and IL-9 impacts ILC2s survival during the *Nippostrongylus brasiliensis* infection [160–162]. An additional protein produced by ILC2s is the epidermal growth factor receptor (EGFR) ligand amphiregulin (Areg) which is important for lung repair after influenza infection in mice [114]. Areg is also produced by skin ILC2s in humans [163] suggesting that ILC2s can drive immune and repair processes in different tissues.

The production of type-2 cytokines by ILC2 can lead to detrimental allergic inflammation; however, it can also promote protective metabolic homeostasis in a physiological context at almost all mucosal and tissue barriers.

ILC discovery is strongly related to the work on helminth expulsion, which resulted in finding a new population of cells with the features of type-2 cells known as ILC2s. ILC2s identification was based on a study of Fallon *et al.* (2006) on helminth expulsion using a murine model of infection of *Nippostrongylus brasilensis* [164]. They suggested that the main source of IL-13 needed for the parasite expulsion and the resistance comes from not type-2 adaptive cells but innate cells which could be accounted for the production of type-2 cytokines. These observations lead finally to the discovery of IL-5 and IL-13 producing $cKIT^+$ $SCA1^+$ innate cells by three different laboratories independently in mouse fat-associated lymphoid structures during infection with the parasite *Nippostrongylus brasiliensis,* that named these cells natural helper cells, innate helper cells (I_h2) or neuocytes [165–167]. These observations on a critical anti-helminth activity of ILC2s in mice were further extended using a murine infection model of *Strongyloides venezuelensis* [168] and subsequently analogous populations were identified in human tissues [114,169].

1.6.3.1. ILC2s and their immunology

Since ILC2 discovery in mice in the gastrointestinal tract [164], these cells have been identified in the liver, adipose tissues, mesenteric lymph nodes and various other anatomical sites such as the respiratory tract and the skin. Interestingly, ILC2s in both mice and humans share a great number of overlapping characteristics: (1) they account for significant production of type 2-cytokines, (2) they are responsible for immediate and fast action upon changes in the microenvironment and (3) ILC2s seem to have a restorative role on epithelial barriers promoting tissue repair [170]. Although ILC2s are scarce in most tissues and blood, they are predominantly embedded in the healthy tissues of the respiratory system and adjacent anatomical sites, such as nasal tonsils [171]. Since obtaining these samples from human lungs is limited ethically, most data on ILC2s come from routine bronchoscopies, tumour surgeries and deceased patients.

Despite the high level of restriction in obtaining lung samples, ILC2s have been described in human pulmonary tissues as $CD127^+$, $KLRG1^+$, and CD117 (c-Kit) low to positive cells upon excluding lineage positive cells [114,169,170]. Furthermore, ILC2 exhibit another molecule CRTH2 (chemoattractant receptor - homologous expressed on Th2 cells) which is involved in binding prostaglandin D_2 (PGD_2) [169]. CRTH2 is a G-coupled protein receptor and CRTH2-PGD2 axis interactions are strongly associated with type-2 cells such as Th2 cells, eosinophils, basophils and epithelial cells which are considered important in allergic inflammation, including asthma [172]. Recent studies show CRTH2 expression on ILC2s in human blood and lung tissues; however, at different levels due to their localisation and function [170]. The enzyme arginase-1 (Arg-1) is another marker of ILC2 differentiation, especially in lung samples. Monticelli *et al.* (2016) have reported that Arg-1 is expressed constitutively in lung ILC2s from mice and humans and it regulates type-2 responses in healthy patients and asthmatics [173,174]. The high numbers of Arg-1 producing ILC2s have been found in patients with chronic lung inflammation, such as idiopathic pulmonary fibrosis (IPF) and chronic obstructive pulmonary disease (COPD) [174].

ILC2s are considered tissue-resident cells; however, the experiments using a mouse model of *Nippostrongylus brasilensis* infection strongly suggest that ILC2s can circulate between the intestine, lungs and liver using the periphery as a vessel (Huang et al. 2018). Huang et al. (2018) documented that inflammatory ILC2s (iILC2s) induced by IL-25 or parasite infection in the intestinal *lamina propria* can enter the circulatory bloodstream via the villus lymphatic endothelium and traffic to different organs in a sphingosine-1-phosphate (S1P) - dependent manner [175]. In their report, they postulate that there are two populations of ILC2s: (1) inflammatory ILC2s (iILC2s) and natural ILC2s (nILC2s). The former is $IL\text{-}25^+$, $KLRG1^{high}$ and lack the ST2 receptor (the receptor for IL-33), while the latter can respond to IL-33 stimulation and seems to play the role of the conventional ILC2s.

The iILC2s seem to be a distinct population of cells that are absent in the lungs. From data on helminth expulsion with IL-25, it is clear that iILC2 originate in the small intestine as intraperitoneal not intranasal inoculation of IL-25 induced the appearance of iILC2s. Interestingly, the experiments with injected antibody labelling showed that iILC2s were labelled on a similar level to the adaptive T cells, suggesting that they had to enter the periphery at some point in time. In contrast, there was no visible staining of nILC2s that could indicate their tissue-resident phenotype [175]. Antibody labelling findings have been supported by imaging studies showing that ILC2s in a state of resting are CD69high. Upon activation with administrated IL-25,

these cells became Ki-67^{high} KLRG1^{+} S1P^{high} CD69^{low} iILC2s that can enter into the lymphatics of the small intestine villi. Since the trafficking of iILC2 cells is in an S1P-dependent manner, experiments with ligand FTY720 (the inhibitor of S1P ligand) resulted in the lack of movement of iILC2s from the intestine into the bloodstream. FTY720 is an immunosuppressant which can elicit lymphopenia and it is usually used in many autoimmune diseases or after an organ transplant [176]. Interestingly, in experiments in *Rag$^{-/-}$* mice treated with FTY720 proved to be lethal in 80% during *Nippostrongylus brasilensis* infection. Intravenous inoculation of iILC2 from RAG-efficient mice exposed to IL-25 provided crucial protection. Of note, migratory iILC2 behaviour parallels the migratory behaviour of T resident memory (T_{rm}) cells which upon activation become CD69^{low} and utilise S1P ligand for crossing into the central lymphatics [177].

1.6.4. Group ILC3 immunology

The ILC3 subset is a RORγt-expressing group of ILCs involved in innate immune responses and regulation of gastrointestinal commensals and lymphoid-associated tissues. These CD127^{+} c-Kit^{+} cells have been found in the *lamina proporia* (LP), the spleen, tonsils in humans and mice [124]. Under acute inflammatory states, high numbers of ILC3s have been found in the lungs, skin and liver [178].

There are several populations of ILC3s in humans and in mice. At least two subsets have been identified regarding different surface expression markers. The first group involves two subsets of ILC3s that express NK-cell associated receptor NKp44 and NKp46 (humans and mice, respectively) and have been named natural-cytotoxicity-receptor-positive (NCR^{+}) or (NCR^{-}) ILC3s cells [67,179]. Another group of ILC3s has been defined based on the chemokine receptor CCR6, and are known as lymphoid tissue-inducer cells (LTi). LTi cells do not express NCR receptors [145]. Functionally, LTi cells are fundamental for the formation of lymphoid structures, such as lymph nodes, the tertiary lymphoid follicles (TLFs) and Payer's patches (crytptopatches) in the gut-associated lymphoid tissues [121,178,179]. The lack of LTi cells or their dysfunctional activity has fatal consequences due to the failure of lymphoid organogenesis.

ILC3s produce cytokines, such as IL-17 and IL-22, upon stimulation with IL-23 produced from myeloid cells stimulated by different PAMPs (pathogen-associated molecular patterns) [145,179]. Stimulation with IL-23 involves the STAT3 signalling pathway and switches on the genes for cardinal ILC3 cytokines, including IL-17A/F and IL-22. IL-22 is the main cytokine associated with ILC3 regulation and IL-22-producing ILC3s are responsible for intestinal stem cell proliferation

and containment of intestinal bacteria [121,180]. The containment of the commensals via IL-22 relies on antibacterial proteins (S100A8, S100A9, Reg3γ, Reg3β) and mucins [145].

Different bacterial, viral, and fungal infection models have been utilised to answer the question of ILC3s role in infections. *In vivo* mouse models using the pathogen *Citrobacter rodentium* have shown that IL-22 producing group 3 ILCs help controlling intestinal inflammation following infection. In this model, ILC3s in RAG-deficient mice were responsible for protection during intestinal inflammation via the production of IL-22 through IL-23 conditioning [181]. IL-23 is the cytokine that stimulates ILC3s to secrete IL-22 but also is crucial for their expansion. Indeed, the depletion of IL-23 results in worse disease outcome and delayed bacterial clearance [182]. A similar approach in mice with intact adaptive responses indicates that ILC3s are not required for host protection [183,184].

In the context of fungal immunity, the mice model of *Candida albicans* infection was used to investigate the non-redundant role of ILC3s in the development of oropharyngeal candidiasis (aka 'thrush'). *Candida albicans* infection can cause a hazardous problem in immunocompromised patients. IL-17-orchestrated immunity against this fungal pathogen has been shown to have a major protective role as IL-17RA–deficient mice fail to control candidiasis from the early onset of infection [185]. The study by Gladator *et al.* (2013) using RAG-1 deficient or Rorc^{-}/$^{-}$ mice found that in the absence of ILC3s, the animals had problems with *Candida albicans* control and clearance in the oral mucosa. In their study, ILC3s take centre stage in defence against that fungal infection through the IL-23/ IL-17 axis [186].

The IL-17 cytokine family (IL-17A and IL17F) has also has emerged as a pivotal player in the pathogenesis of arthritis and psoriasis[185,187]. ILC3s are implicated in a plethora of inflammatory diseases from mouse and human studies. These cells have been likened with rheumatoid arthritis, lupus erythematosus, inflammatory bowel disease (IBD) and Crohn's disease [145]. NCR^{+} and NCR^{-} ILC3s, but not LTi cells, have also been found in the lung of healthy patients and those with various lung diseases, such as cancer, bacterial/viral infections and also patients with COPD and asthma [178].

1.6.5. ILCs in infection and homeostasis

The role of ILCs in homeostasis and controlling different pathogens has been published in numerous studies in mice. As ILCs mimic T cell responses, it remains unclear whether the lack of ILCs impacts survival and controls pathogens or inflammation. Current literature reports that RAG-deficient mice that lack T and B responses have increased the number of different subsets

of ILCs in peripheral blood and tissues suggesting a non-redundant function of these cells in the absence of adaptive immune responses [183].

Although murine models of RAG—deficient mice have been an excellent tool for assessing ILC function what is the biological impact of the ILC lack in the context of human health? A recently published investigation on a cohort of children with severe combined immunodeficiency (SCID) concludes that NKs and ILCs may be dispensable in humans [188]. Patients with SCID die early in childhood and only gene therapy or bone marrow transplantation can stop that fate. SCID children can be divided into two groups regarding the mutation in the genes of interest. The first group suffer from severe immunodeficiency due to mutations in *RAG1* and *RAG2* genes, whereas the second one due to *IL2RG* or *JAK3* mutation. Interestingly, ILC development is spared in the RAG-deficient group; however, those children are as immunocompromised as those from *IL2RG* or *JAK3* group who lack ILCs. The allogeneic hematopoietic stem cell (HSC) transplantation allowed the full reconstitution of ILCs only if myeloablation was performed beforehand, whereas NK cells and ILCs were not reconstituted in patients without intensive myeloablative therapy before HSC transplantation, yet no infectious susceptibility was observed in this cohort, indicating a redundant role of ILCs.

1.6.5.1. ILCs in viral infections

ILCs are among the most recently discovered innate immune cell types that populate every tissue barrier (skin, guts, lungs) and are among the first cells to respond to environmental stimuli [65]. ILCs are essential in regulating innate and adaptive immune responses during respiratory viral infection, as ILC-depleted mice infected with influenza have reduced eosinophilia in BALF and impaired lung function [114]. The importance of ILC responses during early viral infection seems to be critical and it is in concordance with a proposed role of these cells as the ''first responders'' due to the strategic location and ability to sense alarmins produced due to tissue damage or pathogen invasion [117,153].

Weizman *et al*., (2017) show in the mouse model of cytomegalovirus (MCMV) infection that tissue-resident ILC1s are critical for controlling early stages of infection in the initial infection site through the production of IFN-γ in response to IL-12 produced by cDC1 [153]. The authors observed similar results during secondary Sendai virus (SeV) infection four weeks post influenza infection. Interestingly, in this mouse model of heterologous secondary infection, the antiviral activity of $CD8^{+}T_{RM}$ cells occurs much later than previously described [153,189].

1.6.5.2. ILCs and bronchiolitis in children

There is evidence suggesting NK cell and ILC2 involvement in respiratory viral infection in mouse models [123]. Cytotoxic NK cells have antiviral properties in the lungs upon RSV and influenza infection [190,191]. During both viral infections, IFN-γ-producing NK cells have a strong protective function. In the mouse model of RSV, mice depleted of NK cells produce decreased amounts of IFN-γ, promoting type-2 responses. The type-2 responses were dependent on airway epithelial cell-derived IL-25 production [100]. On the other hand, BALB/c mice with depleted NK cells seemed to have significantly higher chances of survival due to decreased LRTI and morbidity associated with less IFN-γ accumulation in the lung during RSV infection [192]. Similarly, Zhou *et al.* (2013) have observed the same effect in mice *in vivo* during influenza infections suggesting that although anti-viral and beneficial to the host, IFN-γ producing NK cells can profoundly increase the pathology of infection [190].

Non-cytotoxic ILCs, ILC2 have been found to increase in number upon respiratory infection in human studies [193,194]. Notably, Nagakamar *et al*., (2016) reported the presence of greater numbers of ILC2s in sputum, BAL and PBMC in children with severe therapy-resistant asthma (STRA) compared to healthy subjects [194]. Valéy *et al*., (2016) have also demonstrated the abundance of ILCs in the peripheral blood of infants and in the cord blood of neonates compared to healthy adults [188]. Little is known about the role of ILC1s and ILC3s in human lungs upon infection even though they were detected in cystic fibrosis [195,196]. The IL-22-producing ILC3 subset seems to be important in respiratory inflammation as it decreases the amount of pro-inflammatory IL-33 in the murine model of allergic inflammation [197].

1.7. Rationale, hypothesis, aims & outline of the thesis

1.7.1. Rationale

It is challenging to investigate immune responses in infants below the age of two due to ethical restrictions in the amount of blood and airway samples obtained. As ILCs are relatively abundant in blood in neonates compared to healthy adults, relatively high numbers in paediatric samples were anticipated [194]. Although cord blood studies suggest there are differences in the frequency of ILCs between neonates and adults [188], the functional differences between these two cohorts are not currently explored. Moreover, the differences in innate immunity between adults and neonates in response to RSV is not very well documented. In this thesis, I investigate the contribution of all members of the ILC family in the immune response against respiratory viral infection in infants. Further understanding of innate immune responses in infants could offer new insights into disease pathogenesis and identify biomarkers and age-related mechanisms that could predict children at high risk of severe bronchiolitis and support the development of new therapeutics.

1.7.2. Research proposal

I propose that ILC frequencies and function are associated with disease severity and aetiology of respiratory infections in children.

Sub-hypothesis 1 ILCs from neonates are functionally different from healthy adult subjects.

Sub-hypothesis 2 Alterations in ILCs frequencies and numbers in blood and airway samples are associated with disease severity, pathogen type and load.

Sub-hypothesis 3 Alterations in ILCs function is associated with disease severity, pathogen type and load.

1.7.3. Aims

The objectives of this project were to establish protocols for ILC enumeration in respiratory and blood samples and to demonstrate the feasibility of detecting ILCs in small volumes of paediatric samples. Secondly, I obtained respiratory mucosal samples and blood from children (infected and ventilated non-infected controls) to enumerate and characterise the functional phenotype of the ILCs from the blood and airways. Thirdly, I aimed to measure soluble inflammatory mediators, such as cytokines, chemokines and other products (perforins, defensins, granzymes, markers of inflammation, damage and remodelling in the airways) which can be produced by or stimulate ILCs. Finally, using ILCs from cord blood I aimed to find out whether ILCs from neonates were at an altered frequency and functionally different to those from healthy adult subjects.

1.7.4. Outline of the thesis

In **Chapter 3.1**, I focused on establishing an optimised multicolour immunophenotyping panel (OMIP) and methodology that would enable me to enumerate different components of the cellular responses in blood and airway samples with low cell numbers by flow cytometry. I utilised different methods for preserving and staining whole blood and airway samples. I optimised the staining panel on blood from healthy adult volunteers using as little as 300 µL of peripheral blood. Based on this optimisation, I was able to select the best methods for immunophenotyping and preserving paediatric samples without losing ILCs and other rare populations of cells. In this chapter, I demonstrated the feasibility of obtaining clinical samples from infants. Finally, I confirmed that by using the optimised methodology I was able to identify ILCs in mucosal and blood samples from infants with bronchiolitis.

In **Chapter 3.2**, I investigated differences in the number and function of different innate and adaptive cells between adults and neonates. I put a particular emphasis on the phenotypical and functional differences in all members of the ILC family (including NK cells), granulocytes and other innate-like $CD3^+$ cells. For enumeration, staining using the OMIP was as performed. To characterise the functional phenotype of ILCs *ex vivo*, intracellular staining panels (ICS) for IFN-γ, IL-13, IL-17A, IL-22, and Granzyme B were developed. Finally, I applied dimension reduction techniques (*t*-SNE and UMAP) to OMIP, ICS and Granzyme B data sets to seek the differences in the topology and clusters of cells using unbiased algorithms. I determined intrinsic differences in ILCs between neonates and adults leading to the generation of distinct immunomes supporting my original sub-hypothesis.

In **Chapter 3.3**, I focused on determining whether the number and function of innate lymphocytes change during bronchiolitis and correlating immune parameters with the severity of disease and other clinical data collected in the Early Life Lung Infection (ELLI) study. I acquired peripheral blood and airway samples from children with severe bronchiolitis in PICU and compared them to healthy, control infants having elective surgery. Using the OMIP and ISC panels, I investigated differences in the number and function of innate and adaptive cells between bronchiolitic and healthy controls. Finally, I measured soluble inflammatory mediators in supernatants of airway samples.

2.

Materials and Methods

2.1. Materials

2.1.1. Consumables

Consumables	Company	Country
1 mL EDTA-coated BD tube	BD Bioscience	UK
10 mL EDTA-coated BD tubes	BD Bioscience	UK
18-gauge winged butterfly needle with a vacutainer system	BD Bioscience	UK
23-gauge winged butterfly needle with a vacutainer system	BD Bioscience	UK
Bijou 7ml sample containers	Greiner Bio-One	AU
EASYstrainer™ cell sieve (100µm)	Greiner Bio-One	AU
EASYstrainer™ cell sieve (40µm)	Greiner Bio-One	AU
CELLSTAR®T175 Flask	Greiner Bio-One	AU
CELLSTAR®T25 Flask	Greiner Bio-One	AU
CELLSTAR®T75 Flask	Greiner Bio-One	AU
Cryos™ freezing tubes (“cryotubes”)	Gilson	USA
DIAMOND Tipack filter pipette tips (10µl, 30µl, 100µl, 200µl)	Gilson	USA
DIAMOND Towerpack pipette tips (1000µl, 200µl)	Gilson	USA
Eppendorf tubes 1.5mL	Greiner Bio-One	AU
Falcon™ tubes (15 mL)	Thermofisher	UK
Falcon™ tubes (50 mL)	Thermofisher	UK
Flow cytometry tubes (FACS tubes)	BD Bioscience	UK
Multicounting10™ Cell counting chamber slides	Immune Systems	UK
Nalagene™ container	Sigma-Aldrich	UK
Nasosorbtion (NS) strips	Hunt Developments	UK
Pasteur pipette	VMR	UK
Rhinoprobe	Arlington Scientific	UK
Suction catheter (tube)	Medical Supplies	UK
U-bottomed 96-well plate	Corning	USA
Wide-bore 2 mL pipette	Thermofisher	UK

Table 2.1 1 Consumables used throughout this thesis.

2.1.2. Reagents

Reagents	Company	Country
BD GolgiPlug™	BD Bioscience	UK
Bovine serum albumin (BSA)	Sigma-Aldrich	UK
Cell staining buffer	BioLegend	UK
DMSO	Sigma-Aldrich	UK
Dulbecco's Modified Eagles Medium (D-MEM)	Sigma-Aldrich	UK
Dulbecco's-PBS (D-PBS)	Sigma-Aldrich	UK
EDTA	Sigma-Aldrich	UK
Ethanol 96% v/v	VWR	UK
Fixation Buffer	BioLegend	UK
Foetal Calf Serum (FCS)	Sigma-Aldrich	UK
Human TruStain FcX™ - Fc Block	BioLegend	UK
Intracellular staining and permeabilsation wash buffer 10x	BioLegend	UK
Ionomycin	Sigma-Aldrich	UK
Isopropanol	Thermofisher	USA
L-glutamine (L-Glu)	Gibco	UK
Lymphopure™	BioLegend	UK
Methanol	VWR	UK
Milliplex immunoassay buffer	Millipore	USA
PBS tablets	Sigma-Aldrich	UK
Penicillin/Streptomycin (P/S)	Sigma-Aldrich	UK
Phorbol 12-myristate 13-acetate (PMA)	Sigma-Aldrich	UK
Phosphate-buffered saline (PBS) 1x	Sigma-Aldrich	UK
Phosphate-buffered saline (PBS) 1x	Sigma-Aldrich	UK
RBC Lysis Buffer (10x)	BioLegend	UK
RBC Lysis/Fixation Solution (10x)	BioLegend	UK
RLT RNA extraction buffer	Qiagen	Germany
RPMI-1640 (Roswel Park Memorial Institute) Medium	Sigma-Aldrich	UK
TransFix™	CalTag	UK
Trypan Blue solution 0.4% w/v	Thermofisher	UK
β-mercaptoethanol (β-ME)	Sigma-Aldrich	UK

Table 2.1 2 'Off-shelf' reagents used in this thesis.

2.1.3. Media and media supplements

Prepared Media and buffers	Content	Final concentration
ACK lysis buffer	Distilled H_2O	-
	$KHCO_3$	10mM
	EDTA	0.1mM
	NH_4Cl	154nM
Dulbecco's Modified Eagles Medium (D-MEM) complete	D-MEM	1x
	FCS	10% v/v
	Streptomycin	100U/mL
	Penicillin	100U/mL
	L-glutamine	2mM
RPMI-1640 complete (R10) medium	RPMI	1x
	FCS	10% v/v
	Streptomycin	100U/mL
	Penicillin	100U/mL
	L-glutamine	2mM
Freezing Media (FM)	FCS	90% v/v
	DMSO	10% v/v
Stimulation Media (SM)	RPMI	1x
	PMA	50ng/mL
	Ionomycin	1 µg/mL
	GolgiPlug™	1 µl

Table 2.1 3 Media and media supplements used in this thesis.

2.1.4. Commercially available kits

Reagents	Company	Country
7-AAD viability staining solution	BioLegend	UK
AbC™ Total Antibody Compensation Bead Kit	Thermofisher	UK
ArC™ Amine Reactive Compensation Bead Kit	Invitrogen	UK
BD CompBead Compensation bead kit	BD Bioscience	USA
CountBright™ Absolute Counting Beads	Thermofisher	UK
CST (cytometry setting and tracking) Research Beads	BD Bioscience	UK

LIVE/DEAD™ Fixable Near-IR Dead Cell Stain Kit	Thermofisher	UK

Table 2.1 4Commercially available kits.

2.1.5. Antibodies for cytometry

Antibody	Clone	Company	Country
Alexa Fluor® 647 anti-human CD294 (CRTH2)	BM16	BioLegend	UK
Alexa Fluor® 700 anti-human CD66b	G10F5	BioLegend	UK
Brilliant Violet 421™ anti-human CD127 (IL-7Rα)	HIL-7R-M21	BD Bioscience	UK
Brilliant Violet 421™ anti-human CD127 (IL-7Rα)	A019D5	BioLegend	UK
Brilliant Violet 510™ anti-human CD123	6H6	BioLegend	UK
Brilliant Violet 510™ anti-human CD14	63D3	BioLegend	UK
Brilliant Violet 510™ anti-human CD19	HIB19	BioLegend	UK
Brilliant Violet 510™ anti-human FcεRIα	AER-37	BioLegend	UK
Brilliant Violet 605™ anti-human CD4	RPA-T4	BioLegend	UK
Brilliant Violet 650™ anti-human CD16	3G8	BioLegend	UK
Brilliant Violet 650™ anti-human CD56 (NCAM)	5.1H11	BioLegend	UK
Brilliant Violet 711™ anti-human CD8	SK1	BioLegend	UK
Brilliant Violet 785™ anti-human TCR Vα7.2	3C10	BioLegend	UK
FITC anti-human CD45	HI30	BioLegend	UK
PE anti-human CD3	OKT3	BioLegend	UK
PE/Cy7 anti-human CD56 (NCAM)	5.1H11	BioLegend	UK
PE/Dazzle™ 594 anti-human CD161	HP-3G10	BioLegend	UK
PerCP/Cy5.5 anti-human CD117 (c-kit)	YB5.B8	BD Bioscience	UK
PerCP/Cy5.5 anti-human CD117 (c-kit)	A3C6E2	BioLegend	UK

Table 2.1 5 Antibodies used for surface staining for OMIP, ICS and Granzyme B panels.

Antibody Intracellular	Clone	Company	Country
BUV395 Mouse Anti-Human IFN-γ (B27)	B27	BD	UK
FITC anti-human IL-22	2G12A41	BioLegend	UK
PE/Cy7 anti-human IL-13	JES10-5A2	BioLegend	UK
Alexa Fluor® 700 anti-human IL-17A	BL168	BioLegend	UK
Alexa Fluor® 700 anti-human Grzm B	QA16A02	BioLegend	UK

Table 2.1 6 Antibodies used for intracellular staining in the ICS and Granzyme B panels.

2.1.6. MSD panels

MSD panels	Company	Country
Chemokine Panel 1 (human) Kits	Meso Scale Discovery ®	USA
Pro-inflammatory Panel 1 (human) Kit	Meso Scale Discovery ®	USA
Th17 Panel1 (human) Kits	Meso Scale Discovery ®	USA
U-plex Metabolic Group 1 (human) Kits	Meso Scale Discovery ®	USA

Table 2.1 7 MSD panels used for the analysis of soluble mediators in airways supernatants.

2.1.7. Equipment and software

Instruments	Company	Country
5-laser-LSRFortessa™ cell analyser	BD Bioscience	UK
Freezer -20°C	VWR	UK
Freezer -80°C	VWR	UK
Heraeus Megafuge 40R	Thermofisher	USA
mLINE® mechanical pipettes	Sartorius	Germany
Sorvall Legend Micro 21 centrifuge	Thermofisher	USA
SubAqua 18 Plus water bath	Grant Instruments	UK
Tissue culture incubator	Binder	Germany
Zeiss Axio Observer inverted widefield microscope	Carl Zeiss Ltd	UK

Table 2.1 8 Equipment used throughout this thesis.

Software	Company	Country
BD FACSDiva™	BD Bioscience	UK
FlowJo v10	BD Bioscience	UK
GraphPad Prism v9.0	GraphPad Software	USA
Microsoft Office 365	Microsoft	USA
R Programming Language	R Foundation for Statistical Computing	Austria

Table 2.1 9 Software used throughout this thesis

2.2. Methods

2.2.1. Early Life Lung Infection (ELLI) study - outline

This PhD is a part of the Early Life Lung Infection (ELLI) study, an on-going established collaboration between paediatric clinicians, research nurses in the Children's Clinical Research Facility (CCRF) and researchers in the Section of Respiratory Infections at Imperial College London [198] (**Figure 2.2.1**). St. Mary's Hospital (SMH) is responsible for the clinical care of many babies with severe respiratory problems. Each winter, there are around 100 babies admitted to paediatric wards of St. Mary's Hospital, London with lower tract respiratory infection (LTRI). Around 40 infants require mechanical ventilation at the Paediatric Intensive Care Unit (PICU) to support them during a lung infection including bronchiolitis. Bronchiolitis is the leading cause of hospitalisation among children (≤ 2 years of age) worldwide. In this work, bronchiolitis was defined according to the American Academy of Paediatrics standard clinical guidelines as an acute respiratory illness with a mixture of rhinitis, wheezing, cough, tachypnoea and hyperinflation [2].

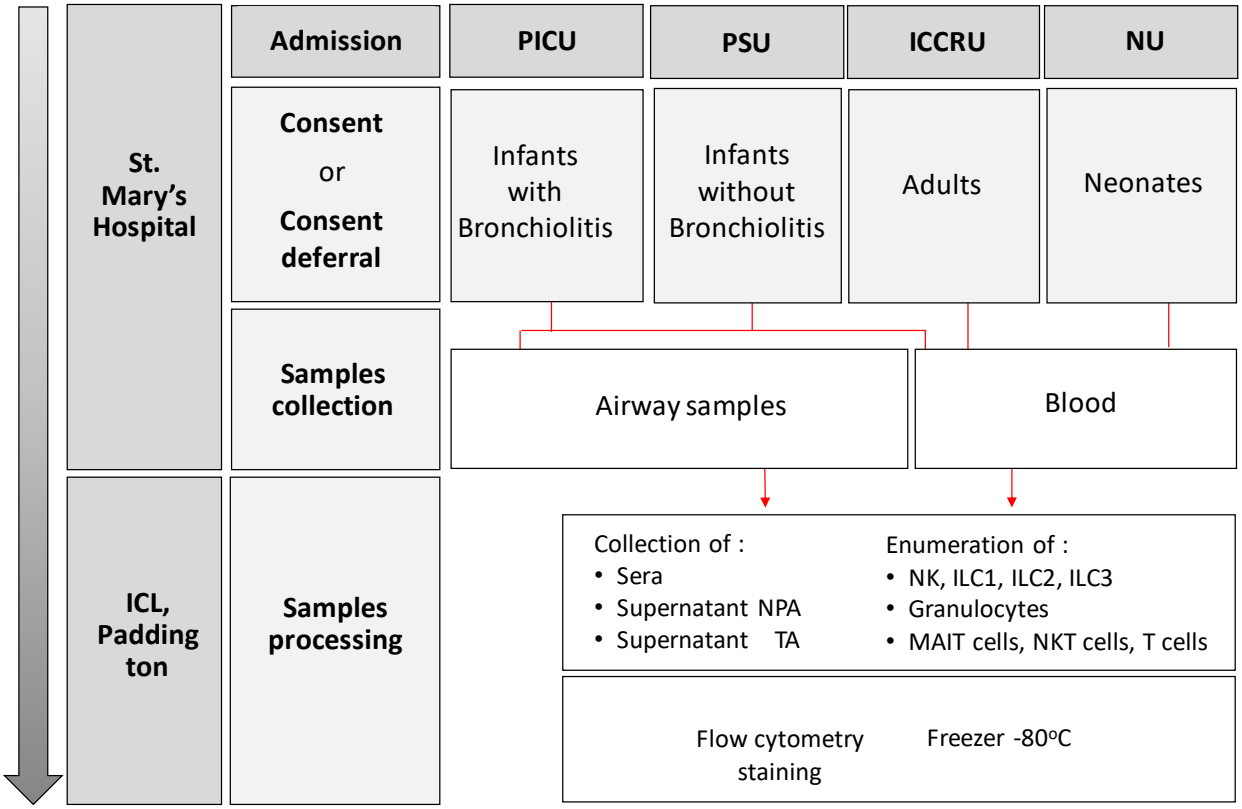


Figure 2.2.1 Clinical workflow in the Paediatric Intensive Care Unit (PICU) and Imperial College London (ICL) laboratories, St. Mary's Campus in the ELLI project.

Abbreviation: ICCRU – Imperial College Clinical Research Facility, ILC – Innate Lymphoid Cells, NU – Neonatal Unit, NPA – Nasopharyngeal aspirates, NK – Natural Killer cells, PICU – Paediatric Intensive Care Unit, PSU – Paediatric Surgery Unit, MAIT – Mucosal associated invariant T cells, TA – Tracheal aspirates.

The ELLI study focuses on understanding pathological mechanisms of upper and lower airway infections in children. We seek to understand how immune responses determine the outcome of the disease and the role and contribution of those responses in bronchiolitis severity and resolution. In summary, the ELLI study will help our understanding of the immune and inflammatory responses to lung infections in children through the measurement and characterisation of inflammatory mediators and cellular immune responses. In addition to studying infants with a respiratory infection, a comparison was made to healthy infants (controls) attending hospital appointments, elective surgery or admitted to PICU for non-respiratory problems.

2.2.2. Ethical Approval (see Appendix)

The first part of this study was performed under the RSV-SAM ethical approval (REC no 15/WM/0343). The majority of work and sample collection was carried out under Early Life Lung Infection (ELLI) study ethics. ELLI was approved by the London – Riverside Research Ethics Committee (REC no 18/LO/1570). Cord blood samples were collected from uncomplicated, term pregnancies (REC no 13/LO/1712) in collaboration with Dr Beth Holder.

2.2.3. Consent (see Appendix)

Written consent was sought from each participant or participant's guardian before entering the study. All participants were provided with the Patient Information Sheet (see Appendix) and signed consent was obtained only after a full explanation of the ELLI study and time allowed for consideration. Participants could refuse to participate in the ELLI study and opt out of any requested samples without giving any reason. We were willing to collect all samples for research purposes where possible; however, it was not necessary to collect all the samples from one child as we were not discriminating on the type of samples collected.

2.2.4. Deferred consent (see Appendix)

A deferred consent approach was utilised in situations when the child's clinical condition needed immediate investigation and the critical situation made discussion of research inappropriate. In these circumstances, the collection of samples for research purposes coincided with the need of the first clinical sample collection. This approach minimised the need to take samples for research purposes and when parents were not initially present. If no consent was given, all samples were destroyed.

2.2.5. Clinical cohort/patients

Children between 2 weeks and 2 years old admitted to the PICU with the requirement of ventilation (Study Group 1) and those without (Study Group 2) were recruited at St Mary's Hospital, London, UK (**Figure 2.2.2**). 'Healthy' paediatric samples (Study Group 2) were collected from infants undergoing elective procedures for non-inflammatory and non-infectious problems such as hernia repair, dental surgery, orchiopexy, hydrocelectomy and repair of hypospadosis.

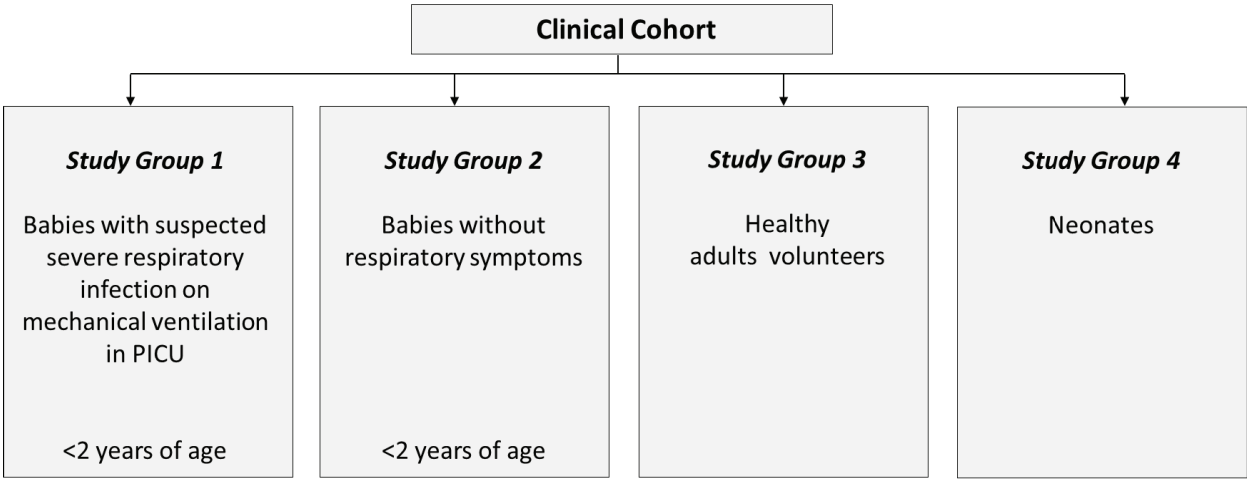


Figure 2.2.2 Flow chart indicating the clinical cohorts involved in the ELLI study.

Samples (Study Groups 1-2) were collected from hospitalised infants as a part of on-going studies in St. Mary's Hospital, London, UK. Samples for Study Groups 3 and 4 (healthy adult volunteers and neonates, respectively) were obtained from healthy adult volunteers or *via* NHSBT-NCI or delivery wards in collaboration with Dr Beth Holder. The following samples were taken: nasosorption (NS), nasopharyngeal aspirate (NPA), tracheal aspirate (TA)and peripheral or cord blood. Samples were collected as early as possible following hospitalisation.

To understand differences between adults (Study Group 3) and neonates (Study Group 4), samples were collected from healthy adult volunteers, and cord blood was obtained *via* NHS Blood Transfer Non-Clinical Issue (NHSBT-NCI) services or delivery wards in collaboration with Dr Beth Holder.

Exclusion Criteria
Infants
- Infants with any local or systemic factor that would influence the safety of nasal sampling - Infants with bleeding disorders or risk of bleeding - Infants taking part in an interventional study - Infants with a limited life expectancy or a decision to limit management - Infants that have received corticosteroid therapy at any time in the past month - Infants with a known immunological disorder - Infants where there is any concern about raised intracranial pressure - Extremely premature infants (<28 weeks) - Significant hypoxia or instability precluding ventilator disconnection - Bilateral indwelling nasal catheters or local nasal pathology preventing access for nasal sampling - Transcutaneous oxygen saturation of <95% on 60% oxygen - Infants with a chronic respiratory condition requiring home oxygen therapy, or recently discharged from NICU or PICU - Pneumothorax (as long as there is no contra-indication to carrying out NPA or nasal SAM sampling, then these children can still be included in the study, but we will not perform tracheal sampling) - Any event which excludes carrying out tracheal aspirate, (e.g.: Significant hypoxia or instability precluding ventilator disconnection) this sample will be missed from the sampling schedule of that study visit - The parents or guardians not able to sign the informed consent form due to limited English or comprehension despite the use of independent interpreter services
Adults
- An adult unwell at the moment of obtaining consent - An adult who might be infected with hepatitis B or hepatitis C - An adult who has a sexual partner who is infected with hepatitis or HIV - An adult who thinks that (s)he might be infected with HIV— the 'AIDS' virus - Anaemic adult or adult receiving treatment for anaemia or iron deficiency - An adult who has given blood in the last month (if more than 100ml is requested)

Table 2.2 1 Exclusion criteria for infants and adults in the ELLI study

Inclusion Criteria
Infants
– Infants aged 2 weeks up to 24 months – Hospitalised infants admitted to the PICU at St. Mary's Hospital, with a suspected respiratory infection – Babies attending routine outpatient appointments, visiting the hospital or undergoing elective surgical procedures – Presentation to the Emergency Department with any upper respiratory tract infection (URTI) – Suspected respiratory infection, admitted to the paediatric wards at St Mary's Hospital. – On a conventional ventilator with an endotracheal tube (ETT) of ≥2.0mmm diameter
Adults
– Adults over 18 years of age

Table 2.2 2 Inclusion criteria for infants and adults in the ELLI study

Cord blood
Inclusion Criteria
– Cord blood from full-term infants (>32 weeks gestation) infants
Exclusion criteria
– The mother not able to sign the informed consent form due to limited English or comprehension despite the use of independent interpreter services – Any illness in the mother or infant – Mother knowingly infected with hepatitis B, hepatitis C or HIV or with a sexual partner who is infected with hepatitis or HIV

Table 2.2 3 Inclusion and exclusion criteria for cord blood in the ELLI study

2.2.6. Clinical data collection

Clinical data were extracted from the medical record onto a standardised form by research nurses. Clinical data include demographic variables, such as sex, age, weight, gestation at delivery, laboratory and microbiology results, need for reintubation, length of mechanical ventilation, length of PICU stay, Pertussis vaccination during pregnancy, gestation at Pertussis vaccination and mode of delivery.

2.2.7. Clinical procedures

Paediatric samples were collected from the clinical cohorts based on the severity and nature of infection and upon consideration of all inclusion and exclusion criteria (**Tables 2.2.1-2.1.3**).

Ethical permission was obtained for the collection of samples from infants from 2 weeks up to 2 years of age, including nasosorbtions (NS), nasopharyngeal aspirate (NPA) tracheal aspirate (TA)[193,198] and different blood samples (peripheral and cord blood) (**Figure 2.1.3**). Samples were collected within 24 hours of admission to PICU or other units.

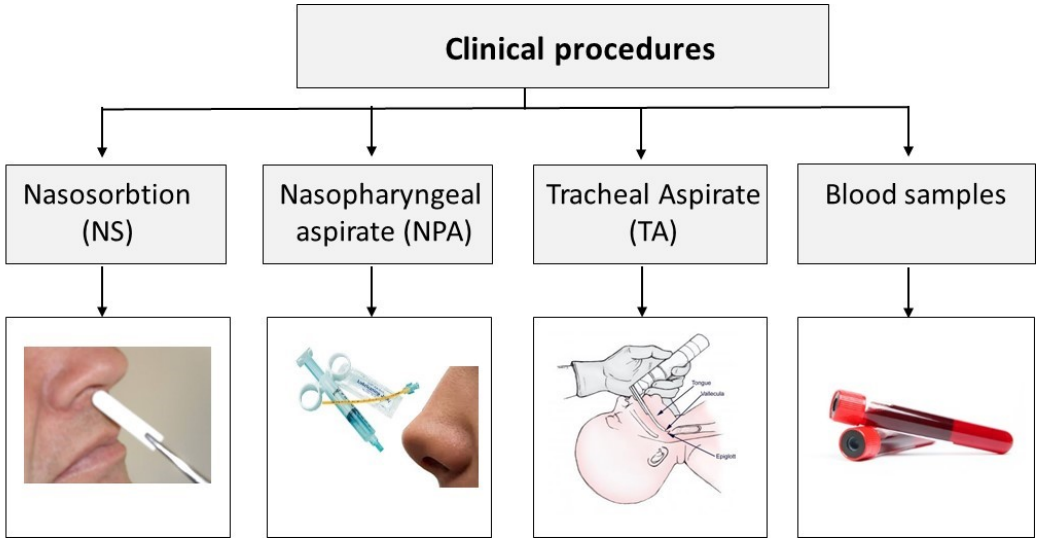


Figure 2.2.3 Flow chart indicating the clinical procedures involved in the ELLI study.

The following samples were allowed to be taken in accordance to the (ELLI) study ethics: nasosorption (NS), nasopharyngeal aspirate (NPA), tracheal aspirate (TA) and peripheral or cord blood. Samples were collected from the clinical cohorts based on the severity and nature of infection as early as possible folowing hospitalisation.

2.2.7.1. Airway samples

2.2.7.1.1. Nasosorbtion (NS)

Nasosorbtion (NS) samples were obtained using CE-marked medical synthetic absorptive matrix strips (SAM, Hunt Developments, UK) [199]. SAMs were utilised to collect mucosal lining fluid from the inferior turbinate of the nose from infants with bronchiolitis [97,198,199]. Due to their low protein binding capacity, SAM strips allow nasal fluid to be easily diluted and then analysed for inflammatory mediators and pathogen load. NS is a non-invasive method for obtaining upper airways samples.

2.2.7.1.2. Nasopharyngeal aspirate (NPA)

NPA is a routine sampling method. NPA samples were obtained by aspiration of the upper airways of congested infants, followed by flushing the suction tubing with saline.

2.2.7.1.3. Tracheal Aspirate (TA)

TA secretions were collected using a suction catheter (tube), which is passed down the tube that goes into the child's windpipe. Infants who required mechanical ventilation are intubated and sedated. This procedure was performed when clinically required as part of the infants 'bronchial

toilet'. These samples allowed a non-invasive study of the lower airway in severely ill and healthy babies.

2.2.7.2. Blood samples

2.2.7.2.1. Infant blood samples

Blood samples were taken from infants with suspected severe respiratory infection in the Paediatric Intensive Care Unit (PICU) requiring mechanical ventilation and infants without respiratory symptoms, visiting the hospital or undergoing elective surgical procedures but also in need of mechanical ventilation.

2.2.7.2.2. Adult blood samples

Blood samples from healthy adults could have been collected on more than one occasion but would not exceed 50 mL at one time or 250 mL in 6 months.

2.2.7.2.3. Cord blood samples

Umbilical cord blood was obtained from the *ex utero* separated placenta in a hospital or *via* NHS Blood Transfer Non-Clinical Issue (NHSBT-NCI) services. Cord blood samples were collected from uncomplicated, term pregnancies in collaboration with Dr Beth Holder and Dr Tom Rice.

2.2.8. Samples collection and processing

2.2.8.1. Fresh blood samples collection

2.2.8.1.1. Adult blood collection

The blood from healthy consenting adult donors was collected by an experienced nurse, doctor or a phlebotomist at the Imperial Clinical Respiratory Research Unit (ICRRU) at St. Mary's Hospital. Typically, 5-10 mL of blood was drawn using a 23-gauge winged butterfly needle with a vacutainer system (BD, UK). All adult blood samples were taken into 10 ml EDTA-coated tubes (BD, UK).

2.2.8.1.2. Infants blood collection

The blood from ill infants was collected by the experienced nurse or a doctor at PICU, St. Mary's Hospital. The blood from healthy infants was collected in the pre-theatre room by the anaesthetist at St. Mary's Hospital. Infants (particularly those in PICU and undergoing surgical procedures) have indwelling vascular catheters enabling blood sampling without the requirement for an additional needle stick. Blood volumes were limited according to clinical guidelines (max 0.8ml per kg of body weight, 0.5 up to 2.5 mL). Blood could be taken from an indwelling vascular catheter, by venepuncture or alternative routes, such as heel prick into 1 ml EDTA-coated BD Microtainer tube (BD, UK).

2.2.8.1.3. Cord blood collection

Umbilical cord blood was collected immediately at birth from full-term infants by the experienced study team member. Umbilical cord blood samples were taken into 10 ml EDTA-coated tubes (BD, UK) using a 23-gauge winged butterfly needle with a vacutainer system (BD, UK).

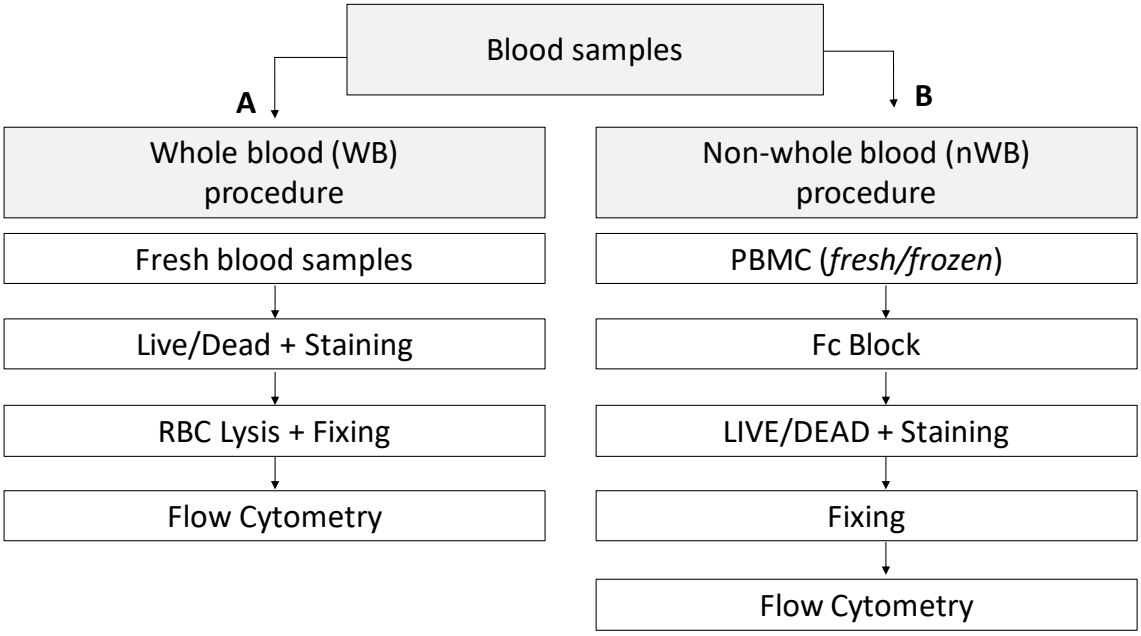


Figure 2.2.4 Strategies for processing blood samples for flow cytometry.

(A) Fresh whole blood (WB) and **(B)** non-whole blood (PBMCs) were stained for flow cytometry analysis. *Abbreviations used:* PBMC – peripheral blood mononuclear cells, RBC - red blood cells; Fc – Fc receptor.

2.2.8.2. Fresh blood sample processing

Anticoagulated, peripheral blood from adults, infants, and cord blood from neonates were stored at 4°C and transported from the ICCRU and the PICU in 4°C temperature-controlled boxes according to the local health and safety standard operating procedures (SOP). Upon arrival at the laboratory (the Section of Respiratory Infection, ICL), blood samples were transferred to a bench-top ice bath and processed within 3 hours. Blood samples were left at room temperature (RT) for a minimum of 30 minutes before further procedures were utilised (**Figure 2.1.4A**).

2.2.8.2.1. Plasma collection

Plasma was obtained from adult, infant and cord blood after a minimum of 30 minutes at RT. Up to 200 µL of adult, cord or infant blood was centrifuged at 400 *x g* for 10 minutes. After centrifugation plasma was aliquoted and stored at –80°C for further analysis.

2.2.8.2.2. PBMC isolation

Anticoagulated whole blood was diluted 1:1 in PBS and then carefully layered over Lymphopure™ (BioLegend, UK) density gradient. For every mL of diluted blood, 0.5 mL of

Lymphopure™ was added. Samples were centrifuged at 800 x *g* for 20 minutes at room temperature (RT). After centrifugation, the layer of PBMCs was removed from the Lymphopure™: plasma interface, carefully collected with a Pasteur pipette into a 15 mL Falcon™ tube, washed in PBS and centrifuged (300 x *g*, 5 minutes). If needed red blood cell lysis was carried out by resuspending the pellet in 9 ml of sterile water for 22 s, after which 1ml of 10 X PBS was added to restore the osmolarity and PBMCs were centrifuged once more (300 x *g*, 5 minutes). The pellet was then resuspended in PBS or R10 media and the total cell number and their viability (trypan blue exclusion) were determined using light microscopy (UK). PBMCs were processed fresh for further analysis, or after freezing (see below) (**Figure 2.1.4A**).

2.2.8.2.3. Freezing samples

After the cell count using a hemocytometer, 5-10 x 10^6 cells were centrifuged at 300 x *g* for 5 minutes and then resuspended in 2 mL of freezing media (FM) (90% v/v FCS (Sigma-Aldrich, UK) 10% DMSO (Sigma-Aldrich, UK). Following resuspension, cells were mixed, aliquoted in 1-mL volume polypropylene freezing tubes with inner caps (Serum tube, Sumitomo Bakelite Co., Tokyo, Japan) and finally placed in a Nalagene™ container (Sigma-Aldrich, UK) for slow freezing to -80^{o}C. After 2 days, cells were transferred into liquid N_2 for long-term storage until use.

2.2.8.2.4. Thawing samples

Frozen PBMCs were thawed as quickly as possible in a water bath at 37°C and then immediately transferred into warm RPMI-1640 complete medium (10% FCS, 100U/mL Penicillin, 100U/mL Streptomycin, 2mM L-Glutamate) utilising a wide-bore 2 mL pipette. 10 mL of complete medium (at 37°C) was used to wash the PBMC. Cells were centrifuged at 300 x *g* for 5 minutes, resuspended in 3 mL of fresh complete media and the total cell number and their viability were determined using the trypan blue dye exclusion method. A further 7 mL of media was added to the thawed cells which were left to rest overnight (O/N) at 37°C, 4% CO_2 in the incubator. The entire thawing procedure was completed routinely within 25 to 30 minutes.

2.2.8.3. Fresh airway samples collection

2.2.8.3.1. NS collection

The NS collection was performed by inserting a synthetic absorptive matrix (SAMs) strip into the nasal cavity avoiding brushing the nasal mucosa. After insertion, contact with mucosal lining fluid (MLF) was achieved by using finger pressure from outside the nose (up to 30 seconds) by a nurse or a clinician. After a 1-minute interval, NS sampling was repeated in the opposing naris. After sampling, SAMs were returned in the collection tubes provided and transported from the hospital in 4°C temperature-controlled boxes [199]. After transport to the laboratory, NS samples

were transferred to the bench-top ice bath and processed within 3 hours for further investigation or freezing.

2.2.8.3.2. NS processing

Nasosorption samples were eluted in two different buffers. NS samples from one naris were eluted in 300µl of Milliplex immunoassay buffer (Millipore, Billerica, USA). The opposite naris NS samples were eluted using 300µl of RLT RNA extraction buffer (Qiagen, Hilden, Germany). In both cases, SAM strips were detached from the nasosorption device using sterile forceps and placed in a 2ml microcentrifuge tube. Nasal fluids were obtained by vortexing the SAMs for 30 seconds in the appropriate buffer. After vortexing, SAMs were transferred into Spin-X column without a membrane (Corning, NY, USA) using sterile forceps and returned to the tube. Finally, tubes were centrifuged (800 x *g*, 20 minutes, 4°C) to elute fluids. The tubes were next placed in a -80°C freezer until further use [97,198,199].

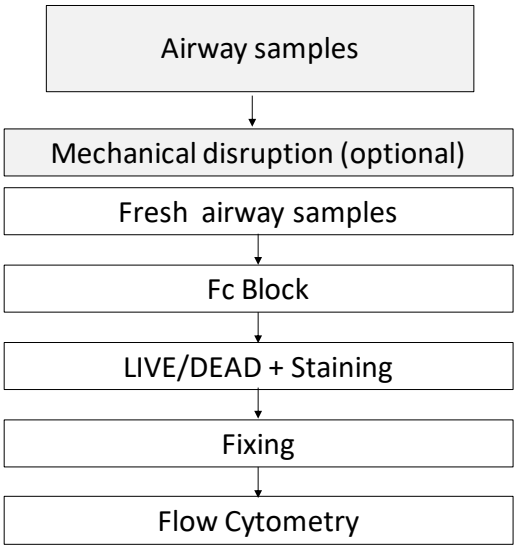


Figure 2.2.5 Airway samples processing, and flow cytometry staining scheme used throughout the study.

Fresh airway samples were immunophenotyped via flow cytometry**.** When rich in mucus samples were mechanically disrupted by using a syringe and a needle to obtain a cellular component. *Abbreviations used*: Fc – Fc receptor.

2.2.8.3.3. NPA and TA sample collections

Following NS, airway samples, such as NPA and TA were collected by an experienced nurse or a clinician at PICU, St. Mary's Hospital. Airway samples (NPA and TA) from healthy infants were collected in the pre-theatre room by the anaesthetist at St. Mary's Hospital. NPA was performed by the suction of secretions from the nasopharynx and by flushing the suction catheter with saline (up to 4 mL) as a part of suctioning routine. TA was obtained from sedated, mechanically ventilated children by flushing up to 1 mL of saline through the suction catheter as a part of the infants 'bronchial toilet' only when clinically indicated. Both NPA and TA samples were collected

into a sterile 15 mL bijous and then transported from the hospital environment in 4°C temperature-controlled boxes.

2.2.8.3.4. NPA and TA sample processing

Upon arrival at the laboratory, NPA and TA samples were transferred to the bench-top ice bath and processed within 3 hours. Firstly, airway samples (NPA and TA) were centrifuged at 800 x *g* for 5 minutes and cell-free airway supernatants (ASN) were carefully aliquoted into Eppendorf tubes (UK) (300 µL per tube) and immediately frozen at –80°C until future analysis. The cellular component was washed with 5 mL of PBS and only if airways samples were very thick, mechanical disruption was utilised [200]. During mechanical disruption, airway samples were homogenised by a gentle rinse up to 10 times through an 18-gauge needle and then samples were filtered using 100-µm and 40-µm cell strainers. If there was not much mucus and the airway samples were clear, simple filtering was carried out. After homogenisation, NPA and TA were centrifuged at 400 x *g* for 5 minutes and the cell suspension was used for flow cytometry analysis (**Figure 2.2.5**).

2.2.9. Assays

2.2.9.1. Flow cytometry

2.2.9.1.1. Surface staining

2.2.9.1.1.1. Fresh whole blood staining

Processed samples were stained with the optimised flow panels [201]. 300 µL of whole blood was carefully aliquoted into flow cytometry tubes (FACS tubes, BD, UK). The prepared mixture of fluorochrome-conjugated antibodies for surface staining and LIVE/DEAD™ Fixable Near-IR dye was added to the blood. The antibody cocktail can be prepared up to 4 weeks in advance without the antibodies changing their properties. Next, samples were vortexed and incubated for 30 minutes at RT with protection from light. After staining, erythrocytes were lysed and fixed with 2 mL of red blood cell (RBC) lysis/fixation solution (BioLegend, UK) diluted in H_2O (1:10) for 10 minutes at RT. After fixing, the level of RBC lysis was estimated under the light and if satisfactory cells were centrifuged at 800 x *g* for 5 minutes at RT. Of note, if the level of RBC lysis is too low, the lysis step was repeated with a reduction in the yield of live cells. Finally, the samples were resuspended in 370 µL of cell staining buffer and stored in the dark, at 4°C until acquisition (no more than 2-3 days later) on a 5-laser-LSRFortessa™ cell analyser (BD Bioscience). CountBright™ absolute counting beads (Invitrogen, UK) were added up to 400 µL just before the acquisition.

2.2.9.1.1.2. Fresh airway samples staining

Freshly obtained cell suspensions from airway samples (see 2.2.8.3.4) were transferred to a U-bottomed 96-well plate (Corning, USA) before staining with the optimised flow panels [201]. In parallel, 300 µL of whole blood was aliquoted into FACS tubes for unstained, LIVE/DEAD and fluorescence minus one (FMO) controls. Firstly, cells were washed with PBS and centrifuged (800 x *g*, 5mins, 4°C). After two washes with PBS, cells were resuspended in 100µL Human TruStain FcX™-Fc Block (Anti-CD16/CD32; Biolegend, UK) diluted 1:50 in cell staining buffer for 10 minutes at 4°C. After Fc-block samples were washed by adding 150 µL of PBS on the top of the Fc-blocked cells and centrifuged at 800 x *g* for 5 minutes Next, the supernatant was removed, and an additional wash was performed with 200µL of PBS followed by centrifugation at 800 x *g* for 5 minutes and removal of the supernatant. Cells were stained with the prepared mixture of fluorochrome-conjugated antibodies for surface staining and LIVE/DEAD™ Fixable Near-IR dye diluted in PBS (1:500) for 30 minutes at 4°C in the dark. All unbound dye was removed by performing a wash with 150 µL of flow staining buffer as above. After staining, cells were resuspended in 100 µL of fresh fixation buffer (Biolegend, UK) and incubated in the dark for 30 minutes at 4°C, or at RT for 20 minutes. Cells were resuspended in 200 µL cell staining buffer. Finally, the samples were transferred to flow cytometry tubes and 170 µL of staining buffer was added. Samples can be stored in the dark, at 4°C (for no more than 2-3 days) until acquisition at which point CountBright™ absolute counting beads (Invitrogen, UK) were added up to 400 µL.

2.2.9.1.2. Intracellular staining

2.2.9.1.2.1. Stimulation of PBMCs

Fresh isolated or thawed PBMCs (1-2.5 x 10^6 cells) were stimulated for at least 3 hours at 37°C with ionomycin (1 µg/mL) and phorbol 12-myristate 13-acetate (PMA) (50 ng/mL) in 3 mL of warm RPMI-1640 complete medium. The unstimulated control was prepared by adding just DMSO. In both cases, 1 µl of GolgiPlug™ (BD, UK) was added for every 1 ml of cell culture (e.g., ~10^6cells/mL) according to the manufacturer's instructions. After the 3-hour stimulation, detection of cytokine-producing cells was performed by immune fluorescent staining with optimized protocols.

2.2.9.1.2.2. Surface staining

After stimulation, cells were transferred to a U-bottomed 96-well plate and washed with PBS and centrifuged (800 x *g*, 5mins, 4°C). After two washes with PBS, cells were resuspended in 100µL Human TruStain FcX™-Fc Block (Anti-CD16/CD32; Biolegend, UK) diluted 1:50 in cell

staining buffer for 10 minutes at 4°C. After Fc-block, samples washed by adding 150 µL of PBS on top of the Fc-blocked cells and centrifuged at 800 x *g* for 5 minutes. After that wash, the supernatant was removed, and additional wash was performed with 200µL of PBS followed by centrifugation at 800 x *g* for 5 minutes and removal of the supernatant. After Fc-blocking step, cells were stained with the prepared mixture of fluorochrome-conjugated antibodies for surface staining and LIVE/DEAD™ Fixable Near-IR dye diluted in PBS (1:500) for 30 minutes at 4^{o}C in the dark. All unbound dye was removed by washingwith 150 µL of flow staining buffer as mentioned above. After staining, cells were resuspended in 100 µL of fresh fixation buffer (Biolegend, UK) and incubated in the dark for 30 minutes at 4^{o}C, or at RT for 20 minutes. After fixing, two further washes were performed, cells were resuspended in 200 µL cell staining buffer and stored O/N at 4^{o}C in the dark until permeabilisation.

2.2.9.1.2.3. Permeabilisation and intracellular staining

After surface staining (see 2.2.9.1.2.2), cells were washed with 150 µL of permeabilization wash buffer (BioLegend, UK) diluted 1 in 10 in dH_2O. After the first wash, samples were incubated with 100 µL of permeabilization wash buffer for 10 minutes at 4^{o}C in the dark. After permeabilization, the prepared mixture of fluorochrome-conjugated antibodies diluted in permeabilization wash buffer was utilised for intracellular staining (60 minutes at 4^{o}C in the dark). After the intracellular staining, cells were washed 1.5 times with permeabilization wash buffer and finally resuspended in 450 µL of cell staining buffer and stored in the dark, at 4^{o}C until acquisition (no more than 2-3 days later) on a 5-laser-LSRFortessa™ cell analyser (BD Bioscience). CountBright™ absolute counting beads (Invitrogen, UK) were added up to 500 µL just before the acquisition.

2.2.9.1.3. Preparation of compensation beads

AbC™ Total Compensation Beads (Thermofisher, UK) and ArC™ Amine Reactive Compensation Beads (Invitrogen, UK) were used to establish the optimal PMT voltages and compensate flow cytometry panels. In either case, beads were prepared in flow cytometry tubes just before cell acquisition. For AbC™ Total Compensation Beads, one drop of each, positive and negative beads were aliquoted to the labelled flow tubes. Next, 0.5-1 µL of each antibody was added to corresponding flow tubes followed by 100 µL of cell staining buffer and incubation for 30 minutes at 4^{o}C in the dark. After incubation, beads were washed with 200 µL of cell staining buffer, centrifuged 800 x *g* for 5 minutes and resuspended in 300 µL of cell staining buffer for flow analysis.

ArC™ Amine Reactive Compensation Beads were utilised for compensation of Live/Dead Near-IR staining. Similarly to AbC™ Total Compensation Beads Kit, one drop of component A was decanted to the labelled flow tube followed by adding 0.5-1 µL LIVE/DEAD™ Fixable Near-IR dye. After incubation for 30 minutes at RT in the dark, ArC™ Amine Reactive Compensation Beads were washed with 2 mL of PBS, centrifuged 800 x *g* for 5 minutes and resuspend in 300 µL of cell staining buffer. Finally, a drop of the second component B of ArC™ Amine Reactive Compensation Bead Kit was added before the acquisition.

2.2.9.1.4. Flow cytometry analysis

A 5-laser-LSRFortessa™ was used to run all cells and beads. AbC™ Total Compensation Beads (Thermofisher, UK) were used to establish the optimal PMT voltages and compensate flow cytometry panels. Additionally, CountBright™ absolute counting beads (Invitrogen, UK) were added and bead count and cell count were determined by gating on beads and cells with indicated markers using FlowJoV10 software (FlowJo, USA). The number of total cells is determined according to the manufacturer's instructions.

The standard procedures were followed for setting up and shutting down the cytometer. To calibrate the laser delay, cytometry setting and tracking (CST) beads were utilised. In addition, to confirm the stability of the settings of the flow cytometer used, CST beads run was performed using the experimental setting during every single experiment.

2.2.9.1.5. Deep immunophenotyping analysis

To improve and verify the manual gating approach, deep immune phenotyping using opt-SNE [202,203] (optimal *t*- stochastic neighbouring embedding, referred later as *t*-SNE) or UMAP[204] (Uniform Manifold Approximation and Projection) were performed. Both techniques are dimension reduction techniques that enable the user to visualize and draw the topological structure of the data by reducing different parameters into two dimensions. *t*-SNE is an algorithm that produces cluster visualisation by assuming Gaussian probability (normal distribution) while UMAP analysis is founded on the geometry and algebraic topology [204,205]. In brief, *t*-SNE preserves the local structure of the data while UMAP claims to preserve both, local and global topology of the dataset with greater run time performance[204]. *t*-SNE and UMAP analysis were computed on FlowJoV10.6 software (FlowJo LLC, USA). The *t*-SNE analysis was performed using 15,000 or 25,000 cells from each FSC file, with 1000 iterations, a perplexity of 30 and a theta of 0.5 [203]. UMAP analysis was computed using 15,000 or 25,000 cells from each FSC file, with hierarchal metric clustering (*Euclidian* distance) with the factor of 15 nearest neighbouring and minimum distance of 0.5. During the process of optimisation *t*-SNE or UMAP

were fed into the FlowSOM clustering algorithm. For each SOM, 8 metacluters and 100 clusters were identified [206].

2.2.9.1.6. Heatmaps, correlograms and PCA visualisations in R

Heatmaps were created using the built-in R function *heatmap()* in *stats* package using row scaling and row and column unsupervised hierarchal metric clustering (*Pearson* distance metric) with *average* cluster method. Pairwise correlations between variables were visualized and computed using *corrplot* in R function where positive correlations are displayed in blue and negative in red. PCAs were created using the *Factorextra* and *FactorMiner* R package where *PCA()* function was used to create the data frame automatically otherwise the R base function *scale()* was used to standardise the data set.

2.2.9.2. Measurement of cytokines via MSD plates

The immune mediators (pg/mL) lower and upper limits of detection (LLOD and ULOD, respectively) for: Interferon-γ (IFN-γ, LLOD=0.235, ULOD=1380), Interleukin-10 (IL-10, LLOD=0.044, ULOD=372), Interleukin-12p70 (IL-12p70, LLOD=0.553, ULOD=515), Interleukin-13 (IL-13, LLOD=2.04, ULOD=460), Interleukin-1β (IL-1β, LLOD=0.248, ULOD=566), Interleukin-2 (IL-2, LLOD=0.59, ULOD=1490), Interleukin-4 (IL-4, LLOD=0.0132, ULOD=234), Interleukin-6 (IL-6, LLOD=0.795, ULOD=767), Interleukin-8 (CXCL8) (IL-8, LLOD=0.0681, ULOD=555), Tumour Necrosis Factor-α (TNF-α, LLOD=0.191, ULOD=390), B-cell activating factor (BAFF, LLOD=1.71, ULOD=4090), Interferon-α2a (IFN-α2a, LLOD=3.68, ULOD=173500), Interferon-β (IFN-β, LLOD=85.1, ULOD=515000), Interleukin-15 (IL-15, LLOD=1.31, ULOD=17500), Interleukin-17E (IL17E, LLOD=3.52, ULOD=37500), Interleukin-29 (IL-29, LLOD=5.61, ULOD=42750), Interleukin-33 (IL-33, LLOD=2.46, ULOD=46950), Interleukin-5 (IL-5, LLOD=2, ULOD=22550), Thymic stromal lymphopoietin (TSLP, LLOD=1.27, ULOD=38850), C-X-C motif chemokine ligand 10 (IP-10, LLOD=1.06, ULOD=2480), Interleukin-17A (IL-17A, LLOD=2.17, ULOD=2900), Interleukin-21 (IL-21, LLOD=0.316, ULOD=1020), Interleukin-22 (IL-22, LLOD=0.315, ULOD=551), Interleukin-23 (IL-23, LLOD=1.26, ULOD=4600), Interleukin-27 (IL-27, LLOD=18.5, ULOD=16100), Macrophage inflammatory protein 3α (MIP-3α, LLOD=0.248, ULOD=962) and Interleukin-31 (IL-31 , LLOD=2.05, ULOD=463) were measured in frozen airway sample supernatants using the Meso Scale platform (Meso Scale Discovery, USA) according to the manufacturer's instructionsand. All LLOD and ULOD lot specific information are provided and available at www.mesoscale.com. Data were expressed as raw values in the figures using a log 10 scale.

2.2.9.3. Statistic and data analysis

Normality tests were performed using the Shapiro-Wilk test showing the non-parametric distribution. Differences between two groups were estimated by Mann-Whitney test for continuous data while *P* values for categorical data were computed by Fisher's exact test. Two group results are presented as a bar and individual subject plots (where the bar represents the median, whiskers represent upper interquartile range and symbols represent each individual). In PCA graphs the group mean point was added in the centre of each group and the point concentration ellipses were drawn around each group mean point using a multivariant t-distribution where the size of the concentration ellipse is in normal probability (95% confidence). All correlations (Heatmap and correlogram formats) were ordered according to hierarchical or non-hierarchal clustering; correlograms represent Pearson's correlation coefficients.

Data from a range of experiments were analysed in part using Microsoft Excel, Office 365™ (Microsoft, Washington, USA). Graphs were generated using GraphPad Prism 9.0 (GraphPad Software, Inc., California, USA), FlowJoV10.6 software (FlowJo LLC, USA) and R: A language and environment for statistical computing (R Foundation for Statistical Computing, Vienna, Austria).

3.

Results

3.1

A 14-colour, 16-antibody panel for immunophenotyping human innate lymphoid, myeloid and T cells in small volumes of whole blood and pediatric airway samples [201]

(See Appendix)

3.1.1. Introduction for Chapter 3.1

Innate immunity is particularly important as it comprises the very first line in defence against a myriad of pathogens, such as viruses and bacteria [188,207]. In early childhood, innate immunity may even be of greater importance regarding limited antigen encounter *in utero*, immature immune responses and low levels of maternal antibodies [10,65]. Innate immunity includes a plethora of soluble components and innate immune cells, such as granulocytes [117], natural killer cells [130] and recently discovered innate lymphoid cells (ILCs) [65]. The latter might play crucial roles in immune homeostasis and tolerance during an invasion by pathogens, such as a respiratory syncytial virus (RSV) [65]. RSV is the most common cause of bronchiolitis in children worldwide. Although RSV-related bronchiolitis has been actively investigated, there are many gaps in understanding of the pathogenesis of this infection [5]. It is believed that age-related differences in innate immune responses and genetic factors, particularly polymorphisms in innate genes can determine the clinical outcome of RSV infection [17]. Poor understanding of immune mechanisms behind bronchiolitis in children opens a window of opportunity for scientists to decode the interplay between the viral and cellular component during this acute lower respiratory infection.

ILCs could play a pivotal role in innate responses to viral bronchiolitis. They populate every tissue barrier (skin, gut, lungs) and are among the first cells to respond to environmental stimuli [65]. Members of the ILC family have classic lymphoid morphology; however, they lack antigen-specific receptors [65,121]. ILCs have been classified into three groups: ILC1s, ILC2s, and ILC3s depending on their function, expression of transcription factors and phenotype.

The first aim of this chapter was to establish an optimised multicolour immunophenotyping panel (OMIP, Swieboda *et al.,* 2019) and methodology that would enable me to enumerate different components of the cellular responses in blood and airway samples with low cell numbers [201]. It was hypothesised that innate cells and in particular ILCs play an important role in early life lung infections. Thus, I placed particular emphasis on identification of all major members of ILC family (ILC1s, including NK cells; ILC2s and ILC3s), T-cells ($CD4^+$ and $CD8^+$), invariant T cells (MAIT and NKT-like cells) and granulocytes (eosinophils and neutrophils). Subsequently, I utilised different methods for preserving and staining the whole blood and airway samples. Based on this optimisation, I was able to decide what the best ways of immunophenotyping and preserving paediatric samples are without losing ILCs and other rare populations of cells, such as NKT-like and MAIT cells. Mucosal-associated invariant T (MAIT) cells are T lymphocytes which respond to riboflavin metabolites [79,81]. On the other hand, natural killer

T (NKT) cells respond to glycolipids. In both cases, these cells are strongly associated with mucosal surfaces and recognition of non-peptide antigens in tissues, such as lungs [83]. As interesting differences in NKT and MAIT cells have been reported between children and healthy adults in a longitudinal study, I incorporated them in the panel believing they might be important in bronchiolitis [84].

The second aim of this chapter was to demonstrate the feasibility of obtaining clinical samples from infants. It is challenging to investigate the adaptive and innate responses in infants below the age of two due to the ethical restriction on sample collection. I optimised the staining panel on blood from healthy adult volunteers using as little as 300 µL of peripheral blood. Studies in neonates and adults have shown ILCs are relatively abundant in cord blood suggesting relatively high numbers of these cells in paediatric samples [194]. The experiments in this chapter demonstrated the feasibility of obtaining whole blood and respiratory samples from children. Finally, I confirmed that using the optimised methodology, I could identify ILCs in mucosal and blood samples from infants with bronchiolitis.

3.1.2. Methods for Chapter 3.1

3.1.2.1. Blood samples collection and processing

Infant blood and blood from healthy consenting adult donors were obtained as described in Materials and Methods **(see Chapter 2).** During optimisation, fresh human blood was processed fresh or frozen in FM (90% FCS, 10% DMSO) or placed in DMSO (up to 10% of added fresh blood). After mixing by inverting, samples were placed in a Nalagene™ container for freezing (**Fig. 3.1.1 A-C**). Additionally, blood samples were stabilised using a stabilising reagent TransFix™ (**Fig. 3.1.1 D**) according to the manufacturer's instructions [208,209]. Fresh, frozen and stabilised blood was characterised by flow cytometry using the optimised panel, also referred to later as OMIP (optimised multicolour immunophenotyping panel).

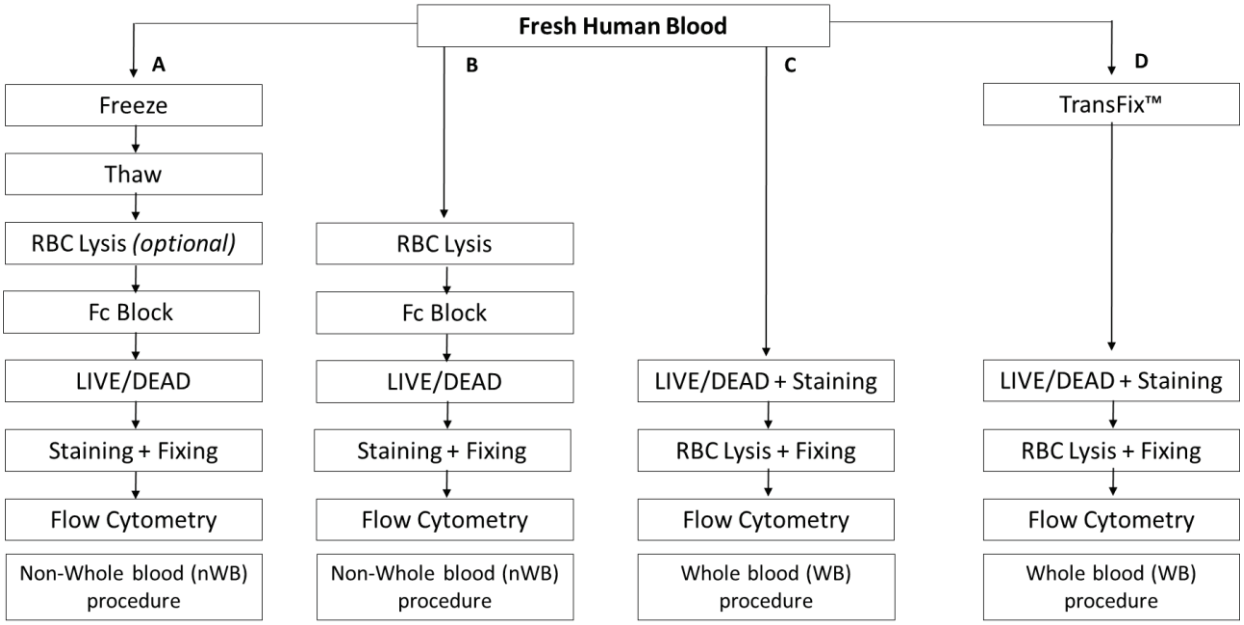


Figure 3.1.1 Strategies for blood sample processing before immunophenotyping using OMIP.

Fresh blood was frozen and stained for flow analysis (**A**) or processed fresh with red blood cell lysis (RBC Lysis) before (**B**) or after (**C**) staining. Fresh whole blood was stabilized using TransFix™ reagent and immunophenotyped (**D**). Non-whole blood (nWB) procedures involve RBC lysis or freezing before immunophenotyping. Abbreviation: Fc – Fc receptor, RBC – red blood cells.

3.1.2.2. Airway samples collection and processing

Nasosorption (NS), nasopharyngeal aspirate (NPA) and tracheal aspirate (TA) were obtained using previously optimised techniques mentioned in Chapter 2 Material and Methods [193,198]. As described before, NPA is a sampling method of upper airways from infants by aspiration of the upper airways of congested infants, followed by flushing the suction tubing with saline. TA is a sampling method of lower airways from infants on mechanical ventilation under sedation. TA secretions were collected using a suction catheter (tube), which is passed down the tube that goes into the child's windpipe.

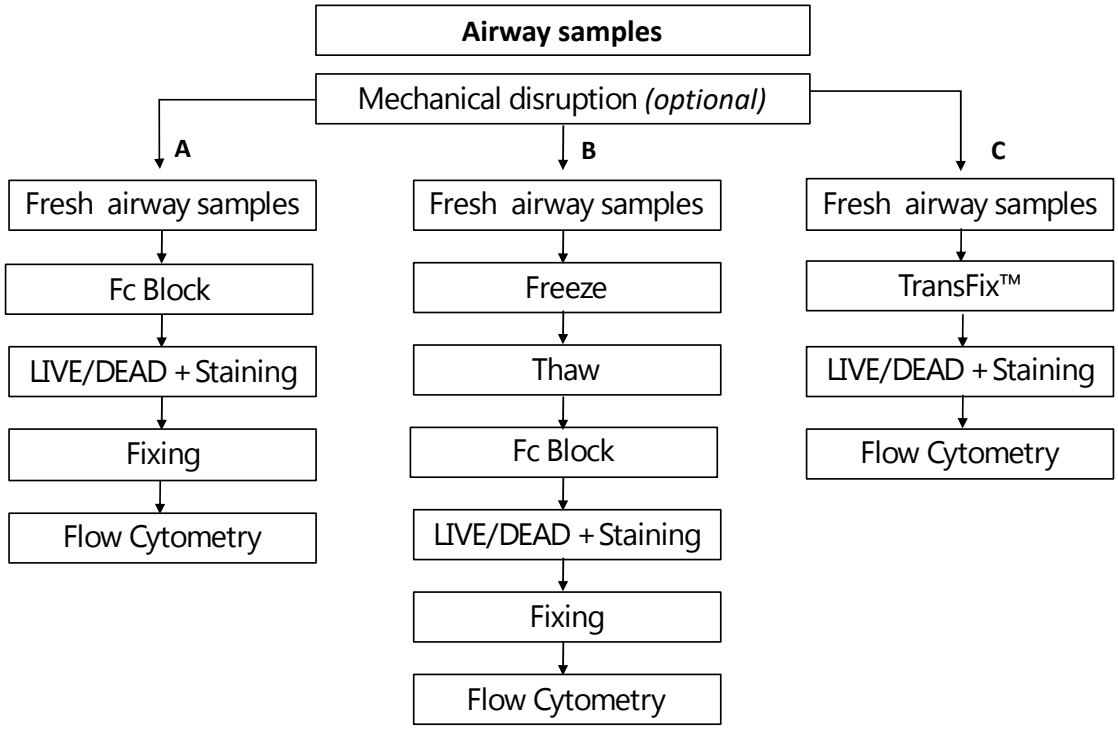


Figure 3.1.2 Strategies for airway sample processing before immunophenotyping.

Fresh (**A**), frozen (**B**) or fresh airway samples stabilised using TransFix™ reagent (**C**) were stained for flow analysis. Mechanical disruption with a syringe and a needle was performed when samples were mucous-rich.

Airway samples (NPA, TA) were processed as described in the Materials and Methods (**Chapter 2, Section 2**) and published literature[200]. During optimisation, the cellular component of airway samples was processed fresh, or after freezing in freezing media (FM, 90% v/v FCS, 10% v/v DMSO) (**Fig. 3.1.2 A and B**). Cells for freezing were mixed and placed in a Nalagene™ container (Sigma-Aldrich, Germany) for slow freezing to -80^{o}C. After 2 days, cells were transferred into liquid N_2 for long-term storage. Alternatively, TA was processed after using a stabilising reagent TransFix™ (CalTag, UK) (**Fig. 3.1.2 C**) according to the manufacturer's instructions.

3.1.3. Flow cytometry and staining procedures during OMIP optimisation

3.1.3.1. Staining protocol for flow cytometry on fresh peripheral blood and blood stabilised with TransFix™

Blood/ Airway samples OMIP			
Antibody	**Clone**	**Supplier**	**Dilution used**
Brilliant Violet 421™ anti-human CD127 (IL-7Rα)	A019D5	BioLegend	1:60
Brilliant Violet 510™ anti-human CD14*	63D3	BioLegend	1:60
Brilliant Violet 510™ anti-human CD19*	HIB19	BioLegend	1:120
Brilliant Violet 510™ anti-human FcεRIα*	AER-37	BioLegend	1:120
Brilliant Violet 510™ anti-human CD123*	6H6	BioLegend	1:300
Brilliant Violet 605™ anti-human CD4	RPA-T4	BioLegend	1:300
Brilliant Violet 650™ anti-human CD16	3G8	BioLegend	1:300
Brilliant Violet 711™ anti-human CD8	SK1	BioLegend	1:300
Brilliant Violet 785™ anti-human TCR Vα7.2	3C10	BioLegend	1:120
FITC anti-human CD45	HI30	BioLegend	1:120
PerCP/Cy5.5 anti-human CD117 (c-kit)	A3C6E2	BioLegend	1:40
PE anti-human CD3**	OKT3	BioLegend	1:120
PE/Dazzle™ 594 anti-human CD161	HP-3G10	BioLegend	1:60
PE/Cy7 anti-human CD56 (NCAM)**	5.1H11	BioLegend	1:120
Alexa Fluor® 647 anti-human CD294 (CRTH2)	BM16	BioLegend	1:40
Alexa Fluor® 700 anti-human CD66b	G10F5	BioLegend	1:300
APCH7/APCCy7 NIR™ Fluorescent reactive dye	-	Invitrogen	1:500

Table 3.1.1 Extracellular antibodies and their concentrations used in the optimised flow cytometry panel.

* Lineage cocktail includes the following antibodies: CD14, CD19, CD123, FcεR1α
**Antibodies used to define lineage negative population, but not part of the lineage cocktail

300 µL of whole blood was aliquoted into FACS tubes (BD, UK). The prepared mixture of fluorochrome-conjugated antibodies for surface staining and LIVE/DEAD IR dye was added to the blood (**Table 3.1.1**) for 30 minutes at RT. After staining, erythrocytes were lysed and fixed with 2 mL of red blood cell (RBC) lysis and fixation solution (BioLegend, UK) diluted in H_2O (1:10) for 10 minutes at RT. After fixing, cells were washed and resuspended in 370µL FACS buffer and kept at 4°C in the dark until they were run on a 5-laser-LSRFortessa™ cell analyser (BD Bioscience). AbC™ Total Compensation Beads (Invitrogen, UK) were used to establish the optimal PMT voltages and to compensate the flow cytometry panel. Additionally, CountBright™ absolute counting beads (Invitrogen, UK) were added up to 400µL total volume and bead count and cell count was determined by gating on beads and cells with indicated markers using FlowJoV10 software (FlowJo, USA). The number of total cells was determined according to the

manufacturer's instructions. In parallel, 300 µL of whole blood was aliquoted into FACS tubes for unstained, LIVE/DEAD and fluorescence minus one (FMO) controls.

3.1.3.2. Staining protocol for OMIP on airway samples, frozen and red-cell-lysed blood

After processing airway **(Fig. 3.1.2 A-C)** and frozen and red-cell-lysed blood samples **(Fig.3.1.1 A and B)** cells were washed with PBS, centrifuged (800 x *g*, 5mins) and were treated for 10 minutes at 4°C with Fc-block (Anti-CD16/CD32; Biolegend, UK). After Fc-blocking staining was performed with directly conjugated antibodies (**Table 3.1.1**) and with the LIVE/DEAD IR dye (Invitrogen, USA) diluted in PBS (1:500) for 30 minutes at 4°C. All unbound dye was removed with FACS buffer and cells were resuspended in 100 µL of fresh fixation buffer (Biolegend, UK) and incubated in the dark for 30 minutes at 4°C, or RT for 20 minutes. All fluorescently labelled surface antibodies were used simultaneously with the optimal concentration of mAb for 30 minutes at 4°C. Next, samples were processed as described above (**Section 3.1.3.1**).

3.1.3.3. Antibodies titration for OMIP on whole blood and airways samples

To determine the amount of antibody that provides the best fluorescence separation in samples, antibody titration was performed (**Fig. 3.1.4 A-B**). To titre antibodies, I used the conditions described above; however, each tube contained only one antibody. Each antibody was tested in a range of dilutions (1:40, 1:60, 1:120, 1:300 or 1:60, 1:120, 1:600, 1:1200). Similarly, the LIVE/DEAD™ Fixable Near-IR Dead Cell Stain (Thermofisher, UK) was titred using a range of dilutions such as 1:100, 1:250, 1:500 and 1:1000 (**Fig. 3.1.7**). Negative control with no antibody was included as well. Samples were run on a 5-laser-LSRFortessa™ cell analyser (**Section 3.1.3.1**). The stain index (SI) was calculated as follows:

$$SI = \frac{(MFI\ positive\ population - MFI\ negative\ population)}{2\ x\ SD\ MFI\ negative\ population}$$

MFI = geometric mean fluorescence intensity, SD = standard deviation.

3.1.3.4. Data acquisition

Processed samples were stained with the optimised flow panel (**Fig. 3.1.3**). A 5-laser-LSRFortessa™ was used to run all cells and beads (400 µL total, resuspended in FACS buffer). The standard procedures were followed for setting up and shutting down the cytometer. To calibrate the laser delay, cytometry setting and tracking (CST) beads were utilised. In addition, to confirm the stability of the settings of the flow cytometer used, a CST beads run was performed using the experimental setting during every single experiment.

3.1.4. Results for Chapter 3.1

3.1.4.1. Design and optimisation of staining panel

To assess the different components of the cellular response in different paediatric and adult samples a 14-multicolour, 17 - parameter flow cytometry panel was designed using 300 µL of adult peripheral blood **(Fig.3.1.3)**. Blood from healthy adult volunteers allowed enumeration of different components of the cellular response. Granulocytes, monocytes and lymphocytes were delineated on FSC/SSC, single, viable and $CD45^+$ cells (**Fig. 3.1.3 A**). Granulocytes were subdivided using CD16 and CD66b surface markers into neutrophils and eosinophils ($CD16^+CD66b^{+/-}$ and $CD16^-CD66b^+$, respectively) (**Fig. 3.1.3 B**). T lymphocytes were defined as $CD3^+CD56^-$ and further subdivided into $CD4^+$ and $CD8^+$ T cells (**Fig. 3.1.3 D-H**). Within $CD4^+$ and $CD8^+$ T cells, prostaglandin D_2 receptor (CRTH2) was used to define Th2 and Tc2 cells, as all type-2 cytokine-producing cells have a high level of expression of this surface cell marker (**Fig. 3.1.3 F-H**). Next, within $CD8^+$ cells, I identified invariant T lymphocytes responsible for the recognition of riboflavin metabolites known as MAIT cells. MAIT cells were defined as $CD161^H$ $V\alpha7.2^+$ -$J\alpha33^+$ (**Fig. 3.1.3 I**). Of note, I could identify $CD56^+$ MAIT cells as $CD3^+$ $CD56^+CD8^+$ CD161H $V\alpha7.2^+$ cells as not all MAIT cells are $CD56^-$ and these cells could be found in the NKT gate **(Fig. 3.1.4)**. In this panel, NK and NKT cells were conventionally defined within the lymphocyte gate as $CD56^+CD3^-$ and $CD56^+CD3^+$ cells, respectively (**Fig. 3.1.3 D**). Within the NK population, $CD56^HCD16^L$ and $CD56^LCD16^H$ subsets were defined with CD56 and CD16 cell markers density (**Fig. 3.1.3 E**). Of note, this staining panel was designed for enumeration of all leukocytes and in particular all major members of the ILC family. ILC populations were identified using a very stringent gating strategy: viable, single, $CD45^+$, lineage negative (CD3, CD14, CD19, CD56, CD123 and $Fc\varepsilon RI\alpha)^-$ and $CD127^+$ (IL-7 receptor-α) cells (**Fig. 3.1.3 C**). Moreover, three main subsets of ILCs (ILC1, ILC2 and ILC3) were delineated using CRTH2 and CD117 (c-Kit) surface markers (**Fig. 3.1.3 C**); ILC1 cells were defined as $CD117^-CRTH2^-$, ILC2 cells as $CRTH2^+$ $CD117^{int}$ and ILC3 as $CD117^+CRTH2^-$.

High dimensional stoichiometry (*t*-SNE, *t*-stochastic neighbouring embedding) analysis was performed on live, single, $CD45^+$ cells to further delineate populations of cells and reduce 17 parameters into two dimensions (*t*-SNE x and *t*-SNE y). Based on this high-dimensional data visualisation analysis, I revealed other unknown or poorly discriminated cell clusters (**Fig. 3.1.3 J**) that I was unable to identify by the standard biaxial gating strategy seen in **Figure 3.1.3 A-I**.

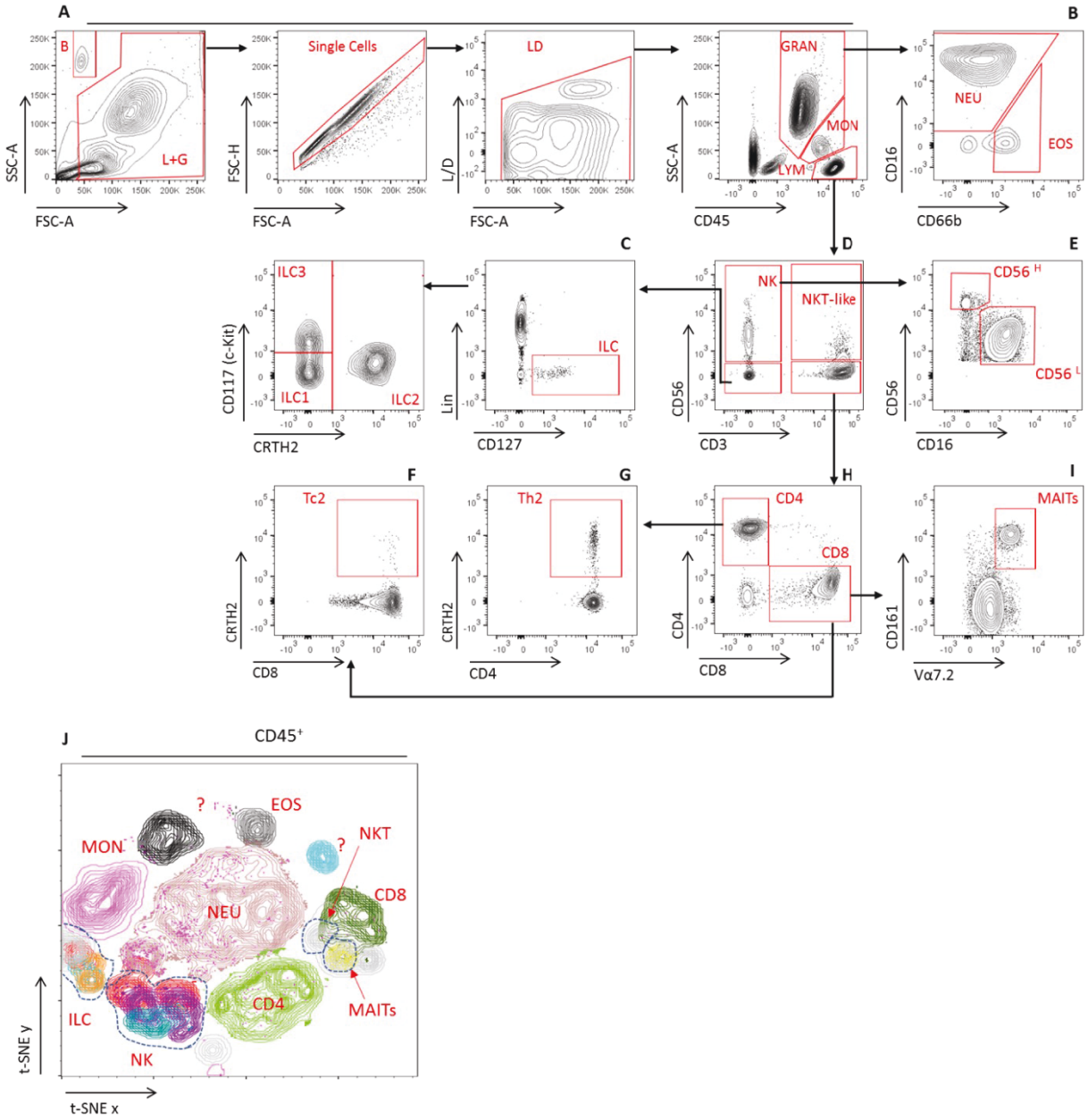


Figure 3.1.3 Example gating strategy and *t*-SNE analysis for visualisation of ILCs (including NK cells), granulocytes, MAIT, NKT-like cells and other T cell populations in paediatric clinical samples.

Cells were delineated using the following gating strategy: FSC/SSC, single, live cells. Granulocytes, monocytes and lymphocytes were gated using FSC and CD45 **(A)**. Within the granulocytes, neutrophils were defined as $CD16^{+}CD66b^{+/-}$ and eosinophils as $CD16^{-}CD66b^{+}$ **(B)**. NK and NKT-like cells were gated within the lymphocyte gate as $CD56^{+}CD3^{-}$ and $CD56^{+}CD3^{+}$ cells, respectively **(D)**. NK cells were further subdivided into $CD56^{H}$ and $CD56^{L}$ populations according to the CD56 and CD16 cell markers **(E)**. T lymphocytes ($CD3^{+}CD56^{-}$) were segregated into $CD4^{+}$ or $CD8^{+}$ T cells **(H)**. Type-2 T cells were defined within the $CD4^{+}$ and $CD8^{+}$ populations using the CRTH2 surface marker **(F, G)**. MAIT cells are $CD161^{H}$ $V\alpha7.2^{+}$ and were gated from live, single, $CD45^{+}$, $CD3^{+}$, $CD8^{+}$ cells **(I)**. ILCs were defined as live, single, $CD45^{+}$, lineage negative (CD3, CD14, CD19, CD56, CD123, $Fc\varepsilon R1\alpha)^{-}$ and $CD127^{+}$ lymphocytes **(C)**; ILC1 cells were defined as $CD117^{-}CRTH2^{-}$, ILC2 cells as $CRTH2^{+}$ $CD117^{int}$ and ILC3 as $CD117^{+}CRTH2^{-}$. Dimensional reduction (t-SNE) analysis for visualization of different cell components of designed flow cytometry panel **(J)**. Abbreviations used: B – counting beads, L+G – lymphocyte and granulocyte gate, LD – live/dead, GRAN – granulocytes, MON – monocytes, LYM – lymphocytes, NEU – neutrophils, EOS – eosinophils, NK – natural killer cells, NKT like – natural killer T –like cells.

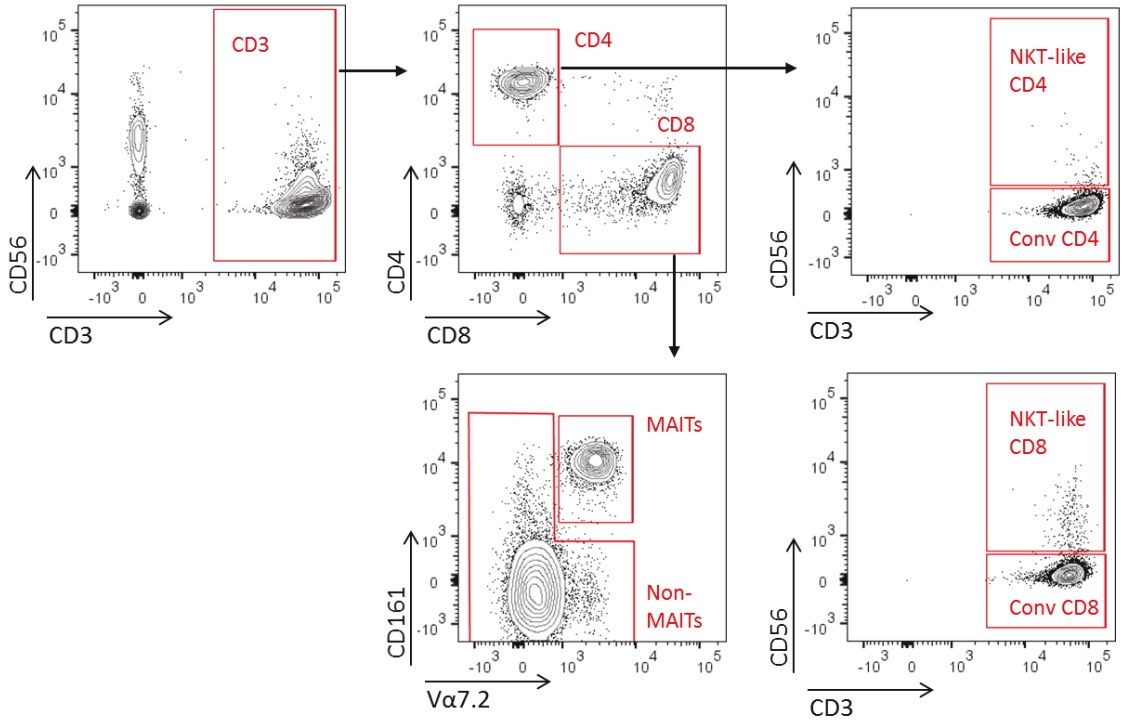


Figure 3.1.4 Exemplified gating strategy on NKT-like cells.

CD45^{+} CD56+ CD3+ lymphocytes are defined as NKT-like cells. Within this population, CD4+, CD8+ and MAIT (CD8^{+} CD161^{H} Vα7.2^{+}) sub-populations can be defined.

As my main aim was to characterise ILCs in-depth, the surface cell markers CD161 and CD127 were used for the identification of ILC subsets. My data strongly supports the notion that CD127 expression varies among different ILC clusters. Similarly, CD161 cell marker was expressed atdifferent levels on different populations of ILCs and this helped me to confirm the identity of ILC2s and ILC3s as they express a high level of CD161 whereas ILC1s do not (**Fig. 3.1.5**).

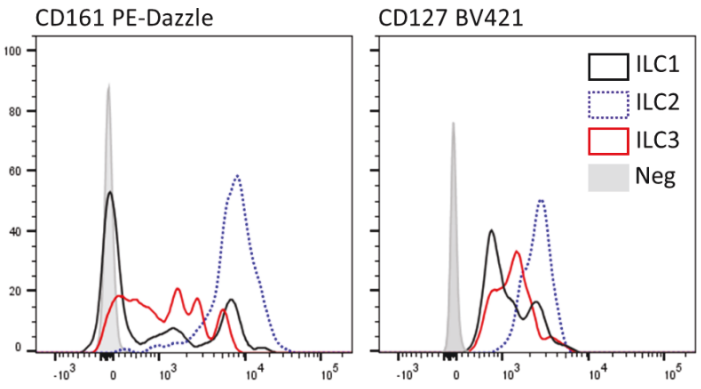


Figure 3.1.5 Histograms of CD161 and CD127 expression on ILCs.

ILCs were defined using the following gating strategy: live, single, CD45^{+}, lineage negative (CD3, CD14, CD19, CD56, CD123, FcεR1α)$^{-}$ and CD127^{+} cells. Histograms show levels of expression of CD161 and CD127 on ILC subsets and FMO controls (Neg).

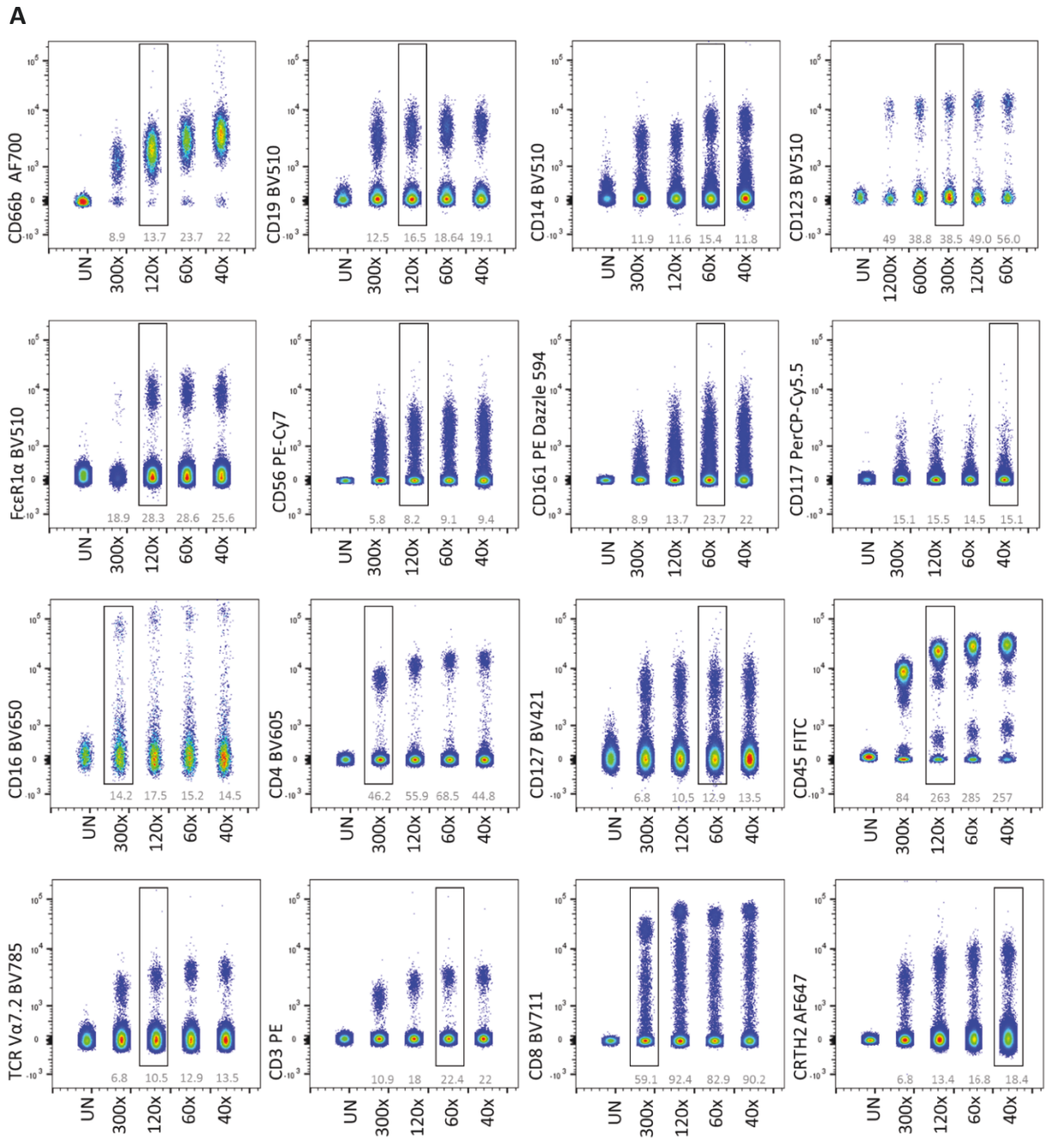


Figure 3.1.6 The histograms showing antibodies titration used in the optimised FACS panel.

(A) All dilutions tested in the experiment (UN, 40x, 60x, 120x, 300x or UN, 60x, 120x, 600x, 1200x) show separation between the negative and positive populations. The visual display shows that the increasing amount of antibody usually increases the separation and fluorescent intensity between the negative and positive populations. The lowest concentration of antibody that gives the highest optimal separation without increasing the signal from the negative population is highlighted with a black square. **(B)** The titration was performed on all antibodies used in optimises FACS panel. Abbreviations used: Ab – antibody, UN – negative staining.

All fluorochrome-conjugated antibodies and Live/Dead reagent (**Fig. 3.1.6B**) were titrated (**Fig. 3.1.6A and Fig. 3.1.7**) on whole blood from healthy adult volunteers according to the manufacturer's instruction. Once optimised, I tested this panel on airways samples (nasopharyngeal aspirates (NPA) and tracheal aspirates (TA) (**Fig. 3.1.8**). After multiple iterations, the final concentrations of antibodies and voltages used were kept the same and no manual PMT alterations were performed between experiments as the optimal separation between positive and negative populations was established.

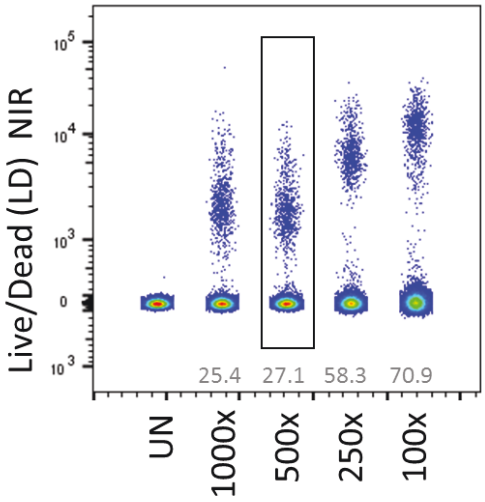
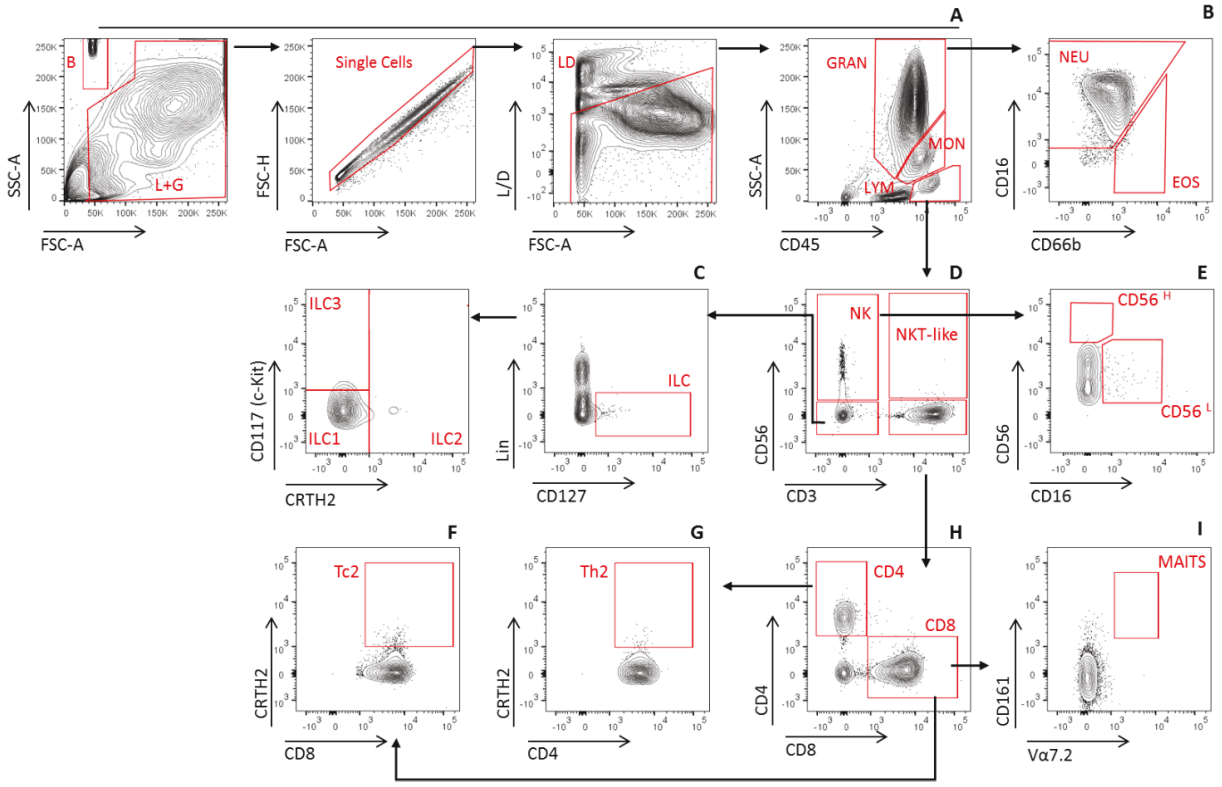


Figure 3.1.7 Live/Dead reagent titration.

LIVE/DEAD™ Fixable Near-IR Dead Cell Stain Kit (L-10119, Thermofisher) was used to eliminate dead cells. The reagent was titrated on whole blood from healthy adult volunteers according to the manufacturer's recommendation.

During the panel optimisation, I determined the fluorescence spread for cell subsets and established the gating boundaries using fluorescence minus one (FMOs) controls for each antibody (**Fig. 3.1.9**). Of note, FMO controls were utilised only if necessary, as the most cells clusters were clearly defined using standard biaxial gating.

NPA


A
B
C
D
E
F
G
H
I
B
L+G
SSC-A
FSC-A
Single Cells
FSC-H
LD
L/D
GRAN
MON
LYM
CD45
NEU
EOS
CD16
CD66b
ILC3
ILC1
ILC2
CD117 (c-Kit)
CRTH2
ILC
Lin
CD127
NK
NKT-like
CD56
CD3
CD56 H
CD56 L
Tc2
Th2
CD4
CD8
MAITS
CD161
Vα7.2

TA

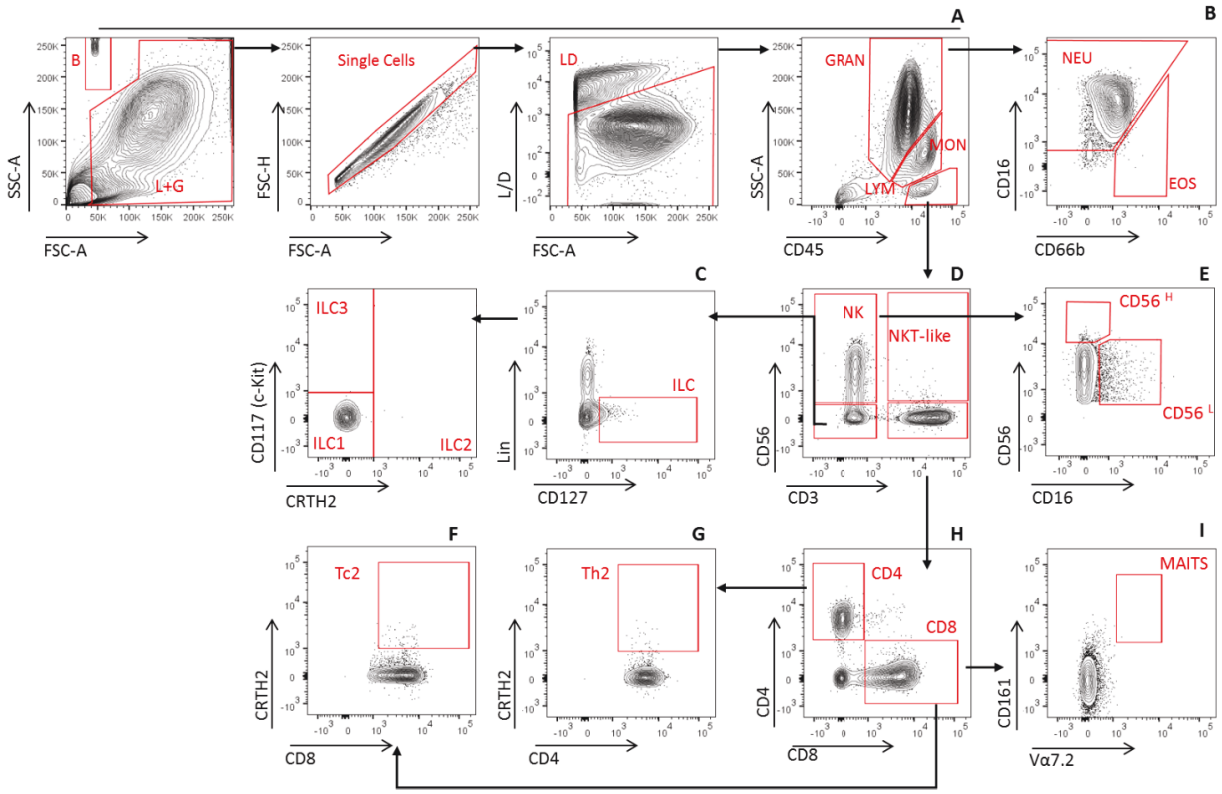

A
B
C
D
E
F
G
H
I
B
L+G
SSC-A
FSC-A
Single Cells
FSC-H
LD
L/D
GRAN
MON
LYM
CD45
NEU
EOS
CD16
CD66b
ILC3
ILC1
ILC2
CD117 (c-Kit)
CRTH2
ILC
Lin
CD127
NK
NKT-like
CD56
CD3
CD56 H
CD56 L
Tc2
Th2
CD4
CD8
MAITS
CD161
Vα7.2

Figure 3.1.8 Gating strategy for enumeration of lymphocytes and granulocytes in paediatric nasopharyngeal aspirate (NPA) and tracheal aspirate (TA).

Cells were delineated using the following gating strategy: FSC/SSC, single, live cells. Granulocytes, monocytes and lymphocytes were gated using FSC and CD45 **(A)**. Within the granulocytes, neutrophils were defined as $CD16^{+}CD66b^{+/-}$ and eosinophils as $CD16^{-}CD66b^{+}$ **(B)**. NK and NKT-like cells were gated within the lymphocyte gate as $CD56^{+}CD3^{-}$ and $CD56^{+}CD3^{+}$ cells, respectively **(D)**. NK cells were further subdivided into $CD56^{H}$ and $CD56^{L}$ populations according to the CD56 and CD16 cell markers **(E)**. T lymphocytes ($CD3^{+}CD56^{-}$) were segregated into CD4+ or CD8+ T cells **(H)**. Type-2 T cells were defined within the $CD4^{+}$ and $CD8^{+}$ populations using the CRTH2 surface marker **(F, G)**. MAIT cells are $CD161^{H}$ $V\alpha7.2^{+}$ and were gated from live, single, $CD45^{+}$, $CD3^{+}$, $CD8^{+}$ cells **(I)**. ILCs were defined as live, single, $CD45^{+}$, lineage negative (CD3, CD14, CD19, CD56, CD123, $Fc\varepsilon R1\alpha)^{-}$ and $CD127^{+}$ lymphocytes **(C)**; ILC1 cells were defined as $CD117^{-}CRTH2^{-}$, ILC2 cells as $CRTH2^{+}$ $CD117^{int}$ and ILC3 as $CD117^{+}CRTH2^{-}$. Abbreviations used: B – counting beads, L+G – lymphocyte and granulocyte gate, LD – live/dead, GRAN – granulocytes, MON – monocytes, LYM – lymphocytes, NEU – neutrophils, EOS – eosinophils, NK – natural killer cells, NKT like – natural killer T –like cells.

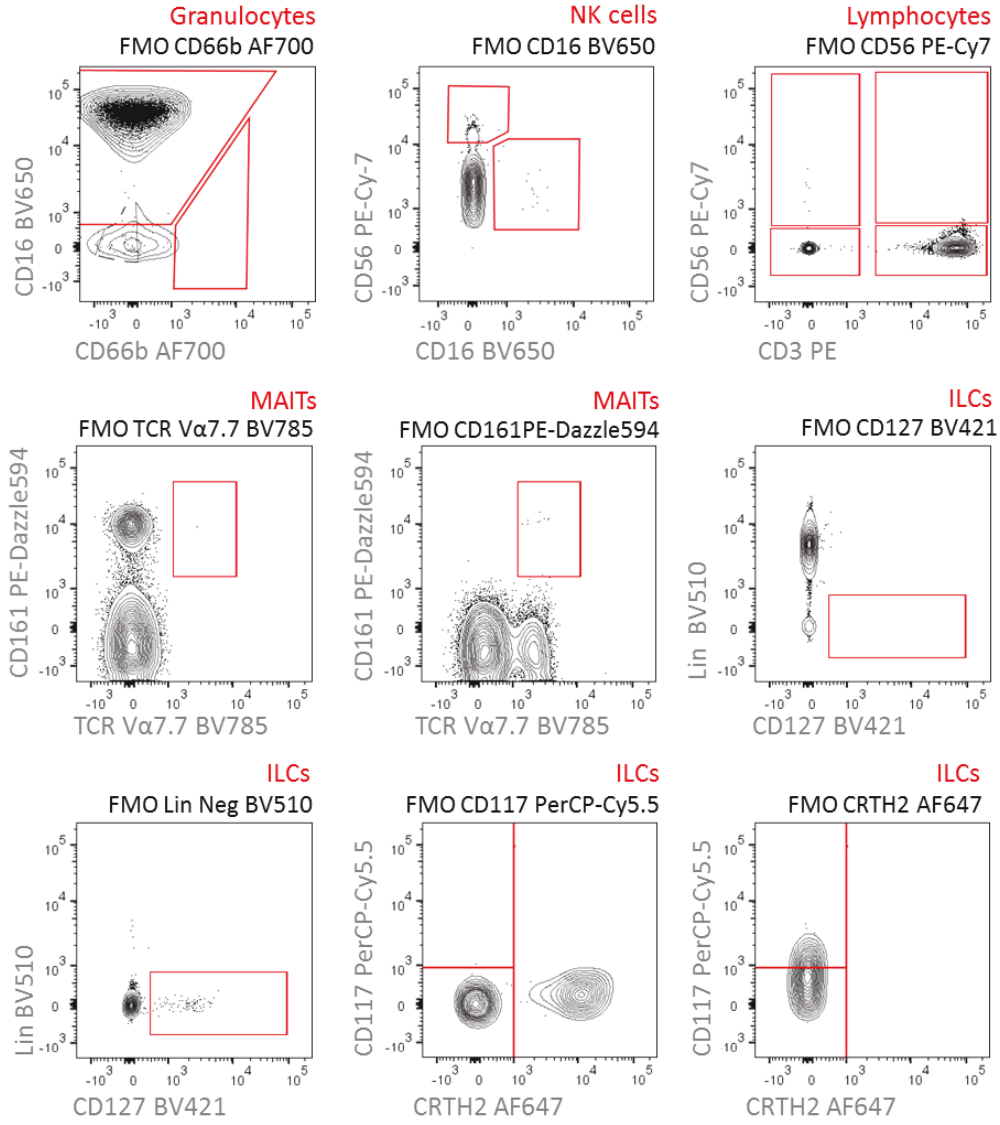


Figure 3.1.9 Fluorescence Minus one controls (FMOs) for Granulocytes, NK cells, MAITs and ILCs.

FMO controls were used to determine fluorescence spread for cell populations and accurately describing gating boundaries. FMO controls were used only when necessary and if cell populations were not clearly defined on the flow plots.

3.1.4.2. Optimisation of staining panel on blood from healthy adult volunteers

3.1.4.2.1. Characterizing the impact of RBC lysis before and after staining on the innate cell populations in whole blood

Whilst most human studies utilise the immunophenotyping of peripheral blood mononuclear cells (PBMCs), I used whole blood immunostaining. The very first part of this project aimed to determine the impact of red blood cell lysis before and after staining to obtain the most applicable and reliable protocol for answering the main aims proposed.

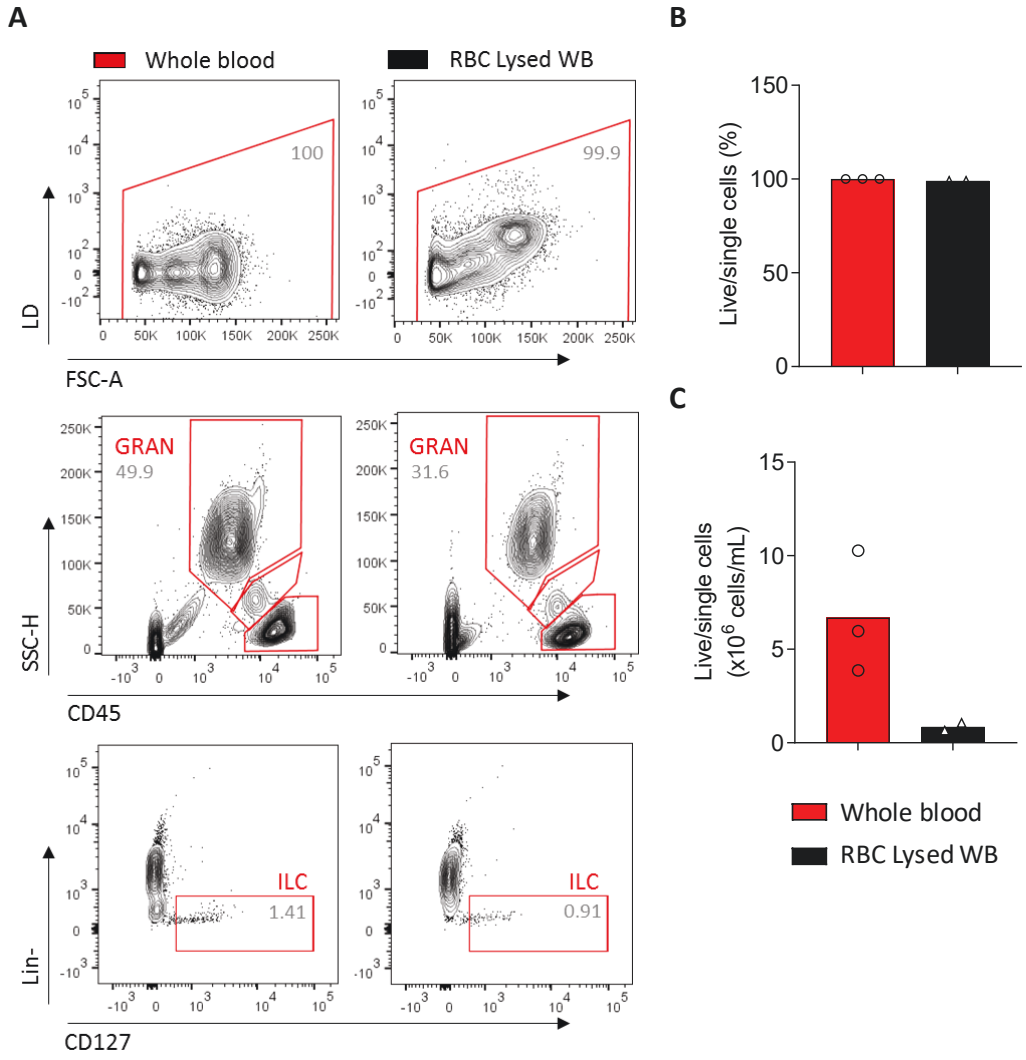


Figure 3.1.10 Comparison of RBC lysis before and after staining protocol on granulocytes, ILCs and a total number of live cells in fresh human blood.

(A) Fresh blood was either stained directly with antibodies and then red blood cells lysis performed (whole blood, red) or red cells were lysed firstly and then stained for immunophenotyping (RBC lysed WB, black). Live/Dead, CD45 positive cells and ILCs were quantified using flow cytometry. The red gates highlight different leukocyte populations including live $Lin^{-}CD127^{+}$ ILCs within $CD3^{-}CD56^{-}$ lymphocytes. Quantification of percentages of live/single **(B)** and total live/single-cell numbers **(C)** in blood using the two different staining protocols. Data show biological replicates using multiple biological samples treated in the same conditions. Abbreviations used: GRAN – granulocytes, LD – Live/Dead, Lin^{-} - lineage negative, RBC– red blood cell, WB – whole blood.

As seen in **Fig. 3.1.10**, RBC lysis before or after staining had an impact on granulocytes and ILCs using these two protocols (**Fig. 3.1.10A**). Although RBC lysis did not affect the percentage of live/single cells (**Fig. 3.1.10A**), it had a profound effect on the total number of live, single cells (**Fig. 3.1.10C**).

3.1.4.2.2. Characterising of the impact of Fc- receptor blocking on RBC-lysed whole blood

Subsequently, the impact of Fc-blocking antibody on lysed whole blood was assessed. Fc-receptors are present on the surface of many hematopoietic cells, such as neutrophils, macrophages, eosinophils and NK cells [210].

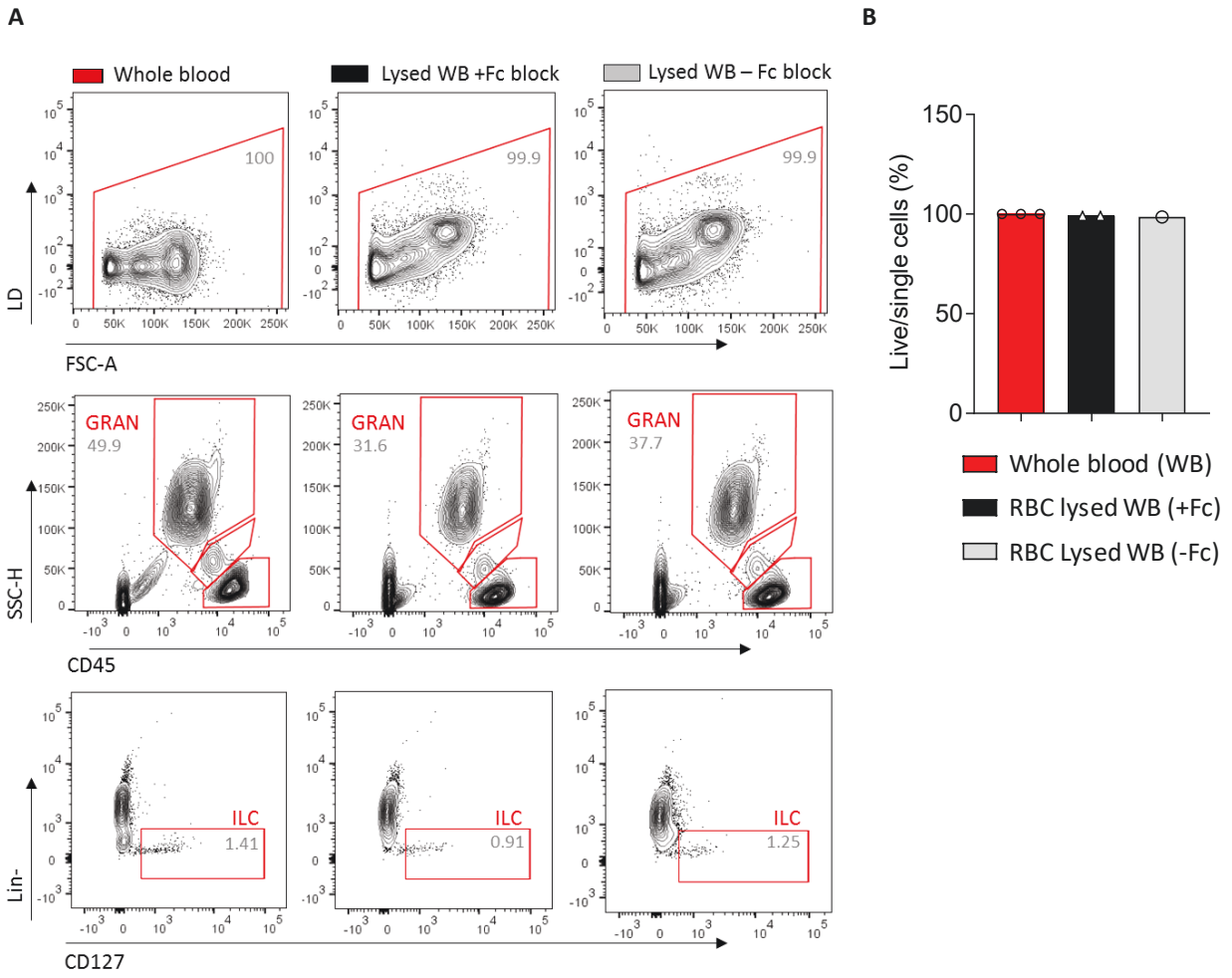


Figure 3.1.11 Impact of Fc blocking on granulocytes and total number of cells in lysed whole blood human samples.

(A) Fresh blood was either stained directly with antibodies and then red blood cells lysis performed (whole blood, red) or red cells were lysed firstly and then sample stained for immunophenotyping (RBC lysed WB, black). Also, RBC lysed WB was either treated with Fc blocking antibody or not, to check the impact of Fc-receptor blocking on FACS staining. **(B)** Quantification of frequencies of live/single cells in whole blood and RBC lysed whole blood samples using different protocols of FACS staining. Data show biological replicates using different biological samples treated in the same conditions. Abbreviations used: GRAN – granulocytes, Fc – Fc blocking antibody, LD – Live/Dead, RBCL – red blood cell lysis, LD – Live/Dead, Lin^- - lineage negative, RBC– red blood cell, WB – whole blood.

As seen on the **Fig. 3.1.11**, the percentages of live, single cells in Fc-blocked lysed blood were similar (~100%) in all conditions (**Fig. 3.1.11B**). Furthermore, the lack of Fc-block did not have an

impact on the ILC population, however, the population of granulocytes slightly diminished in flow plots suggesting the importance of this step in staining RBC-lysed whole blood (**Fig. 3.1.11A**).

3.1.4.2.3. The impact of time and fixative reagent on fluorochrome brightness

I next tried to determine the effect of time (1, 2 or 3 days after staining before analysing by flow cytometry) on FACS staining quality. As can be seen (**Fig. 3.1.12**), there is minimal impact on the percentage (**Fig. 3.1.12B**) and total number (**Fig. 3.1.12C**) of live, single cells up to three days post-staining; and furthermore, the staining allowed the ILC population to be detected. Due to the project's nature, the decision was made that samples would be processed and analysed together, up to three days post-staining to reduce the day-to-day variability of the LSRFortessa™ cell analyser.

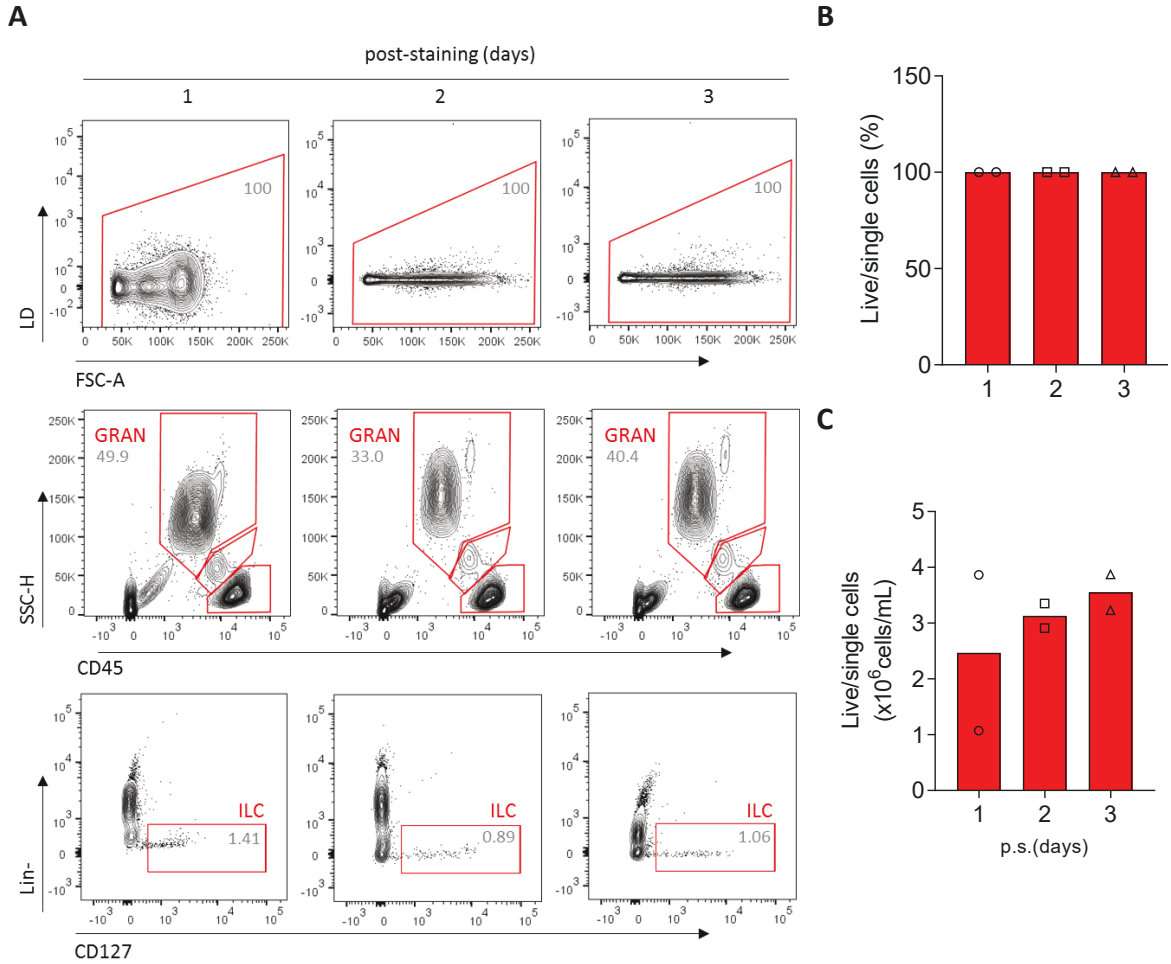


Figure 3.1.12 Stained and fixed blood samples can be left up to three days post-staining before performing flow cytometry analysis.

(A) Fresh whole blood was processed and stained using the optimised FACS panel RBC lysis followed by fixing with RBC lysis and fixing together using the commercial product according to the manufacturer's instruction. After staining samples were kept at 4°C in the dark and analysed using flow cytometry 1, 2 or 3 days post-staining to check the impact of time on fluorochrome brightness. The black circles highlight the granulocyte population. **(B)** Shows the percentage of total live cells while **(C)** shows the number of total live/single cells after 1, 2 and 3 post-staining. Data show biological replicates using different biological samples treated in the same conditions.

Furthermore, a similar result was observed on granulocytes and ILCs populations (**Fig. 3.1.12A**), suggesting that I can analyse different batches of stained samples in one day of the week, reducing a day-to-day variability of the LSRFortessa™ cell analyser.

3.1.4.3. Establishing the effect of controlled-rate cryopreservation on whole blood

In parallel with optimising the panel design on fresh blood, I wanted to test the impact of different methods of processing and freezing on whole blood. I used two different protocols for freezing whole blood (see Materials and Methods section 3.1.2).

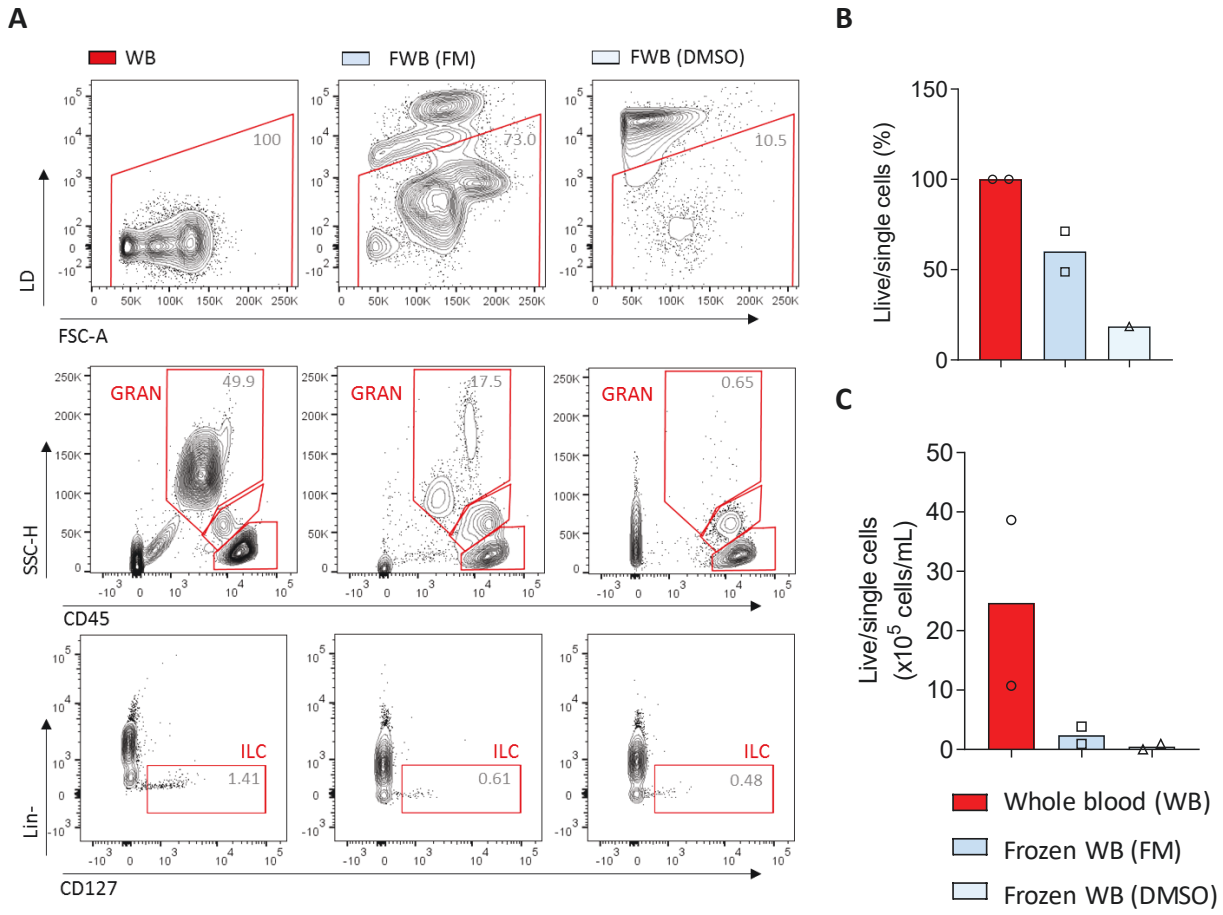


Figure 3.1.13 Controlled – rate freezing and storage in liquid N_2 of fresh whole blood reduces the total number of live cells and the number of granulocytes upon recovery.

(A) Fresh blood was stained directly with antibodies and then red blood cells lysis performed (WB – whole blood, red bar) followed by analysis using flow cytometry. In the case of frozen samples, freezing medium (FM, blue bars) or DMSO (up to 10% of fresh whole blood, light blue bars) were used for the whole blood, long – term storage in N_2 after a controlled – rate freezing using ultralow temperature (-80°C) in a Nalagene™ Mr. Frosty. Thereafter frozen samples were immunophenotyped as described in Materials and Methods. Quantification of percentages of live cells **(B)** and the total number of live cell **(C)** in fresh whole blood and in frozen whole blood (FWB) samples using two different protocols of blood cryopreservation. Live/Dead and CD45 positive cells were quantified using flow cytometry. Data show the biological replicates of different biological samples treated in the same conditions. Abbreviations used: DMSO – dimethyl sulfoxide.

As shown in **Figure 3.1.13B**, I detected a decrease in the percentage of viable cells in both freezing protocols using FM or DMSO (40% and 30% live cells, respectively) compared to fresh

whole blood staining (up to 100%). Notably, in accordance with the percentages, the number of viable cells decreased (**Fig. 3.1.13C**) in both protocols from $2x10^6$ cells/mL in fresh whole blood to $3.6x10^5$ and $9.5x10^4$ cells/mL in the protocols with FM and DMSO, respectively. The reduced recovery of viable cells was reflected in the number of granulocytes and ILCs in frozen samples upon recovery after staining (**Fig. 3.1.13A**).

3.1.4.4. The characterisation a Transfix™-based stabilisation technique on whole blood staining

Subsequently, I assessed the capacity of an antigen-stabilising reagent (TransFix™, **Fig. 3.1.14A**) on different populations of cells in whole blood. TransFix™ is a patented buffer of heavy metal salts and aliphatic aldehyde, which in combination with EDTA works the best [208].

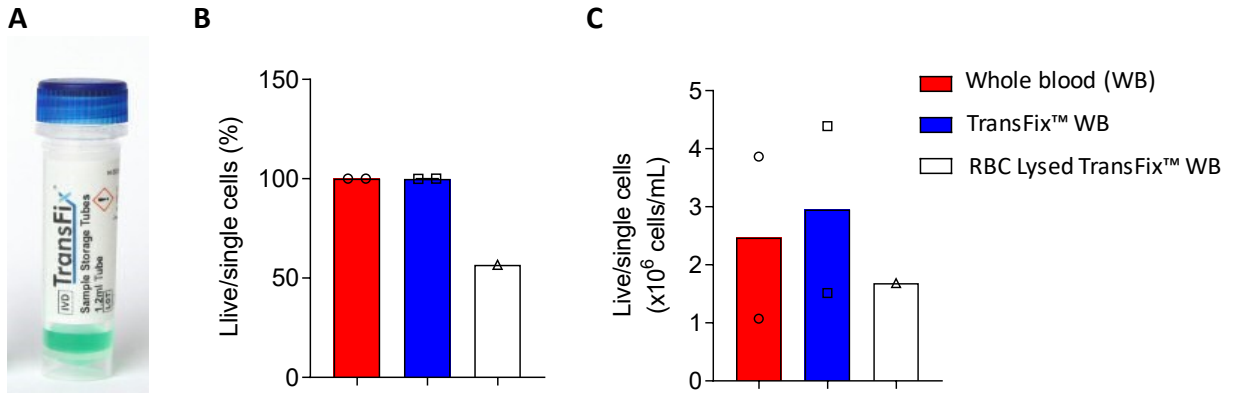


Figure 3.1.14 Comparison of blood processing protocols on whole blood stabilised using a patented Transfix™ reagent.

(A) Blood samples were stabilised using a stabilising reagent TransFix™ (Cytmark, CalTag, UK) according to the manufacturer instructions to check if I can reduce variability in sample analysis due to differences in batches of whole blood. **(B)** The percentages of live/single cells and **(C)** the number of a total live/single cell were quantified in fresh and stabilised blood. Fresh blood was immunophenotyped directly and analysed using flow cytometry (red bar). On the other hand, a stabilised/preserved blood (3 days after TransFix™ addition) was stained directly with antibodies and then red blood cells lysis performed or red cells were lysed firstly and then sample stained for flow cytometry (blue and white bar, respectively) as described in Materials and Methods section. Data show the biological replicates of different biological samples treated in the same conditions.

The first experiments indicated that in blood treated with TransFix™ for three days before staining, the number and the percentage of viable cells were similar to the fresh whole blood (**Fig. 3.1.14 B-C**). Conversely, an RBC lysis before staining of whole blood treated with TransFix™ for 3 days led to decrease in the percentage (~50%) and the number of live cells (down to $1x10^5$ cell/mL) compared to the fresh whole blood and directly stained TransFix™ treated blood (**Fig. 3.1.14 B-C)**.

3.1.4.4.1. Characterising the effect of time on the preservation of whole blood using Transfix™

I also assessed the effect of time on the viability of cells in whole blood stored at 4°C for 0, 1, 2, 3- and 6-days post-treatment with TransFix™ (**Fig. 3.1.15A**). As expected, the immunophenotyping of TransFix™-stabilised blood revealed that the percentages and numbers of viable cells were well preserved particularly in granulocytes and lymphocytes populations up

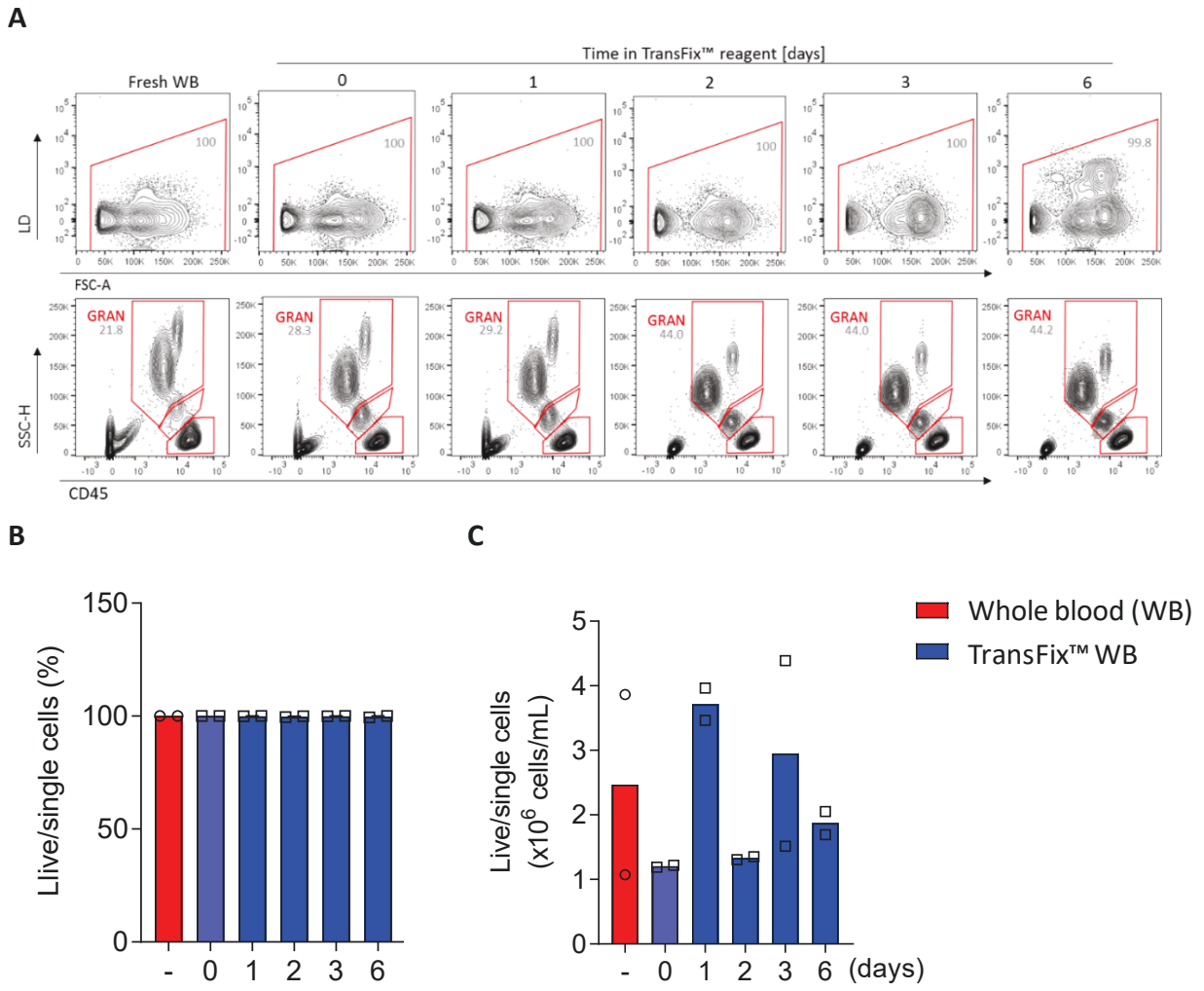


Figure 3.1.15 Transfix™ - a stabilising reagent preserves blood cells and cellular antigens up to 6 days before flow cytometry analysis.

(A) Quantification of live/single cells and CD45 positive cells in fresh whole blood (WB) and stabilised whole blood with Transfix™ using optimised staining protocol. Before immunophenotyping using flow cytometry stabilised blood was preserved in Transfix™ reagent for 0, 1, 2, 3 and 6 days. The enumeration of the percentage of live cells **(B)** and the total number of live cells **(C)** in a fresh and stabilised whole blood with Transfix™. Data show the biological replicates of different biological samples treated in the same conditions.

to 6 days post-treatment (**Fig. 3.1.15 B-C**). Although there were no differences in the percentage and the number of cells, or the brightness of markers expressed on granulocytes, NK/NKT cells, MAIT cells (data not shown), and the total of $Lin^{-}CD127^{+}$ ILCs (**Fig. 3.1.16 B, F**), ILC1s (**Fig. 3.1.16 C, G**) and ILC3s (**Fig. 3.1.16 E, I**), I observed a time-dependent decrease in the brightness of

CRTH2 staining on ILC2s (**Fig. 3.1.16 D, H**). **Figure 3.1.16A** shows changes in CRTH2 staining which plays a pivotal role in the identification of ILC2s [188]. These results were obtained on Transfix™-treated samples and compared to the untreated whole blood sample.

3.1.4.5. Optimisation of the staining panel on paediatric airway samples

In parallel with assessing the best conditions for whole blood staining, the optimised staining panel (**Fig. 3.1.3**) was tested on airway samples from children: nasopharyngeal aspirates (NPA, **Fig. 3.1.9**) and tracheal aspirate (TA, **Fig. 3.1.9**). In both cases, NPA and TA, I investigated the impact of freezing on staining; however, only in the case of TAs was TransFix™ stabilising reagent utilised. As seen in **Fig. 3.1.17**, even though the same number of fresh, frozen and stabilised cells from TA were stained, the total numbers of viable cells reduced in frozen and stabilised samples (**Fig. 3.1.17C**), yet I saw no changes in the percentages of live cells (**Fig. 3.1.17B**). As expected, freezing influenced the viability of populations of lymphocytes and ILCs, decreasing their number. TransFix™-treated TAs were not well preserved, further reducing the viability of lymphocytes and ILCs (**Fig. 3.1.17A**). Next, I sought to investigate the impact of different staining procedures on NPA. **Fig. 3.1.18 B-C** revealed that there were differences between fresh and frozen NPA in terms of quantification of the number (around $4x10^5$ and $3x10^5$ cells/mL, respectively) and the percentage of total live cells (up to ~90% and 50%, respectively). Interestingly, freezing had a strong effect on reducing the population of $CD3^-CD56^-$ lymphocytes to 0.62% from 2.85% in fresh samples and ablating the population of Lin^-CD127^+ ILCs to 0% (**Fig. 3.1.18A**).

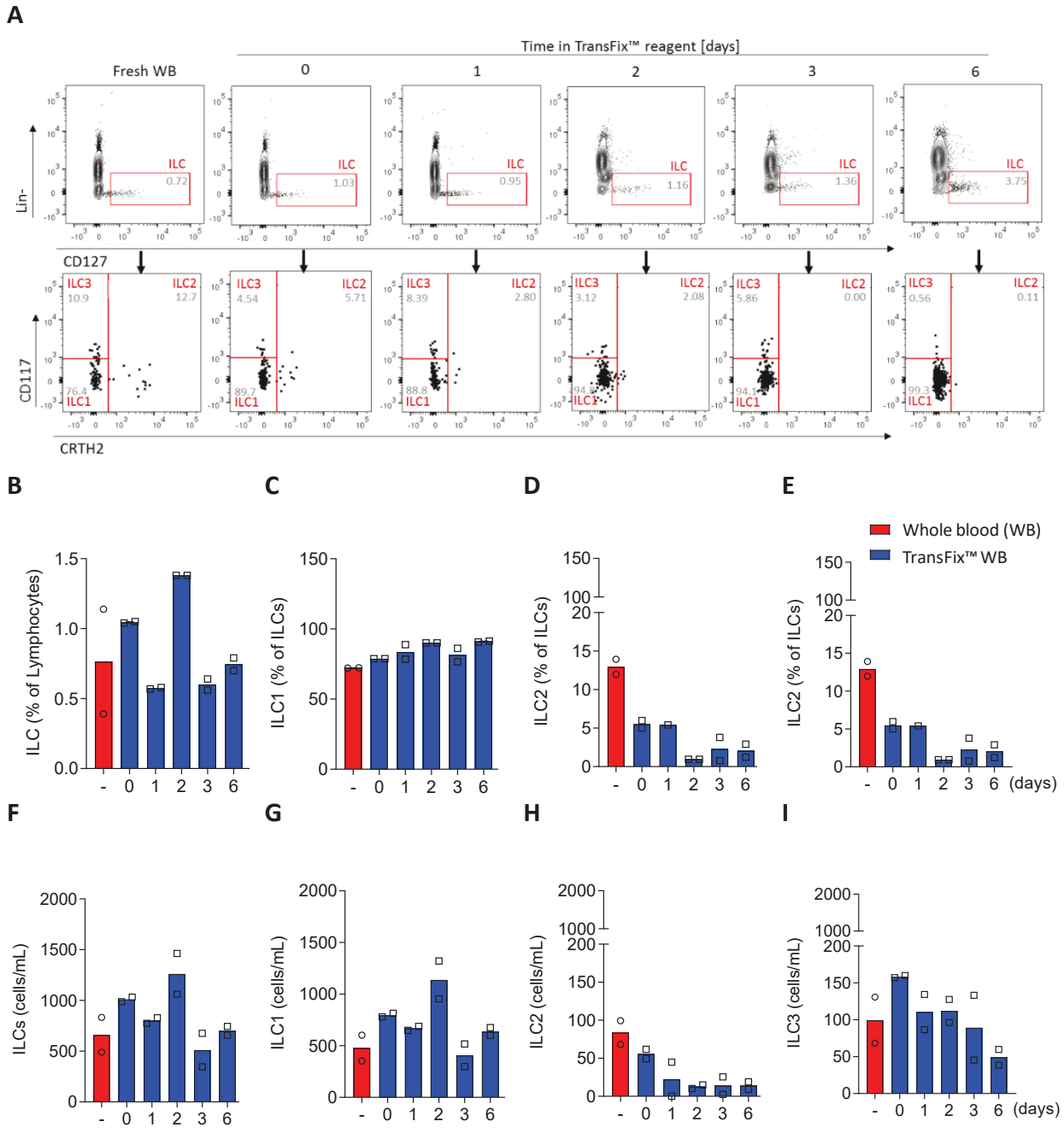


Figure 3.1.16 Blood samples stabilised with Transfix™ show a time-dependent decrease in the brightness of CRTH2 staining on ILCs.

The impact of Transfix™ reagent was measured using means of flow cytometry **(A).** Before immunophenotyping using optimised staining FACS panel stabilised blood (blue bars) was preserved in Transfix™ reagent (0, 1, 2, 3 and 6 days) and compared to the fresh whole blood (red bars). **(B-E)** Show percentages of total ILCs and ILC1, ILC2, ILC3, respectively. **(F-I)** Show enumeration of total cell numbers of ILCs, ILC1, ILC2 and ILC3, respectively. Data show the biological replicates of different biological samples treated in the same conditions.

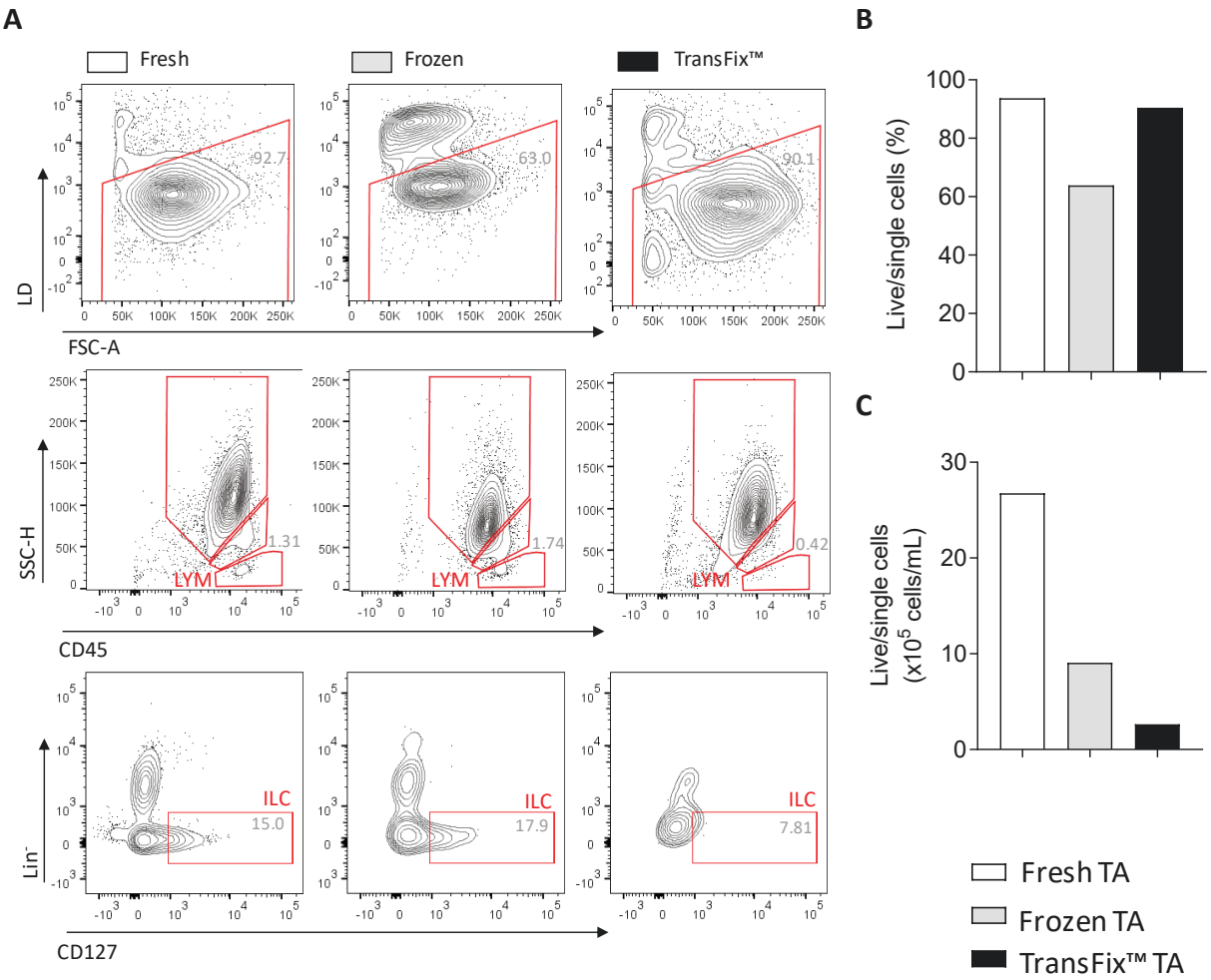


Figure 3.1.17 Comparison of different processing protocols on lymphocyte and ILC number in tracheal aspirate (TA).

1.7 x 10^6 cells from fresh, frozen and TransFix™ - treated TA samples were stained as described in Materials and Methods section. **(A)** The flow plots show the quantification of Live/Dead, CD45 and ILCs in tracheal aspirates. The percentage of live/single cells while **(B)** and the total cell numbers **(C)** were enumerated using flow cytometry in TA samples.

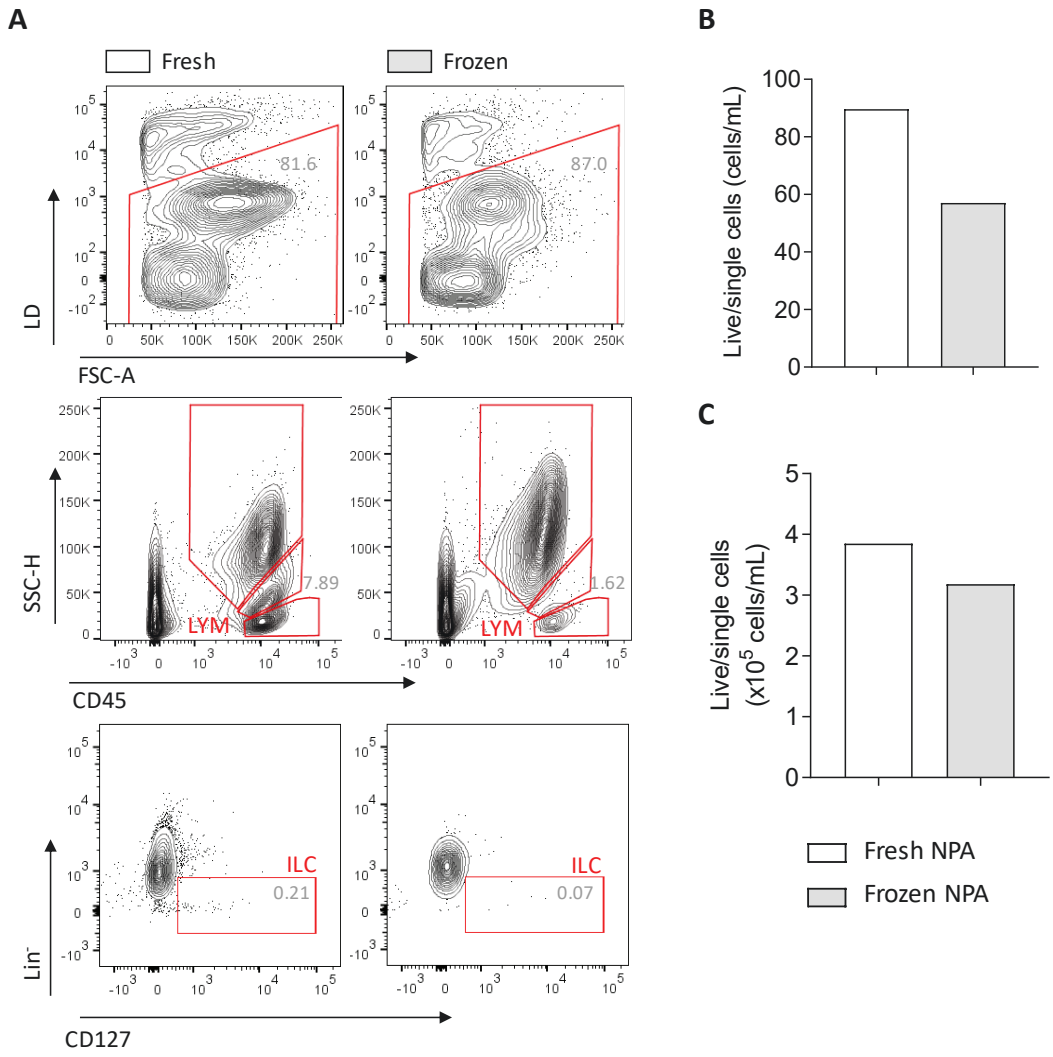


Figure 3.1.18 Comparison of different processing protocols on lymphocytes and ILC number in nasopharyngeal aspirate (NPA) using the optimised FACS panel.

Around 1.2 x 10^6 cells from fresh, frozen NPA samples were stained as described in Materials and Methods section. **(A)** The flow plots show the quantification of Live/Dead, CD45 and ILCs in NPA. The percentage of live cells **(A)** and the total cell numbers **(B)** were enumerated using flow cytometry in NPA samples

3.1.5. Discussion for Chapter 3.1

This project focuses on the role of ILCs during paediatric acute respiratory infections, including RSV-induced bronchiolitis. To understand the association between ILCs and disease severity and lung inflammation during bronchiolitis, the establishment of protocols and methods was prioritised in the first part of this PhD. A 14 – colour, 17 – parameter flow cytometry panel was designed to ensure that many different components of adaptive and innate immunity would be included, such as granulocytes, NK/NKT cells, MAIT cells and, foremost, ILCs [201].

Working on human $CD127^+$ ILCs is challenging as they lack specific markers which define T cells (CD3), B cells (CD19), progenitor cells (CD34), mast cells (FcεR1α) and dendritic cells (CD14, CD1a, CD123, BDCA2); thus, ILCs are known as lineage negative cells [188,211]. To ensure the ILC population purity, a very stringent gating strategy was used: viable, single, $CD45^+$, lineage negative and $CD127^+$ (IL-7 receptor-α) cells. Moreover, there are at least three main subsets of ILCs (ILC1, ILC2 and ILC3) which in this flow cytometry panel were delineated using prostaglandin D_2 receptor (CRTH2) and CD117 (c-Kit) expression [212].

There are many described panels for enumeration of ILCs in peripheral blood samples [211]; however, my flow panel required optimisation for the small blood and airway sample volumes obtainable from infants ≤2-years-old. Compared to this study, human work on ILCs has either been done on healthy children (between 7 and 12 years) [188], healthy adults (age ≥20-65 years) [211] or umbilical cord blood [188]. The work of Nagakumar et al. (2016) on ILCs in patients with severe asthma investigates the effect of illness; nevertheless, it is limited to STRA (severe therapy-resistant asthma) children (≥6 years) or healthy adults [194]. RSV-induced bronchiolitis is the commonest lower respiratory tract disease in children ≤2-years-old [16], thus obtaining blood and airway samples from this cohort was important for this study.

The age challenge adds to the experimental complexity as the number and volume of samples are strictly limited. Most studies have used peripheral blood mononuclear cells (PBMC) to study ILC frequencies; however, I used as little as 300 µL of fresh peripheral blood from healthy adults to optimise OMIP and reflect the challenging situation of the limited amount of blood I can obtain from infants. Pitoiset *et al* (2018) were able to stain regulatory T cells (Tregs) in only 60 µL of whole blood from paediatric patients [213]; however, Tregs are more abundant than ILCs as they comprise approximately 1-5% of all $CD4^+$ T cells in the periphery [214]. In adults' blood, Lin^- $CD127^+$ ILCs represent between 0.1 and 0.01% of circulating lymphocytes. I found that whole blood immunophenotyping not only reduces the processing time but overcame the potential

decrease the number of viable cells observed using other protocols. As a consequence it is likely to give less erroneous results and better quality of data [213].

In preliminary work for this project, the designed flow cytometry panel was evaluated on whole blood which was RBC-lysed before or after staining. I found that RBC lysis after staining is highly effective and I observed increased levels of viable cells (up to $4x10^6$ cells/mL) compared with an RBC-lysis-before staining protocol (<$1x10^6$ cells/mL). The increased cell death in RBC lysed samples might be related to blood cells' natural tendency towards death during the purification, such as PBMC isolation [213] or RBC lysis. Most human studies utilise the immunophenotyping of PBMCs which involves rather time-consuming protocols and numerous steps. In this work, immunostaining of whole blood before RBC lysis/fixation was shown to be superior due to its simplicity and reduction in variability via a shortened staining protocol [215]. Furthermore, immunophenotyping using whole blood excludes the requirement for Fc-blocking due to high level of IgGs in the serum. As Fc-receptors play an important role in immune responses and are detected on many hematopoietic cells, such as neutrophils, macrophages, eosinophils and NK cells [210], Fc-treatment is essential on PBMCs and seems to be important when staining RBC-lysed blood.

Next, I tried to develop an experimental pipeline to preserve whole blood and airway samples (such as NPA and TA), using different cryopreservation methods and blood-stabilising reagent (TransFix™). I aimed to establish protocols that would allow me to 1) process and stain collected blood and airway samples all together using the same batches of antibodies, 2) optimise the use of available resources and 3) eliminate variation due to sample preparation (pipetting errors, temperature variations during the transport).

My results stand contrary to previously published data on whole blood preservation in epidemiologic studies. Stevens *et al.* (2007) successfully developed a cryopreservation method of lymphocytes in whole blood collected to EDTA-coated vacutainers [216]. They obtained a high level of viability of these cells (up to 85%); however, nothing is known about the granulocytes' viability. Clearly, in my hands, frozen whole blood preservation has been unsatisfactory as the recovery of functional, live cells is low with the almost complete death of granulocytes. Following work of Nishimura *et al* (2001), frozen, stored granulocytes die during cryopreservation and only using large volumes of purified granulocytes (400mL of donated peripheral blood, buffy coats), and fixing them with 1 % PFA after thawing, allowed them to significantly prevent this process [217]. Furthermore, long-term storage of cryopreserved granulocytes alters their cytoplasmic,

nuclear and cell surface morphology which might have a negative impact on surface FACS staining [218].

There are no evidence-based protocols for freezing NPA and TA samples. To fill this gap, I compared different protocols for cryopreserving these samples. In my hands, freezing airway samples (NPA and TA) was not successful. Cryopreservation, although a very important tool in studying the immunology of different cells, induces significant changes in the number and viability of cells. Interestingly, I found that the populations of cells affected the most by freezing were lymphocytes including ILCs and to a lesser extent granulocytes. Considering the differences in the total number of cells obtained from fresh and frozen samples, my data suggest that airways samples are less rich in cells; however, if processed fresh the populations of ILCs can be described. The analysis of cryopreserved sputum samples strongly suggests a significant reduction in neutrophils after freezing; however, the viability level for lymphocytes is very high (up to 99%) [219]. Although my data conflicts with other studies, there are many factors which could have an impact on cell recovery, such as washing medium, centrifugation and especially the time of thawing [220].

Subsequently, I was determined to optimise the preservation of blood samples and TA using stabilising reagent Transfix™. TransFix™ is a patented buffer of heavy metal salts and aliphatic aldehyde [208]. According to the published literature and manufacturer's instructions TransFix™-treated whole blood remains stable for up to 10 to 14 days without significant changes in plasma membrane proteins and is particularly suitable for evaluating human lymphocytes using FACS [209,221]. This commercial reagent blocks all apoptotic pathways and seems well suited for the short-term storage of samples [209]. In my hands, TransFix™-stabilisation preserved most of the surface antigens well (granulocytes, NK/NKT and MAIT cells). The most considerable effect was observed on ILCs as a time-dependent decrease in CRTH2 staining was observed. This finding's significance is not understood; however, a progressive time-dependent necrosis-like behaviour was previously reported when working with TransFix™-stabilised granulocytes using transmission electron microscopy (TEM) [209]. Molecular and biochemical investigations of this phenomena are needed and were addressed to the manufacturer.

There is only one paper in which TransFix™ was successfully used for stabilising cells in bronchoalveolar lavage (BAL) to check the neutrophil, macrophage and lymphocyte numbers using Giemsa staining [222]. On the other hand, TransFix™ can prevent cell death and can be used for a flow analysis of lymphocytes in cerebrospinal fluid (CSF) [223]. Unfortunately, I found in my

experiments the stabilising property of TransFix™ to work rather poorly. TransFix™ can work in the presence of EDTA [208]. Interestingly, in my protocols, whole blood was collected in EDTA-coated tubes; however, TA samples were stored in non-EDTA bijou containers, which could explain the poor performance of TransFix™ in airway samples due to the lack of EDTA.

In conclusion, I optimised protocols for enumerating ILCs (NK cells, ILC1, ILC2, ILC3), granulocytes (eosinophils and neutrophils), T – cells ($CD4^+$ and $CD8^+$), MAIT cells and NKT-like cells in blood and airway samples. The detection of ILCs in small volumes of whole blood and paediatric respiratory samples was successfully demonstrated. Finally, the impact of different protocols of cryopreservation and stabilisation of whole blood and airways cells was assessed.

My data clearly show that innate lymphocytes from paediatric samples had to be processed fresh, and this optimised method was applied to all samples collected throughout this study. In brief, 300 µL of fresh peripheral blood is stained for 30 minutes with the antibody cocktail, including live/dead reagent. After staining, blood is lysed to remove red blood cells and data acquisition is performed no more than 3 days later, using counting beads. For fresh paediatric respiratory samples, Fc-blocking is followed by surface staining (including live/dead) and fixation. These studies to optimise the best protocols allowed me to progress to studies directly investigating the importance of ILCs in paediatric bronchiolitis.

3.2

Innate lymphocytes are phenotypically and functionally different between adults and neonates

3.2.1. Introduction for Chapter 3.2

The concept of inborn systems that allow neonates and young infants to respond has been supported for centuries, and it has been known as innatism. Although it is a purely philosophical concept, Plato's innatism supports the notion that we are not a '*tabula rasa*' (blank slate*),* and we are programmed to function in the new hostile environment using different strategies. When born, neonates experience enhanced vulnerability to the microbe-laden world due to increased tolerance to different antigens which is a product of the uterine environment during the pregnancy, a lack of maturity and a skewing towards type 2 immunity [20]. Foetal immunity must have the ability to tolerate the haplo-mismatch of maternal alloantigens which resonates upon early childhood. This innate tolerogenic state was attributed to the concept of immaturity in the T cell compartment but the novel insights into infantile immunity describe it as immune deviant rather than immature or depressed [224].

The concept of immaturity came from the *in vivo* study of neonatal type-1 T cells of mice which upon re-exposure to antigen undergo IL-4-dependent apoptosis [225]. The apoptotic T cell inactivation may allow the tolerance to external and internal antigens. Furthermore, this 'neonatal tolerization' induces immune deviation, not intolerance, observed as skewed immune responses towards type-2 responses and poor type-1 cell responses. The skewed immune response can provide a partial explanation of viral infections such as RSV-related bronchiolitis; however, it does not give an absolute answer. Data obtained from rodents models suggest that an immune response skewed and characterised by the production of type-2 cytokines (IL-4, IL-5 and IL-13) may lead to lung damage and inflammation in RSV-infection [6]. Interestingly, the skewed immune responses observed in neonatal mice are not apparent in human studies of children with malaria, where both type-2 and type-1 immune responses were diminished compared to the adult cohort [226]. To add complexity, in *Mycobacterium bovis* bacillus Calmette-Guerin (BCG) exposure, new-born $CD4^{+}$T cells can be functionally competent in the production of interferon-γ (IFN-γ) on a similar level to their adult counterparts [227].

Neonates experience limited antigen encounter *in utero* [10,20]. In the context of an immature and inexperienced adaptive immune response, innate immunity is likely to be an important part of early life. The activation of epithelial cells and NK cells may be important to fight viral infection *via* the production of IFN-γ in both newborns and adults [100]. ILCs are relatively abundant in blood in neonates compared to healthy adults [194]. ILCs lack antigen-specific receptors and have been classified into three groups: ILC1, ILC2 and ILC3 mirroring the type-1, type-2 and type-17 immune

responses [65,121]. Although cord blood studies suggest there are differences in the frequency of ILCs between neonates and adults [188], the functional differences between these two cohorts are not currently explored.

This chapter investigated differences in the number and function of different innate and adaptive cells between adults and neonates. In this study, clinical samples of cord and peripheral blood from healthy neonates and adults were utilised to demonstrate the differences among the subjects in those two groups. I emphasised the differences in all members of the ILC family (including NK cells), granulocytes, and other innate-like lymphocytes. To identify cell populations staining using an Optimised Multicolour Immunofluorescence Panel (OMIP) [201] was performed. In addition, intracellular staining (ICS) panels for IFN-γ, IL-13, IL-17A, IL-22, and Granzyme B were developed. Finally, I used dimension reduction techniques (*t*-SNE and UMAP) and applied them to the OMIP, ICS and Granzyme B data sets to seek the differences in the topology and clusters of cells using unbiased algorithms. I utilised R programming for PCA, heatmaps and correlation analysis to elucidate the role of different factors (age, sex, weight, vaccination, etc.) on the phenotype and function of ILCs and other innate and adaptive cells.

Elucidation of the ontogeny of innate immune responses in neonates and adults in regards to ILCs biology could offer new insights into age-related mechanisms that could 1) predict children at high risk of developing paediatric infectious diseases, 2) help to identify biomarkers, and 3) may support the development of new therapeutics. Furthermore, this chapter's methodology will elucidate the differences between control and bronchiolitic babies of Chapter 3.3.

3.2.2. Methods for Chapter 3.2

3.2.2.1. Samples collection and processing

Infant blood and blood from healthy consenting adult donors were obtained as described in Chapter 2 (Material and Methods, **Section 2.2.8.1**). Blood samples from healthy adult volunteers and neonates were obtained after written consent from patients or their families was provided (as described in Material and Methods, see Chapter 2). Thus, all healthy adult controls had no infection or any ongoing health problems and cord blood samples were collected from uncomplicated, term pregnancies. The clinical data of the patients' characteristics can be found in Table 3.2.3 and 3.2.4 (**Results section, Chapter 3.2**).

All blood samples were collected no more than 3 hours before arrival in the laboratory. Blood samples were left at room temperature (RT) for a minimum of 30 minutes before further procedures were utilised, including PBMC isolation and staining for flow cytometry.

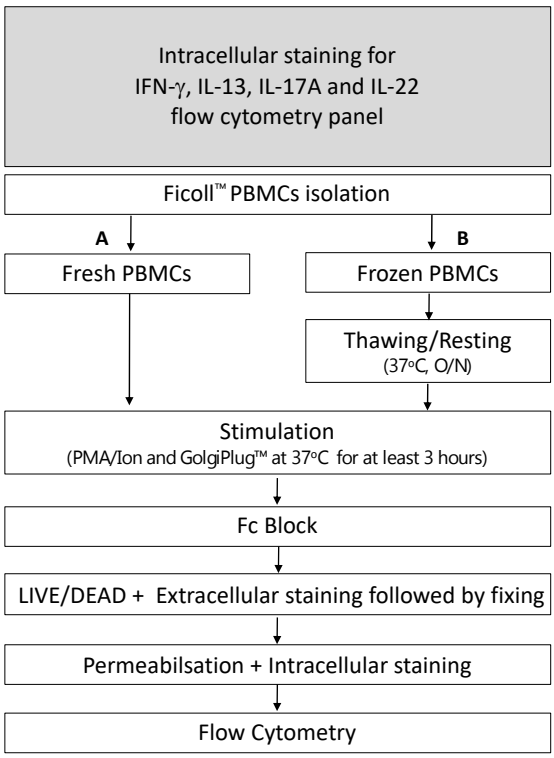


Figure 3.2.1 Alternative strategies for PBMCs staining during ICS panel optimization.

Fresh (**A**) or frozen (**B**) PBMCs were stimulated for 3 hours at 37°C with Ionomycin (1 µg/mL), PMA (50 ng/mL) in warm RPMI-1640 complete medium. The unstimulated control was prepared by adding just DMSO. GolgiPlug™ was added according to the manufacturer's instructions to increase the accumulation of cytokines in the cell via blocking intracellular protein transport processes in the Golgi complex. After blocking and extracellular staining, PBMCs were permeabilized for intracellular staining. *Abbreviations used:* PBMC – peripheral blood mononuclear cells, PMA – phorbol 12-myristate 13-acetate, Ion – Ionomycin, O/N – overnight.

3.2.2.2. The immune cell populations (OMIP) panel

The enumeration of different components of the cellular response (ILCs with NK cells, granulocytes, MAIT, NKT-like cells and other T cell populations) in blood was assessed by a 14-multicolour, 17 - parameter flow cytometry panel [201] (referred to later as OMIP, optimised multicolour immunophenotyping panel). Detailed design and optimisation of this panel can be found in Chapter 3.1 (**Section 3.1.4.1**)

Extracellular antibodies for ICS flow cytometry panel			
Antibody	Clone	Supplier	Dilution used
Brilliant Violet 421™ anti-human CD127 (IL-7Rα)	A019D5	BioLegend	1:60
Brilliant Violet 510™ anti-human CD14*	63D3	BioLegend	1:60
Brilliant Violet 510™ anti-human CD19*	HIB19	BioLegend	1:120
Brilliant Violet 510™ anti-human FcεRIα*	AER-37	BioLegend	1:120
Brilliant Violet 510™ anti-human CD123*	6H6	BioLegend	1:300
Brilliant Violet 605™ anti-human CD4	RPA-T4	BioLegend	1:300
Brilliant Violet 650™ anti-human CD56 (NCAM)**	5.1 H11	BioLegend	1:40
Brilliant Violet 711™ anti-human CD8	SK1	BioLegend	1:300
PerCP/Cy5.5 anti-human CD117 (c-kit)	A3C6E2	BioLegend	1:40
PE anti-human CD3**	OKT3	BioLegend	1:120
Alexa Fluor® 647 anti-human CD294 (CRTH2)	BM16	BioLegend	1:40
APCH7/APCCy7 NIR™ Fluorescent reactive dye***	-	Invitrogen	1:500
Intracellular antibodies for IFN-γ, IL-13, IL-22, IL-17A flow cytometry panel			
BUV395 Mouse Anti-Human IFN-γ (B27)	B27	BD	1:50
FITC anti-human IL-22	2G12A41	BioLegend	1:50
PE/Cy7 anti-human IL-13	JES10-5A2	BioLegend	1:50
Alexa Fluor® 700 anti-human IL-17A	BL168	BioLegend	1:50

Table 3.2.1 Extra- and intracellular antibodies and their concentrations used in the optimised IFN-γ, IL-13, IL-22, IL-17A flow cytometry panel.

* Lineage cocktail includes the following antibodies: CD14, CD19, CD123, FcεR1α
**Antibodies used to define lineage negative population, but not part of the lineage cocktail
*** LIVE\DEAD Near IR-fluorescent reactive dye.

3.2.2.3. Intracellular staining panels for cytokine production

3.2.2.3.1. Optimisation and gating strategy for the IFN-γ, IL-13, IL-17A and IL-22 staining panel

The intracellular staining (ICS) panel was optimised using PBMCs from adult blood (**Fig. 3.2.2**). The panel allowed enumeration of IFN-γ, IL-13, IL-17A, IL-22 producing innate cells such as ILCs (including NK cells) and adaptive CD4, CD8 T cells including invariant T cells (NKT cells) using titrated, fluorochrome-conjugated antibodies for extra- and intracellular staining (**Table 3.2.1**). 1-2.5 x 10^6 fresh (**Fig. 3.2.1 A**) or frozen (**Fig. 3.2.1 B**) PBMCs were stimulated for at least 3 hours

at 37^{o}C in the stimulation cocktail (ionomycin, phorbol 12-myristate 13-acetate (PMA) and GolgiPlug™ in RPMI-1640 complete medium). Unstimulated PBMCs were used as a negative control and prepared by adding just DMSO (**Fig. 3.2.2 II**) (**Fig. 3.2.2 I**). Lymphocytes were gated using FSC-A and SSC-A, single and live cells (**Fig. 3.2.2 A**). Within the lymphocytes gate, NK and NKT cells were gated as CD56^{+}CD3^{-} and CD56^{+}CD3^{+} cells, respectively (**Fig. 3.2.2 E**). NK cells were further subdivided using cell markers IFN-γ, IL-13, IL-17A and IL-22 into IFN-γ^{+} IL-13^{-} and IFN-γ^{-} IL-13^{+} NKs (**Fig. 3.2.2 G**), and IL-17A^{+}IL-22^{-} and IL-17A^{-}IL-22^{+} NK cells without any double-positive cells observed (**Fig. 3.2.2 H**). ILCs were defined as live, single, CD45^{+}, lineage negative (CD3, CD14, CD19, CD56, CD123, FcεR1α)$^{-}$ and CD127^{+} lymphocytes (**Fig. 3.2.2 D**); ILC1 cells were defined as CD117$^{–}$CRTH2$^{–}$, ILC2 cells as CRTH2^{+} CD117^{int} and ILC3 as CD117^{+}CRTH2$^{–}$ (**Fig. 3.2.2 K**). ILCs (CD127^{+}CDLin^{-}) were segregated into IFN-γ^{+} IL-13^{-} ILCs, IFN-γ^{-} IL-13^{+} ILCs (**Fig. 3.2.2 B**), IL-17A^{+}IL-22^{-} ILCs and IL-17A^{-}IL-22^{+} ILCs (**Fig. 3.2.2 C**). Similarly, to total ILCs, ILC1s, ILC2s and ILC3s were further subdivided into IFN-γ^{+} IL-13^{-} ILCs, IFN-γ^{-} IL-13^{+} (**Fig. 3.2.2 I, L, N**) or IL-17A^{+}IL-22^{-} ILCs and IL-17A^{-}IL-22^{+} cells (**Fig. 3.2.2 J, M, O**).

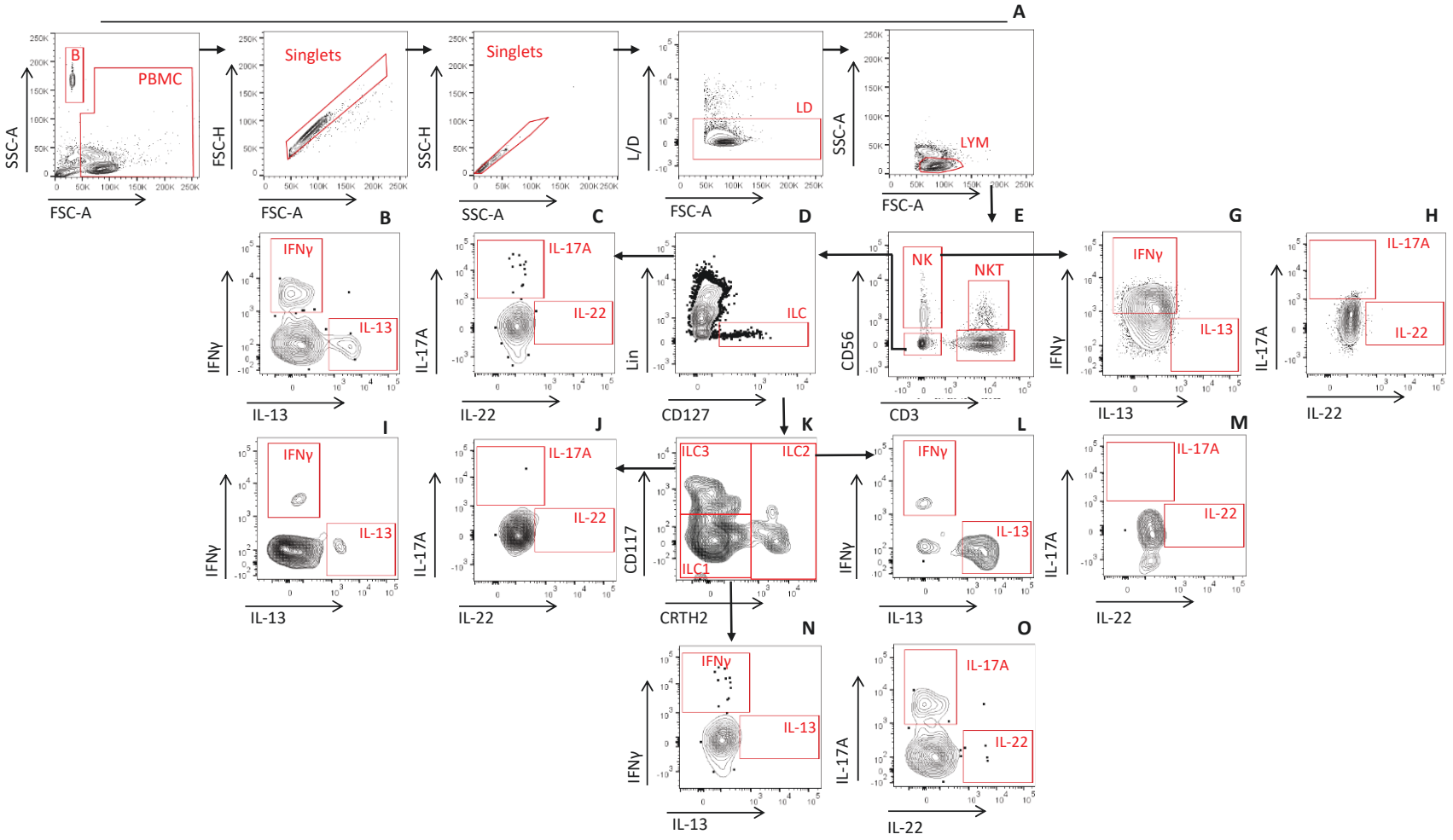
Extracellular antibodies for Granzyme B/CD57 flow cytometry panel			
Antibody Extracellular	Clone	Supplier	Dilution used
Brilliant Violet 605™ anti-human CD4	RPA-T4	BioLegend	1:300
Brilliant Violet 650™ anti-human CD16	3G8	BioLegend	1:300
Brilliant Violet 711™ anti-human CD8	SK1	BioLegend	1:300
FITC anti-human CD45	HNK-1	BioLegend	1:120
PerCP/Cy5.5 anti-human CD57 (HNK-1)	OKT3	BioLegend	1:50
PE anti-human CD3	OKT3	BioLegend	1:120
PE/Cy7 anti-human CD56 (NCAM)	5.1H11	BioLegend	1:120
APCH7/APCCy7 NIR™ Fluorescent reactive dye	-	Invitrogen	1:500
Intracellular antibodies for Granzyme B flow cytometry panel			
Alexa Fluor® 700 anti-human/mouse Grzm B	QA16A02	BioLegend	1:50

Table 3.2.2 Extra- and intracellular antibodies and their concentrations used in the optimised Granzyme B flow cytometry panel.

* LIVE\DEAD Near IR-fluorescent reactive dye.

ICS Panel

I. Stimulated PBMCs



II. **Unstimulated PBMCs**

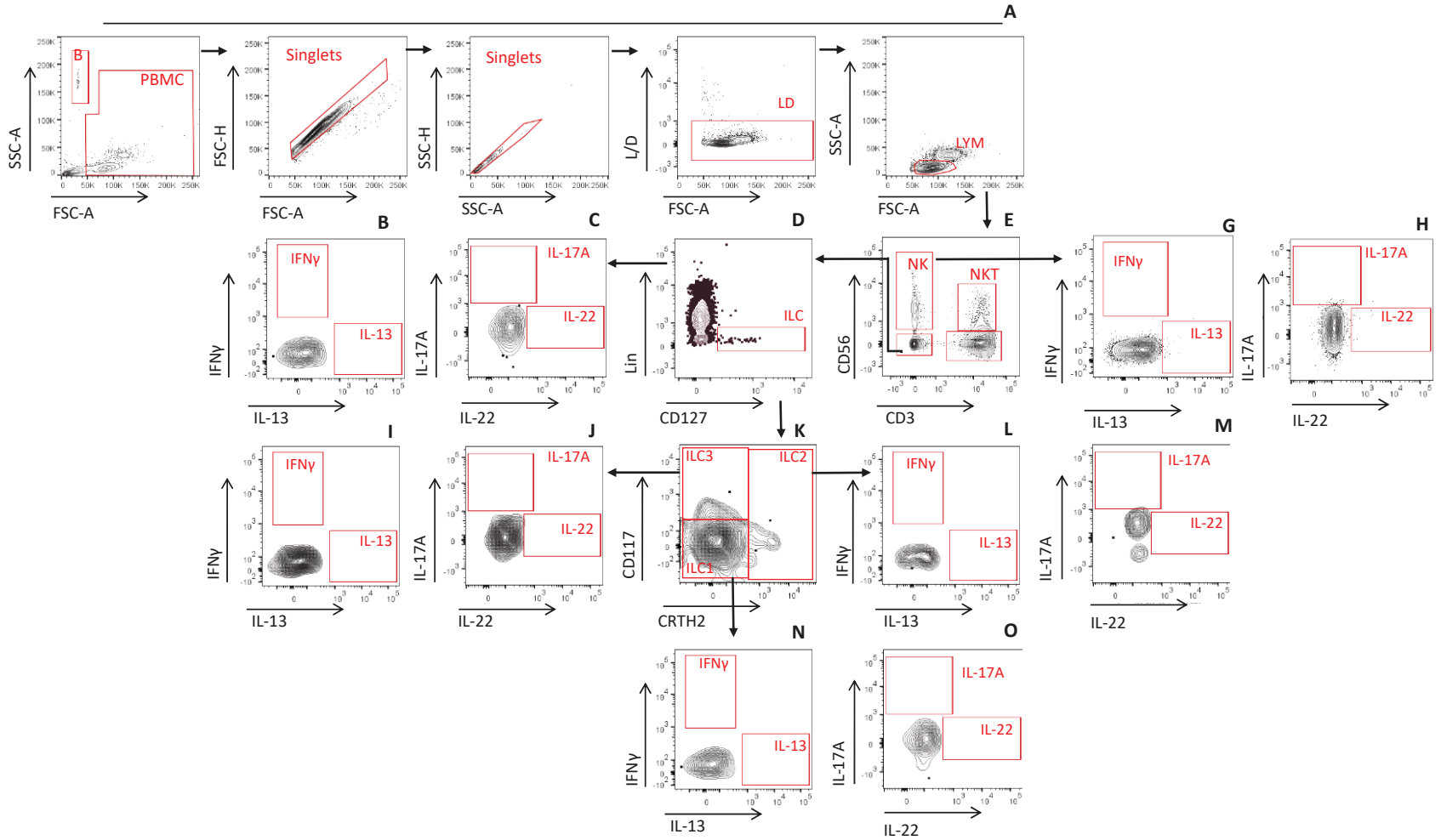


Figure 3.2.2 Example gating strategy for visualisation of IFN-γ, IL-13, IL-17A and IL-22 production (ICS panel) in different populations of ILCs (ILC1, ILC2 and ILC3) and NK cells using (I) stimulated (II) and unstimulated adult PBMCs.

Cells were delineated using the following gating strategy: FSC/SSC, single, live cells. Lymphocytes were gated using FSC-A and SSC-A **(A)**. Within the lymphocyte gate, NK and NKT cells were gated as $CD56^{+}CD3^{-}$ and $CD56^{+}CD3^{+}$ cells, respectively **(E)**. NK cells were further subdivided using cell markers IFN-γ, IL-13, IL-17A and IL-22 into IFN-γ^{+} IL-13^{-} and IFN-γ^{-} IL-13^{+} NKs **(G),** and IL-$17A^{+}$IL-22^{-} and IL-$17A^{-}$IL-22^{+} NK cells **(H)**. ILCs were defined as live, single, $CD45^{+}$, lineage negative (CD3, CD14, CD19, CD56, CD123, FcεR1α)$^{-}$ and $CD127^{+}$ lymphocytes **(D)**; ILC1 cells were defined as $CD117^{-}CRTH2^{-}$, ILC2 cells as $CRTH2^{+}$ $CD117^{int}$ and ILC3 as $CD117^{+}CRTH2^{-}$ **(K).** ILCs ($CD127^{+}CDLin^{-}$) were segregated into IFN-γ^{+} IL-13^{-} ILCs, IFN-γ^{-} IL-13^{+} ILCs **(B)**, IL-$17A^{+}$IL-22^{-} ILCs and IL-$17A^{-}$IL-22^{+} ILCs **(C)**. Similarly, total ILCs, ILC1s, ILC2s and ILC3s were further subdivided into IFN-γ^{+} IL-13^{-} ILCs, IFN-γ^{-} IL-13^{+} **(I, L, N)** or IL-$17A^{+}$IL-22^{-} ILCs and IL-$17A^{-}$IL-22^{+} cells **(J, M, O).** The gating was determined by comparing stimulated PBMCs **(Graph I)** to the unstimulated control **(Graph II)** and fluorescence minus one (FMO) controls (as described in the material and Methods chapter). *Abbreviations used:* B – counting beads, PBMC – peripheral blood mononuclear cells, LD – live/dead, LYM – Lymphocytes, NK – natural killer cells, NKT – natural killer T cells.

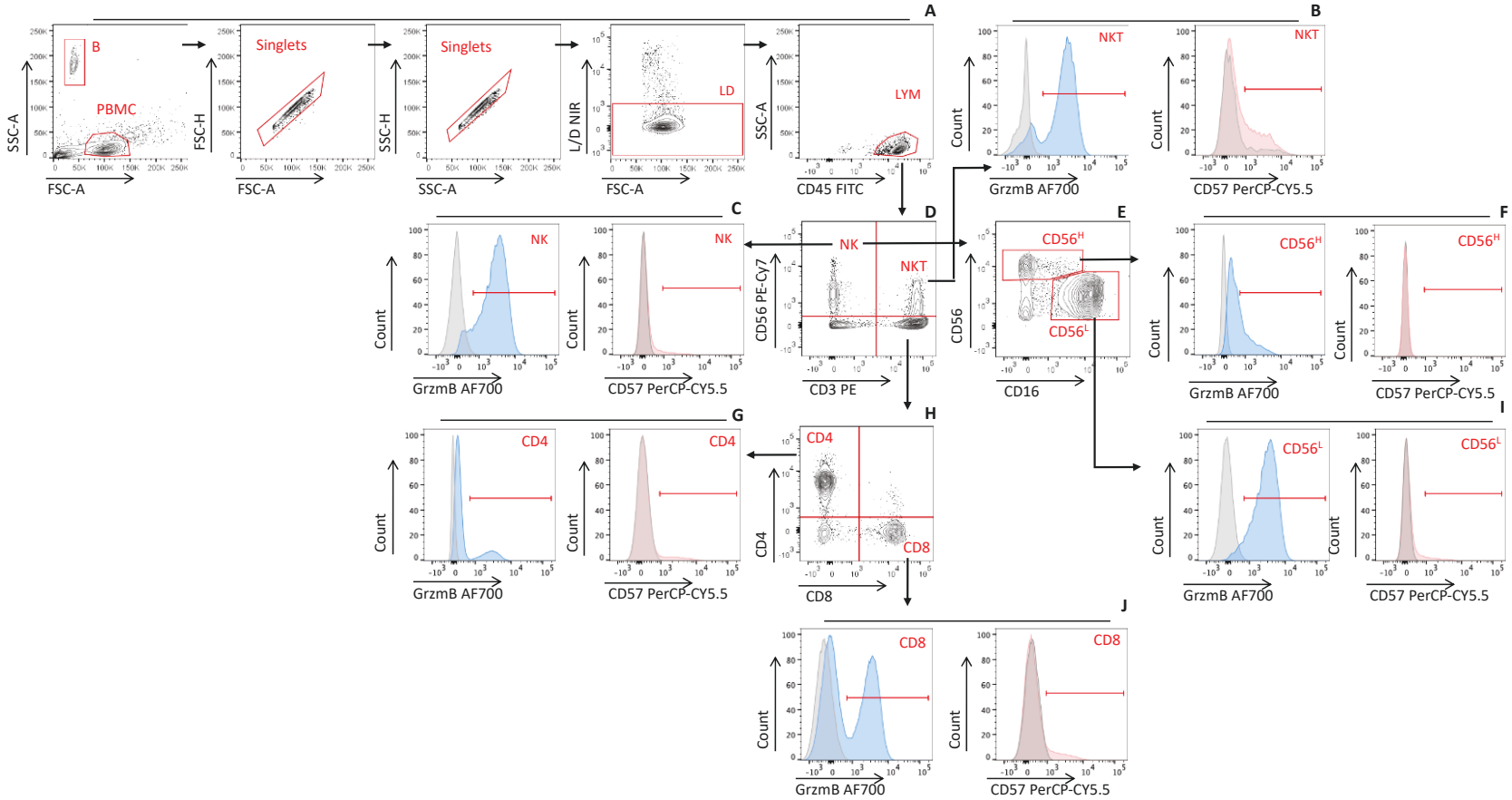


Figure 3.2.3 Example gating strategy for visualisation of Granzyme B production and CD57 expression (ICS panel) in NK, NKT, CD4⁺ and CD8⁺ T cell populations using adult PBMCs.

Cells were delineated using the following gating strategy: FSC/SSC, single, live cells. Lymphocytes were gated using SSC-A and CD45 cell marker **(A)**. Within the lymphocytes, NK and NKT cells were gated as $CD56^{+}CD3^{-}$ and $CD56^{+}CD3^{+}$ cells, respectively **(D)**. NK cells were further subdivided into $CD56^{H}$ and $CD56^{L}$ populations according to the CD56 and CD16 cell markers **(E)**. Within NK cells, $GrzmB^{+}$ NKs and $CD57^{+}$ NK cells were delineated using GrzmB (blue) and CD57 (pink) cell expression markers **(A)**. Similarly, to total NKs, $CD56^{H}$ and $CD56^{L}$ populations were further subdivided into $GrzmB^{+}$ $CD56^{H}$, $CD57^{+}$ $CD56^{H}$ NKs **(F)** and $GrzmB^{+}$ $CD56^{L}$, $CD57^{+}$ $CD56^{L}$ NKs **(I)**. $CD56^{+}CD3^{+}$ NKTs were segregated into $GrzmB^{+}$ NKTs and $CD57^{+}$ NKT cells **(B)**. T lymphocytes ($CD3^{+}CD56^{-}$) were segregated into $CD4^{+}$ or $CD8^{+}$ T cells **(H)**. GrzmB and CD57 cell markers were utilised to further subdivide $CD4^{+}$ or $CD8^{+}$ T cells into $GrzmB^{+}$ $CD4^{+}$, $CD57^{+}$ $CD4^{+}$ cells and $GrzmB^{+}$ $CD8^{+}$, $CD57^{+}$ $CD8^{+}$ cells **(G and J,** respectively**)**. The gating was determined by comparing the stained PBMCs to the unstained control and fluorescence minus one (FMO) controls (grey). *Abbreviations used:* B – counting beads, PBMC – peripheral blood mononuclear cells, LD – live/dead, LYM – Lymphocytes, NK – natural killer cells, NKT – natural killer T cells.

3.2.2.3.2. NK cell function (Granzyme B) staining panel

The functional phenotype of human NK cells, NKT cells, $CD4^+$ and $CD8^+$ T cells for granzyme B production and expression of CD57 allowed me not only to assess the granzyme B producing cells but also to identify the maturational state of those cells [228]. CD57 is known to be a marker of terminal differentiation, anergy and senescence on T cells [229]. The Granzyme B functional panel was established using adult fresh or frozen PBMCs (**Fig. 3.2.3**). Up to 2.5 x 10^6 frozen PBMCs from healthy adult volunteers were stained using titrated, fluorochrome-conjugated antibodies for surface- and intracellular staining (**Table 3.2.2**). For immunophenotyping using the Granzyme B functional panel (**Fig. 3.2.4 A and B**), no stimulation was performed as granzyme B can be found in the granules of cytotoxic T cells and NK cells [228]. Cells were delineated using the following gating strategy: FSC/SSC, single, live cells. Lymphocytes were gated using SSC-A and CD45 (**Fig. 3.2.3 A**). Within the lymphocytes, NK and NKT cells were gated as $CD56^+CD3^-$ and $CD56^+CD3^+$ cells, respectively (**Fig. 3.2.3 D**). NK cells were further subdivided into $CD56^H$ and $CD56^L$ populations according to the CD56 and CD16 cell markers (**Fig. 3.2.3 E**). Within NK cells, $GrzmB^+$ NKs and $CD57^+$ NK cells were delineated using GrzmB (blue) and CD57 (pink) cell expression markers (**Fig. 3.2.3 B, C, F, G, I and J**). Similarly, to total NKs, $CD56^H$ and $CD56^L$ populations were further subdivided into $GrzmB^+$ $CD56^H$, $CD57^+$ $CD56^H$ NKs (**F)** and $GrzmB^+$ $CD56^L$, $CD57^+$ $CD56^L$ NKs (**Fig. 3.2.3 I**). $CD56^+CD3^+$ NKTs were segregated into $GrzmB^+$ NKT cells and $CD57^+$ NKT cells (**Fig. 3.2.3 B**). T lymphocytes ($CD3^+CD56^-$) were segregated into $CD4^+$ or $CD8^+$ T cells (**Fig. 3.2.3 H**). GrzmB and CD57 cell markers were utilised to further subdivide $CD4^+$ or $CD8^+$ T cells into $GrzmB^+$ $CD4^+$, $CD57^+$ $CD4^+$ cells and $GrzmB^+$ $CD8^+$, $CD57^+$ $CD8^+$ cells (**Fig. 3.2.3 G and J,** respectively).

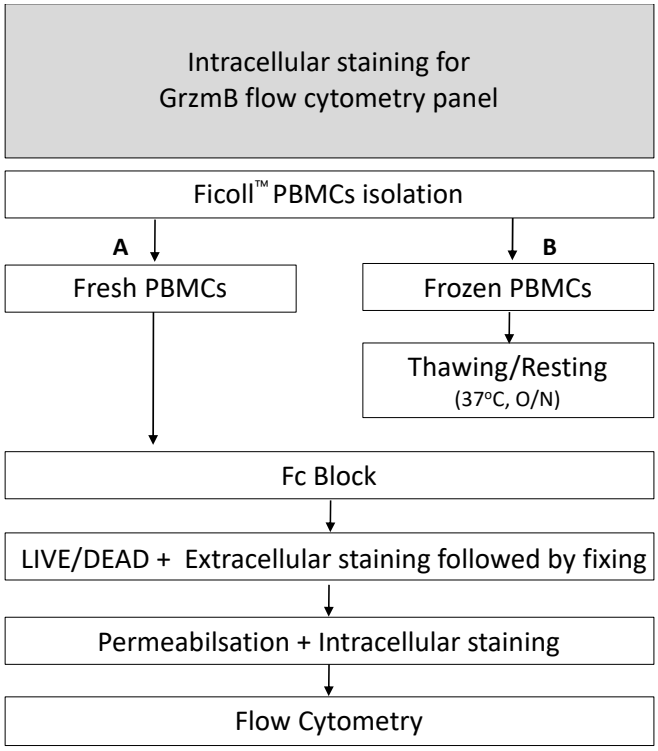


Figure 3.2.4 Alternative strategies for PBMCs staining during Granzyme B panel optimization.

Fresh (**A**) or frozen (**B**) PBMCs were stained using extracellular cell markers then permeabilized and intracellular staining performed as described in the Material and Methods chapter. No stimulation was performed. *Abbreviations used:* PBMC – peripheral blood mononuclear cells.

3.2.2.4. Antibody titration and FMO controls for ICS flow cytometry panels

To determine the amount of antibody for IFN-γ, IL-13, IL-17A, IL-22, granzyme B, CD56 and CD57 in ICS and Granzyme B functional panels titration was performed (**Fig. 3.2.5**). Each antibody was tested at a range of dilutions (20x, 40x, 100x, 300x or 50x, 100x, 250x, 500x) and dilutions were selected to show the best separation between the negative and positive populations. The protocol for titration of antibodies was the same as in Chapter 3.1 (**Section 3.1.3.3**). During the process of optimisation, 2.5 x 10^6 frozen PBMCs from healthy adult volunteers were used for unstained, LIVE/DEAD only and fluorescence minus one (FMO) controls for CD4, ILCs, lymphocytes and NK cells (**Fig. 3.2.6**).

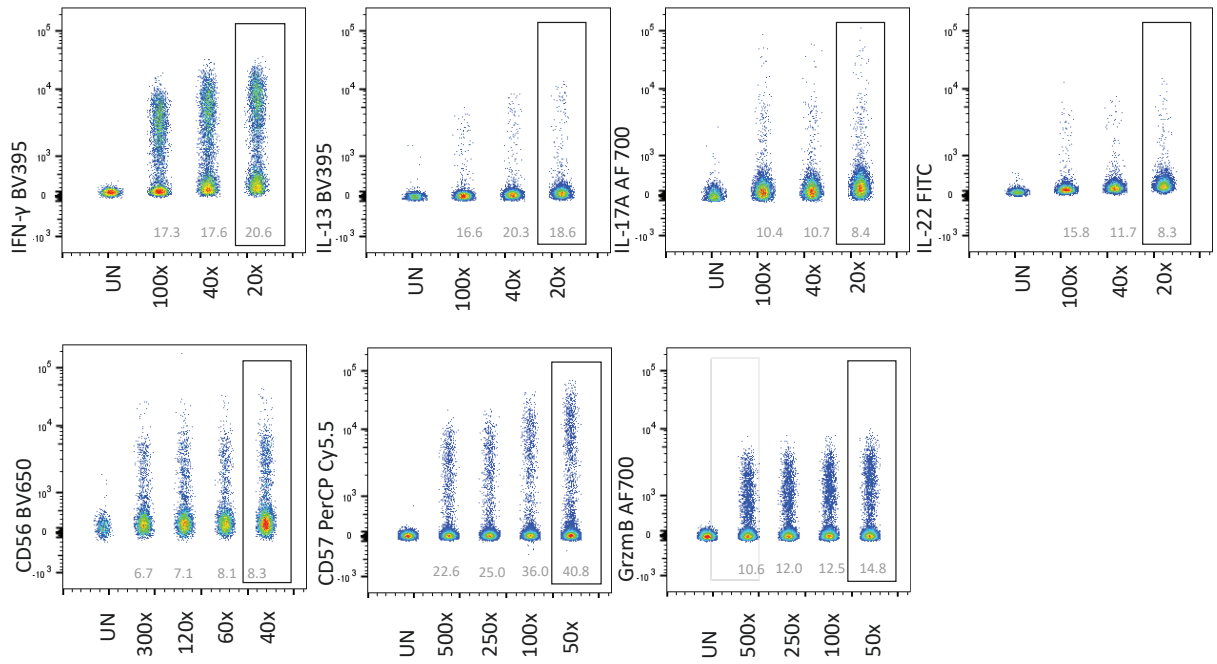


Figure 3.2.5 Titration of antibodies used in optimized ICS and Granzyme B staining panels.

All dilutions tested in the experiment (UN, 20x, 40x, 100x, 300x or UN, 50x, 100x, 250x, 500x) show separation between the negative and positive populations. The visual display shows that increasing the amount of antibody usually increases fluorescence intensity and separation between the negative and positive populations. The concentration of antibody that gives the optimal separation without increasing the signal from the negative population is highlighted with a black square. The stain index is indicated for each dilution. *Abbreviations used*: UN – negative staining.

3.2.2.5. Acquisition of flow cytometric data

A 5-laser-LSRFortessa™ was used to run all cells and AbC™ Total Compensation beads as described in Material and Methods Chapter 2 (**Section 2.2.9.1.4**).

3.2.2.5.1. Deep Immunophenotyping (*t*-SNE and UMAP)

To determine which dimension reduction technique could be applied to the OMIP data set, *t*-SNE and UMAP were compared to check their impact on the topology (on preserving both the local and global distances) and finally, the speed of the computational run time (**Fig. 3.2.7 B and C**). Firstly, an analysis of 135,000 randomly selected CD45+ lymphocytes collected from nine subjects (15,000 per subject) was performed **(Fig. 3.2.7 A**). Then the intensity of expression of CD127, Lin, CD4, CD16, CD8, CD66b, CD3, CD161, CD56, TCR Vα7.2, CD117 and CRTH2 cell markers was measured for *t*-SNE and UMAP (**Fig. 3.2.7 D and E**). Based on these markers' expression, FlowSOM™ clustering analysis allowed classification of cells into seven different populations (Pop1-7) (**Fig. 3.2.7 F**). Use of the manual gating strategy for OMIP (**Fig. 3.2.7 G**) on generated t-SNE and UMAP clusters allowed classification of these clusters into the following cell types: CD4 T cells (yellow), NKT cells (bright blue), monocytes (green), CD8 T cells (orange), neutrophils (ocean blue), eosinophils (magenta), NK cells (bright green), MAIT cells (black), ILC3s

(purple), ILC2s (blue) and ILC1s (red); no ungated cells were shown (**Fig. 3.2.7 G**). Notably, the *t*-SNE and UMAP cell phenotypes identified by the unsupervised FlowSOM™ clustering were comparable with manual gating; however; UMAP allowed better separation, visualisation of the rare populations of ILCs and had greater run time performance when compared to *t*-SNE (**Fig. 3.2.7 G,** right).

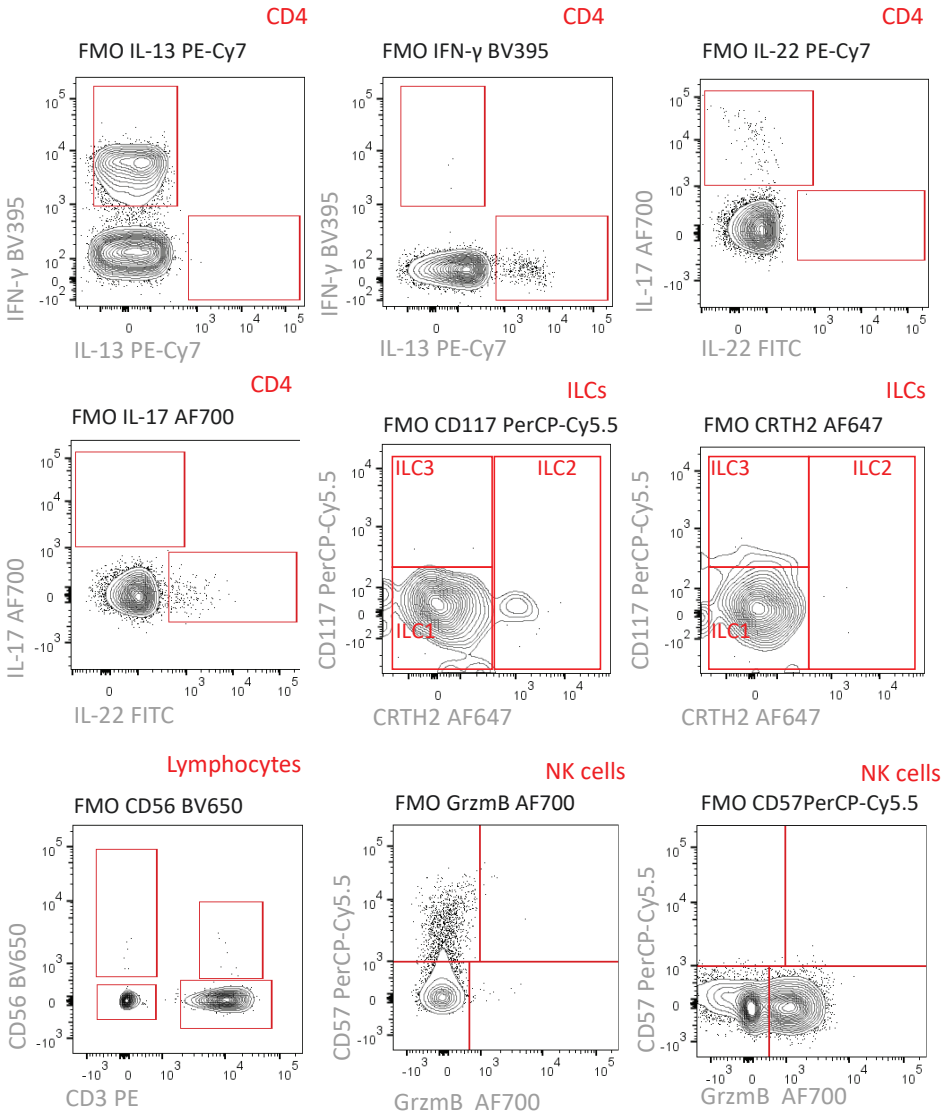


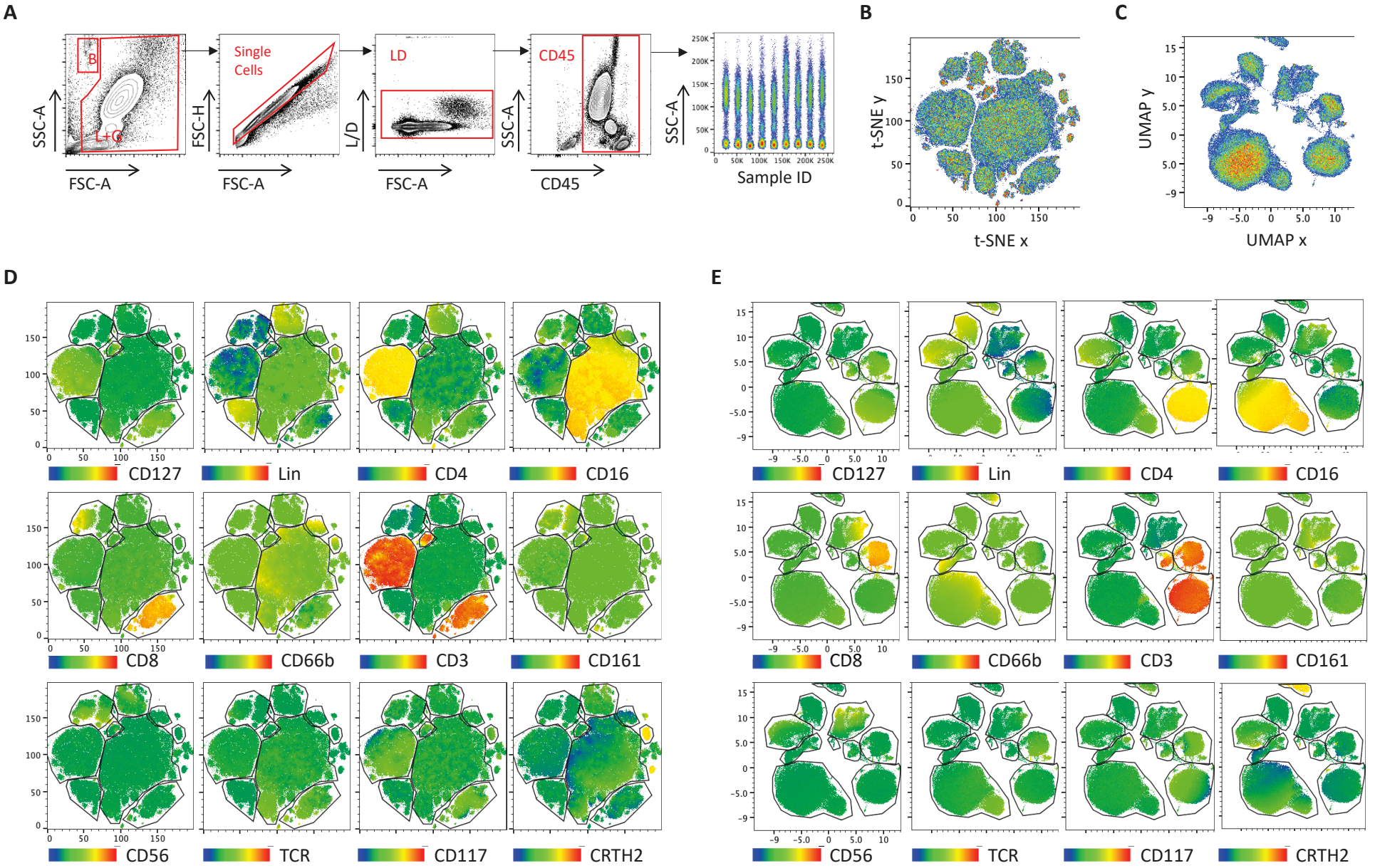
Figure 3.2.6 Extra Fluorescence Minus One controls (FMOs) for CD4, ILCs, Lymphocytes and NK cells utilized in optimized ICS and Granzyme B staining panels.

FMO controls were used to determine fluorescence spread for cell populations and accurately describe gating boundaries. Staining was performed on adult whole blood. Each plot was gated on the cell type indicated in red. *Abbreviations used:* ICS – intracellular staining, NK – natural killer cells, GrzmB – Granzyme B, ILC – innate lymphoid cells.

3.2.2.6. Statistic and data analysis

Differences between two groups were estimated by the Mann-Whitney *U* test for continuous data, while *P* values for categorical data were computed by Fisher's exact test. In PCAs, the group

mean point was added in the centre of each group and the concentration ellipses around each group mean point using a multivariant t-distribution (the size of the concentration ellipse is in the normal probability of 95% confidence). All correlations represent Pearson's correlation coefficients with $P<0.05$ considered significant. Data from a range of experiments were analysed in part using Microsoft Excel, Office 365™ (Microsoft, Washington, USA). Graphs were generated using GraphPad Prism 9.0 (GraphPad Software, Inc., California, USA), FlowJoV10.6 software (FlowJo LLC, USA) and R programming language (R Foundation for Statistical Computing, Vienna, Austria).


A
B
L+G
SSC-A
FSC-A
Single Cells
FSC-H
FSC-A
LD
L/D
FSC-A
CD45
SSC-A
CD45
SSC-A
Sample ID
B
t-SNE y
t-SNE x
C
UMAP y
UMAP x
D
CD127
Lin
CD4
CD16
CD8
CD66b
CD3
CD161
CD56
TCR
CD117
CRTH2
E
CD127
Lin
CD4
CD16
CD8
CD66b
CD3
CD161
CD56
TCR
CD117
CRTH2

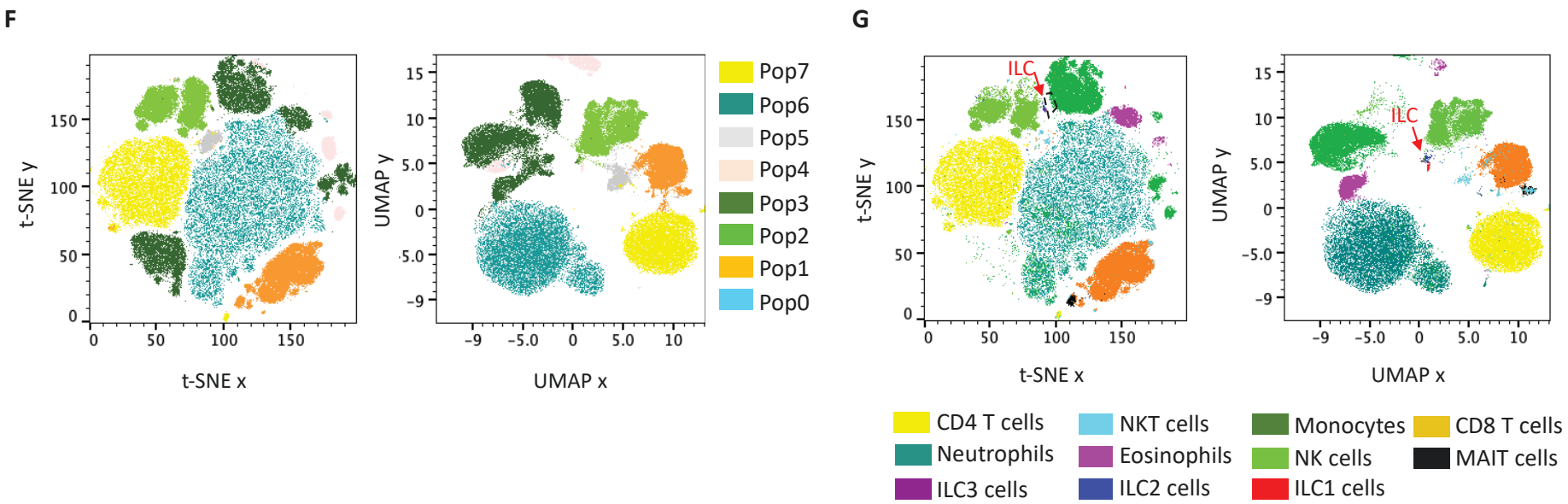


Figure 3.2.7 Comparison of deep immune phenotyping strategies (t-SNE and UMAP) for visualisation of ILCs (including NK cells), granulocytes, MAIT, NKT cells and other T cell populations in whole blood from adults and cord blood from neonates.

(A) Representative manual gating strategy utilised for deep immune phenotyping. Cells were delineated using the following gating strategy: FSC/SSC, single, live cells. Lymphocytes were gated using SSC-A and CD45 cell marker. 15,000 randomly selected CD45$^+$ cells from each subject (*n*=9) were concatenated into a single file containing 135,000 cells for t-SNE (**B)** and UMAP **(C)** analysis. The intensity of CD127, Lin, CD4, CD16, CD8, CD66b, CD3, CD161, CD56, TCR Vα7.2, CD117 and CRTH2 expression in the CD45$^+$ lymphocytes has been compared unsupervised for both t-SNE **(D)** and UMAP **(E)** analysis. The circles (black) around t-SNE and UMAP clusters are based on the intensity of expression of different cells markers in the CD45$^+$ lymphocytes. Based on the expression of the mentioned markers, the generated clusters were subdivided into eight different cell types (Pop0 to Pop7) using FlowSOM™ clustering algorithm **(F)** for both t-SNE and UMAP. After FlowSOM™ clustering, the manual gating strategy from the OMIP was utilised (**G)** allowing the t-SNE and UMAP clusters to be further classified into the following cell types: CD4 T cells (yellow), NKT cells (bright blue), monocytes (green), CD8 T cells (orange), neutrophils (ocean blue), eosinophils (magenta), NK cells (bright green), MAIT cells (black), ILC3s (purple), ILC2s (blue) and ILC1s (red). The population of ILCs is indicated via red arrows. *Abbreviations used:* B – counting beads, PBMC – peripheral blood mononuclear cells, LD – live/dead, LYM – Lymphocytes, NK – natural killer cells, NKT – natural killer T cells, MAITs – mucosal invariant T cells, ILC – innate lymphoid cells, t-SNE – - *t*-distributed Stochastic Neighbour Embedding, UMAP – Uniform Manifold Approximation and Projecti

3.2.3. Results for Chapter 3.2

3.2.3.1. Characteristics of study populations for chapter 3.2

The study participant characteristics are shown in **Figure 3.2.8**. The 36 study participants including healthy adults (*n*=18) and neonates (*n*=18) who provided blood samples are described in **Table 3.2.3**. Both sexes were well represented (*P*=0.7332) in this cohort; adult females (44.4%) and neonatal females (33.4%) (**Table 3.2.3**). From a total of 36 study participants, the OMIP was used on blood samples from 25 subjects, the ICS panel on 19 subjects and the Granzyme B panel on 14 subjects (**Fig. 3.2.8**). The difference between the number of participants in different experiments mirrored the fact that I did not always have enough cells to freeze PBMC for the functional analysis.

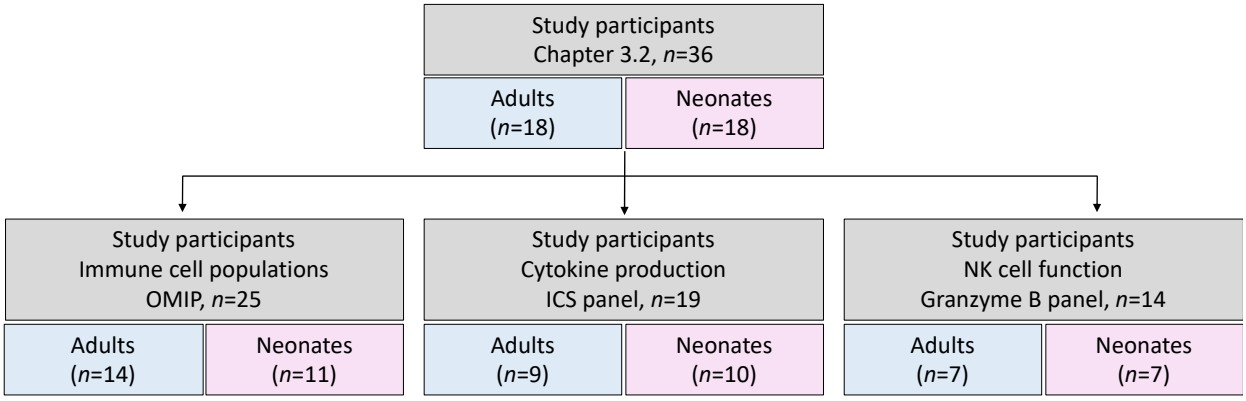


Figure 3.2.8 Flowchart of the study participants used in chapter 3.2

A number of healthy adults (blue, *n*=18) and neonates (pink, *n*=18) used in Chapter 3.2. Graphs depict the number of study participants with data available for the immune cell populations (OMIP), cytokine production (ICS) and Granzyme B panels. From the total of 36 study participants, the flow cytometry data for OMIP were available from 25 subjects, the ICS panel data from 19 subjects and Granzyme B panel data from 14 subjects. *Abbreviations used:* OMIP – Optimised multicolour immunophenotyping panel, ICS – Intracellular staining

	Adults	Neonates (CB)	
Characteristic	*n*=18	*n*=18	*P* value
Age (years), median, (range)	36.6 (22.0-62.0)	0	**0.0001**
Sex, *n* (%)			0.7332
Females	8 (44.4)	6 (33.4)	
Males	10 (55.6)	12 (66.6)	

Table 3.2.3 Adults and neonates' demographics used for Chapter 3.2

Healthy adults and neonates used throughout Chapter 3.2. Patient demographic and clinical information were obtained from the patients' information sheets. Statistical significance was obtained using the Mann-Whitney test for continuous data and Fisher's exact test for categorical data. No adjustment was made for multiple testing. *P* values for continuous data were computed by Mann-Whitney test while *P* values for categorical data were computed by Fisher's exact test. The range is defined as the difference between the highest and lowest value. *Abbreviations used:* CB – cord blood.

Clinical data were available for neonates (**Table 3.2.4**) including medical notes on the sex, weight, gestation at delivery, *Bordetella pertussis* vaccination status (Pertussis, also known as whooping cough) and gestation at vaccination. Pertussis vaccination is considerable as it helps the protection of young babies from the development of whooping cough, which, if particularly severe, might lead to babies death. In brief, getting vaccinated during pregnancy is highly effective in protecting the newborn from developing whooping cough in the first few weeks of their life. Moreover, this information was collected because the cord blood was obtained as part of Beth Holder's study (REC no 13/LO/1712). As the information was available, we checked to see whether it had any influence on neonatal immunity. The neonatal blood samples (cord blood) were collected from term children delivered at ±38.72 (30.43-40.14) weeks gestation in the Neonatal Unit at St. Mary's hospital. Mothers of fourteen babies (77.77%) were vaccinated during ±42.39th (20.14-37.00) week of pregnancy. There were no significant differences between sex and weights of females and males in the neonatal cohort.

	Neonates (CB)
Characteristic	*n*=18
Age (years), Median (range)	0 (0)
Sex, *n* (%)	
Females	6 (33.4)
Males	12 (66.6)
Weight (kg), Median, (range)	
Females	3.53 (4.16-2.64)
Males	3.51 (4.38-2.79)
Premature, *n* (*%*)	
Yes	0 (0)
No	18 (100)
Birthplace, *n* (*%*)	
NU	18 (100)
NICU	0 (0)
Gestation at delivery, wk, Median (range)	38.72 (30.43-40.14)
Pertussis Vaccination during pregnancy (*%*)	
Yes	14 (77.77)
No	4 (22.23)
Gestation at vaccination, wk, median (range)	42.39 (20.14-37)

Table 3.2.4 Demographics and clinical data for neonates used in Chapter 3.2.

Neonates demographic and clinical information were obtained from the neonatal unit. The range is defined as the difference between the highest and lowest value. *Abbreviations used:* CB – cord blood, NU – Neonatal Unit, NICU – Neonatal Intensive Care Unit, wk – week, kg – kilogram.

3.2.3.2. The abundance of different innate and adaptive cells using OMIP in adults and neonates

3.2.3.2.1. OMIP study population characteristics

	Adults	Neonates (CB)	
Characteristic	*n*=14	*n*=11	*P* value
Age (years), median, (range)	32.5 (23.0-62.0)	0	**0.0001**
Sex, *n*			0.4225
Females	6	3	
Males	7	8	

Table 3.2.5 Adults and neonates' demographics used for the immune cell populations (OMIP) panel.

Healthy adults and neonates used for flow cytometric analysis with the OMIP [201]. Patient demographic and clinical information were obtained from the patients' information sheets. Statistical significance was obtained using the Mann-Whitney test for continuous data and Fisher's exact test for categorical data. No adjustment was made for multiple testing. *P* values for continuous data were computed by Mann-Whitney test while *P* values for categorical data were computed by Fisher's exact test. The range is defined as the difference between the highest and lowest value. *Abbreviations used:* CB – cord blood.

	Neonates (CB)
Characteristic	*n*=11
Age (years), Median (range)	0 (0)
Sex, *n* (%)	
Females	3 (27.2)
Males	8 (72.8)
Weight (kg), Median, (range)	
Females	3.45 (4.20-2.79)
Males	3.53 (4.16-2.64)
Premature, *n* (*%*)	
Yes	0 (0)
No	11 (100)
Birthplace, *n* (*%*)	
NU	11 (100)
NICU	0 (0)
Gestation at delivery, wk, Median (range)	39.29 (39-39.86)
Pertussis Vaccination during pregnancy (*%*)	
Yes	10 (90.9)
No	1 (9.01)
Gestation at vaccination, wk, median (range)	42.39 (22-37)

Table 3.2.6 Neonates demographics and clinical data used for the immune cell populations (OMIP) panel.

Neonates demographic and clinical information were obtained from the neonatal unit. The range is defined as the highest and lowest value. *Abbreviations used:* CB – cord blood, NU – Neonatal Unit, NICU – Neonatal Intensive Care Unit, wk – week, kg – kilogram.

In the first part of this study, the abundance of different innate and adaptive cell populations in adults and neonates was determined using the OMIP cohort (**Table 3.2.5**). In this cohort females and males were well represented (*P*=0.4225) with the median age of adults ±32.5 years (23.0-62.0). More clinical data were available for the neonatal patients (**Table 3.2.6**). In the OMIP cohort, neonatal blood samples were collected from term children delivered at ±39.29 (39.43-39.86) weeks gestation. Mothers of ten babies (90.9%) were vaccinated during the ±30th (22.00-37.00) week of pregnancy. The number of females was lower in the neonatal cohort for OMIP compared to adult females; however, there was no significant difference in weights between females and males.

3.2.3.2.2. The abundance of innate cell populations in healthy adults and neonates

Enumeration of circulating granulocytes in healthy adults and neonates

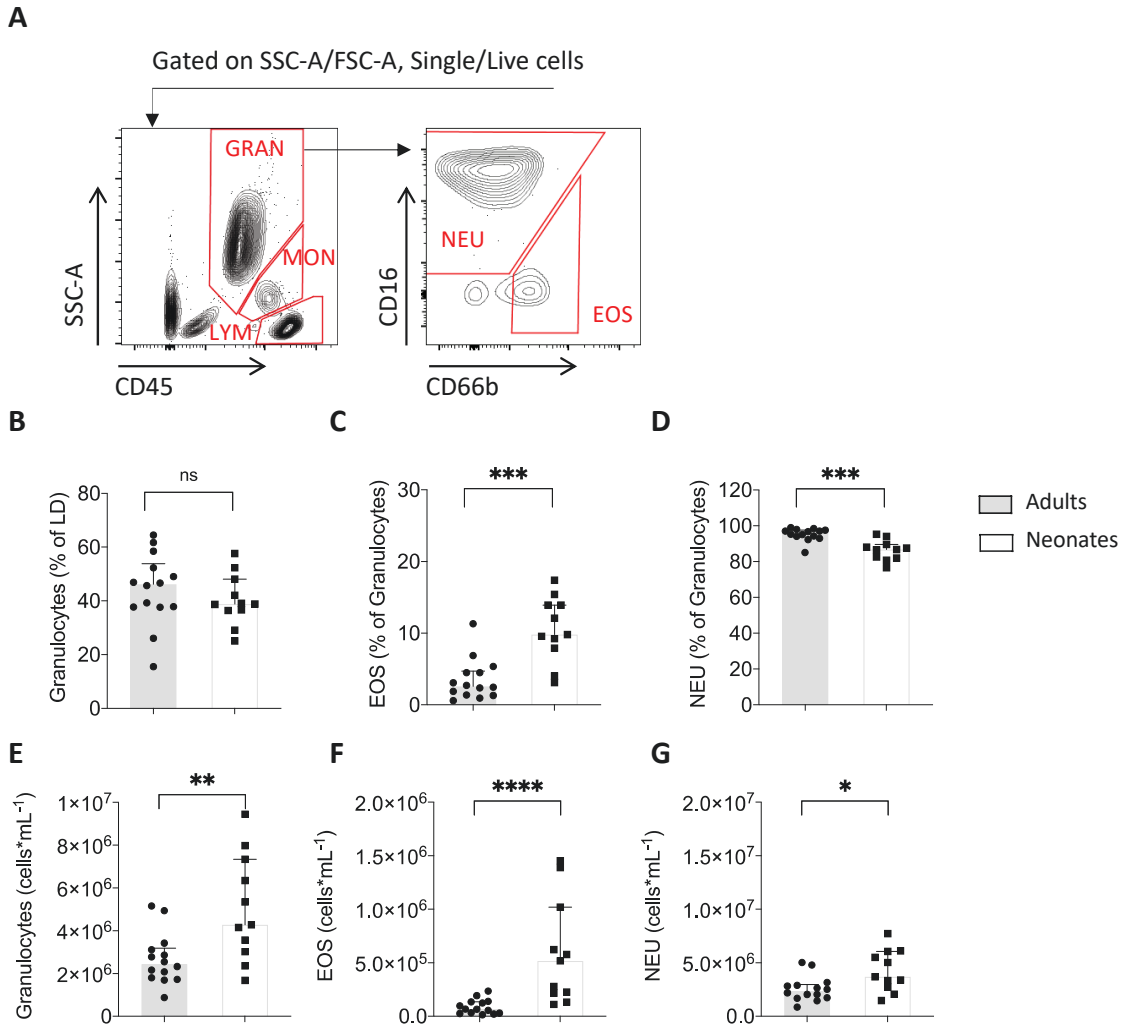


Figure 3.2.9 Abundance of granulocytes in whole blood from healthy adults and neonatal cord blood.

An example of flow cytometry gating for granulocytes in peripheral whole blood from healthy adults. Data are from one experiment but represent more than 30 experiments with similar results **(A)**. Granulocytes were defined within live, single, cells using CD45 expression and SSC-A. Within the granulocytes, neutrophils were defined as $CD16^{+}CD66b^{+/-}$ and eosinophils as $CD16^{-}CD66b^{+}$. Frequency of total granulocytes among live $CD45^{+}$ cells **(B)**, frequency of eosinophils **(C)** and neutrophils **(D)** among granulocytes**,** in the whole blood from healthy adults (*n*=14) and cord blood from neonates (*n*=11)**.** Quantification of granulocytes **(E)**, eosinophils **(F)** and neutrophils **(G)** in the peripheral blood of healthy adults and cord blood from neonates. Data are from 14 (adults) and 11 (neonates) experiments with one subject in each shown as the median with upper interquartile range **(B-G)**. Differences between groups were estimated by Mann-Whitney test (ns, not significant; * $p < 0.05$, ** $p < 0.01$, ***$p < 0.001$ and **** $p < 0.0001$). *Abbreviations used:* GRN – granulocytes, MON –monocytes, LYM – Lymphocytes, EOS – eosinophils, NEU – neutrophils.

To assess the normal abundance of granulocytes (including eosinophils and neutrophils) in the peripheral and cord blood I utilised the gating strategy from the published OMIP [201] (**Fig. 3.2.9**). As seen in **Fig. 3.2.9 A,** granulocytes were defined within live, single, $CD45^{+}$ lymphocytes using SSC-A. Within the granulocytes, neutrophils were defined as $CD16^{+}CD66b^{+/-}$ and eosinophils as $CD16^{-}CD66b^{+}$. Granulocytes were more abundant in the cord blood than peripheral blood (*P*=0.009, 4.28 x 10^{6} and 2.45 x 10^{6} cell per mL, respectively) (**Fig. 3.2.9 E**) but at the same

frequency (**Fig. 3.2.9 B**) among the live leukocytes in the cord blood than peripheral blood. The eosinophils displayed significantly higher total numbers (*P*<0.0001) and were a higher proportion of total granulocytes (*P*=0.02) in cord blood compared to adult blood (**Fig. 3.2.9 C and F**). Similarly, the neutrophil population was significantly increased as a total number (*P*=0.01) but were at a slightly lower proportion of granulocytes (*P*=0.003) in cord compared to adult blood (**Fig. 3.2.9 D and G**).

Enumeration of circulating ILCs in healthy adults and neonates

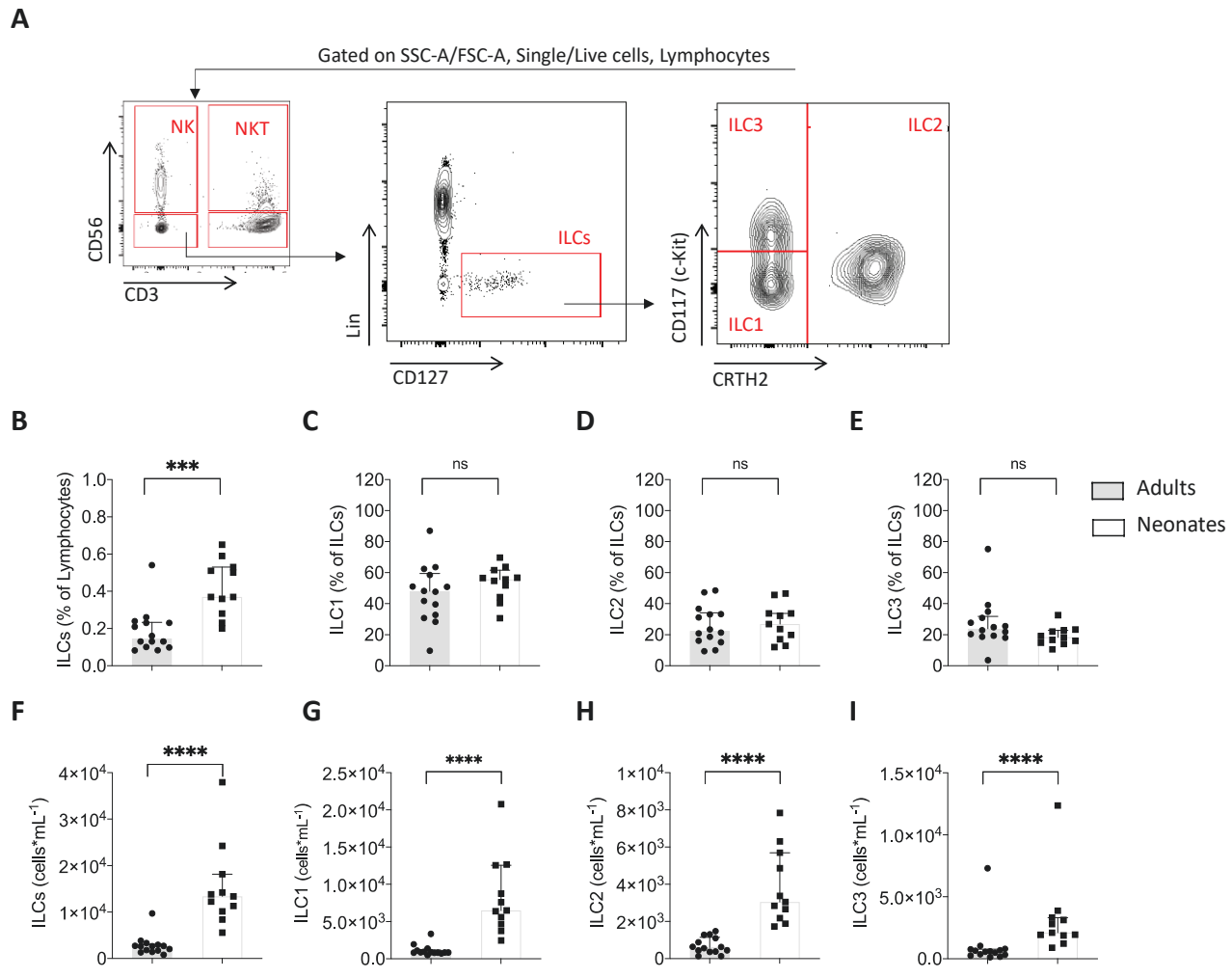


Figure 3.2.10 Abundance of ILCs in the whole blood from healthy adults and cord blood from neonates.

An example of flow cytometry gating for defining ILCs in the peripheral whole blood from healthy adults. Data are from one experiment but represent more than 30 experiments with similar results **(A)**. ILCs were delineated within live, single, $CD45^+$ lymphocytes as lineage negative (CD3, CD14, CD19, CD56, CD123 and $Fc\varepsilon RI\alpha)^-$ and $CD127^+$ (IL-7 receptor-α) cells. The ILC subsets (ILC1, ILC2 and ILC3) were identified using CRTH2 and CD117 (c-Kit) surface markers; ILC1 cells were defined as $CD117^-CRTH2^-$, ILC2 cells as $CRTH2^+$ $CD117^{int}$ and ILC3 as $CD117^+CRTH2^-$ **(A)**. Frequency of total ILCs among live lymphocytes **(B)** and ILC1s **(C)**, ILC2s **(D)**, ILC3s among total ILCs **(E)** in whole blood from healthy adults (*n*=14) and cord blood from neonates (*n*=11)**.** Quantification of total ILCs **(F)**, ILC1s **(G),** ILC2s **(H)** and ILC3 cells **(I)** in the peripheral blood of healthy adults and cord bloods from neonates. Data are from 14 (adults) and 11 (neonates) experiments with one subject in each and are shown as the median with upper interquartile range **(B-I)**. Differences between groups were estimated by Mann-Whitney test (ns, not significant; **** $p < 0.0001$). *Abbreviations used:* NK – natural killer cells, NKT – natural killer T cells, Lin – lineage, CRTH2 – prostaglandin D2 receptor.

Next, I investigated whether there are differences in the distribution of ILCs (excluding NK cells) across those two groups of adults and neonates. Although ILCs are known to be abundant in mucosal sites such as the lungs, gut or skin, they can also be detected in the peripheral blood [151] and cord blood [188]. The typical abundance of ILCs in the adult peripheral and cord blood was assessed by the gating strategy from the OMIP [201]. ILCs were delineated within live, single, $CD45^+$ lymphocytes as lineage negative (CD3, CD14, CD19, CD56, CD123 and FcεRIα)$^-$ and $CD127^+$ (IL-7 receptor-α) cells. The ILC subsets (ILC1, ILC2 and ILC3) were identified using CRTH2 and CD117 (c-Kit) surface markers; ILC1 cells were defined as $CD117^-CRTH2^-$, ILC2 cells as $CRTH2^+$ $CD117^{int}$ and ILC3 as $CD117^+CRTH2^-$ (**Fig. 3.2.10 A**). All ILCs subsets were detected in peripheral and cord blood samples; however, the number and percentage of total ILCs among lymphocytes were lower in adults; the total number of ILCs was only 2.69 x 10^3 cell per mL in adults and 1.34x 10^6 cells per mL in neonates (P<0.0001) (**Fig. 3.2.10 B**) while the frequency of ILCs among peripheral lymphocytes in healthy adults and neonates was ~0.2% and ~0.4%, respectively (P=0.0005) (**Fig. 3.2.10 F**). The ILC1s, ILC2s and ILC3s in the peripheral blood and cord blood had the same frequency among ILCs across the groups (**Fig. 3.2.10 C-E**) and the abundance of all subsets was higher in cord blood (P<0.0005) (**Fig. 3.2.10 G-I**).

Enumeration of circulating NK cells in healthy adults and neonates

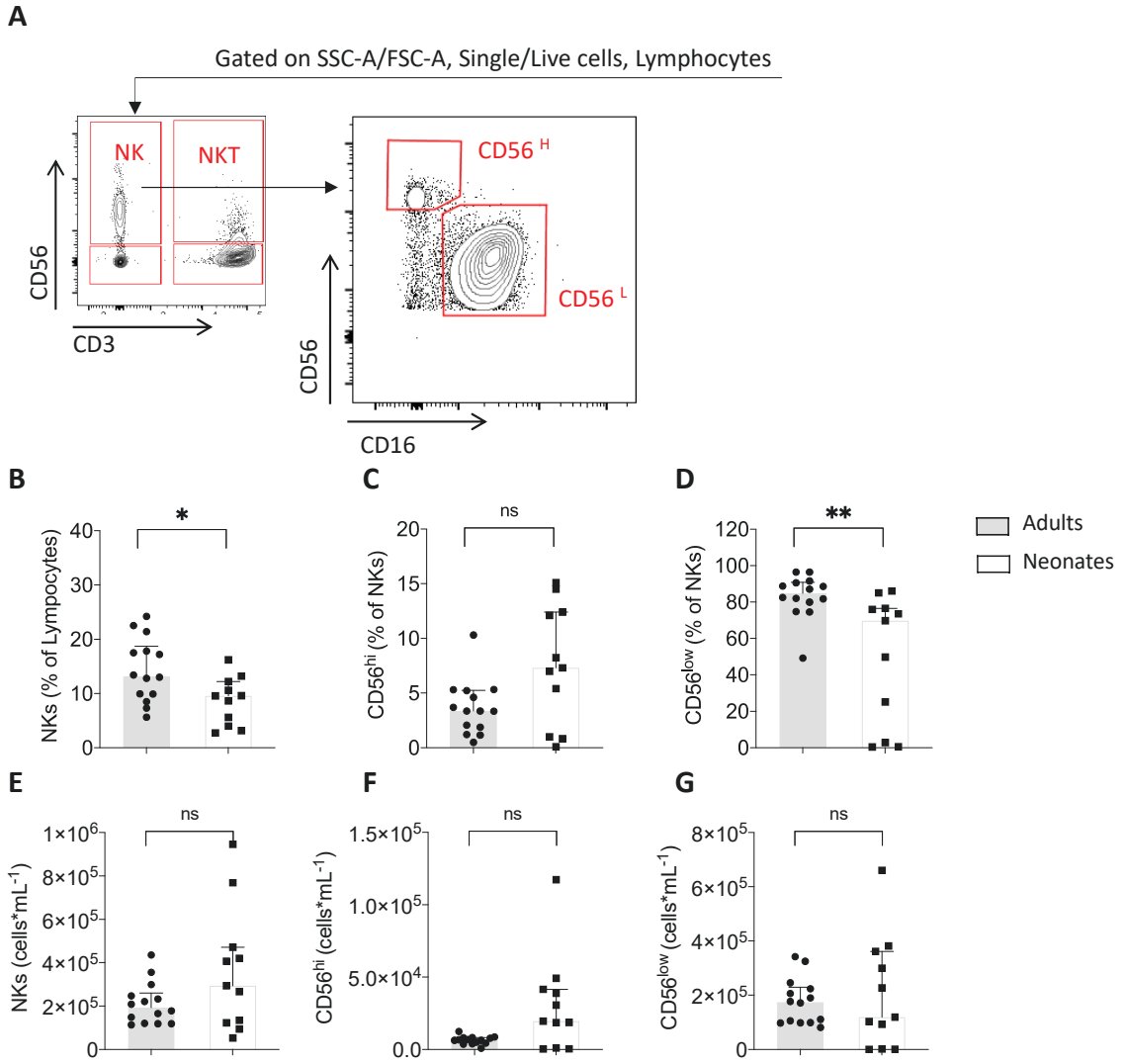


Figure 3.2.11 Abundance of NK cells in whole blood from healthy adults and cord blood from neonates.

An example of flow cytometry gating for NK cells in peripheral whole blood from healthy adults. Data are from one experiment but represent more than 30 experiments with similar results **(A).** NK cells were defined as live, single, $CD45^+$ $CD56^+CD3^-$ lymphocytes. Within the NK cell population, $CD56^HCD16^L$ and $CD56^LCD16^H$ subsets were defined. NKT cells were gated within the lymphocyte gate as $CD56^+CD3^+$ cells **(A)**. Frequency of total $CD56^+CD3^-$ NK cells among live lymphocytes **(B)** and $CD56^HCD16^L$ NKs **(C)** $CD56^LCD16^H$ NKs **(D)** among NK cells in whole blood from healthy adults and cord blood from neonates. Quantification of total $CD56^+CD3^-$ NK cells **(B)** and $CD56^HCD16^L$ **(C)** and $CD56^LCD16^H$ NK cells in the peripheral blood of healthy adults and cord blood from neonates. Data are from 14 (adults) and 11 (neonates) experiments with one subject in each and are shown as the median with upper interquartile range **(B-G)**. Differences between groups were estimated by Mann-Whitney test (ns, not significant; * $p < 0.05$, ** $p < 0.01$). *Abbreviations used:* NK – natural killer cells, NKT – natural killer T cells.

I next determined the normal distribution of NK cells in healthy adults and neonates. Natural killer cells are the most abundant member of the ILC family and can be characterised by their cytotoxic capacity [143]. NK cells were defined as live, single, $CD45^+$ $CD56^+CD3^-$ lymphocytes. Within the NK cell population, $CD56^HCD16^L$ ($CD56^H$) and $CD56^LCD16^H$ (CD56L) subsets were defined (**Fig. 3.2.11 A**). NK cells were detected in the peripheral blood of healthy adults and neonates, shown as the number (**Fig. 3.2.11 E-G**) and the frequency (**Fig. 3.2.11 B-D**) among the live lymphocytes;

however, NK cell frequency as a proportion of lymphocytes was significantly lower in cord blood than adult peripheral blood (P=0.018, 9.5% and 13.2%, respectively). The $CD56^{H}CD16^{L}$ ($CD56^{H}$) and $CD56^{L}CD16^{H}$ ($CD56^{L}$) NK cell subsets displayed similar abundance across the groups; however, $CD56^{L}$ NK cells had a slightly higher frequency among adults' NK cells (P<0.002) (**Fig. 3.2.11 D**).

3.2.3.2.3. The normal abundance of other lymphocyte populations in healthy adults and neonates

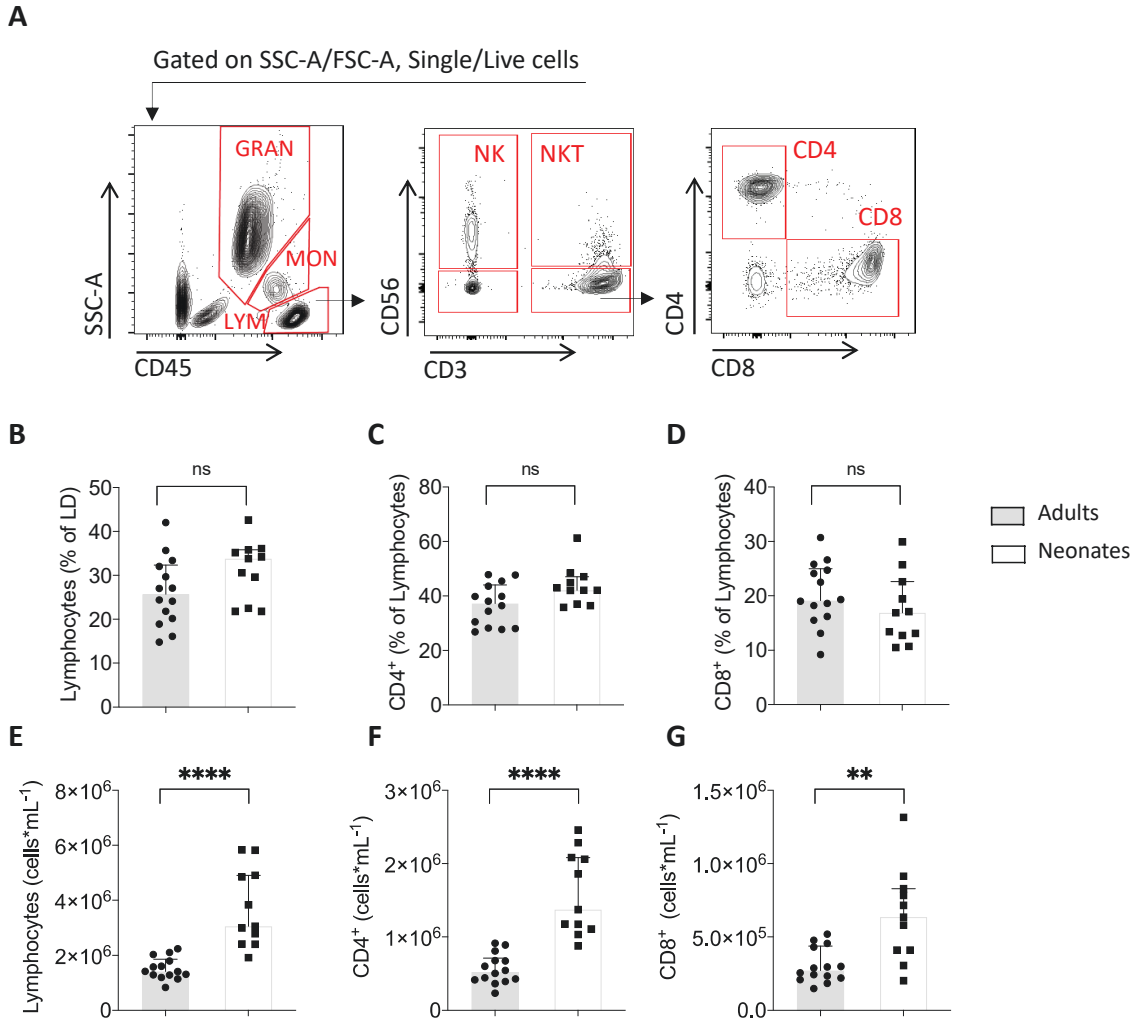


Figure 3.2.12 Abundance of lymphocytes, $CD4^{+}$ and $CD8^{+}$ T cells in whole blood from healthy adults and cord blood from neonates.

An example of flow cytometry gating for lymphocytes, NK, NKT, $CD4^{+}$ or $CD8^{+}$ T cells in peripheral whole blood from healthy adults. Data are from one experiment but represent more than 30 experiments with similar results**(A)**. Lymphocytes were defined within live, single, leukocytes using CD45 expression and SSC-A. Within the lymphocyte gate, NK and NKT-like cells were gated as $CD56^{+}CD3^{-}$ and $CD56^{+}CD3^{+}$ cells, respectively**.** T lymphocytes ($CD3^{+}CD56^{-}$) were segregated into $CD4^{+}$ or $CD8^{+}$ T cells. Frequency of lymphocytes among live $CD45^{+}$ cells **(B)**, $CD4^{+}$ T **(C)** and $CD8^{+}$ T **(D)** cells among lymphocytes in the whole blood from healthy adults (n=14) and cord blood from neonates (n=11)**.** Quantification of lymphocytes **(E)**, $CD4^{+}$ T **(F)** and $CD8^{+}$ T **(G)** cells in the peripheral blood of healthy adults and cord bloods from neonates. Data are from 14 (adults) and 11 (neonates) experiments with one subject in each shown as the median with upper interquartile range **(B-G)**. Differences between groups were estimated by Mann-Whitney test (ns, not significant; ** p < 0.01, **** p < 0.0001). *Abbreviations used:* GRN – granulocytes, MON –monocytes, LYM – lymphocytes, NK – natural killer cells, NKT – natural killer T cells.

The typical abundance of lymphocyte populations in the peripheral and cord blood was assessed using the gating strategy from the OMIP [201]. I focused on establishing the typical values for $CD4^+$ and $CD8^+$ T cells as it seems there is skewed T cell polarization in bronchiolitic infants [224]. Lymphocytes were defined as live, single, $CD45^+$ lymphocytes using SSC-A. Within the lymphocyte gate, NK and NKT cells were gated out and T lymphocytes ($CD3^+CD56^-$) were segregated into $CD4^+$ or $CD8^+$ T cells (**Fig. 3.2.12 A**). Lymphocytes displayed an equivalent frequency of live cells in healthy adults and neonates, and the proportion of $CD4^+$ and $CD8^+$ cells among lymphocytes did not differ (**Fig. 3.2.12 B-D**). Interestingly, all investigated populations were far more abundant in the cord blood of healthy neonates (with median of 3.06×10^6 cell per mL for lymphocytes, 1.3×10^6 cell per mL for CD4 T and 6.3×10^5 cell per mL for CD8 T cells) compared to the adults (with median of 1.41×10^6 cell per mL for lymphocytes, 5.2×10^5 cell per mL for CD4 T and 2.7×10^5 cell per mL for CD8 T cells) **(Fig. 3.2.12 E-F**). The median ratio of CD4positive: CD8 positive cells in adults was 1.88:1 and for neonates it was 2.54:1 with no statistical differences observed between adults and neonates (*P*=0.95).

Subsequently, I determined the MAIT, NKT, Tc2 and Th2 cell populations among the circulatory lymphocytes. The gating strategy is shown in **Figure 3.2.13 A** [201]. T lymphocytes (FSC/SSC, single, live, $CD45^+$, $CD3^+CD56^-$ cells) were segregated into $CD4^+$ or $CD8^+$ T cells. Within $CD4^+$ and $CD8^+$ T cells, the CRTH2 marker was used to define Th2 and Tc2 cells to delineate type-2 cytokine-producing cells. Within $CD8^+$ cells, invariant T lymphocytes responsible for recognition of riboflavin metabolites, known as MAIT cells were defined as $CD161^H$ $V\alpha7.2^+$ [84]. Within the lymphocyte gate, NK and NKT-like cells were gated as $CD56^+CD3^-$ and $CD56^+CD3^+$ cells, respectively (**Fig. 3.2.13 A**). The MAIT, NKT, Tc2 and Th2 subsets remained statistically more abundant in the adult circulatory compared to cord blood (*P*<0.0001) (**Fig. 3.2.13 F-I**), and the frequencies of these cells were higher in adults (*P*<0.0001) (**Fig. 3.2.13 B-E**).

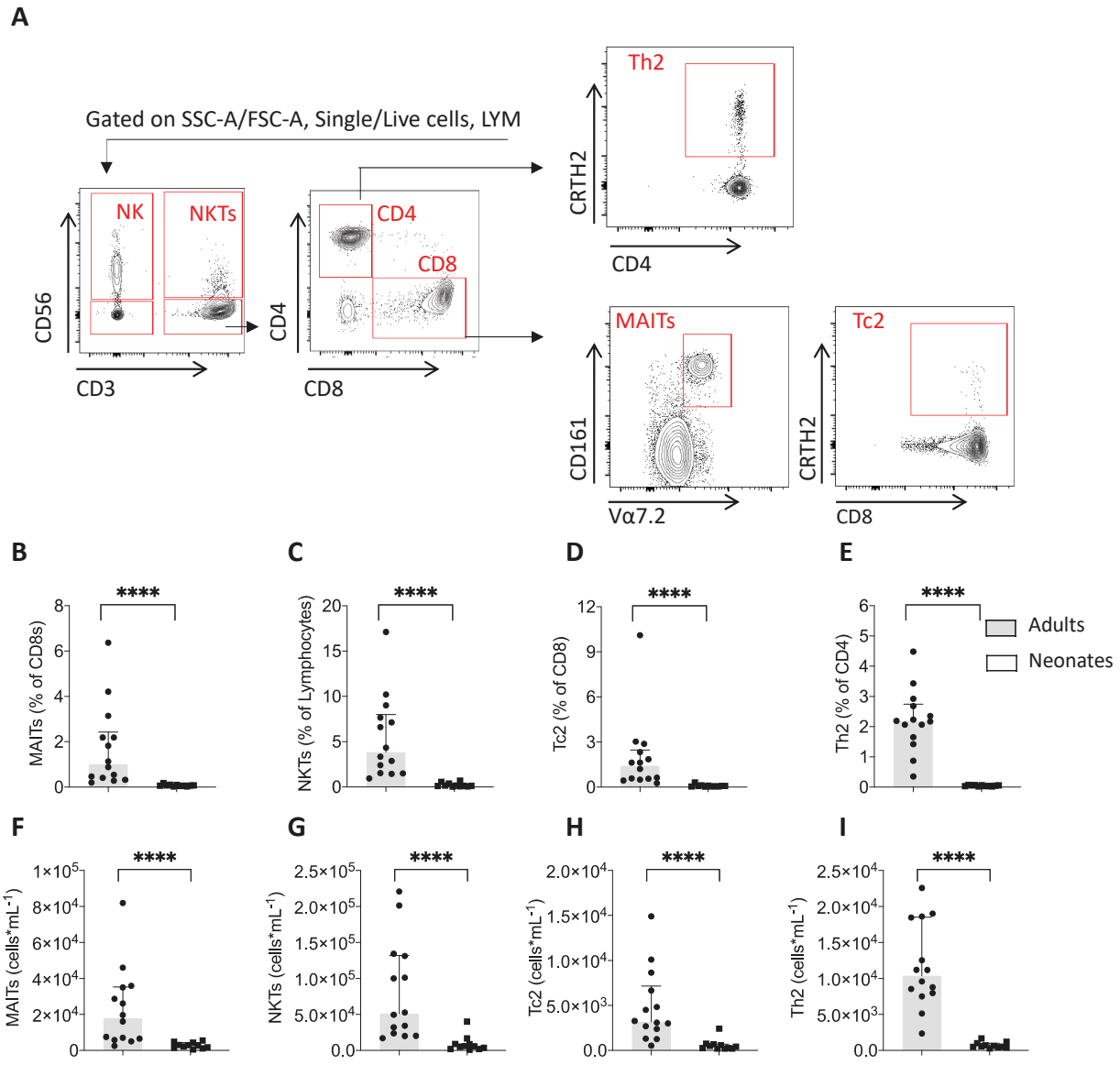


Figure 3.2.13 Abundance of MAIT, NKT, Tc2 and Th2 cells in whole blood from healthy adults and cord blood from neonates.

An example of flow cytometry for MAIT, NKT, Tc2 and Th2 cells in the peripheral whole blood from healthy adults. Data are from one experiment but represent more than 30 experiments with similar results **(A).** T lymphocytes (FSC/SSC, single, live, $CD45^+$, $CD3^+CD56^-$ cells) were segregated into $CD4^+$ or $CD8^+$ T cells. Within $CD4^+$ and $CD8^+$ T cells, the CRTH2 marker was used to define Th2 and Tc2 cells respectively. Within $CD8^+$ cells, MAIT cells were defined as $CD161^H$ $V\alpha7.2^+$ **(A)**. Frequency of total MAITs among live $CD8^+$ T cells **(B)**, $CD56^+CD3^+$ NKTs among lymphocytes **(C),** $CD56^-CD3^+CRTH2^+$ Th2s among CD4+ T cells **(D)** and $CD56^-CD3^+CRTH2^+$ Tc2s among $CD8^+$ T cells **(E)**, in the whole blood from healthy adults (*n*=14) and cord blood from neonates (*n*=11)**.** Quantification of total $CD56^-CD3^+CD8^+CD161^H$ $V\alpha7.2^+$- MAIT **(F)**, $CD56^+CD3^+$ NKT **(G),** $CD56^-CD3^+CD4^+CRTH2^+$ Th2 **(H)** and $CD56^-CD3^+CD8^+CRTH2^+$ Tc2 cells **(I)** cells in the peripheral blood of healthy adults and cord bloods from neonates. Data are from 14 (adults) and 11 (neonates) experiments with one subject in each shown as the median with upper interquartile range **(B-I)**. Differences between groups were estimated by Mann-Whitney test (**** $p < 0.0001$). *Abbreviations used:* LYM – lymphocytes, MAIT – mucosal-associated invariant T cells, NK – natural killer cells, NKT – natural killer T cells, Tc2 – type-2 cytokine-producing CD8s, Th2 – type-2 cytokine-producing CD4s, CRTH2 – prostaglandin D2 receptor.

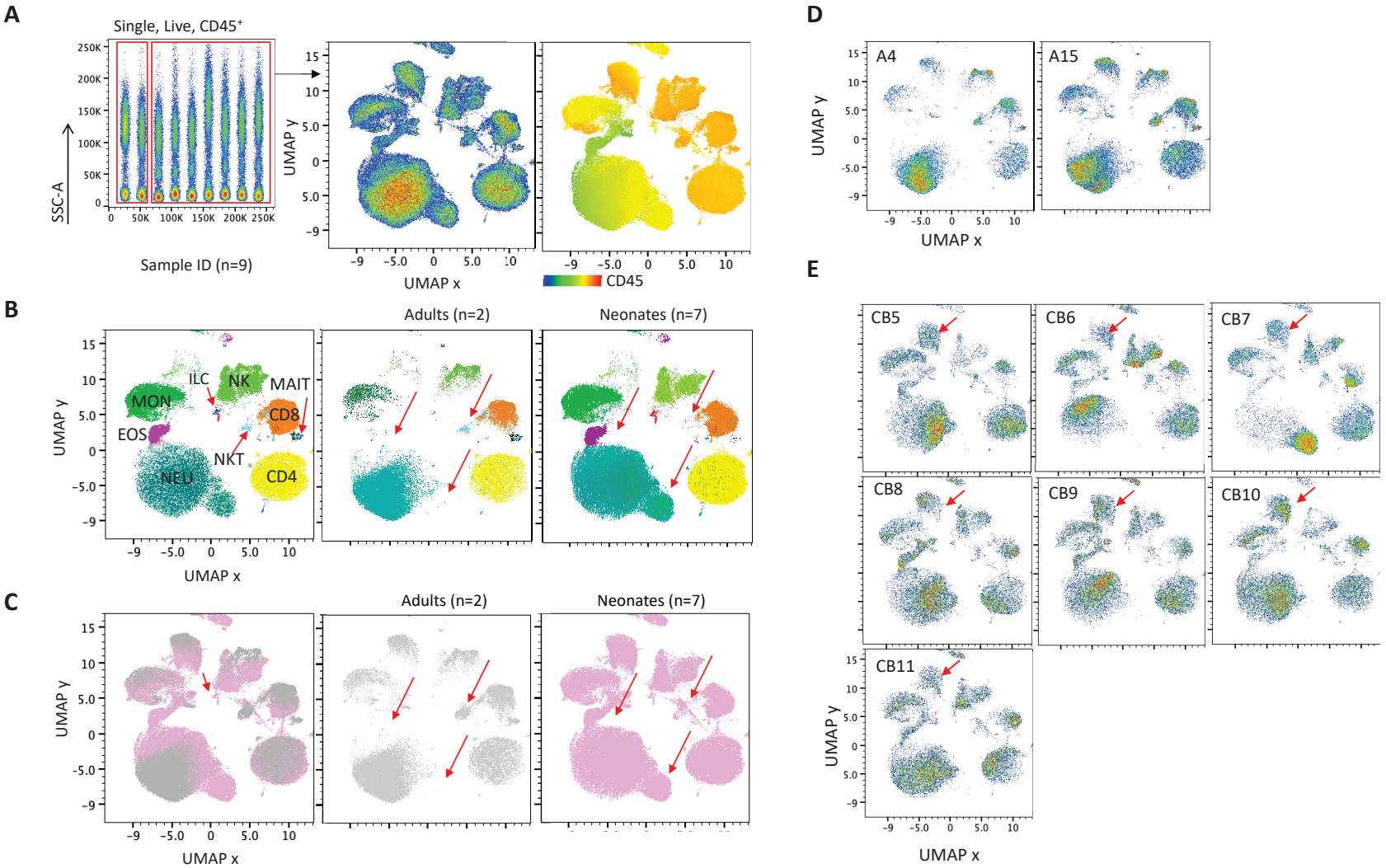


Figure 3.2.14 Deep immune phenotyping of CD45+ populations in whole blood in adults and neonates using UMAP reveals cells alterations.

Representative manual gating strategy utilised for deep immune phenotyping. Cells were delineated using the following gating strategy: FSC/SSC, single, live cells. Lymphocytes were gated using SSC-A and CD45. 15,000 randomly selected $CD45^+$ cells from each subject (*n*=9, left) were concatenated into a single file containing 135,000 cells for UMAP analysis (middle). The intensity of CD45 expression is shown (right). **(B)** The manual gating strategy from the OMIP (see Chapter 3.1) was utilised allowing global UMAP clusters (all subjects pooled) to be classified into the following cell types: CD4 T cells (yellow), NKT cells (bright blue), monocytes (green), CD8 T cells (orange), neutrophils (ocean blue), eosinophils (magenta), NK cells (bright green), MAIT cells (black), ILC3s (purple), ILC2s (blue) and ILC1s (red). The population of ILCs and NKTs are indicated via red arrows (left). Comparison of UMAP representations of clusters for only healthy adult subjects (*n*=2, middle) and neonates (*n*=7, right) coloured by the manual gating strategy used in global UMAP. **(C)** Simplified UMAP projections indicating the differences between cell clusters from all subjects pooled (*n*=9, pink and grey overlaid), only adults (*n*=2, grey) and neonates (*n*=7, pink). The main differences between cell clusters among adults and neonates are depicted using the same orientated red arrows. UMAP visualisation of live $CD45^+$ cell clusters in individual adults **(F)** and neonates **(E)** allowed to depict differences between all subjects. *Abbreviations used:* NEU – neutrophils, EOS – eosinophils, MON – monocytes, LYM – Lymphocytes, NK – natural killer cells, NKT – natural killer T cells, MAITs – mucosal invariant T cells, ILC – innate lymphoid cells, UMAP – Uniform Manifold Approximation and Projection.

3.2.3.2.4. Assessment of immune cell populations by UMAP

After establishing a successful gating strategy for OMIP [201], I next tried to identify the immune cell populations in healthy adults (*n*=2) and neonates (*n*=9) using the deep immune phenotyping technique UMAP[204] (Uniform Manifold Approximation and Projection). This technique allowed me to reduce 16 dimensions (14 colours including FSC-A and SSC-A, **Table 3.1.1**) into two dimensions referred as UMAPx and UMAPy that formed an augmented panel (**Fig. 3.2.14 A,** middle). To reduce dimensions, flow data used for OMIP was utilised from at least 9 experiments on adults and neonates. Prior to UMAP computation, data was sorted using standard biaxial gating including only single, live lymphocytes (**Fig. 3.2.14 A,** left). Lymphocytes were gated using SSC-A and the CD45 cell marker. I performed UMAP analysis on 135,000 randomly selected lymphocytes (15,000 from each subject concatenated into a single file) which highly expressed CD45 (**Fig. 3.2.14 A**, right). The manual gating strategy from the OMIP [201] (see Chapter 3.1) was utilised and allowed global UMAP clusters (all subjects pooled) to be classified into the following cell types: CD4 T cells (yellow), NKT cells (bright blue), monocytes (green), CD8 T cells (orange), neutrophils (ocean blue), eosinophils (magenta), NK cells (bright green), MAIT cells (black), ILC3s (purple), ILC2s (blue) and ILC1s (red). Interestingly, UMAP allowed me to estimate the immune cell composition as in OMIP [201] and investigate phenotypical changes within each cell cluster to picture the diversity and heterogeneity in adults and neonates (**Fig. 3.2.14 B-C**). Based on this visualisation, I identified all cell types in adults; however, there was a lack of invariant T cells (NKT and MAIT cells) in neonates in line with OMIP cell definition. Interestingly, in adults (**Fig. 3.2.14 B**), I observed a lower abundance of eosinophils (magenta) and all subsets of ILCs: ILC1s (red), ILC2s (blue) and ILC3s (purple). Notably, in neonates, I observed a cluster that was shown to share characteristics with stem cells expressing high level of CD117 marker (c-Kit) and it was

present within all neonatal donors within the ungated lineage negative population (**Fig. 3.2.14 E**).

To improve visualisation and investigate the heterogeneity of all subtypes of ILCs (including NK cells), I performed UMAP immunophenotyping on 135,000 FSC/SSC, single, live, $CD45^+$, $CD3^+$, $CD66b^-$ cells (17,000 cells per subject) excluding all granulocytes, monocytes and $CD3^+$ T cell populations (**Fig. 3.2.15 A**). This improved visualisation utilised the same cohort as used in **Figure 3.2.14** and the manual gating strategy from the OMIP [201] (see Chapter 3.1) to screen the clusters. Based on this deep computational analysis and the expression of cell markers, the UMAP clusters were classified into the following cell types: $CD14^+$ $CD19^+$ $CD123^+$ $Fc\varepsilon RI\alpha^+$ lineage+ (yellow), $CD56^+CD3^-$ NK cells (red), $CD56^HCD16^L$ NK cells (grey), $CD56^LCD16^H$ NK (magenta), ILC3s (green), ILC2s (orange) and ILC1s (dark green) (**Fig. 3.2.15 B**). Notably, the phenotypes identified in unsupervised UMAP analysis were similar to manual biaxial gating. As mentioned before, UMAP clusters show changes not only in the cell composition but also depicted phenotypical changes in the cell clusters among cohort participants (**Fig. 3.2.14 D, E**). The main differences between adults and neonates were observed within NK cell, lineage and ILC populations with the most significant reduction observed in lineage and ILC clusters in adults (**Fig. 3.2.15 B-C**). The comparison in the spatial pattern and abundance of NK cells between neonates and adult depicted differences in $CD56^HCD16^L$ NK cells (predominantly in neonates), $CD56^LCD16^H$ NK cells (predominantly in adults).

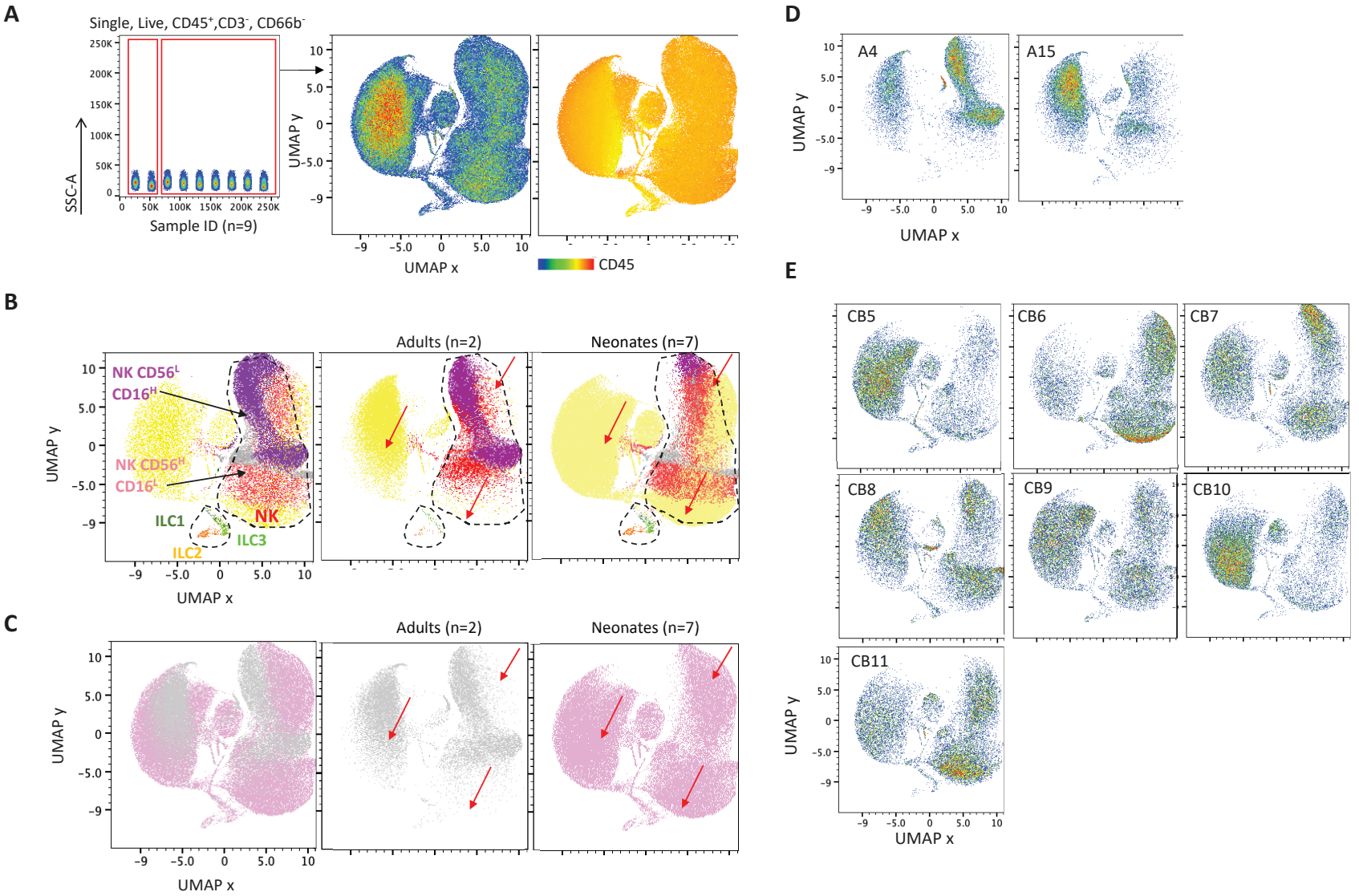


Figure 3.2.15 Deep immune phenotyping of ILCs (including NK cells) in whole blood in adults and neonates using UMAP reveals alterations in cell populations

(A) Representative manual gating strategy utilised for deep immune phenotyping of ILCs. Cells were delineated using the following gating strategy: FSC/SSC, single, live, $CD45^+$, $CD3^-$, $CD66b^-$ lymphocytes (excluding granulocytes, monocytes and T cell populations). 17,000 randomly selected $CD45^+CD3^-CD66b^-$ lymphocytes from each subject (*n*=9) were concatenated into a single file containing 135,000 cells for further UMAP analysis (left). Global UMAP representation of $CD45^+CD3^-CD66b^-$ lymphocytes (middle). The intensity of CD45 cell expression marker is shown (right). **(B)** The manual gating strategy from the OMIP (see Chapter 3.1) was utilised allowing global UMAP clusters (all subjects pooled) to be classified into the following cell types: $CD3^+CD14^+CD19^+CD56^+CD123^+FcεRIα^+$ lineage (yellow), $CD56^+CD3^-$ NK cells (red), $CD56^HCD16^L$ NK cells (grey), $CD56^LCD16^H$ NK (magenta), ILC3s (green), ILC2s (orange) and ILC1s (dark green). Comparison of UMAP representations for only healthy adult subjects (*n*=2, middle) and neonates (*n*=7, right) coloured by the manual gating strategy used in global UMAP. The population of ILCs and NKs are pointed via dashed lines. **(C)** Simplified UMAP projections indicating the differences between cell clusters from all subjects pooled (*n*=9, pink and grey overlaid), only adults (*n*=2, grey) and only neonates (*n*=7, pink). The main differences between cell clusters among adults and neonates are depicted using the same orientated red arrows. UMAP visualisation of live $CD45^+CD3^-CD66b^-$ lymphocyte clusters for each adult individual **(F)** and neonate individual **(E)** to depict differences between all subjects. *Abbreviations used:* NK – natural killer cells, ILC – innate lymphoid cells, UMAP – Uniform Manifold Approximation and Projection

3.2.3.2.5. Assessment of circulatory immune cell populations and their correlations utilising R functions

In parallel with the enumeration of immune cells in adults and neonates using manual and augmented analysis (OMIP and UMAP analysis, respectively) I employed other techniques including heatmaps and principal component of analysis (PCA) in the R programming language. They helped to define and identify the differences between cell populations in adult and cord blood. Both techniques are visualisation techniques that can show the similarities and differences between *n*-number of variables using colour in two dimensions. In heatmaps data are expressed using a colour scale allowing simultaneous visualisation of individuals (samples) and their features (variables). In the first step, hierarchical clustering reorganises data, clustering similar samples together and applies a colour scale for high and low values (red and blue, respectively) to variables. In my hands, hierarchical clustering for each individual in a heatmap format allowed me to visualise differences between different subjects (adults *vs* neonates) using variables such as the frequencies and cell counts of immune cell populations from the flow cytometry data. In heatmaps (**Fig. 3.2.16**), each row represents an individual (sample) (Adults 1-14 and Neonates 15-25) and each column represents the cell population (variable). The rows and columns were ordered according to the hierarchical clustering (as mentioned above), putting similar observations close to each other. In the plots, high values are in red and low values in blue and consist of Pearson correlation coefficients ranging from -4 to 4 (high and low values). The unsupervised hierarchical clustering in the cohort of healthy adults (*n*=14) and neonates (*n*=11) using cell count values revealed subject and sex signatures (only in neonates) (**Fig. 3.2.16 A**). Although, it has to be considered that females were underrepresented in the cohort of neonates compared to males (*n*=3 and *n*=8, respectively). Hierarchical clustering using

percentage –values could not define and identify any sex or subject related signatures in the same cohort (**Fig. 3.2.16 B**). Further exploration stratified cell populations into a cluster related to invariant T cells (MAITs, NKT) and $CD4^+$ and $CD8^+$ T cells expressing CRTH2 (Th2 and Tc2, respectively), which are found at higher numbers in adults. Notably, the sex signature profile was emerging among neonates; females have a higher number of all innate and adaptive cells compared to their male counterparts (**Fig. 3.2.16 A**).

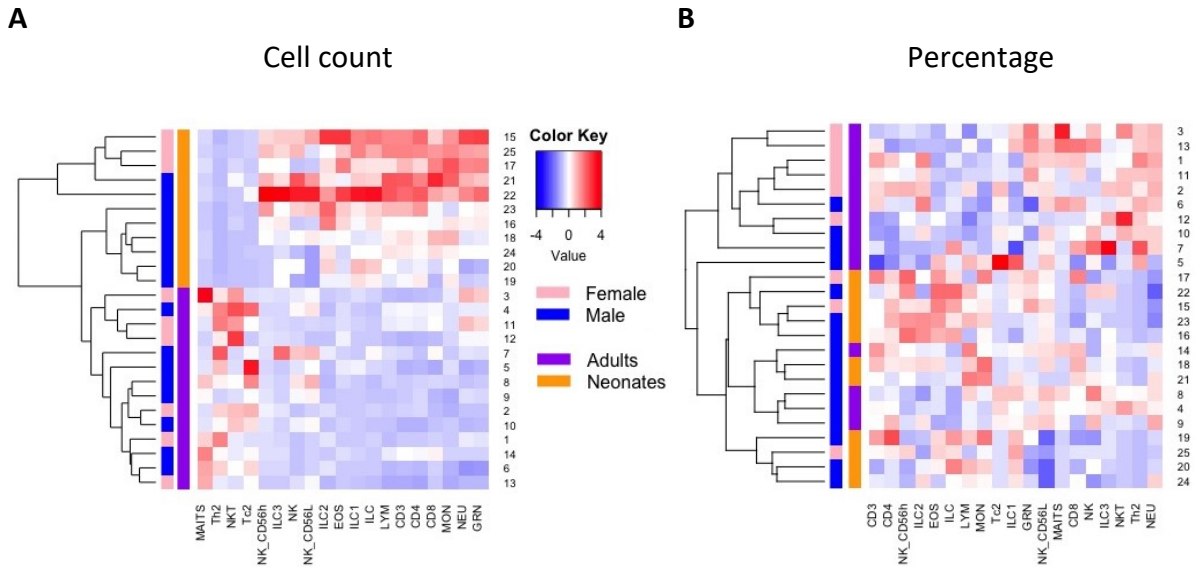


Figure 3.2.16 Hierarchical clustering of the cohort of healthy adults and neonates using heatmaps.

The OMIP cohort signatures (*n*=25) were delivered by comparing total cell counts **(A)** and frequencies **(C)** from healthy adults (*n*=14) and neonates (*n*=11) using the R programming language. Data are displayed in a heatmap format, where each row represents an individual (sample) (Adults 1-14 and Neonates 15-25) and each column represents the cell population (variable). The rows and columns were ordered according to the hierarchical clustering result, putting similar observations close to each other. In the plots above, high values are in red and low values in blue and consist of Pearson correlation coefficients ranging from -4 to 4. Additionally, the rows were annotated according to the subject (Adults, Neonates) and sex (Female, Male) using colours. *Abbreviations used*: NEU – neutrophils, EOS – eosinophils, MON – monocytes, GRN – granulocytes, LYM – Lymphocytes, NK – natural killer cells, NKT – natural killer T cells, MAITs – mucosal invariant T cells, ILC – innate lymphoid cells, Tc2 – type-2 cytokine-producing CD8s, Th2 – type-2 cytokine-producing CD4s.

Using PCA, I showed separation between subjects occurred based on whether the sample was from healthy adults and neonates, but samples did not segregate by sex It also allowed me to establish which cell populations (variables) make the major contribution to driving these differences. In brief, PCA allowed me to reduce the flow cytometry data of different cell populations (dimensions, variables) into basic components, removing all unnecessary dimensions. In my data set, I had 20 distinct cell populations. There were therefore 20 different variables (20 different values for each subject), resulting in a 20-dimension data set. PCA then reduced 20 different dimensions to only two and these dimensions were identified as the principal components (PC): PCA1 (Dim1) and PCA2 (Dim2). Each individual is plotted on the PCA

as a point. PCA was used to determine whether individuals clustered according to their group characteristics (adult vs neonate, or sex); and which cell populations were the drivers of the differences (**Fig. 3.2.17**). The group mean point was added to depict the centre of each group. The point concentration ellipses (red, green, light blue) were added around each group mean point using a multivariant *t*-distribution where the size of the concentration ellipse is the range of normal probability (95% confidence). PCA showed separation according to whether subjects were adult or neonates (when both percentage- and cell count-values were used) (**Fig. 3.2.17 A, C**); females and males were computationally indistinguishable using percentage- and cell count-values (**Fig. 3.2.17 B, D**).

In addition, PCAs allowed the relationship between variables (cell populations) and the PC to be assessed. Cos2 measures the quality of representation of the variables on the PC; the higher cos2 the better the representation of the variable. **Figure 3.2.17 A-D** show cos2 as an arrow for each cell population, with the variables with the highest cos2 values furthest from the origin. Positively and negatively correlated cos2 for variables are shown as arrows on opposite sides of the plot centre. Variables with the largest cos2 values, and which therefore drive the separation of subjects on the PCA plot, are neutrophils, MAIT, Tc2, Th2, NK (including NK $CD56^{low}$) and NKT cells and eosinophils, monocytes, CD4, and $CD56^{high}$ NK cells.

Furthermore, to assess the potential impact of sex (female, male) (**Fig. 3.2.18 A**), weight (above 3.5 kg, below 3.5 kg) (**Fig. 3.2.18 B**), vaccination (No, Yes) (**Fig. 3.2.18 C**) and gestation at vaccination (above 30 wk, below 30wk, NA) (**Fig. 3.2.18 A**) on the cellular composition of peripheral blood in neonates, I performed PCA analysis using percentage-values from the cohort of healthy neonates and found no clustering based on these parameters, indicating that they did not significantly determine differences between individuals.

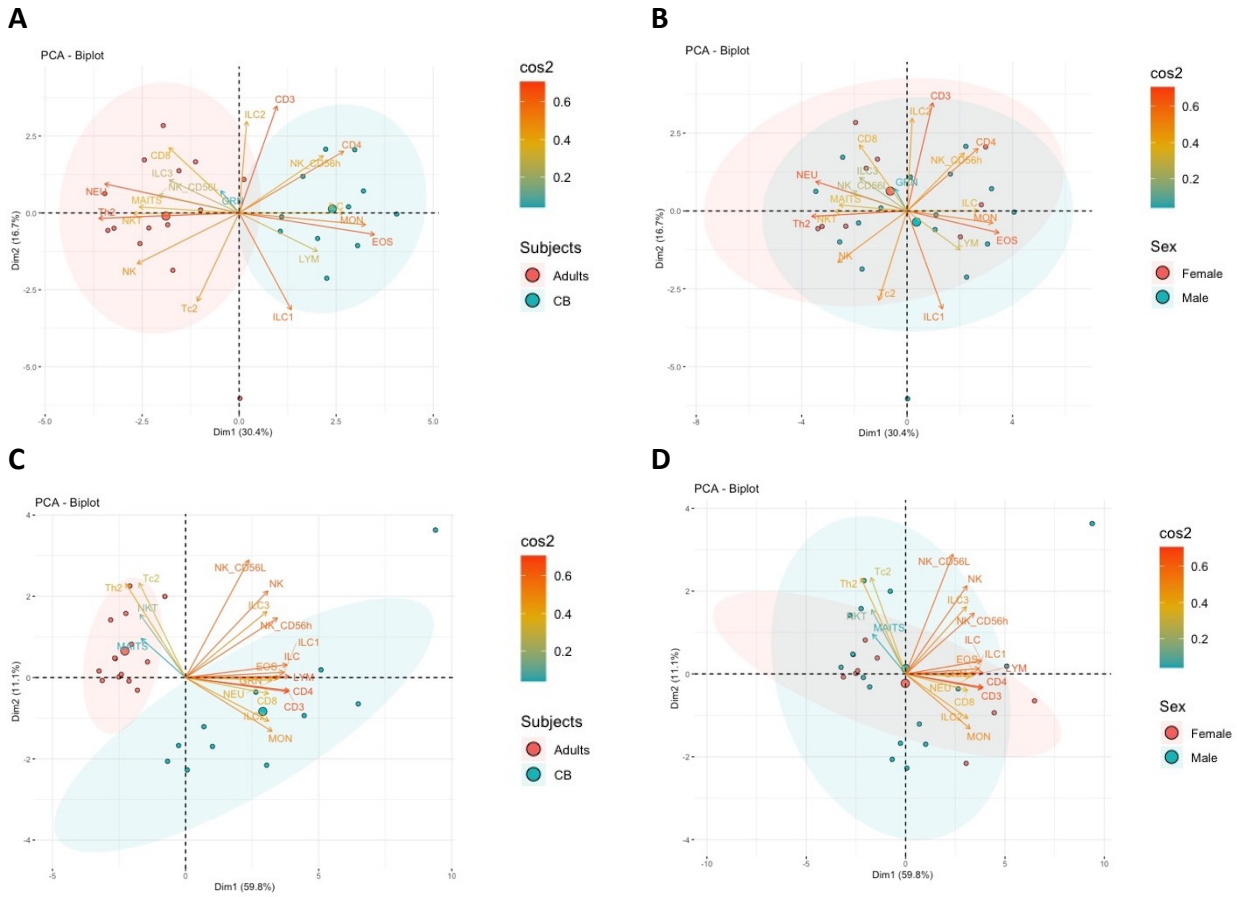


Figure 3.2.17 The separation healthy adults and neonates using PCA but not by differences in sex

Flow cytometric data are displayed as a Principal Component Analysis (PCA), where each individual (*n*=25) is plotted as a point and individuals that are similar are grouped together, comparing the cell frequencies **(A, B)** and total cell numbers **(C, D)** from healthy adults (*n*=14) and neonates (*n*=11) using the R programming language. The subject (Adult, CB) **(A, C**) and sex (Female, Male) **(B, D)** signatures of the cohort are shown. The group mean point (large circle) was added for each group during the process of 'habillage' PCA to depict the centre of each group. The point concentration ellipses (red and light blue) were added around each group mean point using a multivariant t-distribution where the size of the concentration ellipse is in normal probability (95% confidence). Variable correlation plots show the relationship between all variables (arrows). Positively correlated variables (arrows) were grouped together while negatively correlated variables (arrows) were positioned on opposite sides of the plot origin. The distance between variables (arrows) and the origin measures the size of the contribution of each variable to each dimension of PCA. Variables that are away from the origin are well represented on the PCA. The quality of representation on the variable (arrow) on the PCA is called cos2; the higher cos2 the better the representation of the variable. *Abbreviations used:* NEU – neutrophils, EOS – eosinophils, MON – monocytes, LYM – Lymphocytes, NK – natural killer cells, NKT – natural killer T cells, MAITs – mucosal invariant T cells, ILC – innate lymphoid cells, cos2 – square cosine, squared coordinates.

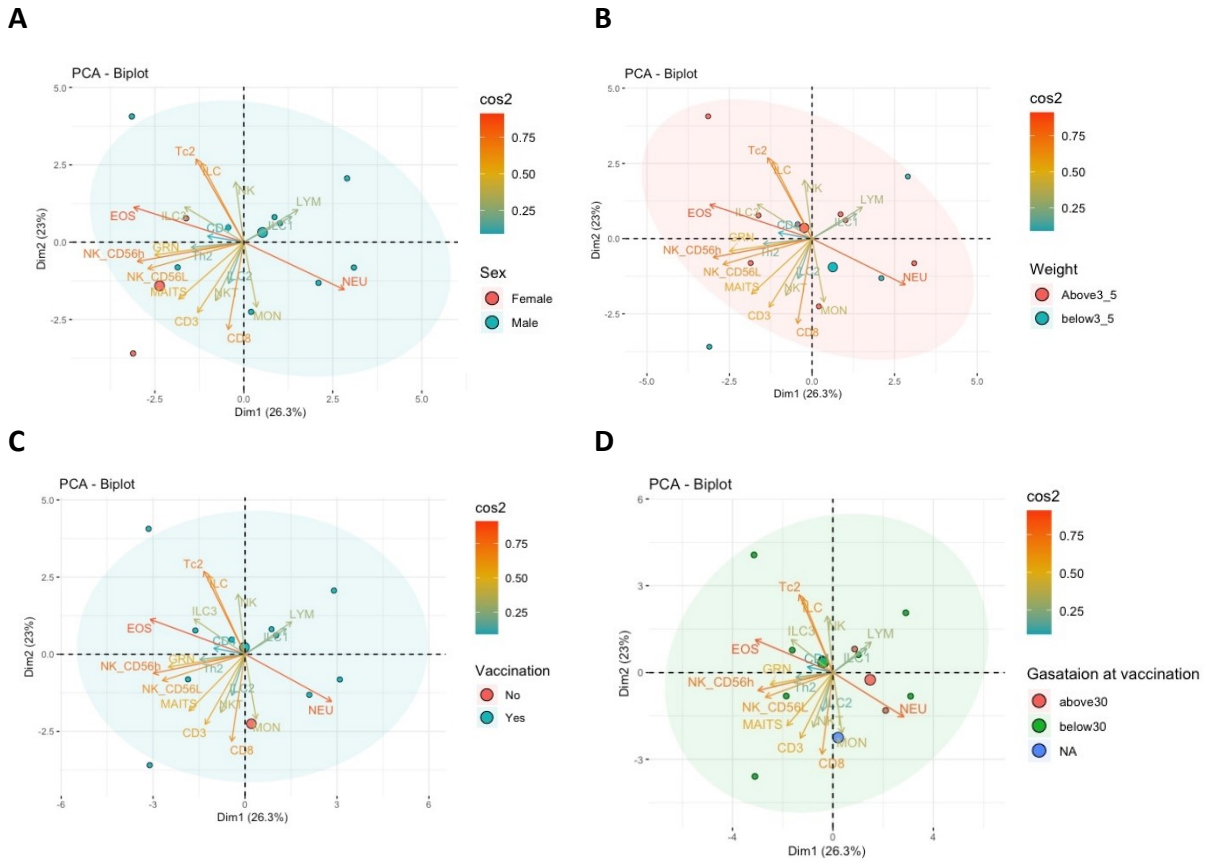


Figure 3.2.18 Neonates do not segregate using PCA by sex, weight, vaccination status and gestational age at vaccination.

(A) The sex (Female, Male), **(B)** weight (above 3.5 kg, below 3.5 kg), **(C)** vaccination (No, Yes) and **(D)** gestation at vaccination (above 30 wk, below 30wk, NA) signatures of the neonatal cohort (*n*=11) were delivered by comparing the frequencies of the cells from optimised OMIP [201] **(A, B, C, D)** using the R programming language. Data are displayed as a Principal Component Analysis (PCA), where each individual is plotted on the PCA as a point and individuals that are similar are grouped together to plot their contribution to the PCA. The group mean point was added for each group during the process of 'habillage' PCA to depict the centre of each group. The point concentration ellipses (red, green, light blue) were added around each group mean point using a multivariant t-distribution where the size of the concentration ellipse is in normal probability (95% confidence). Apart from the contribution of individuals to the plot, variable correlation plots show the relationship between all variables (arrows). Positively correlated variables (arrows) were grouped together while negatively correlated variables (arrows) were positioned on opposite sides of the plot origin. The distance between variables (arrows) and the origin measures the quality of the variables on PCA. Variables that are away from the origin are well represented on the PCA. The quality of representation on the variable (arrow) on the PCA is called cos2; the higher cos2 the better is the representation of the variable. *Abbreviations used*: NEU – neutrophils, EOS – eosinophils, MON – monocytes, LYM – Lymphocytes, NK – natural killer cells, NKT – natural killer T cells, MAITs – mucosal invariant T cells, ILC – innate lymphoid cells, NA – not available, cos2 – square cosine, squared coordinates, kg – kilogram, wk – week.

Taken together, heatmaps and PCA allowed unsupervised clustering of samples based on their cellular composition; however, PCAs showed the comprehensive contribution of each variable to drive the cohort diversity and also the impact of cells populations and other factors on the heterogeneity of the data. As seen in **Fig. 3.2.18 A-D**, I cannot see any variables responsible for driving the diversity in the neonatal cohort when sex, weight, vaccination status or age at vaccination were analysed.

Finally, to dissect potential associations between known clinical features (age, weight, gestation at vaccination, gestation at delivery) and different cell populations, correlation mapping was performed on the cohort of healthy adults (n=14) (**Fig. 3.2.19**) and neonates (**Fig. 3.2.20**) using R programming (Materials and Methods, Chapter 2, **Section 2.2.9.16**). In this analysis, data are displayed in a correlogram format, where positive correlations are displayed in blue and negative correlations in red colour. Colour intensity and the size of the circle are proportional to the correlation coefficients. For all graphs, the correlation matrix was not reordered according to hierarchical clustering. In B and D, correlations with *P*> 0.05 are considered insignificant and were left blank (**Fig. 3.2.19 B, D and Fig. 3.2.20 B, D**). Investigation of correlation in the healthy adults revealed positive correlations between age and Tc2 counts; Th2 and ILC, ILC1, ILC2 counts (**Fig. 3.2.19 B**).

In parallel, I investigated the correlation of cell populations in healthy neonates with clinical parameters (**Fig. 3.2.20 B, D**). A positive correlation was observed between Tc2 cell counts and Th2s, and ILC subsets and Th2s; a negative correlation between age and Tc2, CD8 and neutrophil counts; ILCs and granulocytes (neutrophils, eosinophils) and Th2s and ILCs counts (**Fig. 3.2.19 D**). Although, many correlations were established I focused on innate lymphoid cells and type-2 producing T cells which might be involved in skewing neonates towards type 2 immunity [20]. Interestingly, a great number of potential relationships were identified between immune cell counts but no relationships were found between weight, gestation at vaccination or gestation at delivery and counts of cell populations (except NKT cells and gestation at vaccination) (**Fig. 3.2.20 B**). Notably, Tc2 cell, NKT cell, ILC and CD8+ T cell frequencies were associated with gestation at vaccination (**Fig. 3.2.20 D**).

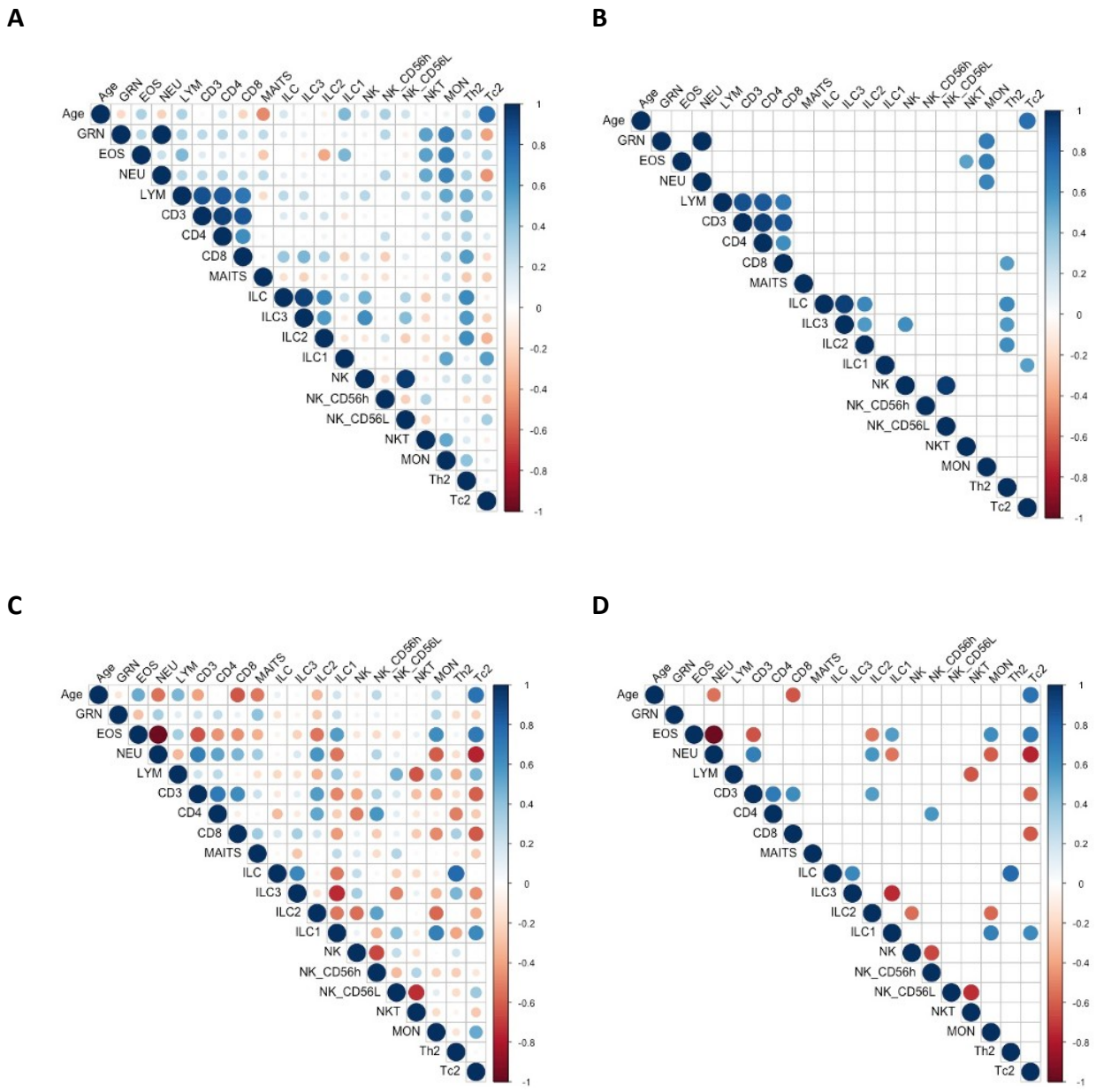


Figure 3.2.19 The correlation between the different cell populations in healthy adults.

The correlation between multiple variables from healthy adults (*n*=14) was derived by comparing total cell counts **(A, B)** or cell frequencies **(C, D)** in whole blood using Pearson parametric correlation test in the R programming language. Data are displayed in a correlogram format, where positive correlations are displayed in blue and negative correlations in red colour. Colour intensity and the size of the circle are proportional to the correlation coefficients. Additionally, on the right side of each correlogram, the legend colour depicts the correlation coefficients and the corresponding colours. The correlation matrix used for all graphs was not reordered according to hierarchical order. Correlations with $p > 0.05$ are considered insignificant and were left blank **(B, D)**. *Abbreviations used*: NEU – neutrophils, EOS – eosinophils, MON – monocytes, GRN – granulocytes, LYM – Lymphocytes, NK – natural killer cells, NKT – natural killer T cells, MAITs – mucosal invariant T cells, ILC – innate lymphoid cells, Th2– type-2 cytokine-producing CD4s, Tc2– type-2 cytokine-producing CD8s.

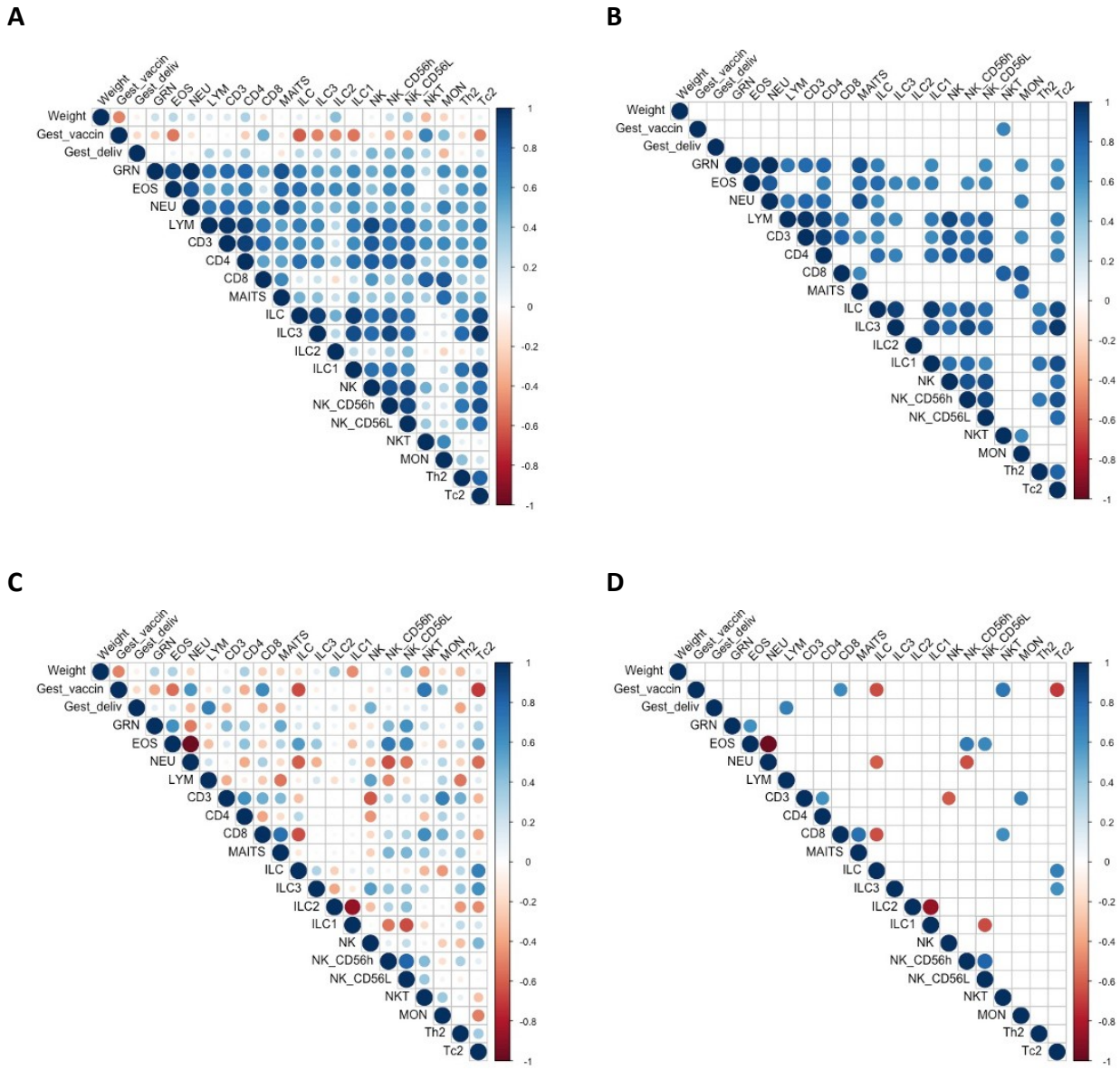


Figure 3.2.20 The correlation between the different cell populations in healthy neonates using correlograms.

The correlation dependence between multiple variables from cord blood from healthy neonates (*n*=11) was derived by comparing total cell counts **(A, B)** or cell frequencies **(C, D)** using Pearson parametric correlation test in the R programming language. Data are displayed in a correlogram format, where positive correlations are in blue and negative correlations are in red. Colour intensity and the size of the circle are proportional to the correlation coefficients. Additionally, in the right side of each correlogram, the legend colour depicts the correlation coefficients and the corresponding colours. The correlation matrix used for all graphs was not reordered according to hierarchical order. Correlations with $p > 0.05$ are considered insignificant and were left blank **(B, D)**. *Abbreviations used*: NEU – neutrophils, EOS – eosinophils, MON – monocytes, GRN – granulocytes, LYM – Lymphocytes, NK – natural killer cells, NKT – natural killer T cells, MAITs – mucosal invariant T cells, ILC – innate lymphoid cells, Th2 – type-2 cytokine-producing CD4s, Tc2 – type-2 cytokine-producing CD8s.

3.2.3.3. The functional phenotype of different innate and adaptive cells determined by intracellular staining for cytokine production

After the enumeration of different immune populations in peripheral and cord blood, the functional phenotype of immune cells was assessed to determine differences between adults and neonates regarding the production of IFN-γ, IL-13, IL-17A and IL-22, the main ILC-related cytokines [230]. 2.5 x 10^6 cells PBMCs from healthy adults and neonates were stimulated for at least 3 hours at 37°C in the stimulation cocktail of ionomycin (1 µg/mL), PMA (50 ng/mL) and GolgiPlug™. The unstimulated, negative control was prepared by adding just DMSO. After stimulation, detection of cytokine-producing cells was performed by staining with an optimized flow cytometry panel (**Fig. 3.2.3 I and II**) as described in Chapter 3.2 (Material and Methods, **Section 2.2.9.1.2-4**).

3.2.3.3.1. Cytokine production (ICS) panel study population

The functional differences in the production of IFN-γ, IL-13, IL-17A and IL-22 were determined using the ICS cohort (*n*=19) in frozen PBMCs from healthy adults (n=9) and neonates (n=10) (**Table 3.2.7**). In this cohort females and males were well represented (*P*=0.3698) with the median age of adults ±38.2 years (26.0-62.0). In neonatal patients, more clinical data was available (sex, weight, gestation at the delivery, *Bordetella pertussis* vaccination and gestation at vaccination) (*n*=10, **Table 3.2.8**). For this study group, the neonatal blood samples were collected from term children (*n*=10, 100%) delivered at ±38.227 (30.43-40.14) weeks at gestation in the Neonatal Unit at St. Mary's hospital. 70% of mothers were vaccinated during week ±29.11 (20.71-37.00) of pregnancy. The proportion of females was 30% in the neonatal cohort with no significant difference in weight between females and males (3.51 and 3.62 kg, respectively).

	Adults	Neonates (CB)	
Characteristic	*n*=9	*n*=10	*P* value
Age (years), median, (range)	38.2 (26.0-62.0)	0	**0.0001**
Sex, *n*			0.3698
Females	5	3	
Males	4	7	

Table 3.2.7 Adults and neonates' demographics used in the optimised IFN-γ, IL-13, IL-22, IL-17A ICS flow cytometry panel.

Healthy adults and neonates used for stimulation of PBMCs and the cytokine production (ICS) flow cytometry analysis for IFN-γ, IL-13, IL-17A and IL-22. Patient demographics and clinical information were obtained from the patients' information sheets. Statistical significance was obtained using the Mann-Whitney test for continuous data and Fisher's exact test for categorical data. No adjustment was made for multiple testing. *P* values for continuous data were computed by Mann-Whitney test while *P* values for categorical data were computed by Fisher's exact test. The range is defined as the difference between the highest and lowest value. *Abbreviations used*: CB – cord blood.

	Neonates (CB)
Characteristic	*n*=10
Age (years), Median (range)	0
Sex, *n* (%)	
Females	3 (30)
Males	7 (70)
Weight (kg), Median, (range)	
Females	3.51 (4.16-2.64)
Males	3.62 (4.38-3.14)
Premature, *n* (*%*)	
Yes	0 (0)
No	10 (100)
Birthplace, *n* (*%*)	
NU	10 (100)
NICU	0 (0)
Gestation at delivery, wk, Median (range)	38.27 (40.14-30.43)
Pertussis Vaccination during pregnancy (*%*)	
Yes	7 (70)
No	3 (30)
Gestation at vaccination, wk, median (range)	29.11 (37-20.71)

Table 3.2.8 Neonates demographics and clinical data used in the optimised IFN-γ, IL-13, IL-22, IL-17A flow cytometry panel.

Neonates demographic and clinical information were obtained from the neonatal unit. The range is defined as the difference between the highest and lowest value. *Abbreviations used*: CB – cord blood, NU – Neonatal Unit, NICU – Neonatal Intensive Care Unit, wk – week, kg – kilogram

3.2.3.3.2. The functional phenotype of innate cell populations in healthy adults and neonates

IFN-γ, IL-13, IL-17A and IL-22 production in circulating NKs and ILCs (ILC1s, ILC2s, ILC3s)

Although cord blood studies suggest there are differences in the frequency of ILCs (including NK cells) between neonates and adult [188], the functional differences between these two cohorts have not been well explored. To get better insights into functional differences between NK cells (**Fig. 3.2.21**) and ILCs populations (**Fig. 3.2.22**), intracellular staining (ICS) was carried out on PBMCs from healthy adult volunteers (n=9) and neonates (n=10) (peripheral and cord blood, respectively). **Figure 3.2.21 A** shows an example of flow cytometry for IFN-γ, IL-13, IL-17A and IL-22 expressing NK cells and total ILCs in PBMCs while **Figure 3.2.22 A** shows IFN-γ, IL-13, IL-17A and IL-22 expressing ILC1s, ILC2s and ILC3s. Lymphocytes were defined within live, single cells using FSC-A and SSC-A. Within the lymphocyte gate, NK cells were gated as $CD56^{+}CD3^{-}$ cells**.** ILCs were delineated within live, single lymphocytes as lineage negative (CD3, CD14, CD19, CD56, CD123 and FcεRIα)$^{-}$ and $CD127^{+}$ (IL-7 receptor-α) cells. Among NK cells and ILCs the populations of IFN-γ, IL-13, IL-17A and IL-22 positive cells were gated. Among ILCs, ILC1, ILC2 and ILC3 were

identified using CRTH2 and CD117 (c-Kit) surface markers; ILC1 cells were defined as $CD117^{-}CRTH2^{-}$, ILC2 cells as $CRTH2^{+}$ $CD117^{int}$ and ILC3 as $CD117^{+}CRTH2^{-}$. Among ILC1s, ILC2s and ILC3s the populations of IFN-γ, IL-13, IL-17A and IL-22 positive cells were identified.

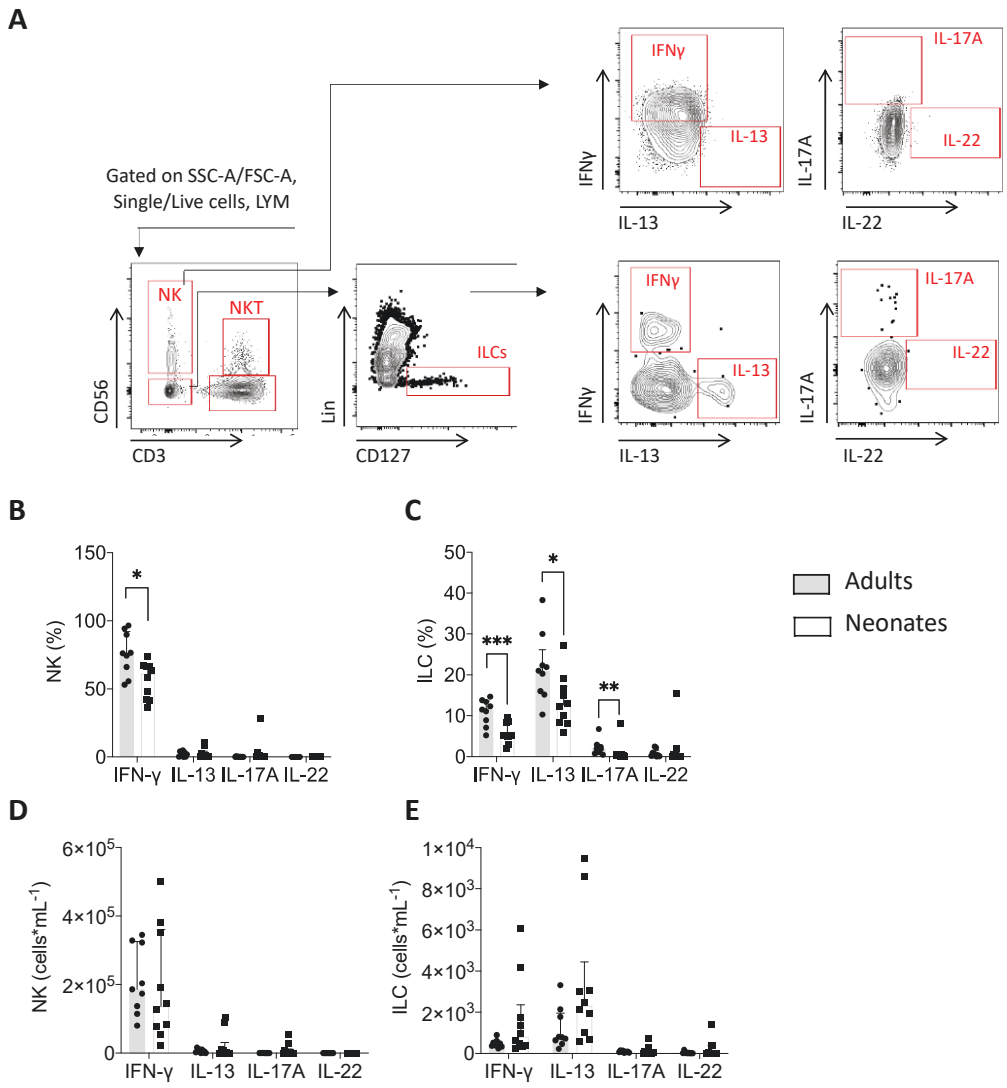


Figure 3.2.21 Comparison of production of signature cytokines in stimulated NKs and ILCs from healthy adult and neonate PBMCs.

PBMC were isolated using Lymphopure® from the blood of healthy adult volunteers (*n*=9) or cord blood of neonates (*n*=10) as described in the Material and Methods. After stimulation of PBMCs with PMA, and ionomycin in the presence of GolgiPlug®, cells were analysed for their cytokine profile using an optimised intracellular staining (ICS) flow cytometry panel. **(A)** An example of flow cytometry for IFN-γ, IL-13, IL-17A and IL-22 expressing NK cells and total ILC in PBMCs**.** Data are from one experiment but represent more than 20 experiments with similar results. Lymphocytes were defined within live, single cells using FSC-A and SSC-A. Within the lymphocyte gate, NK and NKT-like cells were gated as $CD56^{+}CD3^{-}$ and $CD56^{+}CD3^{+}$ cells, respectively**.** ILCs were delineated within live, single, lineage negative (CD3, CD14, CD19, CD56, CD123 and FcεRIα)$^{-}$ and $CD127^{+}$ (IL-7 receptor-α) cells. Among NK cells and ILCs the populations of IFN-γ, IL-13, IL-17A and IL-22 positive cells were gated using a biaxial gating strategy. Frequency of $CD56^{+}CD3^{-}$ NK cells expressing IFN-γ, IL-13, IL-17A and IL-22 **(B)** and Lin^{-} $CD127^{+}$ ILCs expressing IFN-γ, IL-13, IL-17A and IL-22 **(C)**. Quantification of total $CD56^{+}CD3^{-}$ NK cells expressing IFN-γ, IL-13, IL-17A and IL-22 **(D)** and Lin^{-} $CD127^{+}$ ILCs expressing IFN-γ, IL-13, IL-17A and IL-22 **(E)** among live, single lymphocytes. Data are from 9 (adults) or 10 (neonates) experiments with one subject in each shown as the median with upper interquartile range **(B-E)**. Differences between groups were estimated by Mann-Whitney test (* $p < 0.05$, ** $p < 0.01$ and *** $p < 0.001$).

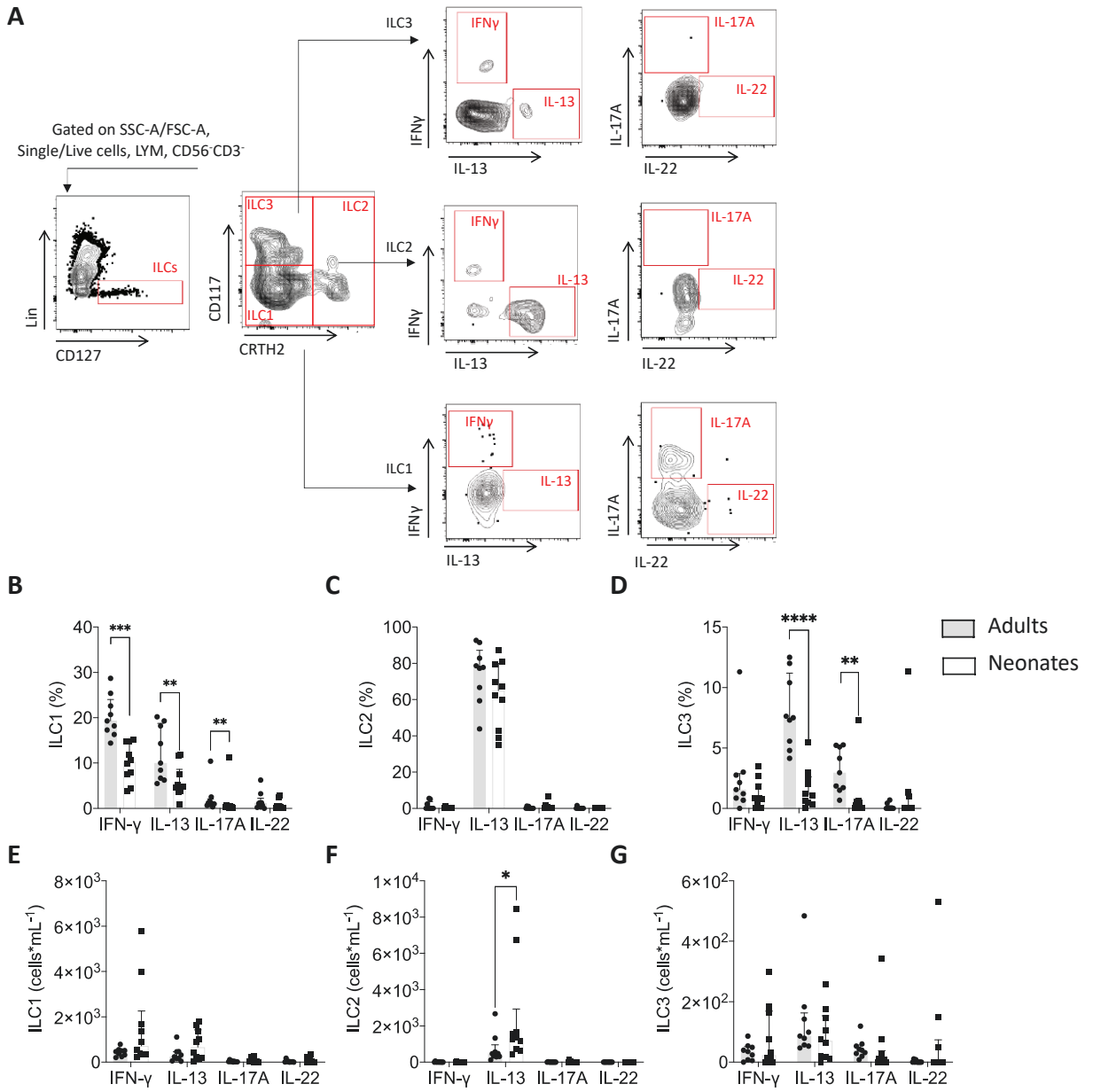


Figure 3.2.22 Comparison of production of signature cytokines in stimulated ILC populations (ILC1s, ILC2s and ILC3s) from healthy adult and neonate PBMCs.

PBMC were isolated using Lymphopure® from the blood of healthy adult volunteers (*n*=9) or cord blood of neonates (*n*=10) as described in the Material and Methods. After stimulation of PBMCs with PMA, and ionomycin in the presence of GolgiPlug®, cells were analysed for their cytokine profile using an optimised intracellular staining (ICS) flow cytometry panel. **(A)** An example of flow cytometry for IFN-γ, IL-13, IL-17A and IL-22 expressing ILC1s, ILC2s and ILC3s in PBMCs**.** Data are from one experiment but represent more than 20 experiments with similar results. Lymphocytes were defined within live, single cells using FSC-A/SSC-A. ILCs were delineated within live, single, lineage negative (CD3, CD14, CD19, CD56, CD123 and FcεRIα)$^-$ and CD127$^+$ (IL-7 receptor-α) cells. The ILC subsets (ILC1, ILC2 and ILC3) were identified using CRTH2 and CD117 (c-Kit) surface markers; ILC1 cells were defined as CD117$^-$CRTH2$^-$, ILC2 cells as CRTH2$^+$ CD117^{int} and ILC3 as CD117$^+$CRTH2$^-$. Among ILC1s, ILC2s and ILC3s the populations of IFN-γ, IL-13, IL-17A and IL-22 cells were gated using a biaxial gating strategy. Frequency of CD117$^-$CRTH2$^-$ ILC1s expressing IFN-γ, IL-13, IL-17A and IL-22 **(B)**, CRTH2$^+$ CD117^{int} ILC2s expressing IFN-γ, IL-13, IL-17A and IL-22 **(C)** and CD117$^+$CRTH2$^-$ ILC3s expressing IFN-γ, IL-13, IL-17A and IL-22 **(D)** among Lin$^-$ CD127$^+$ ILCs. Quantification of total CD117$^-$CRTH2$^-$ILC1s expressing IFN-γ, IL-13, IL-17A and IL-22 **(E)**, CRTH2$^+$ CD117^{int} ILC2s expressing IFN-γ, IL-13, IL-17A and IL-22 **(F)** and CD117$^+$CRTH2$^-$ ILC3s expressing IFN-γ, IL-13, IL-17A and IL-22 **(G)** among live, single lymphocytes. Data are from 9 (adults) or 10 (neonates) experiments with one subject in each shown as the median with upper interquartile range **(B-G)**. Differences between groups were estimated by Mann-Whitney test (ns, not significant; * $p < 0.05$, ** $p < 0.01$ and *** $p < 0.001$).

Stimulation of adult PBMCs resulted in significantly higher frequencies of IFN-γ-producing NK cells (76.2%, *P*=0.0161) and ILCs (11.5%, *P*=0.0015) compared to cord blood cells (**Fig. 3.2.21 B and C**). Furthermore, the frequencies of IL-13 and IL-17 producing ILCs were higher in adult subjects (*P*=0.017 and *P*=0.041, respectively). No differences were observed in the cell numbers for IFN-γ, IL-13, IL-17A and IL-22 producing NK cells and ILCs between adult and cord blood cells (**Fig. 3.2.21 D and E**). Among ILCs, the ILC1 subset was characterised by higher production of IFN-γ in adults (19.3%) compared to neonates (10.2%) (*P*=0.002, **Fig. 3.2.22 B**). IL-13 producing ILC2s were more abundant in neonates (*P*=0.0172, with a median of 1.31 $x10^3$ cells per mL in neonates and 4.72 x 10^2 cell per mL in adults) whereas the frequency of IL-13 production in ILC2s was comparable to adults (*P*=0.211) suggesting that ILC2s are the most functionally mature subset of all ILCs in neonates (**Fig. 3.2.22 C and F**). Finally, the numbers of ILC3s producing IFN-γ, IL-13, IL-17A, and IL-22 were comparable between adults and neonates (**Fig. 3.2.22 G**); however, the frequencies of IL-13 and IL-17 production in ILC3s were significantly higher among adults (*P*<0.0001 and *P*=0.002, respectively).

3.2.3.3.3. The functional phenotype of other lymphocyte populations in healthy adults and neonates

IFN-γ, IL-13, IL-17A and IL-22 production in circulating NKT, $CD4^+$ and $CD8^+$ T cells

Finally, the production of IFN- γ, IL-13, IL-17A, and IL-22 were assessed in NKT, $CD4^+$ and $CD8^+$ T cells using the gating strategy shown in **Figure 3.2.23 A**. NKT cells were gated within the lymphocyte gate as $CD56^+CD3^+$ cells. T lymphocytes ($CD3^+CD56^-$) were segregated into $CD4^+$ or $CD8^+$ T cells. Among NKT, $CD4^+$ or $CD8^+$ T cells, the populations of IFN-γ, IL-13, IL-17A and IL-22 producing cells were identified. Adult $CD4^+$ T cells produced significantly more IFN-γ (*P*<0.0001), IL-13 *P*<0.0001) and IL-17A (*P*=0.0021) compared to neonates (**Fig. 3.2.23 C**). Similarly, around 40% of $CD8^+$ T cells were able to express IFN-γ compared to 5% in their neonatal counterparts (*P*<0.0001, **Fig. 3.2.23 D**). The number of $CD4^+$ T cells producing IFN-γ, IL-13, IL-17A and IL-22 was significantly higher in adults (**Fig. 3.2.23 F**). IFN-γ $CD8^+$ T cells were the most abundant among $CD8^+$ T cells (with a median of 3.34 $x10^5$ cells per mL in adults and 1.93 x 10^4 cells per mL in new-borns) (*P*<0.0001, **Fig. 3.2.23 G**).

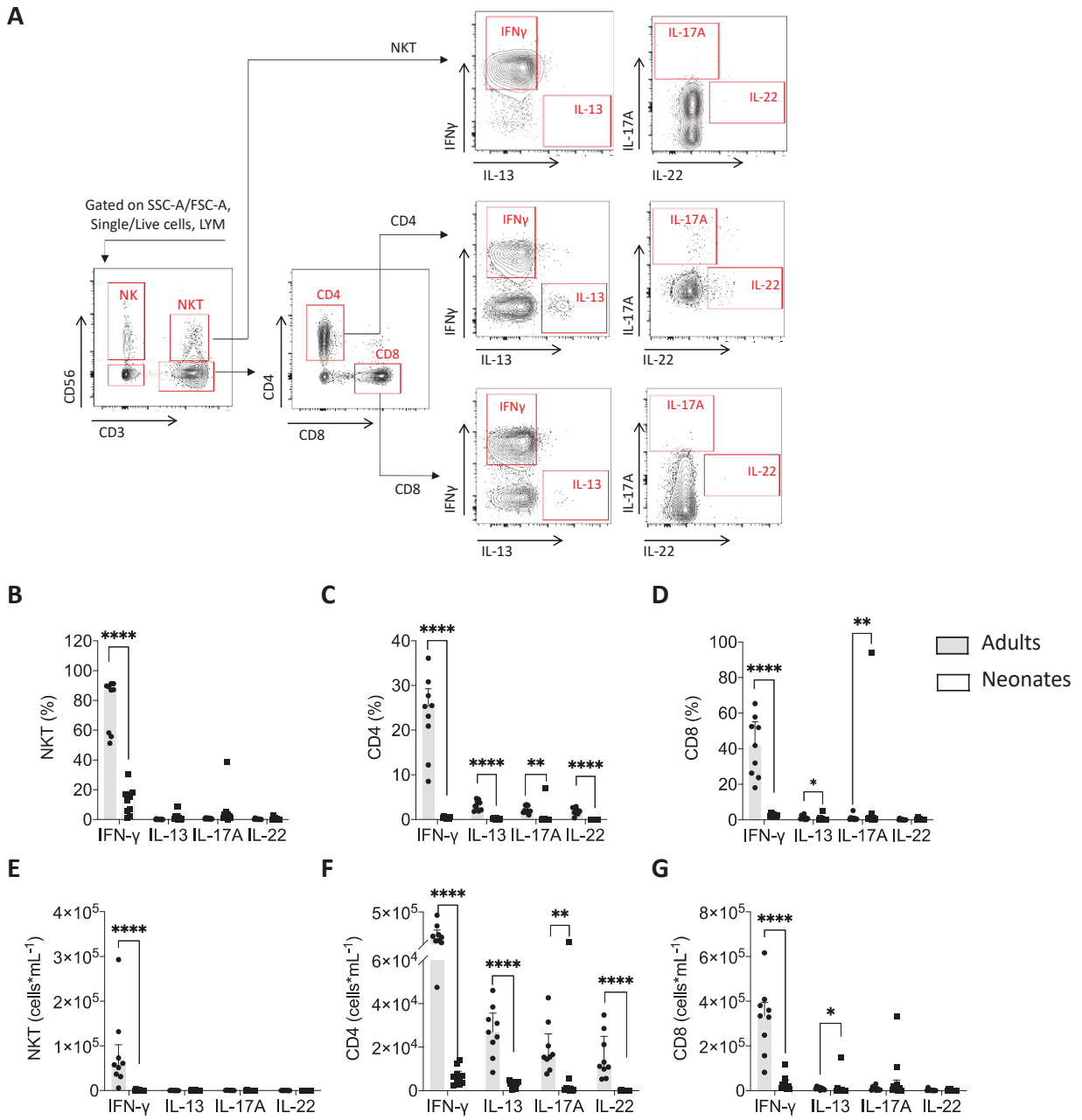


Figure 3.2.23 Comparison of production of signature cytokines in stimulated NKT, CD4$^+$ and CD8$^+$ T cells from healthy adult and neonate PBMCs.

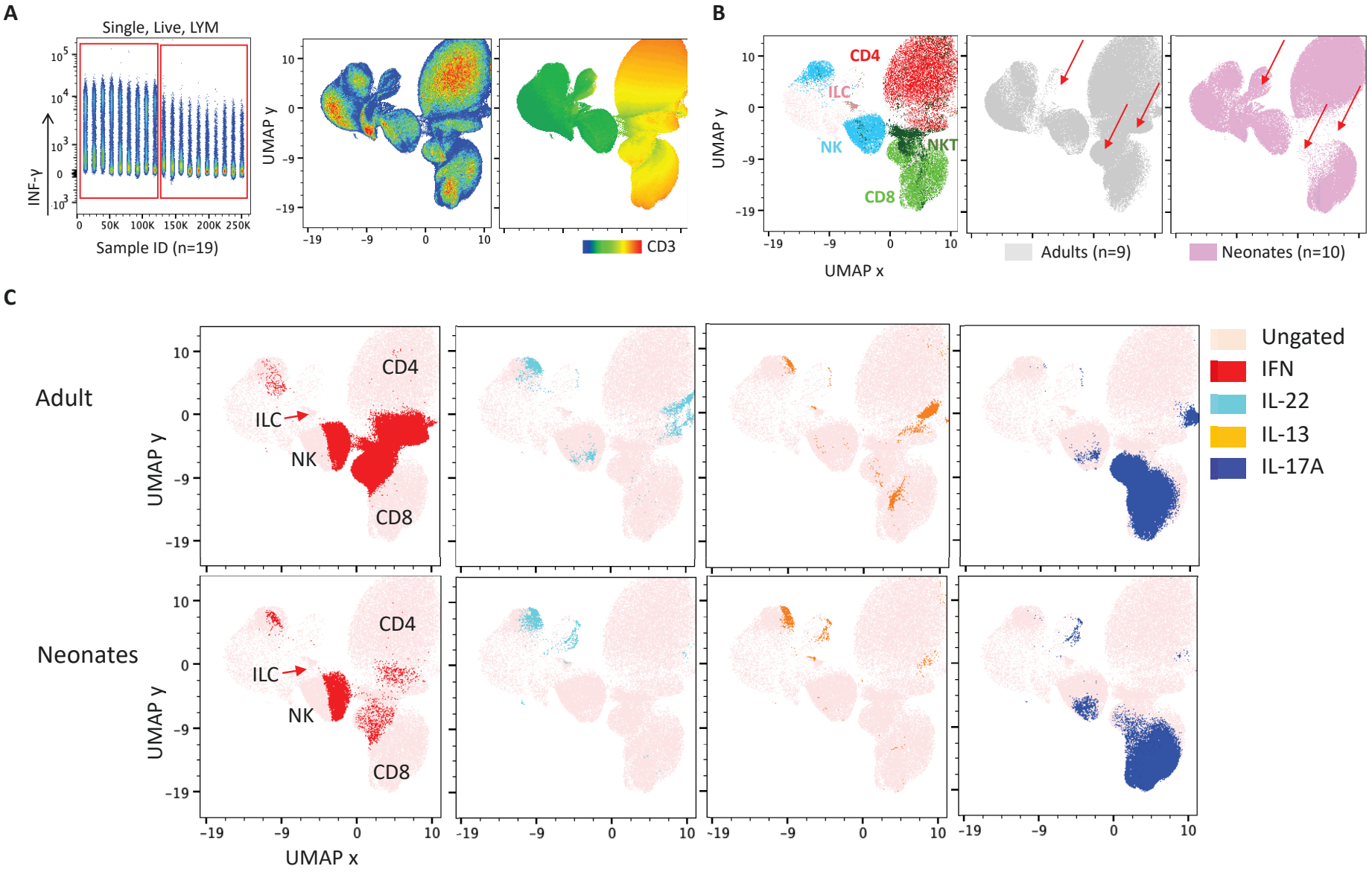
PBMC were isolated using Lymphopure® from the blood of healthy adult volunteers (*n*=9) or cord blood (*n*=10) as described in the Material and Methods chapter. After stimulation of PBMCs with PMA, and ionomycin in the presence of GolgiPlug®, cells were analysed for their cytokine profile using an optimised intracellular staining (ICS) flow cytometry panel. **(A)** An example of flow cytometry for IFN-γ, IL-13, IL-17A and IL-22 expressing NKT, CD4$^+$ or CD8$^+$ T cells in PBMCs. Data are from one experiment but represent more than 20 experiments with similar results. Lymphocytes were defined within live, single, cells using FCS-A/SSC-A. NK and NKT-like cells were gated within the lymphocyte gate as CD56$^+$CD3$^-$ and CD56$^+$CD3$^+$ cells, respectively**.** T lymphocytes (CD3$^+$CD56$^-$) were segregated into CD4$^+$ or CD8$^+$ T cells. Among NKT, CD4$^+$ or CD8$^+$ T cells, the populations of IFN-γ, IL-13, IL-17A and IL-22 cells were gated using biaxial gating. Frequency of CD56$^+$CD3$^+$ NKT cells expressing IFN-γ, IL-13, IL-17A and IL-22 **(B)**, CD56$^-$CD3$^+$CD4$^+$ T cells expressing IFN-γ, IL-13, IL-17A and IL-22 **(C)** and CD56$^-$CD3$^+$CD8$^+$T cells expressing IFN-γ, IL-13, IL-17A and IL-22 **(D)** among live, single, lymphocytes. Quantification of total CD56$^+$CD3$^+$ NKTs expressing IFN-γ, IL-13, IL-17A and IL-22 **(E)**, CD56$^-$CD3$^+$CD4$^+$ T cells expressing IFN-γ, IL-13, IL-17A and IL-22 **(F)** and CD56$^-$CD3$^+$CD8$^+$T cells expressing IFN-γ, IL-13, IL-17A and IL-22 **(G)**. Data are from 9 (adults) or 10 (neonates) experiments with one subject in each shown as the median with upper interquartile range **(B-G)**. Differences between groups were estimated by Mann-Whitney test (* $p < 0.05$, ** $p < 0.01$ and **** $p < 0.0001$). *Abbreviations used:* LYM – lymphocytes, NK – natural killer cells, NKT – natural killer T cells, IL – interleukin, IFN – interferon.

3.2.3.3.4. Assessment of the functional phenotype of circulatory cell populations by UMAP

To gain more insight into functional phenotypes of circulatory cells and ILC (including NK cells), I applied the deep immune phenotyping technique UMAP[204] to the flow cytometry data ICS cohort of healthy adults (*n*=9) and neonates (*n*=10). This analysis allowed me to reduce 15 dimensions (13 colours including FSC-A and SSC-A, **Table 3.1.1**) into two dimensions referred to as UMAPx and UMAPy (**Fig. 3.2.24 A,** middle). Firstly, data were cleaned using standard biaxial gating to include only single, live lymphocytes (**Fig. 3.2.24 A,** left). Lymphocytes were gated using SSC-A and FSC-A. After data cleaning, I performed a UMAP analysis on 570,000 randomly selected lymphocytes (30,000 from each subject concatenated into a single file). These cells can be seen to highly express the CD3 cell marker (**Fig. 3.2.24 A**, right). The manual gating strategy from the ICS panel was utilised to classify global UMAP clusters into the following cell types: CD4 T cells (red), NKT cells (dark green), CD8 T cells (light green), NK cells (blue), ILCs (light brown) (**Fig. 3.2.24 B**). UMAP representations of data highlighted the main differences between cell clusters among adults (grey) and neonates (pink) (**Fig. 3.2.24 B**) in the region of NKT cells, $CD8^+$ and $CD4^+$ T cells. A UMAP map found major regions enriched in adults, but not neonates, with high expression of IFN-γ (red), IL-13 (orange), IL-17A (blue) and IL-22 (light blue) in CD4 and CD8 T cell clusters (**Fig. 3.2.24 C**). Notably, NK cells from adults were highly similar to neonates as they produced the same level of IFN-γ (red) (**Fig. 3.2.24 C**). As mentioned before, UMAP clusters allows not only visualisation of differences in the cell composition but also phenotypical changes in the cell clusters among cohort participants showing that there are changes in the immunomes of adults and neonates (**Fig. 3.2.24 D, E**).

To further define and improve visualisation of differences in the ILCs (including NK cells) in different subjects, I performed UMAP immunophenotyping on 380,000 single, live, $CD3^-$, lin^- lymphocytes (20,000 cells per subject) (**Fig. 3.2.25 A**). This improved visualisation utilised the same cohort as used in **Figure 3.2.24** and the manual gating strategy from the ICS panel (**Fig. 3.2.3**) to classify clusters into the following cell types: NK cells (blue), ILC1s (green), ILC2s (orange), ILC3s (light green) (**Fig. 3.2.25 B**). This UMAP (**Fig. 3.2.25 A**) showed subtle differences to exist in IFN-γ producing cells even though NK cells from adults seem to be similar to neonates (**Fig. 3.2.25 C**). Notably, ILC2s were characterised by robust IL-13 responses in both cohorts. A region of this UMAP corresponding to IL-22+ ILC3s was enriched in in neonates. Finally, UMAP found the changes not only in the cell composition but depicted the phenotypical changes in the

same cell clusters among each of the cohort participants suggesting that immunomes of adults and neonates were different (**Fig. 3.2.25 D, E**).


A
Single, Live, LYM
INF-γ
Sample ID (n=19)
UMAP y
CD3
B
CD4
ILC
NK
NKT
CD8
UMAP x
Adults (n=9)
Neonates (n=10)
C
Adult
Neonates
Ungated
IFN
IL-22
IL-13
IL-17A
UMAP y
UMAP x

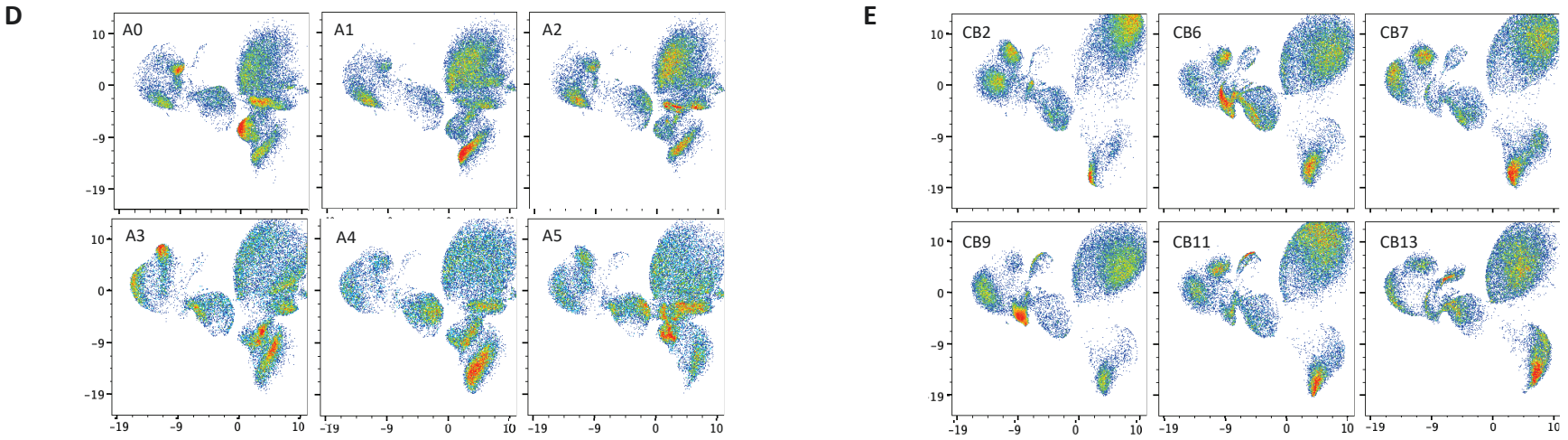
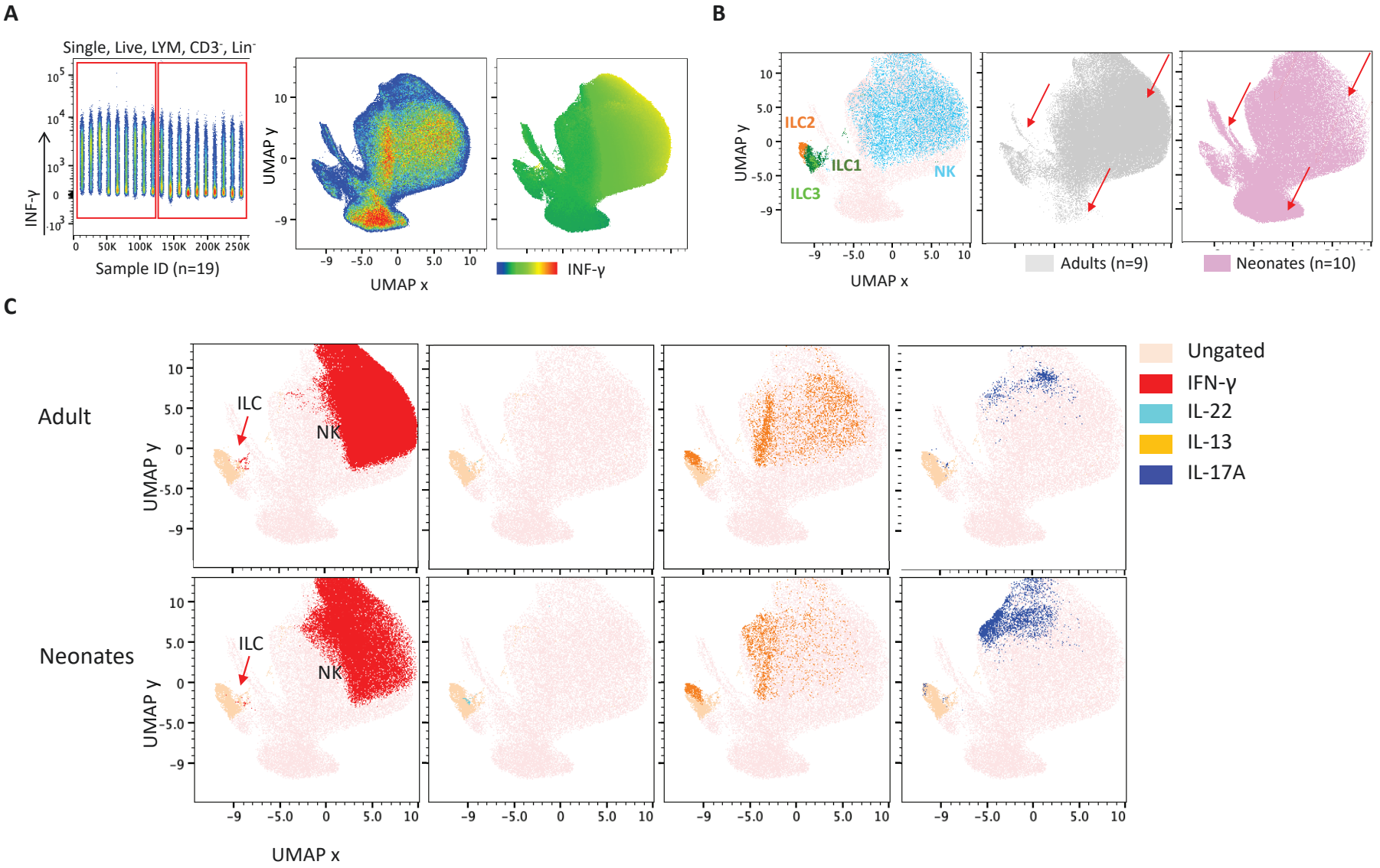


Figure 3.2.24 Deep immune phenotyping of stimulated ILCs (including NK cells), NKT cells and other T cell populations in adult and neonate PBMCs using UMAP reveals alterations in cytokine production

(A) Representative manual gating strategy utilised for immune phenotyping using the ICS panel. Cells were delineated using the following gating strategy: FSC/SSC, single, live cells. Lymphocytes were gated using SSC-A and FSC-A. 30,000 randomly selected lymphocytes from each subject (*n*=19, left) were concatenated into a single file containing 570,000 cells for UMAP analysis (middle). The intensity of the CD3 expression marker was used to identify T lymphocytes (right). **(B)** The manual gating strategy from the ICS panel was utilised allowing global UMAP clusters (all subjects pooled, left) to be classified into the following cell types: CD4 T cells (red), NKT cells (dark green), CD8 T cells (light green), NK cells (blue), ILCs (light brown). Comparison of UMAP representations of clusters for healthy adult subjects (*n*=9, middle) and neonates (*n*=10, right). The main differences between cell clusters among adults (grey) and neonates (pink) are depicted using the same orientated red arrows. **(C)** Simplified UMAP projections indicating the differences in the production of IFN-γ (red), IL-13 (orange), IL-17A (blue) and IL-22 (light blue) in ILC, NK cells, CD4 and CD8 T cell clusters from adults (*n*=9) and neonates (*n*=10). UMAP visualisation of single, live, lymphocytes in individual adults **(D)** and neonates **(E)** allowed depiction of differences between all subjects. Abbreviations used: LYM – Lymphocytes, NK – natural killer cells, NKT – natural killer T cells, ILC – innate lymphoid cells, UMAP – Uniform Manifold Approximation and Projection, IL – interleukin, IFN – interferon.


A
Single, Live, LYM, CD3-, Lin-
INF-γ
Sample ID (n=19)
UMAP y
UMAP x
INF-γ
B
ILC2
ILC1
ILC3
NK
UMAP y
UMAP x
Adults (n=9)
Neonates (n=10)
C
Adult
Neonates
ILC
NK
UMAP y
UMAP x
Ungated
IFN-γ
IL-22
IL-13
IL-17A

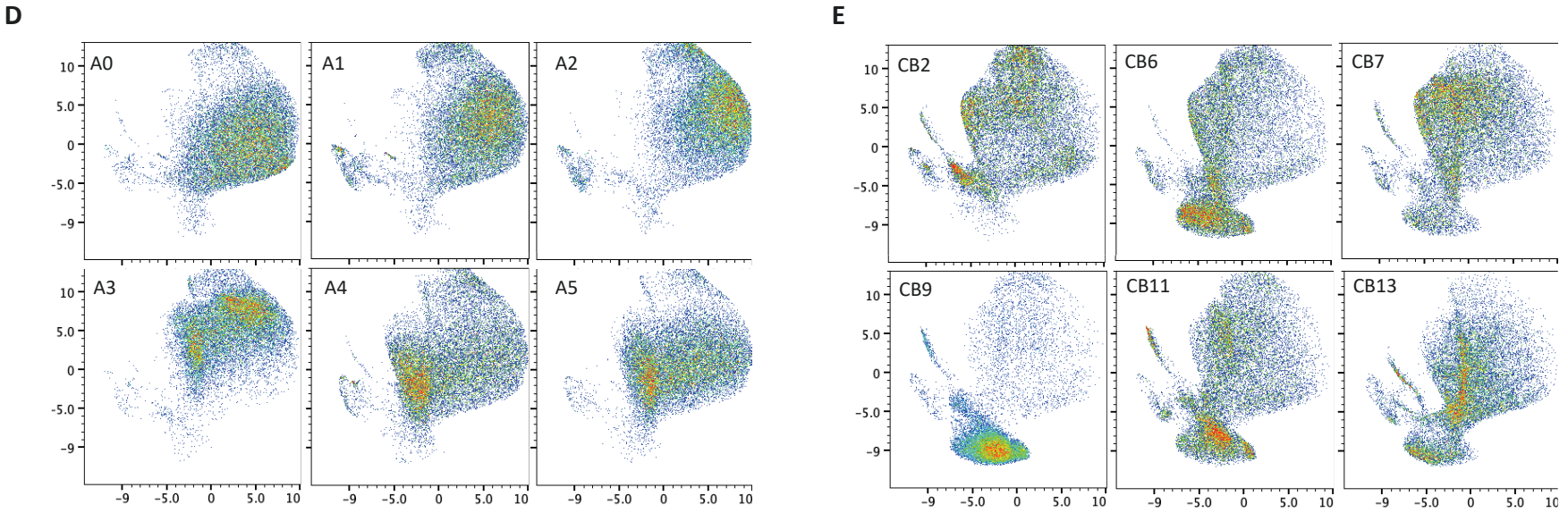


Figure 3.2.25 Deep immune phenotyping of stimulated ILCs (ILC1s, ILC2s and ILC3s) and NK cells in adult and neonate PBMCs using UMAP reveals alterations in the cytokine production.

(A) Representative manual gating strategy utilised for deep immune phenotyping using the ICS panel. Cells were delineated using the following gating strategy: FSC/SSC, single, live cells. Cells were gated using SSC-A/FSC-A, $CD3^-$, Lin^- lymphocytes. 20,000 randomly selected cells from each subject (*n*=19, left) were concatenated into a single file containing 380,000 cells for UMAP analysis (middle). The intensity of IFN-γ expression marker was used to identify IFN-γ^+ lymphocytes (right). **(B)** The manual gating strategy from the ICS panel was utilised allowing global UMAP clusters (all subjects pooled, left) to be classified into the following cell types: NK cells (blue), ILC1s (green), ILC2s (orange), ILC3s (light green). Comparison of UMAP representations of clusters for only healthy adult subjects (*n*=9, middle) and neonates (*n*=10, right). The main differences between cell clusters among adults (grey) and neonates (pink) are depicted using the same orientated red arrows. **(C)** Simplified UMAP projections indicating the differences in the production of IFN-γ (red), IL-13 (orange), IL-17A (blue) and IL-22 (light blue) in ILC1s, ILC2s, ILC3s and NK cell clusters from only adults (*n*=9) and neonates (*n*=10). UMAP visualisation of single, live, $CD3^-$, Lin^- lymphocytes in individual adults **(D)** and neonates **(E)** allowed depiction of differences between all subjects. Abbreviations used: LYM – Lymphocytes, NK – natural killer cells, NKT – natural killer T cells, ILC – innate lymphoid cells, UMAP – Uniform Manifold Approximation and Projection, IL – interleukin, IFN – interferon

3.2.3.3.5. Assessment of circulatory immune cell populations and their correlations utilising R function

In parallel with functional immunophenotyping in adults and neonates using manual and augmented panels (ICS and UMAP analysis, respectively), I employed heatmaps and principal component of analysis (PCA) in the R programming language to better define and identify the differences between adult and cord blood. They again helped me to define and identify the differences between cell populations in circulatory and cord blood. Both techniques are visualisation techniques that can show the similarities and differences between *n*-number of variables using colour in two dimensions. In heatmaps data are expressed using a colour scale allowing simultaneous visualisation of individuals (samples) and their features (variables).

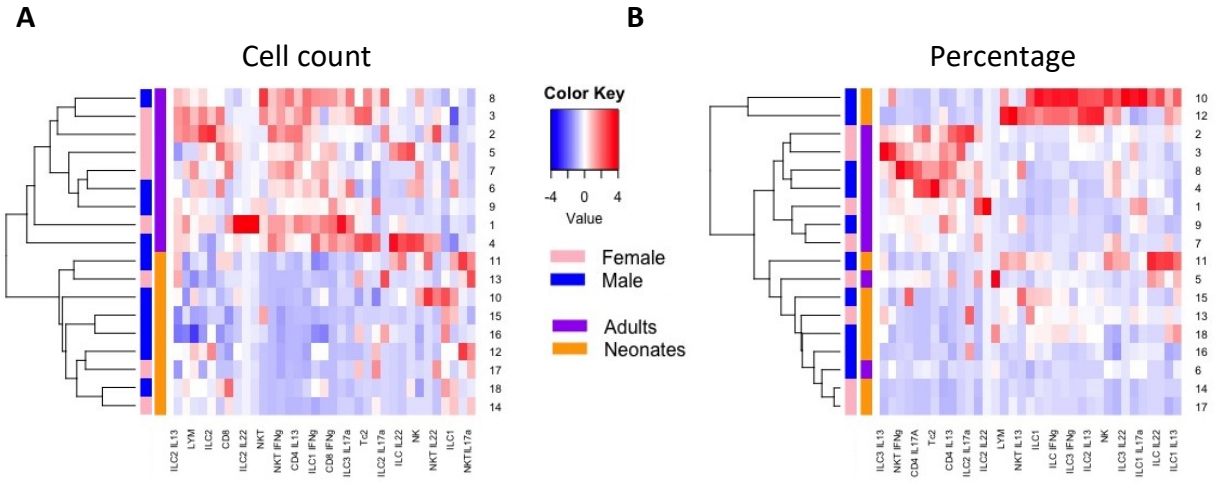


Figure 3.2.26 The hierarchical clustering of subjects in the ICS cohort of healthy adults and neonates using heatmap format.

The ICS cohort signatures (*n*=19) were delivered by comparing total cell counts **(A)** and frequencies **(B)** from healthy adults (*n*=9) and neonates (*n*=10) using the R programming language. Data are displayed in a heatmap format, where each row represents an individual (sample) (Adults 1-9 and Neonates 10-19) and each column represents the cell population (variable). The rows and columns were ordered according to the hierarchical clustering result, putting similar observations close to each other. In the plots above, high values are in red and low values in blue and consist of Pearson correlation coefficients ranging from -4 to 4. Additionally, the rows were annotated according to the subject (Adults, Neonates) and sex (Female, Male) using colours. *Abbreviations used*: NEU – neutrophils, EOS – eosinophils, MON – monocytes, GRN – granulocytes, LYM – Lymphocytes, NK – natural killer cells, NKT – natural killer T cells, MAITs – mucosal invariant T cells, ILC – innate lymphoid cells, Th2– type-2 cytokine-producing CD4s, Tc2 – type-2 cytokine-producing CD8s.

In the first step, hierarchical clustering reorganises data putting similar samples together. The colour scheme is applied to indicate high and low values for variables (red and blue, respectively). The heatmap format was used to visualise flow cytometry data from different subjects using the frequencies and cell counts obtained using the ICS panel. In heatmaps (**Fig. 3.2.26**), each row represents an individual (sample) (adults 1-9 and neonates 10-18) and each column represents the cell population (variable). In the plots above, high values are in red and

low values in blue and consist of Pearson correlation coefficients ranging from -4 to 4. Unsupervised hierarchical clustering in the cohort of healthy adults (*n*=9) and neonates (*n*=10) using cell count values, resulted in clustering according to whether samples were from adults or neonates, but not according to sex, revealing a clear age-related difference in cytokine production in peripheral lymphocytes (**Fig. 3.2.26 A**). Hierarchical clustering using percentage – positive values was not driven by sex or subject related signatures (**Fig. 3.2.26 B**).

PCAs allowed the relationship between individuals and variables (cell populations) to be assessed. The group mean point (large circle) was added to depict the centre of each group. The point concentration ellipses (red and light blue) were added around each group mean point using a multivariant t-distribution where the size of the concentration ellipse indicates the range of normal probability (95% confidence). As seen in **Figure 3.2.27 A-D**, positively and negatively correlated variables (arrows) were positioned on opposite sides of the plot centre. The distance between arrows and the origin measures the quality of the variables on the PC; cell clusters that are away from the origin are well represented in the PC. The quality of representation is called cos2; the higher cos2 the better the representation of the variable.

I applied PCAs to analyse further the relationship between all individuals and the contribution of each variable to the PCA (**Fig. 3.2.27 A and B**). Data has been represented as in **Figure 3.2.17 A-D**. PCAs showed significant separation of subjects into adult and cord blood groups when both percentage- and cell count-values were used. (**Fig. 3.2.27 A, C**). Signatures associated with sex (female, male) were computationally indistinguishable using percentage- and cell count-values (**Fig. 3.2.27 B, D**). The potential impact of sex (female, male), weight (above 3.5 kg, below 3.5 kg), vaccination (No, Yes) and gestation at vaccination (above 30 wk, below 30wk, NA) signatures was analysed in the cohort of healthy neonates only; however, no clustering was found comparing percentage-values (data not shown).

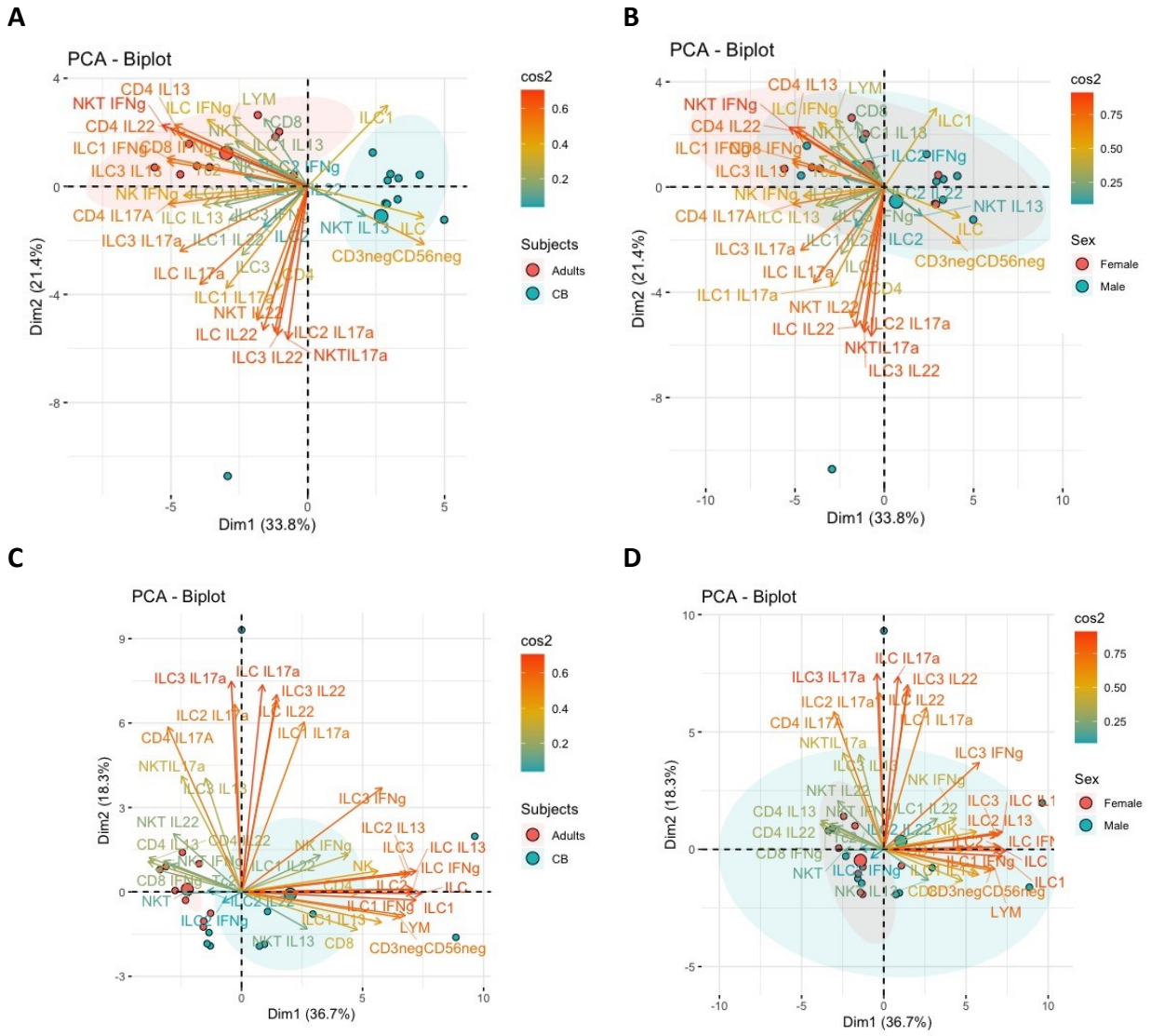


Figure 3.2.27 The separation between healthy adults and neonates using PCA using the ICS cohort.

The subject (Adult, CB) and sex (Female, Male) signatures of the cohort (*n*=19) used for flow cytometry analysis with optimised ICS panel was delivered by comparing the frequencies **(A, B)** and total cell numbers **(C, D)** from healthy adults (*n*=9) and neonates (*n*=10) using the R programming language. Data are displayed as a Principal Component Analysis (PCA), where each individual is plotted on the PCA as a point and individuals that are similar are grouped together to plot their contribution to the PCA. The group mean point was added for each group during the process of 'habillage' PCA to depict the centre of each group. The point concentration ellipses (red and light blue) were added around each group mean point using a multivariant t-distribution where the size of the concentration ellipse is in normal probability (95% confidence). Apart from the contribution of individuals to the plot, variable correlation plots show the relationship between all variables (arrows). Positively correlated variables (arrows) were grouped together while negatively correlated variables (arrows) were positioned on opposite sides of the plot origin. The distance between variables (arrows) and the origin measures the quality of the variables on PCA. Variables that are away from the origin are well represented on the PCA. The quality of representation on the variable (arrow) on the PCA is called cos2; the higher cos2 the better is the representation of the variable. *Abbreviations used*: NEU – neutrophils, EOS – eosinophils, MON – monocytes, LYM – Lymphocytes, NK – natural killer cells, NKT – natural killer T cells, MAITs – mucosal invariant T cells, ILC – innate lymphoid cells, cos2 – square cosine, squared coordinates.

Finally, potential associations between known clinical features (age, weight, gestation at vaccination, gestation at delivery) and different cell populations were dissected by correlation mapping on the ICS cohort of healthy adults (*n*=9) (**Fig. 3.2.28**) and neonates (*n*=10) (**Fig. 3.2.29**) using R (Materials and Methods, Chapter 2, **Section 2.2.9.16**). Data are displayed as correlograms (as described in Section 3.2.3.2.5). Correlations with *P*> 0.05 are considered insignificant and were left blank (**Fig. 3.2.28 B, D** and **Fig. 3.2.29 B, D**). The investigation of correlation dependence in the healthy adults revealed no correlations between changes in immune cells numbers and frequencies and age. The possible relationship between ILC2 and IL-13-producing CD4 T cells was observed in cell frequencies and cell counts which is interesting due to the involvement of those cells in bronchiolitis, asthma and allergic diseases (**Fig. 3.2.28 B and D**). In parallel, I investigated correlations in healthy neonates (**Fig. 3.2.29 A-D**). Interestingly, a great number of potential relationships were identified between immune cells frequencies, but no relationship was found between weight, gestation at vaccination or gestation at delivery and other cell population (except IL-13$^+$ ILC2 cells and gestation at vaccination in cell counts and IL-17$^+$ CD4 cells and gestation at vaccination in cell frequencies) (**Fig. 3.2.29 B and D**, respectively).

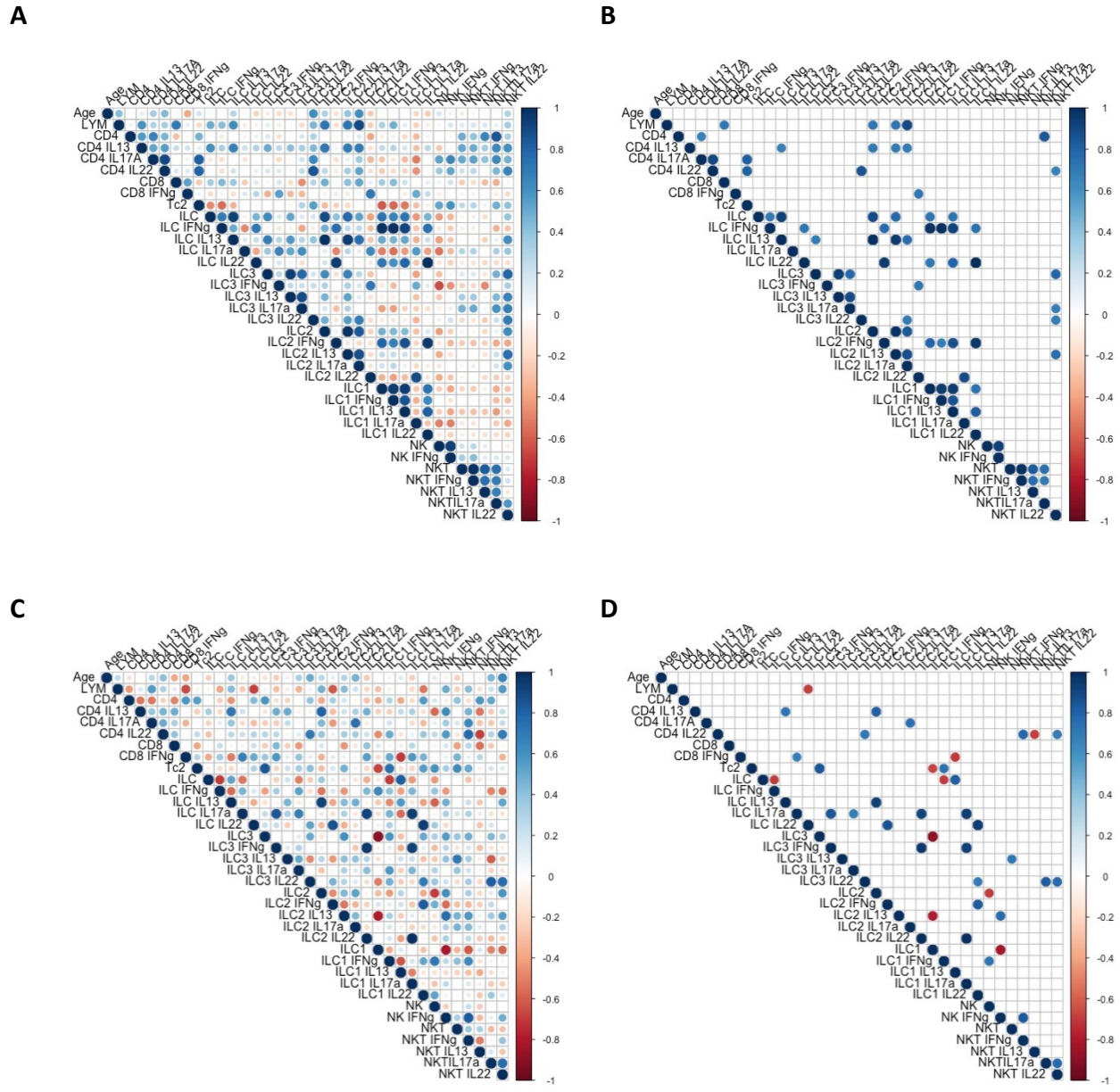


Figure 3.2.28 The correlation between different cell populations in the ICS cohort of healthy adults

The correlation between multiple variables from healthy adults (*n*=9) in the ICS cohort was determined by comparing total cell counts **(A, B)** or cell frequencies **(C, D)** using Pearson parametric correlation test in the R programming language. Data are displayed in a correlogram format, where positive correlations are displayed in blue and negative correlations in red. Colour intensity and the size of the circle are proportional to the correlation coefficients. On the right side of each correlogram, the legend colour depicts the correlation coefficients and the corresponding colours. The correlation matrix used for all graphs was not reordered according to hierarchical order **(A, B, C, D)**. Correlations with $p > 0.05$ are considered insignificant and were left blank **(B, D)**. *Abbreviations used*: NEU – neutrophils, EOS – eosinophils, MON – monocytes, GRN – granulocytes, LYM – Lymphocytes, NK – natural killer cells, NKT – natural killer T cells, MAITs – mucosal invariant T cells, ILC – innate lymphoid cells, Tc2 – type-2 cytokine-producing CD8s, Th2 – type-2 cytokine-producing CD4s.

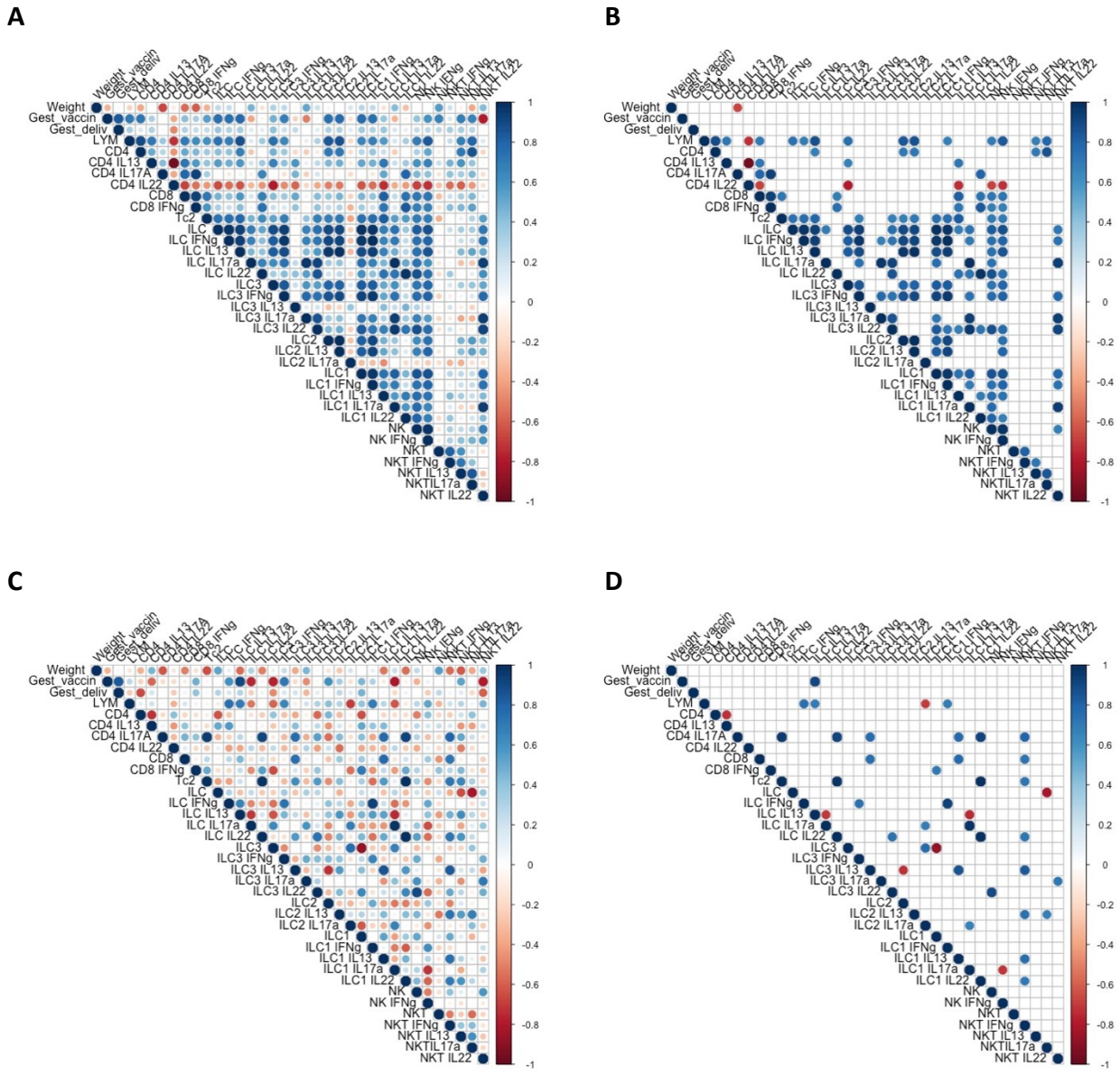


Figure 3.2.29 The correlation between different cell populations in healthy neonates

The correlation between multiple variables from healthy neonates (*n*=11) in the ICS cohort was determined by comparing total cell counts **(A, B)** or cell frequencies **(C, D)** using Pearson parametric correlation test in the R programming language. Data are displayed in a correlogram format, where positive correlations are in blue and negative correlations in red. Colour intensity and the size of the circle are proportional to the correlation coefficients. On the right side of each correlogram, the legend colour depicts the correlation coefficients and the corresponding colours. The correlation matrix used for all graphs was not reordered according to hierarchical order **(A, B, C, D)**. Correlations with $p > 0.05$ are considered insignificant and were left blank **(B, D)**. *Abbreviations used*: NEU – neutrophils, EOS – eosinophils, MON – monocytes, GRN – granulocytes, LYM – Lymphocytes, NK – natural killer cells, NKT – natural killer T cells, MAITs – mucosal invariant T cells, ILC – innate lymphoid cells, Tc2 – type-2 cytokine-producing CD8s, Th2 – type-2 cytokine-producing CD4s

3.2.3.4. NK cell function (Granzyme B production)

Next, I examined the difference between adults and neonates regarding the production of Granzyme B and CD57 expression on NK cells. 2.5 x 10^6 cells PBMCs from healthy adult and neonates were stained using titrated, fluorochrome-conjugated antibodies for surface and intracellular staining (**Table 3.2.2**). Detection of Granzyme B-producing cells was performed by immune fluorescent staining with an optimized flow cytometry panel (**Fig. 3.2.4**) as described (**Section 3.2.2.3.2**).

3.2.3.4.1. NK cell function (Granzyme B) study population

It has been reported that IFN-γ$^+$ NK cells could be in high numbers *post partum* [231]. CD57 is the marker that defines terminally differentiated, mature NK cells with a low level of proliferation and immunosenescence[229]. Differences in the production of granzyme B and CD57 expression were determined in frozen PBMCs from healthy adults (n=7) and neonates (n=7). In this cohort females and males were well represented (*P*=0.999) with the median age of adults ±42 years (27.0-63.0). In neonatal patients, more clinical data was available (sex, weight, gestation at the delivery, *Bordetella pertussis* vaccination and gestation at vaccination) (**Table 3.2.10**). For this study group, the neonatal blood samples were collected from term children delivered at ±28.57 (20.14-37.00) weeks gestation in the Neonatal Unit at St. Mary's hospital. 100% of mothers of neonates were vaccinated during ±39th (38.86-39.57) week of pregnancy. The number of females was lower (29.57%) in the neonatal cohort without significant difference in weights between females and males (3.16 and 3.61 kg, respectively).

	Adults	Neonates (CB)	
Characteristic	*n*=7	*n*=7	*P* value
Age (years), median, (range)	42.0 (27.0-63.0)	0	**0.0001**
Sex, *n*			0.9999
Females	3	2	
Males	4	5	

Table 3.2.9 Demographics of adults and neonates used in the optimised NK cell function (Granzyme B) flow cytometry analysis.

Healthy adults and neonates used for flow cytometry analysis for GrzmB and CD57. Patient demographic and clinical information were obtained from the patients' information sheets. Statistical significance was obtained using the Mann-Whitney test for continuous data and Fisher's exact test for categorical data. No adjustment was made for multiple testing. *P* values for continuous data were computed by Mann-Whitney test while *P* values for categorical data were computed by Fisher's exact test. The range is defined as the difference between the highest and lowest value. *Abbreviations used*: CB – cord blood.

	Neonates (CB)
Characteristic	*n*=7
Age (years), Median	New-borns
Sex, *n* (%)	
Females	2 (28.57)
Males	5 (71.43)
Weight (kg), Median, (range)	
Females	3.16 (3.54-2.79)
Males	3.61 (3.93-2.64)
Premature, *n* (*%*)	
Yes	0 (0)
No	7 (100)
Birthplace, *n* (*%*)	
NU	7 (100)
NICU	0 (0)
Gestation at delivery, wk, Median (range)	28.57 (37.00-20.14)
Pertussis Vaccination during pregnancy (*%*)	
Yes	7 (100)
No	0 (0)
Gestation at vaccination, wk, median (range)	39.00 (39.57-38.86)

Table 3.2.10 Demographics and clinical data of neonates used the NK cell function (Granzyme B) flow cytometry analysis.

Demographic and clinical information were obtained from the neonatal unit. The range is defined as the difference between the highest and lowest value. *Abbreviations used*: CB – cord blood, NU – Neonatal Unit, NICU – Neonatal Intensive Care Unit, wk – week, kg – kilogram.

3.2.3.4.2. The functional phenotype of innate and adaptive cell populations in healthy adults and neonates using the Granzyme B panel

Granzyme B production and CD57 expression in circulating NK cell populations

Figure 3.2.30A is an example of flow cytometry for GrzmB and CD57 expressing NK cells. NK cells were defined as live, single, $CD45^{+}CD56^{+}CD3^{-}$ lymphocytes. Within the NK population, $CD56^{H}CD16^{L}$ ($CD56^{H}$ NK) and $CD56^{L}CD16^{H}$ ($CD56^{L}$ NK) subsets were defined. Histograms show the expression of GrzmB and CD57 in $CD56^{H}CD16^{L}$ and $CD56^{L}CD16^{H}$ NK cells in adults (grey) and neonates (pink). Adults' frequencies of granzyme B producing NK cells were similar to neonatal cord blood (**Fig. 3.2.30 B and D**). The frequencies of $CD57^{+}$ NK cells and were much higher (*P*=0.0006) in adults due to a very low proportion of $CD57^{+}$ $CD56^{L}$ NK cells in neonates (*P*=0.0006) (**Fig. 3.2.30 B and D**). Surprisingly, NK cells producing Grzm B were more abundant in neonates (*P*=0.0379, with a median of 0.62 $x10^{6}$ cells per mL in neonates and 0.1 x 10^{6} cell per mL in adults). The numbers of both $GrzmB^{+}CD56^{L}$ NK cells and $GrzmB^{+}$ $CD56^{H}$ NK cells were higher in neonates compared to adults (**Fig. 3.2.30 G**). Together these data suggest that NK cells are a functionally

active subset in neonates; however, they are not terminally differentiated [229] as they lack the CD57 cell marker.

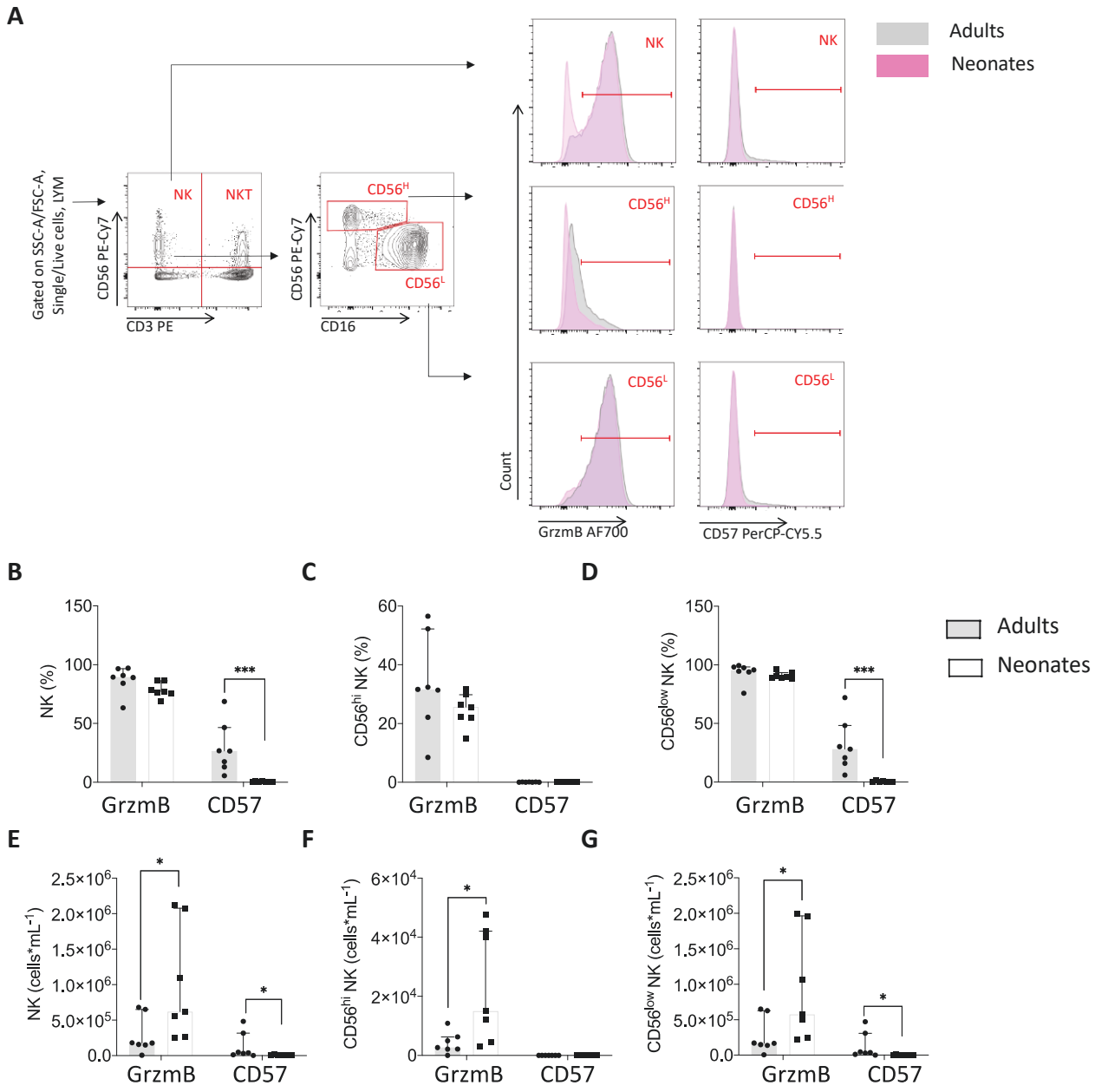


Figure 3.2.30 Comparison of production of Granzyme B and CD57 expression of NK cells from healthy adult and neonatal PBMCs.

PBMC were isolated using Lymphopure® from the blood of healthy adult volunteers (*n*=7) or cord blood of neonates (*n*=7) as described in the Material and Methods. Cells were analysed using the Granzyme B flow cytometry panel. **(A)** A representative example of flow cytometry for GrzmB and CD57 expressing NK cells (including $CD56^{H}CD16^{L}$ and $CD56^{L}CD16^{H}$ NKs)**.** NKs were defined as live, single, $CD45^{+}CD56^{+}CD3^{-}$ lymphocytes. Within the NK population, $CD56^{H}CD16^{L}$ ($CD56^{H}$ NK) and $CD56^{L}CD16^{H}$ ($CD56^{L}$ NK) subsets were defined. Histograms show the expression of GrzmB and CD57 in adults (grey) and neonates (pink) **(A)**. Frequency of total $CD56^{+}CD3^{-}$ NK cells **(B)**, $CD56^{H}CD16^{L}$ NK cells **(C)** and $CD56^{L}CD16^{H}$ NK cells **(D)** expressing GrzmB and CD57**.** Quantification of total $CD56^{+}CD3^{-}$ NK cells **(E)**, $CD56^{H}CD16^{L}$ NK cells **(F)** and $CD56^{L}CD16^{H}$ NK cells **(G)** expressing GrzmB and CD57. Data are shown as the median with upper interquartile range **(B-G)**. Differences between groups were determined by Mann-Whitney test (* $p < 0.05$, *** $p < 0.001$). Abbreviations used: NK – natural killer cells, NKT – natural killer T cells, GrzmB – granzyme B.

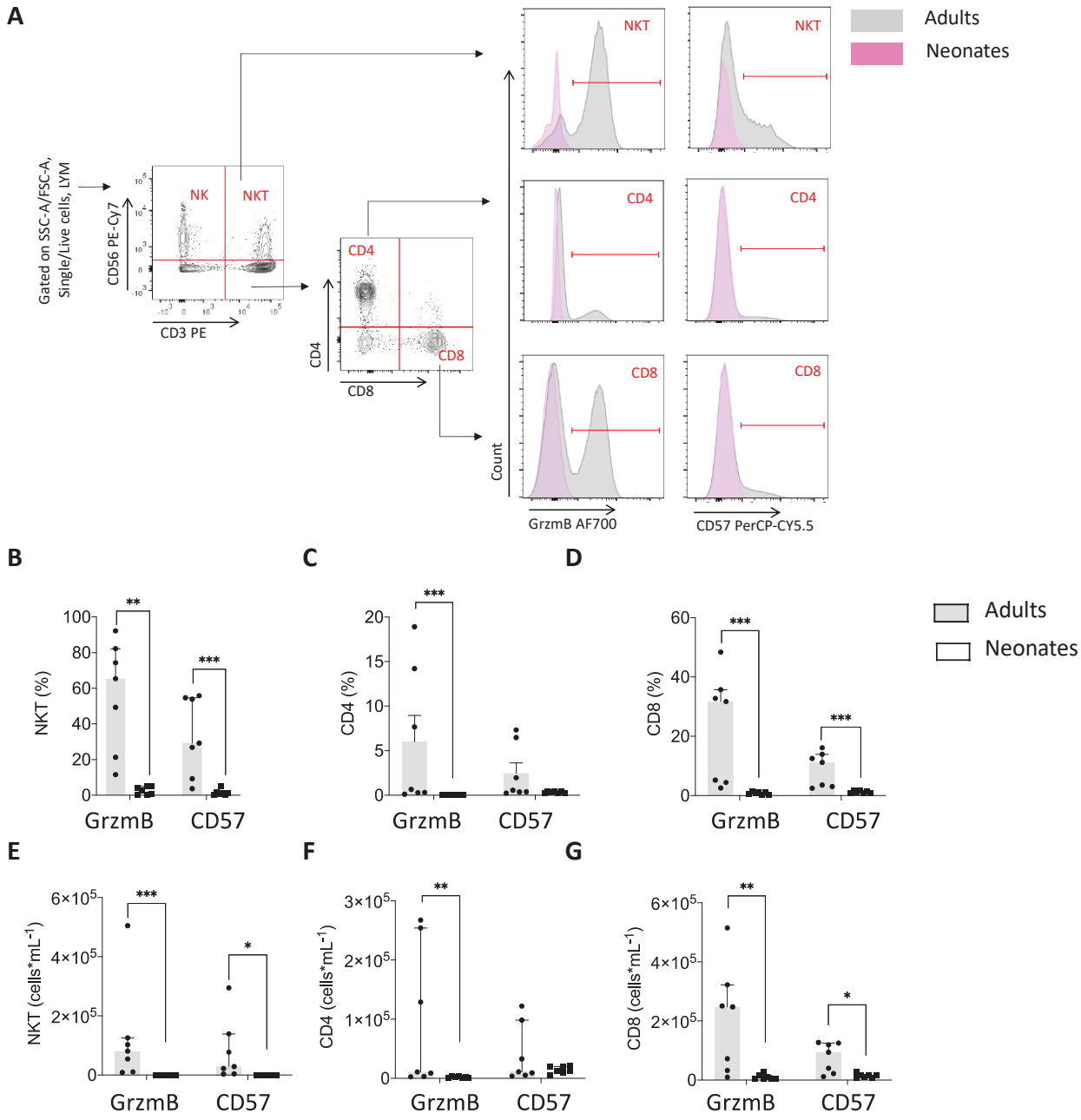


Figure 3.2.31 Comparison of production of Granzyme B and CD57 expression of NKT, CD4 and CD8 T cells from healthy adult and neonate PBMCs.

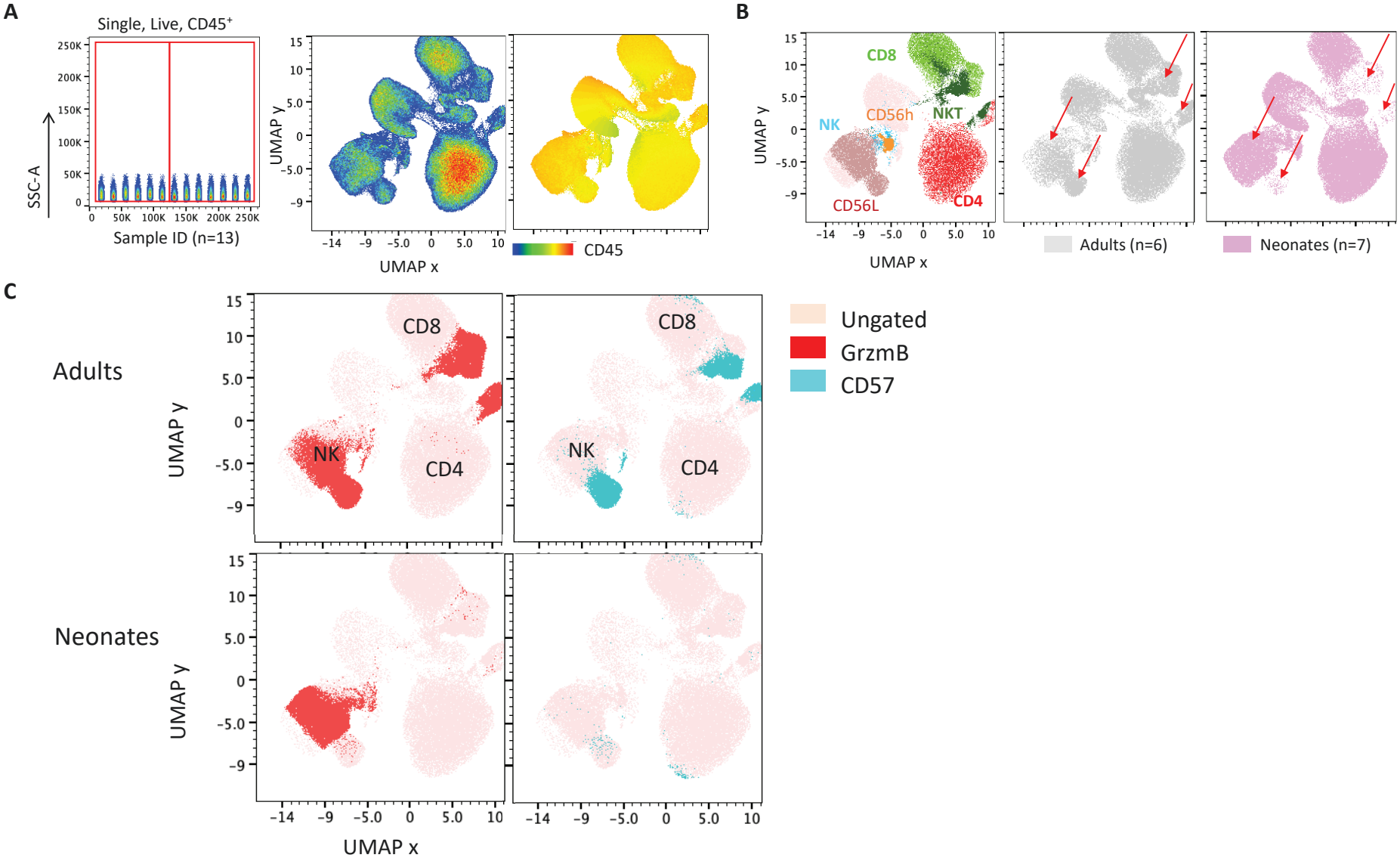
PBMC were isolated using Lymphopure® from the blood of healthy adult volunteers (*n*=7) or cord blood of neonates (*n*=7) as described in the Material and Methods. Cells were analysed using the Granzyme B flow cytometry panel. An example of flow cytometry for GrzmB and CD57 expressing NKT, CD4 and CD8 T cells**.** NKT were defined as live, single, $CD45^+CD56^+CD3^+$ lymphocytes. T lymphocytes ($CD3^+CD56^-$) were segregated into $CD4^+$ or $CD8^+$ T cells. Histograms show the expression of GrzmB and CD57 on NKT, CD4 and CD8 T cells in adults (grey) and neonates (pink) **(A)**. Frequency of total $CD56^+CD3^+$ NKT cells **(B),** $CD56^-CD3^+CD4^+$ T cells **(C)** and $CD56^-CD3^+CD8^+$ T cells **(D)** expressing GrzmB and CD57 in PBMCs from healthy adults (*n*=7) and cord blood from neonates (*n*=7)**.** Quantification of total $CD56^+CD3^+$ NKT **(E)**, $CD56^-CD3^+CD4^+$ **(F)** and $CD56^-CD3^+CD8^+$ cell **(G)** in PBMCs of healthy adults and cord blood from neonates. Data are shown as the median with upper interquartile range **(B-G).** Differences between groups were estimated by Mann-Whitney test (* $p < 0.05$, ** $p < 0.01$, *** $p < 0.001$). Abbreviations used: NK – natural killer cells, NKT – natural killer T cells, GrzmB – granzyme B.

Granzyme B production and CD57 expression in circulating NKT, $CD4^+$ and $CD8^+$ T cell populations

Next, the production of GrzmB and CD57 expression were assessed in NKT, $CD4^+$ and $CD8^+$ T cells using the gating strategy shown in **Figure 3.2.31 A**. NKT cells were gated within the lymphocyte gate as $CD56^+CD3^+$ cells. T lymphocytes ($CD3^+CD56^-$) were segregated into $CD4^+$ or $CD8^+$ T cells. Among NKT, $CD4^+$ or $CD8^+$ T cells, the populations of GrzmB and CD57 positive cells were found. A higher frequency of adult NKT, $CD4^+$ and $CD8^+$ T cells expressed GrzmB compared to neonates (*P*=0.006, *P*=0.0006 and *P*=0.0006, respectively) (**Fig. 3.2.31 A-C**), and the abundance of those populations was greater in adults (**Fig. 3.2.31 E-F**). Furthermore the frequency and numbers of $CD57^+$NK and $CD57^+CD56^{low}$NK cells in neonates were lower compared to their adult counterpart, suggesting that neonatal NK cells are not terminally terminated as adult NK cells (**Fig. 3.2.31 B, D, E, F**).

3.2.3.4.3. Assessment of the functional phenotype of circulatory cell populations by UMAP

In parallel with manual gating, I applied the deep immune phenotyping technique UMAP[204] to analyse granzyme B and CD57 expression in healthy adults and neonates. This analysis allowed me to reduce 11 dimensions (9 colours including FSC-A and SSC-A, **Table 3.2.2**) into two dimensions referred to as UMAPx and UMAPy (**Fig. 3.2.32 A,** middle). Firstly, data were cleaned using standard biaxial gating including only single, live lymphocytes (**Fig. 3.2.32 A,** left). Lymphocytes were gated using SSC-A and CD45. After data cleaning, I performed UMAP analysis on 325,000 randomly selected lymphocytes (25,000 from each subject concatenated into a single file) (**Fig. 3.2.32 A**, right). The manual gating strategy from the Granzyme B panel was utilised to classify global UMAP clusters into the following cell types: CD4 T cells (red), NKT cells (dark green), CD8 T cells (light green), NK cells (blue), CD56h NK cells (orange), CD56L NK cells (light brown) (**Fig. 3.2.32 B**). UMAP representations of data highlighted the main differences between cell clusters among adults (grey) and neonates (pink) (**Fig. 3.2.32 B**). The UMAP map found major regions enriched in adults, but not neonates, with high expression of GrzmB (red) and CD57 (light blue) in all cell clusters (**Fig. 3.2.32 C**). Notably, NK cells from adults were highly similar to neonates as they produced the same level of GrzmB (red); however, neonatal NK cells lack expression of the differentiation cell marker CD57 (light blue) (**Fig. 3.2.32 C**). Regions of GrzmB and CD57 positive NKT cells, $CD8^+$ and $CD4^+$ T cells were found in adults but not neonates suggesting fully matured T cell subsets (**Fig. 3.2.32 C**). UMAP demonstrated the heterogeneity in the same cell clusters among cohort participants (**Fig. 3.2.32 D, E**).


A
Single, Live, CD45+
SSC-A
Sample ID (n=13)
UMAP y
UMAP x
CD45
B
CD8
NK
CD56h
NKT
CD56L
CD4
Adults (n=6)
Neonates (n=7)
C
Adults
Neonates
Ungated
GrzmB
CD57

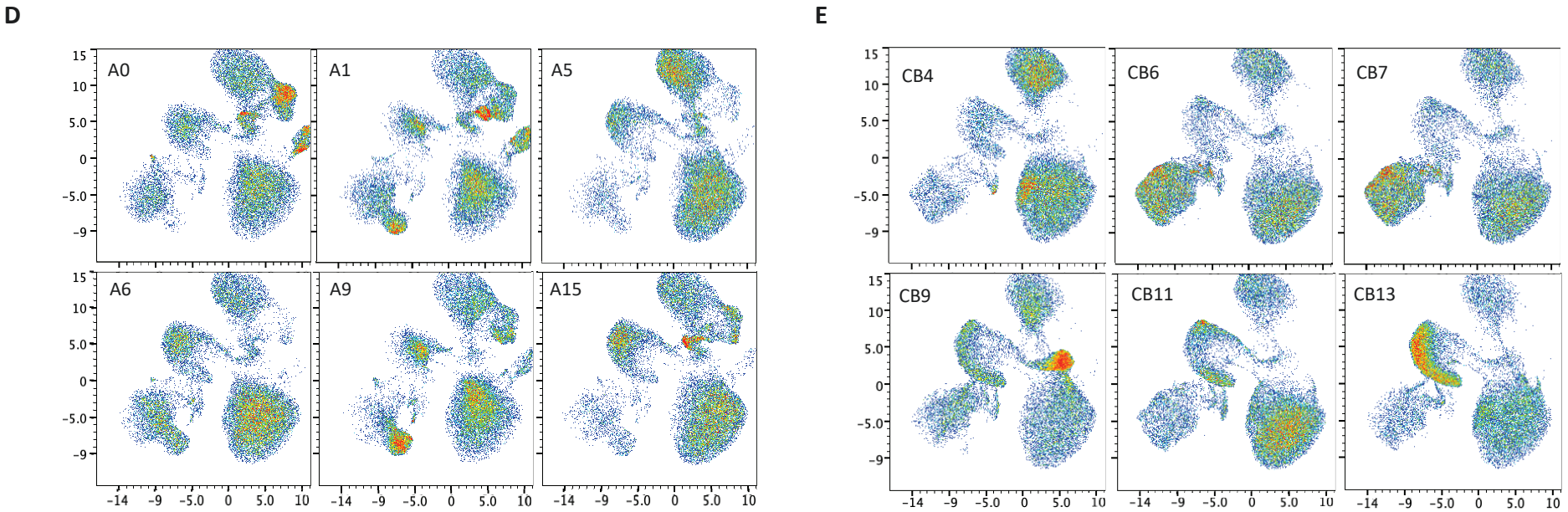


Figure 3.2.32 Deep immune phenotyping of granzyme B and CD57 expressing NK cells, NKT cells and T cell populations in adult and neonatal PBMCs using UMAP.

(A) Representative manual gating strategy utilised for deep immune phenotyping. Cells were delineated using the following gating strategy: FSC/SSC, single, live cells. Lymphocytes were gated using SSC-A and CD45. 25,000 randomly selected $CD45^+$ lymphocytes from each subject (*n*=14, left) were concatenated into a single file containing 325,000 cells for UMAP analysis (middle). The intensity of CD45 expression is shown (right). **(B)** The manual gating strategy from the Granzyme B panel was utilised allowing global UMAP clusters (all subjects pooled, left) to be classified into the following cell types: CD4 T cells (red), NKT cells (dark green), CD8 T cells (light green), NK cells (blue), CD56h (orange), CD56L (light brown). Comparison of UMAP representations of clusters for healthy adult subjects (*n*=7, middle) and neonates (*n*=7, right). The main differences between cell clusters in adults (grey) and neonates (pink) are depicted using the red arrows. **(C)** Simplified UMAP projections indicating the differences in the production of GrzmB (red) and CD57 expression in NK cell, CD4 and CD8 T cell clusters from adults (*n*=7) and neonates (*n*=7). UMAP visualisation of FSC/SSC, single, live, $CD45^+$ lymphocytes in individual adults **(D)** and neonates **(E)** depicts differences between all subjects. Abbreviations used: LYM – Lymphocytes, NK – natural killer cells, NKT – natural killer T cells, ILC – innate lymphoid cells, UMAP – Uniform Manifold Approximation and Projection, GrzmB – granzyme B.

3.2.3.4.4. Assessment of circulatory immune cell populations and their correlations utilising R in the Granzyme B cohort

I employed heatmaps and principal component of analysis (PCA) in the R programming language to better define and identify the differences between adult and cord blood. For the heatmaps, for each individual, variables were visualised on a colour scale with high values in red and low values in blue and consist of Pearson correlation coefficients ranging from -4 to 4 (**Fig. 3.2.33**). Unsupervised hierarchical clustering using cell count values revealed that there are subject (adults and neonates) but not sex (female and male) signatures (**Fig. 3.2.33 A**). Unsupervised hierarchical clustering stratified the subjects into three main clusters: 1) adults with NK cell, NKT cell and CD4 and CD8 T cells expressing CD57 2) neonates with NK cell, NKT cell and CD4 and CD8 T cells expressing a very low-level of CD57 but a high level of GrzmB in NK cells and 3) adults and neonates expressing similar low levels of CD57 and GrzmB (**Fig. 3.2.34 A**). Hierarchical clustering using percentage – positive values defined and identified subject (adults and neonates) signatures with some level of variability due to heterogeneity of human samples; however, segregation into adults and neonates was more explicit compared to cell counts. Adults have a higher frequency of most populations analysed compared to neonates (**Fig. 3.2.34 B**).

PCAs assessed the relationship between subjects and the contribution of each parameter to the PCA (**Fig. 3.2.34 A and B**). Data is represented as described in **Figure 3.2.17 A-D**. PCAs demonstrated distinct adult and cord blood signatures when both percentage- and cell count-values were used, although there is some overlap between groups (**Fig. 3.2.34 A, C**). Notably, samples did not segregate based on sex (female, male) using percentage- and cell count-values (**Fig. 3.2.34 B, D**). The potential impact of sex (female, male), weight (above 3.5 kg, below 3.5 kg), vaccination (No, Yes) and gestation at vaccination (above 30 wk, below 30wk, NA) were analysed in the cohort of healthy neonates; however, no clustering was found when comparing percentage-values (data not shown).

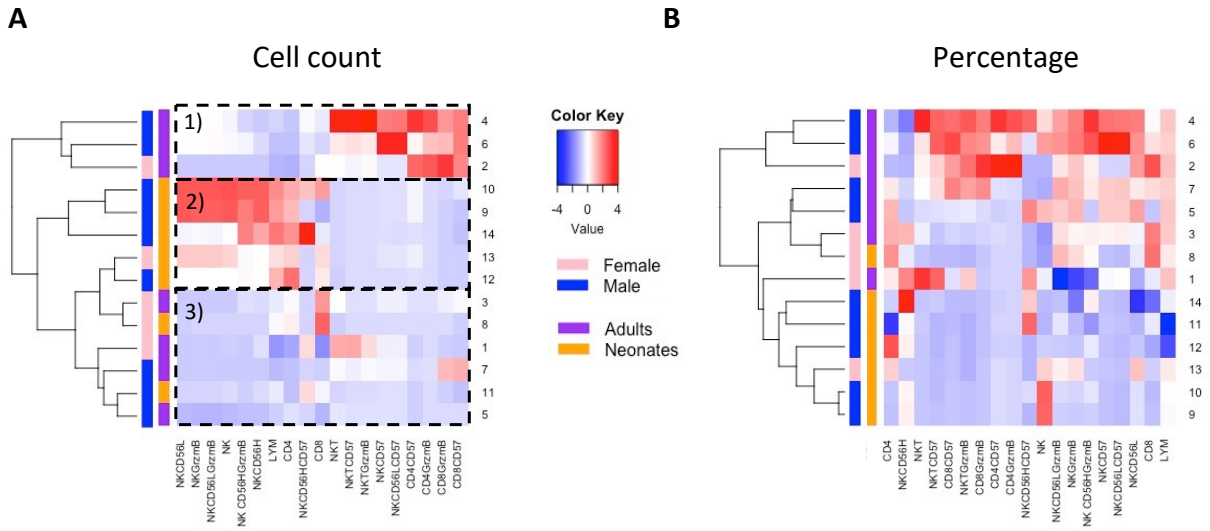


Figure 3.2.33 Hierarchical clustering and subject and sex signatures in the Granzyme B cohort of healthy adults and neonates using the heatmap format.

The ICS cohort signatures (*n*=14) were delivered by comparing total cell counts **(A)** and frequencies **(B)** from healthy adults (*n*=7) and neonates (*n*=7) using the R programming language. Data are displayed in a heatmap format, where each row represents an individual (sample) (Adults 1-7 and Neonates 8-14) and each column represents the cell population (variable). The rows and columns were ordered according to the hierarchical clustering result, putting similar observations close to each other. In the plots above, high values are in red and low values in blue and consist of Pearson correlation coefficients ranging from -4 to 4. Dashed lines are used for displaying subject clusters. Additionally, the rows were annotated according to the subject (Adults, Neonates) and sex (Female, Male) signatures using colours. *Abbreviations used*: GrzmB – granzyme B, LYM – Lymphocytes, NK – natural killer cells, NKT – natural killer T cells.

In the last part, potential associations between known clinical features (age, weight, gestation at vaccination, gestation at delivery) and different cell populations were dissected by correlation mapping on the Granzyme B cohort of healthy adults (*n*=7) (**Fig. 3.2.35 A-D**) and neonates (*n*=7) (**Fig. 3.2.36 A-D**) using R (Materials and Methods, Chapter 2, **Section 2.2.9.16**). Data are displayed as correlograms (as described before Section 3.2.3.2.5). Correlations with *P*> 0.05 are considered insignificant and were left blank (**Fig. 3.2.35 B, D** and **Fig. 3.2.36 B, D**). The investigation of correlation dependence in the healthy adults revealed correlations between changes in CD8 cell numbers and frequencies and age. Furthermore, there was a relationship between $CD56^{H}CD57^{+}$NKs and age observed in cell counts (**Fig. 3.2.35 D**). Interestingly, a great number of potential relationships were identified in immune cells frequencies and numbers in adults (**Fig. 3.2.35 B and D**). In parallel, we investigated correlations in the healthy neonates (**Fig. 3.2.36 A-D**). A negative relationship was found between weight and $Grzmb^{+}$CD4 T cells and a positive relation between gestation at vaccination and $CD57^{+}$CD8 T cells in cell counts (**Fig. 3.2.36 B**). Using frequencies of cells revealed a negative relationship between weight and $Grzmb^{+}$CD4 T and $Grzmb^{+}$CD8 T cells in healthy neonates (**Fig. 3.2.36 D**).

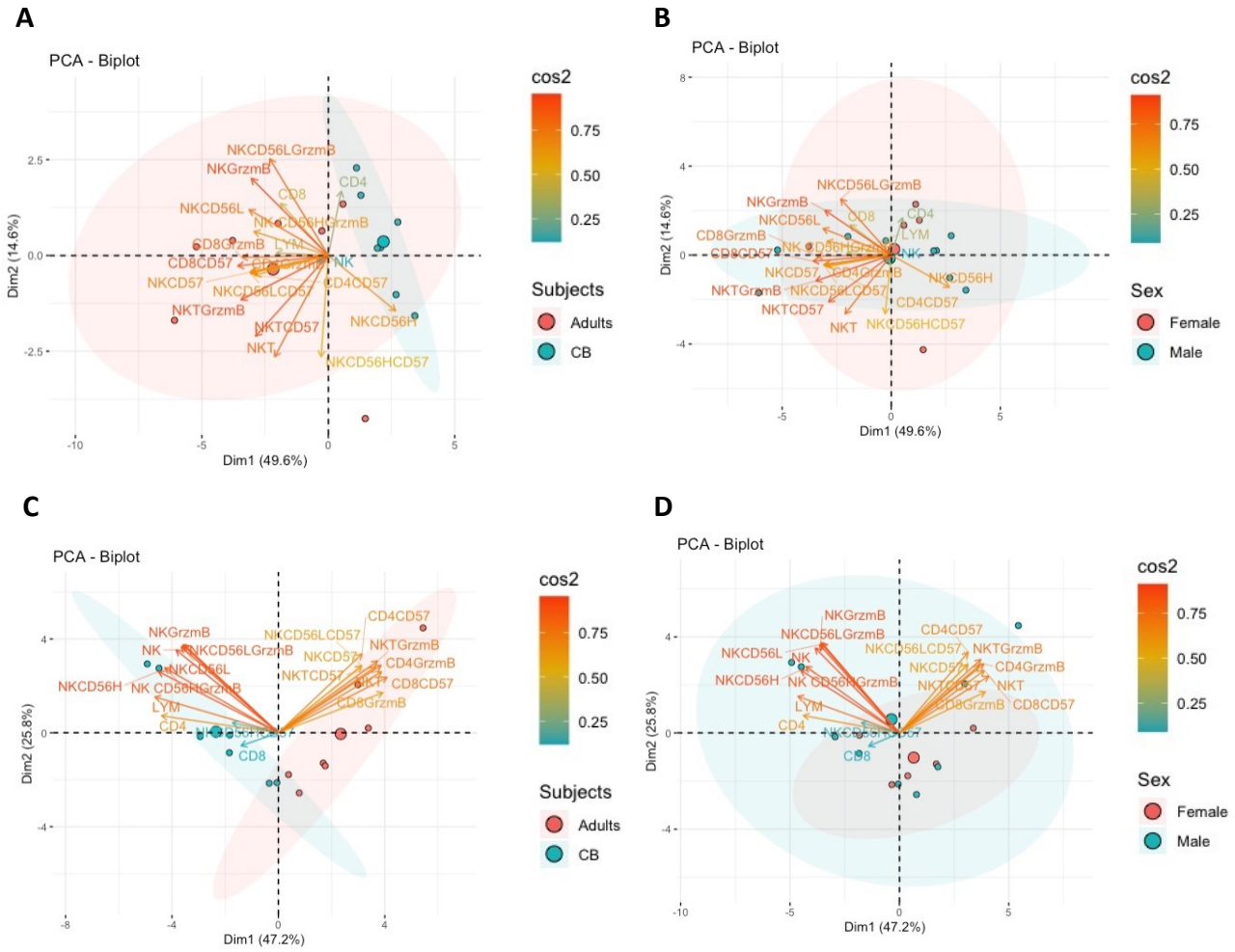


Figure 3.2.34 The separation of healthy adults and neonates using PCA and not by differences in sex in the Granzyme B cohort.

The subject (Adult, CB) and sex (Female, Male) signatures of the cohort (*n*=14) used for flow cytometry analysis with granzyme B panel was delivered by comparing the frequencies **(A, B)** and total cell numbers **(C, D)** from healthy adults (*n*=7) and neonates (*n*=7) using the R programming language. Data are displayed as a Principal Component Analysis (PCA), where each individual is plotted on the PCA as a point and individuals that are similar are grouped together to plot their contribution to the PCA. The group mean point was added for each group during the process of 'habillage' PCA to depict the centre of each group. The point concentration ellipses (red and light blue) were added around each group mean point using a multivariant t-distribution where the size of the concentration ellipse shows normal probability (95% confidence). Plots show the relationship between all variables (arrows). Positively correlated variables (arrows) were grouped together while negatively correlated variables (arrows) were positioned on opposite sides of the plot origin. The distance between variables (arrows) and the origin measures the quality of the variables on PCA. Variables that are away from the origin are well represented on the PCA. The quality of representation on the variable (arrow) on the PCA is called cos2; the higher cos2 the better is the representation of the variable. *Abbreviations used*: GrzmB – granzyme B, LYM – Lymphocytes, NK – natural killer cells, NKT – natural killer T cells, cos2 – square cosine, squared coordinates.

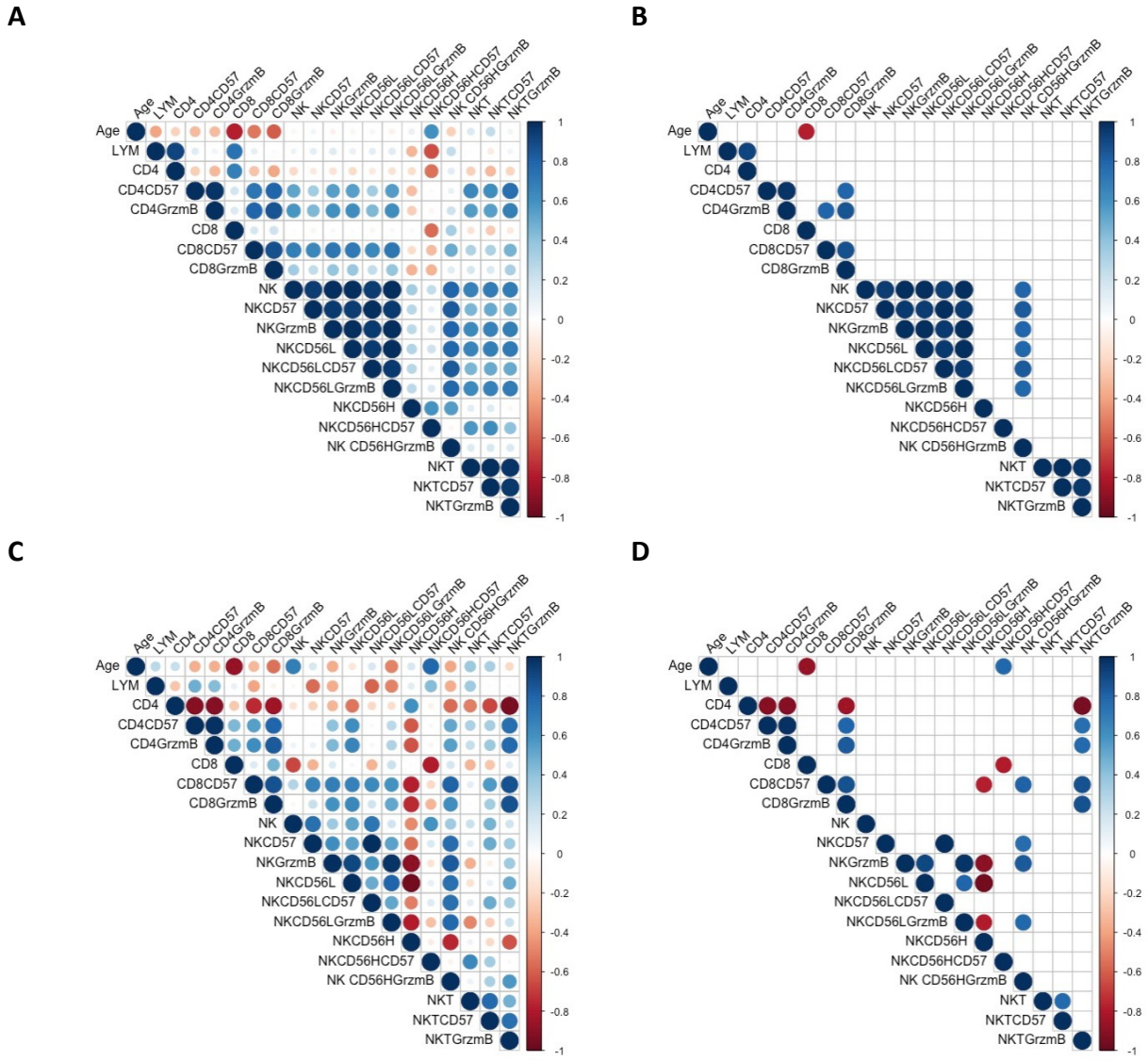


Figure 3.2.35 Correlation between the different cell populations in the Granzyme B cohort of healthy adults

The correlation between multiple variables from healthy adults (*n*=7) in the Granzyme B cohort was delivered by comparing total cell counts **(A, B)** or cell frequencies **(C, D)** using Pearson parametric correlation test in the R programming language. Data are displayed in a correlogram format, where positive correlations are displayed in blue and negative correlations in red. Colour intensity and the size of the circle are proportional to the correlation coefficients. Additionally, on the right side of each correlogram, the legend colour depicts the correlation coefficients and the corresponding colours. The correlation matrix used for all graphs was not reordered according to hierarchical order **(A, B, C, D)**. Correlations with $P > 0.05$ are considered insignificant and were left blank **(B, D)**. *Abbreviations used*: GrzmB – granzyme B, LYM – Lymphocytes, NK – natural killer cells, NKT – natural killer T cells.

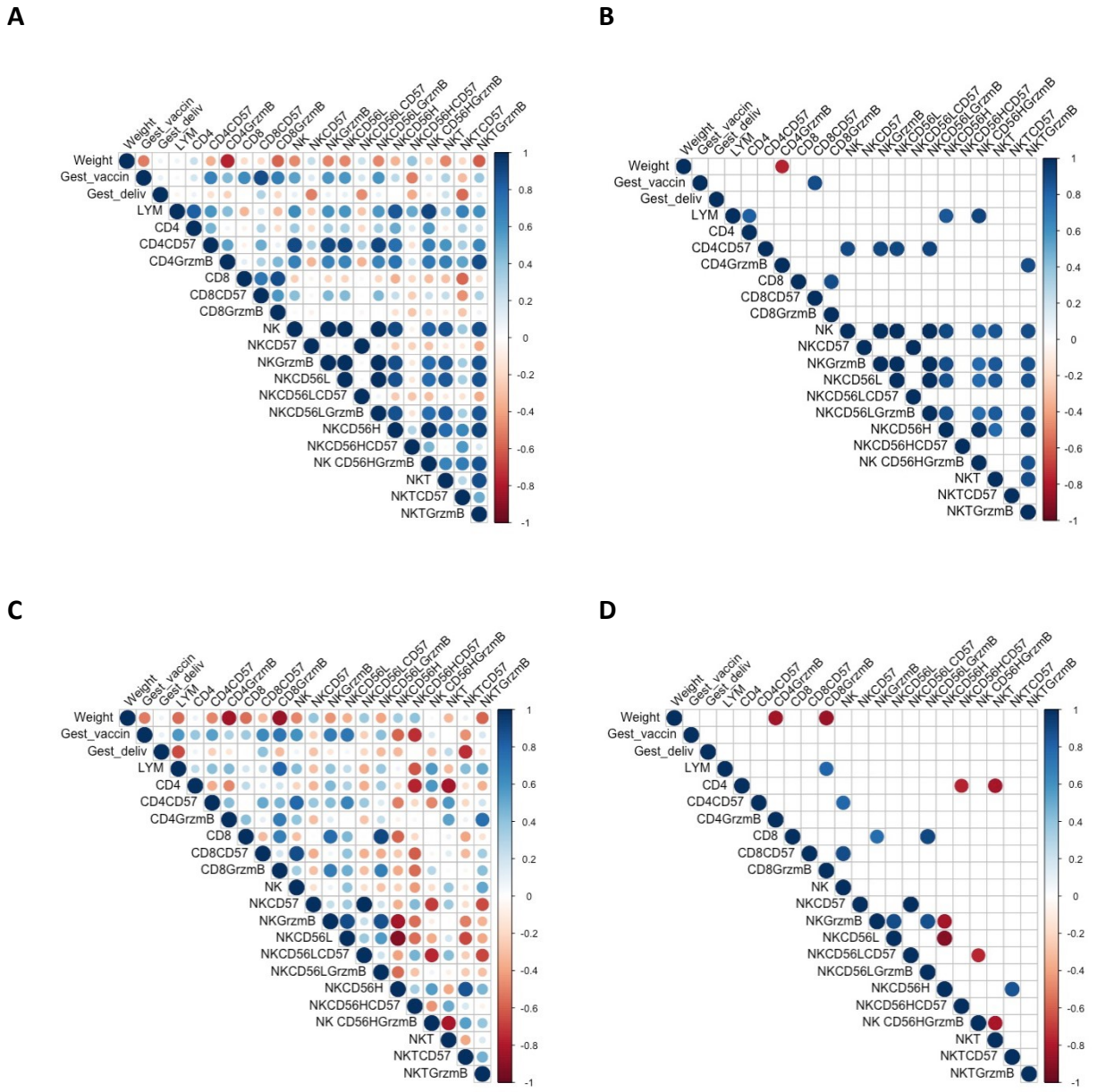


Figure 3.2.36 The correlation between the different cell populations in the Granzyme B cohort of healthy neonates

The correlation between multiple variables from healthy neonates (*n*=7) in the Granzyme B cohort was delivered by comparing total cell counts **(A, B)** or cell frequencies **(C, D)** using Pearson parametric correlation test in the R programming language. Data are displayed in a correlogram format, where positive correlations are in blue and negative correlations in red. Colour intensity and the size of the circle are proportional to the correlation coefficients. Additionally, on the right side of each correlogram, the legend colour depicts the correlation coefficients and the corresponding colours. The correlation matrix used for all graphs was not reordered according to hierarchical order **(A, B, C, D)**. Correlations with $p > 0.05$ are considered insignificant and were left blank **(B, D)**. *Abbreviations used*: GrzmB – granzyme B, LYM – Lymphocytes, NK – natural killer cells, NKT – natural killer T cells.

3.2.4. Discussion for Chapter 3.2

It is acknowledged that neonatal life is a unique time of increased susceptibility to infectious diseases and when the speed of disease progression can be extremely rapid. This phenomenon can be partially explained by the differences in adaptive and innate immunity of neonates in comparison to adults. These differences may contribute to increased morbidity and mortality in early life during infectious diseases such as RSV-related bronchiolitis [6,224].

An ample body of evidence suggests that neonates can mount an effective immune response against environmental insults and a plethora of pathogens, such as bacteria and viruses [188,207]. These effective immune responses are highly regulated by cells of the innate immune system, such as granulocytes [117] and natural killer cells [130]. Recently, another cellular component of innate immunity, innate lymphoid cells (ILCs), has been implicated in guarding against pathogens in early life due to their higher numbers and a higher level of activity in comparison to adulthood [232,233]. Better understanding the differences of ILCs and other components of innate immunity in neonates might help to elucidate the reason for increased susceptibility to diseases when compared to adults.

In this chapter, I focused on differences in the abundance and function of different immune and adaptive cells between adults and neonates. To dissect the differences in numbers of ILCs (including NK cells), granulocytes (neutrophils and eosinophils), $CD3^{+}$T cells, such as CD4+, CD8+ and innate-like lymphocytes (NKT-like and MAIT cells) in the peripheral and cord blood a multiparameter flow cytometry panel (OMIP) was utilised [201]. In parallel, I developed intracellular staining (ICS) functional panels for IFN-γ, IL-13, IL-17A, IL-22 and Granzyme B to determine whether ILCs (including NK cells) differ in their production of these mediators [234]. I also applied powerful tools, such as the Uniform Manifold Approximation and Projection algorithm (UMAP) together with Principal Component of Analysis (PCA), heatmaps and correlograms using the R programming language to gain a better insight into differences between adults and neonates and understand which clinical factors might drive these differences.

After OMIP development, I optimised deep immune phenotyping techniques for characterisation of innate and adaptive cells between adults and neonates. These techniques complemented and validated the manual biaxial gating strategy used. In the first step, I focused on the comparison of *t*-SNE[203] and UMAP[204]. Both techniques use a high-dimension reduction algorithm for visualisation of poly-dimensional cytometric data by locating each cell on a two-

dimension map [203,205]. For this analysis, I used flow cytometric data obtained from the enumeration of immune cells in cord and peripheral blood. Both techniques allowed deeper profiling of immune cells and a better understanding of changes between adult and neonatal immunomes. After comparison of *t*-SNE and UMAP, I found that Uniform Manifold Approximation and Projection algorithm allowed me to achieve better visualisation of flow cytometric data and better preservation of cell clusters' structure in a much shorter run time. UMAP was successfully applied to different cytometric data sets used in this chapter (OMIP, ICS and Granzyme B data sets) and Chapter 3.2.

In accordance with published data, UMAP phenotypic characterisation of blood immune cells demonstrated that invariant T cells (MAITS and NKT-like cells) were increased in adults [84] while eosinophils and ILCs clusters were more strongly projected in neonates [188,235]. Finally, in the neonatal UMAP, I observed a cluster of cells expressing a high level of CD117 which may represent foetal-derived haematopoietic precursors [236,237].

A major strength of this work comes from the fact that I was comparing human neonates and adults when most studies of neonatal immunity are of neonatal mice [225,227]. An important question is how many of those findings from the rodent studies are true in human life? Previously published literature strongly suggests that in some cases the immune responses apparent in mice are not true in early human life and under some circumstances, human neonates are fully competent to develop mature type-1 immune responses in contrast to their murine counterparts [226].

A limitation of this work comes from studying cord blood to understand early life. Considering the variability in cell numbers from different cord blood donors in the context of this study, work with umbilical cord blood can be challenging. Although it is a very important tool to study the immunology of neonates, there are significant factors that can have an impact on the number of particular cells, such as the time of cord blood collection after birth, the temperature during collection and if the phlebotomy was performed before or after the placental delivery [238] - many factors which we could not control or change and which might have an effect on the total cell counts. The factors I aimed to control involved 1) a mode of delivery (caesarean section), 2) a type of anticoagulant used in the study (EDTA) and 3) a frame of time in which it was possible to collect the placenta from the St. Mary's neonatal unit (NU) (approximately 2 hours *post partum*). Olin *et al.* (2018) have demonstrated in a longitudinal study of 100 newborn babies (sampled up to three months after birth) that cord blood might not be the most optimal way of studying

neonatal immunity. In their hands, there were dramatic changes in the development and phenotype of 58 immune cells and 267 plasma proteins in new-borns compared to older infants. However, it is controversial. Cord blood harvested immediately *post partum* and is valuable for scientific work. It contains populations of hematopoietic stem cells that can be utilised to treat certain diseases and immune disorders [238]. Moreover, cord blood and cord blood mononuclear cells (CBMC) have been used to study T cells [84], NK cells [239], DCs [240], granulocytes [241]and other immune cells in early life [241]. Fonceca *et al.* (2017) detected RSV in human cord blood samples using PCR, suggesting *in utero* transmission of RSV to the human foetus and a significant impact on immune development [242]. Bronchiolitis affects children below the age of two, which provides difficulties with obtaining samples in significant volumes. Thus, I used cord blood to (1) remove the technical limitation of obtaining a sufficient amount of blood from neonates,(2) remove the ethical complexity of obtaining blood samples from neonates, and (3) investigate the similarities and differences in the cellular compartment of new-borns compared to adults. Moreover, understanding the precise numbers and frequencies of ILCs in health in neonates can be extremely important as it can be compared to pathological conditions, and specifically bronchiolitis.

Innate cell recruitment is an important part in the response to viral or bacterial infection in the lung [18]. The abundance of leukocytes in the circulation varies with sex, race and age [243]. In the first hours *post partum*, healthy neonates have a high number of granulocytes and in particular neutrophils. Their number decreases slowly throughout the neonatal period [243,244]. By the second week after birth, lymphocytes become predominant; however, there is a gradual decline of all leukocytes throughout childhood, reaching equilibrium by the age of 21 [243,244]. In corroboration with published data, I showed quantitative differences in the number of granulocytes and lymphocytes in neonates compared to adults. Similarly to the published data granulocytes predominate in the new-borns (4.28 x 10^6 cell per mL) compared to lymphocytes (3.06 x 10^6 cell per mL). Furthermore, the correlation analysis indicated evidence of a reduction in frequency of neutrophils across the lifespan in the adult cohort. The age-related decline stands contrary to the published literature in which neutrophil immunosenescence, not the decreased number of those cells was responsible for increased infections in the elderly [245]. Although it was an unexpected observation, the possible explanation is that the adult cohort consisted of predominantly young subjects with a median age of 32 years old and further study with a bigger age range and a number of participants should be used to confirm the result. I observed a higher

number of all leukocytes in new-borns in comparison to adulthood which can be related to the increased white blood cell counts in full-term neonates [243].

Granulocytes are the most frequent cell type throughout the human lifespan [233]. In this study, I was observed an increased frequency of eosinophils and neutrophils in neonates. Although there is a high number of neutrophils when compared to adults, neonatal neutrophils have functional impairments of chemotaxis, migration linked to the decreased expression of cell adhesion molecules (β2 integrins and selectins) and reduced antimicrobial activity as they are not able to form neutrophil extracellular traps (NETs) effectively [20,246]. The elevated number of eosinophils in new-borns has been reported previously and also that the number of those cells and their degranulation activity upon IL-5 stimulation decline with age [235]. Interestingly, eosinophilia seems to be very significant at the beginning of *post-partum* life; however, the role of eosinophils in that part of life has not been studied. The increased number of eosinophils might be related to the skewed type-2 immune responses in the early life; however, hypereosinophilia (>1.0 x 10^6 cells per mL) in the blood of new-born infants might be related to infection with gram-negative bacteria and necrotising enterocolitis (NEC) [247].

In this work, I enumerated of all members of the ILC family (ILC1, ILC2, ILC3) including NK cells as they have been recently categorised as ILCs under new classification [118]. ILCs were identified and characterised as $CD45^+$, lineage negative (Lin^-) $CD127^+$ lymphocytes and NK cells as $CD45^+CD56^+CD3^-$ lymphocytes [201]. ILCs are known to be abundant in mucosal surfaces of lungs, guts or skin [143,248] and according to the published reports they can also be detected in the peripheral blood [151] and cord blood [188]. Although, Lin^- $CD127^+$ILCs have been studied extensively, the difficulty of working with those cells is due to their low number in the periphery and the fact that there are significant variabilities of those cells between patients [169]. Using UMAP visualisation, I showed that significant variabilities of ILCs can be also observed among neonates.

From previously published research it is known that Lin^- $CD127^+$ ILCs represent only between 0.01 and 0.1% of circulating lymphocytes in adult's blood [113] whereas in umbilical cord blood a greater abundance of Lin^- $CD127^+$ ILCs has been reported (from ~0.2% up to 1%) [188]. In my hands, I was able to observe similar differences between neonatal and adult Lin^- $CD127^+$ ILCs when unsupervised UMAP clustering or the manual gating strategy was applied. I demonstrated that ILC1, ILC2 and ILC3 numbers were increased in newborns when compared to adults and their distribution was constant across the cohort. Moreover, in accordance with data from Vély *et al*., (2016) the frequency of ILC1s, ILC2s and ILC3 as a proportion of the ILC population was on an

equivalent level in cord blood and in adult peripheral blood [188]. I show that neonatal ILCs are capable of producing IFN- γ, IL-13, IL-17A, IL-22 after PBMC stimulation with PMA and ionomycin; however, the frequency of IFN- γ^+ ILCs, IL-13^+ILCs and IL-$17A^+$ILCs are lower than in adults. IL-13^+ ILC2s are among the most studied subsets of the ILC family due to their involvement in many diseases such as atopic dermatitis or childhood asthma [249,250]. I showed that the frequencies of IL-13^+ILC2 are comparable between adults and neonates, providing evidence of their maturity in early life. Notably, in neonatal mouse studies, IL-13-producing ILC2s have been reported in a model of childhood asthma upon the viral infection with rhinovirus which may lead to airway hyperresponsiveness (AHR) and mucus production [251]. Similarly, studies of human infants with severe therapy-resistant asthma (STRA) implicate the high numbers of IL-13^+ILC2s in the development of disease through IL-33 stimulation [194,252]. Together with these findings, I showed that ILC2s are fully mature while ILC1s are not able to mount IFN-γ production on the same level as adults. These differences support further the immune deviation theory of new-born immunity being skewed towards type-2 responses. Together, these findings defined the normal abundance and functional phenotyping of the member of ILC family (except NK cells) in homeostasis and proved to be in accordance with previously reported data on adults and neonates [113,151,188]. Understanding the precise numbers and frequencies of ILCs in health in different subjects was extremely important as it allowed me to compare that data to pathological conditions, and specifically bronchiolitis.

Subsequently, I identified and characterised $CD56^+CD3^-$ NK cells in cord and adult blood as they are the cytotoxic arm of the ILC responses. NK cells represent 10-20% of all lymphocytes in adult blood [248]. Interestingly, NK cell frequency elevates to up to 50% in the uterus during pregnancy [253]. Among NK cells two subsets have been identified using CD56 and CD16 cell markers: $CD56^HCD16^L$ and $CD56^LCD16^H$ NK cells [201]. From previously published work it is known that the NK cell counts are high *post partum* with a significant drop by 2-3 times in the first days of life with a further progressive decrease in early childhood, reaching equilibrium by the age of five [231]. In this cohort I observed a tendency towards higher counts of NK cells in cord blood but not on the magnitude observed in published literature and it did not reach significance [231,235].

A clear majority of NK cells were $CD56^LCD16^H$ in both newborns and adults with a significantly higher proportion in adults compared to neonates (~80% and ~50%, respectively). ln agreement with reported data, no differences were observed in the proportions and abundance of $CD56^HCD16^L$ NKs between birth and adult life [231,233]. Notably, the UMAP embedding approach

showed differences in the topography within NK cell clusters from adults and neonates that could imply differences in their functional profile and maturity. In this work, stimulation of neonatal NK cells triggered the production of IFN-γ; however, at a lower level in comparison to adults. Subtle differences in adult and neonate NK cells suggested by UMAP might have an impact on immune deviation in early life. Immune deviation has been the topic of heated discussion of immune cells of newborns, not only NK cells. It is acknowledged that the immunity of newborns is not depressed but rather immunodeviant to protect from the excessive production of cytokines in a microbe-laden world during birth and the first days of life [20,224]. The price of this immune deviation is the higher susceptibility to infections and, ultimately, morbidity and mortality in early life.

The finding that neonatal NK cells produce less IFN-γ compared to adults was not unexpected even though it has been reported that the numbers of those cells can be higher at birth [231]. Followed by this discovery, I investigated the maturity of NK cells by the assessment of Granzyme B production and expression of CD57. CD57 is the marker that defines terminally differentiated, mature NK cells with a low level of proliferation and immunosenescence [229]. I found no $CD57^{+}$NK cells at birth. In previously published reports in human cord blood studies, the lack of CD57 expression was observed in all T cells compartments not only in NK cells [254]. The lack of CD57 on NK cells during the foetal and neonatal time has been linked with the final step in their maturation [229,255]. In this work, I found that CD57 expression was accompanied by functional changes as $CD57^{-}$ NKs were not able to mount Granzyme B production compared to $CD57^{+}$ NK cells. Contrary to UMAP, biaxial gating was not good at depicting functional changes in Granzyme B production of $CD57^{+}$ NKs, $CD57^{+}CD56^{H}CD16^{L}$ NKs and $CD57^{+}CD56^{L}CD16^{H}$ NKs of adults and neonates when compared to $CD57^{-}$ NKs, $CD57^{-}CD56^{H}CD16^{L}$ NKs and $CD57^{-}CD56^{L}CD16^{H}$ NKs.

In this chapter, I focused not only on innate immunity but also established the abundance and function of adaptive immune cells. I showed that the total cell count of lymphocytes, $CD4^{+}$T cells and $CD8^{+}$T cells in newborns is significantly increased compared to adults even though those cells displayed an equivalent ratio and frequency. Furthermore, a key observation from the comparison of adult and neonatal adaptive T cells was the responses of $CD4^{+}$T cells and $CD8^{+}$T cells upon stimulation with PMA and ionomycin. These responses were characterised by the significantly higher production of IFN-γ, IL-13, IL-17A, IL-22 in adult subjects. UMAP embedding approach confirmed the differences in cytokine production, suggesting the identification of a distinct immunome between newborn and adults. Biancotto *et.al.* (2015) defined the

immunome as 'a vastly complex and highly regulated structure that protects against infection and preserves health' [256]. In brief, the immunome includes a set of genes, proteins and numerous types of immune cells that promote the first-line defence against pathogens [256]. This is consistent with observations in *in vivo* and *in vitro* work in murine and human studies suggesting that $CD4^+$T cells and $CD8^+$T might be immunodeviated towards innate immune responses or that neonates lack the antigen exposure to prime their adaptive T cells [224,225].

The differences in the number of lymphocytes between newborns and adults might be a consequence of the composition of the neonatal T cell compartment due to the difference in the differentiation process in foetal and adult thymus [224]. Data from neonatal mice and human studies suggest that in early life, circulatory T cells consist of foetal and adults haematopoietic precursors [236,237]. The number of foetal derived T cells decreases from birth to adulthood; however, the influence of the foetal compartment can explain skewed type-2 immune responses. Adkins *et al.*, (2003) showed in neonatal mice that foetal-derived $CD4^+$ T cells arising from foetal precursors are functionally and phenotypically different compared to the adult-derived $CD4^+$ T cells. The comparison of the Ag-stimulated foetal-derived cells showed higher production of type-2 cytokines compared to adult cells [236]. Interestingly, it has been shown that high levels of CXCL8 production by T effector cells was observed in newborns but not in adult mice [257]. Contrary to Adkins *et al.*, (2003) I measured cytokine production in non-Ag-stimulated T cells, discovering that neonatal adaptive cell responses are immature and the amount of IFN-γ, IL-13, IL-17A, IL-22 are lower when compared to the adult counterpart. These data might suggest that adaptive cell type-1 and type-2 responses are immature rather than increased type-2 responses.

Th2 and Tc2 cells are interesting subsets due to the association of type-2 skewed immune responses in early life. Although, the frequency and total numbers of Th2 cells are low at birth; both human and mouse neonatal studies suggest their rapid expansion upon delivery [224]. Little is known about type-2 cytokine producing $CD8^+$ T cells apart from their involvement in the development of severe eosinophilic asthma. To my knowledge, I demonstrated for the first time a reduced number of Tc2 cells in new-borns, based on both the expression of CRTH2 as a surface marker and measurement of the proportion of CD8+ cells that produce IL-13. The only data available from human studies involve adults with severe eosinophilic asthma[258]. I believe it opens a great window of opportunity for future investigation of those cells in the early life and their role in susceptibility to infections and allergies.

The majority of studies of neonatal T cells focus on the evaluation of main populations of adaptive cells but in my study, I enumerated the innate-like CD3^{+}T lymphocytes (MAIT and NKT-like cells) MAIT and NKT cells are invariant T cells that are strongly associated with mucosal surfaces and can respond to microbial molecules, such as riboflavin (vitamin B products) and glycolipids, respectively [79,81]. In agreement with published studies, I demonstrated that the number and frequencies of invariant T cells in early life were lower compared to adulthood [84]. From human studies, it is also known that neonates have very low numbers of invariant T cells in the periphery. In-depth analysis of the MAIT cells in cord and adult peripheral blood samples indicated that the maturation of Vα7.2^{+}CD161^{high} cells is rapid in the first months of life but their expansion is a rather slow process [84].

Collectively, the low numbers and frequency of MAIT, NKT-like, Th2 and Tc2 cells at birth might be related to the low experience of microbial-derived molecules *in utero*. Rapid transition into the microbe-laden world after birth may be the reason for maturation and expansion with age of invariant T and IL-13-producing T cells.

In this chapter, I applied powerful techniques utilising unbiased algorithms and combined it with multiparameter flow cytometry from OMIP, ISC and Granzyme B datasets and comprehensive clinical datasets to define and identify patterns that could govern differences between neonates and adults. By utilising whole blood and a mononuclear fraction of peripheral blood, I uncovered that the main differences between neonates and adults were driven by the higher numbers of adult MAIT, Th2, Tc2 and NKT-like cells, and, the production of signature cytokines by these cells. I have observed that the main difference in the immunome of adults is correlated with higher numbers of those cells with age in accordance with published literature [84,224]. I found more lymphocytes, neutrophils and eosinophils in neonates. Moreover, there were more ILCs in neonates; however, they produced less IFN-γ but the same levels of IL-13 as adults, which supports the type-2 skewed pattern of innate responses in neonates [225–227]. Furthermore, in my hands neonatal NK cells were less mature and produced lower levels of IFN-γ but the same amount of Granzyme B. Similarly, neonatal adaptive T cell responses are immature and were characterised by much lower production of IFN-γ, IL-13, IL-17A, IL-22 by CD4^{+} and CD8^{+} T cells in neonates. Finally, I demonstrated that the differences between adults and neonates and among neonates are irrespective of sex, weight, vaccination or gestation. Overall, these data suggested that differences between these two cohorts were greatly influenced by a unique pattern of innate and adaptive responses skewed towards type-2 immunity in neonates [225–227].

Interestingly, the adaptive T cell responses were immature and type-2 skewed immune response were predominately driven by the innate cells, such as ILC2s and eosinophils.

In conclusion, the work in this chapter is in agreement with the notion of type-2 driven differences between adults and neonates; however, the concept of neonates being type-2 biased comes from the studies of adaptive T cells. Notably, the comparison of neonate and adult innate functional responses suggests that innate lymphoid cells are mature, and they might play a pivotal role in the neonatal type-2 bias *via* the production of IL-13. What is more, cord blood is a useful tool to help dissect these differences between early life and adulthood in human studies. As pointed out, the study has thus far optimised protocols for intracellular staining for measuring the signature cytokines of all members of the ILC family (IFN-γ, IL-13, IL-17A, IL-22 and Granzyme B) and utilised other analytical tools. These enabling studies allowed me to progress to comprehensive studies of whole blood and airways cells in bronchiolitic infants. Finally, these data demonstrated intrinsic differences in ILCs between neonates and adults leading to the generation of distinct immunomes supporting my original sub-hypothesis.

3.3

Alterations in frequency, number and function of innate lymphocytes in bronchiolitis

3.3.1. Introduction for Chapter 3.3

The most common reason for children under the age of two to be admitted to hospital is a severe lung infection known as bronchiolitis. This is caused by infection with the very common respiratory syncytial virus (RSV), as well as other common respiratory viruses including rhinovirus, which can be spread easily *via* droplets of liquid when someone coughs or sneezes. Importantly, children who have had bronchiolitis are at a higher risk of developing wheeze and asthma later in childhood. There is no vaccine for RSV available and no new treatments have been developed in recent years. An expensive antibody-based immune prophylaxis with Palivizumab™, an anti-RSV-F-protein monoclonal antibody, decreases the number of children in need of hospitalisation; however, its use is limited to those from higher-risk groups (immunodeficient, premature and children with congenital heart and chronic lung diseases) [259].

Innate and adaptive immunity eliminate pathogens and play crucial roles in immune homeostasis and tolerance [65]. There is a continuous debate about the role of adaptive immune responses in infants during severe RSV-induced bronchiolitis. Studies in rodents have demonstrated that $CD4^+$ and $CD8^+$ T cells are involved in the clearance of virus, however, they can be also associated with the development of immunopathology during RSV-infection [5]. In bronchiolitis, the skewed immune responses towards type-2 responses and poor type-1 responses can provide a partial explanation of RSV related disease severity; however, it does not give an absolute answer. Data obtained from murine models suggest that an immune response skewed away from protective type-1 immunity towards type-2 immunity, characterised by the production of type-2 cytokines (IL-4, IL-5 and IL-13), may contribute to lung damage and inflammation in RSV-infection [6], whereas type-1 immunity characterised by the production of IL-2 and interferon-γ (IFN-γ) is related to virus clearance and improved disease outcome [74]. On the other hand, BALB/c mice with depleted NK cells seemed to have significantly higher chances of survival associated with less IFN-γ accumulation in the lung during RSV infection [192]. The same effect was observed in mice *in vivo* during influenza infections suggesting that although anti-viral and beneficial to the host, IFN-γ producing NK cells can profoundly increase the pathology of infection [190]. In humans, the length of hospitalisation is a measure of disease severity, and the severity of disease correlates with viral load[1,260]. This hypothesis is supported by the human viral challenge studies where the severity of the disease is associated with higher viral load [261]. On the other hand, Thwaites *et al.,* (2018) have shown that infants with severe RSV bronchiolitis

had lower viral load and reduced IFN-γ production in nasal lining fluids compared to those with moderate symptoms [97].

Innate immunity may be relatively important in early childhood due to limited antigen encounter *in utero* and an immature adaptive response and where there are low levels of maternal antibodies (matAbs) [10,20]. Furthermore, innate responses and airway epithelial cells play a role in bronchiolitis. RSV has a relatively small cytopathic effect on human respiratory epithelial cells; however, it is important as it is the site of virus replication and the source of type I, III interferons and chemokines [5]. Interferons limit viral load by driving the production of interferon-stimulated genes (ISG) which can be associated with exuberant inflammatory responses to RSV and disease severity [95]. This theory of exuberant and inappropriate immune responses upon RSV infection is supported by studies in children where a higher production of chemotactic mediators recruits innate cells, such as neutrophils and NK cells [97]. Chemokine production also leads to neutrophil infiltration into the lungs of mice infected with RSV [95] and to the airways of bronchiolitic children [98,99]. Apart from neutrophils, the recruitment of monocytes and NK cells is important to reduce the viral load *via* the production of type-1 immune responses [100]. Although bronchiolitis is an inflammation of the airways, the severity of disease does not always correlate with inflammation when measured for example by the level of cytokines. In nasal mucosal lining cytokines can be relatively lower in severe bronchiolitics compared to moderate cases [97].

ILCs are important in regulating innate and adaptive immune responses during respiratory viral infection, as ILC-depleted mice infected with influenza have impaired lung function [114]. Recent studies suggest that the type-2 skewed immune responses can be driven by ILC2s as they have been linked to the exacerbation of type-2 immune responses in respiratory and airway diseases, such as asthma or rhinosinusitis [193,262]. Studies in neonatal mice demonstrated that upon RSV infection there is an influx of pulmonary ILC2s due to the increased production of IL-33 [259]. Although ILC2s are rare they are a rich source of type-2 cytokines during airway inflammation suggesting the critical role of ILC2s in skewing the immune responses from protective type-1 towards type-2 [169]. ILC2s have been found to increase in number upon respiratory infection in human studies [193,194,263]. Nagakamar *et al*., (2016) reported the presence of greater numbers of ILC2s in sputum, BAL and PBMC in children with severe therapy-resistant asthma (STRA) compared to healthy subjects [194]. Vu *et al*., (2019) observed elevated levels of ILC2s in human hospitalised infants infected with RSV in correlation with IL-33 and ILC2s cytokines (IL-13 and IL-4) [263]. The role of ILC1s and ILC3s in human lungs upon infection is not very well documented;

however, these cells seem to be elevated in cystic fibrosis [195,196]. Finally, in a murine model of allergic inflammation, the IL-22-producing ILC3 subset plays a pivotal role in decreasing the amount of pro-inflammatory IL-33 [197].

The aim of this chapter was to establish if the numbers and function of innate lymphocytes are different in infants with bronchiolitis compared to control infants and to correlate these with the severity of disease and other clinical parameters. I acquired peripheral blood and airway samples from children with severe bronchiolitis in PICU and from healthy, control infants having elective surgery.

Firstly, I performed flow cytometry using OMIP [201] on whole blood and airway samples in order to enumerate the immune cell populations including members of the ILC family (ILC1s, including NK cells; ILC2s and ILC3s), granulocytes (eosinophils and neutrophils), T-cells ($CD4^+$ and $CD8^+$) and invariant T cells (MAIT and NKT-like cells).

I used the mononuclear cell fraction of blood for the elucidation of the functional phenotype of immune cells in control and bronchiolitic infants using the optimised ICS panel for IFN-γ, IL-13, IL-17A, IL-22. I measured the production of soluble inflammatory mediators in supernatants of airway samples.

Finally, the data from enumeration and functional phenotyping of cell populations in whole blood and airway samples and cytokine data were correlated retrospectively with clinical data to unravel the immune correlates in infantile bronchiolitis. This analysis of different clinical samples may lead to the discovery of new therapeutics, biomarkers and help to better understand the immune response in severe, viral bronchiolitis.

3.3.2. Methods for Chapter 3.3

3.3.2.1. Sample collection and processing

Blood and airway samples from control and bronchiolitic babies were obtained after written consent from their families was provided (as described in Material and Methods, see **Chapter 2**) under the RSV-SAM (REC no 15/WM/0343) and Early Life Lung Infection (ELLI) study ethical approval (REC no 18/LO/1570). Exclusion and inclusion criteria were established to minimise variability in the data set (**Tables 2.2.1-3**). All healthy controls had no respiratory symptoms, and were visiting the hospital or undergoing elective surgical procedures and required mechanical ventilation; samples from bronchiolitic infants with suspected severe respiratory viral infection were collected from PICU, St. Mary's Hospital, Paddington, London (as described in Material and Methods, see **Chapter 2**) The numbers of participants in this study are shown Table 3.3.1. (**Results section, Chapter 3.3.3.1**).

3.3.2.2. Flow cytometry panels

The enumeration of different cells in blood and airway samples from controls and bronchiolitic infants was assessed by OMIP [201]. Detailed design and optimisation of this panel can be found in Chapter 3.1 (**Section 3.1.4.1**). To assess the functional phenotype of innate and adaptive cell responses in blood and airway samples from controls and bronchiolitic infants the intracellular staining (ICS) functional panel for IFN-γ, IL-13, IL-17A, IL-22 was utilised (detailed design and optimisation of this panel can be found in Chapter 3.2 (**Section 3.2.2.3, Section 3.2.2.3.1 and Section 3.2.2.4**).

3.3.2.3. Analysis flow cytometry

A 5-laser-LSRFortessa™ was used to run all cells and AbC™ Total Compensation beads, as described in Material and Methods Chapter 2 (**Section 2.2.9.1.4**).

3.3.2.3.1. Deep Immunophenotyping of cytometric data (UMAP)

Optimised dimension reduction technique known as UMAP was applied to the data set to determine the topology of the immunome in blood and airway samples from controls and bronchiolitic infants. Detailed design and optimisation of the dimension reduction technique can be found in Chapter 3.2 (**Section 3.2.2.5.1**).

3.3.2.4. Measurement of cytokine levels using the MSD platform

The MSD platform was used for measuring immune mediators in stored frozen supernatants from airway samples. Airway samples were defrosted at least 30 minutes before the experiment and kept on ice. The analysis was performed according to the manufacturer's instructions. Data

are shown as raw values using a log 10 scale. More details can be found in the Materials and Methods Section (**Section 2.2.9.2**).

3.3.2.5. Statistic and data analysis

P values for categorical data were computed by Chi-square test (χ^2 test) or Fisher's exact test. Differences were assessed through the χ^2 test and Fisher's exact test for sample size>5 and <5, respectively. For continuous data, differences between the two groups were estimated by the Mann-Whitney *U* test. Results are presented as bar plots with individual subjects shown (where the bar represents the median, whiskers represent interquartile range and symbols represent each individual). For multiple comparisons, a Kruskal-Wallis test with Dunn's correction was utilised. Three group results are presented as individual subject plots on the logarithmic scale where lines denote median values and error bars are interquartile ranges. In PCAs, the group mean point was added in the centre of each group and the concentration ellipses around each group mean point using a multivariant *t*-distribution (the size of the concentration ellipse is in the normal probability of 95% confidence). All correlations represent Pearson's correlation coefficients with *P*>0.05 considered insignificant. Data from a range of experiments were analysed in part using Microsoft Excel, Office 365™ (Microsoft, Washington, USA). Graphs were generated using GraphPad Prism 9.0 (GraphPad Software, Inc., California, USA), FlowJoV10.6 software (FlowJo LLC, USA) and R programming language (R Foundation for Statistical Computing, Vienna, Austria).

3.3.3. Results for Chapter 3.3

3.3.3.1. Characteristics of study populations for chapter 3.3

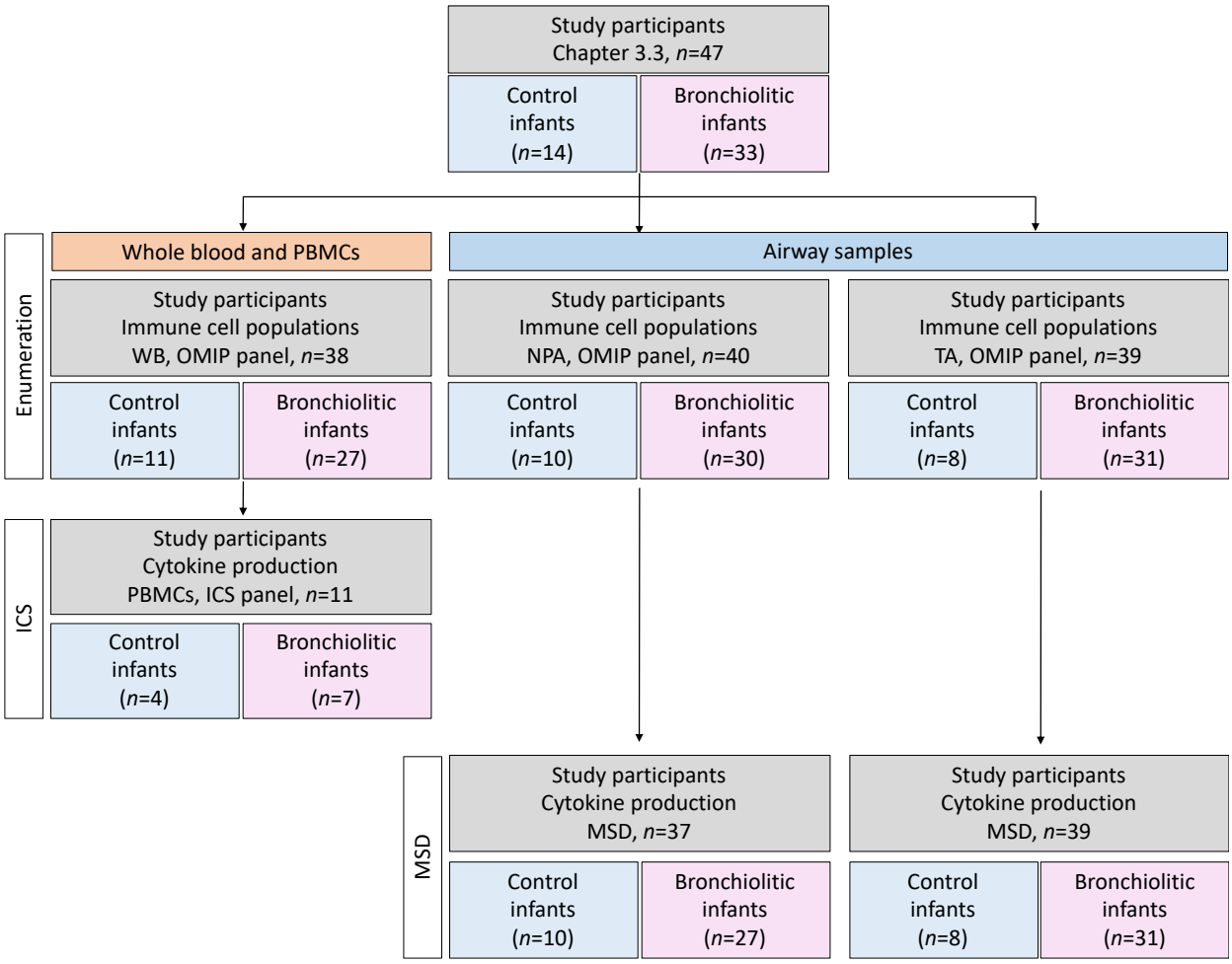


Figure 3.3.1 Flowchart of the study participants used in chapter 3.3

The number of controls (blue, *n*=14) and bronchiolitic infants (pink, *n*=33) used in Chapter 3.3. Graphs depict the number of study participants with data available for OMIP, ICS and MSD analysis. From the total of 47 study participants, the flow cytometry data from WB using OMIP were available from 38 subjects, the NPA data from 40 subjects and TA data from 39 subjects. The flow cytometry data from the ICS panel were available from 11 subjects. The MSD data were available from 37 and 39 subjects (NPA and TA, respectively). Patient data was obtained after written consent using the RSV-SAM study (REC number 15/WM/0343) and the ELLI study (REC Number 18/LO/1570). *Abbreviations used:* OMIP – Optimised multicolour immunophenotyping panel, ICS – Intracellular staining, MSD – Meso scale discovery platform, *n* – number of study participants, PBMC – peripheral blood mononuclear cells, WB – whole blood, NPA – nasopharyngeal aspirates, TA – tracheal aspirates

The study participants' characteristics are shown in **Figure 3.3.1**. The difference between the number of participants in different experiments mirrored the fact that I did not always obtain all samples from this study's subjects. The bronchiolitic patients were stratified according to the viral aetiology of disease: RSV (51.51%), RV (30.30%) and other viruses (18.18%, including Influenza A and B, Adenovirus, CMV, hMPV). At the time of sampling, 33.33% of bronchiolitic infants had bacterial coinfections (*Escherichia coli*, *Klebsiella pneumoniae*, *Staphylococcus aureus*) and other comorbidities. No significant ethnic differences were observed between

control and bronchiolitic groups (*P*=0.19); however, there was a significant difference in the age of infants in the control group with the median age of 216.5 days (range = 18 – 504) compared to the bronchiolitic group (the median age of 66 (range = 36 – 681) (*P*=0.006). Overall, both sexes were represented in this cohort; however, females (7.14%) were underrepresented in the control group compared to bronchiolitic infants (36.6%) (*P*=0.04). There was a significant difference in weights (*P*=0.001) between control and bronchiolitic infants (a median weight of 11.05 and 4.20 kg, respectively). Duration of illness, measured by the length of hospital stay, the length of ventilation and the length of PICU stay were different between groups (*P*<0.001) as most of the control patients were healthy having elective surgery. **Figure 3.3.1** shows the number of study participants with data available for OMIP, ICS and MSD analysis. From the total of 47 study participants, the flow cytometry data from WB using OMIP were available from 38 subjects (**Table 3.3.2**), the NPA data from 40 subjects (**Table 3.3.3**) and TA data from 39 subjects (**Table 3.3.4**). Flow cytometry data for the ICS panel were available from 11 subjects (**Table 3.3.5**). The MSD data were available from 37 and 39 subjects (NPA and TA, respectively) (**Table 3.3.6** and **Table 3.3.7**).

	Control Infants	Bronchiolitic Infants	
Demographic characteristics	*n*=14	*n*=33	*P* value
Age (days); median, (range)	216.50 (18-504)	67.00 (36-681)	**0.006**
Sex; *n* (%)			**0.040**
Females	1 (7.14)	12 (36.36)	
Males	13 (92.86)	21 (61.76)	
Weight (kg); median, (range)	11.05 (2.80-14.30)	4.20 (2.20-10.60)	**0.001**
Ethnicity; *n* (%)			0.190
European	5.00 (35.71)	21.00 (63.63)	
Asian	3.00 (21.42)	7.00 (21.21)	
African (including Afro-Caribbean)	3.00 (21.42)	3.00 (9.09)	
Other	3.00 (21.42)	2.00 (6.06)	
Hospitalisation (days); median, (range)			
Length of hospital stay	1.00 (1.00-2.00)	7.00 (3.00-22.00)	**<0.001**
Length of PICU stay	0.00 (0.00-0.00)	6.00 (3.00-22.00)	**<0.001**
Length of ventilation	1 .00 (1.00-1.00)	6.00 (3.00-22.00)	**<0.001**
Clinical features			NA
Max FiO_2 (%); average, (range)	NA	90.46 (40.00-100)	
PIP (cmH_2O); average, (range)	NA	26.80 (16.00-33.00)	
Aetiology of disease; *n* (%)			NA
RSV	NA	17.00 (51.51)	
RV	NA	10.00 (30.30)	
Other	NA	6.00 (18.18)	
Co-infections; *n* (*%*)			NA
Yes	NA	11.00 (33.33)	
No	NA	22.00 (66.66)	
Comorbidities; *n* (*%*)			NA
Yes	NA	11.00 (33.33)	
No	NA	22.00 (66.66)	
Gestation at delivery			0.537
Not documented; n (%)	5 (35.71)	15 (45.45)	
Documented; *n* (%)	9 (64.29)	18 (54.55)	
Documented (wk); median (range)	32.00 (25.00-41.00)	36.00 (23.00-42.00)	0.484

Table 3.3.1 Control and bronchiolitic infants' demographics used for Chapter 3.3.

Control and bronchiolitic infants used throughout Chapter 3.3. Patient demographic and clinical information were obtained from patients' information sheets. *P* values for continuous data were computed by Mann-Whitney test while *P* values for categorical data were computed by Chi-square test (χ^2 test) or Fisher's exact test. Differences were assessed through χ^2 test and Fisher's exact test for sample size>5 and <5, respectively. Range is defined as the difference between the highest and lowest value. Ethnicity data: European (North/Mid/East-European), Asian (South Asia including India and Pakistan), African (North and Sub-Saharan territories) and other (Middle East, Arabic origin or not stated). Aetiology of disease defines or non-RSV and non-RV viral infection of LRTI such as: Influenza (A and B), Adenovirus, CMV, hMPV. Co-infections are defined as viral (RV, RSV, Influenza A or B, Adenovirus, CMV, hMPV) and bacterial infections (*Escherichia coli*, *Klebsiella pneumoniae*, *Staphylococcus aureus*). *Definition of abbreviation:* PICU – Paediatric Intensive Care Unit, FiO2 – the fraction of inspired oxygen, is defined as the percentage of inhaled oxygen, PIP – Peak Inspiratory Pressure, is the highest amount of pressure in the ventilator circuit when the lungs are filled with air, wk – week, kg – kilogram, NA – not available.

3.3.3.2. The abundance of different innate and adaptive cells in bronchiolitis

3.3.3.2.1. Cohort characteristics for cell enumeration in whole blood

In the first part of this study, the distinction between the abundance of different innate and adaptive cell population between control (*n*=11) and bronchiolitic (*n*=27) infants was determined using whole blood samples (*n*=38, **Table 3.3.2**). In this cohort females and males were well represented (*P*=0.124) with the median age of controls 205 days (range = 18 – 504) and bronchiolitic infants 58 days (range = 36 – 681) (*P*=0.014). There was a significant difference in weights (*P*=0.009) between control and bronchiolitic infants (a median weight of 9.60 and 4.00 kg, respectively). Overall females were well represented; however, females in the control group reached only 9.09% whereas the females were 33.3% of the bronchiolitic cohort. All bronchiolitic patients were stratified according to the viral aetiology of disease: RSV (44.44%), RV (33.33%) and other viruses (22.22%, including Influenza A and B, Adenovirus, CMV, hMPV). At the time of sampling, 29.63% of bronchiolitic infants in the whole blood cohort had bacterial coinfections (*Escherichia coli*, *Klebsiella pneumoniae*, *Staphylococcus aureus*) and 37.03% other comorbidities. Duration of illness, measured by the length of hospital stay, the length of ventilation and the length of PICU stay were different between groups (*P*<0.001) as most of the control patients were healthy having elective surgery.

3.3.3.2.2. Cohort characteristics for cell enumeration in NPA

Similarly, the distinction between the abundance of different innate and adaptive cell population between control (*n*=10) and bronchiolitic (*n*=30) infants was determined using the NPA samples (*n*=40, **Table 3.3.3**). In this cohort females and males were well represented (*P*=0.055) with the median age of controls 216.5 days (range = 100 – 681) and bronchiolitic infants 62.50 days (range = 18 – 504) (*P*=0.007). There was a significant difference in weights (*P*=0.034) between control and bronchiolitic infants (a median weight of 10.15 and 4.10 kg, respectively). Overall females were well represented; however, females reached only 10% of the control group and were 43.33% of the bronchiolitic cohort. All bronchiolitic patients were stratified according to the viral aetiology of disease: RSV (50%), RV (33.33%) and other viruses (16.67%, including Influenza A and B, Adenovirus, CMV, hMPV). At the time of sampling, 36.66% of bronchiolitic infants in NPA cohort had bacterial coinfections (*Escherichia coli*, *Klebsiella pneumoniae*, *Staphylococcus aureus*) and 33.33% other comorbidities. Duration of illness, measured by the length of hospital stay, the length of ventilation and the length of PICU stay were different between groups (*P*<0.001) as most of the control patients were healthy having elective surgery.

3.3.3.2.3. Cohort characteristics for cell enumeration in TA

Finally, the distinction between the abundance of different innate and adaptive cell population between control (*n*=8) and bronchiolitic (*n*=31) infants was determined using the TA samples (*n*=39, **Table 3.3.4**). In this cohort females and males were well represented (*P*=0.121) with the median age of controls 216.5 days (range = 100 – 681) and bronchiolitic infants 67.50 days (range = 18 – 504) (*P*=0.009). There was no significant difference in weights (*P*=0.104) between control and bronchiolitic (a median weight of 10.50 and 4.20 kg, respectively). Overall females were well represented; however, females in the control group reached only 12.5% whereas females were 48.94% of the bronchiolitic cohort. All bronchiolitic patients were stratified according to the viral aetiology of disease: RSV (51.61%), RV (32.25%) and other viruses (16.12%, including Influenza A and B, Adenovirus, CMV, hMPV). At the time of sampling, 35.48% of bronchiolitic infants in TA cohort had bacterial coinfections (*Escherichia coli*, *Klebsiella pneumoniae*, *Staphylococcus aureus*) and 32.25% other comorbidities. Duration of illness, measured by the length of hospital stay, the length of ventilation and the length of PICU stay was different between groups (*P*<0.001) as most of the control patients were healthy having elective surgery.

	Control Infants	Bronchiolitic Infants	
Demographic characteristics	*n*=11	*n*=27	*P* value
Age (days); median, (range)	205.00 (18.00-504.00)	58.00(36.00-681.00)	**0.014**
Sex; *n* (%)			0.124
Females	1.00 (9.09)	9.00 (33.33)	
Males	10.00 (90.91)	18.00 (66.67)	
Weight (kg); median, (range)	9.60 (2.80-14.30)	4.00 (2.20-10.60)	**0.009**
Ethnicity; *n* (%)			0.139
European	4.00 (36.36)	17.00 (62.96)	
Asian	2.00 (18.18)	6.00 (22.22)	
African (including Afro-Caribbean)	2.00 (18.18)	3.00 (11.11)	
Other	3.00 (27.27)	1.00 (3.70)	
Hospitalisation (days); median, (range)			
Length of hospital stay	1.00 (1.00-2.00)	6.00 (3.00-22.00)	**<0.001**
Length of PICU stay	0.00 (0.00-0.00)	6.00 (3.00-21.00)	**<0.001**
Length of ventilation	1 .00 (1.00-1.00)	6.00 (3.00-21.00)	**<0.001**
Clinical features			NA
Max FiO_2 (%); average, (range)	NA	99.81 (40.00-100)	
PIP (cmH_2O); average, (range)	NA	26.18 (16.00-33.00)	
Aetiology of disease; *n* (%)			NA
RSV	NA	12.00 (44.44)	
RV	NA	9.00 (33.33)	
Other	NA	6.00 (22.22)	
Co-infections; *n* (*%*)			NA
Yes	NA	8.00 (29.63)	
No	NA	19.00 (70.37)	
Comorbidities; *n* (*%*)			NA
Yes	NA	10.00 (37.03)	
No	NA	17.00 (62.96)	
Gestation at delivery			0.5076
Not documented; n (%)	4 (36.36)	13 (48.15)	
Documented; *n* (%)	7 (63.64)	14 (51.85)	
Documented (wk); median (range)	31.00 (25.00-38.00)	36.00 (23.00-42.00)	0.4841

Table 3.3.2 Control and bronchiolitic infants' demographics used for whole blood enumeration with immune cell population (OMIP) panel in Chapter 3.3.

Control and bronchiolitic infants used flow cytometry analysis of whole blood with optimised OMIP [201]. Patient demographic and clinical information were obtained from patients' information sheets. *P* values for continuous data were computed by Mann-Whitney test while *P* values for categorical data were computed by Chi-square test (χ^2 test) or Fisher's exact test. Differences were assessed through χ^2 test and Fisher's exact test for sample size>5 and <5, respectively. Range is defined as the difference between the highest and lowest value. Ethnicity data: European (North/Mid/East-European), Asian (South Asia including India and Pakistan), African (North and Sub-Saharan territories) and other (Middle East, Arabic origin or not stated). Aetiology of disease defines or non-RSV and non-RV viral infection of LRTI such as: Influenza (A and B), Adenovirus, CMV, hMPV. Co-infections are defined as viral (RV, RSV, Influenza A or B, Adenovirus, CMV, hMPV) and bacterial infections (*Escherichia coli*, *Klebsiella pneumoniae*, *Staphylococcus aureus*). *Definition of abbreviation:* PICU – Paediatric Intensive Care Unit, FiO2 – the fraction of inspired oxygen, is defined as the percentage of inhaled oxygen, PIP – Peak Inspiratory Pressure, is the highest amount of pressure in the ventilator circuit when the lungs are filled with air, wk=week, kg – kilogram, NA – not available.

	Control Infants	Bronchiolitic Infants	
Demographic characteristics	*n*=10	*n*=30	*P* value
Age (days); median, (range)	216.50 (100-681.00)	62.50(18.00-504.00)	**0.007**
Sex; *n* (%)			**0.055**
Females	1.00 (10.00)	13.00 (43.33)	
Males	9.00 (90.00)	17.00 (56.67)	
Weight (kg); median, (range)	10.15 (2.80-14.30)	4.10 (3.00-10.60)	**0.034**
Ethnicity; *n* (%)			0.264
European	4.00 (40.00)	19.00 (63.33)	
Asian	2.00 (20.00)	6.00 (20.00)	
African (including Afro-Caribbean)	1.00 (10.00)	3.00 (10.00)	
Other	3.00 (30.00)	2.00 (6.67)	
Hospitalisation (days); median, (range)			
Length of hospital stay	2.00 (1.00-2.00)	6.00 (3.00-33.00)	**<0.0001**
Length of PICU stay	0.00 (0.00-0.00)	6.00 (3.00-22.00)	**<0.0001**
Length of ventilation	1 .00 (1.00-1.00)	6.00 (3.00-22.00)	**<0.0001**
Clinical features			NA
Max FiO_2 (%); average, (range)	NA	90.40 (40.00-100)	
PIP (cmH_2O); average, (range)	NA	26.67 (16.00-33.00)	
Aetiology of disease; *n* (%)			NA
RSV	NA	15.00 (50.00)	
RV	NA	10.00 (33.33)	
Other	NA	5.00 (16.67)	
Co-infections; *n* (*%*)			NA
Yes	NA	11.00 (36.66)	
No	NA	19.00 (63.37)	
Comorbidities; *n* (*%*)			NA
Yes	NA	10.00 (33.33)	
No	NA	20.00 (66.67)	
Gestation at delivery			>0.999
Not documented; n (%)	4 (40.00)	12 (40.00)	
Documented; *n* (%)	6 (60.00)	18 (60.00)	
Documented (wk); median (range)	31.50 (25.00-38.00)	36.00 (23.00-42.00)	0.268

Table 3.3.3 Control and bronchiolitic infants' demographics for NPA enumeration with the immune cell population (OMIP) panel in Chapter 3.3.

Control and bronchiolitic infants used flow cytometry analysis of NPA with optimised OMIP [201]. Patient demographic and clinical information were obtained from patients' information sheets. *P* values for continuous data were computed by Mann-Whitney test while *P* values for categorical data were computed by Chi-square test (χ^2 test) or Fisher's exact test. Differences were assessed through χ^2 test and Fisher's exact test for sample size>5 and <5, respectively. Range is defined as the difference between the highest and lowest value. Ethnicity data: European (North/Mid/East-European), Asian (South Asia including India and Pakistan), African (North and Sub-Saharan territories) and other (Middle East, Arabic origin or not stated). Aetiology of disease defines or non-RSV and non-RV viral infection of LRTI such as: Influenza (A and B), Adenovirus, CMV, hMPV. Co-infections are defined as viral (RV, RSV, Influenza A or B, Adenovirus, CMV, hMPV) and bacterial infections (*Escherichia coli*, *Klebsiella pneumoniae*, *Staphylococcus aureus*). *Definition of abbreviation:* PICU – Paediatric Intensive Care Unit, FiO2 – the fraction of inspired oxygen, is defined as the percentage of inhaled oxygen, PIP – Peak Inspiratory Pressure, is the highest amount of pressure in the ventilator circuit when the lungs are filled with air, wk – week, kg – kilogram, NA – not available.

	Control Infants	Bronchiolitic Infants	
Demographic characteristics	*n*=8	*n*=31	*P* value
Age (days); median, (range)	216.50 (100-681.00)	67.00 (18.00-504)	**0.009**
Sex; *n* (%)			0.121
Females	1.00 (12.50)	13.00 (41.94)	
Males	7.00 (87.50)	18.00 (58.06)	
Weight (kg); median, (range)	10.50 (2.80-14.30)	4.20 (3.00-10.60)	0.104
Ethnicity; *n* (%)			0.122
European	3.00 (37.50)	20.00 (64.54)	
Asian	1.00 (12.50)	6.00 (19.34)	
African (including Afro-Caribbean)	1.00 (12.50)	3.00 (9.67)	
Other	3.00 (37.50)	2.00 (6.45)	
Hospitalisation (days); median, (range)			
Length of hospital stay	2.00 (1.00-2.00)	6.00 (3.00-33.00)	**<0.001**
Length of PICU stay	0.00 (0.00-0.00)	6.00 (3.00-22.00)	**<0.001**
Length of ventilation	1 .00 (1.00-1.00)	6.00 (3.00-22.00)	**<0.001**
Clinical features			NA
Max FiO_2 (%); average, (range)	NA	90.76 (40.00-100)	
PIP (cmH_2O); average, (range)	NA	26.29 (16.00-33.00)	
Aetiology of disease; *n* (%)			NA
RSV	NA	16.00 (51.61)	
RV	NA	10.00 (32.25)	
Other	NA	5.00 (16.12)	
Co-infections; *n* (*%*)			NA
Yes	NA	11.00 (35.48)	
No	NA	20.00 (64.51)	
Comorbidities; *n* (*%*)			NA
Yes	NA	10.00 (32.25)	
No	NA	21.00 (67.74)	
Gestation at delivery			0.6817
Not documented; n (%)	4 (40.00)	13 (40.00)	
Documented; *n* (%)	4 (60.00)	18 (60.00)	
Documented (wk); median (range)	29.00 (25.0-37.00)	36.00 (23.00-42.00)	0.1847

Table 3.3.4 Control and bronchiolitic infants' demographics used for TA enumeration with immune cell population (OMIP) panel in Chapter 3.3.

Control and bronchiolitic infants used flow cytometry analysis of TA with optimised OMIP [201]. Patient demographic and clinical information were obtained from patients' information sheets. *P* values for continuous data were computed by Mann-Whitney test while *P* values for categorical data were computed by Chi-square test (χ^2 test) or Fisher's exact test. Differences were assessed through χ^2 test and Fisher's exact test for sample size>5 and <5, respectively. Range is defined as the difference between the highest and lowest value. Ethnicity data: European (North/Mid/East-European), Asian (South Asia including India and Pakistan), African (North and Sub-Saharan territories) and other (Middle East, Arabic origin or not stated). Aetiology of disease defines or non-RSV and non-RV viral infection of LRTI such as: Influenza (A and B), Adenovirus, CMV, hMPV. Co-infections are defined as viral (RV, RSV, Influenza A or B, Adenovirus, CMV, hMPV) and bacterial infections (*Escherichia coli*, *Klebsiella pneumoniae*, *Staphylococcus aureus*). *Definition of abbreviation:* PICU – Paediatric Intensive Care Unit, FiO2 – the fraction of inspired oxygen, is defined as the percentage of inhaled oxygen, PIP – Peak Inspiratory Pressure, is the highest amount of pressure in the ventilator circuit when the lungs are filled with air, wk – week, kg – kilogram, NA – not available.

3.3.3.2.4. The abundance of cell populations in control and bronchiolitic infants in blood and airway samples

Enumeration of granulocytes, lymphocytes and monocytes in control and bronchiolitic infants

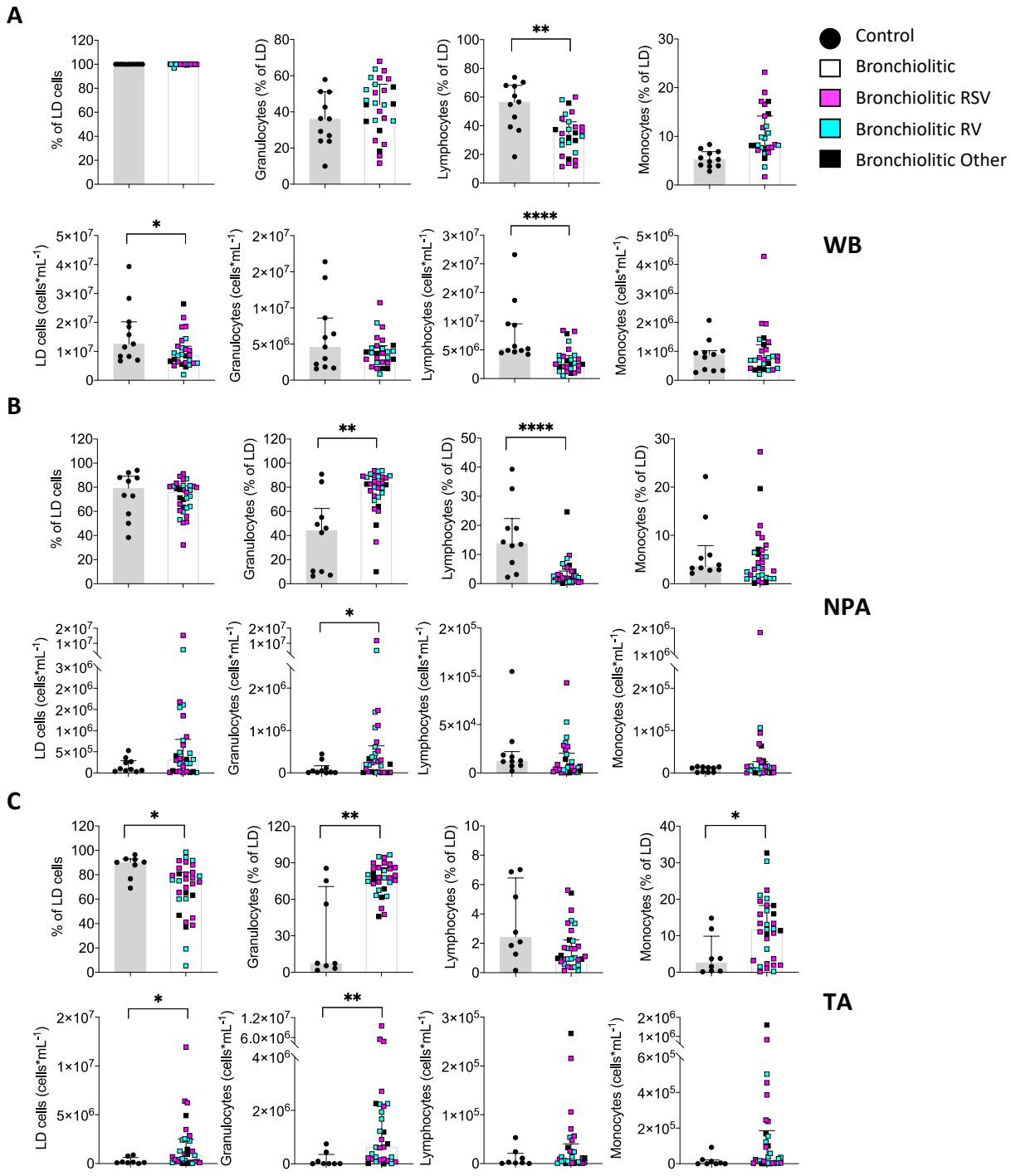


Figure 3.3.2 Abundance of live cells, granulocytes, lymphocytes and monocytes in whole blood and airway samples from control and bronchiolitic infants.

Granulocytes, monocytes and lymphocytes were delineated on live, single and $CD45^+$ cells in the whole blood (*n*=38) **(A)**, NPA (*n*=40) **(B)** and TA (*n*=39) **(C)** from control (*n*=14) and bronchiolitic infants (*n*=33). Graphs show both frequency and quantification of all live cells, granulocytes, lymphocytes and monocytes in the peripheral whole blood **(A)** and airway samples (NPA and TA) **(B-C)**. Data represent more than 40 experimental results shown as the median with upper interquartile range **(A-C)**. Differences between groups were estimated by Mann-Whitney test (* $p < 0.05$, ** $p < 0.01$ and **** $p < 0.0001$). *Abbreviations used:* LD – live, viable cells, *n* – number of study participants, WB – whole blood, NPA – nasopharyngeal aspirates, TA – tracheal aspirates.

I utilised the gating strategy from the published OMIP [201] (**Section 3.1**, **Fig. 3.1.3**). Granulocytes, monocytes and lymphocytes were delineated on live, single and $CD45^+$ cells in whole blood (*n*=38) **(Fig. 3.3.2 A)**, NPA (*n*=40) **(Fig. 3.3.2 B)** and TA (*n*=39) **(Fig. 3.3.2 C)** from control and bronchiolitic infants. Interestingly, in the peripheral blood, I detected a significantly higher number of live cells in control babies compared to the bronchiolitic ones (*P*=0.04, with a median of 1.3 x 10^7 cell per mL and 8.5 x 10^6 cell per mL, respectively) (**Fig. 3.3.2 A**). The decrease of live cells in bronchiolitic infants compared to controls was driven by the fact that the frequency (*P*=0.001, with a median of 57% and 35%, respectively) and a total number (*P*=0.04, with a median of 5.2x 10^6 cells per mL and 2.5 x 10^6 cells per mL, respectively) of lymphocytes were reduced, whereas this trend was not observed for granulocytes and monocytes (**Fig. 3.3.2 A**). In NPAs, similarly to the whole blood samples, the lymphocytes displayed significantly lower frequency in bronchiolitic babies (a median of 14%) compared to control ones (a median of 2%) (*P*<0.0001) (**Fig. 3.3.2 B**). In contrast, the granulocyte population in NPAs from infants with bronchiolitis was significantly higher as a total number (*P*=0.036) and frequency of $CD45^+$ leukocytes (*P*=0.023) compared to controls (**Fig. 3.3.2 B**.). Finally, I investigated TA samples and detected a significantly lower number of live cells in control babies compared to the bronchiolitic ones (*P*=0.0135, with a median of 1.5 x 10^5 cells per mL and 9 x 10^5 cells per mL, respectively) (**Fig. 3.3.2 C**) whilst the opposite trend was observed when the frequencies of live, viable cells of all cells were analysed (*P*=0.012, with a median of 90% for controls and 75% for bronchiolitic infants). The TA monocyte frequency among live CD45+ cells in control and bronchiolitic infants was ~3% and ~12%, respectively (*P*=0.032) (**Fig. 3.3.2 C**).

3.3.3.2.4.1. The abundance of innate cell populations in control and bronchiolitic infants

Enumeration of granulocytes in control and bronchiolitic infants

The role of granulocytes in bronchiolitis is of particular interest as neutrophils are the predominant cell type in the airways of bronchiolitic infants [95]. To assess the abundance of granulocytes (including eosinophils and neutrophils) in the peripheral blood and airway samples (NPA and TA), I utilised the gating strategy from the published OMIP [201] (**Section 3.1**, **Fig. 3.1.3**). Granulocytes were defined within live, single, $CD45^+$ lymphocytes using SSC-A in the whole blood (*n*=38) **(Fig. 3.3.3 A)**, NPA (*n*=40) **(Fig. 3.3.3 B)** and TA (*n*=39) **(Fig. 3.3.3 C)** from control (*n*=14)

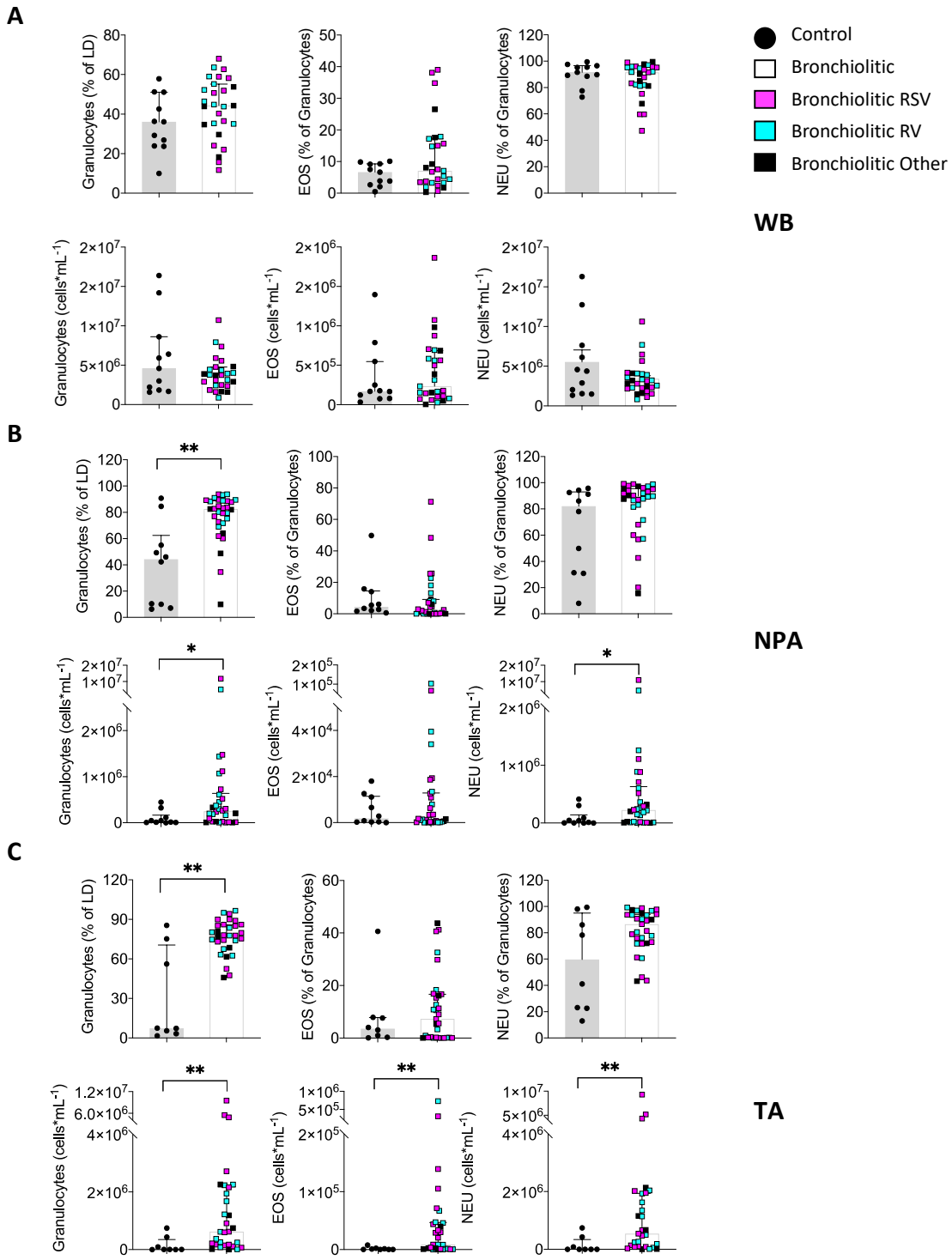


Figure 3.3.3 Abundance of granulocytes in whole blood and airway samples from control and bronchiolitic infants.

Granulocytes, eosinophils and neutrophils were defined in WB (*n*=38) **(A)**, NPA (*n*=40) **(B)** and TA (*n*=39) **(C)** from control (*n*=14) and bronchiolitic infants (*n*=33). Utilizing OMIP [201], granulocytes were delineated as live, single, cells using CD45 and SSC-A; within the granulocytes, neutrophils were defined as $CD16^{+}CD66b^{+/-}$ and eosinophils as $CD16^{-}CD66b^{+}$. Graphs show both quantification and the frequency of total granulocytes among live leukocytes, frequency of eosinophils and neutrophils among granulocytes in the whole blood **(A)** and airway samples (NPA and TA) **(B-C)**. Data represent more than 40 experiments and are shown as the median with upper interquartile range **(A-C)**. Differences between groups were estimated by Mann-Whitney test (* $p < 0.05$ and ** $p < 0.01$). *Abbreviations used:* LD – live, viable cells, *n* – number of study participants, EOS – eosinophils, NEU – neutrophils, WB – whole blood, NPA – nasopharyngeal aspirates, TA – tracheal aspirates.

and bronchiolitic infants (*n*=33). Within the granulocytes, neutrophils were defined as $CD16^{+}CD66b^{+/-}$ and eosinophils as $CD16^{-}CD66b^{+}$. In the peripheral blood, no significant changes were detected in the number and the frequency among the live leukocytes (**Fig. 3.3.3 A**). In the NPAs I observed significantly higher numbers and frequencies of granulocytes (as mentioned in Section 3.3.3.2.4) and significantly higher numbers of neutrophils. In TAs eosinophils and neutrophils were significantly more abundant in bronchiolitic compared to the control cohort. The eosinophils in the TA of bronchiolitic infants displayed significantly higher total numbers (*P*=0.02) with a median of 4.6 x 10^2 cells per mL compared to 8.6 x 10^3 cells per mL in the control group. Similarly, the neutrophil population in the TA of bronchiolitic infants significantly increased compared to control infants (*P*=0.003, with a median of 1.8 x 10^3 and 5.4 x 10^5 cells per mL, respectively). Granulocytes were less abundant in the TAs of controls than bronchiolitic infants, as the number (*P*=0.002, with a median of 6.1 x 10^3 and 6.3 x 10^5 cell per mL, respectively) and also the frequency (*P*=0.002, with a median of 7.3% for controls and 78% for bronchiolitic infants) (**Fig. 3.3.3 C**) among the live leukocytes.

Enumeration of ILCs in control and bronchiolitic infants

Next, I investigated whether there are differences in the populations of ILCs (excluding NK cells) across those two groups of control and bronchiolitic infants. The abundance of ILCs was assessed by the gating strategy from the OMIP [201] (**Section 3.1**, **Fig. 3.1.3**). ILCs were delineated within live, single, $CD45^{+}$ lymphocytes as lineage negative (CD3, CD14, CD19, CD56, CD123 and FcεRIα)$^{-}$ and $CD127^{+}$ (IL-7 receptor-α) cells. All ILCs subsets were detected in peripheral blood from control and bronchiolitic infants; however, the abundance of ILCs, ILC1s, ILC2s and ILC3s was much higher in healthy controls compared to bronchiolitics even though the number of those cells decreases with age [188] (*P*=0.005 with a median of 1.9 x 10^4 cells per mL in control and 5x 10^3 cells per mL in bronchiolitic, *P*=0.0005 with a median of 9 x 10^3 cells per mL in control and 2.5 x 10^3 cells per mL in bronchiolitic, *P*<0.0005 with a median of 4.8 x 10^3 cells per mL in control and 1.5 x 10^3 cells per mL in bronchiolitic and *P*=0.0001 with a median of 2 x 10^3 cells per mL in control and 3.3 x 10^3 cells per mL in bronchiolitic for ILCs, ILC1s, ILC2s and ILC3s, respectively) (**Fig. 3.3.4 A**). Similarly to peripheral blood, in NPA samples, ILCs and ILC1s were less abundant in severely ill infants (*P*=0.025 and *P*=0.045) (**Fig. 3.3.4 B**). Single data points skewing the dataset were observed among healthy control and children with bronchiolitis; however, they did not belong to the same infants. In TAs, although there was a trend towards increased numbers of ILCs in bronchiolitis, no significant differences were detected among patients in the two groups in the

frequency and number of ILCs, ILC1s, ILC2s and ILC3s (**Fig. 3.3.4 C**). Finally, the vast majority of ILCs in the airways were ILC1s and no change in frequencies of these cells as a percentage of total ILCs were observed between bronchiolitic and controls (**Fig. 3.3.4 B, C**).

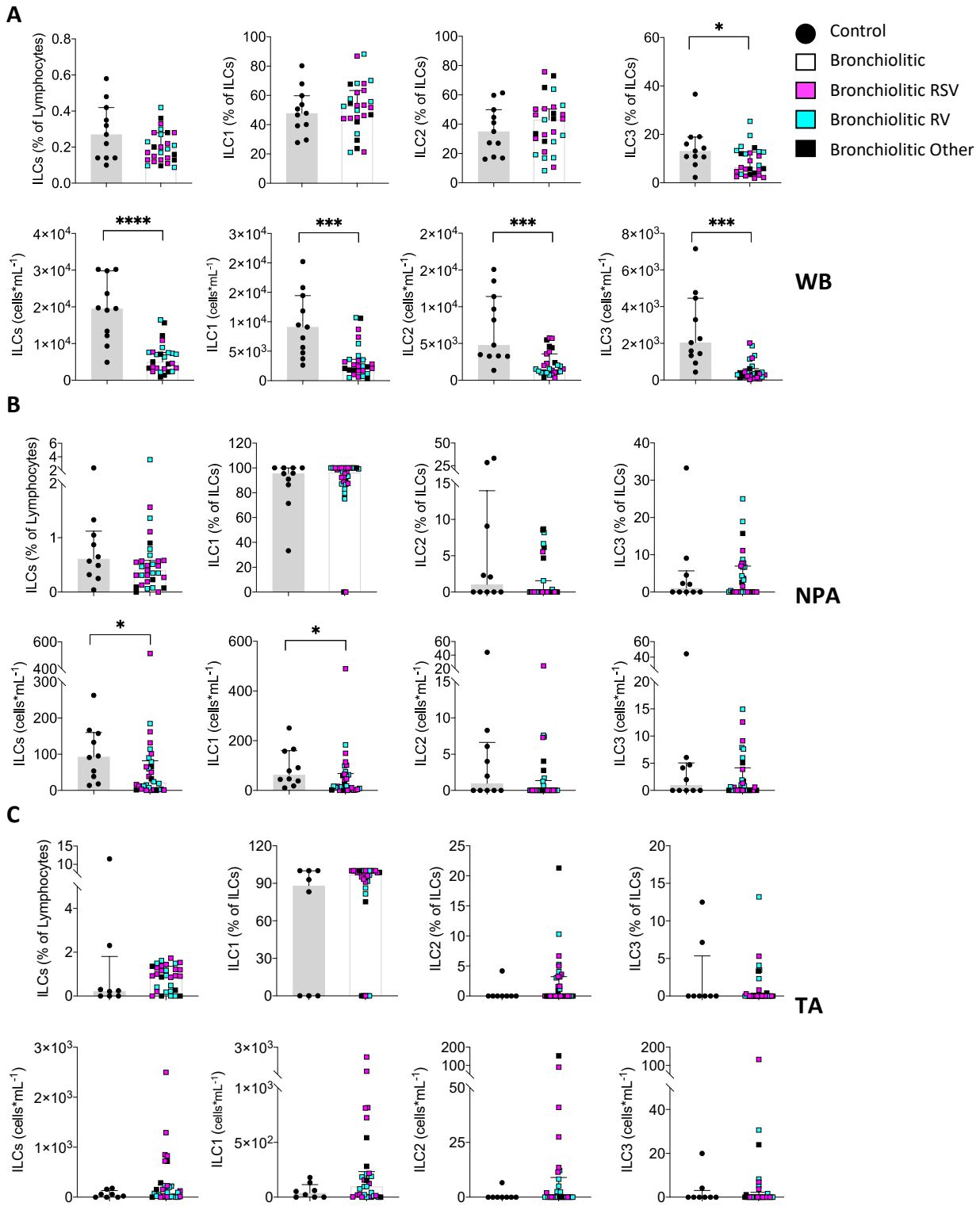


Figure 3.3.4 Abundance of ILCs in whole blood and airway samples from control and bronchiolitic infants.

ILCs in peripheral whole blood (*n*=38) **(A)**, NPA (*n*=40) **(B)** and TA (*n*=39) **(C)** from control (*n*=14) and bronchiolitic infants (*n*=33) were defined using OMIP [201]. ILCs were delineated within live, single, $CD45^+$ lymphocytes as lineage negative (CD3, CD14, CD19, CD56, CD123 and $Fc\varepsilon RI\alpha)^-$ and $CD127^+$ (IL-7 receptor-α) cells. The ILC subsets (ILC1, ILC2 and ILC3) were identified using CRTH2 and CD117 (c-Kit) surface markers; ILC1 cells were defined as $CD117^-CRTH2^-$, ILC2 cells as $CRTH2^+$ $CD117^{int}$ and ILC3 as $CD117^+CRTH2^-$. Graphs show both quantification and the frequency of total ILCs among live lymphocytes and ILC1s, ILC2s, ILC3s among total ILCs in the whole blood **(A)** and airway samples (NPA and TA) **(B-C)**. Data represent more than 40 experiments and are shown as the median with upper interquartile range **(A-C)**. Differences between groups were estimated by Mann-Whitney test (* $p < 0.05$, ** $p < 0.01$ and *** $p < 0.001$). *Abbreviations used: n* – number of study participants, WB – whole blood, NPA – nasopharyngeal aspirates, TA – tracheal aspirates, ILCs – innate lymphoid cells.

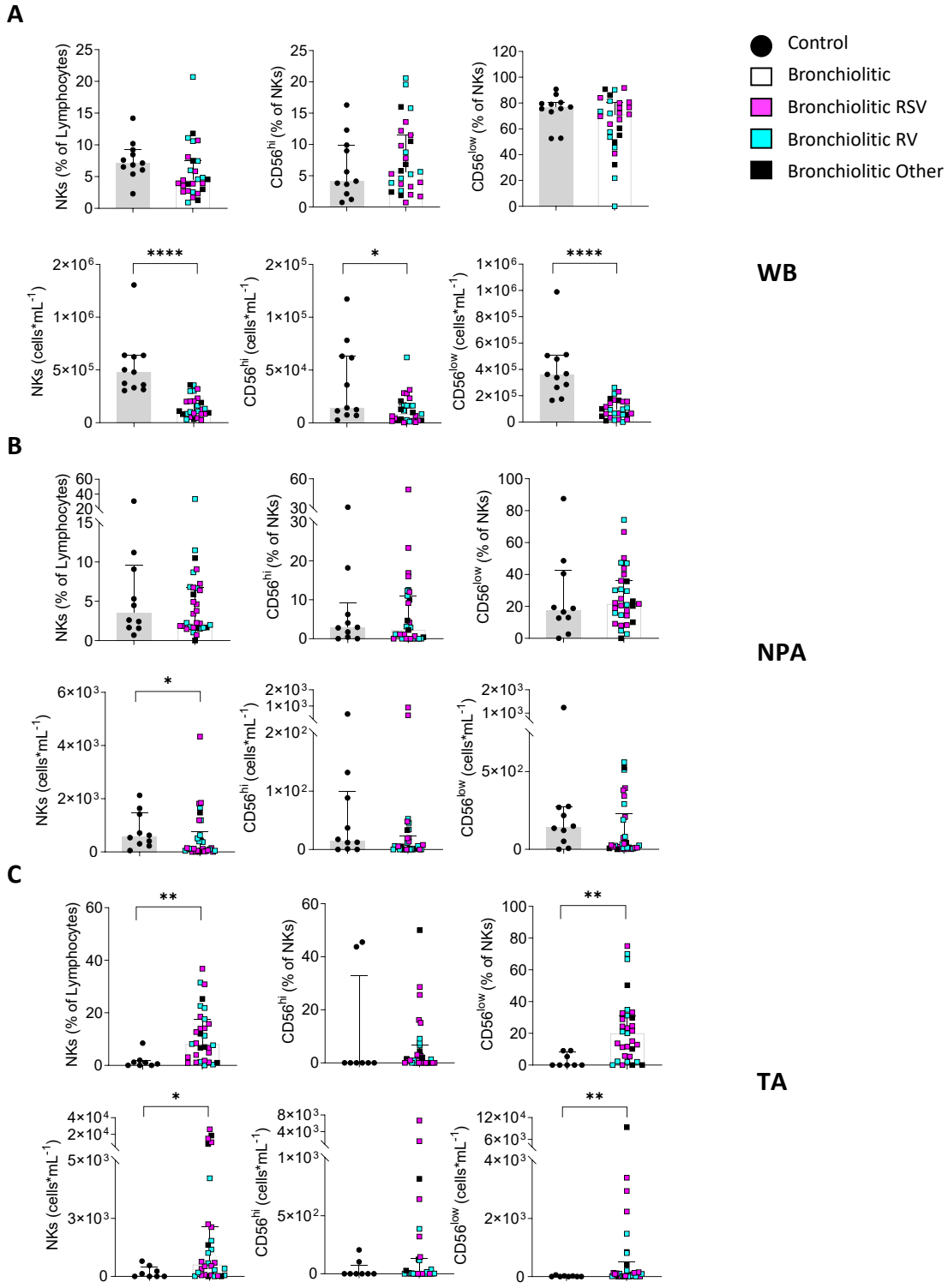


Figure 3.3.5 Abundance of NK cells in whole blood and airway samples from control and bronchiolitic infants.

NK cells in peripheral whole blood (*n*=38) **(A)**, NPA (*n*=40) **(B)** and TA (*n*=39) **(C)** from control (*n*=14) and bronchiolitic infants (*n*=33) were defined using OMIP [201]. NK cells were defined as live, single, $CD45^+$ $CD56^+CD3^-$ lymphocytes. Within the NK cell population, $CD56^HCD16^L$ and $CD56^LCD16^H$ subsets were delineated. Graphs show both quantification and the frequency of $CD56^+CD3^-$ NK cells among live lymphocytes, $CD56^HCD16^L$ NK cells and $CD56^LCD16^H$ NK cells among total NK cells in the whole blood **(A)** and airway samples (NPA and TA) **(B-C)**. Data represent more than 40 experiments and are shown as the median with upper interquartile range **(A-C)**. Differences between groups were estimated by Mann-Whitney test (* $p < 0.05$, ** $p < 0.01$ and **** $p < 0.0001$). *Abbreviations used: n* – number of study participants, WB – whole blood, NPA – nasopharyngeal aspirates, TA – tracheal aspirates, NK – natural killer cells.

I next enumerated NK cells in control and bronchiolitic infants. The abundance of NK cells was assessed using the gating strategy from the published OMIP [201] (**Section 3.1**, **Fig. 3.1.3**). NK cells were defined as live, single, $CD45^+$ $CD56^+CD3^-$ lymphocytes. Within the NK cell population, $CD56^HCD16^L$ ($CD56^H$) and $CD56^LCD16^H$ (CD56L) subsets were defined. In peripheral blood, I detected a significantly higher number of NK cells in control babies compared to the bronchiolitic ones (P<0.0001, with a median of 4.7 x 10^5 cells per mL and 1.1 x 10^5 cells per mL, respectively) (**Fig. 3.3.5 A**). The proportion of $CD56^HCD16^L$ ($CD56^H$) and $CD56^LCD16^H$ ($CD56^L$) subsets remained similar in bronchiolitis and the numbers of both populations were reduced in bronchiolitis (P=0.035 and P<0.0001, respectively) (with a median number of 1.4 x 10^4 $CD56^H$ NK cells per mL for controls and 8.5 x 10^3 cells per mL for bronchiolitics; and a median of 3.6 x 10^5 $CD56^L$ NK cells per mL for controls and 9.3 x 10^4 cells per mL for bronchiolitics) (**Fig. 3.3.5 A**). In NPAs, $CD56^+CD3^-$ NK cells displayed significantly lower cell counts in bronchiolitic babies (a median of 5.8 x 10^2 cells per mL) compared to control ones (a median of 1.2 x 10^2 cells per mL) (P=0.049) (**Fig. 3.3.5 B**). Finally, in TAs I observed a statistically higher number (P=0.019) of NK cells in infants with bronchiolitis and a higher proportion (P=0.002) of those cells (**Fig. 3.3.5 C**). Moreover, the $CD56^HCD16^L$ ($CD56^H$) subset displayed similar numbers in the TA in both groups; however, $CD56^L$ NK cells had a higher abundance (P=0.004) and frequency among NK cells (P=0.001) in the TA in bronchiolitis compared to the control group (**Fig. 3.3.5 C**). Single data points skewing the dataset were observed among healthy control and children with bronchiolitis; however, they did not belong to the same infants (**Fig. 3.3.5 A-C**).

3.3.3.2.4.2. The abundance of adaptive cell populations in controls and bronchiolitics

Enumeration of lymphocytes, $CD4^+$ and $CD8^+$ T cells in control and bronchiolitic infants

I analysed the numbers and frequencies of $CD4^+$ and $CD8^+$ T cells among the lymphocytes in whole blood or airway samples by the gating strategy from the OMIP [201] (**Section 3.1**, **Fig. 3.1.3**). Within the lymphocyte gate, NK and NKT cells were gated out and $CD3^+CD56^-$ T lymphocytes were segregated into $CD4^+$ or $CD8^+$ T cells. As mentioned in Section 3.3.3.2.4 (**Fig. 3.3.2 A-C**, see above), the number and the frequency of lymphocytes were statistically lower in the peripheral blood and NPA but not in TA samples in infants with bronchiolitis. In circulation bronchiolitic infants displayed significantly higher frequencies of $CD4^+$ (P=0.001) whereas $CD8^+$ T cells were statistically lower (P=0.001) as a proportion of lymphocytes when compared to control subjects (**Fig. 3.3.6 A**). Interestingly, both $CD4^+$ and $CD8^+$ T cells populations were far less abundant in the periphery of severely ill infants (with a median of 1.1 x 10^6 cells per mL for CD4 T cells and 4.4 x 10^5 cells per mL for CD8 T cells)

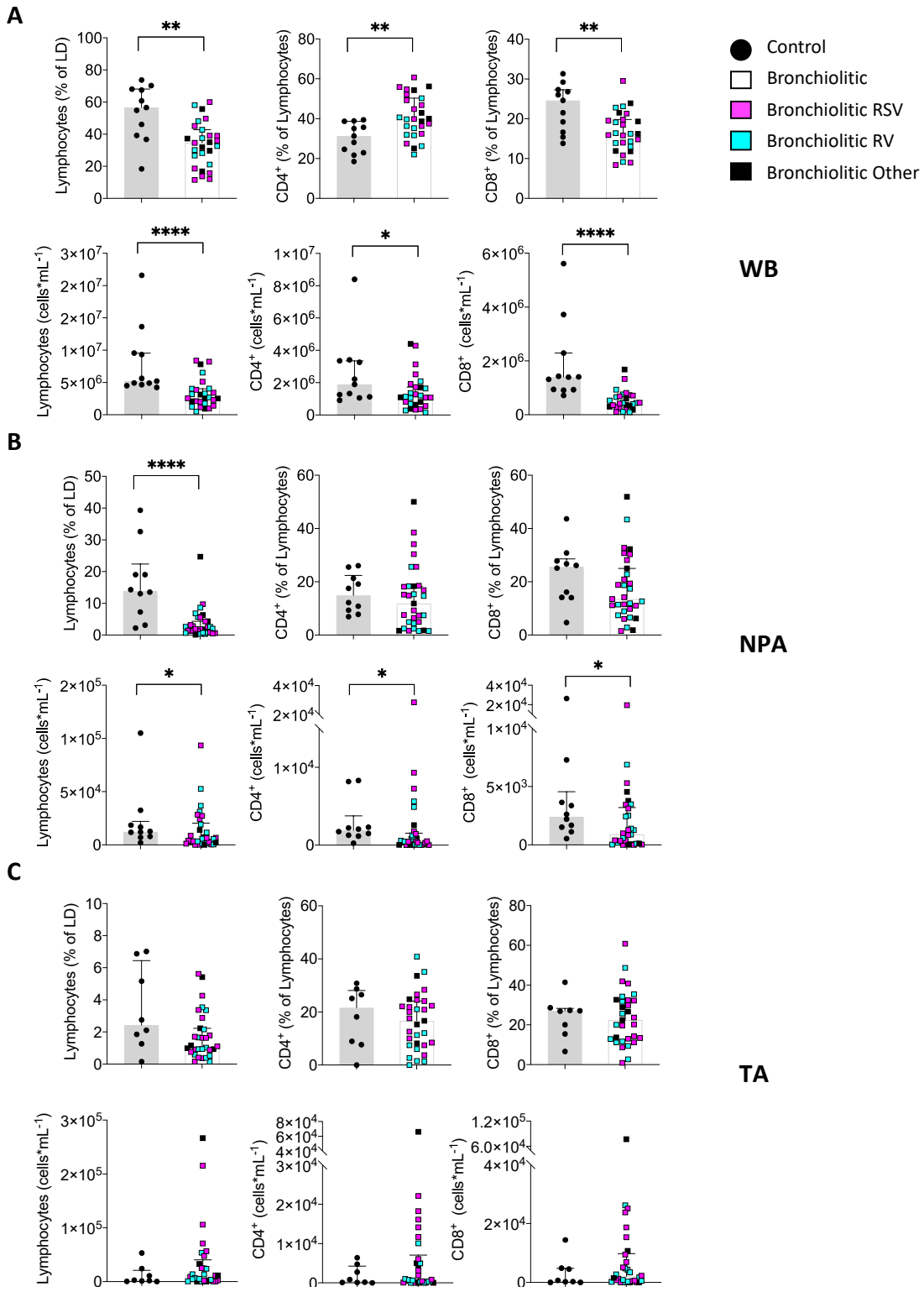


Figure 3.3.6 Abundance of lymphocytes, CD4$^+$ and CD8$^+$ T cells in whole blood and airway samples from control and bronchiolitic infants.

Lymphocytes, CD4$^+$ or CD8$^+$ T cells in peripheral whole blood (*n*=38) **(A)**, NPA (*n*=40) **(B)** and TA (*n*=39) **(C)** from control (*n*=14) and bronchiolitic infants (*n*=33) were defined using OMIP [201]. Using CD45 expression and SSC-A, live, single lymphocytes were delineated. Among the lymphocyte gate, T lymphocytes (CD3$^+$CD56$^-$) were segregated into CD4$^+$ or CD8$^+$ T cells. Graphs shows both quantification and the frequency of total lymphocytes among live leukocytes, frequency of CD4$^+$ and CD8$^+$ T cells among lymphocytes in the whole blood **(A)** and airway samples (NPA and TA) **(B-C)**. Data represent more than 40 experiments and are shown as the median with upper interquartile range **(A-C)**. Differences between groups were estimated by Mann-Whitney test (* $p < 0.05$, ** $p < 0.01$ and **** p

< 0.0001). *Abbreviations used: n* – number of study participants, WB – whole blood, NPA – nasopharyngeal aspirates, TA – tracheal aspirates.

compared to the control infants (with a median of 1.8 x 10^6 cells per mL for CD4 T cells and 1.3 x 10^6 cells per mL for CD8 T cells) (**Fig. 3.3.6 A**). There was a significant difference between the median ratio of CD4 positive:CD8 positive cells in whole blood (P=0.003) between control (1.42:1) and bronchiolitic infants (2.41:1). Similarly to the whole blood, NPA $CD4^+$ and $CD8^+$ T cells populations were less abundant in severely ill infants (with a median of 4.8 x 10^2 cells per mL for CD4 T and 8.9x 10^2 cells per mL for CD8 T cells) compared to the control infants (with a median of 1.9 x 10^3 cells per mL for CD4 T and 2.4 x 10^3 cells per mL for CD8 T cells) (**Fig. 3.3.6 B**). Finally, no differences were detected between groups in the frequency and number of $CD4^+$ and $CD8^+$ T cells populations in the TA (**Fig. 3.3.7 C**); and no difference was observed in the median ratio of CD4 positive:CD8 positive cells between control and bronchiolitic infants in NPA and TA. Moreover, among healthy control and children with bronchiolitis, single data points skewing the data were observed; however, they did not belong to the same infants (**Fig. 3.3.7 A-C**).

Enumeration of MAIT, NKT, Tc2 and Th2 cells in control and bronchiolitic infants

I determined the MAIT, NKT, Tc2 and Th2 cell numbers and frequency among the lymphocytes in the whole blood (*n*=38) (**Figure 3.3.7 A**), NPA (*n*=40) (**Fig. 3.3.7 B**) and TA (*n*=39) (**Fig. 3.3.7 C**) from control (*n*=14) and bronchiolitic infants (*n*=33). The gating strategy from OMIP [201] is shown in **Section 3.1**, **Figure 3.1.3**. The MAIT, NKT, Tc2 and Th2 subsets were statistically more abundant in the periphery of control subjects compared to bronchiolitics (*P*=0.0001, *P*=0.0001, *P*=0.0001, and *P*=0.0001 for MAIT, NKT, Tc2 and Th2 cells, respectively) (**Fig. 3.2.13 A**). In whole blood, only the frequency of MAIT cells was lower in bronchiolitics (a median of 0.18%) compared to controls (a median of 0.07%) (*P*=0.03) and may be explained by age difference (**Fig. 3.3.7 A**). In NPAs, the frequency of Tc2 as a proportion of CD8+ lymphocytes increased significantly in bronchiolitic infants when compared to non-bronchiolitic group (*P*=0.001, with a median of 0.03% and 0.08%, respectively). (**Fig. 3.3.7 B**). Finally, no differences were detected among patients in those two groups in the frequency and number of MAIT, NKT, Tc2 and Th2 T cells subsets in the TA, apart from a higher number of Tc2 cells in infants with bronchiolitis (**Fig. 3.3.7 C**).

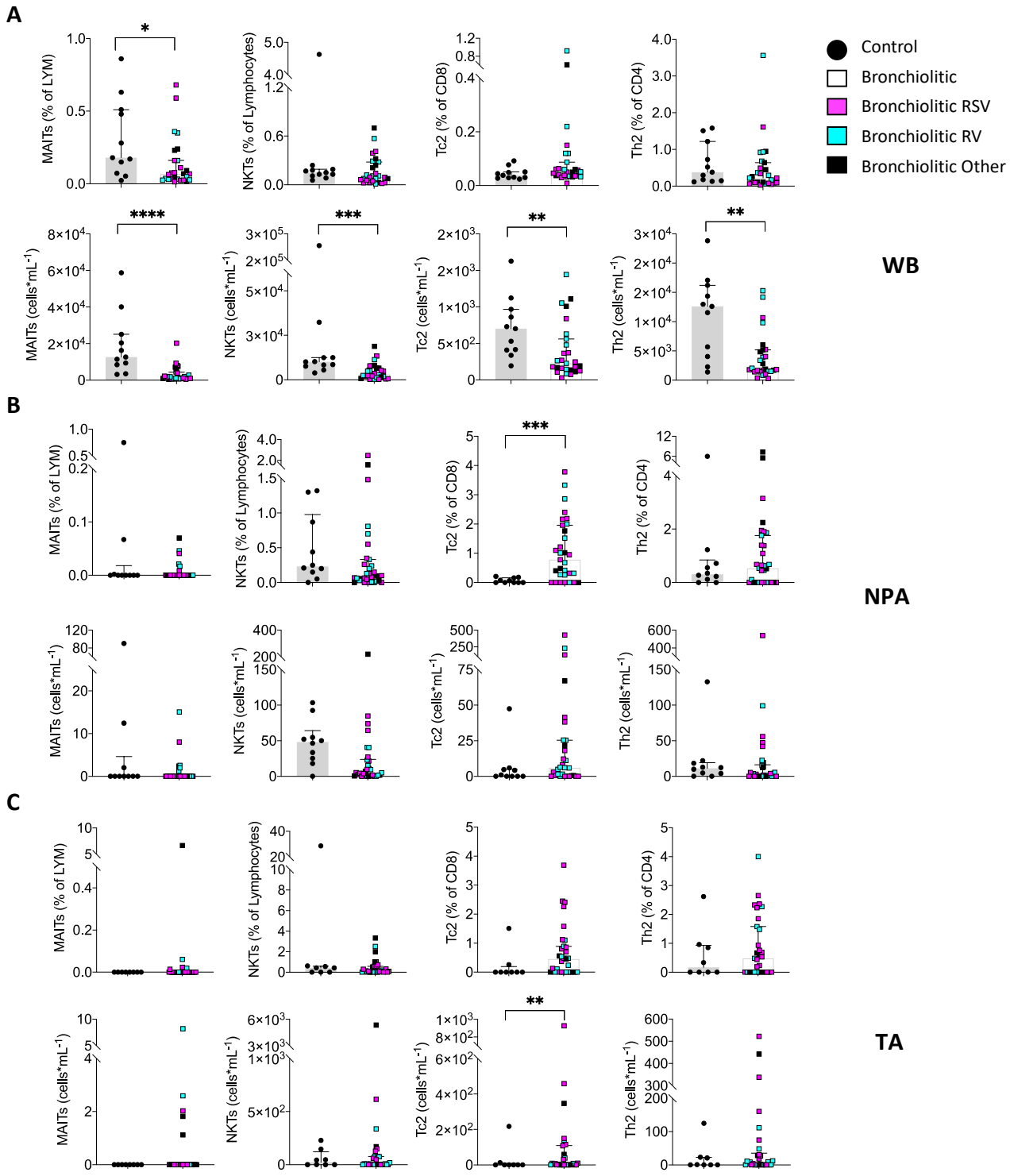


Figure 3.3.7 Abundance of MAIT, NKT, Tc2 and Th2 cells in whole blood and airway samples from control and bronchiolitic infants.

MAIT, NKT, Tc2 and Th2 cells in peripheral whole blood (*n*=38) **(A)**, NPA (*n*=40) **(B)** and TA (*n*=39) **(C)** from control (*n*=14) and bronchiolitic infants (*n*=33) were defined using OMIP [201]. T lymphocytes (FSC/SSC, single, live, $CD45^+$, $CD3^+CD56^-$ cells) were segregated into $CD4^+$ or $CD8^+$ T cells. Within $CD4^+$ and $CD8^+$ T cells, the CRTH2 marker was used to define Th2 and Tc2 cells respectively. Within $CD8^+$ cells, MAIT cells were defined as $CD161^H$ $V\alpha7.2^+$. Graphs show both quantification and the frequency of MAITs, $CD56^+CD3^+$ NKT cellss among lymphocytes, $CD56^-CD3^+CRTH2^+$ Th2s among CD4+ T cells and $CD56^-CD3^+CRTH2^+$ Tc2s among $CD8^+$ T cells in the whole blood **(A)** and airway samples (NPA and TA) **(B-C)**. Data represent more than 40 experiments and are shown as the median with upper interquartile range **(A-C)**. Differences between groups were determined by Mann-Whitney test (* $p < 0.05$, ** $p < 0.01$, ***$p < 0.001$ and **** $p < 0.0001$).

3.3.3.2.5. Assessment of the immunome of bronchiolitic infants by UMAP

I next characterised the immunome in samples from the cohort of control (*n*=12) and bronchiolitic infants (*n*=51) using UMAP [204]. This allowed me to reduce 16 dimensions into two dimensions referred to as UMAPx and UMAPy that formed an augmented panel (**Fig. 3.3.8 A,** middle). To reduce dimensions, flow data used for OMIP [201] (see Chapter 3.1) was utilised from at least 20 experiments; both control and bronchiolitic samples included WB (*n*=21), NPA (*n*=21) and TA (*n*=21). Before UMAP computation, data were cleaned using standard biaxial gating strategy, including only single, live lymphocytes (**Fig. 3.3.8 A,** left). Data cleaning involves selecting the population of cells on which UMAP will be performed using a gating strategy. Data cleaning did not involve removing, replacing or modifying any set of data. Lymphocytes were gated using SSC-A and the CD45 cell marker. After data cleaning, I performed UMAP analysis on 350,000 randomly selected lymphocytes (~5,000 from each subject concatenated into a single file). Expression of CD45 (**Fig. 3.2.14 A**, middle) and CD3 are shown as examples (**Fig 3.2.14 A**, right). The manual gating strategy from the OMIP was utilised to allow global UMAP clusters (all subjects pooled) to be classified into the following cell types: CD4 T cells (yellow), NKT cells (bright blue), monocytes (green), CD8 T cells (orange), neutrophils (ocean blue), eosinophils (magenta), NK cells (bright green), MAIT cells (black), and ILCs (red) (**Fig 3.2.14 B)**. UMAP projections for control and bronchiolitic patients identified pathophysiological alterations in immune cell clusters that are not only disease-specific but also depend on the origin of the sample. Thus, UMAP allowed not only to estimate the immune cell composition as evidenced from gating analysis with OMIP [201] but also to investigate phenotypical, disease-specific changes within each cell cluster in particular for the whole blood, NPA or TA samples among control and bronchiolitic infants (**Fig. 3.3.3.8 C**). Based on visualisation in **Figure 3.3.3.8 C**, I identified that the architecture of the healthy immunome is dysregulated in bronchiolitic WB samples. In the WB, I observed a different structure of neutrophils (ocean blue), eosinophils (magenta) and monocytes (green) with subtle differences in the region of CD3 T cells (**Fig. 3.3.3.8 C**, top). The main differences between cell clusters among controls and bronchiolitic infants are depicted using the red arrows. A UMAP representation of the NPA and TA data highlighted, in line with a two-way comparison, enrichment in the regions of CD66b and CD16 cell markers corresponding to neutrophils (ocean blue), eosinophils (magenta) and monocytes (green) (**Fig. 3.3.3.8 C**). Notably, the bronchiolitic upper (NPA, **Fig. 3.3.3.8 C,** middle) and lower airways (TA, **Fig. 3.3.3.8 C,** bottom) seemed to have higher abundance of eosinophils (magenta), monocytes (green) and a different modular structure of neutrophils (ocean blue).

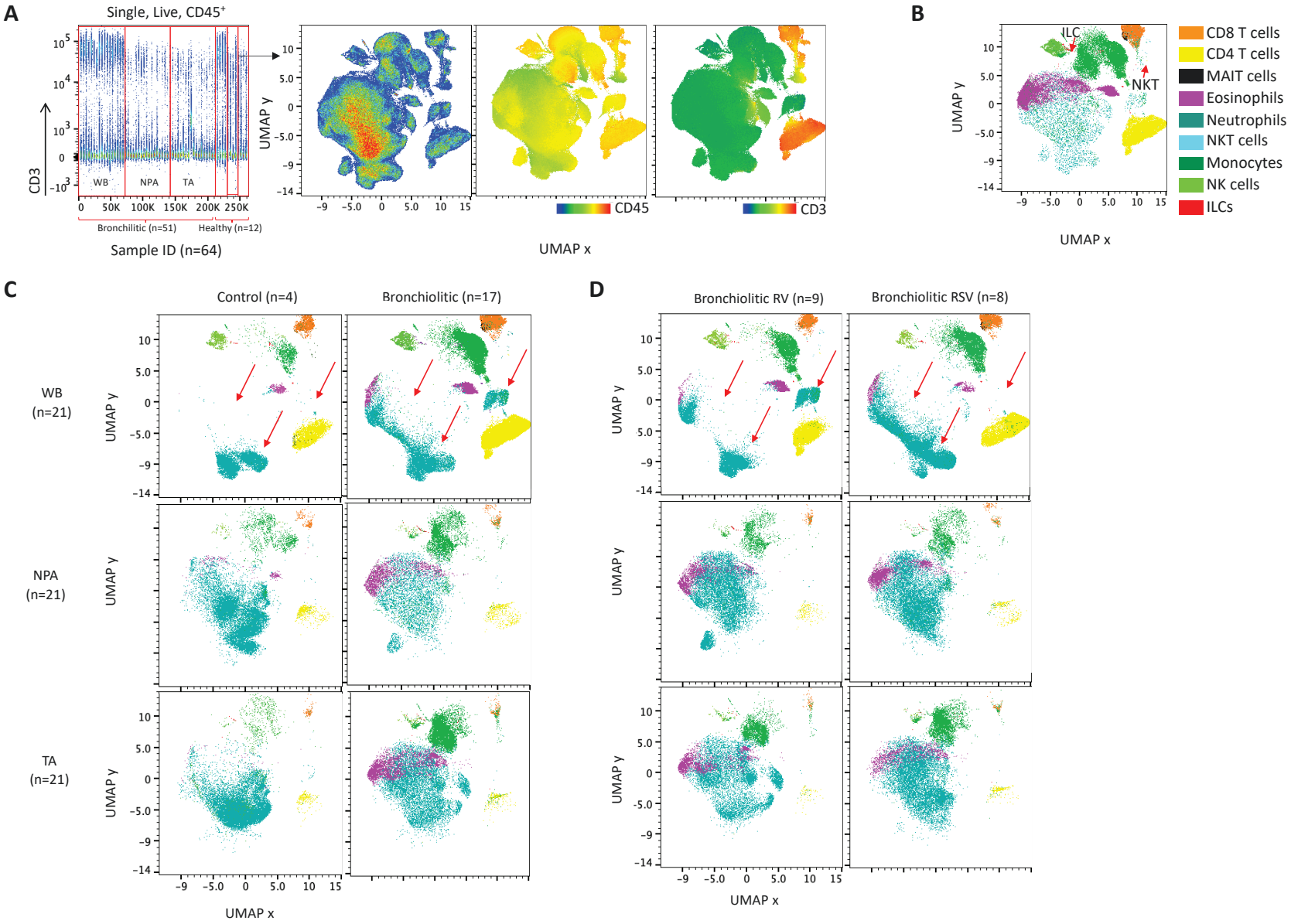

A
Single, Live, CD45+
CD3
WB
NPA
TA
Bronchilitic (n=51)
Healthy (n=12)
Sample ID (n=64)
UMAP y
UMAP x
CD45
CD3
B
ILC
NKT
CD8 T cells
CD4 T cells
MAIT cells
Eosinophils
Neutrophils
NKT cells
Monocytes
NK cells
ILCs
C
Control (n=4)
Bronchiolitic (n=17)
WB (n=21)
NPA (n=21)
TA (n=21)
D
Bronchiolitic RV (n=9)
Bronchiolitic RSV (n=8)

Figure 3.3.8 Deep immune phenotyping of CD45$^+$ populations in whole blood and airway samples from control and bronchiolitic infants using UMAP reveals cell alterations.

(A) Representative manual gating strategy utilised for deep immune phenotyping. Cells were delineated using the following gating strategy: FSC/SSC, single, live cells. Lymphocytes were gated using SSC-A and CD45. Around 5,000 randomly selected CD45$^+$ cells from each control (*n*=12) and bronchiolitic infants (*n*=51) (left) were concatenated into a single file containing 350,000 cells for UMAP analysis (middle). Both, control and bronchiolitic samples included WB (*n*=21), NPA (*n*=21) and TA (*n*=21). The intensity of CD45 and CD3 cell expression marker is shown (middle and right, respectively). **(B)** The manual gating strategy from the OMIP[201] (see Chapter 3.1) was utilised allowing global UMAP clusters (all subjects pooled) to be classified into the following cell types: CD4 T cells (yellow), NKT cells (bright blue), monocytes (green), CD8 T cells (orange), neutrophils (ocean blue), eosinophils (magenta), NK cells (bright green), MAIT cells (black), and ILCs (red). The populations of ILCs and NKT cells are indicated via red arrows (left). **(C)** Comparison of UMAP representations of clusters from WB (*n*=21), NPA (*n*=21) and TA (*n*=21) for both control (*n*=4, left) and bronchiolitic subjects (*n*=17, right) coloured by the manual gating strategy used in global UMAP. **(D)** UMAP comparison of clusters from WB (*n*=17), NPA (*n*=17) and TA (*n*=17) of only bronchiolitic subjects divided into RV bronchiolitic (*n*=9, left) and RSV bronchiolitic (*n*=8, right) coloured by the manual gating strategy used in the global UMAP. The main differences between cell clusters among controls and bronchiolitic infants are depicted using the same orientated red arrows. *Abbreviations used: n* – number of study participants, WB – whole blood, NPA – nasopharyngeal aspirates, TA – tracheal aspirates, NK – natural killer cells, NKT – natural killer T cells, MAITs – mucosal invariant T cells, ILC – innate lymphoid cells, UMAP – Uniform Manifold Approximation and Projection

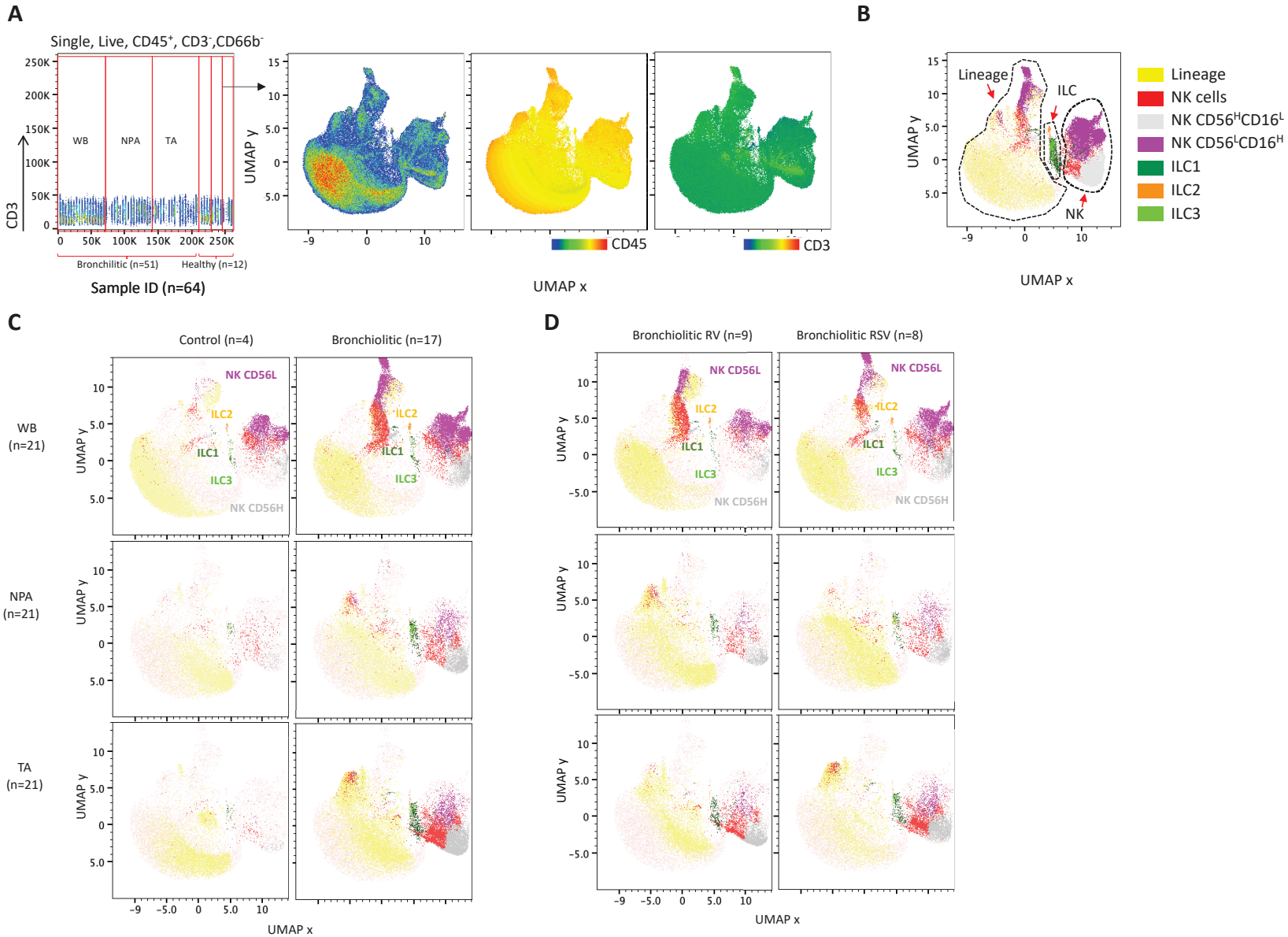

A
Single, Live, CD45+, CD3-,CD66b-
CD3
WB
NPA
TA
Bronchilitic (n=51)
Healthy (n=12)
Sample ID (n=64)
UMAP y
CD45
CD3
UMAP x
B
Lineage
ILC
NK
UMAP y
UMAP x
Lineage
NK cells
NK CD56HCD16L
NK CD56LCD16H
ILC1
ILC2
ILC3
C
Control (n=4)
Bronchiolitic (n=17)
WB (n=21)
NPA (n=21)
TA (n=21)
NK CD56L
ILC2
ILC1
ILC3
NK CD56H
UMAP y
UMAP x
D
Bronchiolitic RV (n=9)
Bronchiolitic RSV (n=8)
NK CD56L
ILC2
ILC1
ILC3
NK CD56H
UMAP y
UMAP x

Figure 3.3. 9 Deep immune phenotyping ILCs (including NK cells) in whole blood and airway samples from control and bronchiolitic infants using UMAP reveals cell alterations.

(A) Representative manual gating strategy utilised for deep immune phenotyping. Cells were delineated using the following gating strategy: FSC/SSC, single, live, $CD45^+$, $CD3^-$, $CD66b^-$ lymphocytes (excluding granulocytes, monocytes and other T cell populations but including lineage). Lymphocytes were gated using SSC-A and CD45 cell marker. Around 3,000 randomly selected $CD45^+CD3^-CD66b^-$ lymphocytes from each control (*n*=12) and bronchiolitic infants (*n*=51) (left) were concatenated into a single file containing 189,000 cells for UMAP analysis (left). Both, control and bronchiolitic samples included WB (*n*=21), NPA (*n*=21) and TA (*n*=21). The intensity of CD45 and CD3 cell expression is shown (middle and right, respectively). **(B)** The manual gating strategy from the OMIP[201] (see Chapter 3.1) was utilised allowing global UMAP clusters (all subjects pooled) to be classified into the following cell types $CD3^+CD14^+CD19^+CD56^+CD123^+Fc\varepsilon RI\alpha^+$ lineage (yellow), $CD56^+CD3^-$ NK cells (red), $CD56^HCD16^L$ NK cells (grey), $CD56^LCD16^H$ NK (magenta), ILC3s (lime green), ILC2s (orange) and ILC1s (dark green).The populations of ILCs, NK cells and Lineage+ cells are indicated via red arrows (left). **(C)** Comparison of UMAP representations of clusters from WB (*n*=21), NPA (*n*=21) and TA (*n*=21) for both control (*n*=4, left) and bronchiolitic subjects (*n*=17, right) coloured by the manual gating strategy used in the global UMAP. **(D)** UMAP comparison of clusters from WB (*n*=17), NPA (*n*=17) and TA (*n*=17) of only bronchiolitic subjects divided into RV bronchiolitic (*n*=9, left) and RSV bronchiolitic (*n*=8, right) coloured by the manual gating strategy used in the global UMAP. The main differences between cell clusters among controls and bronchiolitic infants are depicted using the red arrows. *Abbreviations used: n* – number of study participants, WB – whole blood, NPA – nasopharyngeal aspirates, TA – tracheal aspirates, NK – natural killer cells, ILC – innate lymphoid cells, UMAP – Uniform Manifold Approximation and Projection

To gain more insight into the architecture of the immunome of bronchiolitic children, the global high-dimensional mapping was generated on only bronchiolitic subjects divided into RV bronchiolitic (*n*=9, left) and RSV bronchiolitic (*n*=8, right) coloured by the manual gating strategy used in global UMAP (**Fig. 3.3.3.8 D**). This approach showed that the differences in UMAPs of NPA and TA were very subtle (**Fig. 3.3.3.8 D,** middle and bottom). In contrast, the phenotype of neutrophils, eosinophils and monocytes in whole blood revealed distinct differences between RV and RSV infection (**Fig. 3.3.3.8 D,** top).

Next, to improve visualisation and investigate the heterogeneity of all subtypes of ILCs (including NK cells), I performed UMAP immunophenotyping on 189,000 FSC/SSC, single, live, $CD45^+$, $CD3^-$, $CD66b^-$ lymphocytes (~3 000 cells per subject) excluding all granulocytes, monocytes and $CD3^+$ T cell populations (**Fig. 3.3.9 A**). This improved visualisation utilised the same cohort as used in **Figure 3.3.8** and the manual gating strategy from the OMIP [201] to identify the clusters. UMAP clusters were classified into the following cell types: lineage positive ($CD3^-$ $CD14^+$ $CD19^+$ $CD123^+$ $Fc\varepsilon RI\alpha^+$)(yellow), all $CD56^+CD3^-$ NK cells (red), $CD56^HCD16^L$ NK cells (grey), $CD56^LCD16^H$ NK (magenta), ILC3s (green), ILC2s (orange) and ILC1s (dark green) (all colours were layered in this order) (**Fig. 3.3.9 B**). As mentioned UMAP clusters allowed me to observe differences not only in the cell composition but depicted the phenotypical differences in the same cell clusters between cohorts (**Fig. 3.3.9 C, D**). Interestingly, in bronchiolitic ILCs, I observed higher proportions of all subsets of ILCs: ILC1s (red), ILC2s (blue) and ILC3s (purple) and NK cell clusters in NPA and TA when compared to the healthy controls (**Fig. 3.3.9 C,** middle and bottom). The most striking differences between control and bronchiolitic patients were observed in the WB within $CD56^LCD16^H$ NK cells (magenta), lineage (yellow) but not ILC clusters (**Fig. 3.3.9 C,** top).

The UMAP projection in **Figure 3.3.10 A** identified a major alteration in the $CD56^L$ NK cell cluster (magenta) in bronchiolitic patients; this cluster is typical of the architecture of the WB immunome of RSV- but not RV- bronchiolitis (**Fig. 3.3.9 D,** top). To identify the population characteristics, I performed unsupervised FlowSOM™ clustering analysis and projected it on UMAP to see if the population of $CD56^L$ NK cells can be identified (**Fig. 3.3.10 B**). As expected, eight clusters (Pop0 to Pop7) were generated using self-organising mapping (SOM) algorithm from which cluster Pop7 was identified as the population of interest in the top of the UMAP projection. Pop7 cluster contained $lineage^+$ $CD16^+$ and $CD4^+$ lymphocytes that fell into $CD56^L$ NK cell gate. The biaxial gating strategy was utilised to compare the abundance and frequency of

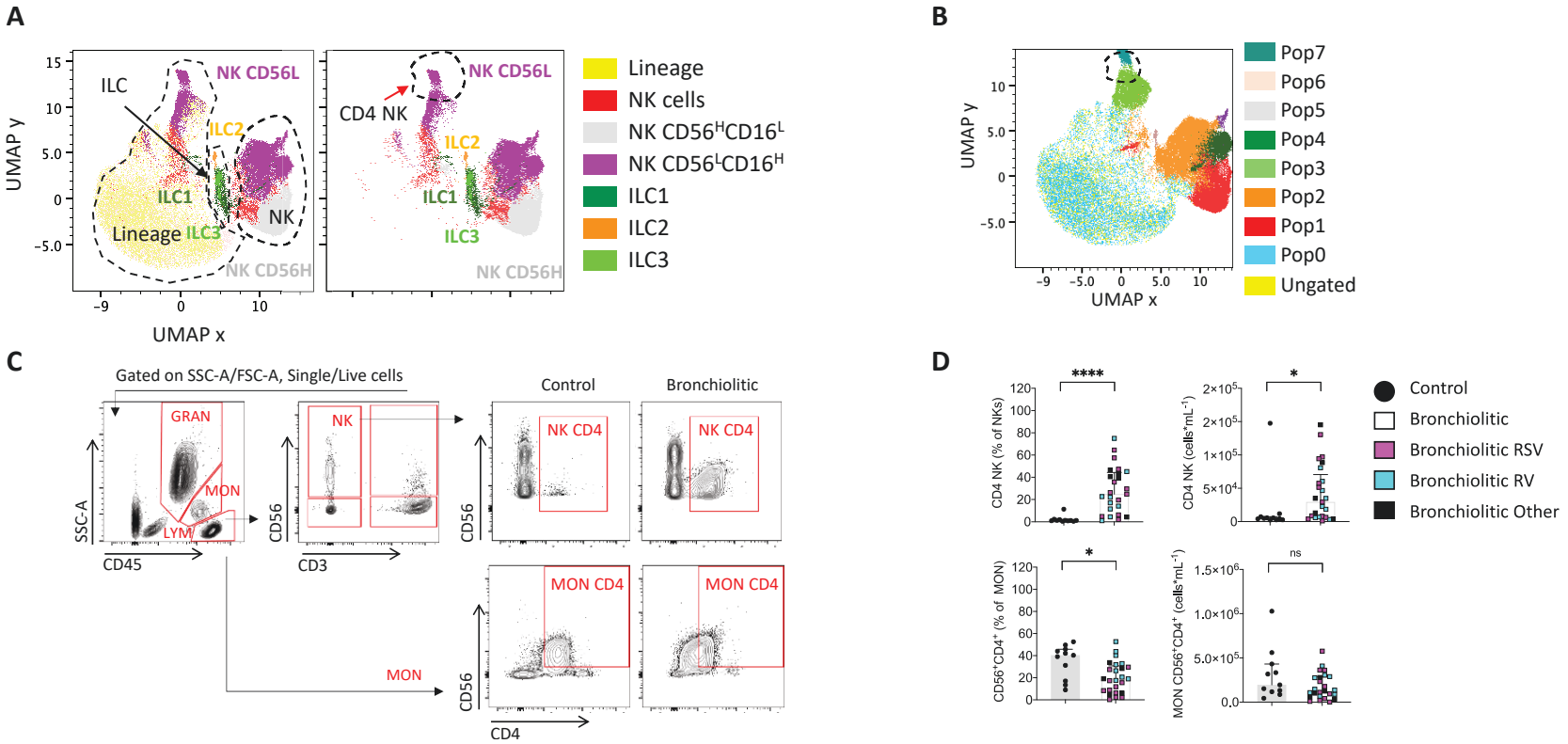


Figure 3.3.10 Deep immune phenotyping ILCs (including NK cells) in whole blood from control and bronchiolitic infants using UMAP reveals cells alterations in CD4⁺ NKs and CD4⁺ monocytes.

(A) The manual gating strategy from the OMIP[201] (see Chapter 3.1) was utilised allowing global UMAP clusters on cells delineated using the following gating strategy: FSC/SSC, single, live, $CD45^+$, $CD3^-$, $CD66b^-$ lymphocytes (excluding granulocytes, monocytes and other T cell populations but including lineage). Around 3,000 randomly selected $CD45^+CD3^-CD66b^-$ lymphocytes from each control (*n*=4) and bronchiolitic infants (*n*=17) were concatenated into a single file containing 63,000 cells for UMAP analysis as seen in the Figure (above). Global UMAP clusters to be classified into the following cell types $CD3^+CD14^+CD19^+CD56^+CD123^+Fc\varepsilon RI\alpha^+$ lineage (yellow), $CD56^+CD3^-$ NK cells (red), $CD56^HCD16^L$ NK cells (grey), $CD56^LCD16^H$ NK (magenta), ILC3s (lime green), ILC2s (orange) and ILC1s (dark green) **(B)** Based on the expression of the mentioned markers, the generated clusters were subdivided into eight different cell types (Pop0 to Pop7) using FlowSOM™ clustering algorithm where the dashed circle represents the cluster of interest **(C)** After FlowSOM™ clustering, the manual, biaxial gating strategy was utilised to compare the abundance of $CD4^+$ monocytes and $CD4^+$ NK cells in whole blood from control (*n*=4) and bronchiolitic infants (*n*=17). Monocytes and lymphocytes were defined within live, single, leukocytes using CD45 expression and SSC-A. Within the monocyte gate, CD4 expressing cells where gated using CD56 and CD4 markers while in the lymphocytes gate, NK cells were gated as $CD56^+CD3^-$. NK cells were further gated using CD56 and CD4 markers. **(D)** Frequency and quantification of $CD4^+$ $CD56^+$ NK and monocytes in the whole blood control (*n*=11) and bronchiolitic infants (*n*=27). Data represent more than 30 experiment results shown as the median with upper interquartile range. Differences between groups were estimated by Mann-Whitney test (ns – not statistical, * $p < 0.05$ and **** $p < 0.0001$)..

those cells. Monocytes, lymphocytes and granulocytes were defined within live, single, leukocytes using CD45 expression and SSC-A. Within lymphocytes $CD56^{+}CD3^{-}$ NK cells were gated, and the expression of CD4 shown using CD56 and CD4 plots (**Fig. 3.3.10 C**). Interestingly, back gating of the $CD4^{+}CD56^{+}$ population onto the SSC-A CD45 plot (data not shown) suggested that this population of cells might alternatively be monocytes which were activated and leaked into the lymphocyte gate and also express CD4 and CD56. Thus, within the monocyte gate, CD56 and CD4 marker expression was determined for both control and bronchiolitic babies (**Fig. 3.3.10 C**). In whole blood, the frequency of $CD4^{+}$ NK cells were increased in bronchiolitis (a median of 1.2%) compared to controls (a median of 25%) (P<0.0001). Similarly, the number of $CD4^{+}$ NK cells showed a similar trend (P=0.01). On the other hand, the frequency of $CD4^{+}$ monocytes decreased from ~40% in controls to ~20% of monocytes in bronchiolitic babies (P=0.012) (**Fig. 3.3.10 D**).

3.3.3.2.6. Assessment of cellular correlations in bronchiolitic infants

Correlation of different cell populations in whole blood, NPA and TA immune profiles

To better understand the association between cells of whole blood and airway samples, I calculated the correlation between cells from the flow cytometric data obtained using OMIP [201] from WB (n=27) (**Fig. 3.3.11 A**), NPA (n=30) (**Fig. 3.3.11 B)** and TA (n=31) (**Fig. 3.3.11 C**) in bronchiolitic children. For this analysis, frequencies of cells were used instead of total cell counts. Data displayed in a correlogram format was delivered by Pearson's correlation using the R programming language where positive correlations are displayed in blue and negative correlations in red colour and then validated using XY plots. I found a significant negative association (r^2=0.895, P<0.001) between the percentages of ILC2s and ILC1s in the whole blood samples but no other ILCs populations (**Fig. 3.3.11 A**, **D**). I also found a negative, significant correlation between the frequency of CD4 T cells and granulocytes (r^2=-0.322, P<0.01) and CD4 T cells and ILC1 (r^2= -0.519, P<0.01) in NPA samples. Finally, I found that granulocytes inversely correlated with monocytes and lymphocytes in TA (r^2=-0.805, P<0.01 and r^2=-0.495, P<0.01, respectively). This analysis allowed me to discover meaningful cellular associations in the immunomes from different compartments such as WB, NPA and TA of bronchiolitic patients.

Correlations between NPA and TA cellular immune profiles

Next, I compared the cellular response between NPA and TA to discover whether the NPA can be utilised to study the lower airways. To better understand if the same cellular responses correlate from different airway samples, I calculated the correlation between the cell populations from NPA and TA in bronchiolitic children (n=30). For this analysis, total cell counts (**Fig. 3.3.12**) and frequencies of cells (**Fig. 3.3.13**) obtained using flow cytometric data generated

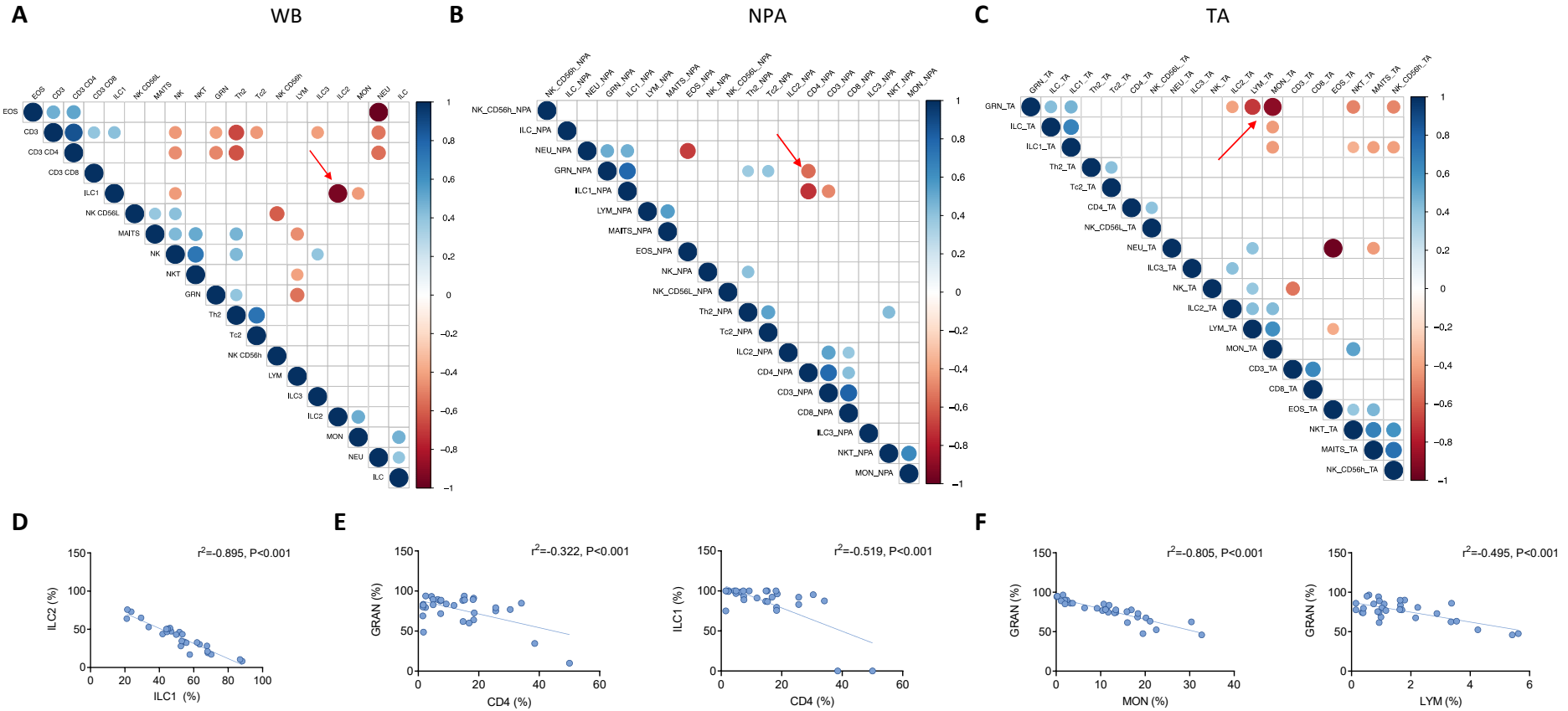
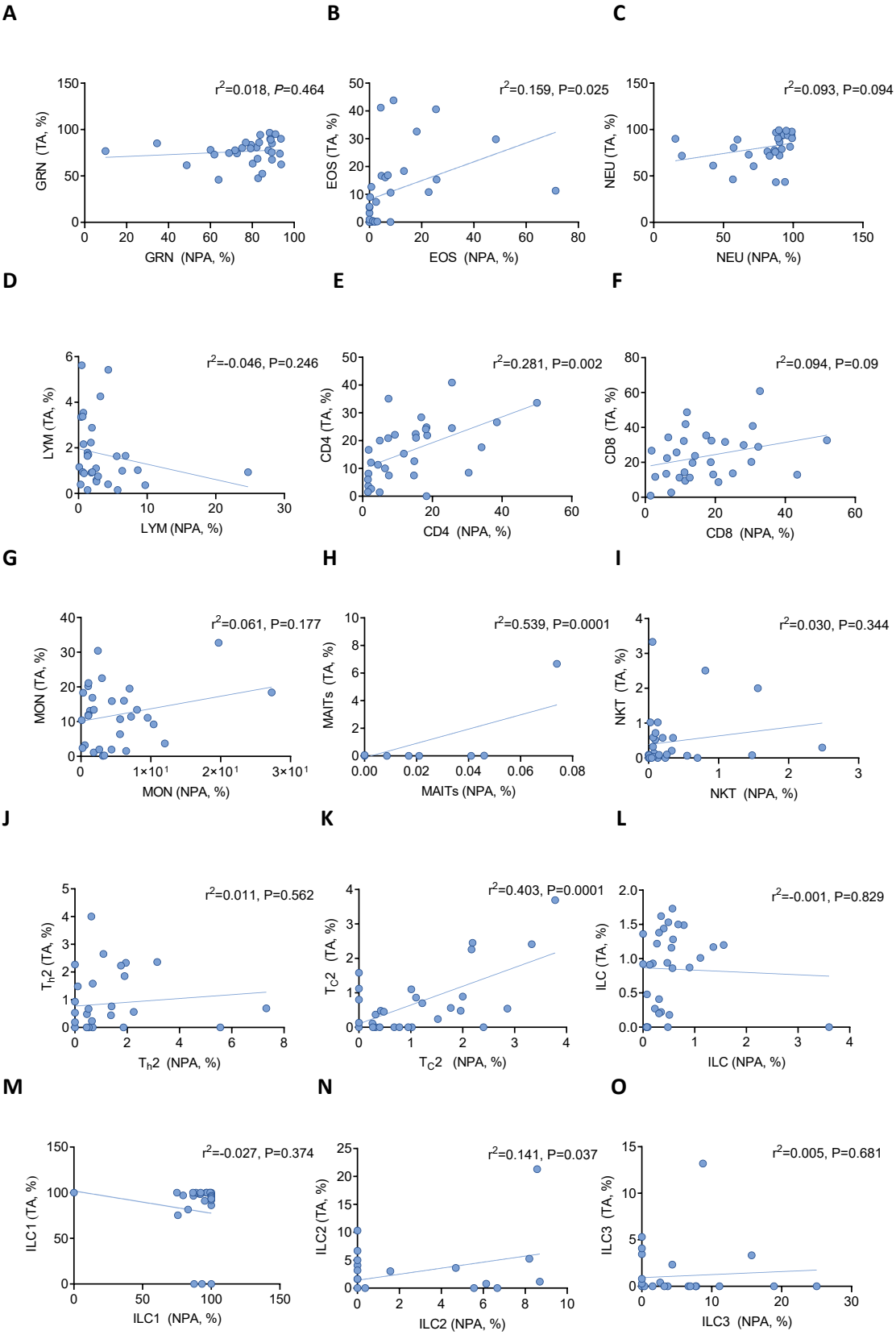


Figure 3.3.11 The correlation between different cell populations in bronchiolitic infants

The correlation between multiple variables from the flow cytometric data obtained using OMIP from the WB (*n*=27) **(A)**, NPA (*n*=30) **(B)** and TA (*n*=31) **(C)** from bronchiolitic infants using correlograms **(A-C)** or XY plots **(D-F)**. Data displayed in a correlogram format was delivered by comparing the frequencies in the whole blood and airway samples using Pearson parametric correlation test in the R programming language where positive correlations are displayed in blue and negative correlations in red colour. The intensity of the colour and the size of the circle are proportional to the correlation coefficients. In the right side of each correlogram, the legend colour depicts the correlation coefficients and the corresponding colours. The correlation matrix used for all graphs was not reordered according to hierarchical order. Correlations with $p > 0.05$ are considered insignificant and were left blank which means there is no linear relation between the variables considered. The strongest correlations are depicted using the red arrows and then validated by using the XY plots **(D-F)**. The relationship between X and Y is summarised by the fitted regression line where r^2 (the correlation squared) shows the proportion of variation in Y explained by X. *Abbreviations used*: NEU – neutrophils, EOS – eosinophils, MON – monocytes, GRN – granulocytes, LYM – Lymphocytes, NK – natural killer cells, NKT – natural killer T cells, MAITs – mucosal invariant T cells, ILC – innate lymphoid cells, Tc2 – type-2 cytokine producing CD4s, Th2 – type-2 cytokine producing CD8s, *n* – number of study participants, WB – whole blood, NPA – nasopharyngeal aspirates, TA – tracheal aspirates.


A
B
C
GRN (TA, %)
GRN (NPA, %)
r²=0.018, P=0.464
EOS (TA, %)
EOS (NPA, %)
r²=0.159, P=0.025
NEU (TA, %)
NEU (NPA, %)
r²=0.093, P=0.094
D
E
F
LYM (TA, %)
LYM (NPA, %)
r²=-0.046, P=0.246
CD4 (TA, %)
CD4 (NPA, %)
r²=0.281, P=0.002
CD8 (TA, %)
CD8 (NPA, %)
r²=0.094, P=0.09
G
H
I
MON (TA, %)
MON (NPA, %)
r²=0.061, P=0.177
MAITs (TA, %)
MAITs (NPA, %)
r²=0.539, P=0.0001
NKT (TA, %)
NKT (NPA, %)
r²=0.030, P=0.344
J
K
L
Th2 (TA, %)
Th2 (NPA, %)
r²=0.011, P=0.562
Tc2 (TA, %)
Tc2 (NPA, %)
r²=0.403, P=0.0001
ILC (TA, %)
ILC (NPA, %)
r²=-0.001, P=0.829
M
N
O
ILC1 (TA, %)
ILC1 (NPA, %)
r²=-0.027, P=0.374
ILC2 (TA, %)
ILC2 (NPA, %)
r²=0.141, P=0.037
ILC3 (TA, %)
ILC3 (NPA, %)
r²=0.005, P=0.681

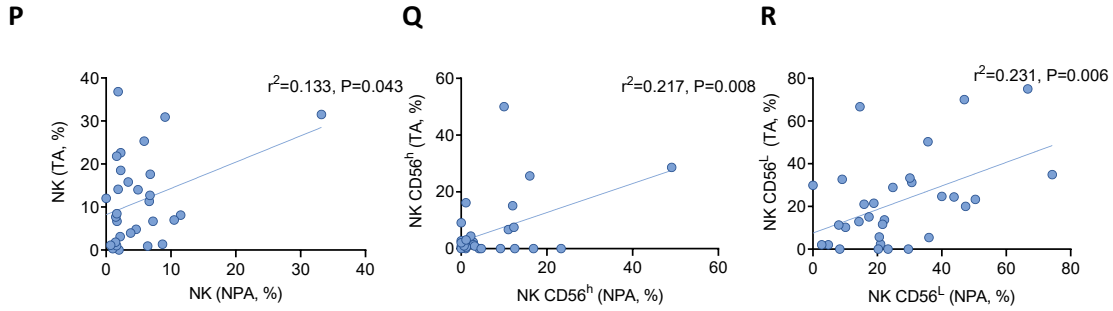
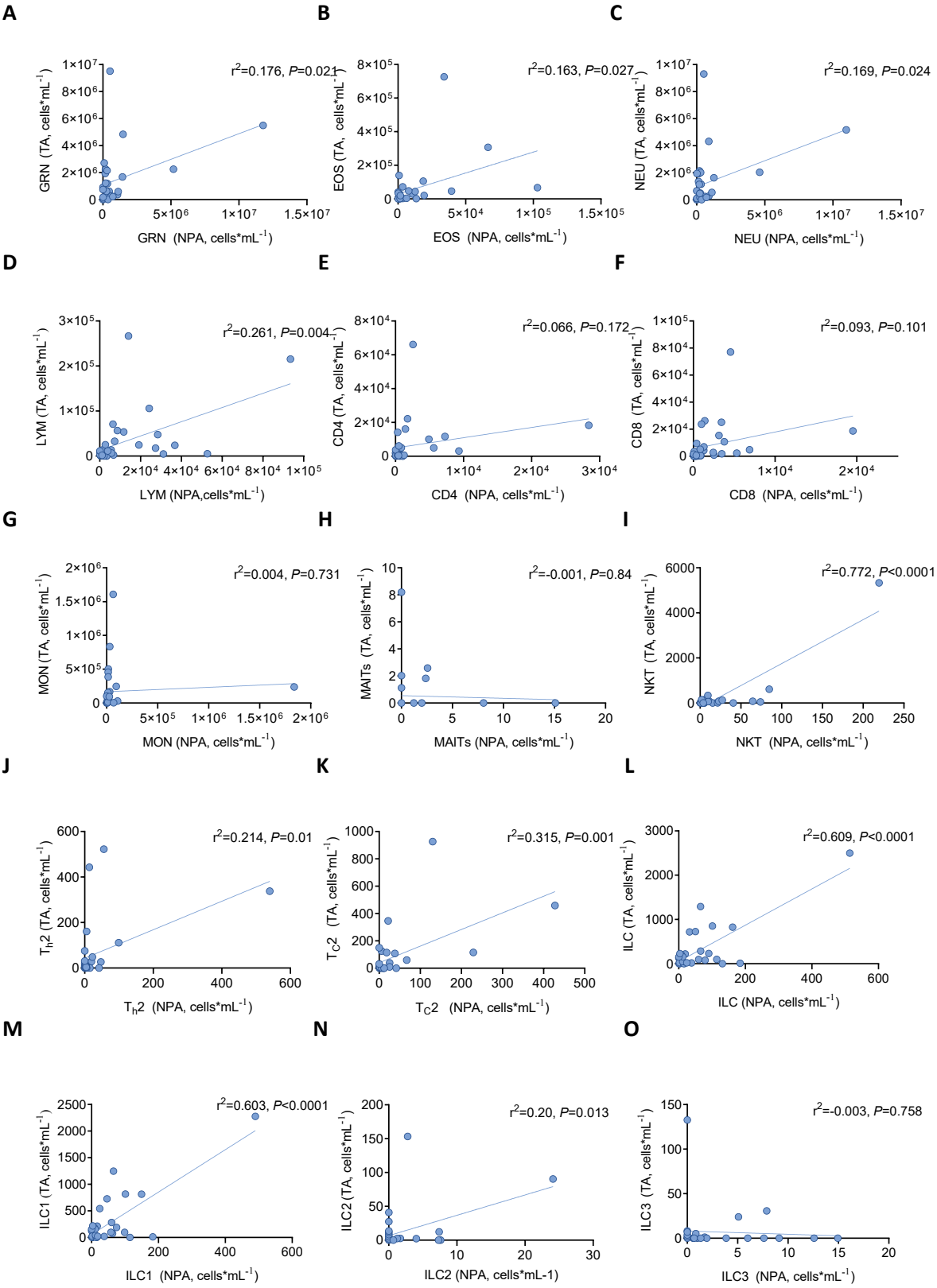


Figure 3.3.12 The correlation dependence between the frequencies of the same cell populations in TA and NPA in the bronchiolitic infants.

The correlation and linear regression between the frequency of cells in TA and NPA from the flow cytometric data obtained using OMIP in bronchiolitic infants (*n*=30) **(A-R)**. Data are displayed in an XY plot format using Pearson parametric correlation test where correlations with $p > 0.05$ considered insignificant. The relationship between X and Y is summarised by the fitted regression line where r^2 (the correlation squared) shows the proportion of variation in Y explained by X. *Abbreviations used*: NEU – neutrophils, EOS – eosinophils, MON – monocytes, GRN – granulocytes, LYM – Lymphocytes, NK – natural killer cells, NKT – natural killer T cells, MAITs – mucosal invariant T cells, ILC – innate lymphoid cells, Th2 – type-2 cytokine-producing CD4s, Tc2 – type-2 cytokine-producing CD8s, *n* – number of study participants, NPA – nasopharyngeal aspirates, TA – tracheal aspirates.


A
B
C
GRN (TA, cells*mL-1)
GRN (NPA, cells*mL-1)
r2=0.176, P=0.021
EOS (TA, cells*mL-1)
EOS (NPA, cells*mL-1)
r2=0.163, P=0.027
NEU (TA, cells*mL-1)
NEU (NPA, cells*mL-1)
r2=0.169, P=0.024
D
E
F
LYM (TA, cells*mL-1)
LYM (NPA,cells*mL-1)
r2=0.261, P=0.004
CD4 (TA, cells*mL-1)
CD4 (NPA, cells*mL-1)
r2=0.066, P=0.172
CD8 (TA, cells*mL-1)
CD8 (NPA, cells*mL-1)
r2=0.093, P=0.101
G
H
I
MON (TA, cells*mL-1)
MON (NPA, cells*mL-1)
r2=0.004, P=0.731
MAITs (TA, cells*mL-1)
MAITs (NPA, cells*mL-1)
r2=-0.001, P=0.84
NKT (TA, cells*mL-1)
NKT (NPA, cells*mL-1)
r2=0.772, P<0.0001
J
K
L
Th2 (TA, cells*mL-1)
Th2 (NPA, cells*mL-1)
r2=0.214, P=0.01
TC2 (TA, cells*mL-1)
TC2 (NPA, cells*mL-1)
r2=0.315, P=0.001
ILC (TA, cells*mL-1)
ILC (NPA, cells*mL-1)
r2=0.609, P<0.0001
M
N
O
ILC1 (TA, cells*mL-1)
ILC1 (NPA, cells*mL-1)
r2=0.603, P<0.0001
ILC2 (TA, cells*mL-1)
ILC2 (NPA, cells*mL-1)
r2=0.20, P=0.013
ILC3 (TA, cells*mL-1)
ILC3 (NPA, cells*mL-1)
r2=-0.003, P=0.758

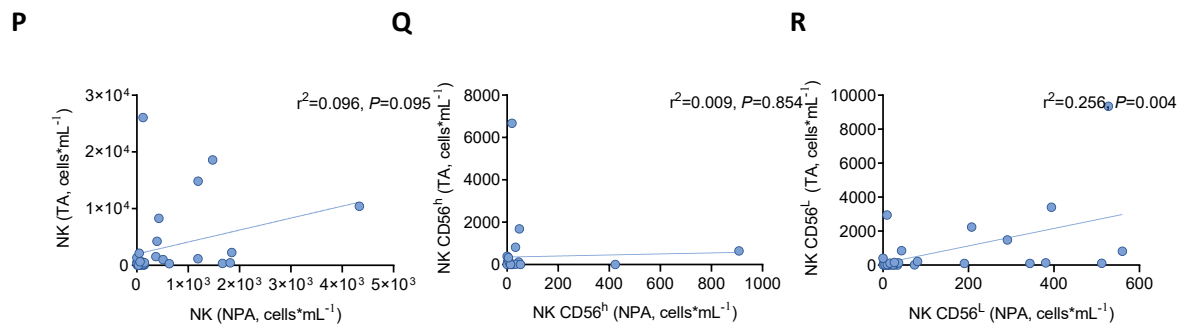


Figure 3.3.13 The correlation dependence between the quantification of the same cell populations in TA and NPA in the bronchiolitic infants.

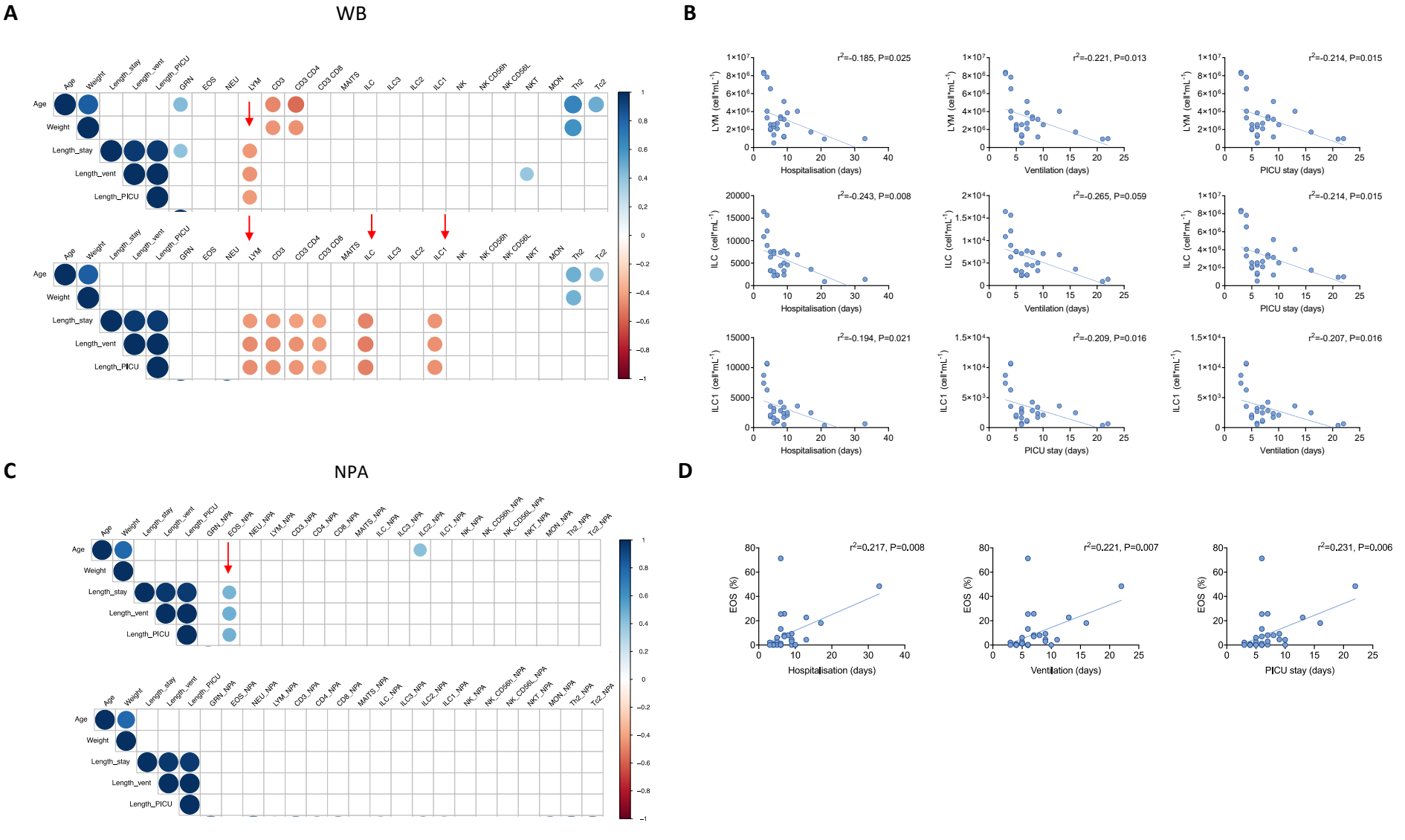
The correlation and linear regression between the quantification of cells in TA and NPA from the flow cytometric data obtained using OMIP in bronchiolitic infants (*n*=30) **(A-R)**. Data are displayed in an XY plot format using Pearson parametric correlation test where correlations with $p > 0.05$ are considered insignificant. The relationship between X and Y is summarised by the fitted regression line where r^2 (the correlation squared) shows the proportion of variation in Y explained by X. *Abbreviations used*: NEU – neutrophils, EOS – eosinophils, MON – monocytes, GRN – granulocytes, LYM – Lymphocytes, NK – natural killer cells, NKT – natural killer T cells, MAITs – mucosal invariant T cells, ILC – innate lymphoid cells, Tc2 – type-2 cytokine-producing CD4s, Th2 – type-2 cytokine-producing CD8s, *n* – number of study participants, NPA – nasopharyngeal aspirates, TA – tracheal aspirates.

by OMIP were correlated and displayed in an XY plot format using Pearson parametric correlation test. In these correlations relationship between the same cell populations in NPA and TA were summarised by a fitted regression line where the correlation squared (r^2) shows the proportion of variation in NPA explained by TA. I found significant correlations between the total cell counts of lymphocytes (r^2=0.261, *P*=0.004), NKT cells (r^2=0.722, *P*<0.0001), Th2 cells (r^2=0.214, *P*=0.01), Tc2 cells (r^2=0.315, *P*=0.001), ILC (r^2=0.609, *P*<0.0001), ILC1 (r^2=0.603, *P*<0.0001), ILC2 (r^2=0.200, *P*<0.013) and $CD56^L$ NK cells (r^2=0.256, *P*<0.004) between TA and NPA (**Fig. 3.3.12 D, I, J,K, L, M, N and R**). I also found positive, significant correlation between frequencies of CD4 T cells (r^2=0.281, *P*=0.002), MAIT cells (r^2=0.539, *P*=0.0001), Tc2 cells (r^2=0.403, *P*=0.0001), NK cells (r^2=0.133, *P*=0.043), CD56h NK cells (r^2=0.217, *P*=0.008) and CD56L NK cells (r^2=0.231, *P*=0.006) between TA and NPA (**Fig. 3.3.13 D, E, H, K, P, Q and R**). This analysis allowed me to identify if there is a similar type of inflammation in the NPA and TA.

Correlation between disease severity and cellular immune profiles

To further define the association between the severity of bronchiolitis and cell populations, I applied the same analytical strategy as mentioned above. The severity of illness, measured by the length of hospital stay, the length of ventilation and the length of PICU stay were correlated with cellular immune profiles obtained from WB (*n*=27) (**Fig. 3.3.14 A, B**), NPA (*n*=30) (**Fig. 3.3.14 C, D**) and TA (*n*=31) (**Fig. 3.3.14 E, F**) from bronchiolitic infants. For this analysis, both total cell counts and frequencies of cells obtained using flow cytometric data generated by OMIP were used. Data were displayed in a correlogram format delivered by Pearson's correlation using R

programming. The most interesting correlations are depicted using the red arrows and then validated by using the XY plots. I found several significant negative associations between the percentages of lymphocytes and the total numbers of lymphocytes (r^2=-0.195, *P*=0.025), ILCs and ILC1 and severity of illness in the whole blood samples (r^2=-0.243, *P*=0.008 and r^2=-0.194, *P*=0.021, respectively) (**Fig. 3.3.14 A, B**). I also found a positive, significant correlation between the frequency of eosinophils and the length of hospital stay (r^2=0.217, *P*=0.008), the length of ventilation (r^2=0.221, *P*=0.007) and the length of PICU stay (r^2=0.231, *P*=0.006) in NPA samples (**Fig. 3.3.14 C, D**). Finally, I found that severity of illness inversely correlated with the frequency of neutrophils and positively with the frequency of eosinophils in the TA (**Fig. 3.3.14 E, F**). This analysis allowed me to discover meaningful cellular associations in WB, NPA and TA with the severity of bronchiolitis.


A
WB
B
C
NPA
D
Age
Weight
Length_stay
Length_vent
Length_PICU
GRN
EOS
NEU
LYM
CD3
CD3 CD4
CD3 CD8
MAITS
ILC
ILC3
ILC2
ILC1
NK
NK CD56h
NK CD56L
NKT
MON
Th2
Tc2
LYM (cell*mL-1)
ILC (cell*mL-1)
ILC1 (cell*mL-1)
EOS (%)
Hospitalisation (days)
Ventilation (days)
PICU stay (days)
r2=-0.185, P=0.025
r2=-0.221, P=0.013
r2=-0.214, P=0.015
r2=-0.243, P=0.008
r2=-0.265, P=0.059
r2=-0.214, P=0.015
r2=-0.194, P=0.021
r2=-0.209, P=0.016
r2=-0.207, P=0.016
r2=0.217, P=0.008
r2=0.221, P=0.007
r2=0.231, P=0.006

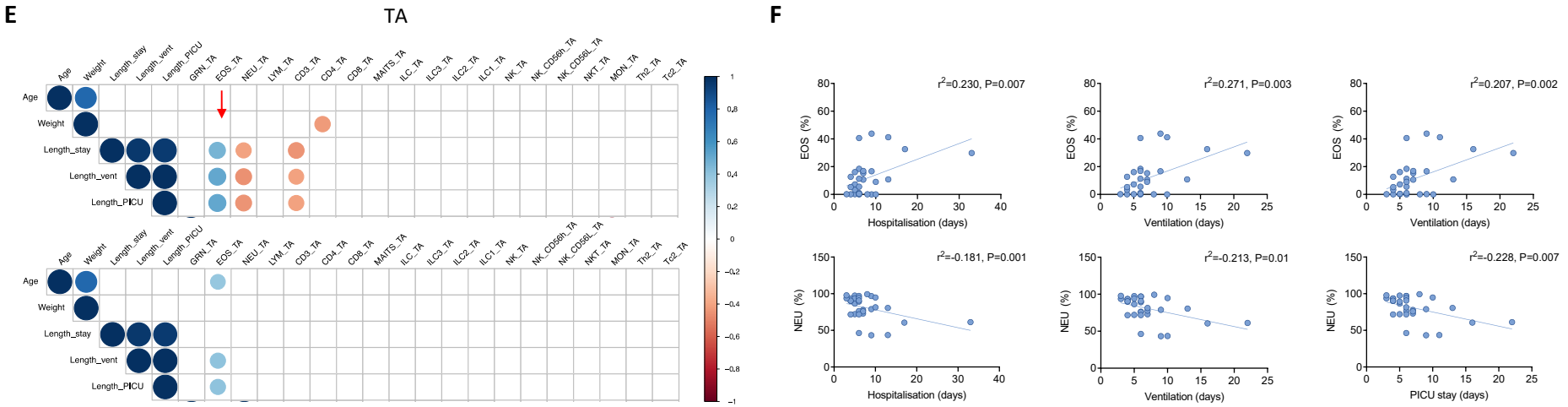


Figure 3.3.14 The correlation between different cell populations and the severity of disease in whole blood and airway samples in bronchiolitic infants.

The correlation dependence between multiple variables from the flow cytometric data obtained using OMIP from the WB (*n*=27) **(A)**, NPA (*n*=30) **(C)** and TA (*n*=31) **(E)** from bronchiolitic infants and the severity of disease measured by the length of hospitalisation stay, the length of ventilation and the length of PICU stay using correlograms. The correlation dependence was delivered by comparing the frequencies and total cell numbers with the clinical data in the whole blood and airway samples using Pearson parametric correlation test in the R programming language. Data are displayed in a correlogram format **(A, C, E)**, where positive correlations are displayed in blue and negative correlations in red colour. The intensity of the colour and the size of the circle are proportional to the correlation coefficients. Additionally, in the right side of each correlogram, the legend colour depicts the correlation coefficients and the corresponding colours. The correlation matrix used for all graphs was not reordered according to hierarchical order. Correlations with $p > 0.05$ are considered insignificant and were left blank which means there is no linear relation between the variables considered. The most interesting correlations are depicted using the red arrows and then validated by using the XY plots **(B, D, F)**. The validation of correlation and linear regression of the flow cytometric data obtained using OMIP from the WB (*n*=27) **(B)**, NPA (*n*=30) **(D)** and TA (*n*=31) **(F)** from bronchiolitic infants and the severity of disease measured by the length of hospitalisation stay, the length of ventilation and the length of PICU stay. The relationship between X and Y is summarised by the fitted regression line where r^2 (the correlation squared) shows the proportion of variation in Y explained by X. *Abbreviations used*: NEU – neutrophils, EOS – eosinophils, MON – monocytes, GRN – granulocytes, LYM – Lymphocytes, NK – natural killer cells, NKT – natural killer T cells, PICU – Paediatric Intensive Care Unit, MAITs – mucosal invariant T cells, ILC – innate lymphoid cells, Th2 – type-2 cytokine-producing CD4s, Tc2– type-2 cytokine-producing CD8s, *n* – number of study participants, WB – whole blood, NPA – nasopharyngeal aspirates, TA – tracheal aspirate

3.3.3.3. The functional phenotype of innate and adaptive PBMCs in bronchiolitis and health

After the enumeration of the architecture of the immunome in bronchiolitic and control infants, the functional phenotype of immune cells was assessed in those two groups to check for differences regarding the production of IFN-γ, IL-13, IL-17A and IL-22, the main ILC-related cytokines [230]. 2x 10^6 PBMCs from control and severely ill infants were stimulated for at least 3 hours at 37^{o}C in the stimulation cocktail of ionomycin (1 μg/mL), PMA (50 ng/mL) and GolgiPlug™. The unstimulated, negative control was prepared by adding just DMSO. After stimulation, detection of cytokine-producing cells was performed by immune fluorescent staining with the optimized flow cytometry panel (**Fig. 3.2.3 I and II**) as described in Chapter 2 (Material and Methods, **Section 2.2.9.1.2-4**).

3.3.3.3.1. Cohort characteristics for the PBMC functional phenotyping

Overall, both sexes were represented in this cohort (*P*=0.194) (**Table 3.3.5**); however, there is a lack of control females (0%) compared to bronchiolitic females (57.14%). The lack of females in the control group was associated with the complexity of obtaining extra blood samples for PBMC and the fact that most infants for elective surgery were males with orchiopexy (Material and Methods, Section 2.2.5). The median age of controls 336.5 days (range = 36 – 594) and bronchiolitic infants 41 days (range = 34 – 243) (*P*=0.178). There was a significant difference in weights (*P*=0.006) between control and bronchiolitic infants (a median weight of 10.85 and 4kg, respectively). All bronchiolitic patients were stratified according to the viral aetiology of disease: RSV (51.14%), RV (28.57%) and other viruses (20.28%, including Influenza A and B, Adenovirus, CMV, hMPV). At the time of sampling, 57.14% of bronchiolitic infants had bacterial coinfections (*Escherichia coli*, *Klebsiella pneumoniae*, *Staphylococcus aureus*) and 28.57% other comorbidities. Duration of illness, measured by the length of hospital stay, the length of ventilation and the length of PICU stay was different between groups (*P*=0.006) as most of the control patients were healthy having elective surgery.

	Control Infants	Bronchiolitic Infants	
Demographic characteristics	*n*=4	*n*=7	*P* value
Age (days); median, (range)	336.50 (36-594.00)	41.00 (34.00-243)	0.178
Sex; *n* (%)			0.194
Females	0.00 (0.00)	4.00 (57.14)	
Males	4.00 (100.00)	3.00 (42.86)	
Weight (kg); median, (range)	10.85 (9.50-13.30)	4.00 (3.00-8.60)	**0.006**
Ethnicity; *n* (%)			0.502
European	3.00 (75.00)	3.00 (42.80)	
Asian	0.00 (0.00)	2.00 (28.57)	
African (including Afro-Caribbean)	1.00 (25.00)	1.00 (14.28)	
Other	0.00 (0.00)	1.00 (14.28)	
Hospitalisation (days); median, (range)			
Length of hospital stay	1.00 (1.00-1.00)	7.00 (5.00-33.00)	**0.006**
Length of PICU stay	0.00 (0.00-0.00)	7.00 (5.00-22.00)	**0.006**
Length of ventilation	1 .00 (1.00-1.00)	6.00 (4.00-22.00)	**0.003**
Clinical features			NA
Max FiO_2 (%); average, (range)	NA	87.14 (52.00-100.00)	
PIP (cmH_2O); average, (range)	NA	27.71 (24.00-33.00)	
Aetiology of disease; *n* (%)			NA
RSV	NA	4.00 (51.14)	
RV	NA	2.00 (28.57)	
Other	NA	1.00 (20.28)	
Co-infections; *n* (*%*)			NA
Yes	NA	4.00 (57.14)	
No	NA	3.00 (42.85)	
Comorbidities; *n* (*%*)			NA
Yes	NA	2.00 (28.57)	
No	NA	5.00 (71.41)	
Gestation at delivery			0.6817
Not documented; n (%)	3 (75.00)	3 (42.80)	
Documented; *n* (%)	1 (25.00)	4 (57.14)	
Documented (wk); median (range)	1.00 (25.00-37.00)	4.00 (23.00-42.00)	NA

Table 3.3.5 Control and bronchiolitic infants' demographics used in the optimised IFN-γ, IL-13, IL-22, IL-17A flow cytometry panel (ICS) for Chapter 3.3.

Control and bronchiolitic infants used for stimulation of PBMCs and ICS flow cytometry analysis for IFN-γ, IL-13, IL-17A and IL-22. Patient demographic and clinical information were obtained from the patients' information sheets. *P* values for continuous data were computed by Mann-Whitney test while *P* values for categorical data were computed Fisher's exact test. Differences were assessed through Fisher's exact test for sample size <5. The range is defined as the difference between the highest and lowest value. Ethnicity data: European (North/Mid/East-European), Asian (South Asia including India and Pakistan), African (North and Sub-Saharan territories) and other (the Middle East, Arabic origin or not stated). Aetiology of disease defines or non-RSV and non-RV viral infection of LRTI such as: Influenza (A and B), Adenovirus, CMV, hMPV. Co-infections are defined as viral (RV, RSV, Influenza A or B, Adenovirus, CMV, hMPV) and bacterial infections (*Escherichia coli*, *Klebsiella pneumoniae*, *Staphylococcus aureus*). *Definition of abbreviation:* PICU – Paediatric Intensive Care Unit, FiO_2 – the fraction of inspired oxygen, is defined as the percentage of inhaled oxygen, PIP – Peak Inspiratory Pressure, is the highest amount of pressure in the ventilator circuit when the lungs are filled with air, wk – week, kg – kilogram, NA – not available.

3.3.3.3.2. Functional phenotyping reveals alterations in cytokine production in NKT and T cells in bronchiolitis

IFN-γ, IL-13, IL-17A and IL-22 production in circulating innate (NK, ILC1s, ILC2s, ILC3s and NKTs) and adaptive (CD4⁺ and CD8⁺ T cells) cell populations

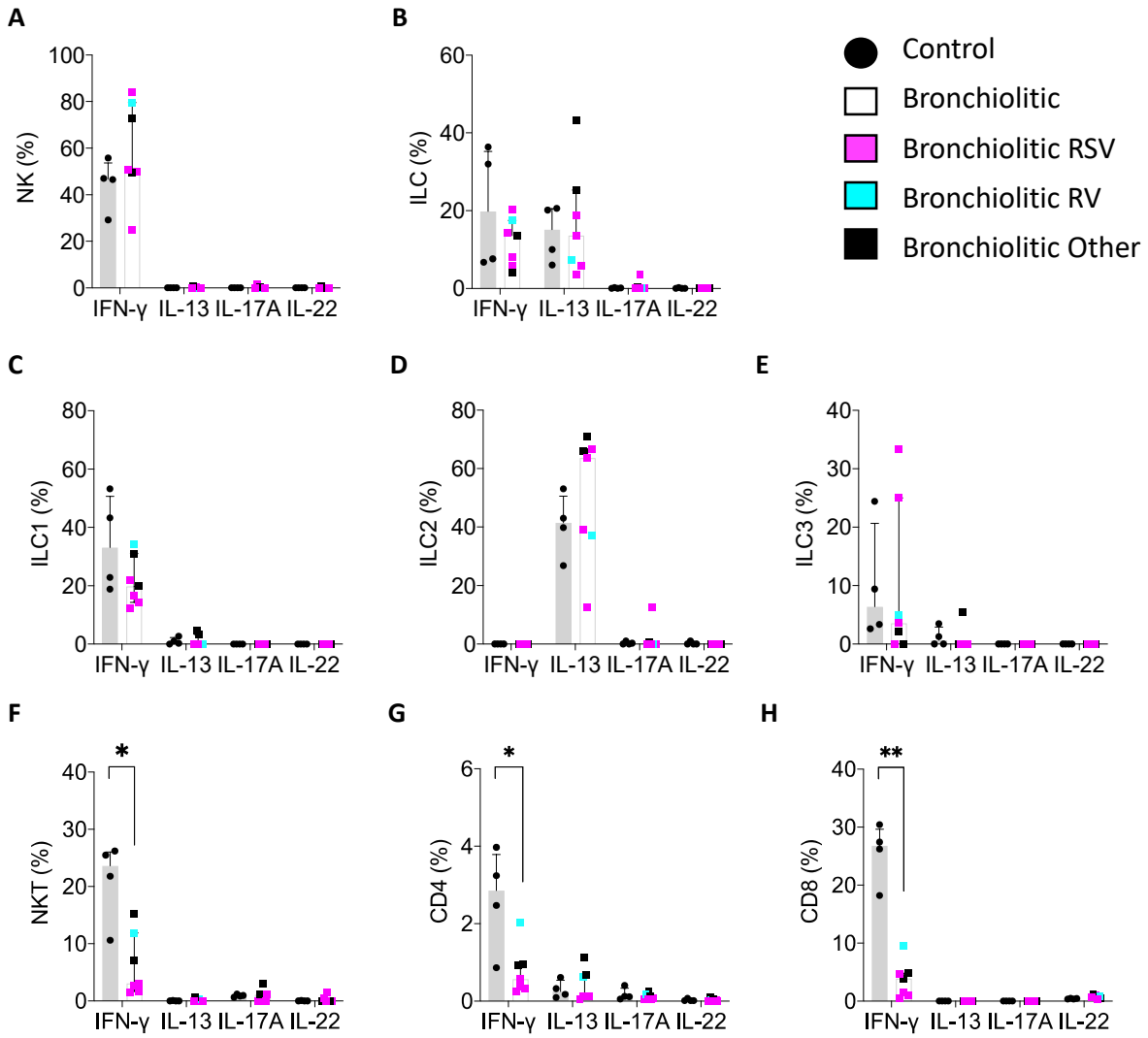


Figure 3.3.15 Comparison of production of signature cytokines in stimulated ILCs (including NKs and ILC1s, ILC2s, ILC3s), NKT, CD4⁺ and CD8⁺ T cells from control and bronchiolitic infants' PBMCs.

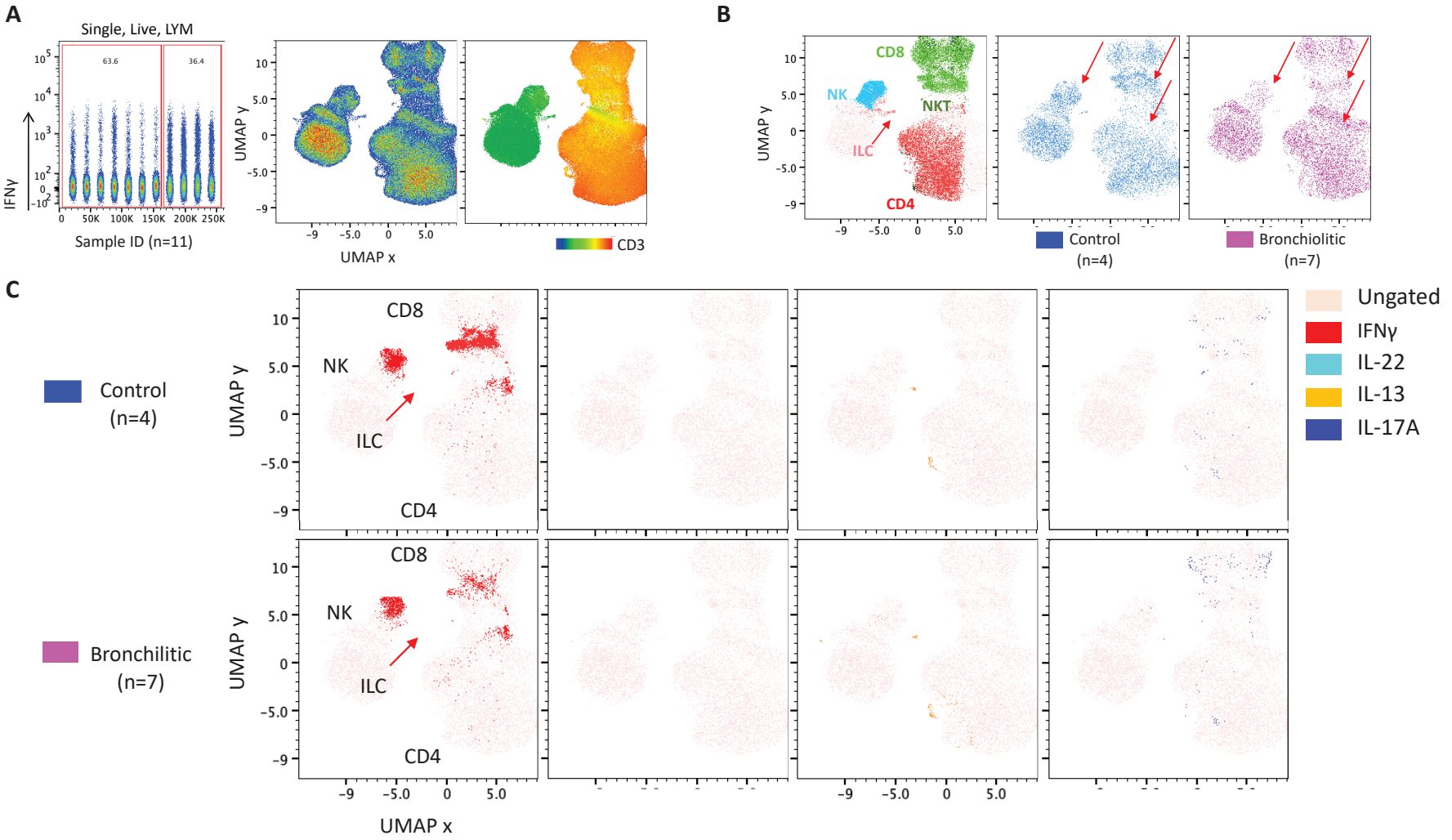
PBMC were isolated using Lymphopure® from the blood of healthy control (*n*=4) or bronchiolitic babies (*n*=7) as described in the Material and Methods chapter. After stimulation of PBMCs with PMA, and ionomycin in the presence of GolgiPlug®, cells were analysed for their cytokine profile using optimised intracellular staining (ICS) flow cytometry panel Chapter 3.2). Lymphocytes were defined as live, single, CD45⁺ lymphocytes using SSC-A. NK and NKT-like cells were gated within the lymphocyte gate as $CD56^{+}CD3^{-}$ and $CD56^{+}CD3^{+}$ cells, respectively. T lymphocytes ($CD3^{+}CD56^{-}$) were segregated into CD4⁺ or CD8⁺ T cells. ILCs were delineated within live, single, CD45⁺ lymphocytes as lineage negative (CD3, CD14, CD19, CD56, CD123 and FcεRIα)⁻ and CD127⁺ (IL-7 receptor-α) cells. Among NK, ILC, NKT, CD4⁺ or CD8⁺ T cells the populations of IFN-γ, IL-13, IL-17A and IL-22 cells were gated using a biaxial gating strategy. Frequency of $CD56^{+}CD3^{-}$ NKs expressing IFN-γ, IL-13, IL-17A and IL-22 **(A)**, $Lin^{-}CD127^{+}$ ILCs expressing IFN-γ, IL-13, IL-17A and IL-22 **(B)**, $CD117^{-}CRTH2^{-}$ ILC1s expressing IFN-γ, IL-13, IL-17A and IL-22 **(C)**, $CRTH2^{+}$ $CD117^{int}$ ILC2s expressing IFN-γ, IL-13, IL-17A and IL-22 **(D)**, $CD117^{+}CRTH2^{-}$ ILC3s expressing IFN-γ, IL-13, IL-17A and IL-22 **(E)**, $CD56^{+}CD3^{+}$ NKTs expressing IFN-γ, IL-13, IL-17A and IL-22 **(F)**, $CD56^{-}CD3^{+}CD4^{+}$ T cells expressing IFN-γ, IL-13, IL-17A and IL-22 **(G)** and $CD56^{-}CD3^{+}CD8^{+}$T cells expressing IFN-γ, IL-13, IL-17A and IL-22 **(H)**. Data are from one experiment from 4 control and 7 bronchiolitic subjects shown as the median with upper interquartile range **(A-H)**. Differences between groups were estimated by Mann-Whitney test (* $p < 0.05$ and ** $p < 0.01$). *Abbreviations used:* LYM – lymphocytes, NK – natural killer cells, NKT – natural killer T cells, ILC – innate lymphoid cells, Lin – lineage, IL – interleukin, IFN – interferon.

To get better insights into functional differences in innate and adaptive immune cells (**Fig. 3.3.15**), intracellular staining cytometry (ISC) (Chapter 3.2, **Fig. 3.2.3**) was carried out on PBMCs from control (n=4) and bronchiolitic patients (n=7). Stimulation of control PBMCs resulted in significantly higher frequencies of IFN-γ-producing NKT cells, a median of 24% compared to only 3% in bronchiolitic infants (*P*=0.024) (**Fig. 3.3.15 F**). Similarly, significantly higher production of IFN-γ was observed in $CD4^+$ (a median of 2.8%) and $CD8^+$ T cells (a median of 27%) from control babies compared to bronchiolitics (~0.57% and ~3.88%, respectively) (**Fig. 3.3.15 G, H**). No differences were observed in the production of IL-13, IL-17A and IL-22 in those adaptive cell populations (**Fig. 3.2.15 D and E**). No difference in the production of IFN-γ, IL-13, IL-17A and IL-22 was observed in innate cells including NK cells, ILC, ILC1, ILC2 and ILC3 (**Fig. 3.2.15 A-E**).

UMAP confirms IFN-γ, IL-13, IL-17A and IL-22 production in the adaptive and innate populations

To gain deeper insights into the flow cytometric data obtained using optimised ICS panel (**Fig. 3.2.3**), UMAP dimensionality reduction was employed. This analysis allowed me to reduce 15 dimensions into two dimensions referred to as UMAPx and UMAPy (**Fig. 3.3.16 A,** middle). To reduce dimensions, FCS files were utilised from at least 11 experiments on bronchiolitic and control PBMCs. Firstly, data were cleaned using standard biaxial gating including only single, live lymphocytes (**Fig. 3.3.16 A,** left). After data cleaning, I performed UMAP analysis on 11,000 randomly selected lymphocytes (~1,000 from each subject concatenated into a single file). CD3 expression is shown **Fig. 3.3.16 A**, right. The manual gating strategy from the ICS panel was utilised allowing global UMAP clusters to be classified into the following cell types: CD4 T cells (red), NKT cells (dark green), CD8 T cells (light green), NK cells (blue), ILCs (light brown) (**Fig. 3.3.16 B**, left). UMAP representations of data highlighted the main differences between cell clusters among controls (blue) and bronchiolitic infants (pink) (**Fig. 3.3.16 B**, middle and right) in the region of NKT cells, $CD8^+$ and $CD4^+$ T cells. A UMAP map found NKT cells, $CD8^+$ and $CD4^+$ T cell regions enriched in control, but not severely ill infants, with high expression of IFN-γ (red) (**Fig. 3.3.16 C**). No differences in the expression of IL-13 (orange), IL-17A (blue) and IL-22 (light blue) were found in CD4 and CD8 T cell clusters (**Fig. 3.3.16 C**).

To further improve visualisation, I investigated differences in the heterogeneity of all subtypes of ILCs (including NK cells), I performed the UMAP immunophenotyping on ~11,000 FSC/SSC, single, live, $CD3^-$, Lin^- cells, $CD56^+$ (1,000 cells per subject) excluding all $CD3^+$ T cell populations (**Fig. 3.3.16 D**). CD56 marker was included deliberately to visualise NK cell populations on UMAP.


A
Single, Live, LYM
63.6
36.4
IFNγ
Sample ID (n=11)
UMAP y
UMAP x
CD3
B
CD8
NK
NKT
ILC
CD4
Control
(n=4)
Bronchiolitic
(n=7)
C
Control
(n=4)
Bronchilitic
(n=7)
Ungated
IFNγ
IL-22
IL-13
IL-17A

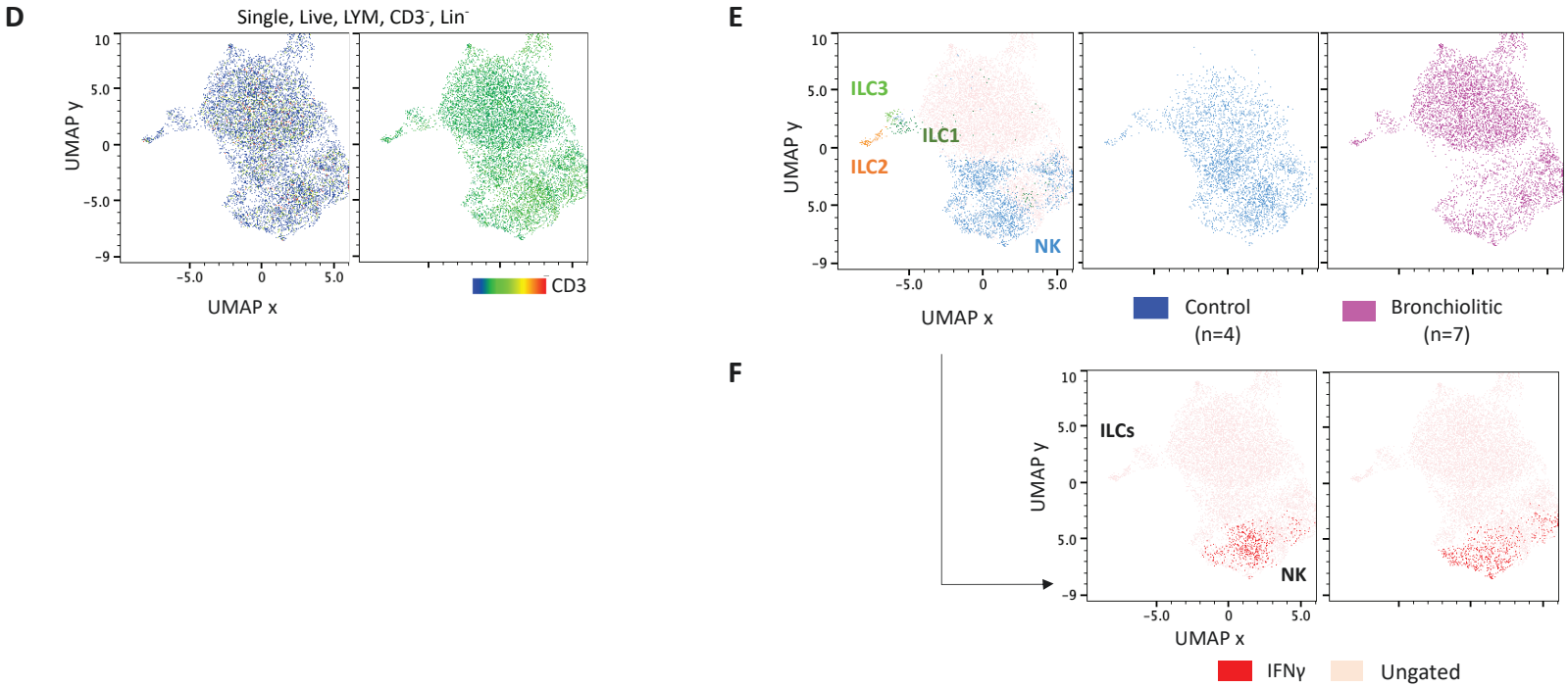


Figure 3.3.16 Deep immune phenotyping of stimulated PBMCs from control and bronchiolitic infants using UMAP reveals alterations in cytokine production in the adaptive but not innate compartment.

(A) Representative manual gating strategy utilised for deep immune phenotyping of cytokine production (ICS) panel. Cells were delineated using the following gating strategy: FSC/SSC, single, live cells. Lymphocytes were gated using SSC-A and FSC-A. The intensity of IFN-γ expression marker was used to identify IFN-γ^+ T lymphocytes (left). 1,000 randomly selected lymphocytes from each subject (*n*=11, left) were concatenated into a single file containing 11,000 cells for UMAP analysis (middle). The intensity of CD3 expression marker is shown (right). **(B)** The manual gating strategy from the ICS panel was utilised allowing global UMAP clusters (all subjects pooled, left) to be classified into the following cell types: CD4 T cells (red), NKT cells (dark green), CD8 T cells (lime green), NK cells (blue), ILCs (light brown). Comparison of UMAP representations of clusters for only control (*n*=7, middle) and bronchiolitic (*n*=4, right). The main differences between cell clusters among control subjects (grey) and bronchiolitic infants (pink) are depicted using the same orientated red arrows. **(C)** Simplified UMAP projections indicating the differences in the production of IFN-γ (red), IL-13 (orange), IL-17A (blue) and IL-22 (light blue) in ILC, NK, CD4 and CD8 T cell clusters from only controls (*n*=4) and bronchiolitics (*n*=7). **(D)** UMAP visualisation of cells delineated using the following gating strategy: FSC/SSC, single, live cells. ILC and NKs were gated using SSC-A/FSC-A, $CD3^-$, Lin^-, $CD56^+$, lymphocytes. 1,000 randomly selected lymphocytes from each subject (*n*=14,) were concatenated into a single file containing 11,000 cells for UMAP analysis (left). The intensity of CD3 expression marker is shown (right). **(E)** The manual gating strategy from the ICS panel was utilised allowing global UMAP clusters (all subjects pooled, left) to be classified into the following cell types: NK cells (blue), ILC1s (green), ILC2s (orange), ILC3s (light green). Comparison of UMAP representations of clusters for control subjects (*n*=4, middle) and bronchiolitic infants (*n*=7, right). **(E)** Simplified UMAP projections indicating the differences in the production of IFN-γ (red), in ILC and NK cell clusters from controls (*n*=7) and bronchiolitics (*n*=4). Abbreviations used: LYM – Lymphocytes, NK – natural killer cells, NKT – natural killer T cells, ILC – innate lymphoid cells, UMAP – Uniform Manifold Approximation and Projection, IL – interleukin, IFN – interferon.

This improved visualisation utilised the same cohort as used in **Figure 3.3.16 A-C** and the manual gating strategy from the ICS panel (**Fig. 3.2.3**) where all clusters were classified into the following cell types: NK cells (blue), ILC1s (green), ILC2s (orange), ILC3s (light green) (**Fig. 3.3.16 E**). This UMAP showed no differences to exist in IFN-γ producing cells between controls and bronchiolitics in the NK cell population (**Fig. 3.3.16 F**).

3.3.3.3.3. Correlations between the age and IFN-γ-producing innate and adaptive cells

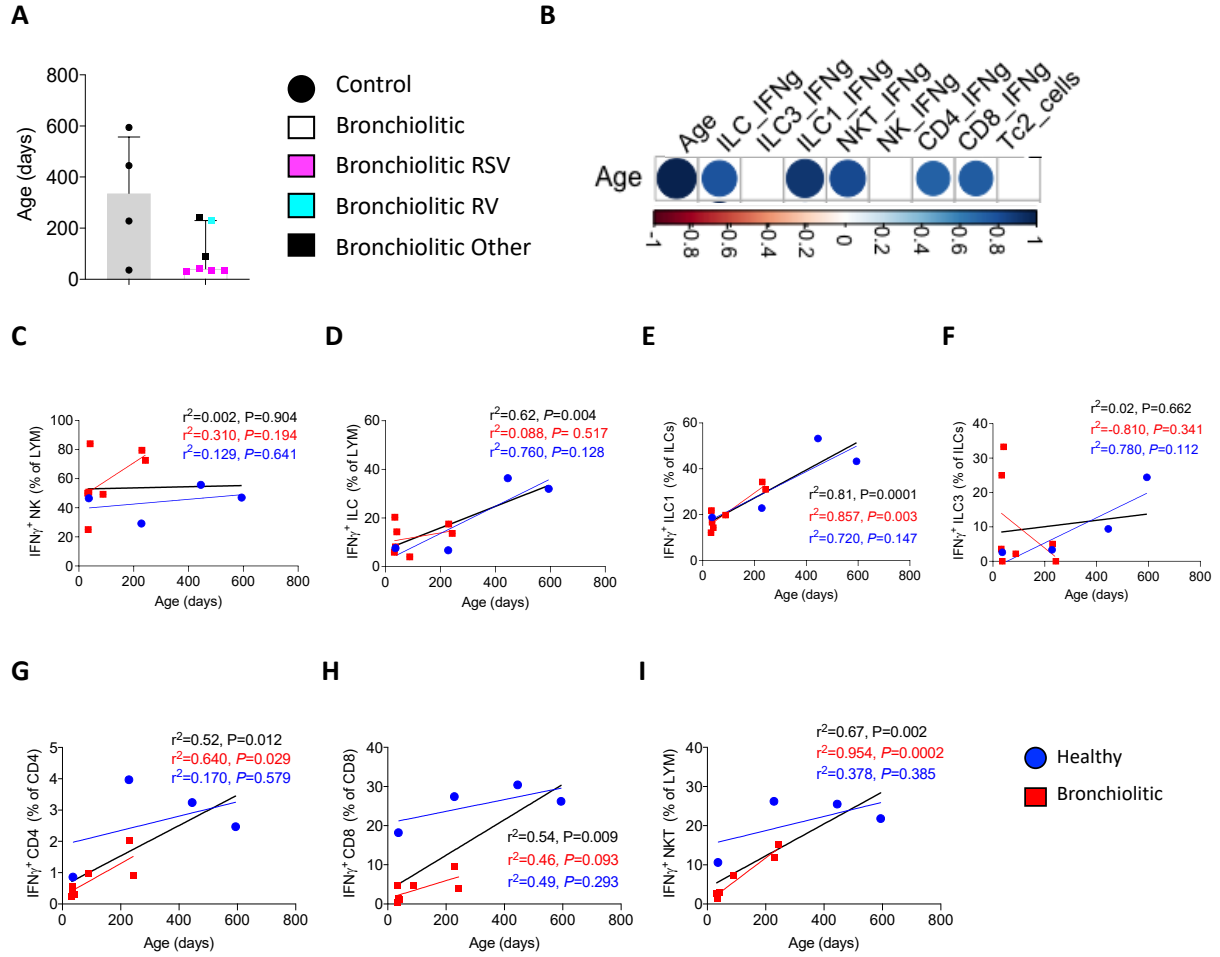


Figure 3.3.17 The differences in IFN-γ-producing CD4, CD8 and NKT cells between control and bronchiolitic infants cannot be explained by age differences.

(A) The age differences in the cytokine production (ICS) cohort (*n*=11) between control (*n*=4) and bronchiolitic (*n*=7) infants. **(B)** The correlation dependence between different cell populations producing IFN-γ and age in the ICS cohort. The correlation and linear regression between the frequency of IFN-γ-producing NK **(C)**, ILC **(D)**, ILC1 **(E)**, ILC3 **(F)**, CD4 **(G)**, CD8 **(H)** and NKT **(I)** cells. Data are displayed in an XY plot format using Pearson parametric correlation test where correlations with $p > 0.05$ are considered insignificant. The relationship between X and Y is summarised by the fitted regression line (blue – controls, red – bronchiolitic and black – control and bronchiolitic subjects) where r^2 (the correlation squared) shows the proportion of variation in Y explained by X. *Abbreviations used*: LYM – Lymphocytes, NK – natural killer cells, NKT – natural killer T cells, ILC – innate lymphoid cells

As seen in **Figure 3.3.17 A,** there is a difference in the median age of controls 336.5 days (range = 36 – 594) to bronchiolitic infants 41 days (range = 34 – 243). Although this difference did not reach a statistical level (*P*=0.178) due to the wide spread of the data, I analysed the correlations

between age and IFN-γ-producing innate and adaptive cells using correlograms (**Fig. 3.3.17 B**) and XY plots (**Fig. 3.3.17 C-I**) with Pearson correlation. As seen in **Figure 3.3.17 B,** I found significant correlations between the age and IFN-γ-producing ILC, ILC1, NKT, $CD4^+$ and $CD8^+$ T cells when control and all bronchiolitic subjects were analysed. This patterns were further confirmed as demonstrated by the correlation and regression line (black) fitted where r^2 explained the production of IFN-γ in ILC (r^2=0.620, *P*=0.004), ILC1 (r^2=0.810, *P*<0.0001), NKT (r^2=0.520, *P*=0.012), $CD4^+$ (r^2=0.540, *P*=0.009)and $CD8^+$ T (r^2=0.670, *P*=0.002) cells was age-dependent. To check if the age can explain the differences in the control versus bronchiolitis group, I performed an independent correlation for both cohorts. The fitted linear regression lines were added (blue – controls, red – bronchiolitic); however, the differences between younger bronchiolitc and older healthy patients cannot be solely explained by the age as the lines stay separated in NKT (**Fig. 3.3.17 I**), $CD4^+$ (**Fig. 3.3.17 G**) and $CD8^+$ T (**Fig. 3.3.17 H**); however, it is important to point out that the numbers used for correlation analysis were very low. To make this analysis robust, the number of subjects would have to be increased above *n*=10 per group.

3.3.3.4. The quantification of mucosal immune mediators in the lower and upper airways

I quantified mucosal inflammatory mediators using a multiplex immunoassay (MSD) in NPA (n=37) and TA (n=39) from healthy and bronchiolitic patients. Detailed information is described in Chapter 2 (Material and Methods, **Section 2.2.9.2**).

3.3.3.4.1. Cohort characteristics of NPA used in immune mediators quantification

To quantify mucosal inflammatory mediators using multiplex immunoassay (MSD) in NPA (*n*=37) I compared cytokines in control (*n*=10) and bronchiolitic (*n*=27) infants (**Table 3.3.6**). In this cohort females and males were well represented (*P*=0.076) with the median age of controls 216.5 days (range = 100 – 681) and bronchiolitic infants 58 days (range = 18 – 504) (*P*=0.002). There was a significant difference in weights (*P*=0.037) between control and bronchiolitic infants (a median weight of 10.15 and 4.20 kg, respectively). Overall females were well represented; however, females in the control group reached only 10% whereas the proportion of females in the bronchiolitic cohort was 43.33%. All bronchiolitic patients were stratified according to the viral aetiology of disease: RSV (51.85%), RV (33.33%) and other viruses (14.81%, including Influenza A and B, Adenovirus, CMV, hMPV). At the time of sampling, 37.03% of bronchiolitic infants in this cohort had bacterial coinfections (*Escherichia coli*, *Klebsiella pneumoniae*, *Staphylococcus aureus*) and 29.62% other comorbidities. Duration of illness, measured by the

length of hospital stay, the length of ventilation and the length of PICU stay was different between groups (*P*<0.001) as most of the control patients were healthy having elective surgery.

3.3.3.4.2. Cohort characteristics of TA used in immune mediators quantification

Next, I quantified mucosal inflammatory mediators using a multiplex immunoassay (MSD) in TA (n=39) by comparing cytokines in control (*n*=8) and bronchiolitic (*n*=31) infants (**Table 3.3.7**. In this cohort females and males were well represented (*P*=0.122) with the median age of controls 216.5 days (range = 100 – 681) and bronchiolitic infants 67 days (range = 18 – 504) (*P*=0.009). There was no difference in weights (*P*=0.105) between control and bronchiolitic (a median weight of 10.50 and 4.20 kg, respectively). Overall females were well represented; however, females in the control group reached only 10% whereas the proportion of females in the bronchiolitic cohort was 43.33%. All bronchiolitic patients were stratified according to the viral aetiology of disease: RSV (51.61%), RV (32.25%) and other viruses (12%, including Influenza A and B, Adenovirus, CMV, hMPV). At the time of sampling, 32.25% of bronchiolitic infants in this cohort had bacterial coinfections (*Escherichia coli*, *Klebsiella pneumoniae*, *Staphylococcus aureus*) and 32.25% other comorbidities. Duration of illness, measured by the length of hospital stay, the length of ventilation and the length of PICU stay was different between groups (*P*<0.001) as most of the control patients were healthy having elective surgery.

	Control Infants	Bronchiolitic Infants	
Demographic characteristics	*n*=10	*n*=27	*P* value
Age (days); median, (range)	216.50 (100-681.00)	58.00(18.00-504.00)	**0.002**
Sex; *n* (%)			0.076
Females	1.00 (10.00)	11.00 (43.33)	
Males	9.00 (90.00)	16.00 (56.67)	
Weight (kg); median, (range)	10.15 (2.80-14.30)	4.20 (3.00-10.60)	**0.037**
Ethnicity; *n* (%)			0.246
European	4.00 (40.00)	18.00 (66.66)	
Asian	2.00 (20.00)	6.00 (22.22)	
African (including Afro-Caribbean)	1.00 (10.00)	1.00 (3.70)	
Other	3.00 (30.00)	2.00 (7.41)	
Hospitalisation (days); median, (range)			
Length of hospital stay	2.00 (1.00-2.00)	6.00 (3.00-17.00)	<0.001
Length of PICU stay	0.00 (0.00-0.00)	6.00 (3.00-16.00)	<0.001
Length of ventilation	1 .00 (1.00-1.00)	6.00 (3.00-22.00)	<0.001
Clinical features			NA
Max FiO_2 (%); average, (range)	NA	92.59 (40.00-100)	
PIP (cmH_2O); average, (range)	NA	25.81 (16.00-33.00)	
Aetiology of disease; *n* (%)			NA
RSV	NA	14.00 (51.85)	
RV	NA	9.00 (33.33)	
Other	NA	4.00 (14.81)	
Co-infections; *n* (*%*)			NA
Yes	NA	10.00 (37.03)	
No	NA	17.00 (62.96)	
Comorbidities; *n* (*%*)			NA
Yes	NA	8.00 (29.62)	
No	NA	19.00 (70.37)	
Gestation at delivery			0.9675
Not documented; n (%)	4 (40.00)	11 (40.74)	
Documented; *n* (%)	6 (60.00)	16 (59.25)	
Documented (wk); median (range)	31.50 (25.00-38.00)	36.00 (23.00-42.00)	0.1394

Table 3.3.6 Control and bronchiolitic infants' demographics used for NPA analysis with MSD platform in Chapter 3.3.

Control and bronchiolitic infants NPAs were analysed using the MSD platform for cytokine production. Patient demographic and clinical information were obtained from the patients' information. *P* values for continuous data were computed by Mann-Whitney test while *P* values for categorical data were computed by Chi-square test (χ^2 test) or Fisher's exact test. Differences were assessed through χ^2 test and Fisher's exact test for sample size>5 and <5, respectively. The range is defined as the difference between the highest and lowest value. Ethnicity data: European (North/Mid/East-European), Asian (South Asia including India and Pakistan), African (North and Sub-Saharan territories) and other (the Middle East, Arabic origin or not stated). Aetiology of disease defines or non-RSV and non-RV viral infection of LRTI such as: Influenza (A and B), Adenovirus, CMV, hMPV. Co-infections are defined as viral (RV, RSV, Influenza A or B, Adenovirus, CMV, hMPV) and bacterial infections (*Escherichia coli*, *Klebsiella pneumoniae*, *Staphylococcus aureus*). *Definition of abbreviation:* PICU – Paediatric Intensive Care Unit, FiO2 – the fraction of inspired oxygen, is defined as the percentage of inhaled oxygen, PIP – Peak Inspiratory Pressure, is the highest amount of pressure in the ventilator circuit when the lungs are filled with air, wk – week, kg – kilogram, NA – not available.

	Control Infants	Bronchiolitic Infants	
Demographic characteristics	*n*=8	*n*=31	*P* value
Age (days); median, (range)	216.50 (100-681.00)	67.00(18.00-504.00)	**0.009**
Sex; *n* (%)			0.122
Females	1.00 (10.00)	13.00 (43.33)	
Males	7.00 (90.00)	18.00 (56.67)	
Weight (kg); median, (range)	10.50 (2.80-14.30)	4.20 (3.00-10.60)	0.105
Ethnicity; *n* (%)			0.123
European	3.00 (37.50)	20.00 (64.51)	
Asian	1.00 (12.50)	6.00 (19.35)	
African (including Afro-Caribbean)	1.00 (12.50)	3.00 (9.60)	
Other	3.00 (37.50)	2.00 (6.45)	
Hospitalisation (days); median, (range)			
Length of hospital stay	2.00 (1.00-2.00)	6.00 (3.00-17.00)	**<0.001**
Length of PICU stay	0.00 (0.00-0.00)	6.00 (3.00-22.00)	**<0.001**
Length of ventilation	1 .00 (1.00-1.00)	6.00 (3.00-22.00)	**<0.001**
Clinical features			NA
Max FiO_2 (%); average, (range)	NA	90.71 (40.00-100)	
PIP (cmH_2O); average, (range)	NA	26.29 (16.00-33.00)	
Aetiology of disease; *n* (%)			NA
RSV	NA	16.00 (51.61)	
RV	NA	10.00 (32.25)	
Other	NA	4.00 (12.00)	
Co-infections; *n* (*%*)			NA
Yes	NA	11.00 (35.48)	
No	NA	20.00 (64.51)	
Comorbidities; *n* (*%*)			NA
Yes	NA	10.00 (32.25)	
No	NA	21.00 (67.74)	
Gestation at delivery			0.6817
Not documented; n (%)	4 (50.00)	13 (40.74)	
Documented; *n* (%)	4 (50.00)	18 (59.25)	
Documented (wk); median (range)	29.00 (25.00-38.00)	36.00 (23.00-42.00)	0.1847

Table 3.3.7 Control and bronchiolitic infants' demographics used for TA analysis with MSD platform in Chapter 3.3.

Control and bronchiolitic infants NPAs were analysed using the MSD platform for cytokine production. Patient demographic and clinical information were obtained from the patients' information sheets. *P* values for continuous data were computed by Mann-Whitney test while *P* values for categorical data were computed by Chi-square test (χ^2 test) or Fisher's exact test. Differences were assessed through χ^2 test and Fisher's exact test for sample size>5 and <5, respectively. The range is defined as the difference between the highest and lowest value. Ethnicity data: European (North/Mid/East-European), Asian (South Asia including India and Pakistan), African (North and Sub-Saharan territories) and other (the Middle East, Arabic origin or not stated). Aetiology of disease defines or non-RSV and non-RV viral infection of LRTI such as: Influenza (A and B), Adenovirus, CMV, hMPV. Co-infections are defined as viral (RV, RSV, Influenza A or B, Adenovirus, CMV, hMPV) and bacterial infections (*Escherichia coli*, *Klebsiella pneumoniae*, *Staphylococcus aureus*). *Definition of abbreviation:* PICU – Paediatric Intensive Care Unit, FiO2 – the fraction of inspired oxygen, is defined as the percentage of inhaled oxygen, PIP – Peak Inspiratory Pressure, is the highest amount of pressure in the ventilator circuit when the lungs are filled with air, wk – week, kg=kilogram, NA – not available.

3.3.3.4.3. Changes in soluble mediators in the airways of control and bronchiolitic patients

Level of selected mediators in the upper airway (NPA) compartment

In the first part, I tried to measure soluble mediators in complex clinical samples collected from upper airways (*n*=37), related as NPA, as described in Chapter 2, Section 2.2.8.3-4. Although extensive efforts have been made to make sure the lowest level of variation in the collected NPAs, the collection of the sample *via* a catheter may result in highly diluted samples and variable dilutions between patients [198]. A multiplex immunoassay (Mesoscale Discovery, aka MSD) was implemented to measure multiple analytes in a tiny volume of clinical samples. This multiplex approach allowed me to measure 25 different soluble mediators (IFN-γ, IL-10, IL-12p70, IL-13, IL-1b, IL-2, IL-4, IL-6, IL-8, TNFα, BAFF, IFN-α2a, IFN-β, IL-15, IL17E, IL-29, IL-33, IL5, TSLP, IP-10, IL-17A, IL-21, IL-22, IL-23, IL-27, MIP-3a and IL-31). As seen in **Figure 3.3.18,** there were significantly higher levels of IFN-γ, IL-10, IL-12p70, IL-13, IL-1b, IL-2, IL-4, IL-6, IL-8, TNFα, BAFF, IL-15, IL-29, IL-5, TSLP, IP-10, MIP-3a and IL-31 (**Fig. 3.3.18 A-K, N, P, R-T, Z and a**, respectively) in the NPA from bronchiolitics relative to healthy controls ($P<0.05$ throughout). No significant differences were measured in the levels of IFN-α2a, IFN-β, IL-17E, IL-33, IL-17A, IL-21, IL-22, IL-23, IL-27 in NPAs between controls (*n*=10) and bronchiolitics (*n*=27). Interestingly, there were no statistical differences between RSV-bronchiolitis (n=14, magenta) compared to RV-bronchiolitis (n=9, light blue) in the production of soluble mediators apart from the level of IL-4 (**Fig. 3.3.18 G**); only IL-4 levels were statistically different between RV- and RSV-bronchiolitic group ($P=0.005$). In addition, the measurement of IL-4, IL-5 and MIP-3a in the NPA samples showed that these cytokine levels are higher in RV-bronchiolitis but not RSV-bronchiolitis ($P=0.002$, $P=0.01$ and $P=0.002$, respectively).

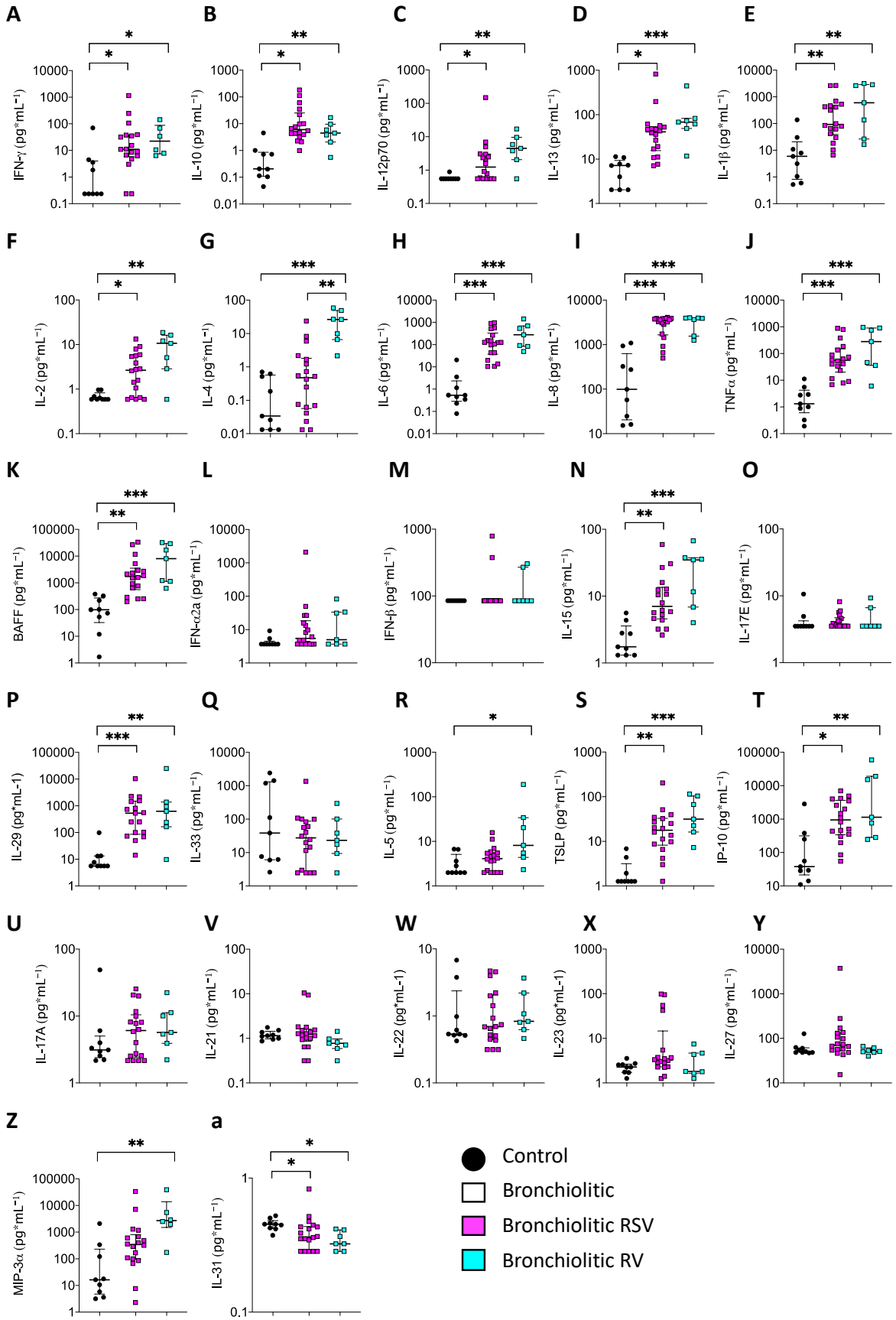


Figure 3.3.18 Soluble mediators in NPA samples from control and bronchiolitic infants

Nasopharyngeal aspirates (NPA) were used to measure soluble mediators in control subjects (*n*=10) and infants with severe bronchiolitis (*n*=27) associated with respiratory syncytial virus (RSV) infection (n=14, magenta) or rhinovirus (RV) infection (n=9, light blue) **(A-a)**. Data were analysed using a Kruskall-Wallis test with Dunns

correction for multiple comparisons (* $p < 0.05$, ** $p < 0.01$, *** $p < 0.001$ and **** $p < 0.0001$). Data are shown as row values on the logarithmic scale where lines denotes median values and error bars are interquartile ranges.

Level of selected mediators in the lower airway (TA) compartment

Subsequently, I measured soluble mediators in samples collected from lower airways (*n*=39), the tracheal aspirate (TA), as described in Chapter 2, Section 2.2.8.3-4. Similarly to NPAs, sample collection *via* suction catheter may result in highly diluted samples and variable dilutions between patients despite extensive effort to minimise variation. A multiplex approach allowed me to measure up to 25 different soluble mediators (IFN-γ, IL-10, IL-12p70, IL-13, IL-1β, IL-2, IL-4, IL-6, IL-8, TNFα, BAFF, IFN-α2a, IFN-β, IL-15, IL17E, IL-29, IL-33, IL5, TSLP, IP-10, IL-17A, IL-21, IL-22, IL-23, IL-27, MIP-3a and IL-31. As seen in the **Figure 3.3.19** there were significantly higher levels of IFN-γ, IL-10, IL-12p70, IL-13, IL-1β, IL-2, IL-4, IL-6, IL-8, TNFα, BAFF, IFN-α2a, IL-15, IL-29, IL-5, TSLP, IP-10 and IL-31 (**Fig. 3.3.19 A-L, N, P, R-T and Z**, respectively) in the measurements from bronchiolitics in relation to heathy controls (P<0.05 throughout). In addition, no significant differences were measured in the levels of IFN-β, IL-17E, IL-33, IL-17A, IL-21, IL-22, IL-23, IL-27 and MIP-3a in NPAs between controls (*n*=8) and bronchiolitics (*n*=31). As seen in NPA, there were no statistical differences between RSV-bronchiolitis (n=16, magenta) compared to RV-bronchiolitis (n=10, light blue) in the production of soluble mediators apart from IL-4 in TAs (**Fig. 3.3.19 G**); only IL-4 levels were statistically different between RV- and RSV-bronchiolitic group (*P*=0.02). In addition, the measurement of IL-5 and IL-31 in TA samples showed that these cytokine levels are higher in RV-bronchiolitis but not RSV-bronchiolits (*P*=0.012 and *P*=0.003, respectively); while IL-4 levels in TAs were elevated in RV- and RSV-bronchiolitis (*P*<0.0001 and *P*=0.004, respectively).

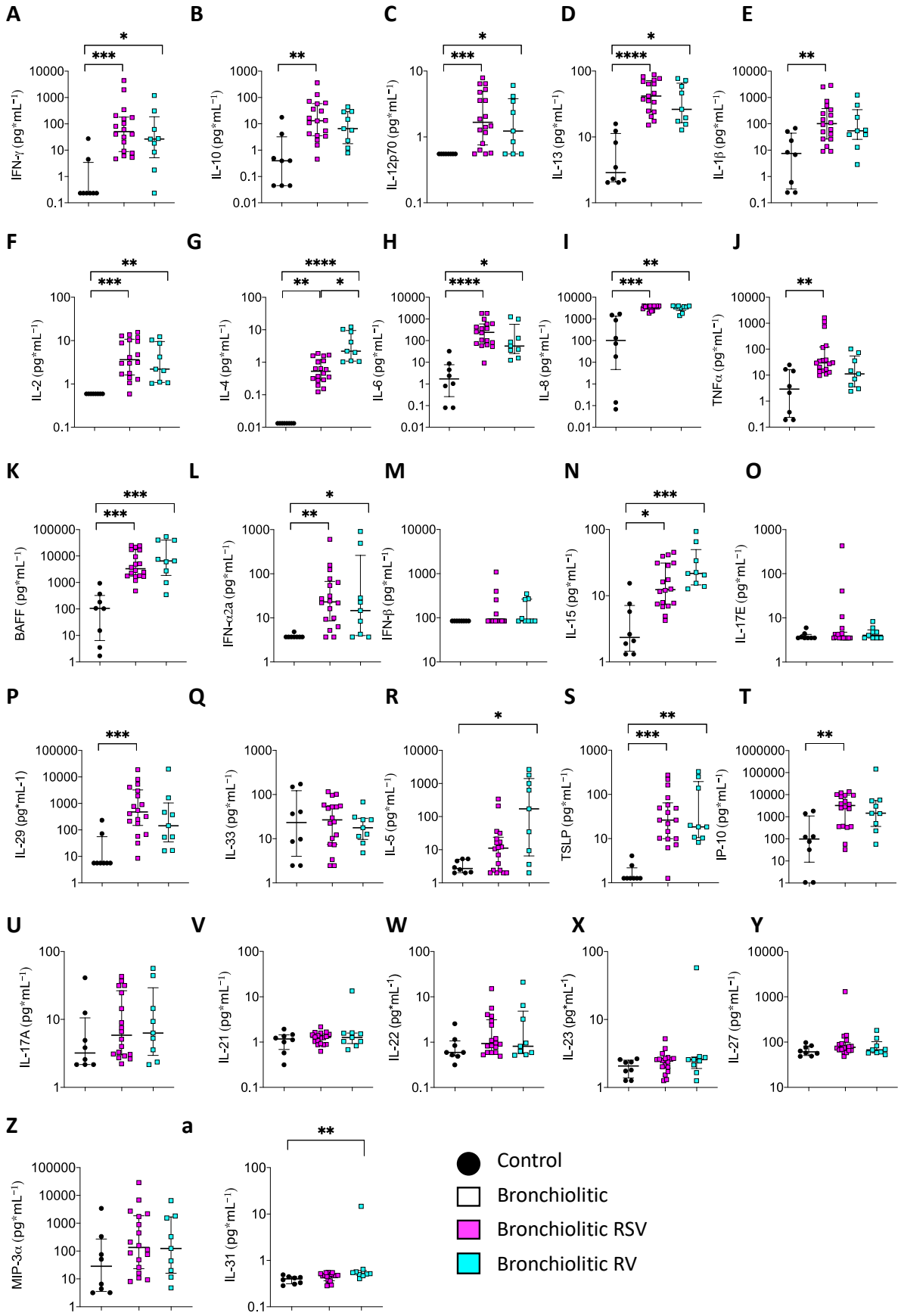


Figure 3.3.19 Soluble mediators in TA samples from bronchiolitic infants

Tracheal aspirates (TA) were used to measure soluble mediators in control subjects (*n*=8) and infants with severe bronchiolitis (*n*=31) associated with respiratory syncytial virus (RSV) infection (n=16, magenta) or rhinovirus (RV) infection (n=10, light blue) **(A-a)**. Data were analysed using a Kruskall-Wallis test with Dunns correction for multiple

comparisons (* $p < 0.05$, ** $p < 0.01$, *** $p < 0.001$and **** $p < 0.0001$). Data are shown on the logarithmic scale where lines denotes median values and error bars are interquartile ranges.

3.3.3.4.4. Cytokine profiles in severe bronchiolitis and healthy controls

After determining the significant differences between healthy and bronchiolitic infants in cytokine production, we next employed heatmaps (**Fig. 3.3.20 and 21**) and principal component of analysis (PCA) (**Fig. 3.3.22**) in the R programming language to better explore the differences in the cytokines profiles in NPA (**Fig. 3.3.20**) and TA (**Fig. 3.3.21**) among severely ill and healthy subjects.

NPA cytokine immune profile in bronchiolitis and health

As seen in **Figure 3.3.20**, I used hierarchical clustering on NPA cytokine levels from both control and bronchiolitic infants (*n*=10 and *n*=27, respectively) (**Fig. 3.3.20 A**) or only among the bronchiolitic infants (n=27) (**Fig. 3.3.20 B**). The hierarchical group comparison identified a set of babies with a very high production of cytokines (in the bronchiolitic cohort) and another one with very low production of these soluble mediators (including both bronchiolitic and control cohort). That heterogeneity among bronchiolitic cohort was not associated with sex (**Fig. 3.3.20 A**). I next assessed the potential impact of viral aetiology, comorbidities, coinfections and again sex on the hierarchical clustering in bronchiolitic infants (**Fig. 3.3.20 B**) with no associations explaining the heterogeneity. This signature was validated by PCA in the NPA cohort (**Fig. 3.3.22 A, C-F**) finding no clustering according to viral aetiology, comorbidities, coinfections and sex; suggesting that the effect of these parameters on cytokine profile was not substantial.

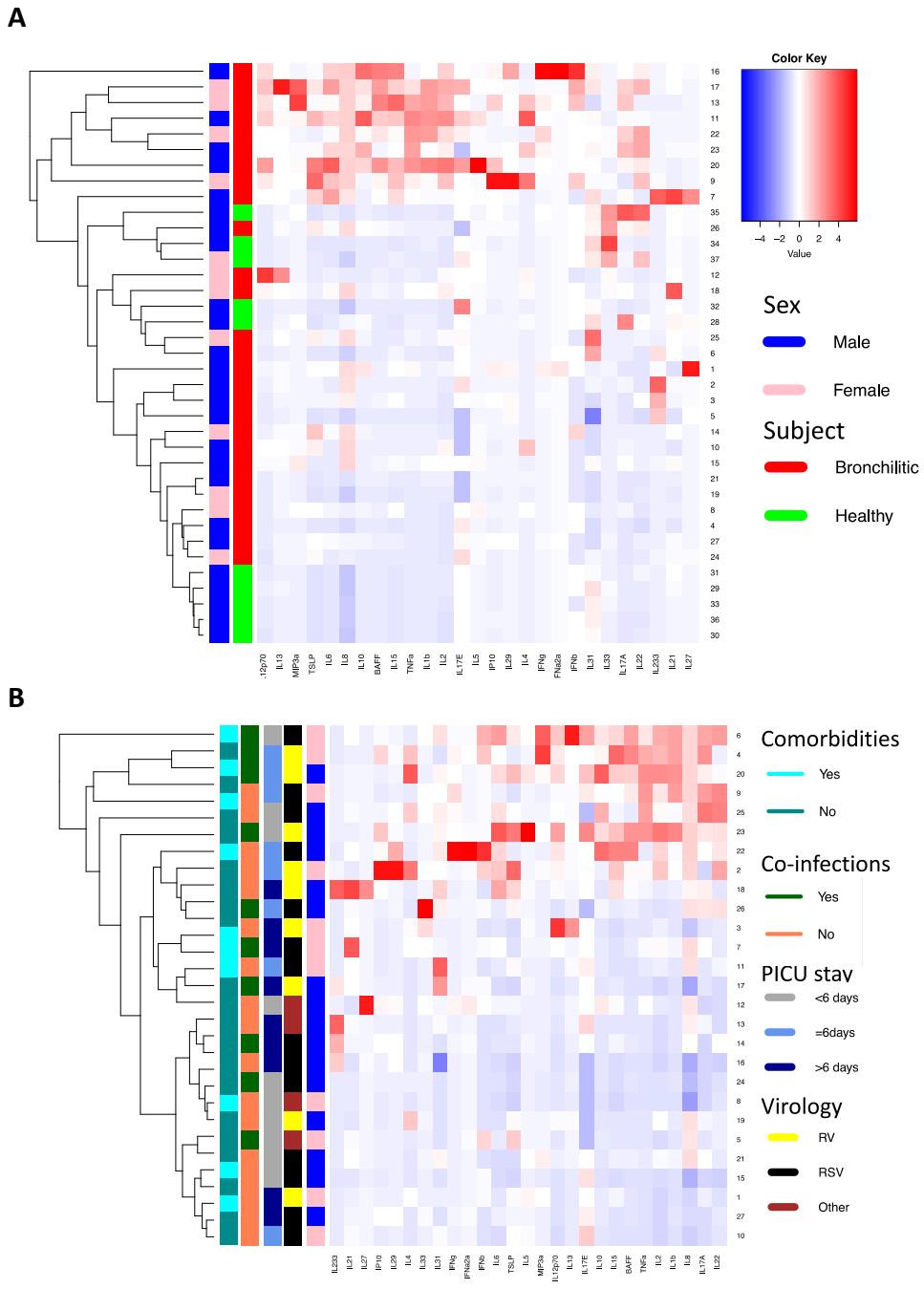


Figure 3.3.20 The hierarchical clustering of the NPA cytokines from control and bronchiolitic infants using heatmap format.

The NPA cytokine (*n*=37) signatures were delivered by comparing cytokine levels from both control and bronchiolitic infants (*n*=10 and *n*=27, respectively) **(A)** and only bronchiolitic infants (*n*=27) **(B)** using the R programming language. Data are displayed in a heatmap format, where each row represents an individual (sample) and each column represents the cytokine (variable). The rows and columns were ordered according to the hierarchical clustering result, putting similar observations close to each other. In the plots above, high values are in red and low values in blue and consist of Pearson correlation coefficients ranging from -5 to 5. Additionally, **(A)** the rows were annotated according to the subject (Control/Healthy, Bronchiolitic) and sex (Female, Male) signatures using colours. **(B)** the rows were annotated according to Viral aetiology (RV, RSV, Other), Comorbidities (Yes/No), Co-infection (Yes/No) and also sex (Female, Male) **(B)** signatures using colours. *Abbreviations used*: *n* – number of study participants, NPA – nasopharyngeal aspirates.

TA cytokine immune profile in bronchiolitis and health

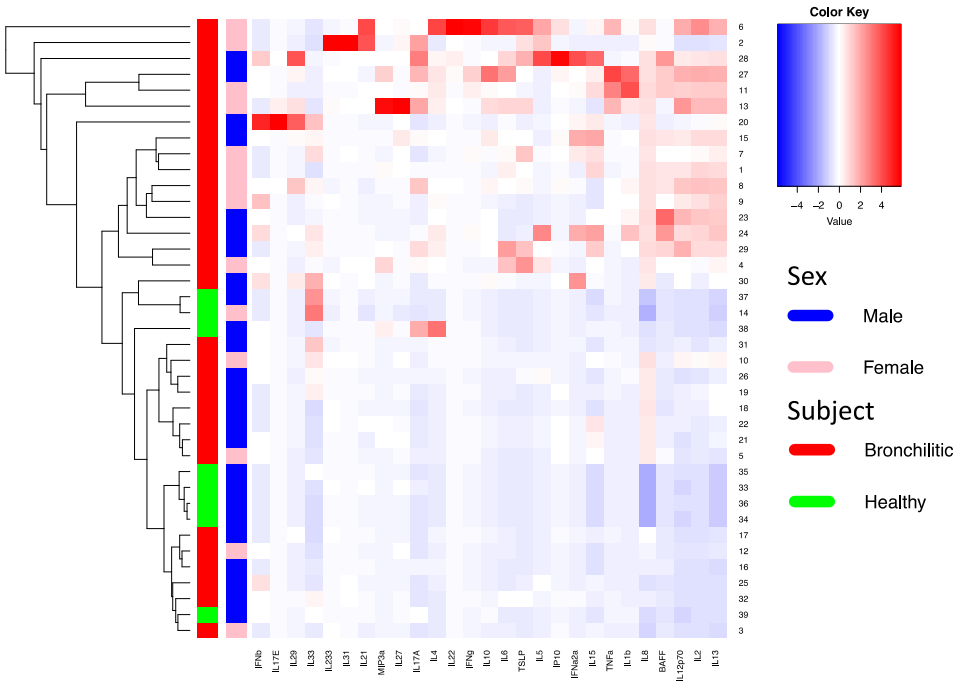
I followed the same approach using hierarchical clustering to define the cytokine profile of the TA cohort (*n*=39) from both control and bronchiolitic infants (*n*=8 and *n*=31, respectively) (**Fig. 3.3.21 A**) or only among the bronchiolitic infants (*n*=31) (**Fig. 3.3.21 B**). The TA profile was similar to the NPA as no substantial associations were found to explain the heterogeneity of the bronchiolitic infants when viral aetiology, comorbidities, coinfections and sex were applied (**Fig. 3.3.21 A and B**). Finally, these signatures were also validated by PCA using the data from the TA cohort (**Fig. 3.3.22 B, G-J**).

3.3.3.4.5. Assessment of cytokine correlations in bronchiolitic infants

Correlations analysis according to age, weight, disease severity

To better understand the association between the age, weight, disease severity and cytokine profiles of airway samples, I calculated the correlations between cytokines from the MSD data (**Fig. 3.3.23**) for NPA (*n*=27) (**Fig. 3.3.23 A, C**) and TA (*n*=31) (**Fig. 3.3.23 B, D**) in bronchiolitic children. For this analysis, data has been displayed in a correlogram format and delivered by Pearson's correlation with hierarchical clustering using the R programming language where positive correlations are displayed in blue and negative correlations in red. I found positive, significant associations between age and NPA cytokines: BAFF, IL-5, IL-15, IL-17A, IL-21, IL-23 and IL-31 and that weight positively correlated with BAFF, IL-5 and IL-15 in upper airways (**Fig. 3.3.23 A**). Moreover, I correlated cytokines in upper airways with the severity of illness, measured by the length of hospital stay, the length of ventilation and the length of PICU stay to discover that IL-21, IL-23, IL-31 positively correlated with the disease severity and IL-33 negatively. (**Fig. 3.3.23 A**). A similar approach was used for TA cytokines (**Fig. 3.3.23 B**). Interestingly, I found a positive correlation between the disease severity and IL-23 but no other cytokines; the weight and IL-10, IL-1β, IL-2 and MIP-3α; and finally, the age and IL-1β, IL-2 and IL-5. Finally, to discover meaningful associations between different cytokines in the airway compartments, I correlated all cytokines in NPA (**Fig. 3.3.23 C**) and TA (**Fig. 3.3.23 D**) using hierarchical clustering. This analysis allowed me to identify any cytokine clusters, for example, related to type-2 or type-1 immune responses.

A



B

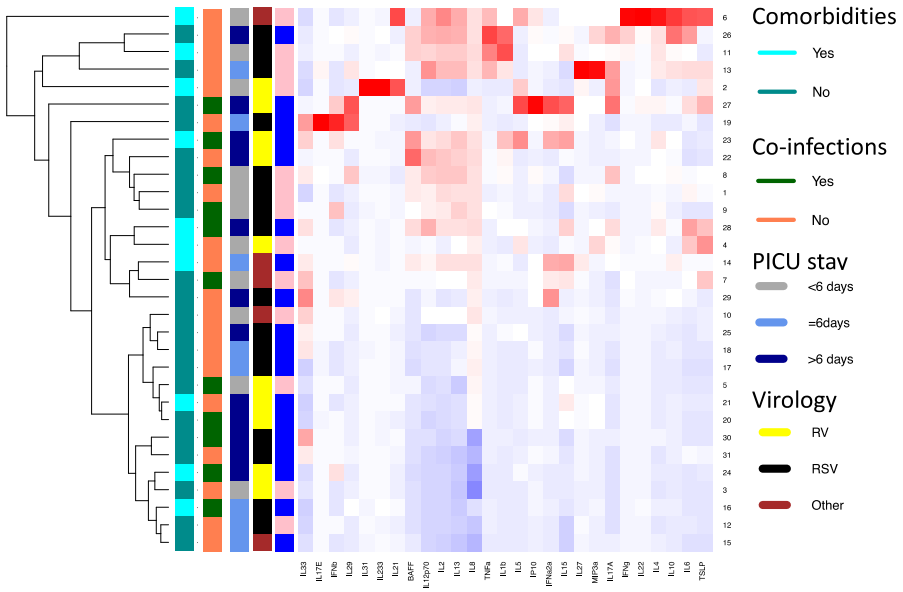


Figure 3.3.21 Hierarchical clustering of cytokines in the TA from control and bronchiolitic infants using a heatmap format.

The TA cytokine (*n*=39) signatures were delivered by comparing cytokine levels from both control and bronchiolitic infants (*n*=8 and *n*=31, respectively) **(A)** and only bronchiolitic infants (*n*=31) **(C)** using the R programming language. Data are displayed in a heatmap format, where each row represents an individual (sample) and each column represents the cell population (variable). The rows and columns were ordered according to the hierarchical clustering result, putting similar observations close to each other. In the plots above, high values are in red and low values in blue and consist of Pearson correlation coefficients ranging from -5 to 5. Additionally, **(A)** the rows were annotated according to the subject (Control/Healthy, Bronchiolitic) and sex (Female, Male) signatures using colours. **(B)** the rows were annotated according to Viral aetiology (RV, RSV, Other), Comorbidities (Yes/No), Co-infection (Yes/No) and also sex (Female, Male) **(B)** signatures using colours. *Abbreviations used*: *n* – number of the study participant, TA – tracheal aspirates.

Correlations between NPA and TA cytokine immune profiles

To better understand if cytokine responses correlate in the upper and lower airways, I calculated the correlation between the same cytokines from NPA and TA in bronchiolitic children (*n*=30) (**Fig. 3.3.24**). In this analysis, correlation relationships between the same cytokines in NPA and TA were summarised by a fitted regression line where the correlation squared (r^2) shows the proportion of variation in NPA explained by TA. I found significant, positive correlations only in seven measured cytokines out of 28 between TA and NPA: IFN-γ (r^2=0.848, *P*<0.0001), IL-10 (r^2=0.403, *P*=0.0004), IL-1β (r^2=0.168, *P*=0.033), IL-2 (r^2=0.192, *P*=0.02), BAFF (r^2=0.184, *P*=0.026), IL-5 (r^2=0.750, *P*<0.0001) and TSLP (r^2=0.389, *P*=0.03) (**Fig. 3.3.24 A, B, E, F, L, S, T**). This analysis allowed me to identify whether the NPA cytokine immune profile reflected the cytokine profile of lower airways measured in the TA.

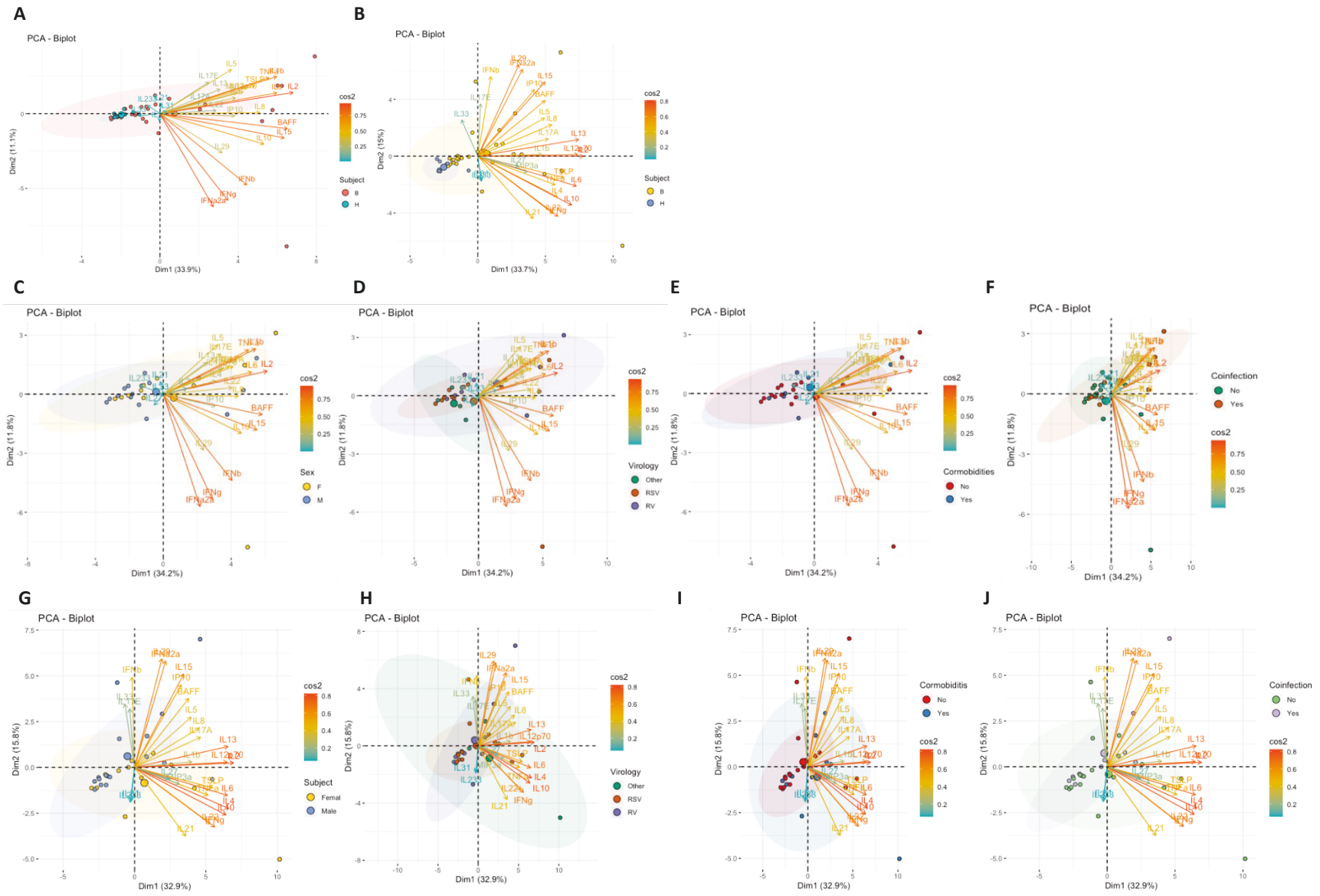

A
PCA - Biplot
Dim1 (33.9%)
Dim2 (11.1%)
cos2
Subject
B
H
B
PCA - Biplot
Dim1 (33.7%)
Dim2 (15%)
cos2
Subject
B
H
C
PCA - Biplot
Dim1 (34.2%)
Dim2 (11.8%)
cos2
Sex
F
M
D
PCA - Biplot
Dim1 (34.2%)
Dim2 (11.8%)
cos2
Virology
Other
RSV
RV
E
PCA - Biplot
Dim1 (34.2%)
Dim2 (11.8%)
cos2
Cormobidities
No
Yes
F
PCA - Biplot
Dim1 (34.2%)
Dim2 (11.8%)
Coinfection
No
Yes
cos2
G
PCA - Biplot
Dim1 (32.9%)
Dim2 (15.8%)
cos2
Subject
Femal
Male
H
PCA - Biplot
Dim1 (32.9%)
Dim2 (15.8%)
cos2
Virology
Other
RSV
RV
I
PCA - Biplot
Dim1 (32.9%)
Dim2 (15.8%)
Cormobiditis
No
Yes
cos2
J
PCA - Biplot
Dim1 (32.9%)
Dim2 (15.8%)
Coinfection
No
Yes
cos2

Figure 3.3.22 Separation between subjects in PCA analysis of cytokine levels is not associated with the health status, sex or the aetiology of the disease.

MSD data are displayed as a Principal Component Analysis (PCA), where each individual is plotted as a point and individuals that are similar are grouped together, comparing the cytokine levels from NPA (*n*=37) and TA (*n*=39) from both control and bronchiolitic infants using the R programming language. The subject health status (Bronchiolitic, Healthy) signatures are shown for NPA **(A)** and TA **(B).** Other signatures such as the sex (Female, Male), viral aetiology (RV, RSV, Other), Comorbidities (Yes/No), Co-infection (Yes/No) are shown for only bronchiolitic NPA **(C-F)** and TA **(G-J)**. The group mean point (large circle) was added for each group during the process of 'habillage' PCA to depict the centre of each group. The point concentration ellipses (red and light blue) were added around each group mean point using a multivariant t-distribution where the size of the concentration ellipse is in normal probability (95% confidence). Variable correlation plots show the relationship between all variables (arrows). Positively correlated variables (arrows) were grouped together while negatively correlated variables (arrows) were positioned on opposite sides of the plot origin. The distance between variables (arrows) and the origin measures the quality of the variables on PCA. Variables that are away from the origin are well represented on the PCA. The quality of representation on the variable (arrow) on the PCA is called cos2; the higher cos2 the better is the representation of the variable. *Abbreviations used:* cos2 – square cosine, squared coordinates, *n* – number of study participants, NPA – nasopharyngeal aspirates, TA – tracheal aspirates

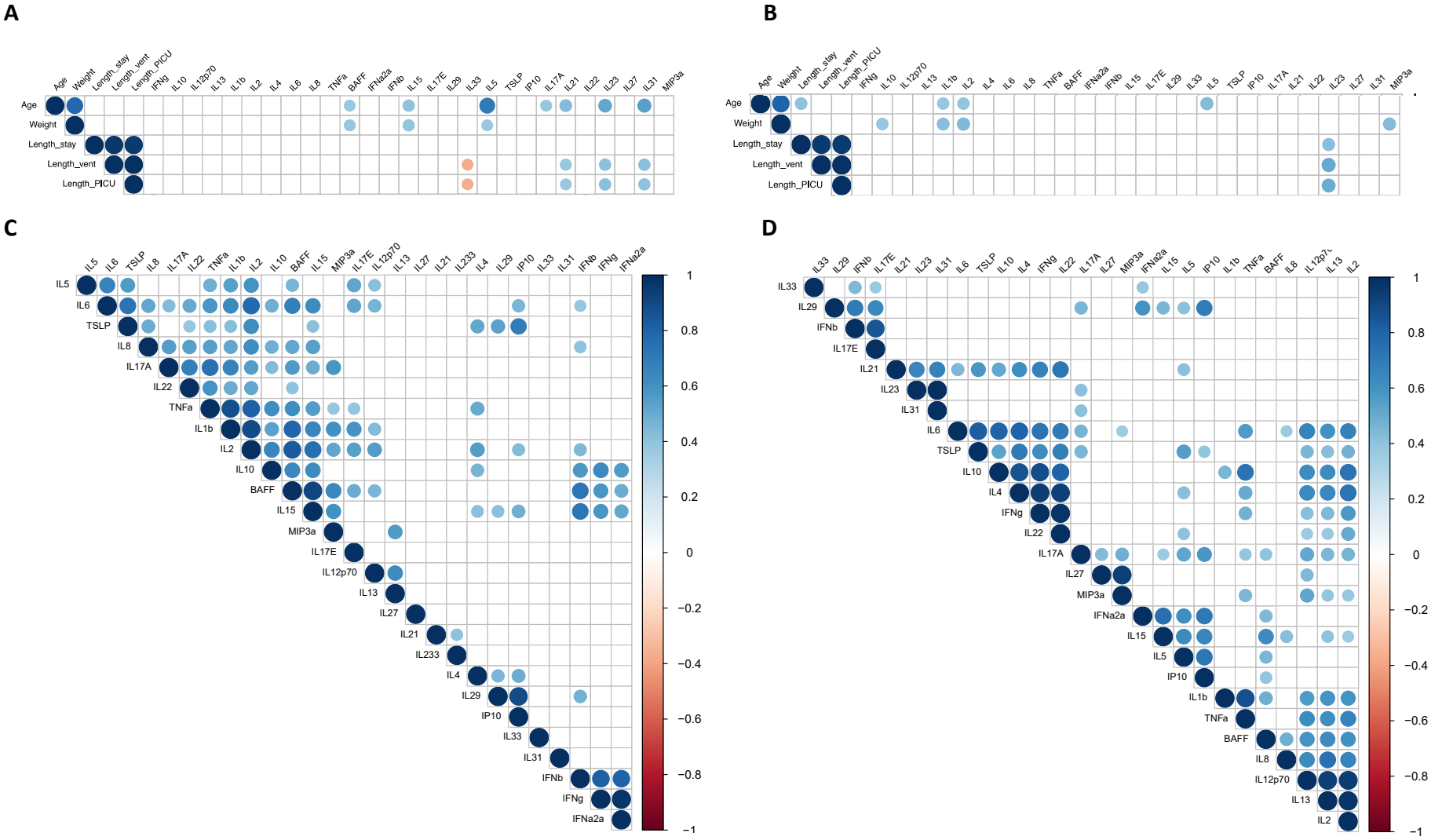

A
Age
Weight
Length_stay
Length_vent
Length_PICU
B
C
D
1
0.8
0.6
0.4
0.2
0
−0.2
−0.4
−0.6
−0.8
−1

Figure 3.3.23 The investigation of the correlation dependence between the cytokine levels and the severity of disease in NPA and TA from bronchiolitic infants using MSD data.

The correlation dependence between multiple variables from the MSD data obtained using NPA (*n*=27) **(A and C)** and TA (*n*=31) **(B and D)** from bronchiolitic infants. **(A)** and **(B)** shows the correlation dependence of the cytokine levels from NPA (A)and TA (B) from bronchiolitic infants and the severity of disease measured by the length of hospitalisation stay, the length of ventilation and the length of PICU stay using correlograms. Additionally, the correlation dependence between all cytokines for data obtained using MSD platform from NPA **(C)** and TA **(D)** from bronchiolitic infants using Pearson parametric correlation test was delivered with the R programming language. Data are displayed in a correlogram format where positive correlations are displayed in blue and negative correlations in red colour. The intensity of the colour and the size of the circle are proportional to the correlation coefficients. Additionally, in the right side of each correlogram, the legend colour depicts the correlation coefficients and the corresponding colours. The correlation matrix used for all graphs was not reordered according to hierarchical order. Correlations with $p > 0.05$ are considered insignificant and were left blank which means there is no linear relation between the variable considered. *Abbreviations used*: PICU – Paediatric Intensive Care Unit, *n* – number of study participants, NPA – nasopharyngeal aspirates, TA – tracheal aspirates

3.3.4. Discussion for Chapter 3.3

Using OMIP, ISC panels and other analytical approaches, I investigated differences in the number and function of innate cells and the adaptive compartment between bronchiolitic and healthy controls. The understanding of innate mucosal immunity in protection against viral infection has been of particular interest in the time of severe acute respiratory syndrome coronavirus 2 (SARS-CoV-2). The role of innate cells and their contribution to defence against emerging and well-known pathogens is lacking [264].

Granulocytes in Bronchiolitis

Strikingly, but not surprisingly, granulocytes were the most abundant cell population in whole blood and airways samples; and the most numerous population of granulocytes were neutrophils. Consistent with these data, previous human studies of lower and upper airway secretions identified neutrophils as the most common component in the airways of bronchiolitic babies [5,99]. However, neutrophils have been reported to be low in the lung parenchyma [99]. MSD data of supernatants from NPA and TA found high levels of CXCL8 which is a chemoattractant for neutrophils [265]. It is believed that neutrophils are drawn to the airway lumen upon chemokine stimulation which explains their presence in high numbers in airway secretions.

Deep immune phenotyping using UMAP allowed me to identify different immune characteristics of the immunomes of healthy and bronchiolitic babies. A UMAP embedding approach found that major regions enriched in bronchiolitis were comprised of neutrophils and eosinophils. Moreover, a UMAP allowed me to observe the changes not only in the cell composition but depicted phenotypic differences in the same clusters between the cohort of healthy and bronchiolitic babies. Therefore, this analysis suggests a change in the phenotype of blood and airway neutrophils in bronchiolitis, which warrants further study.

What is the role of granulocytes? Are they friend or foe during viral infection and the development of severe bronchiolitis? The role of neutrophils in RSV driven disease has been the topic of debate as we do not know if they reflect lung injury and whether they have a detrimental role in viral infections [5]. Massive neutrophil recruitment into the lungs has been observed when mechanical ventilation was involved in the first days of RSV-bronchiolitis in children below the age of six [107]. Data from Lukens *et al*. (2010) of primary RSV infection of 22 infants younger than 52 weeks showed that an influx of neutrophils proceeded the peak of T-cell activation [107]. Furthermore, Habibi *et al*. (2020) have shown that mucosal neutrophilic activation and suppression of IL-17 before exposure of healthy adults to RSV was highly associated with the

predisposition to RSV infection [264]. Although in their study, healthy adult volunteers were inoculated with RSV, not infants, this work has brought into focus the neutrophil involvement in the immunopathogenesis of RSV-infection. In the light of these data and as neutrophils are the most abundant component of the airway infiltrate of bronchiolitic babies [5,99] it would be interesting to see more extensive studies of this innate cell population and their role in infantile bronchiolitis.

In the present study, an increase in eosinophils was detected in the lower airways of bronchiolitic babies. Furthermore, the proportion of airway granulocytes that were eosinophils correlated with disease severity. The role of eosinophils in RSV bronchiolitis is controversial as they are mostly involved in allergic inflammation and allergic diseases [108]. Eosinophil cationic protein (ECP) and eosinophil-derived neurotoxin (EDN) which are products of activated eosinophils have been detected in BAL, NPA and serum of ventilated babies with RSV bronchiolitis [71]. Soukup *et al.*, (2003) have suggested that eosinophils can deactivate RSV by the release of ECP [111]. Therefore, eosinophilic infiltration to the lung mucosa might be important in confining infection; however, it can also be the result of type-2 skewed immune responses which has been associated with severe bronchiolitis.

Innate Lymphoid Cells in Bronchiolitis

In this work, I aimed to understand the contribution of ILCs to the development of viral bronchiolitis. Previously published literature strongly suggests ILCs involvement in viral bronchiolitis in mouse models of viral infection [65 123]. Although the biggest advantage of the animal model is the opportunity to study infection *in vivo*, no animal model can reproduce human pathophysiology [5]. Consequently, we decided to study ILCs in a cohort of bronchiolitic babies and compare it to healthy ones. I firstly used high dimension flow cytometry to enumerate ILCs (including NKs) in different samples in health and disease. I combined it with more extensive profiling using a UMAP embedding mapping. This approach allowed me to find features in bronchiolitic babies not observed among controls when only manual gating was performed.

It was clear from this study there was a much lower abundance of all subsets of circulatory and tissue-resident ILCs in children with bronchiolitis compared to healthy infants, reflecting the general lymphopenia seen in bronchiolitis not only in the $CD3^{+}$T but also $CD3^{-}$ cells when compared to healthy subjects [71]. ILC1 were the predominant ILC subset found in the airways in infants, but surprisingly, I observed a lower number of ILC1s and NK cells in the NPA in

bronchiolitis, although, this was not observed in lower respiratory samples, with an increase in NK cells, particularly the $CD56^{low}$ population in bronchiolitis. Depletion of NK cells has been reported in RSV bronchiolitis and it could have a role in the initial response to RSV infection and during disease. Increased number of those cells in the airways can be the result of NK cell infiltration from the periphery to the side of infection. This infiltration of NK cells may have a protective function against viral infection but may also lead to the lung injury through the production of a high level of IFN-γ and other inflammatory cytokines. Interestingly, IL-15, IL-18, IL-21 and IL-27 have been implicated in NK cell activation, proliferation and secretion of IFN-γ in *ex vivo* work on human PBMCs [266,267]. IL-27 can synergise with IL-15- and IL-18-mediated NK cell activation and lead to the overproduction of IFN-γ, perforin and granzyme B [267]. My cytokine data showed an increase in levels of IL-15 in NPA and TA in bronchiolitis; however, I did not observe high levels of IL-21 or IL-27. IL-15 is produced by a variety of cells including epithelial cells, fibroblasts, monocytes and macrophages and points to the importance of other cells and lung tissue in driving the immunopathology of RSV bronchiolitis.

Moreover, a negative correlation between ILCs and ILC1s and the severity of disease measured by the length of hospitalisation, PICU stay and the length of mechanical ventilation was demonstrated in blood samples. Functionally, I found that ILC and NK cells were equally able to produce cytokines (IFN-γ and IL-13) in control and infants with bronchiolitis. These data are important in the context of viral infections. The non-redundant role of ILC1s and NK cells in protection against viral infections has been studied intensively in rodent models [150,153]. In those models, cytotoxic NK cells have antiviral properties in the lungs upon RSV and influenza infection [190,191]. During both viral infections, IFN-γ-producing NK cells have a strong protective, cytotoxic activity. Moreover, mice depleted of NK cells produce decreased amounts of IFN-γ, promoting type-2 inflammation. The type-2 responses were dependent on airway epithelial cell-derived IL-25 production [100]. Contrary to those data, BALB/c mice with depletion of NK cells seemed to have significantly higher chances of survival due to less IFN-γ accumulation in the lung during RSV infection [192]. Zhou *et al.* (2013) have observed the same effect in mice during influenza infections in which IFN-γ producing NK cells profoundly increased the pathology of infection [190]. Animal models provide great tools to dissect mechanisms of infection; however, they cannot recapitulate human disease.

In this study, it was apparent that ILC2 number is much lower in the periphery of bronchiolitic babies compared to healthy ones. My data stands contrary to the published data on ILC2s in

severe bronchiolitis that correlates high levels of ILC2s with the severe outcome of RSV-bronchiolitis in human babies [263]. Vu *et al*., (2019), have found that ILC2s from NPA of severe patients were increased compared to the mild cohort. One of the most interesting aspects of that study is the demonstration that elevated levels of type 2 cytokines are associated with severity. This finding supports the notion of type-2-biased immune responses which has emerged originally in a mouse model of RSV disease [10]. How this relates to increased levels of ILC2s remains speculative. Although they observed an increase in the frequencies of ILC2s, many data points were zero or on the lower limit of detection (LLOD), perhaps reflecting heterogeneity in the cohort. It is possible that my study was underpowered to detect an increase in ILC2s in a small proportion of infants with bronchiolitis. Moreover, it is difficult to compare it to this work due to the differences in the chosen controls, as this study compared mild and severe RSV infection.

Innate and adaptive lymphocytes in bronchiolitis

I demonstrated that children with severe bronchiolitis had a lower count of live cells in whole blood and nasopharyngeal aspirates (NPA) but not in the tracheal aspirates (TA) compared to healthy controls. The lower numbers of live cells were driven by lymphopenia. I observed lower numbers of all $CD3^+$, $CD4^+$, $CD8^+$ T cells (including Th2 and Tc2) and invariant T cells (NKT and MAITs) in the periphery. It has been reported that children with bronchiolitis who required mechanical ventilation suffered from a T cell lymphopenia when compared to milder cases [71]. A study of $CD4^+$ and $CD8^+$T cells in BALs of young children with severe RSV-bronchiolitis indicated the presence of both cell types in the lower respiratory tract (LRT) with a more numerous population of $CD4^+$T cells [99,268]. Contrary to these data, Kerrin *et al*. (2017) reported no significant changes between RSV bronchiolitis and control children in percentages and numbers of CD4+ and CD8+ T cells from BAL; however, the ratio of CD8 positive:CD4 positive cells was 10-fold higher in bronchiolitic infants [269]. In my hands, no difference was observed in the median ratio of CD8 positive:CD4 positive cells between control and bronchiolitic infants in NPA and TA. Interestingly, I showed no elevation of $CD3^+$, $CD4^+$, $CD8^+$ T cells in the lower airways obtained by TA sampling, apart from an increase in Tc2 numbers in the TA. The possible explanation might be related to the fact that TAs do not reflect what is happening in the lung tissue.

Notably, a defining feature of bronchiolitic immunome was related to a cluster of CD56+ CD3- cells expressing high levels of CD4. These '$CD4^+$NK cells' were largely lacking in controls but also in bronchiolitic infants with RV infection. NK cells can either express or lack CD4 on their surface

[270]. This raised the question of whether these cells were $CD4^+$NK cells or just a problem of manual gating when cleaning samples for a UMAP analysis? The published literature suggested that these CD3-$CD4^+$ cells could be NK cells or monocytes as both populations can be $CD56^+CD4^+$ and the only way to distinguish them would be by using the CD7 cell marker [271]. Using a back-gating strategy, I believe that those cells belong to $CD4^+$ monocytes spilling into the lymphocyte gate upon their activation in RSV- but not RV-bronchiolitis. Although interesting, these data do not allow deeper evaluation of this feature of the bronchiolitic immunome and investigation of this population requires further study.

Cytokine production in bronchiolitis

The functional phenotype of innate and adaptive immune cells was determined by analysis of the production by PMBCs of IFN-γ, IL-13, IL-17A and IL-22, the main ILC-related cytokines [230]. My data indicates that a) IFN-γ responses of $CD4^{+,}$ $CD8^+$ T and NKT cells were lower in bronchiolitic babies, b) IFN-γ production in the innate compartment (NK cells and ILC1) was the same between cohorts and c) bronchiolitic ILC2s produced comparable levels of IL-13 to healthy babies. A UMAP embedding approach confirmed the manual gating strategy revealing the IFN-γ cluster in the region of CD4, CD8 and NKT cells.

In this study, it was only possible to perform functional profiling on PBMCs from peripheral blood of healthy and bronchiolitic babies. I was unable to confirm functional differences in cells in the airways due to the low cell counts in NPA and TA. Despite that limitation, my study has great strengths. Firstly, I compared the IFN-γ, IL-13, IL-17A and IL-22 in the cells from healthy and severely bronchiolitic infants' PMBCs extracted from tiny volumes of peripheral blood (less than 500µL). Secondly, I used the most suitable control of healthy babies to determine differences in functional immunity in health and disease. Finally, I checked the impact of age on the production of IFN-γ to check if the age could explain the differences in the control versus bronchiolitic group. I previously saw an increased in production of IFN-γ in both adaptive and innate compartments with age which might be explained by the progressive expansion of adaptive cells with age and their maturity upon the stimulation with encountered pathogens [224,225]. An independent correlation using linear regression analysis for both cohorts showed that differences in IFN-γ production between bronchiolitic and healthy patients cannot be solely explained by age.

Type-2 responses in bronchiolitis

My data demonstrating lower IFN-γ production by lymphocytes, along with higher numbers of Tc2 cells in the lower airway in bronchiolitis and the correlation of the proportion of eosinophils

with disease severity, support the concept that type-2 immune responses contribute to the immunopathology of bronchiolitis. Although controversial, both murine and human experiments have led to the hypothesis that the polarisation of T cell responses away from the protective type-1 immunity (characterised by IFN-γ production) might be the reason for lung pathology in bronchiolitis [21,69,73]. Interestingly, Schwarze *et al.*, (1999) showed that upon RSV infection CD8 depleted mice did not develop eosinophilia and AHR, suggesting that CD8 T cells, although part of type-1 protective immunity, could be responsible for immunopathology during RSV infection [272]. The early-life type-2 bias may result from intrinsic differences in the adaptive and innate immunity of neonates and contribute to increased morbidity and mortality in early life during viral infections [6,224].

I performed MSD analysis of 29 different cytokines and soluble mediators on supernatants from NPA and TA. Levels of almost all mediators were higher in bronchiolitic babies than controls, including both type-1, type-2 and type-17 associated cytokines. Taken together therefore they cytokine data did not demonstrate clear evidence for a type-2 response. Thwaites *et al*., (2018) did not report an elevation of IL-4 and IL-13 in the upper airways, during RSV-bronchiolitis [199]. In my hands, I observed that IL-4 was elevated in NPAs from RV- but not RSV- bronchiolitic babies which could be a possible explanation of the low level of this cytokine in their study. In contrast to their study, I observed high levels of IL-13 in the upper airways and lower airways of bronchiolitic babies. This observation favours the involvement of type-2 bias in the development of bronchiolitis *via* the production of cardinal type-2 cytokines [6,224]. However, I did not demonstrate an elevation of IL-33 during bronchiolitis; the level of this cytokine was comparable to healthy infants in both upper and lower airways, in contrast with previously published work [263]. The lack of IL-33 could be a possible explanation of low levels of ILC2s in the upper airways [262] but cannot provide the ultimate answer as elevated levels of thymic stromal lymphopoietin (TSLP) were observed in NPA and TA. Since TSLP has been associated with activation of IL-13 production by ILC2s in an adult mouse model of RSV disease [123], is there a possibility that human neonatal ILC2s are activated by IL-33 not TSLP during bronchiolitis? Neonatal epithelial cells secrete IL-33 upon RSV infection in neonatal mice [273], but the ILC2-TSLP axis has not been investigated in neonatal mice infected with RSV. Although interesting, this data further strengthens the suggestion that mouse studies are important but cannot recapitulate what is happening in humans. Moreover, if ILC2s seem to residue in mucosal barriers of lungs, that could be the explanation that I was not able to detect increased levels of those cells in lower and upper

airways. The notion of ILC2s and other cells being stranded in the lung parenchyma could support an important role for cells associated with airway epithelium in the immunopathology of bronchiolitis [99].

The source of cytokines in the NPA and TA supernatants is not clear. Data suggests that inflammatory cells in the lung parenchyma, confined to the airway tissue [99] may be responsible for immunopathology through the production of cytokines in severe RSV-bronchiolitis. Whether this is the case in my study and whether recruited or resident cells of the lung paranchyma might lead to the production of cytokines and skewed immune responses cannot be determined in this study.

Heterogeneity in the immune response in bronchiolitis

Bronchiolitis has been considered as a homogeneous illness by the American Academy of Paediatrics clinical guidelines; however, recent studies identified several clinical phenotypes of this illness suggesting it is not a homogeneous entity but rather a heterogeneous one with different clinical outcomes [2,7]. By enrolling all bronchiolitic babies I did not bias results by choosing only RSV-related bronchiolitic cases. As I did not discriminate based on aetiology of infection, I collected samples from children with rhinovirus (RV)- related disease as well. Mansbach *et al.,* (2012) reported that RSV and RV were associated with up to 84.5% of bronchiolitic cases in a multicentre study of the aetiology of acute viral bronchiolitis using NPA [46]. Similarily, in our cohort of bronchiolitic babies, RSV and RV accounted for approximately 83% of viruses causing severe bronchiolitis using both NPA and TA. Interestingly, in my hands, no difference in cellular immune responses was observed between RSV- and RV-bronchiolitis even though previously published data suggests that immune and inflammatory responses to those two viral agents seem to be different [274]. However, by deep immune phenotyping using UMAP, I identified different immune characteristics of immunomes between RSV and RV bronchiolitic babies. A UMAP embedding approach found major regions enriched in RSV or RV -related bronchiolitis and allowed me to observe the changes not only in the cell composition but depicted the phenotypical changes in the same cell clusters among RV and RSV participants. RSV bronchiolitic patients immunome had a robust neutrophilic cluster together with modest eosinophilic infiltration. On the other hand, the RV immunome was characterised by an eosinophil population and differences in neutrophils. Collectively, this work reports that the lack of differences in the cell counts and frequencies in RSV and RV driven disease; however, by means of deep immune profiling, our data suggest that these two viral agents may lead to

different phenotypes of bronchiolitis in particular when whole blood was used. These data corroborate previously published work which observed different metabolomes [2] and PBMC gene expression profiles [7] in infants infected with RSV compared to RV.

MSD data allowed me to evaluate the impact of different viruses on the cytokine profiles in airway samples. I identified that RV infection is characterised by significantly higher production IL-4, IL-31 and MIP-3α in NPA and TA compared to RSV-driven disease; however, there was no clustering of subjects by viral aetiology (RSV and RV) based on their cytokine or cellular profile (airway and blood samples, respectively) when PCA or heatmap analysis were performed.

Strengths and limitations of this study

Compared to this study, previous human work on ILCs has either been done on healthy children (between 7 and 12 years) [188], healthy adults (age ≥20-65 years) [211] or on umbilical cord blood [188]. While many studies utilise PBMCs for studying the immunity of bronchiolitis, in this study I utilised not only peripheral blood but also nasopharyngeal aspirates (NPA) and tracheal aspirates (TA) (upper and lower airways samples, respectively) to better understand the biological situation *in vivo* of acute bronchiolitis. Although the study of fluids obtained from TA and NPA have been used to study lung problems of neonates and young children [198,275], phenotyping of cells using flow cytometry in those compartments can be limited or very simple due to a range of problems encountered, such as the variability of cell counts in mucosal secretions, day-to-day differences in the collection technique and the amount of sample obtained [198]. However, although suboptimal, NPA and TA sampling methods are less invasive than alternatives such as BAL, and so are recommended as the best tool for sampling in early life. TA, in particular, became the 'gold standard tool' [275]. D'Angio *et al.*, (2002) has also described TA as less complicated than BAL; however, in their hands results obtained from TA sampling did not reflect alveolar compartments [276]. In my lab, Thwaites *et al.*, (2017) have standardised different sampling methods of upper airways suggesting that NPA can be an alternative sampling method to nasosorption (NS) [198,199].

A major achievement of this study is that I compared for the first time the immune responses of severely bronchiolitic babies to the healthy population in the same age range from different airway compartments and whole blood. What is more, I established for the first time the protocols for multiparameter flow cytometry and UMAP embedding approach to elucidate ILCs differences between these two cohorts in whole blood and airways samples. Moreover, I was able to compare upper and lower airway samples and assess the cellular and cytokine responses

between those two compartments using correlation analysis. Although bronchiolitis is a disease of lungs, most data about this disease comes from upper airways sampling due to the complexity of obtaining lower airways samples from very young infants [199,263]. This approach can lead to reaching the wrong conclusions about bronchiolitis so in my hands I tried not to only describe the differences between lower and upper airway samples but also ask questions: can I study upper airways, to understand lung disease? Do the cellular and cytokine responses correlate between those two, anatomically different compartments? I found, not surprisingly, that both NPA and TA are important tools for studying human airways from ethically difficult cohorts of young children. Moreover, these techniques of airways sampling complement each other and represent non-invasive, tolerable, and fast tools in a clinical research environment [198]. Careful optimisation allowed me to establish the cellular and cytokine signatures of upper and lower airways. Using a correlation analysis to compare NPA and TA I demonstrated that lower and upper airways were distinct. I discovered that inflammatory signatures of upper airways were different compared to the lower airways, and the inflammation was not driven by the same cell populations.

In conclusion, using the whole blood but also airway samples I evaluated the cellular and cytokine immune responses in bronchiolitic and healthy infants ≤2-years-old. Using OMIP, ISC panels and other systems of analysis, I investigated differences in the number and function of innate and adaptive cells in bronchiolitic and healthy controls. I put particular emphasis on innate cells such as granulocytes, NK/NKT cells, MAIT cells and, foremost, ILCs. I showed that neutrophilic and eosinophilic infiltration to the lung mucosa might be important in confining infection and eosinophilia was associated with more severe disease. In this study, it was apparent that ILCs numbers are much lower in bronchiolitic babies compared to healthy ones. I observed that bronchiolitis is characterised not only by the $CD3^{+}$T but also by $CD3^{-}$ cells lymphopenia. There was a profoundly lower ability to produce IFN-γ in adaptive, but not innate lymphocytes in bronchiolitis. I also found some evidence for a type-2 skewed immune response during RSV-bronchiolitis, although a broad range of cytokines was elevated in the airways in bronchiolitis. In my hands, I observed that IL-4 was elevated in the airways of RV- but not RSV-infected bronchiolitic babies, and by means of deep immune profiling, I proved the notion that RSV and RV can lead to different phenotypes of bronchiolitis. Finally, I compared for the first time the immune responses in different airways compartments and discovered that inflammatory signatures of upper airways were different to the lower airways, demonstrating

the importance of studying the lower airways to understanding the immune response to RSV infection.

Discussion, future work & concluding summary

In this part of the thesis, the main results will be discussed based upon data obtained from the differences and similarities between adult, neonate, bronchiolitic and healthy infants' immune responses. I studied paediatric, viral bronchiolitis in a cohort of children admitted to a paediatric intensive care unit (PICU) and compared it to healthy children having elective surgery. I focused on elucidating the role of all members of the ILC family but also granulocytes, $CD3^{+}$T cells and other lymphocytes in the development of viral bronchiolitis. I aimed to better understand the role of ILCs in respiratory immunity in children but also to understand their development by comparing their numbers and function in adults and neonates. Elucidation of the ontogeny of innate immune responses in infants could offer new insights into the pathogenesis of the disease, identify biomarkers and age-related mechanisms that could predict children at high risk of severe bronchiolitis and support the development of new therapeutics.

Why ILCs and bronchiolitis?

Bronchiolitis is an acute lung disease of the lower respiratory tract (LRT) affecting mostly infants and young children [1,2]. The most common cause of bronchiolitis is infection with a human respiratory syncytial virus (RSV). RSV is a viral, respiratory agent that infects almost all infants by the age of two and is a financial burden on health services worldwide [10]. Although only 1-3% of infants with RSV require hospitalisation, 2-3% of admitted children require PICU treatment and mechanical ventilation [10,16]. Sadly, a lack of vaccine and an expensive antibody-based immune prophylaxis with Palivizumab™ underline the need for new biomarkers and treatments in bronchiolitis [5,8].

Understanding the role of innate immunity can help to elucidate the mechanisms by which it plays an important role in elimination and tolerance of pathogens, such as RSV in early life infections [65]. Innate immunity may be of relatively great importance in early life due to limited antigen encounter *in utero*, immune deviant adaptive immune responses and low levels of maternal antibodies in early childhood [10,65]. Evidence for the importance of differences in innate immune responses in the clinical outcome of viral bronchiolitis come from associations with polymorphisms in innate genes.

Innate lymphoid cells (ILCs) are the most recently discovered innate immune cells and could play a pivotal role in innate responses to viral bronchiolitis. They populate every tissue barrier (skin, gut, lungs) and are among the first cells to respond to environmental stimuli [65]. The role of ILCs in respiratory immunity is not very well documented. Although there is evidence suggesting their importance in regulating innate and adaptive immune responses to infection in murine models

ILC have been relatively understudied in respiratory infection in humans and particularly in paediatric respiratory infection. This project aimed to define the contribution of all members of the ILC family to the development of viral bronchiolitis. Determining why some children develop bronchiolitis could lead to a better understanding of immunity and the development of new biomarkers and clinical prophylactics.

Tools that matter - OMIP

The first essential step in **Chapter 3.1** was to focus on establishing protocols that would allow me to understand the role of ILCs in the severity of acute lung infection in children. Work on ILCs is challenging as they are lineage negative cells [188,211]. There are at least three main subsets of ILCs (ILC1, ILC2 and ILC3) which I was able to define using the published literature describing cell markers on those cells [188,211,212]. Although there are many described panels for enumeration of ILCs in peripheral blood samples [211], I optimised a flow panel appropriate for the small volume of whole blood and airway samples ethically allowed to be collected from infants ≤2-years-old. Most work on human ILCs has either been done on healthy children [188], healthy adults [211] or on cord blood [188].

The optimised 14-multicolour immunophenotyping panel (OMIP) was designed to make sure that many cellular components of innate immunity were included such as granulocytes, NK/NKT cells, MAIT cells and, foremost, ILCs [201]. Moreover, I included components of adaptive immunity as they have been implicated in playing a pivotal role in bronchiolitis in children [99,268]. During development of the OMIP, I used deep immune phenotyping techniques (*t*-SNE[203] and UMAP[204]) to compliment and validate the manual biaxial gating strategy used in OMIP. Both techniques use a high-dimension reduction algorithm for visualisation of poly-dimensional cytometric data on a two-dimensional map [203,205]. Those techniques allowed deeper profiling of immune cells and better understanding of changes between immunomes in health and disease, in blood and airway samples (**Chapter 3.2** and **Chapter 3.3)**.

Most studies have used peripheral blood mononuclear cells (PBMC) to study ILC. In my hands, 300 µL of fresh, peripheral blood was utilised for OMIP. Limited amounts of blood reflected the ethically challenging situation of obtaining samples from infants. I decided to perform whole blood immunophenotyping to reduce the processing time and to overcome the potential risk of decreasing the number of viable cells and increasing variability, leading to poor quality data in my experiments [213]. I showed that RBC-lysis after staining was highly effective compared with RBC-lysis-before protocols due to decreased cell death. Pitoiset *et al*.,(2018) demonstrated

similar results when staining regulatory T cells (Tregs) in only 60µL of whole blood from paediatric patients [213]. Most human studies utilise the immunophenotyping of PBMCs which involves rather time-consuming and numerous steps. In my hands immunostaining of whole blood before RBC lysis and fixation added simplicity and reduction in a level of variability via a shortened staining protocol [215].

In **Chapter 3.1**, I tried to develop an experimental pipeline for preserving whole blood and airway samples, using a different method of cryopreservation and commercially available stabilising reagent TransFix™. I was determined to establish protocols which would allow me to process and stain collected blood and airway samples all together using the same batches of antibodies, to optimise the use of available resources and eliminate variations due to the preparation of samples (pipetting errors, temperature variations during the transport). Unfortunately, frozen whole blood preservation has been unsatisfactory as the recovery of functional, live cells was low in the population of granulocytes in whole blood contrary to previously published data on whole blood preservation in an epidemiologic study [216].

There are no evidence-based protocols for freezing NPA and TA samples. To fill this gap, I compared different protocols of cryopreserving these samples. Freezing airways samples (NPA and TA) was also not successful. Cryopreservation although a very important tool in studying the immunology of different cells induces significant changes in the number and viability of cells and it is a particularly violent procedure. Although, my data is conflicting with other studies, there are many factors which could have an impact on cell recovery, such as washing medium, centrifugation and especially time of thawing [220].

Subsequently, preservation of whole blood using stabilising reagent was not successful even though TransFix™-stabilisation preserved most of the surface antigens well (granulocytes, NK/NKT and MAIT cells). This commercial reagent blocks all apoptotic pathways which seemed to be ideal for short-term storage of samples [209]. The biggest unexpected effect was observed on ILCs as a time-dependent decrease in CRTH2 staining. The significance of this finding is not understood, however, a progressive time-dependent necrosis-like behaviour was previously reported when working with TransFix™-stabilised granulocytes using transmission electron microscopy (TEM) [209]. Similarly, I found the stabilising property of TransFix™ to work rather poorly on NPA and TA samples. A possible explanation is that TransFix™ is a patented buffer of heavy metal salts and aliphatic aldehyde which needs EDTA [208]. In my protocols, the whole blood was collected in EDTA-coated tubes; however, TA samples were stored in non-EDTA bijoux,

which could explain the poor performance of TransFix™ in airway samples. More studies would be necessary to understand the reason for such a poor performance of TransFix™ on NPA and TA samples.

In conclusion, in **Chapter 3.1** I successfully optimised and published protocols for enumerating ILCs (NK cells, ILC1, ILC2, ILC3) and granulocytes (eosinophils and neutrophils) [201]. We successfully demonstrated the feasibility of detection of ILCs in small volumes of whole blood and respiratory paediatric samples. I assessed the impact of different protocols of cryopreservation and stabilising reagent TransFix™ on the preservation of whole blood and airways samples. Unfortunately, in my hands innate lymphocytes in paediatric samples, blood and airways samples must be processed fresh.

New-borns not so immature

Neonatal immunity is often described as immature or immunodeficient in early life due to impaired function of adaptive immunity among T cells and B cells compared to adults [233]. This limited function contributes to the heightened susceptibility to infection and mortality in young babies. Although the idea of neonatal immunodeficiency is widely acknowledged; it is important to understand to what extent the immune responses of new-borns and young children are immature or just different? Can these immune responses be compared to adults? In 1996, the understanding of neonatal immunity was revolutionised by the discovery that neonatal mice can mount T-cell responses *in vivo* when re-exposed to the same antigens on a similar level to the adult counterparts [277,278]. This discovery started a discussion about the immune deviation of infant immunity which, however, looks like it might be immature it is in fact perfectly balanced to protect infants from exuberant immune responses in the microbe-laden world. What is more, enhanced type-2 immune status of neonates can have remodelling and reparative functions *post partum* [232].

In **Chapter 3.2**, I showed differences in the abundance and function of different immune and adaptive cells between adults and neonates. I investigated the differences in numbers of all ILC members, granulocytes, $CD3^{+}$T cells and other innate-like lymphocytes in the peripheral and cord blood using the multiparameter flow cytometry (OMIP) from **Chapter 3.1** [201]. I successfully developed intracellular staining (ICS) functional panels for IFN-γ, IL-13, IL-17A, IL-22 and Granzyme B to determine whether ILCs are capable of producing a range of cytokines and proteases in accordance to the published literature [234]. Subsequently, I applied a Uniform Manifold Approximation and Projection algorithm (UMAP) together with Principal Component

of Analysis (PCA), heatmaps and correlograms in the R programming language to gain an insight into differences between adults and neonates and understand which clinical factors might drive these differences.

It is well known that the normal abundance of leukocytes in circulation varies with sex, race but also age [243]. In the early hours of *post partum*, healthy neonates have a high number of granulocytes such as neutrophils. Their number decreases slowly throughout the neonatal period [243,244]. Moreover, by the second week after birth, lymphocytes become predominant; however, there is a gradual decline of all leukocytes throughout childhood, reaching equilibrium by the age of 21 [243,244]. In agreement with this, I observed higher numbers of all leukocytes in new-borns in comparison to adulthood [243].

In **Chapter 3.2**, I determined eosinophil and neutrophil numbers in the neonate cohort. Although there are a high number of neutrophils when compared to adults, it is acknowledged that from the qualitative standpoint neonatal neutrophils and eosinophils have a functional impairment. Reduced chemotaxis and antimicrobial activity of neutrophils have been reported in neonates [20,246]. Similarly, elevated number of eosinophils in new-borns has been reported previously but their activity and number decline with age [235]. As suggested before, eosinophilia might be related to skewed type-2 immune responses in early life.

Using biaxial gating and UMAP visualisation, I showed that significant variabilities of ILCs were observed among adults and neonates. I observed similar differences between neonatal and adult Lin^{-} $CD127^{+}$ ILCs when unsupervised UMAP clustering or manual gating strategy were applied. I successfully demonstrated that ILC1, ILC2 and ILC3 numbers were increased in newborns when compared to adults in accordance with previously published data [188]. I showed that the numbers of IL-13^{+}ILC2 are comparable between adults and neonates, providing evidence of their maturity in early life. The frequency of IFN-γ^{+} ILCs, IL-13^{+} ILCs and IL-$17A^{+}$ ILCs are slightly lower than in adults. Together, these findings defined the normal abundance and functional phenotype of all members of the ILC family (except NK cells) in accordance with previously published reports on adults and neonates [113,151,188]. In this cohort, I observed a tendency towards higher counts of NK cells in cord blood but not on the magnitude observed in the published literature [231,235]. I demonstrated a lower frequencies of NK cells, $CD56^{L}CD16^{H}$ NKs but not $CD56^{H}CD16^{L}$ NKs in cord blood when compared to healthy adults. Understanding the precise numbers and frequencies of ILCs (including NK cells) in health in different subjects was extremely important as it allowed to compare that data to the pathological conditions.

The differences in the number of lymphocytes between new-borns and adults might be the consequence of the composition of the neonatal T cell compartment due to the difference in the differentiation process in foetal and adult thymus [224]. I showed that the total cell count of lymphocytes, $CD4^+$T cells and $CD8^+$T cells in new-borns is significantly increased compared to adults. The key observation from the comparison of adult and neonatal adaptive T cells was that neonates do not have the robust cytokine responses observed in adults. From *in vivo* and *in vitro* work in mice and human studies, the lack of the antigen exposure to prime adaptive T cells in order to mount proper IFN-γ, IL-13, IL-17A, IL-22 response could be a possible explanation [224,225].

In agreement with published studies, I demonstrated that the number and frequencies of invariant T cells in early life were lower compared to adulthood [84]. To my knowledge, my work is the first report of type-2 cytokine-producing $CD8^+$ T cells in neonates. Little is known about Tc2 apart from their involvement in the development of severe eosinophilic asthma [258]. I demonstrated for the first time a reduced number of Tc2 cells in new-borns. Together, the low numbers and frequency of MAIT, NKT-like, Th2 and Tc2 cells at birth might be related to a limited experience of microbial-derived molecules *in utero*. Rapid transition into the microbe-laden world after birth may be the reason for maturation and expansion with age of invariant T and IL-13-producing $CD3^+$T cells.

In conclusion, in this chapter, I observed that the main difference in the immunome of adults is correlated with higher numbers of invariant T cells with age in accordance with published literature [84,224]. I demonstrated that immune differences in cell distribution and cytokine patterns using UMAP supports the biaxial gating strategy of OMIP. Moreover, the differences between adults and neonates and among neonates are irrespective of sex, weight, vaccination or gestation. Overall, these data suggested that differences between these two cohorts are greatly influenced by the unique pattern of innate and adaptive responses skewed towards type-2 immunity in neonates leading to the generation of distinct immunomes [225–227].

Ye olde bronchiolitis and ILCs - new kids on the block

The most common reason for children under the age of two to be admitted to the hospital is a severe lung infection known as bronchiolitis. Bronchiolitis is most frequently caused by the very common infections respiratory syncytial virus (RSV) and rhinovirus (RV). Innate and adaptive immunity eliminate pathogens and play crucial roles in immune homeostasis and tolerance against pathogens, such as RSV [65]. ILCs populate in abundance every tissue barrier such as skin, guts and lungs. Recently, the members of ILC family have been studied in paediatric bronchiolitis

due to their strategic location and fast responsiveness to environmental stimuli and pathogens [65].

In **Chapter 3.3**, I utilised not only peripheral blood but also nasopharyngeal aspirates (NPA) and tracheal aspirates (TA) (upper and lower airways samples, respectively) to better understand the biological situation *in vivo* of acute bronchiolitis. Most studies have used PBMCs for exploring the immunity of bronchiolitis [188,211]. Although suboptimal, the study of fluids obtained from TA and NPA has been previously used to study the lung problems of neonates and young children [198,275]. I performed immunophenotyping in those compartments successfully even though it has been reported as rather challenging [198]. I found that both NPA and TA are important tools for studying human airways of young children in a clinical setting. NPA and TA techniques of airways sampling complement each other and are non-invasive, tolerable, and fast tools in a clinical research environment [198].

Strikingly, but not surprisingly, in this study, granulocytes were the most abundant cell type in whole blood and airways samples; the most numerous populations of granulocytes were neutrophils. Consistent with these data, previous human studies of lower and upper airways secretions identified neutrophils as the most common component in the airways of bronchiolitic babies [5,99]. The role of neutrophils in RSV driven disease has been the topic of debate as we do not know if they reflect lung injury and what their role is in viral infections [5]. Neutrophils may contribute to tissue damage in RSV-bronchiolitis in children below the age of six [107]. The neutrophilic infiltration and inflammatory mediators are very often associated with lung injury due to infection [105] but also mechanical ventilation [106]. Moreover, neutrophilia did not correlate with the severity of the disease. In contrast the proportion of granulocytes that were eosinophils correlated with disease severity. The role of eosinophils in RSV bronchiolitis is controversial as they are mostly involved in allergic inflammation and allergic diseases [108]. Soukup *et al.*, (2003) have suggested that eosinophils can deactivate the RSV virus by the release of ECP [111]. Therefore, eosinophilic infiltration to the lung mucosa might be important in confining infection; however, it is associated with type-2 skewed immune responses which have been associated with severe bronchiolitis.

Neutrophilic infiltration and inflammatory mediators are very often associated with lung injury due to infection [105] but also mechanical ventilation [106]. In the multicentre study Hennus *et al.*, (2013) showed that mechanical aspiration drives enhanced inflammatory responses in RSV-bronchiolitic patients measured in the NPA within 24 hours [106]. Plötz *et al*., (2002) demonstrated

that mechanical ventilation can elicit the changes in the cytokine immune responses in TA and blood samples in healthy children [279]. In the recent SARS-CoV-2019 outbreak the post-ventilation barotrauma became the point of heated debate about the role of ventilation in the immunopathology of lungs [64]. Although the impact of ventilation is undeniable, in this study higher level of mediators were observed in bronchiolitic children with shorter hospital stay and length of ventilation when heatmaps analysis was performed. These data is supported by other studies in which ventilation was associated with lower mediator levels and did not impact the severity of disease [199].

Previously published literature strongly suggests ILC involvement in viral bronchiolitis in mouse models of viral infection [65] [123]. Although the biggest advantage of the animal model is the opportunity to study infection *in vivo*, no animal model can reproduce human pathophysiology [5]. It was clear from this study that there was a much lower abundance of all subsets of circulatory and tissue-resident ILCs in children with bronchiolitis compared to healthy infants. ILC1 were by far the most frequent ILC family member in the airways. I observed a lower number of ILC1s and NK cells in NPA in bronchiolitis. The ILC1 deficiency in upper airways was not observed in lower respiratory samples (TA) of bronchiolitic infants. Interestingly, a negative correlation between ILCs and ILC1s and the severity of disease measured by the length of hospitalisation, PICU stay and the length of mechanical ventilation was demonstrated. The non-redundant role of ILC1s and NK cells in protection against viral infections has been studied intensively in rodent models [150,153].

It was apparent that ILC2 number is much lower in blood in bronchiolitic babies compared to healthy ones. My data stands contrary to the published data on ILC2s in severe bronchiolitis [263]. In their work Vu *et al*., (2019) found that ILC2s from NPA of severe patients were increased compared to the mild cohort. An interesting aspect of their study was the demonstration of elevated levels of type 2 cytokines and its association with disease severity. This finding further supports the notion of type-2-biased immune responses in bronchiolitis [10]. Contrary to this study my cytokine data did not demonstrate clear evidence of a type-2 response in severe bronchiolitis compared to healthy controls.

Subsequently, I demonstrated that children with severe bronchiolitis had a lower count of live cells in whole blood and nasopharyngeal aspirates (NPA) but not in the tracheal aspirates (TA). The lower numbers of live cells were driven by lymphopenia. The recruitment of peripheral blood cells into the lung tissue might cause lymphopenia. Data suggests that cells confined to

the airway tissue might be accountable for producing high levels of cytokines and the development of lung immunopathology [99]. I observed lower numbers of all $CD3^+$, $CD4^+$, $CD8^+$ T cells, invariant T cells (NKT and MAITs) and type 2 T cells (Th2 and Tc2) in the periphery in accordance with published data on ventilated children [71]. These data support my observations of lower numbers of $CD3^+$ T cells in the upper airways but not in the lower airways in bronchiolitis. I showed no elevation of $CD3^+$, $CD4^+$, $CD8^+$ T cell in the lower airways obtained by TA sampling from severely bronchiolitic infants. In other human studies of $CD4^+$ and $CD8^+$T cells in BALs of young children with RSV-bronchiolitis, the presence of both cell types in the lower respiratory tract (LRT) with a more numerous population of $CD4^+$T cells was apparent [99,268].

The functional phenotype of innate and adaptive immune cells was assessed in bronchiolitic and healthy infants to determine the production in PMBCs of IFN-γ, IL-13, IL-17A and IL-22, the main ILC-related cytokines [230]. My data indicate that a) IFN-γ responses of $CD4^+$, $CD8^+$ T and NKT cells were decreased in bronchiolitic babies, b) IFN-γ production in the innate compartment was the same between cohorts and c) bronchiolitic ILC2s produced comparable levels of IL-13 to healthy babies. These data support the relevance of type-2 immune responses in the immunopathology of bronchiolitis [21,69,73].

The functional profile of cells in the lower and upper airways could not be done due to their limited numbers in the samples. To check the inflammatory profile, I performed MSD analysis of 29 different cytokines and soluble mediators on supernatants from NPA and TA. Levels of almost all mediators were increased in bronchiolitic babies compared to healthy controls. Taken together my cytokine data did not demonstrate clear evidence for type-2 or type-1 responses in bronchiolitis, but instead for a mixed response involving both type 1 and type 2 cytokines.

In conclusion, I successfully evaluated the cellular and cytokine immune responses in bronchiolitic and healthy infants ≤2-years-old using the whole blood and airway samples. It was apparent that ILC numbers are much lower in blood and airways in bronchiolitic babies compared to healthy ones. I propose that bronchiolitis is characterised not only by the $CD3^+$T but also by $CD3^-$ cells lymphopenia. It was clear that ILC2s were able to mount a production of IL-13 which could be a possible explanation of lower numbers of ILC1s in bronchiolitis compared to healthy controls. Increased levels of type-2 cytokines such as IL-4, IL-13 and IL-5 can lead to skewed type-2 immune responses during bronchiolitis which has been associated with severe bronchiolitis. I proved the notion that RSV and RV can lead to different phenotypes of bronchiolitis. Finally, I compared for the first time the immune responses of severely

bronchiolitic babies to the healthy population in the same age range from different airway compartments and whole blood and discovered that inflammatory signatures of upper airways were different compared to the lower airways, and, the inflammation was not driven by the same cell populations.

Future work

The data presented in this work supports the hypothesis that ILCs are associated with disease severity in children with acute lower respiratory tract infections because I show a negative correlation between the frequencies of ILCs in blood and the severity of disease measured by the length of hospital stay, the length of ventilation and PICU stay. Moreover, bronchiolitis was characterised by systemic ILC-peania as the abundance of total ILCs, ILC1s, ILC2s and ILC3s was significantly lower. Similarly to peripheral blood, the lower numbers of ILCs, ILC1 and NK cells were observed in upper airway samples. Thus, alterations in ILC numbers in bronchiolitis characterised by systemic and upper airway ILC depletion might play a pivotal role in developing the disease. I proposed that alterations in ILC function are associated with disease severity; however, ILCs from bronchiolitis patients could produce IFN-γ and IL-13 on a similar level to healthy controls. Although I proposed that alterations in pathogen type can lead to different phenotypes of bronchiolitis and I observed differences in IL-4 production between RSV and RV, more work needs to be done to check the impact of aetiology on the severity of bronchiolitis as this study might have been underpowered to identify differences between those viruses. Finally, I hypothesised that ILCs from adults are functionally different from healthy neonates; however, my data suggest that neonatal ILCs are mature and they can produce the same level of cytokines as adult ILCs.

Although I demonstrated the importance of studying these cells in contributing to the development of viral bronchiolitis, I believe that future work should involve some of the following aims: viral load, cytokine storm, functional changes of airway ILCs and involvement of other innate cells (neutrophils and monocytes) in bronchiolitis.

In this thesis, I reported an increase of almost all cytokines and soluble mediators in the airways of children with bronchiolitis. All mediators for type-1, type-2 and type-17 associated cytokines were increased but it is still not clear whether a so-called ‘cytokine storm’ can be associated with respiratory failure, as children with a high level of cytokines did not seem to be the ones who had a long PICU stay or were ventilated for the longest time. Thwaites *et al*., (2018) reported a similar finding in their studies; however, they also cast doubt on the role of viral load [199]. As I

collected nasosorptions, NPAs and TAs, it will be important to assess viral load in upper and lower airways and to correlate it with clinical parameters and the measured cellular and cytokine responses.

I do not know the cellular source of many of the cytokines I measured in bronchiolitis. There may be production from recruited inflammatory cells or resident cells in the lung parenchyma and airways, or the epithelium itself could be a source of cytokines [99]. It would be interesting to establish the source of cytokines; however, due to the ethical complexity, it might be difficult or even impossible to collect the airway tissues from bronchiolitic and control babies. In future studies, I could utilise well-differentiated primary paediatric airway epithelial cell cultures (WD-PAEC), a very well - established model of RSV infection used by the Power group [280]. WD-PAEC are derived from nasal or bronchial brushes and can be a surrogate model for RSV infection. What is more, using nasal-derived WD-PAEC from children without and with severe and mild bronchiolitis I could establish intrinsic differences in the production of cytokines *ex vivo* in these cohorts.

In this work using OMIP [201], I was, unfortunately, unable to demonstrate functional and phenotypical changes in other innate cell types, such as neutrophils, monocytes or γδT cells. Although flow cytometry is evolving rapidly, at the beginning of this project I was confined by the limitations of the equipment I used for establishing immunophenotyping panels. I focused on ILCs and some invariant T-like cells; however, it would be interesting to investigate other rare lymphocytes such as γδT cells which have been associated with epithelial surfaces of the lung, gut and other mucosal surfaces [281].

This work and previous human studies of lower and upper airways secretions identified neutrophils as the most common component in the airways of bronchiolitic babies [5,99]. However, what is the role of granulocytes, and neutrophils in particular in the development of bronchiolitis? Others have reported heterogeneity of neutrophils in bronchiolitis (based on CD16 and CD62L expression) [7]. I believe that this presents an opportunity to further study the phenotype of neutrophils in the airways and peripheral blood in bronchiolitis and it could help to elucidate this innate cell population's role in infantile bronchiolitis. Apart from neutrophils other myeloid cells known as Myeloid-Derived Suppressor Cells (MDSCs) have been reported. MDSCs seem to have high suppressive properties [282]. In mouse studies MDSCs transferred into adults from new born mice could suppress allergic lung inflammation. As neonatal MDSCs have

been reported to express high levels of s100a8/9, an antimicrobial protein [283], we would aim to identify the role of MDSCs in infantile bronchiolitis.

In my observations, I reported an increase of $CD4^+CD56^+$ cells in bronchiolitic babies. The published literature suggested that these cells could be genuinely NK cells or monocytes as both populations are $CD56^+CD4^+$; however, the only way to distinguish them would be by using the CD7 cell marker [271]. I believe that those cells belong to $CD4^+$ monocytes spilling into the lymphocyte gate upon their activation in RSV- bronchiolitis. Although interesting, my data did not allow to evaluate the role of monocytes in bronchiolitis. It would be important to do deeper immunophenotyping of monocytes in the blood and airways during RSV-infection as it was clear that there were changes in this cluster of cells.

Finally, it is difficult to compare this work to other studies due to the differences in the chosen controls. To check the role of ILCs in viral bronchiolitis I focused on severely ill and healthy children. This data on ILC2s stands contrary to the published data on ILC2s using mild and severe cases of RSV bronchiolitis [263]. In my hands, it was clear that I observed lower numbers of those cells in bronchiolitic babies compared to healthy controls. Would bronchiolitic babies benefit from an increased level of ILC2s? ILC data cast doubt on the proposed explanation of the severity of disease with an increased number of ILCs. It would be important to increase the number of children involved in the study and include milder patients to show a clear picture of bronchiolitis using mild and severe cases and compare them to healthy patients. Moreover, it would be important to assess whether infants who got bronchiolitis already lack ILCs or are the lower numbers of ILCs due to the infection? A big prospective study could address this; however, it would have to involve a significant number of children enrolled in the study before the development of the disease. Although possible, it would be logistically and financially challenging.

Conclusions & final remarks

In this work, I characterised the immune cellular responses in different cohorts of new-borns, healthy infants, bronchiolitic babies and adults by using the optimised multiparameter immunophenotyping panel (OMIP) [201]. In the first part of this study, I chose to compare cellular and functional immune profiles of neonates and adults. I believe that even though cord blood may differ from peripheral blood of babies and infants, cord blood studies of neonatal immunity allowed me to remove the technical limitation of obtaining a sufficient amount of blood, and the ethical complexity of obtaining blood samples from neonates. The big volumes of cord blood allowed me to investigate the similarities and differences of the cellular compartment of new-borns and then compare it to adults' peripheral blood. The comparison of adults and neonates allowed to conclude that neonates are not immature but rather immune deviant towards type-2 immunity. This immune deviation characterised by eosinophilia and mature ILC2s producing a high level of IL-13^{+} could help to understand the role of type-2 immunity in immunomodulation during infection. I propose that new-born immunity being skewed towards type-2 responses is an evolutionary way of protecting developing tissues against excessive inflammation and ultimately may help to protect against infection.

Only a minority of infants become severely ill when infected with respiratory viruses. It seems that neonates are perfectly capable of mounting protective innate and adaptive responses even if they seem different from those of adults. I believe that enhanced type-2 immune status of neonates may be beneficial in that it may contribute to tissue remodelling and reparative function and stop exuberant inflammatory responses in the pathogen-laden world *post partum* [232]. Of course, from the clinical point of view, type-2 skewing of T cell responses, far from type-1 immunity and characterised by low IFN-γ production, might have an impact on severity and susceptibility to viral infections in early life. In adults, type-1 immunity may be much more important as the adaptive responses are fully developed and organs have fully grown which from an evolutionary point of view allows the type-2 immunity to be switched on for reparative function only to stop the development of allergic diseases characterised by remodelling and inflammation [284].

The major strength of this study however comes from the comparison of immunity in different compartments in healthy and bronchiolitic babies. Although bronchiolitis is the disease of lungs, most data about this disease comes from upper airways sampling due to the complexity of obtaining lower airways samples from very young infants [199,263] or has been studied using PBMCs

[198,275]. I successfully utilised not only peripheral blood but also upper and lower airways samples (NPA and TA, respectively) to better understand the biological situation *in vivo* of acute bronchiolitis. Although the investigation of fluids obtained from TA and NPA have been used to study lung conditions of neonates and young children [198,275], the phenotyping of cells using flow cytometry in those compartments has not been successful [198]. I proved that NPA and TA can be 'gold standard' methods used to study respiratory inflammation. Interestingly, results obtained from TA sampling did not reflect nasopharyngeal compartments. In the hospital environment, NPA and TA methods are less invasive than BAL sampling and are highly recommended for sampling in early life infection where sampling is ethically and methodically difficult. Careful optimisation allowed me to establish the cellular and cytokine signatures of upper and lower airways; however, using correlation analysis, I concluded that inflammatory signatures of upper airways were different to the lower airways, and inflammation was not driven by the same cell populations.

Another crucial strength of this work comes from the fact that I was looking in human cohorts when many of studies of neonatal immunity come from neonatal mouse studies [225,227]. Although interesting how much of these data can recapitulate what is happening in humans? Previously published literature strongly suggests that the immune responses apparent in mice are not valid in early human life and under some circumstances, human neonates are fully competent to develop mature type-1 immune responses in contrast to their murine counterparts [226]. In bronchiolitis, animal models provide great tools to dissect mechanisms of infection; however, cannot provide an ultimate answer. I believe that in this study I demonstrated that the severity of bronchiolitis may be associated with type-2 cytokines supporting the murine models of RSV-bronchiolitis.

Even though different metabolomes [2] and PBMC gene expression profiles [7] have been described in infants infected with either RSV or RV- bronchiolitis, I showed that the manual gating strategy did not allow me to observe differences between different type of cells in these two cohorts of bronchiolitic babies. From the clinical point of view, this could partially explain why bronchiolitis is still considered as a homogeneous illness by the American Academy of Paediatrics clinical guidelines [2,7]. By using the deep immune phenotyping (UMAP) on the cytometric data, and IL-4 differences using MSD data I identified different immune characteristics of immunomes between RSV and RV bronchiolitic babies. Collectively this data strongly suggests that in the

future, flow cytometry in combination with a more powerful analytical tool could provide the answer about differences in RV and RSV bronchiolitis.

This thesis focused on the aspect of innate immunology regarding the ILC family members in the context of neonatal and bronchiolitic immunity. I successfully demonstrated that it is possible to work on rare populations of cells in difficult to obtain and process clinical samples. The complexity of paediatric material in addition to the immunophenotyping of rare innate cells makes this work rather crucial for understanding of ILC biology in bronchiolitis. If we understand what drives severe bronchiolitis in children, we might develop interventions to help paediatricians and clinicians prevent children from developing severe disease. Moreover, finding which cytokines are associated with bronchiolitis, could facilitate development of therapeutic antibody-based drugs that could be used to treat bronchiolitis.

As mentioned before, only one paper has studied the role of ILC2s in bronchiolitis using NPA samples [263]. Although they observed an increase in the frequencies of ILC2s, it is difficult to compare it to my work due to the differences in the chosen controls. As for them, I support the notion that elevated levels of type 2 cytokines might play a role in severity but in my setting ILCs numbers were lower in bronchiolitic babies when compared to healthy controls. The important questions are: what is the plausible scientific explanation of ILCs role in bronchiolitis? What is the relation between ILCs, innate and adaptive cells and finally disease severity? In my hands, a negative correlation between ILCs and ILC1s and the severity of disease was demonstrated so would bronchiolitic babies benefit from an increased level of ILCs? Do ILC2s drive the bronchiolitis *via* the production of a high level of type-2 cytokines even though they are significantly lower in the severe bronchiolitis? Or do ILC1s protect during the severe bronchiolitis? These important questions show how little we still understand when it comes to ILCs and bronchiolitis. Essential data to answer these questions would involve future functional immunophenotyping of ILCs and other cells in the upper and lower airways and the involvement of other controls such as mild bronchiolitis patients.

Bibliography

1. Smyth Rosalind L, Openshaw, P. J. M. Bronchiolitis. Lancet Respir. Med. 368, 312–22 (2006).
2. Stewart, C. J. et al. Respiratory Syncytial Virus and Rhinovirus Bronchiolitis Are Associated with Distinct Metabolic Pathways. J. Infect. Dis. 217, 1160–1169 (2018).
3. Smith, D. K. et al. Respiratory syncytial virus bronchiolitis in children. Am. Fam. Physician 95, 94–99 (2017).
4. Smith, C. M. et al. Ciliary dyskinesia is an early feature of respiratory syncytial virus infection. Eur. Respir. J. 43, 485–496 (2014).
5. Openshaw, P. J. M. et al. Protective and Harmful Immunity to RSV Infection. 501–532 (2017) doi:10.1146/annurev-immunol-051116-052206.
6. Rey-Jurado, E. & Kalergis, A. M. Immunological features of respiratory syncytial virus-caused pneumonia-implications for vaccine design. Int. J. Mol. Sci. 18, (2017).
7. Dumas, O. et al. A clustering approach to identify severe bronchiolitis profiles in children. Thorax 25, 289–313 (2016).
8. Zorc, J. J. & Hall, C. B. Bronchiolitis: Recent Evidence on Diagnosis and Management. Pediatrics 125, 342–349 (2010).
9. Hall, C. B. et al. The Burden of Respiratory Syncytial Virus Infection in Young Children. N. Engl. J. Med. 360, 588–598 (2009).
10. Lambert, L. et al. Immunity to RSV in early-life. Front. Immunol. 5, 1–14 (2014).
11. WHO. WHO Consultation on respiratory syncytial virus (RSV) vaccine development. http://www.who.int/immunization/research/meetings_workshops/rsv_vaccine_development/en/ (2015).
12. Karron, R. A. & Black, R. E. Determining the burden of respiratory syncytial virus disease: The known and the unknown. Lancet 390, 917–918 (2017).
13. Amand, C. et al. Healthcare resource use and economic burden attributable to respiratory syncytial virus in the United States: A claims database analysis. BMC Health Serv. Res. 18, 1–15 (2018).
14. Paramore, L. C. et al. Economic impact of respiratory syncytial virus-related illness in the US: An analysis of national databases. Pharmacoeconomics 22, 275–284 (2004).
15. Øymar, K. et al. Acute bronchiolitis in infants, a review. Scand. J. Trauma. Resusc. Emerg. Med. 22, 1–10 (2014).
16. McNamara, PS. et al. Production of chemokines in the lungs of infants with severe respiratory syncytial virus bronchiolitis. J Infect Dis. 191, 1225–32. (2005).
17. Thomsen, S. F. et al. Increased Concordance of Severe Respiratory Syncytial Virus Infection in Identical Twins. Pediatrics 121, 493–496 (2008).
18. Culley, F. J. & Lambert, L. Innate Immunity to Infection in the Neonatal Lung. (2017).
19. Castilow, E. M. et al. Understanding respiratory syncytial virus (RSV) vaccine-enhanced disease. Immunol. Res. 39, 225–239 (2007).
20. Levy, O. Innate immunity of the newborn: Basic mechanisms and clinical correlates. Nat. Rev. Immunol. 7, 379–390 (2007).
21. Chanock, R. et al. Recovery from infants with respiratory illness of a virus related to chimpanzee coryza agent (CCA): Isolation, properties and characterization. Am. J. Epidemiol. 66, 281–290 (1957).
22. Belongia, E. A. et al. Clinical Features, Severity, and Incidence of RSV Illness During 12 Consecutive Seasons in a Community Cohort of Adults ≥ 60 Years Old. (2018) doi:10.1093/ofid/ofy316.
23. Battles, M. B. & McLellan, J. S. Respiratory syncytial virus entry and how to block it. Nat. Rev. Microbiol. 1 (2019) doi:10.1038/s41579-019-0149-x.
24. Jorquera, P. A. et al. Human respiratory syncytial virus: An introduction. Methods Mol. Biol. 1442, 1–12 (2016).
25. Borchers, A. T. et al. Respiratory syncytial virus - A comprehensive review. Clin. Rev. Allergy Immunol. 45, 331–379 (2013).
26. Battles, M. B. & McLellan, J. S. Respiratory syncytial virus entry and how to block it. Nat. Rev. Microbiol. 17, 233–245 (2019).
27. Bitko, V. et al. Nonstructural Proteins of Respiratory Syncytial Virus Suppress Premature Apoptosis by an NF- B-Dependent, Interferon-Independent Mechanism and Facilitate Virus Growth. J. Virol. 81, 1786–1795 (2007).
28. Spann, K. M. et al. Effects of Nonstructural Proteins NS1 and NS2 of Human Respiratory Syncytial Virus on Interferon Regulatory Factor 3, NF- B, and Proinflammatory Cytokines. J. Virol. 79, 5353–5362 (2005).
29. Collins, P. L. et al. Transcription elongation factor of respiratory syncytial virus, a nonsegmented negative-strand RNA virus. Proc. Natl. Acad. Sci. U. S. A. 93, 81–85 (1996).

30. Cheng, X. et al. Overexpression of the M2-2 Protein of Respiratory Syncytial Virus Inhibits Viral Replication. J. Virol. 79, 13943–13952 (2005).
31. Castagné, N. et al. Biochemical characterization of the respiratory syncytial virus P-P and P-N protein complexes and localization of the P protein oligomerization domain. J. Gen. Virol. 85, 1643–1653 (2004).
32. Collins, P. L. & Graham, B. S. Viral and Host Factors in Human Respiratory Syncytial Virus Pathogenesis. J. Virol. 82, 2040–2055 (2008).
33. Gan, S. W. et al. The small hydrophobic protein of the human respiratory syncytial virus forms pentameric ion channels. J. Biol. Chem. 287, 24671–24689 (2012).
34. Hendricks, D. A. et al. Appearance of a soluble form of the G protein of respiratory syncytial virus in fluids of infected cells. J. Gen. Virol. 68, 1705–1714 (1987).
35. Mufson, M. A. et al. Two distinct subtypes of human respiratory syncytial virus. J. Gen. Virol. 66, 2111–2124 (1985).
36. Malero, J. et al. Structural, antigenic and immunogenic features of respiratory syncytial virus glycoproteins relevant for vaccine development. Vaccine 176, 461–468 (2017).
37. Tripp, R. A. et al. CX3C chemokine mimicry by respiratory syncytial virus G glycoprotein. Nat. Immunol. 2, 732–738 (2001).
38. Collins, P. L. & Mottet, G. Oligomerization and post-translational processing of glycoprotein G of human respiratory syncytial virus: altered O-glycosylation in the presence of brefeldin A. J. Gen. Virol. 73, 849–863 (1992).
39. Griffiths, C. D. et al. IGF1R is an entry receptor for respiratory syncytial virus. Nature 583, 615–619 (2020).
40. Tayyari, F. et al. Identification of nucleolin as a cellular receptor for human respiratory syncytial virus. Nat. Med. 17, 1132–1135 (2011).
41. Wright, P. F. Progress in the Prevention and Treatment of RSV Infection. N. Engl. J. Med. 371, 775–776 (2014).
42. Rincheval, V. et al. Functional organization of cytoplasmic inclusion bodies in cells infected by respiratory syncytial virus. Nat. Commun. 8, 1–11 (2017).
43. Mehedi, M. et al. Actin-Related Protein 2 (ARP2) and Virus-Induced Filopodia Facilitate Human Respiratory Syncytial Virus Spread. PLoS Pathog. 12, 1–35 (2016).
44. Krarup, A. et al. A highly stable prefusion RSV F vaccine derived from structural analysis of the fusion mechanism. Nat. Commun. 6, (2015).
45. Mansbach, J. M. et al. Children hospitalized with rhinovirus bronchiolitis have asthma- like characteristics. J Pediatr. 172, 202–204 (2017).
46. Mansbach, J. M. et al. Prospective multicenter study of viral etiology and hospital length of stay in children with severe bronchiolitis. Arch. Pediatr. Adolesc. Med. 166, 700–706 (2012).
47. Van Den Hoogen, B. G. et al. A newly discovered human pneumovirus isolated from young children with respiratory tract disease. Nat. Med. 7, 719–724 (2001).
48. Panda, S. et al. Human metapneumovirus: Review of an important respiratory pathogen. International Journal of Infectious Diseases vol. 25 45–52 (2014).
49. Lin, J.-Y. et al. Viral and host proteins involved in picornavirus life cycle. J. Biomed. Sci. 16, 103 (2009).
50. Jacobs, S. E. et al. Human rhinoviruses. Clin. Microbiol. Rev. 26, 135–62 (2013).
51. Stepanova, E. et al. Overview of human rhinovirus immunogenic epitopes for rational vaccine design. Expert Rev. Vaccines 18, 877–880 (2019).
52. Kelly, J. T. & Busse, W. W. Host immune responses to rhinovirus: mechanisms in asthma. J. Allergy Clin. Immunol. 122, 671–82; quiz 683–4 (2008).
53. Mousnier, A. et al. Human Rhinovirus 16 Causes Golgi Apparatus Fragmentation without Blocking Protein Secretion. J. Virol. 88, 11671–85 (2014).
54. Palmenberg, A. C. et al. Analysis of the complete genome sequences of human rhinovirus. J. Allergy Clin. Immunol. 125, 1190–9; quiz 1200–1 (2010).
55. Ditt, V. et al. Respiratory infections by HMPV and RSV are clinically indistinguishable but induce different host response in aged individuals. PLoS One 6, 1–9 (2011).
56. Rao, B. L. et al. First detection of human metapneumovirus in children with acute respiratory infection in India: A preliminary report [1]. J. Clin. Microbiol. 42, 5961–5962 (2004).
57. Sherman, A. C. et al. The future of flu: A review of the human challenge model and systems biology for advancement of influenza vaccinology. Front. Cell. Infect. Microbiol. 9, 1–9 (2019).
58. Bashir, U. et al. Respiratory syncytial virus and influenza are the key viral pathogens in children <2 years hospitalized with bronchiolitis and pneumonia in Islamabad Pakistan. Arch. Virol. 162, 763–773 (2017).
59. Bouvier, N. M. & Palese, P. The biology of influenza viruses. European J. Org. Chem. 2018, 619–626 (2018).
60. Royston, L. & Tapparel, C. Rhinoviruses and respiratory enteroviruses: Not as simple as ABC. Viruses 8, (2016).

61. Renois, F. et al. Enterovirus 68 in pediatric patients hospitalized for acute airway diseases. J. Clin. Microbiol. 51, 640–643 (2013).
62. Haagmans, B. L. & Osterhaus, A. D. M. E. Coronaviruses and their therapy. Antiviral Res. 71, 397–403 (2006).
63. Kristoffersen, A. W. et al. Coronavirus causes lower respiratory tract infections less frequently than RSV in hospitalized Norwegian children. Pediatr. Infect. Dis. J. 30, 279–283 (2011).
64. Mathew, D. et al. Deep immune profiling of COVID-19 patients reveals patient heterogeneity and distinct immunotypes with implications for therapeutic interventions. bioRxiv Prepr. Serv. Biol. (2020) doi:10.1101/2020.05.20.106401.
65. Klose, C. S. N. & Artis, D. Innate lymphoid cells as regulators of immunity, inflammation and tissue homeostasis. Nat. Immunol. 17, 765–74 (2016).
66. Johnson, J. E. et al. The histopathology of fatal untreated human respiratory syncytial virus infection. Mod. Pathol. 20, 108–119 (2007).
67. Vivier, E. et al. Innate Lymphoid Cells: 10 Years On. Cell 174, 1054–1066 (2018).
68. Glatzová, D. & Cebecauer, M. Dual role of CD4 in peripheral T lymphocytes. Front. Immunol. 10, (2019).
69. Kim, H. W. et al. Respiratory Syncytial Virus Disease in Infants Prior adminstration of antigenic Inactivated vaccine. Am. J. Epidemiol. 89, 422–434 (1969).
70. Christiaansen, A. F. et al. The CD4 T cell response to respiratory syncytial virus infection. Immunol. Res. 59, 109–117 (2014).
71. Russell, C. D. et al. The Human Immune Response to Respiratory Syncytial Virus Infection. Clin. Microbiol. Rev. 30, 481–502 (2017).
72. de Souza, A. P. D. et al. Respiratory syncytial virus induces phosphorylation of mTOR at ser2448 in CD8 T cells from nasal washes of infected infants. Clin. Exp. Immunol. 183, 248–257 (2016).
73. Graham, B. S. et al. Role of T lymphocyte subsets in the pathogenesis of primary infection and rechallenge with respiratory syncytial virus in mice. J. Clin. Invest. 88, 1026–1033 (1991).
74. Cahn, A. et al. Safety, tolerability, pharmacokinetics and pharmacodynamics of GSK2239633, a CC-chemokine receptor 4 antagonist, in healthy male subjects: results from an open-label and from a randomised study. BMC Pharmacol. Toxicol. 14, 14 (2013).
75. Shevach, E. M. et al. The lifestyle of naturally occurring CD4+ CD25+ Foxp3+ regulatory T cells. Immunol. Rev. 212, 60–73 (2006).
76. Shevach, E. M. Review Mechanisms of Foxp3 + T Regulatory Cell-Mediated Suppression. Immunity 30, 636–645 (2009).
77. Loebbermann, J. et al. Regulatory T cells expressing granzyme B play a critical role in controlling lung inflammation during acute viral infection. Mucosal Immunol. 5, 161–72 (2012).
78. Lee, D. C. et al. CD25+ natural regulatory T cells are critical in limiting innate and adaptive immunity and resolving disease following respiratory syncytial virus infection. J Virol 84, 8790–8798 (2010).
79. Ghazarian, L. et al. Mucosal-associated invariant T cell interactions with commensal and pathogenic bacteria: Potential role in antimicrobial immunity in the child. Front. Immunol. 8, 1–8 (2017).
80. Peng, L. et al. Altered phenotypic and functional characteristics of CD3+CD56+ NKT-like cells in human gastric cancer. Oncotarget 7, (2016).
81. Wang, H. & Hogquist, K. A. How MAIT cells get their start. Nat. Immunol. 17, 1238–1240 (2016).
82. Dhodapkar M.V. et al. Type II Natural Killer T (NKT) Cells And Their Emerging Role In Health And Diseases. J. Immunol. Methods 198, 1015–1021 (2017).
83. Chandra, S. et al. Development of Asthma in Inner-City Children: Possible Roles of MAIT Cells and Variation in the Home Environment. J. Immunol. 200, 1995–2003 (2018).
84. Ben Youssef, G. et al. Ontogeny of human mucosal-associated invariant T cells and related T cell subsets. J. Exp. Med. 215, 459–479 (2018).
85. Vazquez, M. et al. B cells responses and cytokine production are regulated by their immune microenvironment. Cytokine 176, 139–148 (2016).
86. Browne, E. P. Regulation of B-cell responses by Toll-like receptors. Immunology 136, 370–379 (2012).
87. Häusser-Kinzel, S. & Weber, M. S. The role of B cells and antibodies in multiple sclerosis, neuromyelitis optica, and related disorders. Front. Immunol. 10, (2019).
88. Habibi, M. S. et al. Impaired antibody-mediated protection and defective iga b-cell memory in experimental infection of adults with respiratory syncytial virus. Am. J. Respir. Crit. Care Med. 191, 1040–1049 (2015).
89. Dorshkind, K. & Montecino-Rodriguez, E. Fetal B-cell lymphopoiesis and the emergence of B-1-cell potential. Nat. Rev. Immunol. 7, 213–219 (2007).
90. Griffin, D. O. et al. Human B1 cells in umbilical cord and adult peripheral blood express the novel phenotype CD20+CD27+CD43+CD70-. J. Exp. Med. 208, 67–80 (2011).

91. Williams, J. V. et al. The human neonatal B cell response to respiratory syncytial virus uses a biased antibody variable gene repertoire that lacks somatic mutations. Mol. Immunol. 47, 407–414 (2009).
92. Wu, N. H. et al. The differentiated airway epithelium infected by influenza viruses maintains the barrier function despite a dramatic loss of ciliated cells. Sci. Rep. 6, 1–12 (2016).
93. Garofalo, R. P. & Haeberle, H. Epithelial regulation of innate immunity to respiratory syncytial virus. Am. J. Respir. Cell Mol. Biol. 23, 581–585 (2000).
94. Zhang, L. et al. Respiratory Syncytial Virus Infection of Human Airway EpithelialCells Is Polarized, Specific to Ciliated Cells, and withoutObvious Cytopathology. J. Virol. 76, 5654–5666 (2002).
95. Goritzka, M. et al. Alveolar macrophage–derived type I interferons orchestrate innate immunity to RSV through recruitment of antiviral monocytes. J. Exp. Med. 212, 699–714 (2015).
96. LeVine, A. M. et al. Surfactant protein-A enhances respiratory syncytial virus clearance in vivo. J. Clin. Invest. 103, 1015–1021 (1999).
97. Thwaites, R. S. et al. Reduced nasal viral load and IFN responses in infants with RSV bronchiolitis and respiratory failure. 1–46 (2018) doi:10.1164/rccm.201712-2567OC.
98. McNamara, P. S. et al. Bronchoalveolar lavage cellularity in infants with severe respiratory syncytial virus bronchiolitis. Arch Dis Child. 922–926 (2003).
99. Everard, M. L. et al. Analysis of cells obtained by bronchial lavage of infants with respiratory syncytial virus infection. Arch. Dis. Child. 71, 428–432 (1994).
100. Kaiko, G. E. et al. NK Cell Deficiency Predisposes to Viral-Induced Th2-Type Allergic Inflammation via Epithelial-Derived IL-25. J. Immunol. 185, 4681–4690 (2010).
101. Grunwell, J. R. et al. Neutrophil Dysfunction in the Airways of Children with Acute Respiratory Failure Due to Lower Respiratory Tract Viral and Bacterial Coinfections. Sci. Rep. 9, 1–13 (2019).
102. Toussaint, M. et al. Host DNA released by NETosis promotes rhinovirus-induced type-2 allergic asthma exacerbation. Nat. Med. (2017) doi:10.1038/nm.4332.
103. Adrover, J. M. et al. Programmed 'disarming' of the neutrophil proteome reduces the magnitude of inflammation. Nat. Immunol. (2020) doi:10.1038/s41590-019-0571-2.
104. de Bont, C. M. et al.. NETosis, complement, and coagulation: a triangular relationship. Cell. Mol. Immunol. 16, 19–27 (2019).
105. Halfhide, C. P. et al. Respiratory syncytial virus binds and undergoes transcription in neutrophils from the blood and airways of infants with severe bronchiolitis. J. Infect. Dis. 204, 451–458 (2011).
106. Hennus, M. P. et al. Mechanical ventilation drives inflammation in severe viral bronchiolitis. PLoS One 8, 8–12 (2013).
107. Lukens, M. V. et al. A Systemic Neutrophil Response Precedes Robust CD8+ T-Cell Activation during Natural Respiratory Syncytial Virus Infection in Infants. J. Virol. 84, 2374–2383 (2010).
108. Lindemans, C. A. et al. Systemic eosinophil response induced by respiratory syncytial virus. Clin. Exp. Immunol. 144, 409–417 (2006).
109. Eng, S. S. & Defelice, M. L. The role and immunobiology of eosinophils in the respiratory system: A comprehensive review. Clin. Rev. Allergy Immunol. 50, 140–158 (2016).
110. Kawasaki, Y. et al. Serum regulated upon activation, normal T cell expressed and presumably secreted concentrations and eosinophils in respiratory syncytial virus infection. Pediatr. Int. 48, 257–260 (2006).
111. Soukup, J. M. & Becker, S. Role of monocytes and eosinophils in human respiratory syncytial virus infection in vitro. Clin. Immunol. 107, 178–185 (2003).
112. Jans, J. et al. Siglec-1 inhibits RSV-induced interferon gamma production by adult T cells in contrast to newborn T cells. Eur. J. Immunol. 48, 621–631 (2018).
113. Bernink, J. H. et al. Human type 1 innate lymphoid cells accumulate in inflamed mucosal tissues. Nat. Immunol. 14, 221–229 (2013).
114. Monticelli, L. a. & Artis, D. Innate lymphoid cells promote lung tissue homeostasis following acute influenza virus infection. Nat. Immunol. 12, 1045–1054 (2011).
115. Kiessling, R. et al. „Natural" killer cells in the mouse. II. Cytotoxic cells with specificity for mouse Moloney leukemia cells. Characteristics of the killer cell. Eur. J. Immunol. 5, 117–121 (1975).
116. Mebius, R. E. et al. Developing lymph nodes collect CD4+CD3- LTβ+ cells that can differentiate to APC, NK cells, and follicular cells but not T or B cells. Immunity 7, 493–504 (1997).
117. Artis, D. & Spits, H. The biology of innate lymphoid cells. Nature 517, 293–301 (2015).
118. Spits, H. et al. Innate lymphoid cells-a proposal for uniform nomenclature. Nat. Rev. Immunol. 13, 145–149 (2013).
119. Yokota, Y. et al. Development of peripheral lymphoid organs and natural killer cells depends on the helix-loop-helix inhibitor Id2. Nature 397, 702–706 (1999).
120. Eberl, G. et al. Innate lymphoid cells: A new paradigm in immunology. Science (80-.). 348, (2015).

121. Ebbo, M. et al. Innate lymphoid cells: major players in inflammatory diseases. Nat. Rev. Immunol. 17, 665–678 (2017).
122. Spits, H. & Cupedo, T. Innate lymphoid cells: Emerging insights in development, lineage relationships, and function. Annu. Rev. Immunol. 30, 647–675 (2012).
123. Stier, M. T. et al. Respiratory syncytial virus infection activates IL-13–producing group 2 innate lymphoid cells through thymic stromal lymphopoietin. J. Allergy Clin. Immunol. 138, 814-824.e11 (2016).
124. Montaldo, E. et al. Group 3 innate lymphoid cells (ILC3s): Origin, differentiation, and plasticity in humans and mice. Eur. J. Immunol. 45, 2171–2182 (2015).
125. Li, S., Bostick, J. W. & Zhou, L. Regulation of innate lymphoid cells by aryl hydrocarbon receptor. Front. Immunol. 8, (2018).
126. Seehus, C. R. et al. Alternative activation generates IL-10 producing type 2 innate lymphoid cells. Nat. Commun. 8, (2017).
127. Gury-BenAri, M. et al. The Spectrum and Regulatory Landscape of Intestinal Innate Lymphoid Cells Are Shaped by the Microbiome. Cell 166, 1231-1246.e13 (2016).
128. Serafini, N. et al. Transcriptional regulation of innate lymphoid cell fate. Nat. Rev. Immunol. 15, 415–428 (2015).
129. Bernink, J. H. et al. Human type 1 innate lymphoid cells accumulate in inflamed mucosal tissues. Nat. Immunol. 14, 221–229 (2013).
130. Culley, F. J. Natural killer cells in infection and inflammation of the lung. doi:10.1111/j.1365-2567.2009.03167.x.
131. Zhang, Y. et al. In vivo kinetics of human natural killer cells: The effects of ageing and acute and chronic viral infection. Immunology 121, 258–265 (2007).
132. Caligiuri, M. A. Human natural killer cells. Blood 112, 461–469 (2008).
133. Gardiner, C. M. & Finlay, D. K. What fuels natural killers? Metabolism and NK cell responses. Front. Immunol. 8, (2017).
134. Freud, A. G. et al. The Broad Spectrum of Human Natural Killer Cell Diversity. Immunity 47, 820–833 (2017).
135. Crinier, A. et al. High-Dimensional Single-Cell Analysis Identifies Organ-Specific Signatures and Conserved NK Cell Subsets in Humans and Mice. Immunity 49, 971-986.e5 (2018).
136. Long, E. O. Ready for Prime Time: NK Cell Priming by Dendritic Cells. Immunity 26, 385–387 (2007).
137. Lucas, M. et al. Dendritic Cells Prime Natural Killer Cells by trans-Presenting Interleukin 15. Immunity 26, 503–517 (2007).
138. Lanier, L. L. NK cell receptors. Annu. Rev. Immunol. 16, 359–393 (1998).
139. Topham, N. J. & Hewitt, E. W. Natural killer cell cytotoxicity: How do they pull the trigger? Immunology 128, 7–15 (2009).
140. Takeda, K. et al. TRAIL identifies immature natural killer cells in newborn mice and adult mouse liver. Blood 105, 2082–2089 (2005).
141. Orange, J. S. & Ballas, Z. K. Natural killer cells in human health and disease. Clin. Immunol. 118, 1–10 (2006).
142. Robinette, M. L. et al. Transcriptional programs define molecular characteristics of innate lymphoid cell classes and subsets. Nat. Immunol. 16, 306–317 (2015).
143. Simoni, Y. et al. Human Innate Lymphoid Cell Subsets Possess Human Innate Lymphoid Cell Subsets Possess Tissue-Type Based Heterogeneity in Phenotype and Frequency. Immunity 46, 148–161 (2017).
144. Fuchs, A. et al. Intraepithelial type 1 innate lymphoid cells are a unique subset of il-12- and il-15-responsive IFN-γ-producing cells. Immunity 38, 769–781 (2013).
145. Ahmet Eken, H. D.-A. Innate Lymphoid Cells (Non-NK ILCs). Agric. Biol. Sci. Grain Legum. (2016) doi:10.5772/711.
146. Cortez, V. S. & Colonna, M. Diversity and function of group 1 innate lymphoid cells. Immunol. Lett. 179, 19–24 (2016).
147. Chea, S. et al. CXCR6 Expression Is Important for Retention and Circulation of ILC Precursors. Mediators Inflamm. 2015, (2015).
148. Cella, M. et al. Subsets of ILC3−ILC1-like cells generate a diversity spectrum of innate lymphoid cells in human mucosal tissues. Nat. Immunol. 20, (2019).
149. Jozwik, A. et al. RSV-specific airway resident memory CD8+ T cells and differential disease severity after experimental human infection. Nat. Commun. 6, 1–15 (2015).
150. Klose, C. S. N. et al. Differentiation of type 1 ILCs from a common progenitor to all helper-like innate lymphoid cell lineages. Cell 157, 340–356 (2014).
151. Klose, C. S. N. et al. A T-bet gradient controls the fate and function of CCR6-RORγt + innate lymphoid cells. Nature 494, 261–265 (2013).
152. Abt, M. C. et al. Innate immune defenses mediated by two ilc subsets are critical for protection against acute clostridium difficile infection. Cell Host Microbe 18, 27–37 (2015).

153. Weizman, O. E. et al. ILC1 Confer Early Host Protection at Initial Sites of Viral Infection. Cell 171, 795-808.e12 (2017).
154. Kim, B. S. et al. TSLP elicits IL-33-independent innate lymphoid cell responses to promote skin inflammation. Sci. Transl. Med. 5, (2013).
155. Diefenbach, A. et al. Development, differentiation and diversity of innate lymphoid cells. Immunity 41, 354–365 (2014).
156. Hwang, Y. Y. & Mckenzie, A. N. J. Innate Lymphoid Cells in Immunity and Disease. 785, (2013).
157. Fort, M. M. et al. IL-25 Induces IL-4, IL-5, and IL-13 and Th2-associated pathologies in vivo. Immunity 15, 985–995 (2001).
158. Moro, K. et al. Isolation and analysis of group 2 innate lymphoid cells in mice. Nat. Protoc. 10, 792–806 (2015).
159. Halim, T. Y. F. et al. Lung Natural Helper Cells Are a Critical Source of Th2 Cell-Type Cytokines in Protease Allergen-Induced Airway Inflammation. Immunity 36, 451–463 (2012).
160. Wilhelm, C. & Stockinger, B. Innate lymphoid cells and type 2 (Th2) mediated immune responses - pathogenic or beneficial? Front. Immunol. 2, 2–5 (2011).
161. Licona-Limón, P. et al. TH2, allergy and group 2 innate lymphoid cells. Nat. Immunol. 14, 536–542 (2013).
162. Turner, J. E. et al. IL-9-mediated survival of type 2 innate lymphoid cells promotes damage control in helminth-induced lung inflammation. J. Exp. Med. 210, 2951–2965 (2013).
163. Salimi, M. et al. A role for IL-25 and IL-33-driven type-2 innate lymphoid cells in atopic dermatitis. J. Exp. Med. 210, 2939–2950 (2013).
164. Fallon, P. G. et al. Identification of an interleukin (IL)-25–dependent cell population that provides IL-4, IL-5, and IL-13 at the onset of helminth expulsion. J. Exp. Med. 203, 1105–1116 (2006).
165. Moro, K. et al. Innate production of TH 2 cytokines by adipose tissue-associated c-Kit+ Sca-1+ lymphoid cells. Nature 463, 540–544 (2010).
166. Neill, D. R. et al. Nuocytes represent a new innate effector leukocyte that mediates type-2 immunity. Nature 464, 1367–1370 (2010).
167. Price, A. E. et al. Systemically dispersed innate IL-13-expressing cells in type 2 immunity. Proc. Natl. Acad. Sci. U. S. A. 107, 11489–11494 (2010).
168. Yasuda, K. et al. Contribution of IL-33-activated type II innate lymphoid cells to pulmonary eosinophilia in intestinal nematode-infected mice. Proc. Natl. Acad. Sci. U. S. A. 109, 3451–3456 (2012).
169. Mjösberg, J. M. et al. Human IL-25- and IL-33-responsive type 2 innate lymphoid cells are defined by expression of CRTH2 and CD161. Nat. Immunol. 12, 1055–1062 (2011).
170. Mindt, B. C. et al. Group 2 innate lymphoid cells in pulmonary immunity and tissue homeostasis. Front. Immunol. in press, 1–17 (2018).
171. Mjösberg, J. et al. The Transcription Factor GATA3 Is Essential for the Function of Human Type 2 Innate Lymphoid Cells. Immunity 37, 649–659 (2012).
172. Singh, P. B. et al. MicroRNA regulation of type 2 innate lymphoid cell homeostasis and function in allergic inflammation. J. Exp. Med. 214, 3627–3643 (2017).
173. Bando, J. K. et al. M. Type 2 innate lymphoid cells constitutively express arginase-I in the naïve and inflamed lung. J. Leukoc. Biol. 94, 877–884 (2013).
174. Monticelli, L. A. et al. Checkpoint Controlling Type 2 Inflammation. 17, 656–665 (2016).
175. Huang, Y. et al. S1P-dependent interorgan trafficking of group 2 innate lymphoid cells supports host defense. Science (80-.). 359, 114–119 (2018).
176. Brinkmann, V. et al. The immune modulator FTY720 targets sphingosine 1-phosphate receptors. J. Biol. Chem. 277, 21453–21457 (2002).
177. Germain, R. N. & Huang, Y. ILC2s — resident lymphocytes pre-adapted to a specific tissue or migratory effectors that adapt to where they move? Curr. Opin. Immunol. 56, 76–81 (2019).
178. Barlow, J. L. & Mckenzie, A. N. J. Innate Lymphoid Cells of the Lung. Annu. Rev. Physiol. 429–52 (2019).
179. Melo-Gonzalez, F. & Hepworth, R. Functional and phenotypic heterogeneity of group 3 innate lymphoid cells. 265–275 (2016) doi:10.1111/imm.12697.
180. Hepworth, M. R. et al. Group 3 innate lymphoid cells mediate intestinal selection of commensal bacteria-specific CD4+ T cells. 348, 1031–1035 (2015).
181. Song, C. et al. Unique and redundant functions of NKp46+ ILC3s in models of intestinal inflammation. J. Exp. Med. 212, 1869–1882 (2015).
182. Zheng, Y. et al. Interleukin-22 mediates early host defense against attaching and effacing bacterial pathogens. Nat. Med. 14, 282–289 (2008).
183. Sawa, S. et al. RORγt+ innate lymphoid cells regulate intestinal homeostasis by integrating negative signals from the symbiotic microbiota. Nat. Immunol. 12, 320–328 (2011).

184. Rankin, L. C. et al. Complementarity and redundancy of IL-22-producing innate lymphoid cells. Nat. Immunol. 17, 179–186 (2016).
185. Conti, H. R. et al. Th17 cells and IL-17 receptor signaling are essential for mucosal host defense against oral candidiasis. J. Exp. Med. 206, 299–311 (2009).
186. Gladiator, A. et al. Cutting Edge: IL-17–Secreting Innate Lymphoid Cells Are Essential for Host Defense against Fungal Infection. J. Immunol. 190, 521–525 (2013).
187. McGeachy, M. J. et al. The IL-17 Family of Cytokines in Health and Disease. Immunity 50, 892–906 (2019).
188. Vély, F. et al. Evidence of innate lymphoid cell redundancy in humans. Nat. Immunol. 17, 1291–1299 (2016).
189. Ariotti, S. et al. Skin-resident memory CD8+ T cells trigger a state of tissue-wide pathogen alert. Science (80). 346, 101–105 (2014).
190. Zhou, G. et al. NK cells exacerbate the pathology of influenza virus infection in mice. Eur. J. Immunol. 43, 929–938 (2013).
191. Ascough, S. et al. Induction and Subversion of Human Protective Immunity: Contrasting Influenza and Respiratory Syncytial Virus. Front. Immunol. 9, 323 (2018).
192. Li, F. et al. Natural Killer Cells Are Involved in Acute Lung Immune Injury Caused by Respiratory Syncytial Virus Infection. J. Virol. 86, 2251–2258 (2012).
193. Dhariwal, J. et al. Mucosal Type 2 Innate Lymphoid Cells Are a Key Component of the Allergic Response to Aeroallergens. Am. J. Respir. Crit. Care Med. 195, 1586–1596 (2017).
194. Nagakumar, P. et al. Type 2 innate lymphoid cells in induced sputum from children with severe asthma. J. Allergy Clin. Immunol. 137, 624–626 (2016).
195. Hazenberg, M. D. & Spits, H. Review Article Human innate lymphoid cells. Blood 124, 700–710 (2014).
196. Wilson, M. S. et al. Bleomycin and IL-1β–mediated pulmonary fibrosis is IL-17A dependent. J. Exp. Med. 207, 535–552 (2010).
197. Taube, C. et al. IL-22 is produced by innate lymphoid cells and limits inflammation in allergic airway disease. PLoS One 6, (2011).
198. Thwaites, R. S. et al. Nasosorption as a minimally invasive sampling procedure: Mucosal viral load and inflammation in primary RSV bronchiolitis. J. Infect. Dis. 215, 1240–1244 (2017).
199. Thwaites, R. S. et al. Absorption of nasal and bronchial fluids: Precision sampling of the human respiratory mucosa and laboratory processing of samples. J. Vis. Exp. 2018, 1–8 (2018).
200. Hector, A. et al. Novel method to process cystic fibrosis sputum for determination of oxidative state. Respiration 80, 393–400 (2010).
201. Swieboda, D. et al. OMIP-062: A 14-Color, 16-Antibody Panel for Immunophenotyping Human Innate Lymphoid, Myeloid and T Cells in Small Volumes of Whole Blood and Pediatric Airway Samples. Cytom. Part A (2019) doi:10.1002/cyto.a.23907.
202. Scheltema, N. M. et al. RSV prevention in infancy and asthma in later life – Authors' reply. Lancet Respir. Med. 6, e33 (2018).
203. Belkina, A. C. et al. Automated optimized parameters for T-distributed stochastic neighbor embedding improve visualization and analysis of large datasets. Nat. Commun. 10, 1–12 (2019).
204. McInnes, L. et al. UMAP: Uniform Manifold Approximation and Projection for Dimension Reduction. (2018).
205. Van der matten, L. & Hinton Geoffry. Visualizing Data using t-SNE. New Sci. 164, 10 (1999).
206. Van Gassen, S. et al. FlowSOM: Using self-organizing maps for visualization and interpretation of cytometry data. Cytom. Part A 87, 636–645 (2015).
207. Zuniga, E. I. et al. A. Innate and Adaptive Immune Regulation During Chronic Viral Infections. Annu. Rev. Virol. 2, 573–597 (2015).
208. De Jongste, A. H. et al. Use of TransFixTM cerebrospinal fluid storage tubes prevents cellular loss and enhances flow cytometric detection of malignant hematological cells after 18 hours of storage. Cytom. Part B - Clin. Cytom. 86, 272–279 (2014).
209. Canonico, B. et al. Evaluation of leukocyte stabilisation in TransFix®-treated blood samples by flow cytometry and transmission electron microscopy. J. Immunol. Methods 295, 67–78 (2004).
210. Masuda, A. et al. Role of Fc Receptors as a therapeutic target. Inflamm. Allergy Drug Targets 8, 80–6 (2009).
211. Björklund, Å. K. et al. The heterogeneity of human CD127+ innate lymphoid cells revealed by single-cell RNA sequencing. Nat. Immunol. 17, 451–460 (2016).
212. Wallrapp, A. et al. The neuropeptide NMU amplifies ILC2-driven allergic lung inflammation. Nature 549, 351–356 (2017).
213. Pitoiset, F. et al. A standardized flow cytometry procedure for the monitoring of regulatory T cells in clinical trials. Cytom. Part B Clin. Cytom. 348–355 (2018) doi:10.1002/bab.1342.This.
214. Kondělková, K. et al. Regulatory T cells (TREG) and their roles in immune system with respect to immunopathological disorders. Acta Medica (Hradec Kralove) 53, 73–7 (2010).

215. Streitz, M. et al. Standardization of whole blood immune phenotype monitoring for clinical trials: panels and methods from the ONE study. Transplant. Res. 2, 17 (2013).
216. Stevens, V. L. et al. Cryopreservation of whole blood samples collected in the field for a large epidemiologic study. Cancer Epidemiol. Biomarkers Prev. 16, 2160–2163 (2007).
217. Nishimura, M. et al. Frozen-stored granulocytes can be used for an immunofluorescence test to detect granulocyte antibodies. Transfusion (2001).
218. Sinclair, F. & Boonlayangoor, S. Cryopreservation of human Granulocytes: Study of Granulocytes Function and Ultrastructure. 56, 237–246 (1980).
219. Brooks, C. R. et al. Identifying leukocyte populations in fresh and cryopreserved sputum using flow cytometry. Cytom. Part B - Clin. Cytom. 84 B, 104–113 (2013).
220. Costantini, A. et al. Effects of cryopreservation on lymphocyte immunophenotype and function. J. Immunol. Methods 278, 145–155 (2003).
221. Cytomark. Cellular Antigen Stabilising Reagent. CalTag 2016 (2016).
222. Noël, A. et al. Effects of inhaled nano-TiO2 aerosols showing two distinct agglomeration states on rat lungs. Toxicol. Lett. 214, 109–119 (2012).
223. Rajab, A. et al. Ten-color 15-antibody flow cytometry panel for immunophenotyping of lymphocyte population. Int. J. Lab. Hematol. 39, 76–85 (2017).
224. Adkins, B. et al. Neonatal adaptive immunity comes of age. Nat. Rev. Immunol. 4, 553–564 (2004).
225. Li, L. et al. IL-4 utilizes an alternative receptor to drive apoptosis of Th1 cells and skews neonatal immunity toward Th2. Immunity 20, 429–440 (2004).
226. Xainli, J. et al. Age-Dependent Cellular Immune Responses to Plasmodium vivax Duffy Binding Protein in Humans. J. Immunol. 169, 3200–3207 (2002).
227. Vekemans, J. et al. Neonatal bacillus Calmette-Guérin vaccination induces adult-like IFN-γ production by CD4+ T lymphocytes. Eur. J. Immunol. 31, 1531–1535 (2001).
228. Costanzo, M. C. et al. OMIP-027: Functional analysis of human natural killer cells. Cytom. Part A 87, 803–805 (2015).
229. Nielsen, C. M. et al. Functional significance of CD57 expression on human NK cells and relevance to disease. Front. Immunol. 4, 163–180 (2013).
230. Salimi, M. et al. A role for IL-25 and IL-33–driven type-2 innate lymphoid cells in atopic dermatitis. J. Exp. Med. 210, 2939–2950 (2013).
231. Guilmot, A. et.al. Natural killer cell responses to infections in early life. J. Innate Immun. 3, 280–288 (2011).
232. Kotas, M. E. & Locksley, R. M. Why Innate Lymphoid Cells? Immunity 48, 1081–1090 (2018).
233. Yu, J. C. et al. Innate Immunity of Neonates and Infants. Front. Immunol. 9, (2018).
234. Lim, A. I. et al. Systemic Human ILC Precursors Provide a Substrate for Tissue ILC Differentiation. Cell 168, 1086-1100.e10 (2017).
235. Georgountzou, A. & Papadopoulos, N. G. Postnatal innate immune development: From birth to adulthood. Front. Immunol. 8, 1–16 (2017).
236. Adkins, B. Peripheral CD4 + Lymphocytes Derived from Fetal versus Adult Thymic Precursors Differ Phenotypically and Functionally . J. Immunol. 171, 5157–5164 (2003).
237. Prescott, S. L. et al. Transplacental priming of the human immune system to environmental allergens: universal skewing of initial T cell responses toward the Th2 cytokine profile. J. Immunol. 160, 4730–7 (1998).
238. Mayani, H. et.al. Cord blood research, banking, and transplantation: achievements, challenges, and perspectives. Bone Marrow Transplant. 55, 48–61 (2020).
239. Dalle, J. H. et al. Characterization of cord blood natural killer cells: Implications for transplantation and neonatal infections. Pediatr. Res. 57, 649–655 (2005).
240. Papaioannou, N. E. et.al. Understanding the functional properties of neonatal dendritic cells: A doorway to enhance vaccine effectiveness? Front. Immunol. 10, 1–8 (2019).
241. Carolina, A. et al. Blood cells profile in umbilical coed of late preterm and term newborns. Revi Paul Pediatr 37, 264–274 (2019).
242. Fonceca, A. M. et al. Infective respiratory syncytial virus is present in human cord blood samples and most prevalent during winter months. PLoS One 12, 1–10 (2017).
243. Bao, W. et.al. Normative distribution of complete blood count from early childhood through adolescence: The Bogalusa heart study. Preventive Medicine vol. 22 825–837 (1993).
244. Schmutz, N. et.al. Expected ranges for blood neutrophil concentrations of neonates: The Manroe and Mouzinho charts revisited. J. Perinatol. 28, 275–281 (2008).
245. Wenisch, C. et.al. Effect of age on human neutrophil function. J. Leukoc. Biol. 67, 40–45 (2000).
246. Carr, R. Neutrophil production and function in newborn infants. Br. J. Haematol. 2000, 110, 18–28 (2000).

247. Shumer, D.E. et.al. Early Persistent Blood Eosinophilia in Necrotizing Enterocolitis is a Predictor of Late Complications. Neonatology 108, 137–142 (2015).
248. Simoni, Y. & Newell, E. W. Dissecting human ILC heterogeneity: more than just three subsets. Immunology 153, 297–303 (2018).
249. Kim, B. S. & David, A. Group 2 innate lymphoid cells in disease. Int. Immunol. dxv050 (2015) doi:10.1093/intimm/dxv050.
250. Smith, S. G. et al. Increased numbers of activated group 2 innate lymphoid cells in the airways of patients with severe asthma and persistent airway eosinophilia. J. Allergy Clin. Immunol. 137, 75-86.e8 (2016).
251. Hong, J. Y. et al. Neonatal rhinovirus induces mucous metaplasia and airways hyperresponsiveness through IL-25 and type 2 innate lymphoid cells. J. Allergy Clin. Immunol. 134, 429-439.e8 (2014).
252. Bal, S. M. et al. IL-1β, IL-4 and IL-12 control the fate of group 2 innate lymphoid cells in human airway inflammation in the lungs. Nat. Immunol. 17, 636–645 (2016).
253. Xu, Y. et al. Innate lymphoid cells at the human maternal-fetal interface in spontaneous preterm labor. Am. J. Reprod. Immunol. 79, 1–12 (2018).
254. Weekes, M. P. et al. Large clonal expansions of human virus-specific memory cytotoxic T lymphocytes within the CD57+ CD28- CD8+ T-cell population. Immunology 98, 443–449 (1999).
255. Björkström, N. K. et al. Expression patterns of NKG2A, KIR, and CD57 define a process of CD56 dim NK-cell differentiation uncoupled from NK-cell education. Blood 116, 3853–3864 (2010).
256. Biancotto, A. & McCoy, P. J. Studying the Human Immunome: The Complexity of Comprehensive Leukocyte Immunophenotyping. Curr Top Microbiol Immunol 377, 23–60 (2015).
257. Gibbons, D. et al. Interleukin-8 (CXCL8) production is a signatory T cell effector function of human newborn infants. Nat. Med. 20, 1206–1210 (2014).
258. Hilvering, B. et al. Synergistic activation of pro-inflammatory type-2 CD8+ T lymphocytes by lipid mediators in severe eosinophilic asthma. Mucosal Immunol. 1 (2018) doi:10.1038/s41385-018-0049-9.
259. You, D. et.al. Crawling with Virus: Translational Insights from a Neonatal Mouse Model on the Pathogenesis of Respiratory Syncytial Virus in Infants. J. Virol. 90, 2–4 (2016).
260. Houben, B.M.L. et.al. Disease Severity and Viral Load Are Correlated in Infants With Primary Respiratory Syncytial Virus Infection in the Community M.L. Anticancer Res. 30, 4799–4804 (2010).
261. DeVincenzo, J. P. et al. Viral load drives disease in humans experimentally infected with respiratory syncytial virus. Am. J. Respir. Crit. Care Med. 182, 1305–1314 (2010).
262. Poposki, J. A. et al. Group 2 innate lymphoid cells are elevated and activated in chronic rhinosinusitis with nasal polyps. Immun. Inflamm. Dis. 5, 233–243 (2017).
263. Vu LD et al. Elevated Levels of Type 2 Respiratory Innate Lymphoid Cells in Human Infants with Severe RSV Bronchiolitis. Am J Respir Crit Care Med. 105, 9817–9822 (2019).
264. Habibi, M. S. et al. Neutrophilic inflammation in the respiratory mucosa predisposes to RSV infection. Science 370, (2020).
265. Kanegasaki, S. et al. A novel optical assay system for the quantitative measurement of chemotaxis. J. Immunol. Methods 282, 1–11 (2003).
266. Denman, C. J. et al. Membrane-bound IL-21 promotes sustained Ex Vivo proliferation of human natural killer cells. PLoS One 7, (2012).
267. Choi, Y. H. et al. IL-27 enhances IL-15/IL-18-mediated activation of human natural killer cells. J. Immunother. Cancer 7, 1–12 (2019).
268. Heidema, J. et al. CD8 + T Cell Responses in Bronchoalveolar Lavage Fluid and Peripheral Blood Mononuclear Cells of Infants with Severe Primary Respiratory Syncytial Virus Infections. J. Immunol. 179, 8410–8417 (2007).
269. Kerrin, A. et al. Differential lower airway dendritic cell patterns May reveal distinct endotypes of RSV bronchiolitis. Thorax 72, 620–627 (2017).
270. Li, N. et al. Mass cytometry reveals innate lymphoid cell differentiation pathways in the human fetal intestine. J. Exp. Med. jem.20171934 (2018) doi:10.1084/jem.20171934.
271. Milush, J. M. et al. Functionally distinct subsets of human NK cells and monocyte/DC-like cells identified by coexpression of CD56, CD7, and CD4. Blood 114, 4823–4831 (2009).
272. Schwarze, J. et al. CD8 T cells are essential in the development of respiratory syncytial virus-induced lung eosinophilia and airway hyperresponsiveness. J. Immunol. 162, 4207–11 (1999).
273. Saravia, J. et al. Respiratory Syncytial Virus Disease Is Mediated by Age-Variable IL-33. PLoS Pathog. 11, 1–17 (2015).
274. Vandini, S. et al. Immune and inflammatory response in bronchiolitis due to respiratory Syncytial Virus and Rhinovirus infections in infants. Paediatr. Respir. Rev. 24, 60–64 (2017).
275. Kalantar, K. L. et al. Metagenomic comparison of tracheal aspirate and mini-bronchial alveolar lavage for assessment of respiratory microbiota. Am. J. Physiol. - Lung Cell. Mol. Physiol. 316, L578–L584 (2019).

276. D'Angio, C. T. et al. Comparison of tracheal aspirate and bronchoalveolar lavage specimens from premature infants. Biol. Neonate 82, 145–149 (2002).
277. Forsthuber, T. et al. Induction of TH1 and TH2 immunity in neonatal mice. Science (80-). 271, 1728–1730 (1996).
278. Sarzotti, M. et al. Induction of protective CTL responses in newborn mice by a murine retrovirus. Science (80). 271, 1726–1728 (1996).
279. Plötz, F. B. et al. Mechanical ventilation alters the immune response in children without lung pathology. Intensive Care Med. 28, 486–492 (2002).
280. Broadbent, L. et al. Comparative primary paediatric nasal epithelial cell culture differentiation and RSV-induced cytopathogenesis following culture in two commercial media. PLoS One 15, 1–12 (2020).
281. Van Acker, H. H. et al. CD56 in the immune system: More than a marker for cytotoxicity? Front. Immunol. 8, 1–9 (2017).
282. Bronte, V. et al. Recommendations for myeloid-derived suppressor cell nomenclature and characterization standards. Nat. Commun. 7, (2016).
283. He, Y. M. et al. Transitory presence of myeloid-derived suppressor cells in neonates is critical for control of inflammation. Nat. Med. 24, 224–231 (2018).
284. Jackson, D. J. & Johnston, S. L. The role of viruses in acute exacerbations of asthma. J. Allergy Clin. Immunol. 125, 1178–87; quiz 1188–9 (2010).

Appendix

ELLI Ethical Approval

Ymchwil Iechyd a Gofal Cymru
Health and Care Research Wales

NHS
Health Research Authority

Dr Simon Nadel
Consultant in Paediatric Intensive Care
NHS, St Mary's Hospital, Paediatric Intensive Care Unit
Queen Elizabeth Queen Mother (QEQM) building
London
W2 1NY

Email: hra.approval@nhs.net
Research-permissions@wales.nhs.uk

26 November 2018

Dear Dr Nadel

HRA and Health and Care Research Wales (HCRW) Approval Letter

Study title:	**Immune responses in early life lung infection**
IRAS project ID:	**245152**
Protocol number:	**18M4545**
REC reference:	**18/LO/1570**
Sponsor	**Joint Research Compliance Office, Imperial College London**

I am pleased to confirm that HRA and Health and Care Research Wales (HCRW) Approval has been given for the above referenced study, on the basis described in the application form, protocol, supporting documentation and any clarifications received. You should not expect to receive anything further relating to this application.

How should I continue to work with participating NHS organisations in England and Wales?
You should now provide a copy of this letter to all participating NHS organisations in England and Wales, as well as any documentation that has been updated as a result of the assessment.

This is a single site study sponsored by the site. The sponsor R&D office will confirm to you when the study can start following issue of HRA and HCRW Approval.

It is important that you involve both the research management function (e.g. R&D office) supporting each organisation and the local research team (where there is one) in setting up your study. Contact details of the research management function for each organisation can be accessed here.

How should I work with participating NHS/HSC organisations in Northern Ireland and Scotland?
HRA and HCRW Approval does not apply to NHS/HSC organisations within the devolved administrations of Northern Ireland and Scotland.

If you indicated in your IRAS form that you do have participating organisations in either of these devolved administrations, the final document set and the study wide governance report (including this letter) has been sent to the coordinating centre of each participating nation. You should work with the relevant national coordinating functions to ensure any nation specific checks are complete, and with each site so that they are able to give management permission for the study to begin.

Please see IRAS Help for information on working with NHS/HSC organisations in Northern Ireland and Scotland.

How should I work with participating non-NHS organisations?
HRA and HCRW Approval does not apply to non-NHS organisations. You should work with your non-NHS organisations to obtain local agreement in accordance with their procedures.

What are my notification responsibilities during the study?
The document "*After Ethical Review – guidance for sponsors and investigators*", issued with your REC favourable opinion, gives detailed guidance on reporting expectations for studies, including:

- Registration of research
- Notifying amendments
- Notifying the end of the study

The HRA website also provides guidance on these topics, and is updated in the light of changes in reporting expectations or procedures.

I am a participating NHS organisation in England or Wales. What should I do once I receive this letter?
You should work with the applicant and sponsor to complete any outstanding arrangements so you are able to confirm capacity and capability in line with the information provided in this letter.

The sponsor contact for this application is as follows:

Name: Dawid Swieboda
Tel: 020 7594 3855
Email: d.swieboda@imperial.ac.uk

Who should I contact for further information?
Please do not hesitate to contact me for assistance with this application. My contact details are below.

Your IRAS project ID is **245152**. Please quote this on all correspondence.

Yours sincerely,

Steph Blacklock
Senior Assessor

Email: hra.approval@nhs.net

Copy to: *Miss Ruth Nicholson, Imperial College London, Sponsor Contact*

List of Documents

The final document set assessed and approved by HRA and HCRW Approval is listed below.

Document	*Version*	*Date*
Copies of advertisement materials for research participants	1.0	18 April 2018
Costing template (commercial projects) [NIHR CRN portfolio Application Form ELLI]		13 August 2018
Evidence of Sponsor insurance or indemnity (non NHS Sponsors only) [Sponsorship and Insurance registration Form]		24 July 2017
IRAS Application Form [IRAS_Form_14082018]		14 August 2018
Letter from funder [MRC Asthma UK Founder letter]		16 October 2017
Letter from sponsor [Letter of sposorship]		15 May 2018
Letter from statistician [ELLI Study Statistical letter]		16 October 2018
Letters of invitation to participant [Email for Healthy Volunteers asking for extra blood ELLI]	1.0	18 April 2018
Other [PIS Healthy Adults ELLI]		10 August 2018
Other [Ryan Thwaites CV]		24 July 2018
Other [Fiona Culley CV]	V 2	13 August 2018
Other [The REC response letter]		26 October 2018
Other [PIS Healthy Adults ELLI clean]	V 1.0	16 October 2018
Other [PIS Parents Guardians ELLI uninfected clean]	V 2.0	16 October 2018
Other [PIS Parents Guardians ELLI infected clean]	V 2.0	16 October 2018
Other [Consent Parents Guardians ELLI clean]	V 2.0	16 October 2018
Other [Consent Cord blood Elli clean]	v 2.0	16 October 2018
Other [PIS Cord Blood ELLI]	V 2.0	16 October 2018
Other [PIS Healthy Adults ELLI]	V 2.0	16 October 2018
Other [PIS Parents Guardians ELLI infected]	V 2.0	16 October 2018
Other [PIS Parents Guardians ELLI uninfected]	V 2.0	16 October 2018
Other [Consent Parents Guardians ELLI]	V 2.0	16 October 2018
Other [Consent Cord Blood ELLI]	V 2.0	16 October 2018
Other [Consent Healthy Adults ELLI]	V 2.0	16 October 2018
Participant consent form [Consent Adult Volunteers clean]	V 2.0	16 October 2018
Participant information sheet (PIS) [PIS Cord Blood ELLI clean]	V 2.0	16 October 2018
Research protocol or project proposal [ELLI Study]	1.0	10 August 2018
Summary CV for Chief Investigator (CI) [Simon Nadel (CI) CV]		24 August 2018
Summary CV for student [CV Dawid Swieboda PhD]		24 August 2018
Summary CV for supervisor (student research) [CV Peter Openshaw Supervisor]		24 August 2018

IRAS project ID	245152

Summary of assessment

The following information provides assurance to you, the sponsor and the NHS in England and Wales that the study, as assessed for HRA and HCRW Approval, is compliant with relevant standards. It also provides information and clarification, where appropriate, to participating NHS organisations in England and Wales to assist in assessing, arranging and confirming capacity and capability.

Assessment criteria

Section	Assessment Criteria	Compliant with Standards	Comments
1.1	IRAS application completed correctly	Yes	No comments
2.1	Participant information/consent documents and consent process	Yes	No comments
3.1	Protocol assessment	Yes	No comments
4.1	Allocation of responsibilities and rights are agreed and documented	Yes	Although formal confirmation of capacity and capability is not expected of all or some organisations participating in this study, and such organisations would therefore be assumed to have confirmed their capacity and capability should they not respond to the contrary, we would ask that these organisations pro-actively engage with the sponsor in order to confirm at as early a date as possible. Confirmation in such cases should be by email to the CI and Sponsor confirming participation based on the relevant Statement of Activities and information within this letter.
4.2	Insurance/indemnity arrangements assessed	Yes	No comments
4.3	Financial arrangements assessed	Yes	No comments

Section	Assessment Criteria	Compliant with Standards	Comments
5.1	Compliance with the Data Protection Act and data security issues assessed	Yes	No comments
5.2	CTIMPS – Arrangements for compliance with the Clinical Trials Regulations assessed	Not Applicable	No comments
5.3	Compliance with any applicable laws or regulations	Yes	No comments
6.1	NHS Research Ethics Committee favourable opinion received for applicable studies	Yes	No comments
6.2	CTIMPS – Clinical Trials Authorisation (CTA) letter received	Not Applicable	No comments
6.3	Devices – MHRA notice of no objection received	Not Applicable	No comments
6.4	Other regulatory approvals and authorisations received	Not Applicable	No comments

Participating NHS Organisations in England and Wales

This provides detail on the types of participating NHS organisations in the study and a statement as to whether the activities at all organisations are the same or different.
If this study is subsequently extended to other NHS organisation(s) in England or Wales, an amendment should be submitted, with a Statement of Activities and Schedule of Events for the newly participating NHS organisation(s) in England or Wales. If chief investigators, sponsors or principal investigators are asked to complete site level forms for participating NHS organisations in England and Wales which are not provided in IRAS, the HRA or HCRW websites, the chief investigator, sponsor or principal investigator should notify the HRA immediately at hra.approval@nhs.net or HCRW at Research-permissions@wales.nhs.uk. We will work with these organisations to achieve a consistent approach to information provision.

Principal Investigator Suitability

This confirms whether the sponsor position on whether a PI, LC or neither should be in place is correct for each type of participating NHS organisation in England and Wales, and the minimum expectations for education, training and experience that PIs should meet (where applicable).
Principal Investigator is expected. GCP training is not a generic training expectation, in line with the HRA/HCRW/MHRA statement on training expectations.

HR Good Practice Resource Pack Expectations

This confirms the HR Good Practice Resource Pack expectations for the study and the pre-engagement checks that should and should not be undertaken
No HR Good Practice arrangements are expected.

Other Information to Aid Study Set-up

This details any other information that may be helpful to sponsors and participating NHS organisations in England and Wales to aid study set-up.
The applicant has indicated that they intend to apply for inclusion on the NIHR CRN Portfolio.

Imperial College London

Imperial College Healthcare NHS Trust

Use patient label

Patient name:

DOB:

Number:

CONSENT FORM
Parents or Guardians

Department
Respiratory Infection
Imperial College London
St Mary's Campus
Wright-Fleming Institute
Norfolk Place
London W2 1PG

Early Life Lung Infection Study

Principal investigator: Dr Simon Nadel

		Please initial each box
1	I confirm that I have read and understood the participant information sheet dated ……. (version …….) for the above study and been given a copy to keep. I have had the opportunity to ask questions and have had these answered satisfactorily.	
2	I understand that participation is voluntary, and that I am free to withdraw consent at any time, without giving any reason and without my child/baby's medical care or legal rights being affected.	
3	I understand that sections of any of my child/baby's hospital notes and data collected during the study may be looked at by responsible individuals from Imperial College, Imperial College Healthcare NHS Trust or from regulatory authorities, where it is relevant to my taking part in this research. I give permission for these individuals to access my child's records.	
4	I agree to the taking of nasal absorption from my child/baby as described in the patient information sheet. I understand that this would be voluntary and that I am free to withdraw consent at any time, without giving any reason and without my child/baby's medical care or legal rights being affected.	
5	I agree to the taking of nasopharyngeal aspirates from my child/baby as described on the patient information sheet. I understand that this would be voluntary and that I am free to withdraw consent at any time, without giving any reason and without my child/baby's medical care or legal rights being affected.	
6	I agree to the taking of blood samples from my child/baby as described on the patient information sheet. I understand that this would be voluntary and that I am free to withdraw consent at any time, without giving any reason and without my child/baby's medical care or legal rights being affected.	
7	I agree to the taking of some extra blood samples as described in the patient information sheet. I understand that this would be voluntary and that I am free to withdraw consent at any time, without giving any reason and and without my child/baby's medical care or legal rights being affected	

8	I agree to the taking of airway samples from my child/baby: and realise that this will only be carried out if my baby is already being ventilated on the Paediatric Intensive Care Unit (PICU) or babies having elective surgery in theatre.	
9	I agree to the taking of nasal micro curettage samples as described in the patient information sheet: and realise that this will only be carried out if my baby is already sedated on the Paediatric Intensive Care Unit (PICU).	
10	I agree to the use of my child/baby's blood, nasal and airway samples for genetic analysis (although I understand I will not be told of the results). If I do not agree to genetic analysis, then I can choose NOT to initial this box.	
11	I agree that samples taken during this study can be used in the future for any ethically-approved studies.	
12	I agree that samples collected during this study may be shared with research partners in the UK for ethically-approved studies.	
13	I agree that samples collected during this study may be shared with research partners outside the UK for ethically-approved studies in the EEA and outside the EEA area.	
14	I agree for my child/baby to take part in this research project.	

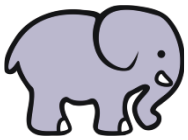
_____	_____	_____
Name of Parent or Guardian	Signature	Date
_____	_____	_____
Name of Person taking consent	Signature	Date
_____	_____	_____
Principal Investigator	Signature	Date

1 copy for subject; 1 copy for Principal Investigator; 1 copy to be kept with study notes.

Imperial College London

Imperial College Healthcare NHS Trust

Early Life Lung Infection (ELLI) study
The Immune Response to Lung Infection in Infants



Principal Clinical Investigator: Dr Simon Nadel
Consultant Paediatrician and Head of the Paediatric Intensive Care Unit (PICU)

St Mary's Hospital, 7th Floor, Queen Elizabeth the Queen Mother (QEQM) Building
South Wharf Road, Paddington, LONDON W2 1NY

Telephone: 02033126466.
Email: s.nadel@imperial.nhs.uk

PARTICIPANT INFORMATION SHEET
HEALTHY ADULT VOLUNTEERS

Introduction

We are inviting you to consider taking part in a research study of babies with respiratory infections. We are recruiting healthy adult volunteers to allow us to compare immune responses in babies with those in adults.

Before you decide, we would like to explain what the study is about and what joining the study involves. Please take time to read the following information and ask us about anything that is not clear or if you would like more information.

Why is the study being done?

Chest infections are common in the early years of life. The vast majority of babies have mild symptoms such as a runny nose or cough, but a small number of babies suffer from severe breathing difficulties requiring hospitalisation, and a small number of these are so unwell that they need to be helped with their breathing by use of a mechanical ventilator.

In addition to studying babies and children with suspected chest infection, we will take samples from healthy adult volunteers in order to compare immune responses in babies to those in adults.

Do I have to take part?

It is up to you to decide whether or not you take part. If you agree, you will be given this information sheet to keep and you will be asked to sign a consent form. You do not have to agree to give samples nor need to explain why, should you choose not to donate. Any personal information provided by you in connection with the donation will be held in confidence and in line with the College Data Protection Policy.

For reasons of safety, you should not donate if:

- You are unwell at the moment
- You know, or think that you might be infected with hepatitis B or hepatitis C
- You know, or think that you might be infected with HIV— the 'AIDS' virus
- You have a sexual partner who is infected with hepatitis or HIV
- You are anaemic or receiving treatment for anaemia or iron deficiency
- You have donated 250ml or more of blood in the last 6 months

What will happen in this study?

We will collect blood samples and samples from your nose.

What samples are being taken in the research study?

1. **Nasal "paper" absorption (nasosorption):** A small strip of absorbent material that looks and feels like soft blotting paper will be used to absorb moisture from the inside surface of the nostril. This special sterile absorptive "paper" will be placed inside the nostril and left for a period of about 30 seconds before being removed. Putting the paper in can tickle and cause you to sneeze and perhaps make your eyes water a little. However, it is not painful and has proved to be a very safe method. We hope to use the moisture collected on the paper to look for viruses, immune cells and chemicals produced which can be important during the infection process so we can understand the body's response to infection. We would like to take a sample from each nostril, or 2 samples from the same nostril. We may do this more than once.

2. **Micro Curettage:** To obtain a sample of cells lining the airways we will use a rhinoprobe to collect a small sample of cells from inside the nose. This may cause slight transient pain or discomfort and perhaps make your eyes water a little.

3. **Blood samples:** We will typically collect a 5-10 ml blood sample (up to 50mls - a glass full). This will be taken by a trained phlebotomist using a needle from a vein in your arm. We may ask you to donate blood on more than one occasion. If so, not more than 250ml will be collected in 6 months.

   You can opt out of any sample type(s) being collected at any point.

Genetic Analysis

As part of a sub-study we may look at your genetic material (DNA and RNA). We would like to do this in both samples from your nose and in the blood sample. These samples will be used to measure genes that reflect your immune response. You should not expect to receive the results

of any tests on your genetics. This genetic data will be handled in a careful and confidential manner in compliance with regulations for such tests.

If you are agreeable, we will store your samples in an anonymised form for future research in compliance with the Human Tissue Act 2004.

What are the possible benefits of taking part?
There will not be any direct benefit for you in taking part in this study. However, the information gained from your participation in this study may help to improve the diagnosis and treatment of unwell children in the future.

What are the possible disadvantages to taking part?

There are few disadvantages to taking part in this study. The study will involve taking samples from your nose. This will be done in a gentle way by experienced staff but may cause minor discomfort. In the event of the blood sample being taken, the small volume being taken will not make any difference to your well-being. You may experience some bruising at the site where the needle is put in and occasionally people feel faint when blood is taken, but these are the only significant risks involved.

Will the information be kept confidential?

All information collected during the course of the research will be kept strictly confidential.

Imperial College London is the sponsor for this study based in the United Kingdom. We will be using information from you in order to undertake this study and will act as the data controller for this study. This means that we are responsible for looking after your information and using it properly. Imperial College London will keep identifiable information about you.
Your rights to access, change or move your information are limited, as we need to manage your information in specific ways in order for the research to be reliable and accurate. If you withdraw from the study, we will keep the information about you that we have already obtained. To safeguard your rights, we will use the minimum personally-identifiable information possible.
You can find out more about how we use your information from Dr Simon Nadel. Telephone: 02033126466. Email: s.nadel@imperial.nhs.uk.

Imperial College London will collect information from you for this research study in accordance with our instructions. Imperial College London will use your name and contact details to contact you about the research study, and make sure that relevant information about the study is recorded for your care, and to oversee the quality of the study. Individuals from Imperial College London and regulatory organisations may look at your research records to check the accuracy of the research study. The only people in Imperial College London who will have access to information that identifies you will be people who need to contact you to request further samples or audit the data collection process. Imperial College London will keep identifiable information about you from this study for 10 years after the study has finished.

When you agree to take part in a research study, the information about your health and care may be provided to researchers running other research studies in this organisation and in other organisations. These organisations may be universities, NHS organisations or companies involved in health and care research in this country or abroad. Your information will only be used by organisations and researchers to conduct research in accordance with the UK Policy Framework

for Health and Social Care Research. This information will not identify you and will not be combined with other information in a way that could identify you. The information will only be used for the purpose of health and care research, and cannot be used to contact you or to affect your care. It will not be used to make decisions about future services available to you, such as insurance.

What will happen to the results of the research study?

Results of this research may be published in scientific journals and presented at scientific medical conferences. Your privacy will be protected and you will not be identified in any report or publication. We would not expect to contact you with any results.

Who is organising and funding the research?

The research is being run by the Department of Paediatrics and the Respiratory Infection Section at Imperial College and Imperial College NHS Healthcare Trust. This research is funded from within the Department of Paediatrics, the National Heart and Lung Institute, the Imperial College Biomedical Research Cluster, the Medical Research Council and Asthma UK.

Who has reviewed the study?

This study has been reviewed and given a favourable opinion by the National Research Ethics Committee.

What if there is a problem?

Imperial College London holds insurance policies which apply to this study. If you experience serious and enduring harm or injury as a result of taking part in this study, you may be eligible to claim compensation without having to prove that Imperial College is at fault. This does not affect your legal rights to seek compensation. If you are harmed due to someone's negligence, then you may have grounds for a legal action. Regardless of this, if you wish to complain, or have any concerns about any aspect of the way you have been treated during the course of this study then you should immediately inform the Investigator (Dr Simon Nadel, The Principal investigator). The normal National Health Service complaints mechanisms are also available to you. If you are still not satisfied with the response, you may contact the Imperial AHSC Joint Research Compliance Office.

Where can I find out more about research in general?

There is currently no single organisation for this in the UK, however INVOLVE is a national advisory group, funded by the National Institute for Health Research (NIHR). Its role is to support and promote active public involvement in NHS, public health and social care research. Contact details are in the next paragraph.

What could I do to help researchers use my own experience more when they are planning their next project?

Do you want to get more involved and help researchers improve future project ideas and research information leaflets? Please contact "People in Research – Opportunities for public involvement in research" http://www.peopleinresearch.org/. If you would like to help, you can also contact INVOLVE which is a national advisory group, funded by the National Institute for Health Research (NIHR). Its role is to support and promote active public involvement in NHS,

public health and social care research. http://www.invo.org.uk/ or Wessex House, Upper Market Street, Eastleigh, Hampshire, SO50 9FD, Telephone: 02380 595628. Email: involve@nihr.ac.uk

The ELLI research team wish to thank you for considering participating in this study.

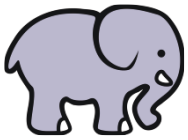
Study Team Contact Telephone Numbers: Dr Simon Nadel, Telephone 02033126466

ELLI PIS Parents and guardians (Infected) V3.0

Imperial College London

Imperial College Healthcare NHS Trust

Early Life Lung Infection (ELLI) study
The Immune Response to Lung Infection in Infants



Principal Clinical Investigator: Dr Simon Nadel
Consultant Paediatrician and Head of the Paediatric Intensive Care Unit (PICU)

St Mary's Hospital, 7th Floor, Queen Elizabeth the Queen Mother (QEQM) Building
South Wharf Road, Paddington, LONDON W2 1NY

Telephone: 02033126466.
Email: s.nadel@imperial.nhs.uk

PARTICIPANT INFORMATION SHEET
Parents or Guardians of
Babies with Respiratory Infection

Introduction

We are inviting you to consider your child taking part in a research study of babies with respiratory infections. Babies of up to 24 months of age are eligible to take part.

We are recruiting babies that have come to St. Mary's Hospital. This includes babies that are attending the emergency department, being treated on the paediatric wards or being treated on the Paediatric Intensive Care Unit (PICU).

Before you decide, we would like to explain what the study is about and what joining the study involves. Please take time to read the following information and ask us about anything that is not clear or if you would like more information.

Why is the study being done?

Chest infections are common in the early years of life. The vast majority of babies have mild symptoms such as a runny nose or cough, but a small number of babies suffer from severe breathing difficulties requiring hospitalisation, and a small number of these are so unwell that they need to be helped with their breathing by use of a mechanical ventilator.

We would like to take samples of mucous from your child's nose and a blood sample. For children in the Paediatric Intensive Care Unit (PICU) on a mechanical ventilator, we will also collect a sample of mucus from their lungs. With these samples we will look at the immune response to the infection, with the aim of discovering why some infants become more unwell.

Does my child have to take part?

It is up to you to decide whether or not your child takes part. If you agree, you will be given this information sheet to keep and you will be asked to sign a consent form. If you decide for your child not to take part, their care will not be affected in any way. They will continue to receive the same treatment, that is, whatever treatment his or her doctors decide is best. Even if you agree for your baby to enter the study, you may withdraw your consent at any time. You don't have to give a reason and it will not affect your child's care.

What will happen to my baby in the study?

We will take some specimens from your child's nose. Additionally we would like to take blood samples that will be used for our research.

Babies that are being treated on PICU and are on a mechanical ventilator routinely have regular suction to remove excess secretions from their lungs and to make the baby more comfortable. We would like to keep these secretions, which are otherwise thrown away.

What are the different kinds of samples being taken in the research study?

1. **Nasal "paper" absorption (nasosorption):** A small strip of absorbent material that looks and feels like soft blotting paper will be used to absorb moisture from the inside surface of the nostril. This special sterile absorptive "paper" will be placed inside the nostril of the baby and left for a period of about 30 seconds before being removed. Putting the paper in can tickle and cause the baby to sneeze and perhaps make baby's eyes water a little. However, it is not painful and has proved to be a very safe method, having been studied in many babies. We hope to use the moisture collected on the paper to look for viruses and bacteria, immune cells and chemicals produced during the infection process so we can understand the body's response to the infection. We would like to take a sample from each nostril, or 2 samples from the same nostril. We will do this no more than twice a day.

2. **Nasopharyngeal aspiration (NPA):** This method is routinely performed on babies in hospital. It involves using a suction catheter (tube) to take fluid from the back of the nose. This may cause your baby some discomfort, but this is a routine method used to suction a baby with a blocked nose. It is also used to collect fluid from the nose which can be used to look for viruses and bacteria, immune cells and chemicals produced by the body in response to infection.

3. **Blood samples:** We would like to take samples of up to 2.5ml (half a teaspoon) of blood. These samples will be used to look at the immune response to infection. A blood sample may have already been taken from your baby for clinical tests. If so, we would like to request consent to use any extra blood which is not needed for these tests, for our research.

4. **Airway samples: This will only be performed on mechanically ventilated infants in PICU.** When a child needs intensive care and supportive mechanical ventilation it is routine care to clear the airways of any secretions/fluid. A suction catheter (tube) is passed down the tube that goes into the child's windpipe, and excess secretions are removed. We would like to collect this fluid and perform the same tests as we do in the fluid collected from the nose.

5. **Micro Curettage: This will only be performed on sedated infants in PICU.** To obtain a sample of cells lining the airways we will use a rhinoprobe to collect a small sample of cells from inside the nose.

You can opt out of any sample type(s) being collected at any point.

Genetic Analysis

As part of a sub-study we would like you to consider allowing us to look at your baby's genetic material (DNA and RNA). We would like to do this in both samples from your baby's airways and, if collected, by analysing a blood sample. These samples will be used to measure genes that reflect your baby's immune response. You should not expect to receive the results of any tests on your baby's genetics. This genetic data will be handled in a careful and confidential manner in compliance with regulations for such tests.

If you are agreeable, we will store your baby's samples in an anonymised form for future research in compliance with the Human Tissue Act 2004.

What are the possible benefits of taking part?
We do not think there will be any direct benefit for your child in taking part in this study. However, the information gained from your child's participation in this study may help to improve the diagnosis and treatment of unwell children in the future.

What are the possible disadvantages to taking part?
There are few disadvantages to taking part in this study. The study will involve taking samples from your child's nose and from the lower airway (in children in PICU and on a mechanical ventilator). These will be taken as outlined above on a daily basis, and this will be done in a gentle way by experienced nursing or medical staff. The small volume of blood being taken will not make any difference to your child's well-being. If your child is in PICU and on a mechanical

ventilator, then the airway sample is collected as part of routine airway care that involves suction of secretions. In this case your child will be continuously monitored, so any change in your child's oxygen level or condition during the procedure will cause us to stop the procedure.

Will the information be kept confidential?

We will record details of your child's condition, including details from the hospital medical notes. All information collected during the course of the research will be kept strictly confidential. Any information about your child that leaves the hospital will have the name and address removed so that they cannot be identified from it.

We will record details of your child's condition, including details from the hospital medical notes. All information collected during the course of the research will be kept strictly confidential. Any information about your child that leaves the hospital will have the name and address removed so that they cannot be identified from it.

Imperial College London is the sponsor for this study based in the United Kingdom. We will be using information from your child and/or your child's medical records in order to undertake this study and will act as the data controller for this study. This means that we are responsible for looking after your child's information and using it properly. Imperial College London will keep identifiable information about your child.
Your rights to access, change or move your child's information are limited, as we need to manage your child's information in specific ways in order for the research to be reliable and accurate. If you withdraw your child from the study, we will keep the information about your child that we have already obtained. To safeguard your child's rights, we will use the minimum personally-identifiable information possible.

You can find out more about how we use your information from Dr Simon Nadel Telephone: 02033126466. Email: s.nadel@imperial.nhs.uk.

Imperial College Healthcare NHS Trust will collect information from your child's medical records for this research study in accordance with our instructions. Imperial College Healthcare NHS Trust will keep your and your child's name, NHS number and contact details confidential and will not pass this information to Imperial College London. Imperial College Healthcare NHS Trust will use this information as needed, to contact you or your child about the research study, and make sure that relevant information about the study is recorded for your child's care, and to oversee the quality of the study. Certain individuals from Imperial College London and regulatory organisations may look at your child's medical and research records to check the accuracy of the research study. Imperial College London will only receive information without any identifying information. The people who analyse the information will not be able to identify you or your child and will not be able to find out your or your child's name, NHS number or contact details. Imperial College Healthcare NHS Trust will keep identifiable information about you and your child from this study for 10 years after the study has finished.

When you agree for your child to take part in a research study, the information about your child's health and care may be provided to researchers running other research studies in this organisation and in other organisations. These organisations may be universities, NHS organisations or companies involved in health and care research in this country or abroad. Your child's information will only be used by organisations and researchers to conduct research

in accordance with the UK Policy Framework for Health and Social Care Research.
This information will not identify you or your child and will not be combined with other information in a way that could identify you or your child. The information will only be used for the purpose of health and care research, and cannot be used to contact you or your child or to affect your child's care. It will not be used to make decisions about future services available to you or your child, such as insurance.

What will happen to the results of the research study?

Results of this research may be published in scientific journals and presented at scientific medical conferences. Your child's privacy will be protected and they will not be identified in any report or publication.

Who is organising and funding the research?

The research is being run by the Department of Paediatrics and the Respiratory Infection Section at Imperial College London and Imperial College NHS Healthcare Trust. This research is funded from within the Department of Paediatrics, the National Heart and Lung Institute, the Imperial College Biomedical Research Cluster, the Medical Research Council and Asthma UK.

Who has reviewed the study?

This study has been reviewed and given a favourable opinion by the National Research Ethics Committee.

What if there is a problem?

Imperial College London holds insurance policies which apply to this study. If you experience serious and enduring harm or injury as a result of taking part in this study, you may be eligible to claim compensation without having to prove that Imperial College is at fault. This does not affect your legal rights to seek compensation.

If you are harmed due to someone's negligence, then you may have grounds for a legal action. Regardless of this, if you wish to complain, or have any concerns about any aspect of the way you have been treated during the course of this study then you should immediately inform the Investigator (Dr Simon Nadel, The Principal investigator). The normal National Health Service complaints mechanisms are also available to you. If you are still not satisfied with the response, you may contact the Imperial AHSC Joint Research Compliance Office.

Where can I find out more about research in general?

There is currently no single organisation for this in the UK, however INVOLVE is a national advisory group, funded by the National Institute for Health Research (NIHR). Its role is to support

and promote active public involvement in NHS, public health and social care research. Contact details are in the next paragraph.

What could I do to help researchers use my own experience more when they are planning their next project?

Do you want to get more involved and help researchers improve future project ideas and research information leaflets? Please contact "People in Research – Opportunities for public involvement in research" http://www.peopleinresearch.org/. If you would like to help, you can also contact INVOLVE which is a national advisory group, funded by the National Institute for Health Research (NIHR). Its role is to support and promote active public involvement in NHS, public health and social care research. http://www.invo.org.uk/ or Wessex House, Upper Market Street, Eastleigh, Hampshire, SO50 9FD, Telephone: 02380 595628. Email: involve@nihr.ac.uk

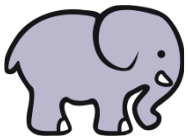
The ELLI research team wish to thank you and your baby for considering participating in this study.

Study Team Contact Telephone Number: Dr Simon Nadel, Telephone 02033126466

Imperial College London

Imperial College Healthcare NHS Trust

Early Life Lung Infection (ELLI) study
The Immune Response to Lung Infection in Infants



Principal Clinical Investigator: Dr Simon Nadel
Consultant Paediatrician and Head of the Paediatric Intensive Care Unit (PICU)

St Mary's Hospital, 7th Floor, Queen Elizabeth the Queen Mother (QEQM) Building
South Wharf Road, Paddington, LONDON W2 1NY

Telephone: 02033126466.
Email: s.nadel@imperial.nhs.uk

PARTICIPANT INFORMATION SHEET
Parents or Guardians of
Babies with Respiratory Infection

Introduction

We are inviting you to consider your child taking part in a research study of babies with respiratory infections. Babies of up to 24 months of age are eligible to take part.

We are recruiting babies that have come to St. Mary's Hospital. This includes babies that are attending the emergency department, being treated on the paediatric wards or being treated on the Paediatric Intensive Care Unit (PICU).

Before you decide, we would like to explain what the study is about and what joining the study involves. Please take time to read the following information and ask us about anything that is not clear or if you would like more information.

Why is the study being done?

Chest infections are common in the early years of life. The vast majority of babies have mild symptoms such as a runny nose or cough, but a small number of babies suffer from severe breathing difficulties requiring hospitalisation, and a small number of these are so unwell that they need to be helped with their breathing by use of a mechanical ventilator.

We would like to take samples of mucous from your child's nose and a blood sample. For children in the Paediatric Intensive Care Unit (PICU) on a mechanical ventilator, we will also collect a sample of mucus from their lungs. With these samples we will look at the immune response to the infection, with the aim of discovering why some infants become more unwell.

Does my child have to take part?

It is up to you to decide whether or not your child takes part. If you agree, you will be given this information sheet to keep and you will be asked to sign a consent form. If you decide for your child not to take part, their care will not be affected in any way. They will continue to receive the same treatment, that is, whatever treatment his or her doctors decide is best. Even if you agree for your baby to enter the study, you may withdraw your consent at any time. You don't have to give a reason and it will not affect your child's care.

What will happen to my baby in the study?

We will take some specimens from your child's nose. Additionally we would like to take blood samples that will be used for our research.

Babies that are being treated on PICU and are on a mechanical ventilator routinely have regular suction to remove excess secretions from their lungs and to make the baby more comfortable. We would like to keep these secretions, which are otherwise thrown away.

What are the different kinds of samples being taken in the research study?

1. **Nasal "paper" absorption (nasosorption):** A small strip of absorbent material that looks and feels like soft blotting paper will be used to absorb moisture from the inside surface of the nostril. This special sterile absorptive "paper" will be placed inside the nostril of the baby and left for a period of about 30 seconds before being removed. Putting the

paper in can tickle and cause the baby to sneeze and perhaps make baby's eyes water a little. However, it is not painful and has proved to be a very safe method, having been studied in many babies. We hope to use the moisture collected on the paper to look for viruses and bacteria, immune cells and chemicals produced during the infection process so we can understand the body's response to the infection. We would like to take a sample from each nostril, or 2 samples from the same nostril. We will do this no more than twice a day.

2. **Nasopharyngeal aspiration (NPA):** This method is routinely performed on babies in hospital. It involves using a suction catheter (tube) to take fluid from the back of the nose. This may cause your baby some discomfort, but this is a routine method used to suction a baby with a blocked nose. It is also used to collect fluid from the nose which can be used to look for viruses and bacteria, immune cells and chemicals produced by the body in response to infection.

3. **Blood samples:** We would like to take samples of up to 2.5ml (half a teaspoon) of blood. These samples will be used to look at the immune response to infection. A blood sample may have already been taken from your baby for clinical tests. If so, we would like to request consent to use any extra blood which is not needed for these tests, for our research.

4. **Airway samples: This will only be performed on mechanically ventilated infants in PICU.** When a child needs intensive care and supportive mechanical ventilation it is routine care to clear the airways of any secretions/fluid. A suction catheter (tube) is passed down the tube that goes into the child's windpipe, and excess secretions are removed. We would like to collect this fluid and perform the same tests as we do in the fluid collected from the nose.

5. **Micro Curettage: This will only be performed on sedated infants in PICU.** To obtain a sample of cells lining the airways we will use a rhinoprobe to collect a small sample of cells from inside the nose.

You can opt out of any sample type(s) being collected at any point.

Genetic Analysis

As part of a sub-study we would like you to consider allowing us to look at your baby's genetic material (DNA and RNA). We would like to do this in both samples from your baby's airways and, if collected, by analysing a blood sample. These samples will be used to measure genes that reflect your baby's immune response. You should not expect to receive the results of any tests on your baby's genetics. This genetic data will be handled in a careful and confidential manner in compliance with regulations for such tests.

If you are agreeable, we will store your baby's samples in an anonymised form for future research in compliance with the Human Tissue Act 2004.

What are the possible benefits of taking part?
We do not think there will be any direct benefit for your child in taking part in this study. However, the information gained from your child's participation in this study may help to improve the diagnosis and treatment of unwell children in the future.

What are the possible disadvantages to taking part?

There are few disadvantages to taking part in this study. The study will involve taking samples from your child's nose and from the lower airway (in children in PICU and on a mechanical ventilator). These will be taken as outlined above on a daily basis, and this will be done in a gentle way by experienced nursing or medical staff. The small volume of blood being taken will not make any difference to your child's well-being. If your child is in PICU and on a mechanical ventilator, then the airway sample is collected as part of routine airway care that involves suction of secretions. In this case your child will be continuously monitored, so any change in your child's oxygen level or condition during the procedure will cause us to stop the procedure.

Will the information be kept confidential?

We will record details of your child's condition, including details from the hospital medical notes. All information collected during the course of the research will be kept strictly confidential. Any information about your child that leaves the hospital will have the name and address removed so that they cannot be identified from it.

We will record details of your child's condition, including details from the hospital medical notes. All information collected during the course of the research will be kept strictly confidential. Any information about your child that leaves the hospital will have the name and address removed so that they cannot be identified from it.

Imperial College London is the sponsor for this study based in the United Kingdom. We will be using information from your child and/or your child's medical records in order to undertake this study and will act as the data controller for this study. This means that we are responsible for looking after your child's information and using it properly. Imperial College London will keep identifiable information about your child.
Your rights to access, change or move your child's information are limited, as we need to manage your child's information in specific ways in order for the research to be reliable and accurate. If you withdraw your child from the study, we will keep the information about your child that we have already obtained. To safeguard your child's rights, we will use the minimum personally-identifiable information possible.

You can find out more about how we use your information from Dr Simon Nadel Telephone: 02033126466. Email: s.nadel@imperial.nhs.uk.

Imperial College Healthcare NHS Trust will collect information from your child's medical records for this research study in accordance with our instructions. Imperial College Healthcare NHS Trust will keep your and your child's name, NHS number and contact details confidential and will not pass this information to Imperial College London. Imperial College Healthcare NHS Trust will use this information as needed, to contact you or your child about the research study, and make sure that relevant information about the study is recorded for your child's care, and to oversee the quality of the study. Certain individuals from Imperial College London and regulatory organisations may look at your child's medical and research records to check the accuracy of the research study. Imperial College London will only receive information without any identifying information. The people who analyse the information will not be able to identify you or your child and will not be able to find out your or your child's name, NHS

number or contact details. Imperial College Healthcare NHS Trust will keep identifiable information about you and your child from this study for 10 years after the study has finished.

When you agree for your child to take part in a research study, the information about your child's health and care may be provided to researchers running other research studies in this organisation and in other organisations. These organisations may be universities, NHS organisations or companies involved in health and care research in this country or abroad. Your child's information will only be used by organisations and researchers to conduct research in accordance with the UK Policy Framework for Health and Social Care Research.
This information will not identify you or your child and will not be combined with other information in a way that could identify you or your child. The information will only be used for the purpose of health and care research, and cannot be used to contact you or your child or to affect your child's care. It will not be used to make decisions about future services available to you or your child, such as insurance.

What will happen to the results of the research study?

Results of this research may be published in scientific journals and presented at scientific medical conferences. Your child's privacy will be protected and they will not be identified in any report or publication.

Who is organising and funding the research?

The research is being run by the Department of Paediatrics and the Respiratory Infection Section at Imperial College London and Imperial College NHS Healthcare Trust. This research is funded from within the Department of Paediatrics, the National Heart and Lung Institute, the Imperial College Biomedical Research Cluster, the Medical Research Council and Asthma UK.

Who has reviewed the study?

This study has been reviewed and given a favourable opinion by the National Research Ethics Committee.

What if there is a problem?

Imperial College London holds insurance policies which apply to this study. If you experience serious and enduring harm or injury as a result of taking part in this study, you may be eligible to claim compensation without having to prove that Imperial College is at fault. This does not affect your legal rights to seek compensation.

If you are harmed due to someone's negligence, then you may have grounds for a legal action. Regardless of this, if you wish to complain, or have any concerns about any aspect of the way you have been treated during the course of this study then you should immediately inform the Investigator (Dr Simon Nadel, The Principal investigator). The normal National Health Service complaints mechanisms are also available to you. If you are still not satisfied with the response, you may contact the Imperial AHSC Joint Research Compliance Office.

Where can I find out more about research in general?

There is currently no single organisation for this in the UK, however INVOLVE is a national advisory group, funded by the National Institute for Health Research (NIHR). Its role is to support and promote active public involvement in NHS, public health and social care research. Contact details are in the next paragraph.

What could I do to help researchers use my own experience more when they are planning their next project?

Do you want to get more involved and help researchers improve future project ideas and research information leaflets? Please contact "People in Research – Opportunities for public involvement in research" http://www.peopleinresearch.org/. If you would like to help, you can also contact INVOLVE which is a national advisory group, funded by the National Institute for Health Research (NIHR). Its role is to support and promote active public involvement in NHS, public health and social care research. http://www.invo.org.uk/ or Wessex House, Upper Market Street, Eastleigh, Hampshire, SO50 9FD, Telephone: 02380 595628. Email: involve@nihr.ac.uk

The ELLI research team wish to thank you and your baby for considering participating in this study.

Study Team Contact Telephone Number: Dr Simon Nadel, Telephone 02033126466

Imperial College London

Imperial College Healthcare NHS Trust

Early Life Lung Infection (ELLI) Study
The Immune Response to Lung Infection in Infants

Imperial College investigators:
Simon Nadel (Principal Investigator), Jethro Herberg, Ryan Thwaites, Dawid Swieboda, Fiona Culley, Trevor Hansel, Peter Openshaw

Abbreviations

ALRI: Acute lower respiratory infections
DNA: deoxyribonucleic acid
MLF: mucosal lining fluid
NPA: nasopharyngeal aspirate
NS: nasosorption with a soft absorptive material
SAM: synthetic absorptive matrix
RSV: respiratory syncytial virus
PICU: paediatric intensive care unit
qPCR: quantitative polymerase chain reaction
NP: nasopharyngeal
NAC: nasal allergen challenge
RTI: respiratory tract infection
mRNA: messenger ribonucleic acid
SNP: Single nucleotide polymorphism
URTI: upper respiratory tract infections
TA: Tracheal aspirate

INTRODUCTION

Early Life Lung Infections

Respiratory infections are the leading single cause of hospitalisation of infants worldwide and are caused by a number of different viruses and bacteria. Globally, the leading cause of severe acute lower respiratory infections (ALRIs, lung infections) in this age group is respiratory syncytial virus (RSV) . Only a minority of infants develop severe disease following a respiratory viral infection, and most children admitted to hospital with ALRI are previously healthy. Prematurity is the main known risk factor for severe disease but there are no predictive biomarkers of disease severity (3). Current treatments for bronchiolitis are largely supportive and no new effective treatments have been developed in recent years. There is no vaccine to prevent RSV infection.

Severe Respiratory Infection at St Mary's Hospital

St. Mary's Hospital is responsible for the clinical care of many babies with severe respiratory infection. Of the babies that attend the Emergency Department (ED) with upper respiratory tract infections (URTI) each winter, over 100 are admitted to the paediatric wards with lung infections. Around 40 babies a year require mechanical ventilation on the Paediatric Intensive Care Unit (PICU) to support them during a lung infection. Although the clinical burden is large, most babies respond well to treatment and mortality is rare.

Study of respiratory infection in infants

Studies of the upper and lower airways of human infants with lung infections are required to definitively understand pathological mechanisms. We seek to understand how the immune inflammatory response during lung infections contributes to disease severity and resolution. Furthermore, we will determine whether the genes of the infant or the infecting virus or bacteria contribute to the outcome of infection.

ALTI is associated with an inflammatory response in the lungs, however, the mechanisms which promote this inflammation, and the nature of the association with viral and bacterial loads are controversial (2,4). The adaptive immune system of infants is generally less developed than in adults(5). Genomic association studies and mechanistic studies of the immune response to RSV point to the importance of the early immune response in determining the outcome of infection (6,7). A weak or ineffective innate response may lead to an elevated pathogen load and allow infection to reach the lower airways (6). Excessive or inappropriate activation of the immune system may promote harmful inflammation (8).

Sample collection

Nasal fluid: We have recently developed the use of nasosorption (NS) using synthetic absorptive matrix (SAM) strips as a minimally invasive method for obtaining samples of airway fluid from infants with bronchiolitis(9). The SAM strips, which have CE marking, were developed in conjunction with a specialist medical device manufacturing company (Hunt Developments (Midhurst, West Sussex). SAMs look and feel like blotting paper and are placed into a nostril and gently held in place for around 30 seconds during which they absorb mucosal lining fluid from the inferior turbinate. SAMs have a low protein binding capacity, allowing fluid to be eluted followed by highly sensitive analysis of airway inflammatory mediators and pathogen load. Importantly, it is minimally distressing for the infant, and samples can be collected at regular intervals over extended periods of time.

Nasopharyngeal aspirate (NPA): In this routine sampling method, NPA samples are obtained by aspiration of the upper airways of congested infants, followed by flushing the suction tubing with saline.

Tracheal aspirate: Infants who require mechanical ventilation are intubated and sedated. In ventilated infants, lower airway samples can be obtained during routine tracheal aspiration. This is performed when clinically required as part of the infants 'bronchial toilet'. This sample allows non-invasive study of the lower airway in severely ill babies.

Micro curettage: To obtain samples of cells lining the airways of infants we will employ a Rhinoprobe to obtain a pinhead of mucosal tissue from the nose.

Blood samples: Infants (particularly dose in PICU) may have indwelling vascular catheters which enable blood sampling without the requirement for an additional needle stick. Blood volumes will be limited according to clinical guidelines (max 0.8ml per kg of body weight). Blood may be taken from indwelling vascular, by venepuncture or alternative routes such as heel prick.

In the case of blood taken from healthy adult volunteers, blood samples may be taken on more than one occasion but will not exceed 50ml at one time or 250ml in 6 months.

Blood may also be obtained from umbilical cord, with collection made from the *ex utero* separated placenta.

Readouts

Analysis of the airway infection

Viral load in airway samples may be obtained by quantitative polymerase chain reaction (qPCR). Viral load of RSV correlates with disease severity in infected infants (4,5). We may also carry out genomic analysis of viral infection. In addition, we may perform culture to identify bacterial

infections and assess the microbiota by microbial genome evaluation. This will fully characterise the microbes present in the airways, including those causing a bacterial and viral co-infection.

Analysis of inflammatory mediators

To determine the extent and nature of the inflammatory response to infection, soluble mediators will be measured by single or multiplex analysis in mucosal lining fluid obtained by nasosorption (NS), NPA and tracheal aspirate as well as in blood. We may also measure levels of pathogen specific antibodies in these samples.

Analysis of the cellular immune response

NPA, tracheal aspirate, nasal curettage and blood samples will undergo processing to obtain cells for analysis of the cellular immune and inflammatory response. Cells may be analysed by flow cytometry, imaging or functional assays, and their gene expression determined.

Genetics

Host genetics may play in important roles in infectious disease outcome. Sequencing of the patient samples may be carried out to identify genetic aetiologies of severe respiratory infections. Gene expression analysis may be performed on blood or airway samples.

Summary

In summary, this study will analyse the immune and inflammatory response to lung infections in infants. We shall additionally measure and characterise the infectious agent and clinically characterise the infection. We shall also assess the genetics of babies included in this study, to see if they may be particularly vulnerable to severe lung infections. Comparison may be made of infant and adult immune responses.

AIMS

The study involves obtaining nasal samples from babies with suspected respiratory infection in the Emergency Department (ED), as well as those admitted to the paediatric wards and PICU at St. Mary's Hospital, London. This will help us to understand the host response during respiratory infections in infants both hospitalised and in the community.

In addition, we shall take samples from infants attending hospital for outpatient appointments, routine elective surgery and admitted to PICU for non-respiratory diagnoses, as controls. To

understand the differences in the immune system in infants compared to adults, we will also collect control samples from adult volunteers and cord blood.

The specific aims are:

1. To measure inflammatory mediators, such as cytokines and antibodies, in the airways and serum of infants with respiratory infection.
2. To characterise the inflammatory cellular infiltrate into the airways and cells in the blood, in terms of cell types, their activation status and their function, particularly innate lymphoid cells, such as natural killer (NK) cells, and granulocytes including eosinophils.
3. To measure gene expression in the airway and blood cells.
4. To determine the infecting virus, measure viral load and viral genotype.
5. To characterise bacterial infection where present and the microbiota in the airways.
6. To determine the differences in immune cell function in adults and infants.
7. To determine the genotype of infected infants to assess if there is a genetic predisposition to severe respiratory infections.
8. To correlate these parameters with clinical parameters including severity and outcome, and to compare infants with RSV infection to infants with non-RSV infection, mild infection and uninfected control infants, and to compare infant and adult samples.

ENDPOINTS

To characterise the inflammatory and immune response to respiratory infection in infants.

PRIMARY ENDPOINT:

Inflammatory mediator production and inflammatory cell infiltrate in the airways.

SECONDARY ENDPOINTS

1. Comparison of the immune response in the blood and airways, as determined by production of inflammatory mediators, antibodies, and the cellular phenotype, numbers and function. Comparison of cells and mediators in the blood and airways of adults and infants.

2. Infection status: This study will include babies with upper respiratory tract infections (URTI) as well as those with severe ALRI. We will include those with RSV and non-RSV infections.

The nature of the viral infection and/or bacterial infection may be unknown at the time of recruitment. In addition, we will measure viral load and may genotype the infecting virus(es). The microbiota of infants may also be characterised to determine whether this is associated with clinical infection and to identify bacterial co-infection.

3. Gene expression: Measurement of gene expression in cells from the airways and blood.

4. Genetics: To establish whether there is a genetic predisposition to severe respiratory infection. To carry out genetic analysis by targeted gene sequencing, next generation sequencing or whole genome single nucleotide polymorphism (SNP) typing in order to evaluate any genetic deficiencies.

STUDY DESIGN

Type of Study: Research project

Duration: 5 years starting in July 2018.

Identification of patients: We shall obtain our study groups from patients attending St. Mary's Hospital, London and healthy adult volunteers who would like to participate in the study. We will recruit healthy adult volunteers via poster and by word of mouth. We might contact healthy adult volunteers for some extra samples via email if consent was given.

Consent:

Consent to enter the study will be sought from each participant or participant's parents or guardians only after a full explanation has been given, an information leaflet offered and time allowed for consideration. Signed consent will be obtained. Participants can opt out of any requested samples without giving any reason. It is not necessary to collect all the samples from one child as we will not discriminate on type of samples collected, however, where possible and parents are willing we would like to obtain as many samples as possible for research purposes. The right of the participant, parent or guardian to refuse to participate without giving reasons will be respected. We will request consent for future research use of samples in other ethically approved studies. The ELLI study may use samples previously obtained in earlier ethically approved studies where consent for future use of samples was obtained.

Deferred consent: In circumstances where the child's clinical condition necessitates immediate investigation and management, we will use a 'deferred consent approach', such that blood tests are carried out before written consent is obtained, through collection of research samples at the

same time as the first clinical samples are taken. This will minimise the need to take samples for research purposes. This may be appropriate in emergency admissions if parents are not initially present, or a critical situation makes discussion of research inappropriate. Parents or guardians will be approached at the earliest opportunity after sample collection to seek consent and assent. If no consent is given, all samples taken will be destroyed. No other samples will be collected until consent is obtained. The blood sample volumes in this study are small and would not constitute a harmful intervention.

Sampling of patients:

- Typically a single blood sample will be taken from infants when bloods are taken for clinical purposes. Exceptionally further samples may be taken and whenever possible these will coincide with clinical draws. Blood samples may be taken for research purposes once weekly from infants from PICU or Wards for up to 2 weeks or until discharge; exceptionally up to 2 further blood samples may be collected per week but only if samples are required for clinical purposes.

  Clinical blood samples may be obtained prior to written consent owing to urgent clinical need. Consent will be obtained at the earliest opportunity and study investigation carried out on left over sample once clinical tests are completed.
- Nasal aspirates will typically be collected once, but further samples may be obtained for up to 2 weeks or until discharge.
- Tracheal aspirates are routinely taken twice daily as part of the care of intubated infants and are discarded. Typically, we will collect one sample per infant, but further samples may be collected if required, for up to 2 weeks or until discharge.
- NS samples may be taken up to twice daily for up to 2 weeks or until discharge.
- Microcurettage samples will typically be taken only once and only from sedated infants, but exceptionally may be taken twice.
- Cord blood sample will be donated once.
- Adults will donate blood, two nasosorption samples and microcurettage once, but may be contacted again to request further donation.

Number and types of Subjects:

A total of 7 groups (up to the total of 50 UK sample size)

Details of each group and sampling are given below:

1. Study Group 1: Babies with suspected respiratory tract infection (RTI) in the ED:

Nasosorption (NS)

Nasopharangeal aspirate (NPA)

Blood sample for research purposes

2. Study Group 2: Babies with suspected respiratory infection admitted to paediatric wards:

NS

NPA

Blood sample for research purposes

3. Study Group 3: Babies with suspected severe respiratory infection in PICU requiring mechanical ventilation:

NS

NPA

Nasal curettage

Tracheal aspirate (TA)

Blood sample for research purposes

4. Study Group 4: Babies without respiratory symptoms, attending routine outpatient appointments, visiting the hospital or undergoing elective surgical procedures:

Nasosorption (NS)

NPA

Nasal curettage

Tracheal aspirate (TA)

Blood sample for research purposes

5. Study Group 5: Babies without respiratory infection but requiring mechanical ventilation in PICU :

NS

NPA

Nasal curettage

Tracheal aspirate (TA)

Blood sample for research purposes

As far as possible, control groups will be sex and age matched to Groups 1 and 2 *ie* infants from 0-6 months will be recruited, as well as older infants up to age 2.

6. Adult Control Group

Healthy adult volunteers.

Blood may be taken on more than one occasion, typically 5-10 ml (up to 200ml) at a time and no more than 250ml in 6 months.

Nasosorption.

Nasal curettage.

7. Cord blood.

Blood from *ex utero* umbilical cord following maternal consent. Cord blood may be from full term infants or from premature (<32 weeks gestation) infants.

PROCEDURES

Nasosorption: SAM strips will be placed inside each of the nostrils for 30 seconds. We will place the SAM on the inferior aspect of the inferior turbinate and middle turbinate. There is minimal discomfort in sampling in these areas. This is a well-tolerated, non-invasive procedure without the need for local anaesthetic.

Nasopharyngeal aspirate: NPA will be carried out after the nasosorption has been performed. NPAs will be collected using a standardized protocol (9-11). The child is supine, and a small suction catheter is used to take fluid from the back of the nose directly with no saline flush. This is a routine method used to suction babies with a blocked nose in clinical practice. Sampling will have to consider the impact of nasogastric and other tubes in the airway. If both NS and NPA samples have to be taken from the same nostril there should be a 5 min interval between these samples. Parents can opt-out of this procedure at each sampling visit.

Tracheal aspirate: Routine clearance of excess mucus by suction through the endotracheal tube. We will keep this aspirate that is usually discarded.

Micro curettage: We will employ a Rhinoprobe to obtain a pinhead of mucosal tissue. This does not require local anaesthesia and will only be performed on sedated infants in PICU, or on adult volunteers.

Blood sampling: Blood will be taken and used to measure markers of infection and inflammation, together with genetic analysis (subject to consent). A maximum of 0.8ml per kg (typically 0.5ml – 2.5ml) will be taken from infants.

Up to 50ml (typically 5-10 ml) of blood will be taken at one time from healthy adults. No more than 250ml will be collected in 6 months.

Genetics Methods for DNA and gene expression (RNA)

i. **Sample collection** Blood and airway samples from the baby will be collected and genetic material extracted

ii. **Sample processing** To carry out genetic analysis from DNA/RNA isolated from infants by targeted gene sequencing, next generation sequencing or whole genome SNP typing in order to evaluate any genetic deficiencies.

iii. **Data Collection** It will be necessary to collect demographic and clinical data from the families to define clearly clinical phenotypes. This will include data on age, sex, ethnicity and clinical details relating to the phenotype. These clinical data will be provided by collaborating clinicians.

Sample storage: All samples will be stored in the specially allocated freezers in ICRRU and Respiratory Infection section at Imperial College London. After the ELLI study if there are any samples left, they will be stored securely and used for another study with appropriate ethics.

Confidentiality: Personal identifiable data arising from the study will be kept on manual paper files in a secure records room at the ICRRU and on NHS computers. Personal data will be kept in pseudo-anonymised form with a link code which can be used to refer to the participants information. This link code will only be available to the clinical research team. Data arising from the study, for publication or dissemination will retain no link to the original participant, and participants will not be identifiable from any published or disseminated materials. Personal data will only be electronically transmitted through secure NHS computers. Only suitably qualified members of the clinical research team will have access to the personal data of the study participants. Anonymised, non-identifiable, information may be shared with academic collaborators.

INCLUSION AND EXCLUSION CRITERIA

Group 1 and Group 2

Inclusion Criteria

- Infants aged 2 weeks-24 months
- Presentation to the Emergency Department with any suspected upper respiratory tract infection (URTI).

  OR
- Suspected respiratory infection, admitted to the paediatric wards at St Mary's Hospital.

Exclusion Criteria

- Any local or systemic factor that would influence the safety of nasal sampling
- Bilateral indwelling nasal catheters or local nasal pathology preventing access for nasal sampling
- Bleeding disorders or risk of bleeding
- The baby is taking part in an interventional study
- The parents or guardians not able to sign the informed consent form due to limited English or comprehension despite the use of independent interpreter services
- Limited life expectancy of the baby or a decision to limit management.
- Infants received corticosteroid therapy at any time in the past month
- Infants with a chronic respiratory condition requiring home oxygen therapy, or recently discharged from NICU or PICU
- Extremely premature infants (<28 weeks)
- Infants with a known immunological disorder

Group 3

Inclusion criteria

- Hospitalised infants admitted to the PICU at St. Mary's Hospital, aged 2 weeks-24 months with suspected respiratory infection
- On a conventional ventilator with an Endotracheal Tube (ETT) of $\geq$2.0mmm diameter

Exclusion criteria

In addition to those listed for Groups 1 and 2

- Significant hypoxia or instability precluding ventilator disconnection
- Transcutaneous oxygen saturation of <95% on 60% oxygen
- In the case of any event which excludes carrying out tracheal aspirate, (e.g.: Significant hypoxia or instability precluding ventilator disconnection) this sample will be missed from the sampling schedule of that study visit
- Pneumothorax (As long as there is no contra-indication to carrying out NPA or nasal SAM sampling, then these children can still be included in the study, but we will not perform tracheal sampling)

Control Group 1

Inclusion criteria

- Babies, aged 2 weeks-24 months, attending routine outpatient appointments, visiting the hospital or undergoing elective surgical procedures.

Exclusion criteria

- Any respiratory symptoms
- All other exclusion criteria are the same as Groups 1 and 2

Control Group 2

Inclusion criteria

- Infants aged 2 weeks-24 months.
- Infants ventilated on the PICU for any condition
- Confirmed negative for infection by PCR of respiratory tract samples

Exclusion Criteria

- All exclusions are the same as Group 3
- In addition – any concern about raised intracranial pressure

Healthy Adult Volunteers

Inclusion criteria

Adults over 18 years of age.

Exclusion Criteria

Volunteers will be asked to exclude themselves from donation according to the following criteria -

- You are unwell at the moment
- You know, or think that you might be infected with hepatitis B or hepatitis C
- You know, or think that you might be infected with HIV— the 'AIDS' virus
- You have a sexual partner who is infected with hepatitis or HIV
- You are anaemic or receiving treatment for anaemia or iron deficiency

Volunteers may be asked to donate more than once. A maximum volume of 50ml will be taken at any one time, and a maximum of 250ml within a 6-month period.

Volunteers not able to sign the informed consent form due to limited English or comprehension despite the use of independent interpreter services.

Umbilical Cord Blood

Inclusion criteria

- Cord blood may be from full term infants or from premature (<32 weeks gestation) infants

Exclusion criteria

- The mother not able to sign the informed consent form due to limited English or comprehension despite the use of independent interpreter services
- Any illness in the mother or infant.
- Mother knowingly infected with hepatitis B, hepatitis C or HIV or with a sexual partner who is infected with hepatitis or HIV.

DATA STORAGE

After a participant has been recruited to the study, their healthcare records will be reviewed by the clinical research team to confirm that the inclusion/exclusion criteria are met. This research team are not part of the direct healthcare team but are suitably qualified.

Personally, identifiable data arising from the study will be kept on manual paper files in a secure records room at the ICRRU and on NHS computers. This records room has a combination lock

code only known to the clinical research team. This records room is further contained in a secure area of the ICRRU which requires swipe-card access. Paediatric clinical data will also be stored in the paediatric research facility, accessible only by qualified staff. Only anonymised data will be transmitted from the clinical research team to the non-clinical research staff.

Personal data will only be electronically transmitted through secure NHS computers. Personal data will be kept in pseudo-anonymised form with a link code which can be used to refer to the participants information. This link code will only be available to the clinical research team. Individuals will only be identified on the database by their unique alphanumeric identifier; data relating to the subjects' names to this identifier will be stored separately. Data arising from the study, for publication or dissemination will retain no link to the original participant, and participants will not be identifiable from any published or disseminated materials. Only suitably qualified members of the clinical research team will have access to the personal data of the study participants. Anonymised, non-identifiable, information may be shared with academic collaborators. Involvement of collaborators may be required for some in-depth data analyses arising from the study. These collaborators may be based in the EEA or further abroad. Only non-identifiable data will be shared with collaborators.

Where consent has previously been given, prospective healthy adult volunteers may be contacted by post, telephone or email.

Data and all appropriate documentation will be stored for a minimum of 10 years after the completion of the study, including the follow-up period.

DATA ANALYSIS

The cellular immune response will be analysed by flow cytometry using appropriate software for data analysis (eg Flojo). Data including levels of inflammatory mediators (e.g. cytokines as pg/ml), cell phenotypes and function and gene expression across the patient groups will be analysed using a number of available statistical packages for the assessment of research data, including GraphPad Prism, SPSS and 'R' software. Statistical analysis will be performed to demonstrate significance of levels of individual biomarkers and molecular signatures. Data will be assessed for normal (Gaussian) distribution using D'AgostinoPearosn omnibus normality tests or Shapiro-Wilk normality tests and will be analysed as either parametric or nonparametric data, as relevant. Analysis techniques will include ANOVA, T-tests in addition to logistic regression and principal-component analyses.

Data will be presented as:
• Raw data: linear and log plots as appropriate
• Box-whisker plots: median/quartile/range
• Heat maps to show correlation between levels

WITHDRAWAL CRITERIA

Any clinically significant side effects during procedures or withdrawal of consent by the parents or guardians of participants.

ADVERSE EVENTS

DEFINITIONS

Adverse Event (AE): any untoward medical occurrence in a patient or clinical study subject.

Serious Adverse Event (SAE): any untoward and unexpected medical occurrence or effect that:

- **Results in death**
- **Is life-threatening** – *refers to an event in which the subject was at risk of death at the time of the event; it does not refer to an event which hypothetically might have caused death if it were more severe*
- **Requires hospitalisation, or prolongation of existing inpatients' hospitalisation**
- **Results in persistent or significant disability or incapacity**
- **Is a congenital anomaly or birth defect?**

Medical judgement should be exercised in deciding whether an AE is serious in other situations. Important AEs that are not immediately life-threatening or do not result in death or hospitalisation but may jeopardise the subject or may require intervention to prevent one of the other outcomes listed in the definition above, should also be considered serious.

REPORTING PROCEDURES

All adverse events should be reported. Depending on the nature of the event the reporting procedures below should be followed. Any questions concerning adverse event reporting should be directed to the Chief Investigator in the first instance.

Non-serious AEs

All such events, whether expected or not, should be recorded.

Serious AEs

An SAE form should be completed and faxed to the Chief Investigator within 24 hours. However, relapse and death due to hospitalisations for elective treatment of a pre-existing condition do not need reporting as SAEs.

All SAEs should be reported to the REC where in the opinion of the Chief Investigator, the event was:

- 'related', i.e. resulted from the administration of any of the research procedures; and
- 'unexpected', i.e. an event that is not listed in the protocol as an expected occurrence

Reports of related and unexpected SAEs should be submitted within 15 days of the Chief Investigator becoming aware of the event, using the NRES SAE form for non-IMP studies. The Chief Investigator must also notify the Sponsor of all SAEs.

Local investigators should report any SAEs as required by their Local Research Ethics Committee, Sponsor and/or Research & Development Office.

Contact details for reporting SAEs
Fax: 020 331 25750, attention Dr Simon Nadel
Please send SAE forms to:
St, Mary's Hospital,
7th Floor, Queen Elizabeth the Queen Mother Building,
Paddington
London
W2 1NY
Tel: 020 78866077 (Mon to Fri 09.00 – 17.00)

ASSESSMENT AND FOLLOW-UP

When sampling is well tolerated there will not be follow up of patients, and the patients will not generally be informed of the result of analyses.

REGULATORY ISSUES

ETHICS APPROVAL

The Study Coordination Centre has obtained approval from the London-Riverside Research Ethics Committee (REC) and Health Regulator Authority (HRA). The study must also receive confirmation of capacity and capability from each participating NHS Trust before accepting participants into the study or any research activity is carried out. The study will be conducted in accordance with the recommendations for physicians involved in research on human subjects adopted by the 18th World Medical Assembly, Helsinki 1964 and later revisions.

CONSENT

Consent to enter the study must be sought from each participant or participant's parents or guardians only after a full explanation has been given, an information leaflet offered and time allowed for consideration. Signed consent should be obtained. The right of the participant, parent or guardian to refuse to participate without giving reasons must be respected. After the participant has entered the study the clinician remains free to give alternative treatment to that specified in the protocol at any stage if he/she feels it is in the participant's best interest, but the reasons for doing so should be recorded. In these cases the participants remain within the study for the purposes of follow-up and data analysis. All participants, parents and guardians are free to withdraw at any time from the protocol without giving reasons and without prejudicing further treatment.

CONFIDENTIALITY

The Chief Investigator will preserve the confidentiality of participants taking part in the study and is registered under the Data Protection Act.

INDEMNITY

Imperial College London holds negligent harm and non-negligent harm insurance policies which apply to this study.

SPONSOR

Imperial College London will act as the main Sponsor for this study. Delegated responsibilities will be assigned to the NHS trusts taking part in this study.

PARTICIPANT REIMBURSMENT

There will be no reimbursement for participating in this study as samples are taken opportunistically.

FUNDING

This study is supported by funding from the Biomedical Research Council and a PhD studentship awarded to David Swieboda by the MRC-Asthma UK Centre in Allergic Mechanisms of Asthma.

AUDITS

The study may be subject to inspection and audit by Imperial College London under their remit as sponsor and other regulatory bodies to ensure adherence to GCP and the UK Policy Framework for Health and Social Care Research.

STUDY MANAGEMENT

The day-to-day management of the study will be co-ordinated through Dr. Simon Nadel, consultant paediatrician and intensivist.

PUBLICATION POLICY

Our aim is to ensure the full dissemination of all study results in medical publications of the highest impact and citation factor. Individual subjects will be strictly anonymised.

REFERENCES

1. Hall, C.B., E.A. Simoes, and L.J. Anderson, Clinical and epidemiologic features of respiratory syncytial virus. Curr Top Microbiol Immunol, 2013. 372: p. 39-57.
2. Shi, T., et al., Global, regional, and national disease burden estimates of acute lower respiratory infections due to respiratory syncytial virus in young children in 2015: a systematic review and modelling study. Lancet, 2017.
3. Hall, C.B., et al., The burden of respiratory syncytial virus infection in young children. N Engl J Med, 2009. 360(6): p. 588-98.
4. Houben, M.L., et al., Disease severity and viral load are correlated in infants with primary respiratory syncytial virus infection in the community. J Med Virol, 2010. 82(7): p. 1266-71.
5. El Saleeby, C.M., et al., Respiratory syncytial virus load, viral dynamics, and disease severity in previously healthy naturally infected children. J Infect Dis, 2011. 204(7): p. 996-1002.
6. Lambert, L., et al., Immunity to RSV in early-life. 2014.
7. Openshaw, P.J., et al., Protective and Harmful Immunity to Respiratory Syncytial Virus Infection. Annual Review of Immunology, 2017. 35(1).
8. Legg, J.P., et al., Type 1 and type 2 cytokine imbalance in acute respiratory syncytial virus bronchiolitis. Am J Respir Crit Care Med, 2003. 168(6): p. 633-9.
9. Thwaites, R.S., et al., Nasosorption as a Minimally Invasive Sampling Procedure: Mucosal Viral Load and Inflammation in Primary RSV Bronchiolitis. J Infect Dis, 2017. 215(8): p. 1240-1244.
10. Hasegawa, K., et al., Respiratory syncytial virus genomic load and disease severity among children hospitalized with bronchiolitis: multicenter cohort studies in the United States and Finland. J Infect Dis, 2015. 211(10): p. 1550-9.
11. Mansbach, J.M., et al., Prospective multicenter study of viral etiology and hospital length of stay in children with severe bronchiolitis. Arch Pediatr Adolesc Med, 2012. 166(8): p. 700-6.

Figure permission from Nature Springer

MOLECULAR BIOSCIENCES
College of Natural Sciences

100 E 24th Street, NHB 2.606 • A5000 • Austin, Texas 78712 • 512-471-5105 • FAX 512-471-1218
molecularbiosci.utexas.edu

January 30, 2020

David Swieboda
Imperial College London
Faculty of Medicine
St. Mary's Campus
London W2 1PG

Dear David,

You have my permission to use Figure 1 from our Nat Reviews Microbiology paper (Nat Rev Microbiol. 2019 Apr;17(4):233-245) in your thesis. I'm glad you like it!

Sincerely,

Jason S. McLellan, Ph.D.
Associate Professor of Molecular Biosciences

SPRINGER NATURE LICENSE
TERMS AND CONDITIONS

Jan 30, 2020

This Agreement between Imperial College London -- Sawid Swieboda ("You") and Springer Nature ("Springer Nature") consists of your license details and the terms and conditions provided by Springer Nature and Copyright Clearance Center.

License Number	4758721048281
License date	Jan 30, 2020
Licensed Content Publisher	Springer Nature
Licensed Content Publication	Nature Reviews Microbiology
Licensed Content Title	Respiratory syncytial virus entry and how to block it
Licensed Content Author	Michael B. Battles et al
Licensed Content Date	Feb 5, 2019
Type of Use	Thesis/Dissertation
Requestor type	academic/university or research institute
Format	print and electronic
Portion	figures/tables/illustrations
Number of figures/tables/illustrations	1
High-res required	no

Will you be translating?	no
Circulation/distribution	1 - 29
Author of this Springer Nature content	no
Title	ILC in viral bronchiolitis
Institution name	Imperial College London
Expected presentation date	Jan 2020
Order reference number	RSV
Portions	Fig. 1: Respiratory syncytial virus virion
Requestor Location	Imperial College London West Kensington London, W14 9NU United Kingdom Attn: Imperial College London
Total	0.00 USD

Terms and Conditions

Springer Nature Customer Service Centre GmbH
Terms and Conditions

This agreement sets out the terms and conditions of the licence (the **Licence**) between you and **Springer Nature Customer Service Centre GmbH** (the **Licensor**). By clicking 'accept' and completing the transaction for the material (**Licensed Material**), you also confirm your acceptance of these terms and conditions.

1. Grant of License

1. 1. The Licensor grants you a personal, non-exclusive, non-transferable, world-wide licence to reproduce the Licensed Material for the purpose specified in your order only. Licences are granted for the specific use requested in the order and for no other

use, subject to the conditions below.

1. 2. The Licensor warrants that it has, to the best of its knowledge, the rights to license reuse of the Licensed Material. However, you should ensure that the material you are requesting is original to the Licensor and does not carry the copyright of another entity (as credited in the published version).

1. 3. If the credit line on any part of the material you have requested indicates that it was reprinted or adapted with permission from another source, then you should also seek permission from that source to reuse the material.

2. Scope of Licence

2. 1. You may only use the Licensed Content in the manner and to the extent permitted by these Ts&Cs and any applicable laws.

2. 2. A separate licence may be required for any additional use of the Licensed Material, e.g. where a licence has been purchased for print only use, separate permission must be obtained for electronic re-use. Similarly, a licence is only valid in the language selected and does not apply for editions in other languages unless additional translation rights have been granted separately in the licence. Any content owned by third parties are expressly excluded from the licence.

2. 3. Similarly, rights for additional components such as custom editions and derivatives require additional permission and may be subject to an additional fee. Please apply to Journalpermissions@springernature.com/bookpermissions@springernature.com for these rights.

2. 4. Where permission has been granted **free of charge** for material in print, permission may also be granted for any electronic version of that work, provided that the material is incidental to your work as a whole and that the electronic version is essentially equivalent to, or substitutes for, the print version.

2. 5. An alternative scope of licence may apply to signatories of the STM Permissions Guidelines, as amended from time to time.

3. Duration of Licence

3. 1. A licence for is valid from the date of purchase ('Licence Date') at the end of the relevant period in the below table:

Scope of Licence	Duration of Licence
Post on a website	12 months
Presentations	12 months
Books and journals	Lifetime of the edition in the language purchased

4. Acknowledgement

4. 1. The Licensor's permission must be acknowledged next to the Licenced Material in print. In electronic form, this acknowledgement must be visible at the same time as the figures/tables/illustrations or abstract, and must be hyperlinked to the journal/book's homepage. Our required acknowledgement format is in the Appendix below.

5. Restrictions on use

5. 1. Use of the Licensed Material may be permitted for incidental promotional use and minor editing privileges e.g. minor adaptations of single figures, changes of format, colour and/or style where the adaptation is credited as set out in Appendix 1 below. Any other changes including but not limited to, cropping, adapting, omitting material that affect the meaning, intention or moral rights of the author are strictly prohibited.

5. 2. You must not use any Licensed Material as part of any design or trademark.

5. 3. Licensed Material may be used in Open Access Publications (OAP) before publication by Springer Nature, but any Licensed Material must be removed from OAP sites prior to final publication.

6. Ownership of Rights

6. 1. Licensed Material remains the property of either Licensor or the relevant third party and any rights not explicitly granted herein are expressly reserved.

7. Warranty

IN NO EVENT SHALL LICENSOR BE LIABLE TO YOU OR ANY OTHER PARTY OR ANY OTHER PERSON OR FOR ANY SPECIAL, CONSEQUENTIAL, INCIDENTAL OR INDIRECT DAMAGES, HOWEVER CAUSED, ARISING OUT OF OR IN CONNECTION WITH THE DOWNLOADING, VIEWING OR USE OF THE MATERIALS REGARDLESS OF THE FORM OF ACTION, WHETHER FOR BREACH OF CONTRACT, BREACH OF WARRANTY, TORT, NEGLIGENCE, INFRINGEMENT OR OTHERWISE (INCLUDING, WITHOUT LIMITATION, DAMAGES BASED ON LOSS OF PROFITS, DATA, FILES, USE, BUSINESS OPPORTUNITY OR CLAIMS OF THIRD PARTIES), AND
WHETHER OR NOT THE PARTY HAS BEEN ADVISED OF THE POSSIBILITY OF SUCH DAMAGES. THIS LIMITATION SHALL APPLY NOTWITHSTANDING ANY FAILURE OF ESSENTIAL PURPOSE OF ANY LIMITED REMEDY PROVIDED HEREIN.

8. Limitations

8. 1. ***BOOKS ONLY:*** Where **'reuse in a dissertation/thesis'** has been selected the following terms apply: Print rights of the final author's accepted manuscript (for clarity, NOT the published version) for up to 100 copies, electronic rights for use only on a

personal website or institutional repository as defined by the Sherpa guideline (www.sherpa.ac.uk/romeo/).

9. Termination and Cancellation

9. 1. Licences will expire after the period shown in Clause 3 (above).

9. 2. Licensee reserves the right to terminate the Licence in the event that payment is not received in full or if there has been a breach of this agreement by you.

Appendix 1 — Acknowledgements:

For Journal Content:
Reprinted by permission from **[the Licensor]**: **[Journal Publisher** (e.g. Nature/Springer/Palgrave)] **[JOURNAL NAME] [REFERENCE CITATION** (Article name, Author(s) Name), **[COPYRIGHT]** (year of publication)

For **Advance Online Publication papers:**
Reprinted by permission from **[the Licensor]**: **[Journal Publisher** (e.g. Nature/Springer/Palgrave)] **[JOURNAL NAME] [REFERENCE CITATION** (Article name, Author(s) Name), **[COPYRIGHT]** (year of publication), advance online publication, day month year (doi: 10.1038/sj.[JOURNAL ACRONYM].)

For Adaptations/Translations:
Adapted/Translated by permission from **[the Licensor]**: **[Journal Publisher** (e.g. Nature/Springer/Palgrave)] **[JOURNAL NAME] [REFERENCE CITATION** (Article name, Author(s) Name), **[COPYRIGHT]** (year of publication)

Note: For any republication from the British Journal of Cancer, the following credit line style applies:

Reprinted/adapted/translated by permission from **[the Licensor]**: on behalf of Cancer Research UK: : **[Journal Publisher** (e.g. Nature/Springer/Palgrave)] **[JOURNAL NAME] [REFERENCE CITATION** (Article name, Author(s) Name), **[COPYRIGHT]** (year of publication)

For **Advance Online Publication** papers:
Reprinted by permission from The **[the Licensor]**: on behalf of Cancer Research UK: **[Journal Publisher** (e.g. Nature/Springer/Palgrave)] **[JOURNAL NAME] [REFERENCE CITATION** (Article name, Author(s) Name), **[COPYRIGHT]** (year of publication), advance online publication, day month year (doi: 10.1038/sj.[JOURNAL ACRONYM])

For Book content:
Reprinted/adapted by permission from **[the Licensor]**: **[Book Publisher** (e.g. Palgrave Macmillan, Springer etc) **[Book Title]** by **[Book author**(s)] **[COPYRIGHT]** (year of publication)

Other Conditions:

Version 1.2

Questions? customercare@copyright.com or +1-855-239-3415 (toll free in the US) or +1-978-646-2777.

Publication OMIP-062

ISAC CYTOMETRY
Journal of Quantitative Cell Science PART A

MIFlowCyt

OMIP-062: A 14-Color, 16-Antibody Panel for Immunophenotyping Human Innate Lymphoid, Myeloid and T Cells in Small Volumes of Whole Blood and Pediatric Airway Samples

Dawid Swieboda,[1,2] Yanping Guo,[1] Sophie Sagawe,[1] Ryan S. Thwaites,[1] Simon Nadel,[3] Peter J.M. Openshaw,[1,2] Fiona J. Culley[1,2*]

[1]National Heart and Lung Institute, Imperial College London, London, UK
[2]Asthma UK Centre in Allergic Mechanisms of Asthma, London, UK
[3]Paediatric Intensive Care Unit, St Mary's Hospital, Imperial College Healthcare NHS Trust, London, UK

Received 21 June 2019; Revised 17 September 2019; Accepted 19 September 2019

Grant sponsor: Asthma UK Centre in Allergic Mechanisms of Asthma, Grant number: AUK-BC-2015-01; Grant sponsor: Imperial College Healthcare NHS Trust Biomedical Research Centre, Grant number: RDA02 and P82570; Grant sponsor: The Wellcome Trust, Grant number: 109008/Z/15/A

Additional Supporting Information may be found in the online version of this article.

*Correspondence to: Fiona J. Culley, NHLI, Faculty of Medicine, Imperial College London, St Mary's Campus, London, W2 1PG, UK Email: f.culley@imperial.ac.uk

Published online 21 October 2019 in Wiley Online Library (wileyonlinelibrary.com)

DOI: 10.1002/cyto.a.23907

© 2019 The Authors. *Cytometry Part A* published by Wiley Periodicals, Inc. on behalf of International Society for Advancement of Cytometry.

This is an open access article under the terms of the Creative Commons Attribution License, which permits use, distribution and reproduction in any medium, provided the original work is properly cited.

ISAC

Purpose and Sample Types

This 14-color, 16-antibody OMIP was designed for enumeration of leukocyte responses in pediatric samples, where sample volumes and cell numbers can be very low. Leukocytes identified by this panel include all major members of the innate lymphoid cell (ILC) family (ILC1s, ILC2s, and ILC3s), natural killer cells (NK cells), granulocytes (neutrophils and eosinophils), T-cells ($CD4^+$ and $CD8^+$), mucosal-associated invariant T cells (MAIT cells) and NKT-like cells. The protocol was optimized using small volumes of peripheral blood and validated in airway samples obtained from children (< 2 years of age) admitted to a pediatric intensive care unit (PICU). Given this backdrop, this OMIP is widely applicable to clinical research using low volume or paucicellular samples, such as studies of innate and adaptive immune responses in infants and children, with potential clinical application in diagnostics and monitoring of patients by pediatricians.

Background

The immaturity of the immune system in early life renders infants vulnerable to infectious diseases, particularly those of the gastrointestinal and respiratory tracts. According to the World Health Organization, acute lower respiratory tract infections are the leading cause of death and hospitalization in children globally (1). How the immune system matures in early life is not fully understood. A better understanding of the nature of the immune and inflammatory response to infection in infants and why some infants develop disease could help to identify new clinical biomarkers, treatments, and prophylactics.

One of the major hurdles in the field of neonatal and pediatric immunology is obtaining relevant samples, which is limited by ethical restrictions on the volume and number of samples that can be taken. As a result, much of our understanding of cellular immunity in infants comes from studies of umbilical cord blood. Less is known about immunity in more mature infants, and less still is known about immunity to infection at mucosal sites, such as the lung (2–4). Moreover, the use of invasive procedures to obtain, for example, lower airway samples cannot be justified in healthy infants. It is important, therefore, that techniques are developed that facilitate the characterization of the immune response in small-volume and paucicellular samples, particularly from sites of infection where sampling is limited. In designing this OMIP (5) we focused on developing a panel to enumerate the innate lymphoid cell (ILC), granulocyte and T-cell responses in infants, particularly those with a lung infection (Table 1). To reflect the challenging situation of limited amounts of blood

and airway samples from infants we optimized this panel using a small volume (300 µl) of adult peripheral blood. Pitoiset et al. (2018) were able to detect regulatory T cells (Tregs) in as little as 60 µl of whole blood from children (6) and others have demonstrated the feasibility of detecting T cell subsets and Type 2 ILCs within pediatric airway samples (7,8).

The recently discovered ILCs have been implicated in playing a pivotal role in immune responses to viral and bacterial pathogens, and they are particularly abundant at mucosal sites (9–11). There are three main subsets of ILC; ILC1s, ILC2s, and ILC3s, which may mirror $CD4^+$ T helper 1 (Th1), Th2, and Th17 subsets, whereas NK cells may complement the cytokine profile and function of $CD8^+$ T cells (12). ILCs comprise only 0.1 to 0.01% of lymphocytes in adult blood (13) and most published methods for detection of ILCs are optimized on relatively large volumes of peripheral blood, however, since ILCs are relatively abundant in children we anticipated relatively high frequencies in small volume pediatric samples (8,14,15). Immunophenotyping ILCs can be challenging as they are defined as lineage negative lymphocytes, which lack specific markers, including CD3 (T cells), CD19 (B cells), CD34 (progenitor cells), FcεR1α (mast cells) and CD1a, CD123, BDCA2 (plasmacytoid dendritic cells, pDC) (15,16). Accordingly, while designing this panel we made sure that a very stringent gating strategy was utilized to obtain a pure ILC subset. We used biaxial gating to delineate ILCs as lineage negative, CD127 (IL-7 receptor-α) positive, live lymphocytes. We distinguished ILC subsets using surface expression of prostaglandin D_2 receptor chemoattractant receptor-homologous molecule expressed on Th2 cells (CRTH2) and CD117 (c-Kit) (8,10,17). In designing this OMIP other components of the cellular immune response were included, which gives this panel broad applicability to other pediatric clinical studies. These were myeloid cells (neutrophils, eosinophils), invariant T cells (mucosal invariant T cells (MAITs) and NKT-like cells) and adaptive T cells ($CD4^+$ and $CD8^+$). By immunophenotyping whole blood, rather than peripheral blood mononuclear cells (PBMC), we reduced the processing time and retained granulocyte populations. All fluorochrome-conjugated antibodies were titrated during panel optimization and are listed in Table 2.

Cells were delineated using the following gating strategy: FSC/SSC, single cells, live cells. Granulocytes, monocytes, and lymphocytes were gated using FSC and the CD45 cell marker

Table 1. Summary table

PURPOSE	MYELOID AND INNATE/ADAPTIVE LYMPHOID COMPREHENSIVE IMMUNOPHENOTYPING
Cell types	Whole peripheral blood, cord blood, PBMCs, nasal aspirate, and tracheal aspirate samples
Species	Human
Cross-reference	OMIP-55, OMIP-007, OMIP-27, OMIP-029, OMIP-038, OMIP-039

Table 2. Antibodies used in the optimized multicolor immunofluorescence panel (OMIP-062)

ANTIBODY	FLUOROCHROME	AB CLONE	PURPOSE
CD127 (IL-7Rα)	BV421	A019D5	ILCs
CD14[1]	BV510	63D3	Lineage
CD19[1]	BV510	HIB19	Lineage
FcεRIα[1]	BV510	AER-37 (CRA-1)	Lineage
CD123[1]	BV510	6H6	Lineage
CD4	BV605	RPA-T4	$CD4^+$ T cells
CD16	BV650	3G8	NK cells/ neutrophils
CD8	BV711	SK1	$CD8^+$ T cells
TCR Vα7.2	BV785	3C10	MAIT cells
CD45	FITC	HI30	Leukocytes
CD117 (c-kit)	PerCP-Cy5.5	A3C6E2	ILC3
CD3[2]	PE	OKT3	T cells
CD161	PE-Dazzle	HP-3G10	MAIT cells
CD56 (NCAM)[2]	PE-Cy7	5.1H11	NK/NKT-like cells
CD294 (CRTH2)	AF647	BM16	ILC2/Th2/ Tc2 subsets
CD66b	AF700	G10F5	Eosinophils
Live/Dead	Near IR-fluorescent reactive dye	n/a	Viability

[1] Lineage cocktail includes the following antibodies: CD14, CD19, CD123, FcεR1α.
[2] Antibodies used to define the lineage negative population, but not part of the lineage cocktail.

(Fig. 1A). Within the granulocyte population, neutrophils were defined as $CD16^{H}CD66b^{+/-}$ and eosinophils as $CD16^{+/-}CD66b^{+}$ (Fig. 1B). Within the lymphocyte gate, the markers CD56 and CD3 were used to identify NK cells ($CD56^+CD3^-$), conventional T lymphocytes ($CD3^+CD56^-$) and NKT-like cells ($CD56^+CD3^+$) (Fig. 1D) (18–20). NK cells were further subdivided into $CD56^{H}CD16^{L}$ and $CD56^{L}CD16^{H}$ populations according to the CD56 and CD16 density (Fig. 1E). T lymphocytes ($CD3^+CD56^-$) were segregated into $CD4^+$ or $CD8^+$ T cells (Fig. 1H). Th2 and Tc2 cells were defined within the $CD4^+$ and $CD8^+$ T cell subsets, respectively, using the CRTH2 surface marker, as these Type-2 cytokine-producing cells express high levels of CRTH2 (8,21) (Fig. 1F,G). Within $CD8^+$ T cells, we also identified MAIT cells. MAIT cells are invariant T lymphocytes which respond to riboflavin metabolites in the context of the MHC class I related molecule MR1 (22,23). MAIT cells were identified within the $CD3^+CD56^-CD8^+$ gate as $CD161^{H}Vα7.2^+$cells (Fig. 1I). NKT cells are conventionally described as $CD3^+CD56^+$ lymphocytes (24,25), however, the use of these markers alone defines a heterogeneous population of lymphocytes, which we designate here as "NKT-like" cells. CD56 can be expressed by many $CD3^+$ lymphocyte subpopulations, including invariant NKT cells (iNKT cells), and some γδ

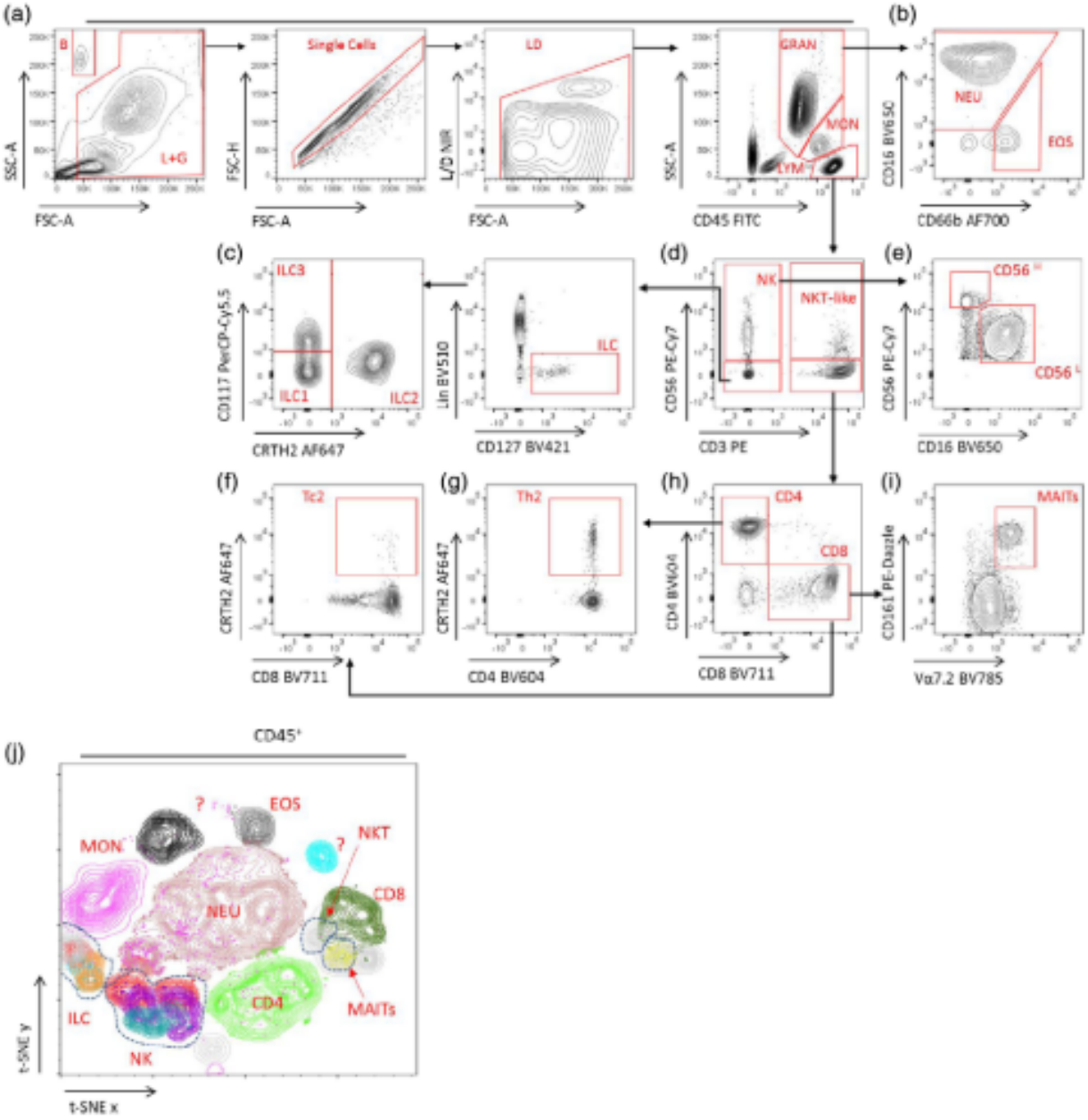


Figure 1. Example gating strategy and t-SNE analysis for visualization of ILCs (including NK cells), granulocytes, MAIT, NKT-like cells, and other T cell populations in pediatric clinical samples. Abbreviations: B, counting beads; L + G, lymphocyte and granulocyte gate; LD, live/dead; GRAN, granulocytes; MON, monocytes; LYM, lymphocytes; NEU, neutrophils; EOS, eosinophils; ILC, innate lymphoid cells; MAIT, mucosal-associated invariant T cells; NK, natural killer cells; NKT-like, natural killer T like cells; ?, Unidentified populations. [Color figure can be viewed at wileyonlinelibrary.com]

T cells and MAIT cells (which have previously been described as mucosal NKT cells) (26,27). Strategies to define these subpopulations are discussed further in the Supporting Information (Part B). Finally, ILCs were defined using the following gating strategy: live, single, $CD45^+$ lymphocytes, lineage (CD3, CD56, CD14, CD19, CD123, FcεR1α) negative, and $CD127^+$ cells (Fig. 1C); ILC1s were defined as $CD117^-CRTH2^-$, ILC2s as $CRTH2^+$ $CD117^{int}$, and ILC3s as $CD117^+CRTH2^-$ (15,28).

To further analyze different populations of cells in this OMIP, unbiased high dimensional stoichiometry (t-SNE) analysis was performed on live, single, $CD45^+$ cells incorporating the lymphocyte, granulocyte, and monocyte gates

(Fig. 1J). In this example, t-SNE not only revealed that all the populations of cells segregated according to the gating strategy illustrated in Figure 1A–I but additionally discriminated distinct or poorly defined populations. Therefore, this 14-color flow panel can be used to delineate other unknown populations using high-dimensional data visualization techniques (29).

Following optimization on adult peripheral blood, we confirmed that the panel was suitable for staining umbilical cord blood, and peripheral blood, tracheal aspirate, and nasal aspirate samples from infants. The inclusion of CD45 in the panel allowed us to separate leukocytes from structural cells, such as epithelial cells, found in airway samples. Concentrations of antibodies were kept the same for analysis of different samples as they gave the same optimal separation between positive and negative populations; however, the protocol for staining airway samples was more methodically complicated and included the use of Fc block. Counting beads were included to allow absolute counts of cell numbers. Detailed information on the panel development and optimization can be found in the Supporting Information (Part B).

Human Samples

All blood and airway samples were collected from subjects after gaining written consent. Some samples were collected as a part of the Early Life Lung Infection (ELLI) and RSV-SAM studies, at St. Mary's Hospital, London. The use of all human tissue samples was approved by the Health Research Authority (HRA) and Health and Care Research Wales (HCRW) Ethics Committee (REC numbers 18/LO/1570; 15/WM/0343 and 13/LO/1712) and in accordance with the Declaration of Helsinki 1964.

Similarity to Other OMIPs

OMIP-55 cross-references to the ILC immunophenotyping; OMIP-007, OMIP-027, and OMIP-029, OMIP-38 and OMIP-039 include phenotypic analysis of NK cells.

Acknowledgments

We thank the St. Mary's Flow Cytometry Core Facility for support and instrumentation during the design of this panel. We are particularly thankful to Prof Beate Kampmann, Dr Beth Holder, Dr Tom Rice, and Sara Barnett for providing cord blood samples. We would like to thank Prof Trevor Hansel for valuable discussions. Finally, we are grateful to research nurses Sarah Darnell, Sobia Mustafa, Ladan Ali, Amina Abdulla, and Suzanne Laing for collecting pediatric samples. This article is independent research funded by the National Institute for Health Research (NIHR) Biomedical Research Centre (BRC) based at Imperial College Healthcare NHS Trust and Imperial College London. The views expressed in this publication are those of the authors and not necessarily those of the NHS, the National Institute for Health Research or the Department of Health.

Conflict of interest

The authors have no conflicts of interest to declare.

Funding

Research Support: Asthma UK Centre in Allergic Mechanisms of Asthma, Imperial College London; Grant number: AUK-BC-2015-01; National Institute for Health Research (NIHR) Biomedical Research Centre (BRC) based at Imperial College Healthcare NHS Trust and Imperial College London; Grant numbers: RDA02 and P82570, The Wellcome Trust; Grant number: 109008/Z/15/A.

Literature Cited

1. WHO. WHO Consultation on respiratory syncytial virus (RSV) vaccine development 2015.
2. Adkins B, Leclerc C, Marshall-Clarke S. Neonatal adaptive immunity comes of age. Nat Rev Immunol 2004;4:553–564.
3. Lambert L, Sagfors AM, Openshaw PJM, Culley FJ. Immunity to RSV in early life. Front Immunol 2014;5:1–14.
4. Yu JC, Khodadadi H, Malik A, Davidson B, Salles ÉDSL, Bhatia J, Hale VL, Baban B. Innate immunity of neonates and infants. Front Immunol 2018;9:1759.
5. Mahnke Y, Chattopadhyay P, Roederer M. Publication of optimized multicolor immunofluorescence panels. Cytom Part A 2010;77:814–818.
6. Pitoiset F, Barbié M, Monneret G, Braudeau C, Pochard P, Pellegrin I, Tranet J, Labuletie M, Klatzmann D, Rosenzwajg M. A standardized flow cytometry procedure for the monitoring of regulatory T cells in clinical trials. Cytom Part B 2018;94:777–782.
7. Connors TJ, Baird JS, Yopes MC, Zens KD, Pethe K, Ravindranath TM, et al. Developmental regulation of effector and resident memory T cell generation during pediatric viral respiratory tract infection. J Immunol 2018;201(2):432–439.
8. Nagakumar P, Denney L, Fleming L, Bush A, Lloyd CM, Saglani S. Type 2 innate lymphoid cells in induced sputum from children with severe asthma. J Allergy Clin Immunol 2016;137:624–626.
9. Bernink JH, Peters CP, Munneke M, Te Velde AA, Meijer SL, Weijer K, Hreggvidsdottir HS, Heinsbroek SE, Legrand N, Buskens CJ, et al. Human type 1 innate lymphoid cells accumulate in inflamed mucosal tissues. Nat Immunol 2013;14:221–229.
10. Dharwal J, Cameron A, Trujillo-Torralbo M-B, del Rosario A, Bakhsoliani E, Paulsen M, Jackson DJ, Edwards MR, BMJ R, Cousins DJ, et al. Mucosal type 2 innate lymphoid cells are a key component of the allergic response to aeroallergens. Am J Respir Crit Care Med 2017;195:1586–1596.
11. Eisman NM, Hamrawi S, Maghazachi AA. Innate lymphoid cells (ILCs) as mediators of inflammation, release of cytokines and lytic molecules. Toxins (Basel) 2017;9:1–18.
12. Ebbo M, Crinier A, Vély F, Vivier E. Innate lymphoid cells: Major players in inflammatory diseases. Nat Rev Immunol 2017;17:665–678.
13. Hazenberg MD, Spits H. Human innate lymphoid cells. Blood 2014;124:700–710.
14. Björklund ÅK, Forkel M, Picelli S, Konya V, Theorell J, Friberg D, Sandberg R, Mjösberg J. The heterogeneity of human CD127+ innate lymphoid cells revealed by single-cell RNA sequencing. Nat Immunol 2016;17:451–460.
15. Vély F, Barlogis V, Vallentin B, Neven B, Piperoglou C, Ebbo M, et al. Evidence of innate lymphoid cell redundancy in humans. Nat Immunol 2016;17:1291–1299.
16. Simoni Y, Fehlings M, Kloverpris HN, Tan IB, Ginhoux F, Newell EW. Human innate lymphoid cell subsets possess human innate lymphoid cell subsets possess tissue-type based heterogeneity in phenotype and frequency. Immunity 2017;46:148–161.
17. Wallrapp A, Riesenfeld SJ, Burkett PR, Abdulnour R-EE, Nyman J, Dionne D, Hofree M, Cuoco MS, Rodman C, Farouq D, et al. The neuropeptide NMU amplifies ILC2-driven allergic lung inflammation. Nature 2017;549:351–356.
18. Costanzo MC, Creegan M, Lal KG, Eller MA. OMIP-027: Functional analysis of human natural killer cells. Cytom Part A 2015;87:803–805.
19. Mahnke YD, Beddall MH, Roederer M. OMIP-029: Human NK-cell phenotypization. Cytom Part A 2015;87:986–988.
20. Eller MA, Currier JR. OMIP-007: Phenotypic analysis of human natural killer cells. Cytom Part A 2012;81A:447–449.
21. Höverling B, Hinks TSC, Stöger L, Marchi E, Salimi M, Shrimankar R, Liu W, Chen W, Luo J, Go S, et al. Synergistic activation of pro-inflammatory type-2 CD8+ T lymphocytes by lipid mediators in severe eosinophilic asthma. Mucosal Immunol 2018;11:1408–1419.
22. Wang H, Hogquist KA. How MAIT cells get their start. Nat Immunol 2016;17:1238–1240.
23. Godfrey DI, Koay HF, McCluskey J, Gherardin NA. The biology and functional importance of MAIT cells. Nat Immunol 2019;20:1110–1128.